THE NONLINEAR DIRAC EQUATION IN BOSE-EINSTEIN CONDENSATES

by

Laith H. Haddad

ARTHUR LAKES LIBRARY
COLORADO SCHOOL OF MINES
GOLDEN, CO 80401

ProQuest Number: 10797419

All rights reserved

INFORMATION TO ALL USERS
The quality of this reproduction is dependent upon the quality of the copy submitted.

In the unlikely event that the author did not send a complete manuscript
and there are missing pages, these will be noted. Also, if material had to be removed,
a note will indicate the deletion.



ProQuest 10797419

Published by ProQuest LLC (2019). Copyright of the Dissertation is held by the Author.

All rights reserved.
This work is protected against unauthorized copying under Title 17, United States Code
Microform Edition © ProQuest LLC.

ProQuest LLC.
789 East Eisenhower Parkway
P.O. Box 1346
Ann Arbor, MI 48106 – 1346

© **Copyright by Laith H. Haddad, 2012**

All Rights Reserved

A thesis submitted to the Faculty and the Board of Trustees of the Colorado School of Mines in partial fulfillment of the requirements for the degree of Doctor of Philosophy (Condensed Matter Theory).

Golden, Colorado

Date 8/29/2012

Signed: _____

Laith H. Haddad

Signed: _____

Dr. Lincoln D. Carr

Thesis Advisor

Golden, Colorado

Date 8/29/2012

Signed: _____

Dr. Thomas E. Furtak

Professor and Head

Department of Physics

ABSTRACT

In this thesis, we study the theory of ultracold atoms in two-dimensional (2D) optical lattices, focusing in particular on honeycomb lattices, the same lattice geometry as in graphene. We study the case of a Bose-Einstein condensate (BEC) located at the Dirac points of the reciprocal honeycomb lattice, whose mean-field theory is described by the nonlinear Dirac equation (NLDE), analogous to the nonlinear Schrödinger equation (NLSE) for ordinary unconstrained BECs in three-dimensions (3D). Physically, the NLDE describes relativistic quasi-particles which travel at speeds 10 orders of magnitude slower than the speed of light, a feature which allows access to relativistic phenomena in the laboratory. We derive the NLDE in coordinate space and recover the same chiral structure and linear dispersion as for electrons in graphene, but from an intuitive microscopic lattice perspective. Symmetries of the NLDE are discussed in detail and compared with those of NLDEs found in the particle physics and mathematics literature. We determine the low-energy theory by deriving, then solving the *relativistic linear stability equations* (RLSE). These are the relativistic analogs of the Bogoliubov-de Gennes equations (BdGE) and describe quasi-particle fluctuations and their associated energy eigenvalues for a BEC near the Dirac point, or Brillouin zone edge, of a honeycomb lattice.

Foundational issues regarding the NLDE are explored, in order to better understand both the context of the NLDE in relation to the NLSE as well as in terms of spin statistics. We give a microscopic physical explanation for the transition from fundamental bosons to Dirac spinors. Similar to graphene, there is a Berry phase associated with rotations in the honeycomb lattice BEC, and we explain this feature in relation to the spin-statistics theorem. We explore reductions of the NLDE to the cubic NLSE with additional correction terms, and study symmetry breaking in this

model in addition to soliton and vortex solutions. By including all Dirac points of the honeycomb lattice, we find that the reduced NLDE maps to the nonlinear sigma model. Lagrangian and energy functional approaches are treated, which provide useful insights into the NLDE.

To place the NLDE on solid experimental ground, we define all relevant physical parameters and show how they relate back to those of ordinary BECs. We do this by deriving the parameter renormalizations which occur under dimensional reduction from 3D to 2D, in addition to the effect of the periodic honeycomb lattice. All of the constraints and approximations needed to observe the NLDE physics are delineated, and a consistent range of values is determined for all of our parameters. To realize NLDE physics along with relativistic vortex excitations, we propose a multistep process using a spin-dependent lattice potential to turn off and on a mass gap, Bragg scattering to transfer condensed atoms to the Dirac points, and Gaussian and Laguerre-Gaussian laser beams to excite the vortices. The combined use of a spin-dependent lattice and Bragg scattering allows for the transfer of atoms to a zero-group velocity state at the Dirac point, resulting in a metastable non-equilibrium BEC removed from the lattice ground state.

Solitons in the NLDE are realized by tightening the harmonic trap in one of the planar directions, which produces either an armchair or zigzig pattern in the remaining spatial degree of freedom of the honeycomb lattice, similar to the geometry of graphene nanoribbons. We call the resulting (1+1)-dimensional NLDEs the armchair NLDE and zigzag NLDE, respectively; their solutions are isomorphic under a complex Pauli rotation. We obtain, by purely analytical means, an extended array of bright solitons. In addition, using a numerical shooting method we obtain the ground state and excited states for a gray line soliton in the presence of a weak harmonic potential. Confinement along the direction of the line soliton leads to spatially quantized states, and the resulting spectra for chemical potential versus particle interaction are com-

puted. Another important consequence of spatial confinement is the appearance of Klein-tunneling in regions where the potential becomes large. We give a detailed explanation of how Klein-tunneling occurs in the NLDE, and contrast this with systems described by the NLSE.

We find that quantized vortices occur in the full $(2+1)$-dimensional NLDE in any of seven possible types, distinguished by different combinations of phase winding number and asymptotic radial forms for each of the spinor components. We obtain analytical and numerical topological and non-topological vortex solutions for arbitrary phase winding number, which include skyrmion and half-quantum vortices, both characterized by a nontrivial pseudospin structure. In the case of unit phase winding, we obtain a singly wound vortex in one spinor component, and a soliton in the other component residing at the core of the vortex. These solutions are analogous to the coreless vortices studied in non-relativistic spinor BECs governed by the well-known vector NLSE. Similar to the case of solitons, we study our vortices in the presence of a radial confining potential, and determine the resulting spectra for the ground state and radial excited states for all of our vortices.

We have extended our study of localized solutions to the general case of a non-zero mass gap in the NLDE, which can be implemented in the honeycomb lattice using a variety of methods, but most readily by breaking the degeneracy between the A and B hexagonal sublattices of the honeycomb lattice. We derive a general method for translating solitons and vortices, embedded in the continuous spectrum, into the gap region, i.e., a mapping from embedded to gap-solitons. The presence of a gap in the spectrum allows for more general massive NLDEs. In particular, we uncover a mapping from a subspace of the NLDE to the massive Thirring model, an extensively studied integrable model, thus revealing a subspace of the NLDE possessing enhanced symmetry.

The first order corrections to mean-field theory are obtained via the RLSE. We derive the RLSE from first principles, by considering quantum fluctuations at each lattice site, then diagonalizing the resulting Hamiltonian and imposing the tight-binding and long-wavelength limits. We analyze the low-energy structure for the case of a uniform BEC by solving the RLSE to obtain quasi-particle coherence factors and frequencies, and find that quasi-particle emission has a distinctive Cherenkov directional and momentum signature when the BEC is displaced from the Dirac point. To add formal rigor to our results, we present a thorough analysis of Wannier expansions of the condensate wavefunction and quasi-particle states at the lattice level, and show that our results depend, to lowest order, on the quality of phase coherence from site-to-site and on a well defined local particle density. In the same vein, we study the mapping of local rotation, quantum, and unitary operators in the honeycomb lattice from the lattice scale to the continuum limit, and obtain the result that discrete rotation matrices acting on the lattice map to $SU(2)$ operations in the continuum limit. Application of the RLSE to soliton and vortex states yields spatial structure for quasi-particle functions, highly localized around the soliton peaks, or dips, and near the vortex cores. The RLSE reveal Nambu-Goldstone modes associated with symmetry breaking. We find that, for the case of a BEC of ^{87}Rb atoms, most solitons and vortices are stable over the lifetime of the BEC.

The full many-body Hamiltonian for bosons near the Dirac points of the honeycomb lattice is derived in detail in both the linear and quadratic momentum approximations using nearest neighbor hopping for both derivations. The linear part of the Hamiltonian describes the full quantum mechanical theory for excitations closest to the Dirac points, and is identical to the Hamiltonian for massless Dirac fermions. The next order correction describes quantum excitations with quadratic dispersion associated with bending of the Dirac cone away from the Dirac points.

TABLE OF CONTENTS

ABSTRACT iii

LIST OF FIGURES xvi

LIST OF TABLES xviii

LIST OF SYMBOLS xix

LIST OF ABBREVIATIONS xxi

ACKNOWLEDGMENTS xxii

DEDICATION xxiii

CHAPTER 1 INTRODUCTION 1

1.1 Mean-field Theory and the Nonlinear Schrödinger Equation 4

1.2 Bogoliubov Theory 7

1.3 Reduction from Three Dimensions to Two Dimensions 9

1.4 Bose-Einstein Condensates in Two-Dimensional Optical Lattices 10

1.5 Cold Atom Interactions in Optical Lattices and Magnetic Traps 16

1.6 The Linear and Nonlinear Dirac Equations 18

1.7 Nonlinear Dirac Equations in Condensed Matter and Cold Atomic Gases 25

1.8 Connections to Optics and Applied Mathematics 27

1.9 Approximations and Constraints Involved in the Nonlinear Dirac Equation 28

1.10 Solution Methods for the Nonlinear Dirac Equation 29

1.11 Overview of Thesis 32

CHAPTER 2 THE NONLINEAR DIRAC EQUATION IN BOSE-EINSTEIN CONDENSATES: FOUNDATION AND SYMMETRIES 37

2.1 Introduction 38

2.2 The Nonlinear Dirac Equation 40

2.2.1 Two-Component Spinor Form of the NLDE 40

2.3 Maximally Compact Form of the NLDE 50

2.4 Symmetries and Constraints 52

2.4.1 Locality 53

2.4.2 Poincaré Symmetry 53

2.4.3 Hermiticity 58

2.4.4 Current Conservation 58

2.4.5 Chiral Current 59

2.4.6 Universality 60

2.4.7 Discrete Symmetries 60

2.4.8 Parity 60

2.4.9 Charge Conjugation 61

2.4.10 Time Reversal 62

2.5 Discussion and Conclusions 63

CHAPTER 3 FOUNDATIONAL TOPICS IN THE NONLINEAR DIRAC EQUATION: SPINOR FORMALISM, SPIN-STATISTICS, LAGRANGIAN ANALYSIS, AND REDUCTION TO THE NONLINEAR SCHRÖDINGER EQUATION 67

3.1 Introduction 67

3.2 The Spin-Statistics Theorem and Honeycomb Lattice Elementary Excitations 68

3.3 Spinor Formalism in the Dirac Equation 72

3.3.1 Energy Versus Chiral Representation 72

3.3.2 Lorentz Non-Covariance of the NLDE 75

3.4 Lagrangian and Energy Functional of the Nonlinear Dirac Equation . . 79

3.4.1 Lagrangian Analysis 80

3.4.2 Energy Functional Analysis for Relativistic Vortices 84

3.5 Reduction of the Time-Dependent NLDE to the Time-Dependent NLSE with Correction Terms 86

3.5.1 One-Dimensional Case 87

3.5.2 Topological Solitons 88

3.5.3 Soliton Energy 92

3.5.4 Nonlinear Sigma Model 95

3.5.5 Two-Dimensional Case 95

3.6 Conclusion 100

CHAPTER 4 RELATIVISTIC LINEAR STABILITY EQUATIONS FOR THE NONLINEAR DIRAC EQUATION IN BOSE-EINSTEIN CONDENSATES 103

4.1 Introduction 104

4.2 Derivation of the RLSE 107

4.3 Physical Parameters and Regimes 109

4.4 Uniformly Moving Condensate 110

4.5 Cherenkov Radiation 112

4.6 Nonlinear Localized Modes 113

4.7 Localized Mode Stability 115

4.8 Conclusion 119

CHAPTER 5 ESTABLISHING THE RELATIVISTIC LINEAR STABILITY EQUATIONS: MICROSCOPIC LATTICE DERIVATION, TRANSITION OF OPERATORS FROM LATTICE TO CONTINUUM, PROPERTIES OF SPINOR COHERENCE FACTORS AND INTERACTING GROUND STATE 121

5.1 Introduction 121

5.2 Standard Theory for a Free Condensate 121

5.3 Bogoliubov Theory for a Condensate at Dirac Point of a Honeycomb Lattice 127

5.3.1 Transition of Operators Between Lattice and Continuum Limits 135

5.3.2 The Tight-Binding Limit Form of Bogoliubov Transformations 138

5.3.3 Derivation of the Constraint Equations for the Lattice: Relativistic Linear Stability Equations 142

5.4 Calculation of RLSE Eigenvalues and Coherence Factors for a Uniform Condensate 145

5.5 Derivation of Condensate Phase Gradient Terms 146

5.6 Energy Eigenvalues 151

5.7 Limits of Quasi-Particle Energy 154

5.7.1 Directional Behavior of the Energy 155

5.8 Coherence Factors for Uniform Background 158

5.9 Interacting Ground-State 162

5.10 General Properties of the RLSE, Quasi-Particle States, and Energies . 163

5.11 Symmetries of the RLSE 164

5.12 Normalization of Quasi-Particle States 165

5.13 Positive and Negative Energy States: Lattice Versus Interaction Effects 167

5.14 Analytical Solutions of the RLSE for Arbitrary Vortex Background . 170

5.15 Conclusion 175

CHAPTER 6 THE NONLINEAR DIRAC EQUATION: RELATIVISTIC VORTICES AND EXPERIMENTAL REALIZATION IN BOSE-EINSTEIN CONDENSATES 177

6.1 Main Text 178

6.2 Supplementary Materials 187

CHAPTER 7 THE NONLINEAR DIRAC EQUATION: METASTABLE RELATIVISTIC VORTICES IN A BOSE-EINSTEIN CONDENSATE 193

7.1 Introduction 194

7.2 Experimental Realization of the NLDE 198

7.2.1 Renormalized Parameters and Physical Constraints 200

7.2.2 Transition from 3D to 2D NLSE 200

7.2.3 Derivation of NLDE from 2D NLSE. 202

7.2.3.1 Normalization Condition. 203

7.2.3.2 Renormalized Atomic Interaction. 204

7.2.3.3 Natural Parameters of the NLDE 204

7.2.4 Physical Constraints 205

7.2.5 Lattice Construction 208

7.2.6 Preparing a BEC at a Dirac Point 209

7.2.7 Coherent Transfer Between Sublattices 212

7.2.8 Creation of Vortices 215

7.2.9 Coherent Transfer Between Dirac Points by Bragg Scattering . 217

7.3 Vortex Solutions of the NLDE 218

7.3.1 Asymptotic Bessel Solutions for Large Phase Winding 220

7.3.2 Numerical Shooting Method for Vortices with Arbitrary Phase Winding and Chemical Potential 222

7.3.3 Algebraic Solutions for Zero Chemical Potential and Phase Winding Greater than One 224

7.3.4 Algebraic Solutions for Zero and Unit Phase Winding 227

7.3.5 Ring-Vortex/Soliton. 227

7.3.6 Vortex/Soliton. 229

7.3.7 Skyrmion Solutions 230

7.3.8 Anderson-Toulouse Skyrmions 232

7.3.9 Mermin-Ho Skyrmions 232

7.3.10 Half-Quantum Vortices 233

7.4 Spectra for Relativistic Vortices 235

7.4.1 Ground State and Radial Excitations of Unconfined Vortices . 236

7.4.2 Solutions for Unit Phase Winding 238

7.4.3 Solutions for Phase Winding Greater than One 239

7.4.4 Special Case of Zero Chemical Potential: Localized Ring-Vortices 240

7.4.5 Discrete Eigenvalue Spectra for Vortices in a Weak Harmonic Trap 241

7.5 Relativistic Linear Stability Equations 243

7.5.1 Derivation 245

7.5.2 First Method - Tight-Binding Limit Followed by Diagonalization of the Quasi-Particle Hamiltonian 248

7.5.3 Second Method - Diagonalize the Quasi-Particle Hamiltonian then Impose Tight-Binding 253

7.5.4 Proof of NLDE Limit to NLSE 255

7.5.5 Proof of RLSE limit to BdGE 257

7.6 Stability of Vortex Solutions 258

7.6.1 Solving the RLSE 259

7.6.2 Computing Vortex Lifetimes 261

7.7 Conclusion 264

7.8 Appendix A: Convergence of Numerical Solutions of the NLDE and RLSE 266

CHAPTER 8 THE NONLINEAR DIRAC EQUATION: RELATIVISTIC SOLITONS AND MASS GAPS 269

8.1 Introduction 270

8.2 Soliton Solutions of the NLDE 273

8.3 Bright Soliton Train 275

8.3.1 Soliton Expansion and Conserved Charges 277

8.3.2 Numerical Solitons 280

8.4 Mass Gaps for the NLDE 282

8.4.1 General Embedded and Gap Solitons 283

8.4.2 Mapping to the Integrable Thirring Model 285

8.4.3 Derivation of the Mapping 285

8.4.4 NLDE Gap Solitons from the Thirring Mapping 287

8.4.5 Implications of the Mapping: Integrability of a Relativistic Subspace of Solutions 288

8.5 Stability of Soliton Solutions 290

8.5.1 Linear Eigenvalues 291

8.5.2 Computing the Line Soliton Lifetime 291

8.6 Soliton Spectra in a Harmonic Trap 293

8.6.1 Quantized Excitations 293

8.6.2 Eigenvalue Spectra and Macroscopic Klein-Tunneling 294

8.7 Conclusion 301

8.8 Appendix A: Continuous Spectrum of the NLDE 302

8.8.1 Four-Spinor Spectrum 302

8.8.2 Resonances at $k = 0$ 303

8.8.3 Two-Spinor Spectrum 304

8.8.4 Static Solutions for Zero Chemical Potential 304

8.8.5 Resonances at $k = 0$ 305

CHAPTER 9 EFFECTIVE QUANTUM FIELD THEORY FOR BOSONS IN THE HONEYCOMB LATTICE 307

9.1 Introduction 308

9.2 Microscopic Derivation of the Many-body Hamiltonian for Bosons in a Honeycomb Lattice 308

9.2.1 First-Order Nearest-Neighbor Hopping 308

9.2.2 Second-Order Nearest-Neighbor Hopping Correction 313

9.3 Continuum Quantum Field Theory 319

9.4 Conclusion 326

CHAPTER 10 CONCLUSIONS AND OUTLOOK 329

REFERENCES CITED 335

LIST OF FIGURES

Figure 2.1 Characterization of a honeycomb lattice. 41

Figure 4.1 The honeycomb optical lattice 106

Figure 4.2 Localized solutions of the NLDE 114

Figure 4.3 Lowest quasi-particle excitation for the vortex/soliton configuration. 116

Figure 6.1 Bragg scattering in a spin-dependent honeycomb lattice. 181

Figure 6.2 Coherent transfer between sublattices A and B 182

Figure 6.3 Relativistic vortices. 183

Figure 7.1 The honeycomb optical lattice 199

Figure 7.2 Convergence of numerical vortex for $\ell = 2$ 224

Figure 7.3 Connection of ring-vortex solution to free particle Bessel solution 225

Figure 7.4 Phase and density for the Bessel topological vortex for $\ell = 4$ . . 226

Figure 7.5 Phase and density for the $\ell = 4$ numerical topological vortex . . 227

Figure 7.6 NLDE vortex radial solutions 228

Figure 7.7 Phase and density for the $\ell = 2$ ring-vortex 229

Figure 7.8 Phase and density for the $\ell = 1$ ring-vortex/soliton 230

Figure 7.9 Phase and density for the $\ell = 1$ vortex/soliton 232

Figure 7.10 Phase and density for the $\ell = 1$ Anderson-Toulouse skyrmion . . 233

Figure 7.11 NLDE vortex radial solutions 234

Figure 7.12 Phase and density for the $\ell = 1$ Mermin-Ho skyrmion 236

Figure 7.13 Phase and density for the half-quantum vortex solutions 237

Figure 7.14 Radial excited states for $\ell = 1$ 238

Figure 7.15 Radial profiles for $\ell = 1$ flat solution 240

Figure 7.16 Radial ring-vortex states for $\ell = 2$ topological solution in the harmonic trap 242

Figure 7.17 Anomalous mode frequencies for the vortex/soliton 260

Figure 7.18 Imaginary parts of the five lowest quasi-particle excitation energies for the ring/vortex solution 261

Figure 7.19 Convergence of RLSE for the vortex/soliton 267

Figure 7.20 Convergence of the $l = 2$ ring-vortex solution 267

Figure 8.1 Quasi-one-dimensional BEC in a honeycomb optical lattice with harmonic confinement 271

Figure 8.2 Optical lattice nanoribbons 272

Figure 8.3 Bright soliton train 277

Figure 8.4 Numerical solutions of the NLDE 281

Figure 8.5 Soliton densities 282

Figure 8.6 Real and imaginary parts of Thirring solutions 289

Figure 8.7 Numerical shooting results for the line soliton 295

Figure 8.8 Numerical shooting results for the line soliton in a harmonic trap 296

Figure 8.9 Ground state of the line soliton in a trap with soft boundary . . 299

Figure 8.10 Discrete spectra of the line soliton in a harmonic trap 300

LIST OF TABLES

Table 5.1 Character of Negative Norm Excitations. The dots indicate that the same condition applies as in the previous line. 169

Table 5.2 Character of Positive Norm Excitations. The dots indicate that the same condition applies as in the previous line. 169

Table 6.1 Physical parameters and constraints for the NLDE typical for a BEC of ^{87}Rb atoms. 179

Table 6.2 Vortex solutions of the NLDE. 187

Table 7.1 Physical Parameters for the NLDE typical for a BEC of ^{87}Rb atoms. 201

Table 7.2 Vortex solutions of the NLDE. 235

Table 7.3 Numbers for computing spectra of $\ell = 2$ topological vortex *ground state* solution 244

Table 7.4 Stability properties of NLDE vortices 262

LIST OF SYMBOLS

Planck's constant . . . . . $\hbar$

Boltzmann's constant . . . . . k_B

atomic mass . . . . . M

number of atoms in the system . . . . . N

wavenumber of laser light . . . . . k_L

lattice constant . . . . . a

lattice recoil energy . . . . . E_R

lattice potential depth . . . . . V_0

hopping energy . . . . . t_h

s-wave scattering length . . . . . a_s

average particle density . . . . . $\bar{n}$

two-body interaction . . . . . g

healing length . . . . . ξ

speed of sound in a Bose-Einstein condensate . . . . . c_s

two-dimensional renormalized speed of sound . . . . . $c_{s,\mathrm{2D}}$

two-dimensional renormalized healing length . . . . . ξ_{2D}

transverse trapping frequency . . . . . ω_z

transverse oscillator length . . . . . L_z

two-dimensional average particle density . . . . . $\bar{n}_{\mathrm{2D}}$

effective speed of light in the honeycomb lattice . . . . . c_l

Dirac kinetic coefficient . . . . . $\bar{c}_l$

coefficient of the Dirac cubic nonlinearity . . . . . U

Dirac healing length . . . . . ξ_{Dirac}

Dirac spinor wavefunction . . . . . Ψ

spinor component wavefunction for A or B sublattice . . . . . $\psi_{A(B)}$

quasi-particle spatial functions . . . . . u_j, v_j

spinor quasi-particle spatial functions . . . . . $\mathbf{u_j}$, $\mathbf{v_j}$

Dirac kinetic operator . . . . . $\mathcal{D}$

gradient operator . . . . . ∇

Minkowski space-time metric . . . . . $g^{\mu\nu}$

Dirac matrices . . . . . γ^{μ}

Pauli matrices . . . . . σ^{μ}

LIST OF ABBREVIATIONS

Bose-Einstein Condensate . . . . . BEC

Nonlinear Dirac Equation . . . . . NLDE

Relativistic Linear Stability Equations . . . . . RLSE

Nonlinear Schrödinger Equation . . . . . NLSE

Bogoliubov-de Gennes Equations . . . . . BdGE

Quantum Electrodynamics . . . . . QED

Berezinkii-Koserlitz-Thouless . . . . . BKT

Unitary Group of Degree 1 . . . . . $U(1)$

Special Unitary Group of Degree 2 . . . . . $SU(2)$

Special Linear Group of Degree 2 Over the Complex Numbers . . . . . $SL(2, C)$

Four Dimensional Representation of $SL(2, C)$ . . . . . $D^{(1/2,1/2)}$

Spin group of dimension n . . . . . $Spin(n)$

General linear group of degree n over the real numbers . . . . . $GL(n, \mathbb{R})$

General linear group of degree n over the complex numbers . . . . . $GL(n, \mathbb{C})$

Charge-Parity-Time Transformation . . . . . CPT

ACKNOWLEDGMENTS

First, I would like to thank my advisor Lincoln Carr for his enthusiasm, insight, creative fervor, and contagious adventurous spirit which have supplied me with hope and inspiration during the long hours deriving equations. Though he has been a helpful guide to me in terms of the technical details of my work, it is the positive energy that surrounds him that has been an indispensable component to my success. I am grateful for his choice of research project which somehow was a perfect fit to my experience and personal inclinations. I attribute our first meeting to fate but subsequent direction in my research to Lincoln's depth and breadth of knowledge of physics.

I would also like to acknowledge the help and support of Michael Wall. He is not only an immensely gifted physicist, but also a person of the heart for whom I have great respect. The discussions we have had over the past few years continue to inspire me and fill me with new ideas. I have enjoyed the time spent with other students at CSM as well. Majed Alotaibi, Erman Bekaroglu, Miguel Ángel García March and others who have enriched my time at CSM.

I dedicate this thesis to my daughter Alyssa and to my mother and father, my brothers and sister, and to my friends. I also dedicate it to my uncle and grandmother. They are in my thoughts and in my heart during every moment of my work.

" Look for the stars, you'll say that there are none; Look up a second time, and, one by one, You mark them twinkling out with silvery light, And wonder how they could elude the sight! "

-William Wordsworth

CHAPTER 1

INTRODUCTION

Since the earliest experiments with laser cooling of atoms and in particular with the creation [1–3] of the first Bose-Einstein condensate (BEC),[1] we have seen an explosion of theoretical and experimental work in the field of cold atomic gases [4–18]. Contributions have come from a diverse array of fields in theoretical and experimental physics, physical chemistry, and applied mathematics [19]. Major areas of impact include nonlinear optics [20–22], physics of the Bose-Einstein condensate to Bardeen-Cooper-Schrieffer superconductivity crossover (BEC-BCS) [23–25], and the dynamics of quantum vortices [26–29]. Advances in the engineering of trapped cold atoms in optical lattices have extended our reach into such exotic aspects of matter as topological insulators, spintronics, and meta-materials. On the mathematics side, our understanding of nonlinear partial differential equations, rooted in mathematics as well as in nonlinear physics, has been vigorously stimulated by the increased interest in BECs [30–32]. As a product of the strong interdisciplinary nature of these topics and the increased ability to manipulate atoms, a new unifying theme is gradually emerging. This is the study of condensed matter and particle physics analogs or simply *quantum analogs*: the modeling of foundational problems in physics using constructions of cold atomic gases [8, 33, 34].

Several developments have made it easier to explore these analogies. For example, with the construction of optical lattices we are now able to model a wide range of condensed matter systems [5, 8]. We can control impurities to a degree not possible in experiments with ordinary crystals. Precise Feshbach resonance tuning allows us

[1]The 2001 Nobel prize for physics was awarded for the discovery of the BEC to Carl Wieman and Eric Cornell at the University of Colorado at Boulder NIST-JILA lab, and to Wolfgang Ketterle at Massachusetts Institute of Technology.

to control the sign, strength, and symmetry of atomic interactions [35]. A variety of periodic systems of ultracold bosonic [36] or fermionic [37] atoms and molecules have been constructed via optical lattices. Spinor condensates which rely on the hyperfine structure of alkali atoms to create a macroscopic pseudospin, are particularly relevant to our work and provide a practical method for constructing multi-component BECs with interesting topologies [38–44]. Such condensates were first realized experimentally for the upper and lower hyperfine states of ^{87}Rb atoms [9, 45], and soon followed for the case of three hyperfine orientations $m_F = 1, 0, -1$ for the $F = 1$ ground state of sodium [10, 46]. In particular, for the case of ^{87}Rb, the angular momentum of the nucleus, $I = 3/2$, and the outer electron, $J = 1/2$, allow for two possible values of the total angular momentum $F = 1, 2$. When the various hyperfine states labeled by the z-components m_F are weakly coupled, this gives rise to interpenetrating superfluids [45, 47].

Our work on BECs in honeycomb lattices connects to important contemporary topics in fundamental and applied physics. In 2004, the first stable monolayer of graphite, graphene, was realized in the laboratory [48–51].[2] The creation of graphene is an exciting new development for two reasons. First, from a technological standpoint its electronic spectrum allows for high mobility of charge carriers, making graphene a good candidate for future replacement of silicon in computing technology. Moreover, at low energies, graphene's honeycomb lattice structure and linear dispersion means that charge carriers are chiral and propagate as massless Dirac fermions at an effective speed of light $c_{\text{eff}} = v_F \simeq c/300$, where v_F is the Fermi velocity. In contrast, we show that a BEC in a honeycomb lattice exhibits relativistic Dirac physics at a velocity 10 orders of magnitude slower than the speed of light. This gives us tabletop access to slow relativistic quantum phenomena [52].

[2]The 2010 Nobel prize for physics was awarded to Andre Geim and Konstantin Novoselov at the University of Manchester for their work in isolating flakes of graphene.

The problems which we explore in this thesis were inspired by the condensed matter/particle physics connection and involve theoretical studies beginning with the optical lattice counterpart of graphene in which ultracold bosonic atoms replace electrons, but retaining graphene's characteristic honeycomb lattice. We obtain the same result as that found in the graphene literature [53, 54], namely that the bipartite structure of the lattice induces a chiral structure on the order parameter as well as reproducing the linear Dirac dispersion [52]. This similarity to graphene is purely due to the honeycomb lattice geometry. However, a significant difference in our case is that, by including contact interactions for bosons, we have obtained a *nonlinear Dirac equation* (NLDE) for the BEC order parameter.

Our model is an ideal starting point for bridging condensed matter systems to various phenomenological models where Dirac fermions can be strongly coupled to other fields or to themselves, as well as gaining a deeper understanding of the fundamental distinction between bosons and fermions. Our studies take place specifically within the context of soliton and vortex solutions of the NLDE. Nonlinear Dirac theories have been used to describe such exotic phenomena as low energy fermions at the intersections of D-branes in string theory using Jona-Lasinio and Gross-Neveu models [55, 56]. These are phenomenological QCD models in that asymptotic freedom and dynamical mass generation are generic features. Other examples include BCS theory with mediating phonons integrated out, weak interactions in the Standard Model and the study of the renormalization of quantum field theories in the large N limit.

In this introduction, we present several topics which provide important background material key to understanding and motivating the work in this thesis. In Sec. 1.1, we review the basic idea behind mean-field theory, a paradigm which is central to the NLDE. In particular, we review the nonlinear Schrödinger equation which is fundamentally connected to the NLDE. Bogoliubov theory is another foundational topic which underlies our work. In Sec. 1.2, we review the motivating assumptions

and physical results obtained through Bogoliubov's method. The physical results presented in this thesis pertain to 2D systems, or to quasi-1D systems. In Sec. 1.3 we explain how dimensional reduction takes place from both the physical as well mathematical perspective. In Sec. 1.4, we review BECs in 2D systems through concepts such as superfluidity and the BKT transition, as well as concepts fundamental to optical lattice cold atoms, such as the Bose-Hubbard model. In Sec. 1.5, we discuss interactions of cold atoms in magnetic fields and optical lattices. In Sec. 1.6, we review the basics of Dirac theory and present some history and motivation behind the nonlinear Dirac equation. In Sec. 1.7, we provide a context for the NLDE as it occurs in optical lattices. in Sec. 1.8, we look at some contemporary fields of research in optics and applied mathematics where the NLDE plays a key role. In Sec. 1.9, the approximations and constraints needed to observe NLDE physics are discussed. Finally, methods for obtaining vortex and soliton solutions of the NLDE are outlined in Sec. 1.10.

1.1 Mean-field Theory and the Nonlinear Schrödinger Equation

The standard approach to mean-field theory was originally developed by Bogoliubov in 1947, and then Gross and Pitaevskii (1961) [57–59]. A succinct explanation is provided in Ref. [27]. The mean-field approach provides a useful paradigm for computing the properties of a Bose gas when most of the particles are in the ground state of the system, i.e, under BEC conditions with minimal depletion. To develop mean-field theory for bosons, one starts from the full many-body Hamiltonian for interacting bosons under the approximation of contact interactions, appropriate to low energy s-wave scattering,

$$\hat{H} = \int d\mathbf{r}\, \hat{\psi}^\dagger(\mathbf{r}) \left[-\frac{\hbar^2}{2m}\nabla^2 + V_{\text{ext}}(\mathbf{r}) \right] \hat{\psi}(\mathbf{r}) + \frac{1}{2}\frac{4\pi\hbar^2 a_s}{m} \int d\mathbf{r}\, \hat{\psi}^\dagger(\mathbf{r})\hat{\psi}^\dagger(\mathbf{r})\hat{\psi}(\mathbf{r})\hat{\psi}(\mathbf{r}) \,, \quad (1.1)$$

where $\hat{\psi}^\dagger$ ($\hat{\psi}$) represents the field operator which creates (destroys) a particle at the spatial point $\mathbf{r}$, V_{ext} is an external potential, and a_s and m are the s-wave scattering length and mass for the constituent bosons. The field operator in Eq. (1.1) pertains to bosonic atoms, so that the bosonic commutation relations apply,

$$\left[\hat{\psi}(\mathbf{r}),\, \hat{\psi}^\dagger(\mathbf{r}')\right] = \delta(\mathbf{r} - \mathbf{r}'). \tag{1.2}$$

We will see that in our work V_{ext} is the periodic lattice potential throughout the thesis, plus an additional harmonic trap in Chapters 7 and 8. The time evolution of the field operator $\hat{\psi}$ is obtained according to the Heisenberg prescription $i\hbar\,\partial\hat{\psi}/\partial t = [\hat{\psi},\, \hat{H}]$, whereby one obtains the equation of motion

$$i\hbar\frac{\partial}{\partial t}\hat{\psi}(\mathbf{r},t) = \left[-\frac{\hbar^2}{2m}\nabla^2 + V_{\text{ext}}(\mathbf{r})\right]\hat{\psi}(\mathbf{r},t) + \frac{4\pi\hbar^2 a_s}{m}\,\hat{\psi}^\dagger(\mathbf{r},t)\hat{\psi}(\mathbf{r},t)\,\hat{\psi}(\mathbf{r},t)\,, \tag{1.3}$$

where we have used the bosonic field commutation relations for $\hat{\psi}$ in Eq. (1.2). The field operator is then expressed as a sum of condensate and noncondensate particle operators

$$\hat{\psi}(\mathbf{r},t) = \hat{\Psi}(\mathbf{r},t) + \hat{\varphi}(\mathbf{r},t)\,, \tag{1.4}$$

where $\hat{\Psi}$ represents the condensate and $\hat{\varphi}$ the non-condensate part.

At this point one assumes a dilute Bose gas so that most of the particles are in the ground state condensate, i.e., that $N - N_0 \ll N$, where N is the total number of particles and N_0 is the number of particles in the condensate. Assuming weak interactions, the condensate can then be approximately represented by a classical field instead of a quantum operator due to $U(1)$ symmetry breaking and an approximate coherent state.[3] Thus we can replace the operator $\hat{\Psi}(\mathbf{r},t)$ by a complex scalar function, namely the expectation value $\Psi(\mathbf{r},t) \equiv \langle\hat{\Psi}(\mathbf{r},t)\rangle$. Taking the expectation value

[3]Here we do not consider a perfect coherent state as such states do not conserve particle number [60].

of Eq. (1.3) and using the mean-field decomposition [61] for products of operators $\langle \ldots \hat{\psi}^\dagger \ldots \hat{\psi} \ldots \rangle = \ldots \langle \hat{\psi}^\dagger \rangle \ldots \langle \hat{\psi} \rangle \ldots$, Eq. (1.3) becomes

$$i\hbar \frac{\partial}{\partial t}\Psi(\mathbf{r},t) = \left[-\frac{\hbar^2}{2m}\nabla^2 + V_{\text{ext}}(\mathbf{r})\right]\Psi(\mathbf{r},t) + \frac{4\pi\hbar^2 a_s}{m}\,|\Psi(\mathbf{r},t)|^2\,\Psi(\mathbf{r},t)\,. \tag{1.5}$$

Equation (1.5) is the Gross-Pitaevskii equation (GPE), or nonlinear Schrödinger equation (NLSE) [58, 59] for the evolution of the complex function $\Psi(\mathbf{r},t)$ with cubic nonlinearity, interacting with the external potential $V_{\text{ext}}(\mathbf{r})$.

When dealing with excitations of a Bose gas in the ground state of a lattice, we require a discrete version of Eq. (1.5), the discrete nonlinear Schrödinger (DNLS) equation [62]. The nature of the DNLS can be pedagogically demonstrated for the case where $V_{\text{ext}}(x) = V_{\text{lat}}(x)$ is a one-dimensional periodic lattice potential, and for the moment we ignore the other two spatial dimensions y, z. The mean-field wavefunction can then be expanded in terms of Bloch functions, $\Psi_{k,\alpha}(x) = e^{ikx}u_{k\alpha}(x)$, where k is the Bloch wavevector and α refers to the energy band, or alternatively in terms of Wannier functions which are localized functions around the lattice sites. Defined explicitly in terms of Bloch functions, the Wannier functions which we take to be real are

$$w_{n\alpha}(x - nL) = \sqrt{\frac{L}{2\pi}}\int_{-\pi/L}^{\pi/L} dk\,\Psi_{k\alpha}(x)e^{-inkL}\,, \tag{1.6}$$

where L is the period of the potential and n refers to the nth lattice position. These functions form a complete orthonormal set so that any solution of the NLSE can be expressed as $\Psi(x,t) = \sum_{n\alpha} c_{n\alpha}(t)w_{n\alpha}(x)$. Upon substitution into the NLSE, multiplying through by $w_{n\alpha}$ and integrating over x gives the result

$$i\hbar\frac{d}{dt}c_{n\alpha} = -\frac{\hbar^2}{2m}\sum_{n_1\alpha_1} c_{n_1\alpha_1}\int dx\, w_{n\alpha}\frac{d^2}{dx^2}w_{n_1\alpha_1} + \sum_{n_1\alpha_1} c_{n_1\alpha_1}\int dx\, w_{n\alpha}V_{\rm lat}w_{n_1\alpha_1}$$
$$+ \; g\sum_{n_1n_2n_3\alpha_1\alpha_2\alpha_3} c^*_{n_1\alpha_1}c_{n_2\alpha_2}c_{n_3\alpha_3}\int dx\, w_{n\alpha}w_{n_1\alpha_1}w_{n_2\alpha_2}w_{n_3\alpha_3}\,, \qquad (1.7)$$

where the interaction strength is defined as $g \equiv 4\pi a_s\hbar^2/m$. If we consider only nearest-neighbor interactions where the potential wells at the lattice sites are deep and well localized around each site, then $w_{n\alpha}$ and its second derivative are large only near each site. Restricting the sums to the same band α, we obtain the DNLS in the tight-binding limit,

$$i\hbar\frac{d}{dt}c_{n\alpha} = \qquad (1.8)$$
$$\langle n,\alpha|H_0|n,\alpha\rangle c_{n\alpha} + \langle n,\alpha|H_0|n+1,\alpha\rangle(c_{n+1\alpha}+c_{n-1\alpha}) + g\,W^{nnnn}_{\alpha\alpha\alpha\alpha}|c_{n\alpha}|^2c_{n\alpha}\,,$$

where the kinetic, lattice potential, and interaction overlap integrals are encapsulated in the coefficients of the amplitudes $c_{n,\alpha}$ in Eq. (1.9) using the definitions

$$H_0 = -\frac{\hbar^2}{2m}\frac{d^2}{dx^2} + V_{\rm lat}(x)\,, \quad W^{nn_1n_2n_3}_{\alpha\alpha_1\alpha_2\alpha_3} = \int dx\, w_{n\alpha}w_{n_1\alpha_1}w_{n_2\alpha_2}w_{n_3\alpha_3}\,. \qquad (1.9)$$

Interesting applications of the DNLS can be found in Ref. [63].

1.2 Bogoliubov Theory

Mean-field theory can be improved by incorporating quantum fluctuations as a perturbation. In particular, the Bogoliubov method [57] starts from Eq. (1.4), then substitutes the mean-field for the condensate operator $\hat{\Psi}$, where the noncondensate term represents small quantum fluctuations around the mean-field. Retaining the small operator term $\hat{\varphi}(\mathbf{r})$ in Eq. (1.4) as an addition to the mean-field component, is called the Bogoliubov shift [64], and reflects the assumption that the condensate is the dominant part of the wavefunction. From Eqs. (1.2)-(1.4), we see that the

bosonic nature of $\hat{\psi}(\mathbf{r})$ implies the commutation relation $\left[\hat{\varphi}(\mathbf{r}),\, \hat{\varphi}^{\dagger}(\mathbf{r}')\right] = \delta(\mathbf{r}-\mathbf{r}')$, for the fluctuations. Next, the mean-field limit of Eq. (1.4) is substituted into the full many-body Hamiltonian, Eq. (1.1), wherein we neglect terms beyond second order in $\hat{\varphi}(\mathbf{r})$, consistent with the assumption of small depletion of the condensate. Moreover, the terms first order in the operator are eliminated by the fact that the mean-field satisfies the NLSE. Thus, Eq. (1.1) reduces to a quadratic form in $\hat{\varphi}(\mathbf{r})$, which is then diagonalizable by a convenient unitary transformation. This step is called the canonical Bogoliubov transformation, and has the general form $\hat{\varphi}(\mathbf{r}) = \sum_j \left[u_j(\mathbf{r})\hat{\alpha}_j - v_j^*(\mathbf{r})\hat{\alpha}_j^{\dagger}\right]$, where the summation is over momentum states j, and the spatial functions u_j and v_j will depend on the profile of the condensate $\Psi(\mathbf{r})$. The operators $\hat{\alpha}_j(\mathbf{r})$ and $\hat{\alpha}_j^{\dagger}(\mathbf{r})$ have a physical interpretation as quasi-particle and quasi-hole operators [65].

The particle-hole picture derives naturally from the fact that the interacting ground state is a superposition of single-particle states covering a spread in momentum values subject to momentum conservation. This is true because the ground state is formed out of momentum-conserving interactions. A full treatment for general nonuniform $\Psi(\mathbf{r})$ can be found in Ref. [66]. Requiring unitarity forces a normalization condition and completeness relations on u_j and v_j,

$$\sum_j{}' \left[u_j(\mathbf{r})\, u_j^*(\mathbf{r}') \;-\; v_j^*(\mathbf{r})\, v_j(\mathbf{r}')\right] \;=\; \delta(\mathbf{r},\mathbf{r}')\,, \tag{1.10}$$

$$\sum_j{}' \left[u_j(\mathbf{r})\, v_j^*(\mathbf{r}') \;-\; v_j^*(\mathbf{r}')\, u_j(\mathbf{r}')\right] \;=\; 0\,, \tag{1.11}$$

$$\sum_j{}' \left[u_j^*(\mathbf{r})\, v_j(\mathbf{r}') \;-\; v_j(\mathbf{r})\, u_j^*(\mathbf{r}')\right] \;=\; 0\,, \tag{1.12}$$

where the prime notation on the summation indicates exclusion of the ground state. Equations (1.10)-(1.11) are key conditions when diagonalizing the Hamiltonian. The Bogoliubov rotation mixes the Fourier terms in the plane-wave expansion of $\hat{\varphi}(\mathbf{r})$, so

that the quantum aspect of the interactions in Eq. (1.1) get absorbed into the collective quasi-particle excitations. This is evident by examining the final transformed Hamiltonian

$$\hat{H} = \int d\mathbf{r}\, \Psi^*(\mathbf{r}) \left[\hat{H}_0 - \mu + \frac{g}{2}\,|\Psi(\mathbf{r})|^2\right] \Psi(\mathbf{r}) - \sum_j{}' E_j \int d\mathbf{r}\, |v_j(\mathbf{r})|^2 + \sum_j{}' E_j\, \hat{\alpha}_j^\dagger \hat{\alpha}_j . \quad (1.13)$$

The first term is the mean-field contribution, the second term is a correction to the mean-field theory, and the third term is the quantum contribution from the quasi-particle excitations. Note that at finite temperature additional terms will appear in Eq. (7.111), as Bogoliubov theory treats the particular regime $T \ll T_c$ where temperatures are well below the critical temperature for BEC. In Chapter 5 of this thesis, we provide a rigorous proof of the discussion in this section. A good introduction to Bogoliubov theory and symmetry breaking can be found in Ref. [67].

1.3 Reduction from Three Dimensions to Two Dimensions

In this thesis, we study BECs in quasi-2D systems [68, 69]. In a realistic setting, this means that the BEC is tightly confined in one direction and loosely confined in the other two directions. More precisely stated, we require magnetic trapping along the z-direction to be such that excitations along this direction have much higher energy, by at least an order of magnitude, compared to the lowest excitations in the x and y-directions. A fundamental part of our work involves calculating the precise renormalization of all the relevant physical parameters when transitioning from the standard 3D BEC to a 2D system. Note that in addition to this step, we must also account for a renormalization due to the presence of the optical lattice potential, which introduces an additional length scale from the lattice constant. Thus, we work out the full physical picture in 2D, confident that any point in a particular calculation we can map back to the 3D system.

Strict confinement in the z-direction demands a clear separation between the characteristic length scales associated with the interaction g, the average particle density $\bar{n}$, and the width of the BEC in the z-direction L_z. Note that throughout this thesis we consider only the case where $g > 0$. The separation of length scales is expressed in the inequality $a_s \ll L_z \lesssim \xi$, where the transverse oscillator length is determined by the oscillator frequency through $L_z \equiv (\hbar/M\omega_z)^{1/2}$, and the mass M of the individual particles. The healing length in the BEC sets the upper bound and is defined as $\xi \equiv (8\pi\bar{n}a_s)^{-1/2}$. Note that two length scales appear here: one is the scattering length a_s and the other is the healing length ξ, which incorporates the particle density $\bar{n} \equiv N/V$, where N is the number of particles in the system and V is the corresponding volume. A second condition is that the size of the condensate along the large directions, defined by a radius R, is much larger than the transverse direction L_z, $R \gg L_z$, which for low temperatures and low energy stationary states and dynamics, forces any accessible momentum states to lie only along the planar direction of the BEC. Based on this discussion, we can separate the full 3D condensate wavefunction into longitudinal and transverse parts, $f(x, y)$ and $h(z)$, respectively, so that $\Psi(\mathbf{r}, t) = (AL_z)^{-1/2} f(x, y)h(z)e^{-i\mu t/\hbar}$, where A is the area πR^2 and μ is the chemical potential of the system. The reduction is completed by integrating over the transverse direction z then redefining parameters to recover the 2D NLSE. In Chapters 6 and 7, we explain how the interaction g is modified to obtain g_{2D} along with a full detailed analysis of our dimensional reduction procedure with complete definitions of physical parameters.

1.4 Bose-Einstein Condensates in Two-Dimensional Optical Lattices

Bose-Einstein condensation was initially observed in dilute atomic gases of sodium, lithium, and rubidium.[4] Other elements which have been now Bose-condensed include

[4]We point out that the lithium observation was only confirmed two years after rubidium and sodium.

hydrogen, chromium, ytterbium, the alkali metals potassium and cesium, in addition to the alkaline earth metals calcium and strontium, as well as dysprosium. The BEC is typically observed at particle densities of $10^{12}\,\mathrm{cm}^{-3}$ to $10^{14}\,\mathrm{cm}^{-3}$ and as high as $10^{15}\,\mathrm{cm}^{-3}$ and at temperatures less than a microKelvin and as low as tens of picoKelvin [70]. The cooling process occurs along a two step path: laser cooling followed by evaporative cooling. The latter step allows higher energy atoms to leave the system while further cooling the remaining atoms. Laser cooling is based on the use of the Doppler effect for atoms interacting with a laser beam. To see this, we consider two oppositely directed beams of the same frequency just below the frequency of an atomic transition. An atom stationary with respect to both beams will absorb an equal number of photons, of the same energy, from either direction. Thus no net momentum change of the atom is observed. The key point here is that the atomic absorption rate depends on the frequency of the absorbed light, so that we can capitalize on the Doppler shift that occurs for motion towards or away from the direction of a beam. The result is that an atom with a net velocity in one direction will experience a frictional force opposite the direction of motion.

Two pervasive features which underlie our work are the concepts of condensation and superfluidity. The Bose-Einstein condensate is synonymous with the breaking of global $U(1)$ symmetry [30, 31], resulting in long-range phase coherence, whereas superfluidity derives from the BEC state but has more notions associated with it, such as the Hess-Fairbanks effect [71]. Generally, the condensate phase refers to a macroscopic number of particles residing in one single-particle state, whereas superfluidity refers to the response of particles to a velocity boost. We can understand the meaning of $U(1)$ symmetry breaking by returning to the Hamiltonian in Eq. (1.1). It is symmetric under a global phase transformation, i.e., the transformation $\hat{\psi} \rightarrow e^{i\alpha}\hat{\psi}$ leaves the Hamiltonian unchanged, where α is a real constant. This symmetry is described by the unitary group of degree one, or $U(1)$. It is in some ways implied in

Eq. (1.1) that since we are working with the full many-body theory, the principle of phase-density uncertainty is at work, and that in general the Hilbert space connected to the field operator $\hat{\psi}$ is associated with a completely random phase. As we have seen, the mean-field step which exchanges the condensate operator for a complex wavefunction implies a completely well defined phase: the phase has acquired a non-zero expectation value. This type of formal symmetry breaking is physically realized in the case of a BEC, where the ground state of the system does not share the same global $U(1)$ symmetry of the underlying Hamiltonian.

These concepts become more tenuous when the constituent bosons are confined in an optical lattice, since here macroscopic atomic coherence can be disrupted by the periodic potential of the lattice. Nevertheless, one finds that BECs do indeed occur in such systems as long as the lattice is shallow enough to avoid the Mott insulating phase. In the lattice setting, particle interactions U and hopping t_h give rise to two distinct phases associated with the strong and weak interaction limits $U/t_h \gg 1$ and $U/t_h \ll 1$. When interactions are strong, particles tend not to occupy the same sites, and we find that particle number is well defined at each site, with large uncertainty in the phase. This defines a Mott insulator: shifting particles around is energetically costly. For weak interactions, hopping is dominant so that the total energy of the system is lowered when particles move freely through the lattice. In this case, on-site particle number is uncertain, while the phase is well defined. This state defines a superfluid with velocity defined as the gradient of the phase $\mathbf{v} \equiv (\hbar/M)\nabla\Phi$, which we discuss later in Section 1.4. Of critical importance to BEC stability is the strict 2D confinement which destroys long-range order as expounded in the Mermin-Wagner theorem [72]. For a thorough treatment of the physics of cold atoms see Ref. [7] and the review article [4]. For a good review on the theory of cold bosons in optical lattices see Ref. [64], and [73, 74] for a treatments on 2D systems.

A quantum fluid may be described in terms of its normal versus superfluid fractions f_n and f_s, the former pertaining to the viscous part and the latter referring to that part of the fluid which flows unimpeded [75]. In particular, one precise way to define the superfluid state is in terms of changes in the matter wave interference, i.e., decoherence, quantified by the energetic cost of adding twists to the macroscopic phase Φ of the BEC, where the macroscopically occupied wavefunction Ψ may be expressed in terms of the density and phase $\Psi(\mathbf{r}) = \sqrt{\rho(\mathbf{r})}\, e^{i\Phi(\mathbf{r})}$ [76]. The velocity field which describes superfluid flow is the usual phase gradient $\mathbf{v} \equiv (\hbar/M)\nabla\Phi$.

The BEC ground state energy E_0 is invariant under global changes in Φ but not local, spatially dependent ones. The energetic cost δE_Φ of adding small local variations in Φ is interpreted as the additional kinetic energy due to the superfluid flow. In the 1D linear approximation this leads to an expression for the superfluid fraction $f_s = 4\pi^2(E_\Phi - E_0)/(NE_R\Delta\Phi^2)$, where N is the total number of particles, $\Delta\Phi$ is the phase variation over the lattice spacing a, and $E_R = \hbar^2/(2Ma^2)$ is the lattice recoil energy, i.e., the kinetic energy characterized by the periodicity of the lattice [76]. In all of the problems we present in this thesis, we work in the long-wavelength limit so that Φ is the phase of the complex Bloch factor and plays a central role in vortices as the quantized winding around the core.

Closely related to the use of on-site localized atomic states is the notion of the tight-binding approximation. Physically, this refers to the optical regime in which a particle's potential energy inside a single well is much larger than the characteristic kinetic energy imparted to it by the lattice. This can be stated precisely as $V_0/E_R \gg 1$, in terms of the lattice depth V_0 and the recoil energy E_R, where M is the mass of the constituent bosons and k is the wavenumber of the laser light making up the lattice. In our work we consider $1 \gg V_0/E_R \lesssim 20$: the lower bound is to satisfy the tight-binding limit, while the upper bound comes from satisfying the various physical constraints in our problem, including avoiding a Mott-insulating transition. The tight-

binding limit allows for a many-body description in terms of the nearest-neighbor hopping picture where bosons reside mainly at individual lattice sites and tunneling to adjacent sites is accounted for by including the strength of overlap between adjacent Wannier peaks [62] encapsulated in the hopping energy t_h. Typically, the hopping parameter t_h is computed using the semiclassical approximation, which provides an accurate treatment such that $t_h \equiv 1.861\,(V_0/E_R)^{3/4}\,E_R \exp\!\left(-1.582\sqrt{V_0/E_R}\right)$ [77].

The Bose-Hubbard model (BHM) is consistent with this picture, which we obtain as an intermediate stage of our derivation of the nonlinear Dirac equation, and rely on extensively well as the foundation of many of our other calculations. The derivation of the BHM proceeds from the full many-body Hamiltonian for an interacting Bose gas in a periodic external potential, followed by the assumption of tight-binding, which allows for a Wannier basis expansion of spatially dependent terms. Finally, we integrate over the spatial coordinates which leads to a discrete lattice Hamiltonian. We present this derivation in detail in Chapter 2.2.1. Explicitly, the BHM is embodied in the Hamiltonian

$$\hat{H} = -t_h \sum_{\langle i,j \rangle} \left(\hat{b}_i^\dagger \hat{b}_j + \hat{b}_j^\dagger \hat{b}_i \right) + \frac{U}{2} \sum_i \hat{n}_i(\hat{n}_i - 1) - \mu \sum_i \hat{n}_i \,, \tag{1.14}$$

where $\hat{b}_i^\dagger$ ($\hat{b}_i$) creates (destroys) a boson at lattice site i, and $\hat{n}_i \equiv \hat{b}_i^\dagger \hat{b}_i$ counts the number of atoms at the ith site. The first term in Eq. (1.14) describes particle hopping between nearest neighbor sites, indicated by the $\langle i, j \rangle$ subscript on the summation, the second term describes on-site particle interactions, and the third term is the chemical potential term. Note that hopping is controlled by the strength t_h,[5] and interactions by the strength U, both encapsulating the microscopic continuum spatial aspects of the physics. Competition between the hopping and interaction strengths leads to the well-known superfluid to Mott insulator transition [36, 79], a prototypical

[5]The usual notation is t [78], but we use t_h to distinguish hopping from time t; another common notation is J for hopping, which we opt not to use.

example of a quantum phase transition (QPT) [80] observed in experiments [36]. Note that Eq. (1.14) is valid for arbitrary spatial dimensions. In particular, for the 2D honeycomb lattice, the BHM is expressed by the Dirac-Bose-Hubbard Hamiltonian which we derive in Chapter 2, specifically in Eq. (2.10).

One unique feature of two-dimensional (2D) systems at finite temperatures is the absence of condensation in the formal sense, i.e., a configuration with infinite phase coherence. At nonzero temperature, long-wavelength thermal fluctuations destroy the long-range order in a sample. This occurs in the interacting as well as non-interacting case, and one must instead be content with a quasi-condensate order characterized by phase coherence on finite length scales. In this case, the one-body correlation function decays algebraically as opposed to exponential decay for the ordinary uncondensed state. Nevertheless, the vortex and soliton structures which we deal with have characteristic healing lengths which are small compared to the size of the regions of coherence, and hence this limitation does not impose any noticeable restrictions on our results.

The transition from ordinary to superfluid phase in 2D was originally predicted by Berezinskii [81] and by Kosterlitz and Thouless (BKT) [82], and has been confirmed for several macroscopic quantum systems [74]. A wide variety of 2D phenomena exhibit this property including superfluid liquid helium films [83], superconductivity in arrays of Josephson junctions [84], and collisions in 2D atomic hydrogen [11]. The microscopic mechanism underlying the BKT transition is that of bound, oppositely rotating pairs of vortices below a critical temperature T_c, contrasted with a proliferation of unbound individual vortices above T_c which destroy the long-range order. The precise mechanism of the transition hinges on the abrupt phase dislocations which occur at the core of a vortex contrary to the slowly varying phase interference fringes coming from ordinary fluctuations in Φ.

Recently, it was shown that the BKT phase transition is a generic feature of a large class of $(2+1)$-dimensional models which bridge non-relativistic and relativistic many-body physics [85]. This new type of phase transition was obtained via holographic duality, thus the term *holographic BKT* has been coined. The honeycomb optical lattice provides an ideal setting for studying the binding and unbinding of exotic relativistic vortices not found in ordinary 2D BECs, and the associated BKT transition at finite or zero temperature. Although we do not treat the full dynamics of vortices in this thesis, our investigations into vortex solutions and their stability properties provide the framework for further research into such phenomena as BKT type transitions for relativistic systems. The underlying lattice allows for a large variety of distinct vortices, and these are expected to play a central role in the corresponding superfluid phase transition. To study BKT in our system requires a specific relationship for our length scales. We would require that the BEC sample size R (radius), 2D healing length ξ, and lattice constant a satisfy the inequality $a \ll \xi \ll R$. The first inequality pertains to the long wavelength approximation on the lattice, while the second ensures that vortices are microscopic in relation to the sample size. Incidentally, we adhere to this condition throughout our work.

1.5 Cold Atom Interactions in Optical Lattices and Magnetic Traps

In our work we consider samples of cold atoms confined in magnetic traps. Magnetic trapping of neutral atoms occurs through the Zeeman effect, which comes from the interaction between electronic and nuclear spin magnetic moments and an external applied magnetic field. For low-strength magnetic fields, Zeeman energies are small compared with hyperfine splitting, in which case the energy may be written as

$$E(F, m_F) = E(F) + m_F g_F \mu_B B\,, \tag{1.15}$$

expressed to first order in the magnetic field B, where g_F is the Landé g factor, $E(F)$ is the energy in the absence of an external magnetic field, F is the total spin, and m_F is the z-component of the total spin. The states which interest us are the ones for which $F = I - 1/2$ with $m_F = -(I - 1/2)$, since they have negative magnetic moments and are therefore amenable to magnetic trapping. A negative magnetic moment means that atoms in such states will be forced towards a local minimum when placed in an inhomogeneous magnetic field. Thus, the magnetic configuration of interest is one with a local minimum, either a zero or a non-zero value of $|\mathbf{B}|$. The quadrupole trap is an example of the former and the Ioffe-Pritchard trap is an example of the latter. Detailed explanations of the various types of traps may be found in Ref. [7].

In the presence of a spatially varying electric field, neutral atoms experience a force due to the polarization of their electronic charge distribution. For an inhomogeneous time-varying electric field, the gradient of the shift in atomic energy gives rise to the dipole force

$$\mathbf{F}_{\text{dipole}} = -\nabla V(\mathbf{r}) = \frac{1}{2}\alpha'(\omega)\nabla\langle\mathcal{E}(\mathbf{r},t)^2\rangle_t\,, \tag{1.16}$$

where the bracketed quantity is the time-average of the applied electric field and $\alpha'(\omega)$ is the frequency dependent atomic polarizability. This is referred to as the AC Stark shift. The direction of the polarizability is aligned with the electric field at low frequencies (red-detuned) and anti-aligned for frequencies above critical atomic transitions (blue-detuned). Thus, just below or above a resonance, the atom is forced towards high-field regions and low-field regions, respectively. This leads directly to the notion of using interfering laser beams to create standing waves with alternating regions of peaks and zeros in the electric field. The resulting periodic optical lattice potential can be used to trap atoms either at the regions of strong or weak electric field for the red-detuning versus blue-detuning case. In Figure 1.1(a), we illustrate

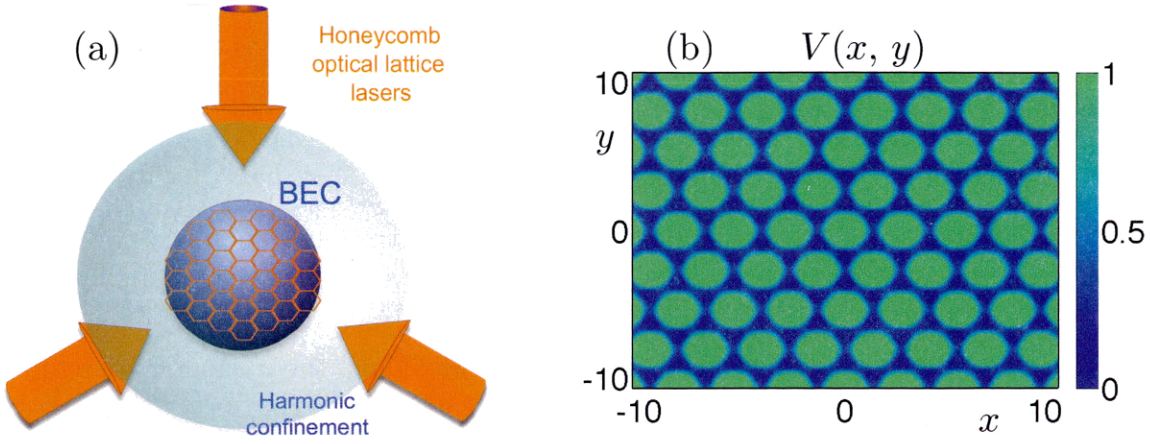

Figure 1.1: (color online) *BEC in a honeycomb optical lattice with harmonic confinement.* (a) Depiction of the lattice beams and lattice (orange), the BEC (dark blue), and the harmonic confining potential (light blue). (b) Two-dimensional honeycomb lattice potential.

the BEC with honeycomb lattice and harmonic potential. In Figure 1.1(b), a plot of the 2D honeycomb potential is shown.

1.6 The Linear and Nonlinear Dirac Equations

Several versions of the nonlinear Dirac equation have been around for decades and have typically been attempts to formulate effective theories of relativistic interacting fermions subject to Poincaré covariance, colloquially known as the principle of relativity. As such, they contain the kinetic terms consistent with the usual noninteracting theory, plus additional terms which model the interactions formed from contracting Poincaré invariant quantities. Here we review some of the main features of standard Dirac theory, with complete treatments found in Ref. [86] and [87].

Historically, the motivation behind the Dirac equation was part of a drive to understand the quantum mechanics of particles traveling at relativistic velocities. The starting point was the consideration of the various deficiencies of the Klein-Gordon equation, a theory of relativistic particles plagued with seeming inconsistencies of negative probability densities. Dirac's approach was to search for an equation linear

in the time derivative as well as the spatial ones, and he thus came upon the gamma matrices. His motivation was based partly on a deep intuition about the way physics equations should look. This appeal to aesthetics was the source of his creative inspiration so it is not surprising that the Dirac equation should exhibit a rich mathematical structure. The Dirac equation for a particle of mass m is

$$(i\hbar\gamma^{\mu}\partial_{\mu} - mc)\Psi(\mathbf{r},t) = 0\,, \tag{1.17}$$

where the first term contains the familiar first-order contraction of space-times derivatives with the 4×4 gamma matrices. Equation (1.17) is the standard form used in relativistic physics where the space-time coordinates are in the covariant form (ct, x, y, z). Using this notation the kinetic and mass terms in Eq. (1.17) have dimensions of momentum. In the chiral representation, the Dirac matrices are

$$\gamma^0 \equiv \begin{pmatrix} \mathbf{0} & \mathbf{1} \\ \mathbf{1} & \mathbf{0} \end{pmatrix}, \gamma^1 \equiv \begin{pmatrix} \mathbf{0} & \sigma^x \\ -\sigma^x & \mathbf{0} \end{pmatrix}, \gamma^2 = \begin{pmatrix} \mathbf{0} & \sigma^y \\ -\sigma^y & \mathbf{0} \end{pmatrix}, \gamma^3 = \begin{pmatrix} \mathbf{0} & \sigma^z \\ -\sigma^z & \mathbf{0} \end{pmatrix}, \tag{1.18}$$

where the σ^i are the 2×2 Pauli matrices

$$\sigma^x \equiv \begin{pmatrix} 0 & 1 \\ 1 & 0 \end{pmatrix}, \quad \sigma^y \equiv \begin{pmatrix} 0 & -i \\ i & 0 \end{pmatrix}, \quad \sigma^z = \begin{pmatrix} 1 & 0 \\ 0 & -1 \end{pmatrix}. \tag{1.19}$$

The associated plane-wave four-spinor solutions for Ψ are

$$\Psi_1 = e^{i(\mathbf{p}\cdot\mathbf{r} - Et)/\hbar} \begin{pmatrix} 1 \\ \frac{(p_x + i\,p_y)c}{E + mc^2} \\ 0 \\ 0 \end{pmatrix}, \quad \Psi_2 = e^{i(\mathbf{p}\cdot\mathbf{r} - Et)/\hbar} \begin{pmatrix} 0 \\ 0 \\ 1 \\ \frac{(p_x + i\,p_y)c}{-(E + mc^2)} \end{pmatrix}, \tag{1.20}$$

where Ψ_1 and Ψ_2 give the positive and negative helicity eigenstates, respectively, at the extreme relativistic limit, i.e., when $E \gg mc^2$. In a similar way we find the negative energy eigenstates to be

$$\Psi_3 = e^{i(\mathbf{p}\cdot\mathbf{r}-Et)/\hbar}\begin{pmatrix} 1 \\ \frac{(p_x+ip_y)c}{-(E+mc^2)} \\ 0 \\ 0 \end{pmatrix}, \quad \Psi_4 = e^{i(\mathbf{p}\cdot\mathbf{r}-Et)/\hbar}\begin{pmatrix} 0 \\ 0 \\ 1 \\ \frac{(p_x+ip_y)c}{E+mc^2} \end{pmatrix}, \tag{1.21}$$

where Ψ_3 and Ψ_4 give the positive and negative helicity eigenstates in the extreme relativistic limit. The total relativistic energy squared is given by $E^2 = p^2c^2 + m^2c^4$.

Dirac obtained Eq. (1.17) by essentially taking the square root of the Klein-Gordon equation. In order for this method to work out, the coefficients in the equation were found to be matrices, rather than scalars, with dimensionality of at least 4×4 and complex valued entries. Consequently, the wavefunction $\Psi(\mathbf{r}, t)$ must be a 4-component object with complex entries which transforms under a spin representation of the Poincaré group. The gamma matrices are found to obey anti-commutation relations: $\{\gamma^\mu, \gamma^\nu\} = 2\eta^{\mu\nu}$, where $\eta^{\mu\nu}$ is the Minkowski metric. Objects that satisfy such relations are said to form a *Clifford algebra.*

On a deeper level, the algebraic structure of the Dirac equation is a consequence of invariance under the Poincaré group: the set of all space-time translations, rotations and relativistic boosts. In fact, the states or particles associated with any theory that is consistent with special relativity naturally fall into categories according to the way they transform under the Poincaré group. Thus, states will fall into the various irreducible representations of the Poincaré group, the Lorentz group in particular (the subgroup consisting of rotations and boosts), labeled by spin values: 0, 1/2, 1, 3/2, and so on. Integer values describe bosons, and indicate the number of factors of the Poincaré transformation required to transform the single particle state: spin 0 = scalar; spin 1 = vector; spin 2 = rank 2 tensor, etc. Half-integer values denote fermions and correspond to the particular spin representation of the Poincaré group. In particular, solutions to the Dirac equation are in the fundamental spin-1/2 representation. Generally, an equation is invariant under Poincaré transformations if all of

its terms transform with the same numbers of factors of the Poincaré group or factors of its spinor representation. This idea is illustrated in further detail in Chapter 3.3, where we work out the Poincaré structure of our nonlinear Dirac equation.

In high energy physics, the mass term in the Dirac equation has an intuitive meaning as the minimum energy needed to produce real (non-virtual) particles during collisions. The analogous concept for periodic condensed matter systems is the *mass gap*, i.e., the finite gap which separates two energy bands. In a crystal, the gap appears at the edge of the reciprocal lattice when the periodic particle density undergoes a rigid spatial translation by half the period of the lattice, while keeping the crystal momentum fixed. The energy shift is just the energy difference that comes from shifting the position of the density peaks from the minima to the maxima of the background lattice potential. Graphene represents a semi-metal, as there is no gap due to the bands crossing at the Dirac point; the NLDE also has no gap. The crossing is due to degeneracy in A and B sublattices. A staggered lattice or other method that breaks the degeneracy of A and B sublattices can be used to deform the Dirac point and open up a band gap. In Chapter 8.4, we introduce the different mass gaps for the NLDE and obtain gap solitons. Although mass gaps are easy to implement in optical lattices, for simplicity, we focus here on the Dirac equation with the mass term set to zero, $m = 0$ in Eq. (1.17). This describes the behavior of massive fermions in the extreme relativistic limit, as well as the flow of charge carriers in graphene and cold bosonic and fermionic atoms in honeycomb-optical-lattice condensed matter systems.

There are two key representations of the gamma matrices, each one emphasizing one of two extreme perspectives. In the *energy* representation, the upper and lower 2-spinors which make up ψ are positive and negative-energy eigenstates, respectively: changing from positive to negative energy does not mix the 2-spinors. On the other hand, in the *chiral* representation, the upper and lower 2-spinors are positive and negative-helicity eigenstates: changing from positive to negative helicity does not

mix these 2-spinors. This is explained in mathematical detail in the first part of Chapter 3.3. Helicity measures the projection of spin in the direction of momentum and the helicity operator is exactly the nonzero 2×2 subspace of the kinetic part of the massless Dirac Hamiltonian – off diagonal subspaces in the energy representation and diagonal subspaces in the chiral representation. Interestingly, there is an elegant formulation of the massless Dirac equation in 2D as the simplest example of a supersymmetric theory, namely $N = 2$ supersymmetry [88]. The two generators or supercharges, indicated by the N-value, are the nonzero 2×2 subspaces of the Hamiltonian.

The earliest versions of the NLDE were motivated by the need to reduce the complexity of subatomic phenomena down to workable models which one could solve using well know mathematical tools. As the use of complicated field theoretic methods became the mainstay for describing relativistic interactions, various other methods were developed in parallel. Phenomenological models were developed in which complicated quantum effects could be encapsulated into nonlinear terms which were incorporated into semiclassical field equations. Such effective models offered the advantage of being intuitive as well as easier to work with, while still retaining some of the essential physics of the full theory. Among the most notable nonlinear modifications of the Dirac equation were the nonlinear spinor models proposed by D. D. Ivanenko [89], W. Heisenberg [90, 91], R. Finkelstein [92, 93], and F. Gürsey [94]. These were designed to account for the self-energy of the electron in the ambient electromagnetic background.

Remarkably, the techniques developed for solving a wide variety of NLDEs have also been used to construct multi-parameter families of exact solutions for many other nonlinear systems [95]. Systems of partial differential equations which have been solved using nonlinear Dirac techniques include Dirac-d'Alembert, Maxwell-Dirac, d'Alembert-eikonal, $SU(2)$ Yang-Mills, and Lévy-Leblond among others. A

good review of these methods can be found in Ref. [95]. The NLDE has been applied to many contemporary problems as well. In optics, for example, the NLDE has been used as an effective description of Maxwell's equations in the slowly varying envelope approximation for photonic crystals [96]. From a mathematical standpoint, classifications of stationary solutions of NLDEs are generally restricted to $(3+1)$-dimensions, and to classes of nonlinear terms of the form $F(\psi)\psi$, where $F \in C^2(\mathbb{C}^4, \mathbb{R})$, $\psi : \mathbb{R}^3 \to \mathbb{C}^4$, and commonly $F(\psi) \equiv \lambda(|\psi\bar{\psi}|^\alpha + b|\bar{\psi}\gamma^5\psi|^\beta)$, with $1 < \alpha, \beta < 3/2\,;\ \lambda, b > 0$ [95, 97, 98]. Note that in this form $F(\psi)\psi$ is Poincaré invariant, whereas for the NLDE which we study in this thesis the nonlinearity does not factor in the same way. An exception to this is the case of NLDE in optics which breaks Poincaré covariance. It is important to point out that our NLDE arises naturally out of BECs in honeycomb optical lattices, whereas other NLDEs were purely theoretical constructs.

Formal mathematical treatments of the NLDE focus on defining the bounds, stability, and scope of well-posedness from a purely theoretical standpoint [98–102], while other treatments focus more on explicit solutions by capitalizing on the symmetries of the NLDE [95, 103]. A rigorous exposition of the various nonlinearities which preserve Poincaré invariance can be found in Ref. [97], where the NLDEs are classified by the degree of the nonlinearity and the number of derivatives it contains. For a good introduction to the subject of NLDEs see Ref. [104].

In the literature, one generically encounters the NLDE in a condensed form expressed as

$$i\hbar\,\partial_t\Psi \;-\; D_m\Psi \;+\; G(\Psi) = 0\,, \tag{1.22}$$

where the notation $G(\Psi)$ indicates a functional of Ψ, and contains the interaction terms. The form of Eq. (1.22) differs from that of Eq. (1.17) in that the space and time derivatives have been separated as a first step towards obtaining explicit solutions. Note that in Eq. (1.22) the space-time coordinates are $(t,\, x,\, y,\, z)$. In addition, we

have defined $D_m \equiv -i\hbar c\,\gamma^j\partial_j + mc^2$, which contains the spatial derivatives contracted with gamma matrices ($j = 1, 2, 3$) and includes the mass gap structure indicated by the subscript m. The mass term is just the subtraction of a constant from the derivative terms. The nonlinear terms are contained in the functional $G \in C^1(\mathbb{C}^4, \mathbb{C})$. The usual analysis is to consider stationary solutions, i.e., a separation of variables between time and space, for which solutions to Eq. (1.22) are of the form: $\Psi(\mathbf{r}, t) = e^{-i\omega t}\psi(\mathbf{r})$, where ψ is also a four-spinor and solves the time-independent NLDE,

$$-\hbar\omega\,\psi \;-\; D_m\,\psi \;+\; G(\psi) \;=\; 0\,, \tag{1.23}$$

where we retain the same notation as in Eq. (1.22). The functional $G(\psi)$ is parametrized by the interaction strength U. In the literature, the nonlinear terms in $G(\psi)$ are constrained to be a Poincaré invariant (usually scalar or vector quantities) to coincide with most particle physics models. It is important to state that Poincaré invariance places a strong restriction on the form of $G(\psi)$ and these types of NLDEs only admit localized solutions for eigenvalues inside the gap, $0 < \hbar\omega < mc^2$, and nonexistence of localized solutions for $|\omega| > 1$ [105, 106]. This is because invariance under a general Poincaré transformation forces the radial amplitudes within each of the upper and lower two-spinors of ψ to be equal, which greatly limits the variety of possible combinations in the derivative terms. However, for the NLDE that we obtain, this severe restriction is lifted and the form of the equations allow for localized eigenvalues within the continuous spectrum, i.e., for $\hbar|\omega| \geq mc^2$, as well as inside the gap, $-mc^2 < \hbar\omega < mc^2$.

One also encounters the nonlinear Dirac operator as $D_{m,U} = D_m - \tilde{G}(\psi)$ such that Eq. (1.22) is

$$D_{m,U}\,\psi \;-\; \omega\,\psi = 0\,. \tag{1.24}$$

This is indeed possible even though the range of $D_{m,U}$ depends on elements of the domain [107, 108]. The nonlinear Dirac equation can be derived from a variational principle with the corresponding action being given by

$$I^{\omega}(\psi) = \int_{\mathbb{R}^2} d^2x \left[\frac{1}{2} \left(\psi^{\dagger}, D_m \psi \right) - \frac{1}{4} \omega \, \psi^{\dagger} \psi - \bar{G}(\psi) \right], \tag{1.25}$$

where $\bar{G}$ is the functional integral of G, i.e. $G(\psi) = \frac{\delta}{\delta \psi} \bar{G}$, the contraction $\left(\psi^{\dagger}, D_m \psi \right)$ is the L^2 contraction defined by

$$(\psi, \psi')_{L^2} = \int_{\mathbb{R}^2} d^2x \, \bar{\psi} \, \psi' \, . \tag{1.26}$$

Eq. (1.23) is the Euler-Lagrange equation associated with Eq. (1.25). It is important to note that since the spectrum of D_m is not positive-definite, solutions of Eq. (1.23) do not minimize Eq. (1.25), that is, the spectrum of the NLDE is not bounded below: there is no ground state in the strict sense.

1.7 Nonlinear Dirac Equations in Condensed Matter and Cold Atomic Gases

As we show in this thesis, the NLDE can be realized by forming a BEC in the lowest Bloch band of a honeycomb optical lattice [109]. The lattice is constructed using three sets of interfering laser beams in a plane while tightly trapping atoms in the vertical direction to obtain a quasi-2D system. Atoms are condensed into the lowest energy state of the lattice and then transferred to the Dirac points by Bragg scattering combined with a series of switching steps to turn off and on interactions of the atomic hyperfine states with the lattice laser beams. This method allows for a stable transfer of atoms to the Dirac points. An alternative approach involves an adiabatic acceleration of the lattice to get the BEC to the Dirac points, but the first approach eliminates potential dynamical instabilities which may arise from a moving

lattice. It should be noted that the Dirac point is maintained in the presence of the shallow harmonic trapping potential [110]. As described in Sec. 1.5, the laser interference pattern interacts with the atoms of the condensate via the AC Stark effect, thus creating a two-dimensional periodic potential; as described in Chapter 7, the third spatial dimension frozen out by a tightly confining potential in that direction [74].

From a theoretical standpoint, as shown in Chapt. 2, the NLDE is derived by starting from the second quantized Hamiltonian for a weakly interacting bosonic gas in two spatial dimensions and then imposing the tight-binding limit which involves expressing the bosonic field operators in terms of Wannier functions, a natural basis for periodic systems. Upon integrating over the two spatial degrees of freedom keeping only nearest neighbor tunneling, the Hamiltonian reduces to a discrete lattice form: the Bose-Hubbard model for the honeycomb lattice. Translating to the edge of the Brillouin zone and taking the expectation value with respect to on-site coherent states (which projects from a second quantized theory down to a mean-field one), and finally, taking the continuum limit produces the NLDE. By taking a superposition of theories for two opposite Dirac points, we obtain the full NLDE [52]. The nonlinear interactions are proportional to the density of the BEC and each term contains factors of the same spinor component – nonlinear terms do not couple different spinor components. Similar equations have been vigorously studied in the literature, in the context of particle and nuclear theory [111–114] as well as in nonlinear dynamics and applied mathematics [95, 115–119], but our particular version of the NLDE had not been studied before in connection with BECs or otherwise, and there was no experimental realization of any NLDE in any field before our work in 2009 [52]. In Chapts. 2 and 8, we obtain massless and massive versions of the NLDE as well as zigzag and armchair forms of the 1D NLDE, all with the same form for the nonlinear terms.

1.8 Connections to Optics and Applied Mathematics

A major area of research into NLDE physics outside of cold atoms is the study of diabolical points in optics. This concept originated in a combination of experiments where a randomly polarized ray of light traveling through a biaxial crystal exhibits cone shaped diffraction due to a singularity in k space from the polarization of the beam. More recently, inspired by conical Dirac points in honeycomb lattices, there has been much interest in obtaining diabolical point structures for optical waves traveling in honeycomb photonic crystals [120]. These have been studied numerically and have been experimentally detected. Other topics based on relativistic physics of Dirac points have also been investigated in honeycomb photonic crystals, such as symmetry breaking in the Dirac cone [121] and P-T symmetry, as well as problems in nonlinear physics such as gap solitons [120], which play an important role in our work. Another field where the honeycomb lattice structure is used to get Dirac dispersion is in an acoustic setting [122].

Partly because of the nonlinearity associated with conical diffraction, research in applied mathematics has also been stimulated. From the mathematical point of view, conical diffraction arises in the nonlinear Schrödinger equation when the external potential has a honeycomb shape. Both analytical derivations and numerical simulations for the wave envelope of Bloch modes in a honeycomb lattice potential have confirmed conical diffraction. Such approaches work directly from the NLSE, and show that the dynamics of the wave envelope is governed by the NLDE [123]. Significantly, the results of Ablowitz, Nixon, and Zhu show that when tight-binding in the lowest band is assumed, conical diffraction is maintained in the presence of nonlinearity [20, 123].

Investigations into nonlinear Dirac physics using numerical methods based on the NLSE and accounting for higher band structure beyond the lowest band, have also been implemented [32]. These calculations reveal that nonlinearity alters the structure

of the Dirac cone by changing the topology at the Dirac points for arbitrarily small interaction, suggesting a breakdown of the superfluid phase. These results provide key insights into Dirac point structure when the tight-binding, lowest band approximation does not hold. However, as long as lattice parameters and interactions are chosen such that the lowest-band approximation is warranted, it is our contention that the integrity of the Dirac cone will be preserved. A numerical investigation of NLDE vs. full NLSE with honeycomb lattice dynamics to support our scaling arguments is reserved for future work. In addition, another intriguing method worth mentioning for simulating the 1D NLDE is by using a single trapped ion which can be shown to mimic a free relativistic quantum particle [124].

1.9 Approximations and Constraints Involved in the Nonlinear Dirac Equation

Realization of the NLDE physics requires that several physical constraints are satisfied. For example, we have already touched on the problem of dimensional reduction, which, as we have seen, determines an upper bound on the order of magnitude of the s-wave scattering length, and a lower bound on the oblateness of the condensate, for a given value of the particle density. The density $\bar{n}$ and its dimensionally reduced form $\bar{n}_{2D} \equiv L_z \bar{n}$, are central, and appear in the definitions of many important quantities and their renormalized counterparts. The constraints which need to be satisfied can be broken down into categories involving the following sets of physical quantities: the energies and lengths for the 3D to 2D reduction; the characteristic speeds of the 2D lattice theory versus the unconfined 3D theory; the relative strengths of interactions to hopping between lattice sites must be correctly tuned for a stable superfluid state; quasi-particle, Dirac point, and lattice recoil momenta are interrelated to ensure that the Dirac cone and long-wavelength limits are valid and the relative strength of the potential depth to the recoil energy of the lattice to ensure that the lowest-band and tight-binding approximations hold.

Several length and energy parameters are fundamental to the NLDE, with other composite quantities formed from these. The fundamental lengths are the transverse width and longitudinal radius of the BEC, L_z and $R_\perp$, the honeycomb lattice constant a, the s-wave scattering length a_s, and the average inter-particle distance $\bar{n}^{-1/3}$. The fundamental energy scales are determined by the lattice depth V_0, the thermal Boltzmann energy $k_B T$, and the chemical potential of the system μ. All of these parameters are related in a complicated way through the constraints, with the region of validity for the NLDE lying within the boundaries defined by these constraints. For example, the following offers one consistent set of length parameter values for a BEC made up of ^{87}Rb atoms in a honeycomb lattice, to support the NLDE: $L_z = 3.0\,\mu$m, $R_\perp = 55.0\,\mu$m, $a = 0.55\,\mu$m, $a_s = 5.77\,$nm, and $\bar{n}^{-1/3} = (1 \times 10^{16}\,\mathrm{m}^{-3})^{-1/3} = 4.64\,\mu$m. Values of the energy parameters consistent with these lengths are $V_0 = 2.60\,\mu$K, $k_B T = 8.0\,$nK, and $\mu = 2.36\,$nK. A complete description of NLDE parameters and constraints can be found in Chapters 6 and 7 of this thesis, specifically in Tables 6.1 and 7.1.

1.10 Solution Methods for the Nonlinear Dirac Equation

The stationary localized solutions of the NLDE we obtain fall into either of two categories: two-dimensional vortices and one-dimensional solitons. Vortices are characterized by having a core defined by a phase jump, or singularity, with quantized rotational angular momentum circulating around the core. Our soliton solutions solve the 1D NLDE obtained by integrating out one of the planar spatial directions. Physically, this arises when the trap length in one direction is made small compared to the other direction. To obtain these solutions in the chiral representation of the NLDE, we start by splitting the full four-spinor NLDE into two equivalent sets of coupled equations for each pair of two-spinors, and specialize to stationary wavefunctions to arrive at:

$$\mu\,\psi_A + i\,\hbar c_l\,\mathcal{D}^*\psi_B - U\,|\psi_A|^2\,\psi_A = 0 \quad (1.27)$$
$$\mu\,\psi_B + i\,\hbar c_l\,\mathcal{D}\,\psi_A - U\,|\psi_B|^2\,\psi_B = 0\,, \quad (1.28)$$

where μ is the chemical potential, c_l is the effective speed of light, U is the interaction strength, and $\mathcal{D} \equiv (\partial_x + i\,\partial_y)$ is the Dirac differential operator.

We obtain soliton solutions to Eqs. (1.28) by freezing out one spatial dimension as stated above. Retaining only the y-direction in Eqs. (1.28) results in equations for propagation in the armchair geometry of nanoribbon, whereas retaining the x-direction gives the zigzag geometry analogous to the two forms of graphene nanoribbon geometries. We then express the wavefunction in terms of envelope and internal component functions: $\Psi(x) = \eta(x)\,[\cos\varphi(x),\, \sin\varphi(x)]^T$, where we let x denote either direction in Eq. (1.28). This step allows us to obtain a formal integral for η in terms of φ, for which an exact solution is obtained when $\mu = 0$. For more general soliton solutions ($\mu \neq 0$), we find solutions for which φ is approximately linear in x. We show that such approximate solutions are valid as long as φ is a slowly varying function in x. The second method that we use to obtain soliton solutions is to expand the envelope η in a power series in the quantity $\cos^4\varphi + \sin^4\varphi$. We find this to be a natural expansion argument given the way that it appears in the transformed version of Eqs. (1.28). By solving consistently for the expansion coefficients, we are able to obtain solutions which are more general than those obtained by the first method. An important property of the series solution is that the terms connect to the solutions for slowly varying φ above, when the parameters U and μ are appropriately tuned. When a mass gap is turned on, a mapping of a subclass of NLDE solutions to the massive Thirring model is possible. The massive Thirring model is was originally formulated as a low energy effective theory of interacting fermions, integrable at both classical and quantum mechanical levels [125, 126]. The advantage of this mapping is that properties and solutions of the Thirring system are well understood and may then

be translated to the NLDE. We find that NLDE solutions obtained by this method are qualitatively similar to the bright solitons obtained through the slowly varying φ method.

We obtain seven different types of vortices by a variety of analytical methods. To obtain vortex solutions, we first express Eqs. (1.28) in plane-polar coordinates, then factor out the quantized angular dependence from the solution to arrive at two coupled first order equations for the radial parts $f_A(r)$ and $f_B(r)$ of the component wavefunctions $\psi_A(r,\theta)$ and $\psi_B(r,\theta)$. Our first method uses an asymptotic Bessel expansion, which matches the asymptotic form of the vortex near the core and far from the core, and gives us an approximate solution for large winding number, in addition to deeper insight into the effect of the nonlinearity on solutions. A second method is to write f_A and f_B as general algebraic expressions in the radial coordinate r, up to arbitrary parameters. Substituting into the NLDE allows us to solve for the extra parameters in a consistent manner. The algebraic method leads to a large class of solutions for any winding number ℓ. Specifically, when $\ell = 1$, solutions exist for the case $\mu = 0$ and for $\mu > 0$, in the form of a vortex with bright soliton at the core: a ring-vortex with vanishing tail for the first case, and a vortex with asymptotically constant (non-zero) tail for the second case. For $\ell > 1$, we find algebraic closed forms with chemical potential $\mu = 0$, characterized by an asymptotically vanishing tail at large r. These are general ring vortices where both spinor solutions vanish at the core. For $\ell = 1$, we also find skyrmions and half-quantum vortices by expressing the wavefunction in terms of the envelope and internal spinor parts, $\eta(r)$ and $\varphi(r)$, similar to the 1D case, then solving the resulting nonlinear system in η and φ.

Numerical solutions for both solitons and vortices are also obtained. In the case of vortices, we first separate the quantized angular part from the radial part, then solve the 1D radial equation by discretizing the derivatives using forward-backward finite differencing and tuning the number of grid points until the desired precision of

convergence is obtained. We use numerical shooting by first expanding the solution in a power series near the peak of the soliton, or the core of the vortex, then from this we derive the behavior of the solution near that point. The vortex solution must vanish at the core because of the angular momentum term, which adds an additional condition on the wavefunction.

1.11 Overview of Thesis

This thesis is organized such that most chapters are separate articles published (Chapters 2, 4), presently under review (Chapters 6, 8), or soon to be submitted in a peer-reviewed journal (Chapters 7, 9). Some additional material is included in Chapters 3 and 5 for overall clarity. The bibliography is placed at the end of the thesis as many references are common to more than one chapter. The nature of the work in this thesis is interdisciplinary and in general we adhere to the same notation throughout consistent with condensed matter physics. The notation and definitions for physical constants are summarized in Chapter 7.2.1 in particular in Table 7.1. However, in certain places it is sometimes more convenient to use notation more in line with high energy physics where covariance is explicit. This is done in order to help bridge the gap between condensed matter and particle physics. In this overview, we will address deviations from the standard notation of Table 7.1 for each chapter.

In Chapter 2, we derive the NLDE for BECs in honeycomb lattices and provide a thorough symmetry analysis with comparison to the standard Dirac theory. This section sets the foundation for the rest of the material in this thesis by providing a rigorous derivation of the NLDE using well established tools of many-body theory founded on coherent states for lattices. The section on symmetries clearly categorizes our theory within the larger NLDE picture. The properties of the NLDE under Poincaré transformations pertains to the full 2D equations, in contrast to the 1D problem which is treated later in the thesis. In this chapter the derivations use explicit notation for physical parameters which include the effective speed of light

c_l and Planck's constant $\hbar$ with the usual $(2+1)$-dimensional coordinate notation (t, x, y). In places where we want to emphasize the covariance of the NLDE, we use the coordinate form $(c_l t, x, , y)$. The derivation and resulting NLDE is unique and appears here in the context of BECs for the first time.

In Chapter 3, we study additional fundamental topics in the NLDE. We summarize the key points of the standard Dirac formalism, and provide a detailed analysis of the structure of the NLDE. The Lagrangian formulation is presented and analyzed with a view towards obtaining localized soliton and vortex solutions in addition to a connecting to the nonlinear sigma model. We place the NLDE within established mean-field theory by showing how it reduces to the NLSE with correction terms, and study the soliton and vortex landscape of the corrected NLSE. These additional correction terms result in a completely new type of NLSE. In addition, we address a fundamental issue regarding spin-statistics. The spin-statistics theorem provides the step which relates the geometric phase associated with Dirac points to the quasi-particle operator statistics and clarifies how Dirac physics describing fermions can arise out of a weakly interacting Bose gas. Our model offers a novel method for realizing a transition from Bose to Fermi statisitics.

Chapter 4 provides an overview and first look at localized solutions of the NLDE and the relativistic linear stability equations (RLSE), which determine the first order effect of quantum fluctuations on arbitrary solutions of the NLDE. Experimental signatures such as Cherenkov radiation and preliminary lifetime calculations are obtained naturally from the RLSE. The interplay between quantum effects contained in the Dirac dispersion and particle interactions reveal two low energy regimes defined by, first, the lattice spacing, and second, the 2D renormalized healing length, the length scale set by the strength of the 2D two-body interactions. Fluctuations much larger than both the healing length and the lattice spacing behave as composite Dirac particles. Such fluctuations are large enough that interactions blur the individual chi-

ral Dirac quasi-particles set up by the bipartite lattice. The chiral Dirac structure is recovered for fluctuations with wavelengths comparable to the healing length but still much larger than the lattice spacing. The RLSE are a completely new set of equations derived for quasi-relativistic systems in BECs.

In Chapter 5, we provide the full detailed calculations of the RLSE eigenvalues and the quasi-particle coherence factors for the case of a uniform condensate. We present topics unique to this thesis which include symmetries of the RLSE, derivations of the quasi-particle normalization conditions, classification of the different types of spinor quasi-particle excitations, and approximate analytical solutions for general vortex backgrounds.

In Chapter 6, we present the parameters and constraints key to observing Dirac physics in BECs, along with the experimental procedures for setting up the optical lattice, establishing the BEC at the Dirac points, and exciting the desired vortex states. All of these topics are unique in that our experimental studies and particular solutions in the context of honeycomb lattice BECs at Dirac points have not been presented before. By accessing the internal atomic hyperfine degrees of freedom, we show that our method allows one to populate Dirac points with a stable macroscopic sample of cold bosonic atoms. We include a first look at topics such as vortex structure and spectra. The notation in this chapter is based on Table 7.1 with the exception of the general length scale r_0 which is used to denote either the scale set by the interaction $\hbar c_l/U$, or that set by the chemical potential $\hbar c_l/\mu$.

Chapter 7 explores the complete vortex landscape for the full 2D NLDE. The NLDE allows for seven distinct types of vortices distinguished by their phase winding number and their asymptotic radial behavior far from the core. The macroscopic phase encircling a vortex core may involve the internal spinor degrees of freedom, as in the case of our skyrmions, or may only pertain to the overall phase, as in many other NLDE solutions. Significantly, the 2D lattice allows for a half-quantum

vortex with half-integer phase winding. We present detailed analysis of analytical and numerical vortex solutions, including stability analysis by solving the RLSE for vortex backgrounds and calculating spectra for bound states in a weak confining potential. The solutions, stability studies and spectra are new since our particular form of NLDE is novel.

In Chapter 8, we solve the one-dimensional (1D) version of the NLDE and investigate the types of gaps possible in this physical setup. For the case of zero gap, we obtain solitons by a direct method, a soliton series expansion method, and by numerical shooting. The first two methods provide consistency cross-checks for bright-solitons, and the series method in particular gives us insight into possible integrability of the 1D NLDE. Numerical shooting gives us a dark soliton solution not accessed through the first two methods. We calculate lifetimes by solving the 1D RLSE to obtain the quasi-particle amplitudes and energies. The inclusion of a mass gap reveals two mappings: one from the massive NLDE to the massive Thirring model and another from the massless NLDE to the massive NLDE. From a practical point of view, these mappings establish a dictionary translating from readily obtained soliton solutions in one theory to new solutions in another. We encounter the topic of integrability here, since the massive Thirring is well known to be integrable. Finally, the discrete spectra which we obtain for bound solitons in a harmonic trap clearly delineate the energetic signature for the gray solitons. The calculation of bound states leads directly into the physics of Klein-tunneling, a feature of relativistic fermions not yet observed in high-energy experiments.

In Chapter 9, we establish a quantum field theory at the Dirac points of the lattice obtain the new result that bosons are described by a relativistic quantum field theory for Dirac spinors. In addition, we derive the full many-body Hamiltonian for bosons in the honeycomb lattice. We obtain the first-order momentum contribution which gives the full quantum theory for a massless Dirac spinor. In addition, we compute

the second order correction term beyond the linear Dirac theory. This term describes deviations from the linear approximation, and gives the quadratic contribution to the dispersion in the associated mean-field theory. By using Hubbard-Stratonovich decomposition, we derive the continuum quantum field theory at the Dirac points and obtain the Lagrangian for interacting relativistic Dirac spinors.

Finally, in Chapter 10 we conclude by presenting several topics for future research in the NLDE.

CHAPTER 2

THE NONLINEAR DIRAC EQUATION IN BOSE-EINSTEIN CONDENSATES: FOUNDATION AND SYMMETRIES

Publication: L. H. Haddad and Lincoln D. Carr, Physica D: Nonlinear Phenomena, **238**, 1413-1421 (2011).

Abstract

We show that Bose-Einstein condensates in a honeycomb optical lattice are described by a nonlinear Dirac equation in the long wavelength, mean field limit. Unlike nonlinear Dirac equations posited by particle theorists, which are designed to preserve the principle of relativity, i.e., Poincaré covariance, the nonlinear Dirac equation for Bose-Einstein condensates breaks this symmetry. We present a rigorous derivation of the nonlinear Dirac equation from first principles. We provide a thorough discussion of all symmetries broken and maintained.

2.1 Introduction

Recently the first truly two-dimensional (2D) solid state material, graphene, was created in the laboratory [127, 128]. One of the most exciting aspects of this novel material is that long wavelength excitations are described by a Dirac equation for massless particles, with a "speed of light" equal to the Fermi velocity $v_F \simeq c/300$ [48]. Thus one can study relativistic phenomena at very low velocities in an experiment far more accessible than a particle accelerator. The lattice structure of graphene has also led to insights into exotic features such as the integral and fractional quantum hall effects [129]. The only real requirement to obtain this equation is the honeycomb lattice structure of the graphene [16, 130–132]. One can therefore consider any solid state system constructed on a honeycomb lattice, including artificial systems, in order to study relativistic phenomena in novel materials accessible in tabletop experiments.

The most precise, cleanest, most controllable artificial solid state system is ultra-cold atoms in optical lattices. Such systems have no impurities and no disorder unless specifically added in by hand. They are very versatile: they can be constructed of both bosons and fermions, of atoms and/or diatomic molecules, and can even have a pseudospin structure. Their temperature, interactions, and symmetries can be controlled externally. Moreover, 2D physics has recently been of great interest in this context, in the form of the Berzinskii-Kosterlitz-Thouless crossover [74], and 2D systems underpinned by lattices are immediately available in experiments. Instead of considering ultra-cold fermions, which could be used to produce an near-exact analog of graphene [133], we consider ultra-cold bosons. Other bosonic systems have been studied in Refs. [70, 134–136], as well as systems composed of fractional numbers of fermions of relevance to condensed matter as well as relativistic quantum field theory [137, 138] . Systems of ultra-cold fermions have been used to study Bosonic statistics and interactions lead to a new feature in the massless Dirac equation known in graphene: a naturally occurring nonlinear term, giving rise to a *nonlinear Dirac*

equation. An important distinction should be made regarding preparation. For the case of graphene it is the Fermi energy that brings the system to the Dirac point. To bring the BEC to the Dirac point involves creating the condensate first then adiabatically turning on the lasers in such a way as to create a moving lattice relative to the condensate thus resulting in a condensate with nonzero lattice momentum [70].

The study of nonlinear phenomena in ultra-cold atoms, especially in Bose-Einstein condensates (BECs) [4, 6], has been enormously fruitful. The recent text edited by Kevrekidis, Frantzeskakis, and Carretero-González provides an excellent summary of this field [19]. The nonlinear mean field description given by the nonlinear Schrodinger equation (NLSE) has been very accurate in the majority of experiments on BECs. Vector and non-local generalization of the NLSE have also proven useful. In optical lattices, the mean field description remains accurate provided the lasers creating the standing wave which is the optical lattice are not too intense, and the dimensionality of the system is greater than one [139, 140].

In this article, we present a completely new class of nonlinear phenomena in BECs, based on the nonlinear Dirac equation (NLDE). Nonlinear Dirac equations have a long history in the literature, particularly in the context of particle and nuclear theory [111–114], but also in applied mathematics and nonlinear dynamics [95, 115–119]. As nonlinearity is a ubiquitous aspect of Nature, it is natural to ask how nonlinearity might appear in a relativistic setting. However, this line of questioning has been strongly constrained by modeling, rather than first principles. That is, there is no standard first principle of quantum electrodynamics (QED) which is nonlinear. So, the approach has been to require symmetry constraints in nonlinear models. One of these constraints is the principle of relativity, i.e., Poincaré covariance. Poincaré symmetry includes rotations, translations, and Lorentz boosts.In contrast, our NLDE is not a model: it is derived from first principles for a weakly interacting bosonic gas in the presence of a honeycomb optical lattice. We show that Poincaré symmetry is

naturally broken by the nonlinearity inherent in this system. Given that this form of nonlinearity, which depends only on the local condensate density, is one of the most common throughout nature, it is important to recognize that the principle of relativity may be broken by small nonlinearities even at a fundamental level, for example of QED [49, 141]. Thus, we suggest a new direction of investigation in particle physics of possible nonlinearities as well as providing a natural context in artificial solid state systems for the NLDE.

This article is outlined as follows. In Sec. 2.2.1 we provide a rigorous derivation of the NLDE from first principles. In Sec. 2.4 we discuss both discrete and continuous symmetries common to relativistic systems, providing a clear physical interpretation in the present context. Finally, in Sec. 2.5 we conclude.

2.2 The Nonlinear Dirac Equation

2.2.1 Two-Component Spinor Form of the NLDE

The second quantized Hamiltonian for a weakly interacting bosonic gas in two spatial dimensions is

$$\hat{H} = \int d^2r\, \hat{\psi}^\dagger H_0 \hat{\psi} + \frac{g}{2}\int d^2r\, \hat{\psi}^\dagger\hat{\psi}^\dagger\hat{\psi}\hat{\psi}\,, \tag{2.1}$$

$$H_0 \equiv -\frac{\hbar^2}{2m}\nabla^2 + V(\vec{r})\,. \tag{2.2}$$

The bosonic field operators $\hat{\psi} = \hat{\psi}(\vec{r},t)$ obey bosonic commutation relations in the Heisenberg picture. In Eq. (9.1), $g \equiv 4\pi\hbar^2 a_s/2m$ is the coupling strength for binary contact interactions with a_s the s-wave scattering length and m the atomic mass. The external potential $V(\vec{r})$ is a honeycomb lattice formed by standing waves of three sets of counter-propagating laser beams [133]. The atoms experience this potential via the AC Stark effect. We assume that the third spatial dimension is frozen out by a tightly confining potential which is locally harmonic, as in Ref. [74]. Quasiparticle excitations are perturbations around the Dirac points and have energy $E = \hbar k v_f$ that must be

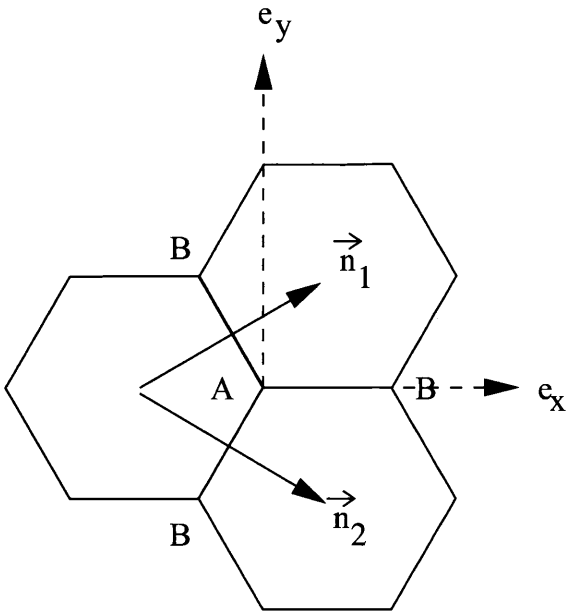

(a) Hexagonal lattice structure

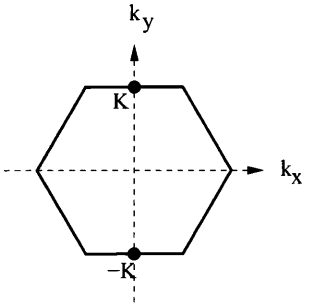

(b) Reciprocal lattice

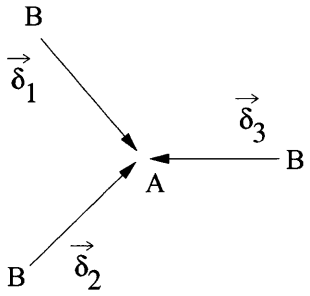

(c) Nearest neighbor displacement vectors

Figure 2.1: Characterization of a honeycomb lattice.

compared to excitations in the third direction. Excitations along the 2D plane can be made arbitrarily small so that $\hbar k v_f \gg \hbar k_3$, or simply that, $L_{1,2} \gg L_3$; length scales for excitations along the plane must be larger than the vertical trap length. The honeycomb lattice has two sites in the lattice unit cell. We refer to the resulting two degenerate sublattices as A and B. Expanding in terms of Bloch states belonging to A or B sites of the honeycomb lattice, as shown in Figure 2.1, we can break up the bosonic field operator into a sum over the two sublattices:

$$\hat{\psi} = \hat{\psi}_A + \hat{\psi}_B \,, \tag{2.3}$$

$$\hat{\psi}_A \equiv \sum_A \hat{a}\, e^{i\vec{k}\cdot(\vec{r}-\vec{r}_A)} u(\vec{r}-\vec{r}_A) \,, \tag{2.4}$$

$$\hat{\psi}_B \equiv \sum_B \hat{b}\, e^{i\vec{k}\cdot(\vec{r}-\vec{r}_B)} u(\vec{r}-\vec{r}_B) \,, \tag{2.5}$$

where $\hat{a}$ and $\hat{b}$ are the time-dependent destruction operators at A and B sites respectively and $\vec{r}_A$ and $\vec{r}_B$ are the positions of A and B sites respectively.The spatial dependence is then encapsulated outside the operator in the exponential and the functions u. The summation indices indicate sums over A or B sites.Inserting Eq. (9.3) into Eq. (9.1), the Hamiltonian can be rewritten

$$\begin{aligned} \hat{H} = & \int d^2r \Big[(\hat{\psi}_A^\dagger + \hat{\psi}_B^\dagger) H_0 (\hat{\psi}_A + \hat{\psi}_B) \\ & + \frac{g}{2} (\hat{\psi}_A^\dagger + \hat{\psi}_B^\dagger)(\hat{\psi}_A^\dagger + \hat{\psi}_B^\dagger)(\hat{\psi}_A + \hat{\psi}_B)(\hat{\psi}_A + \hat{\psi}_B) \Big] \,. \end{aligned} \tag{2.6}$$

In the integral over H_0, imposing the restriction of nearest-neighbor interactions in the tight-binding, lowest band approximation eliminates all A-A and B-B transitions except for on-site kinetic and potential terms; the latter can be neglected as an overall self-energy. Then only integrals involving neighboring A-B sites remain in the sum. Similarly, in the interaction term only on-site terms are non-negligible, i.e., overlap of functions u belonging to the same site. Specifically, the terms dropped from the summation are integrals of products of four onsite localized wavefunctions with at least one belonging to a different site than the others. They are of the form $\int d^3r u_{0_i}^* u_{0_j}^* u_{0_k} u_{0_l}$. Since we are performing all calculations in the tight-binding approximation we neglect all such terms unless i = j = k = l . Note that the hopping integral is $t_h = -\int d^3r u_0^*(\mathbf{r} - \mathbf{R_i}) \hat{H}_0 u_0(\mathbf{r} - \mathbf{R_j})$, where i and j refer to nearest neighbor sites.

Thus in the tight-binding, lowest band approximation, Eqs. (9.4)-(9.5) are substituted into Eq. (2.6) to yield:

$$
\begin{aligned}
\hat{H} &= \int d^2r \sum_{<A,B>} \Big[\hat{a}^\dagger \, e^{-i\vec{k}\cdot\vec{\chi}_A} u(\vec{\chi}_A) H_0 \hat{a} \, e^{i\vec{k}\cdot\vec{\chi}_A} u(\vec{\chi}_A) \\
&\quad + \hat{a}^\dagger \, e^{-i\vec{k}\cdot\vec{\chi}_A} u(\vec{\chi}_A) H_0 \hat{b} \, e^{i\vec{k}\cdot\vec{\chi}_B} u(\vec{\chi}_B) \\
&\quad + \hat{b}^\dagger \, e^{-i\vec{k}\cdot\vec{\chi}_B} u(\vec{\chi}_B) H_0 \hat{a} \, e^{i\vec{k}\cdot\vec{\chi}_A} u(\vec{\chi}_A) \\
&\quad + \hat{b}^\dagger \, e^{-i\vec{k}\cdot\vec{\chi}_B} u(\vec{\chi}_B) H_0 \hat{b} \, e^{i\vec{k}\cdot\vec{\chi}_B} u(\vec{\chi}_B) \Big] \\
&\quad + \frac{g}{2} \int d^2r \sum_A \hat{a}^\dagger \hat{a}^\dagger \hat{a} \hat{a} \, [u(\vec{\chi}_A)]^4 \\
&\quad + \frac{g}{2} \int d^2r \sum_B \hat{b}^\dagger \hat{b}^\dagger \hat{b} \hat{b} [u(\vec{\chi}_B)]^4 \, , \qquad (2.7) \\
\vec{\chi}_A &\equiv \vec{r} - \vec{r}_A \, , \quad \vec{\chi}_B \equiv \vec{r} - \vec{r}_B \, , \quad \vec{\chi}_{AB} = \vec{r}_A - \vec{r}_B \, . \qquad (2.8)
\end{aligned}
$$

Isolating the integrals by pulling out all sums and terms not dependent on $\vec{r}$, Eq. (9.6) becomes

$$
\begin{aligned}
\hat{H} &= \sum_{<A,B>} \Big[\hat{a}^\dagger \hat{b} \, e^{i\vec{k}\cdot\vec{\chi}_{AB}} \int d^2r e^{-i\vec{k}\cdot\vec{r}} u(\vec{\chi}_A) H_0 e^{i\vec{k}\cdot\vec{r}} u(\vec{\chi}_B) \\
&\quad + \hat{b}^\dagger \hat{a} \, e^{-i\vec{k}\cdot\vec{\chi}_{AB}} \int d^2r e^{-i\vec{k}\cdot\vec{r}} u(\vec{\chi}_B) H_0 e^{i\vec{k}\cdot\vec{r}} u(\vec{\chi}_A) \Big] \\
&\quad + \sum_A \hat{a}^\dagger \hat{a} \int d^2r e^{-i\vec{k}\cdot\vec{r}} u(\vec{\chi}_A) H_0 e^{i\vec{k}\cdot\vec{r}} u(\vec{\chi}_A) \\
&\quad + \sum_B \hat{b}^\dagger \hat{b} \int d^2r e^{-i\vec{k}\cdot\vec{r}} u(\vec{\chi}_B) H_0 e^{i\vec{k}\cdot\vec{r}} u(\vec{\chi}_B) \\
&\quad + \frac{g}{2} \sum_A \hat{a}^\dagger \hat{a}^\dagger \hat{a} \hat{a} \int d^2r [u(\vec{\chi}_A)]^4 \\
&\quad + \frac{g}{2} \sum_B \hat{b}^\dagger \hat{b}^\dagger \hat{b} \hat{b} \int d^2r [u(\vec{\chi}_B)]^4 \, , \qquad (2.9)
\end{aligned}
$$

Finally, we redefine the spatial integrals in Eq. (9.23) as hopping energy t_h and interaction energy U, respectively, as is standard for the Hubbard Hamiltonian [142, 143]:

$$
\begin{aligned}
\hat{H} &= -t_h \sum_{<A,B>} \left[\hat{a}^\dagger \hat{b} \, e^{i\vec{k}\cdot(\vec{r}_A - \vec{r}_B)} + \hat{b}^\dagger \hat{a} \, e^{-i\vec{k}\cdot(\vec{r}_A - \vec{r}_B)} \right] \\
&\quad + \frac{U}{2} \sum_A \hat{a}^\dagger \hat{a}^\dagger \hat{a} \hat{a} + \frac{U}{2} \sum_B \hat{b}^\dagger \hat{b}^\dagger \hat{b} \hat{b} \qquad (2.10)
\end{aligned}
$$

ARTHUR LAKES LIBRARY
COLORADO SCHOOL OF MINES
GOLDEN CO 80401

The bracketed A and B summation index signifies a sum over nearest-neighbor A and B sites. The terms proportional to $\hat{a}^\dagger\hat{a}$ and $\hat{b}^\dagger\hat{b}$ just count the total number of atoms in the system, and have been neglected in Eq. (2.10) as an overall constant. Equation (2.10) is the Hubbard Hamiltonian divided into two degenerate sublattices A and B, appropriate to the honeycomb optical lattice.

In order to work towards the nonlinear Dirac equation, we calculate the time evolution of $\hat{a}$ and $\hat{b}$ according to the standard Heisenberg picture prescription. This is similar to the approach taken by Pitaevskii in his landmark paper which first obtained the NLSE, or Gross-Pitaevskii equation [59]. The Heisenberg equation of motion is

$$i\hbar\,\partial_t\hat{a}_k = [\hat{a}_k, \hat{H}]\,. \tag{2.11}$$

The operator $\hat{a}_k$, which destroys a boson at site k, satisfies the bosonic commutation relation

$$[\hat{a}_k, \hat{a}^\dagger_{k'}] = \delta_{kk'}\,. \tag{2.12}$$

Then the commutator with the on-site interaction terms reduces to

$$[\hat{a}_k, \hat{a}^\dagger_k\hat{a}^\dagger_k\hat{a}_k\hat{a}_k] = \hat{a}_k\hat{a}^\dagger_k\hat{a}^\dagger_k\hat{a}_k\hat{a}_k - \hat{a}^\dagger_k\hat{a}^\dagger_k\hat{a}_k\hat{a}_k\hat{a}_k. \tag{2.13}$$

Taking the first product on the right and commuting the furthermost left $\hat{a}$ through according to Eq. (2.12), one finds

$$\hat{a}_k\hat{a}^\dagger_k\hat{a}^\dagger_k\hat{a}_k\hat{a}_k = 2\hat{a}^\dagger_k\hat{a}_k\hat{a}_k + \hat{a}^\dagger_k\hat{a}^\dagger_k\hat{a}_k\hat{a}_k\hat{a}_k.$$

Substituting Eq. (2.14) into Eq. (2.13), one obtains

$$[\hat{a}_k, \hat{a}^\dagger_k\hat{a}^\dagger_k\hat{a}_k\hat{a}_k] = 2\hat{a}^\dagger_k\hat{a}_k\hat{a}_k\,. \tag{2.14}$$

Substituting Eq. (2.14) into Eq. (2.11) and the Hubbard Hamiltonian Eq. (2.10), one finds

$$
\begin{aligned}
i\hbar\,\partial_t \hat{a}_k &= -t_h \Big[\hat{b}_k\, e^{i\vec{k}\cdot(\vec{r}_{A_k}-\vec{r}_{B_k})} + \hat{b}_{k-n_1}\, e^{i\vec{k}\cdot(\vec{r}_{A_k}-\vec{r}_{B_{k-n_1}})} \\
&\quad + \hat{b}_{k-n_2}\, e^{i\vec{k}\cdot(\vec{r}_{A_k}-\vec{r}_{B_{k-n_2}})}\Big] + U\hat{a}_k^\dagger \hat{a}_k \hat{a}_k\,, \qquad (2.15)
\end{aligned}
$$

where the first three terms on the right hand side represent transitions from the three B-sites nearest the k^{th}site of the A sublattice and $\vec{n}_1$ and $\vec{n}_2$ are primitive cell translation vectors for the reciprocal lattice, as shown in Figure 2.1.

In a similar fashion as Eqs. (2.11)-(2.15), we arrive at the an expression of the same form for the B sublattice,

$$
\begin{aligned}
i\hbar\partial_t \hat{b}_k &= -t_h \Big[\hat{a}_k\, e^{-i\vec{k}\cdot(\vec{r}_{A_k}-\vec{r}_{B_k})} + \hat{a}_{k+n_1}\, e^{-i\vec{k}\cdot(\vec{r}_{A_{k+n_1}}-\vec{r}_{B_k})} \\
&\quad + \hat{a}_{k+n_2}\, e^{-i\vec{k}\cdot(\vec{r}_{A_{k+n_2}}-\vec{r}_{B_k})}\Big] + U\hat{b}_k^\dagger \hat{b}_k \hat{b}_k. \qquad (2.16)
\end{aligned}
$$

Continuing to follow Pitaevskii's method, we next calculate the time rate of change of the expectation value of Eqs. (2.15) and (2.16) with respect to on-site coherent states. A tensor product over sites of such coherent states is also assumed [139]. A more formal, careful treatment of finite number states, rather than coherent states, has been worked out in the literature (see [12] and references therein). Either way, we obtain coupled equations of motion for discrete, on-site, complex-valued amplitudes. For simplicity of notation we take

$$
a_k \equiv < \hat{a}_k >\,, \quad b_k \equiv < \hat{b}_k > \,. \qquad (2.17)
$$

Inserting the nearest-neighbor vectors $\vec{\delta}_1$, $\vec{\delta}_2$, and $\vec{\delta}_3$ in the exponentials in Eqs. (2.15) and (2.16), as shown in Figure 2.1, we obtain

$$
\begin{aligned}
i\hbar\,\dot{a}_k &= -t_h(b_k\, e^{i\vec{k}\cdot\vec{\delta}_3} + b_{k-n_1}\, e^{i\vec{k}\cdot\vec{\delta}_1} + b_{k-n_2}\, e^{i\vec{k}\cdot\vec{\delta}_2}) \\
&\quad + U a_k^* a_k a_k\,, \qquad (2.18) \\
i\hbar\,\dot{b}_k &= -t_h(a_k\, e^{-i\vec{k}\cdot\vec{\delta}_3} + a_{k+n_1}\, e^{-i\vec{k}\cdot\vec{\delta}_1} + a_{k+n_2}\, e^{-i\vec{k}\cdot\vec{\delta}_2}) \\
&\quad + U b_k^* b_k b_k\,, \qquad (2.19)
\end{aligned}
$$

where n_1 and n_2 in the indices label the lattice sites in the two directions of the primitive-cell translation vectors $\vec{n}_1$ and $\vec{n}_2$.

The NLDE is derived around the linear band crossings between the A and B sublattices at the Brillouin zone corners [50], called the *Dirac cones* in the graphene literature [48]. To this end, we insert particular values for the the nearest-neighbor displacement vectors $\vec{\delta}$ and evaluate $\vec{k}$ at the Brillouin zone corner, defined by $\vec{k} = \vec{K} = (0, 4\pi/3)$, $\vec{\delta}_1 = (\frac{1}{2\sqrt{3}}, -\frac{1}{2})$, $\vec{\delta}_2 = (\frac{1}{2\sqrt{3}}, \frac{1}{2})$, $\vec{\delta}_3 = (-\frac{1}{\sqrt{3}}, 0)$. Then Eqs. (2.18)-(2.19) become

$$\begin{aligned} i\hbar\,\dot{a}_k &= -t_h(b_k\,e^0 + b_{k-n_1}\,e^{-i2\pi/3} + b_{k-n_2}\,e^{i2\pi/3}) \\ &\quad +U a_k^* a_k a_k\,. \end{aligned} \tag{2.20}$$

Reducing the exponentials,

$$\begin{aligned} i\hbar\,\dot{a}_k &= -t_h[b_k + b_{k-n_1}(-1/2 - i\sqrt{3}/2) \\ &\quad +b_{k-n_2}(-1/2 + i\sqrt{3}/2)] + U a_k^* a_k a_k\,. \end{aligned} \tag{2.21}$$

In anticipation of taking the long wavelength, continuum limit, as is necessary to obtain the NLDE, we group terms appropriately in order to construct discrete versions of derivatives. We demonstrate this procedure for Eq. (2.20) only, as it is identical in form for Eq. (2.21). Grouping terms in Eq. (2.20),

$$\begin{aligned} i\hbar\,\dot{a}_k &= -t_h[b_k + (b_k - b_{k-n_1})(1/2 + i\sqrt{3}/2) \\ &\quad -b_k(1/2 + i\sqrt{3}/2) + (b_k - b_{k-n_2})(1/2 - i\sqrt{3}/2) \\ &\quad -b_k(1/2 - i\sqrt{3}/2)] + U a_k^* a_k a_k\,, \end{aligned} \tag{2.22}$$

which reduces to

$$\begin{aligned} i\hbar\dot{a}_k &= -t_h[(b_k - b_{k-n_1})(1/2 + i\sqrt{3}/2) \\ &\quad +(b_k - b_{k-n_2})(1/2 - i\sqrt{3}/2)] + U a_k^* a_k a_k\,. \end{aligned} \tag{2.23}$$

At this point it is appropriate to elaborate on the meaning of the c-valued a_j and b_j in our derivation. To explain the physics here we borrow from the molecular orbital model of graphene. In this language we say that the Π-bonding and anti-bonding orbitals correspond to the valence and conduction bands respectively. Bringing the system in the vicinity of the Dirac point corresponds to a continuous distortion of the bonding and ant-bonding orbitals where, at the Dirac point, they become indistinguishable. It is standard in the literature to examine perturbations near the Dirac point by linearizing the states in momentum space. This we will also do. But our approach departs from the usual in that we have averaged with respect to coherent states in the tight-binding limit and are thus effectively left with a theory in position space where the fundamental length scale is the lattice spacing. Since Eq. (2.23) results from evaluating our equations at the Dirac point, small perturbations in momentum correspond to long wavelength modes which involve little change in nearby a_j and b_j amplitudes. Since amplitude changes are small on the order of the lattice spacing we can equivalently recast our equation using continuous functions for the onsite amplitudes provided the momentum of the perturbation satisfies the condition that $p \ll h/d$ where h is Planck's constant and d is the lattice spacing.

Taking the continuum limit and replacing the discrete quantities a_k and b_k by the continuous functions $\psi_A = \psi_A(\vec{r})$ and $\psi_B = \psi_B(\vec{r})$, we arrive at

$$\begin{aligned} i\hbar\dot{\psi_A} &= -t_h\left[\frac{\partial\psi_B}{\partial n_1}(1/2+i\sqrt{3}/2)+\frac{\partial\psi_B}{\partial n_2}(1/2-i\sqrt{3}/2)\right] \\ &\quad +U\psi_A^*\psi_A\psi_A\,. \end{aligned} \tag{2.24}$$

where the partial derivatives are in the directions of the unit-cell vectors $\vec{n}_1$ and $\vec{n}_2$. With a little trigonometry we find that the unit-cell vectors are

$$\vec{n}_1 = \cos(\pi/6)\hat{e}_x - \sin(\pi/6)\hat{e}_y = \sqrt{3}/2\hat{e}_x - 1/2\hat{e}_y\,, \tag{2.25}$$

$$\vec{n}_2 = \cos(\pi/6)\hat{e}_x + \sin(\pi/6)\hat{e}_y = \sqrt{3}/2\hat{e}_x + 1/2\hat{e}_y\,. \tag{2.26}$$

Up to now the "hat" symbol (accent circumflex) has been reserved for operators alone. However, in Eqs. (2.25)-(2.26) we use this symbol to indicate a unit vector in the x and y directions. Thus

$$\begin{aligned} \partial_{n_1} &= \vec{n_1} \cdot \vec{\bigtriangledown} = (\sqrt{3}/2)\partial_x - (1/2)\partial_y \,, & (2.27) \\ \partial_{n_2} &= \vec{n_2} \cdot \vec{\bigtriangledown} = (\sqrt{3}/2)\partial_x + (1/2)\partial_y \,. & (2.28) \end{aligned}$$

Substituting Eqs. (2.27)-(2.28) into Eq. (2.24),

$$\begin{aligned} i\hbar\dot{\psi_A} &= -t\Big[(\sqrt{3}/2\partial_x - 1/2\partial_y)\psi_B(1/2 + i\sqrt{3}/2) \\ &\quad +(\sqrt{3}/2\partial_x + 1/2\partial_y)\psi_B(1/2 - i\sqrt{3}/2)\Big] \\ &\quad +U\psi_A^*\psi_A\psi_A \,. \end{aligned} \tag{2.29}$$

Further simplification of Eq. (2.29) leads to

$$i\hbar\dot{\psi_A} = -t_h\sqrt{3}/2(\partial_x\psi_B - i\partial_y\psi_B) + U\psi_A^*\psi_A\psi_A \tag{2.30}$$

Similarly, for the continuum limit of $b_k \to \psi_B = \psi_B(\vec{r})$,

$$i\hbar\dot{\psi_B} = -t_h\sqrt{3}/2(-\partial_x\psi_A - i\partial_y\psi_A) + U\psi_B^*\psi_B\psi_B \,. \tag{2.31}$$

Eqs (2.30)-(2.31) are in fact massless Dirac equations with an added nonlinear term. To put this in a more familiar form, we use Pauli matrix notation. To this end, one must rename the coordinate axes so that $x \to y$, and, in order to preserve the handedness of the coordinate system, $y \to -x$. We also reinsert the lattice constant a; note that a is unrelated to the s-wave scattering length a_s briefly mentioned in the definition of g following Eq. (9.1). Thus $\partial_x \to \partial_y$ and $\partial_y \to -\partial_x$. Then Eqs. (2.30)-(2.31) become

$$\begin{aligned} i\hbar\dot{\psi_A} &= -t_h a\sqrt{3}/2(\partial_y\psi_B + i\partial_x\psi_B) + U\psi_A^*\psi_A\psi_A \,, & (2.32) \\ i\hbar\dot{\psi_B} &= -t_h a\sqrt{3}/2(-\partial_y\psi_A + i\partial_x\psi_A) + U\psi_B^*\psi_B\psi_B \,, & (2.33) \end{aligned}$$

or in matrix form,

$$i\hbar \begin{pmatrix} \dot{\psi}_A \\ \dot{\psi}_B \end{pmatrix} = \frac{-it_h a\sqrt{3}}{2} \begin{pmatrix} 0 & \partial_x - i\partial_y \\ \partial_x + i\partial_y & 0 \end{pmatrix} \begin{pmatrix} \psi_A \\ \psi_B \end{pmatrix} + U \begin{pmatrix} \psi_A^* \psi_A \psi_A \\ \psi_B^* \psi_B \psi_B \end{pmatrix} . \quad (2.34)$$

We can write Eq. (2.34) more compactly in terms of Pauli matrices $(\sigma_1, \sigma_2) = \vec{\sigma}$,

$$i\hbar \begin{pmatrix} \dot{\psi}_A \\ \dot{\psi}_B \end{pmatrix} = \frac{-it_h a\sqrt{3}}{2} \vec{\sigma} \cdot \vec{\bigtriangledown} \begin{pmatrix} \psi_A \\ \psi_B \end{pmatrix} + U \begin{pmatrix} \psi_A^* \psi_A \psi_A \\ \psi_B^* \psi_B \psi_B \end{pmatrix} . \quad (2.35)$$

Equation (2.35) is the NLDE. However, we can make one further step by expressing Eq. (2.35) in a more covariant looking form as follows in (2+1) dimensions:

$$(i\sigma_0 \partial_t + ic_l \vec{\sigma} \cdot \vec{\nabla}) \begin{pmatrix} \psi_A \\ \psi_B \end{pmatrix} - U \begin{pmatrix} \psi_A^* \psi_A \psi_A \\ \psi_B^* \psi_B \psi_B \end{pmatrix} = 0 , \quad (2.36)$$

where $\vec{\sigma}$ and $\vec{\nabla}$ are restricted to the $x - y$ plane. In Eq. (2.36),

$$c_l \equiv t_h a\sqrt{3}/2\hbar \quad (2.37)$$

is an effective speed of light of the condensate in the lattice[144, 145] (in graphene it would be replaced with the Fermi velocity [48]). This velocity is an effective speed of light for excitations of the NLDE in our QED_{2+1} theory. Experimental values of c_l in BECs are on the order of cm/s, ten orders of magnitude slower than the speed of light in a vacuum. Note also that in Eq. (2.36) U has now absorbed a factor of $1/\hbar$. Finally, a few additional definitions lead to a nicely compact form for the NLDE. Let

$$A \equiv \begin{pmatrix} 1 & 0 \\ 0 & 0 \end{pmatrix}, B \equiv \begin{pmatrix} 0 & 0 \\ 0 & 1 \end{pmatrix}, \psi \equiv \begin{pmatrix} \psi_A \\ \psi_B \end{pmatrix}, \bar{\psi} \equiv \begin{pmatrix} \psi_A^*, \psi_B^* \end{pmatrix}. \quad (2.38)$$

With the choice of metric which raises and lowers space-time indices restricted to (2+1) dimensions,

$$g^{\mu\nu} = \begin{pmatrix} 1 & 0 & 0 \\ 0 & -1 & 0 \\ 0 & 0 & -1 \end{pmatrix} , \quad (2.39)$$

Eq. (2.36) becomes

$$(i\sigma^{\mu}\partial_{\mu} - U\bar{\psi}A\psi A - U\bar{\psi}B\psi B)\psi = 0\,, \tag{2.40}$$

where the standard Einstein summation rule is in effect, $\mu \in \{0, 1, 2\}$ in keeping with (2+1) dimensions, and the units are chosen such that $c_l = 1$.

2.3 Maximally Compact Form of the NLDE

In Sec. 2.2 we developed ψ, a two-dimensional complex object which brings to mind one member of a pair of Weyl-spinors in the (1/2,1/2) chiral representation of the Dirac algebra used to describe massless neutrinos in the standard QED_{3+1} theory. Such a treatment is appropriate for any neutral Dirac fermion viewed in the extreme relativistic frame. In order to make the connection clear we must find the second member of the pair of Weyl-spinors and verify that the mapping is true. A thorough treatment of the mapping of QED_{3+1} into the QED_{2+1} theory of graphene is contained in [51] and references therein. We will continue to restrict ourselves to (2+1) dimensions in the following.To this end, we seek to put the NLDE into a form consistent with the standard compact four-component spinor notation for the linear Dirac equation

$$i\gamma^{\mu}\partial_{\mu}\Psi = 0\,. \tag{2.41}$$

We point out that this notation is not only standard but more appropriate if the quasi-particles, i.e., the long-wavelength excitations, develop a non-zero effective mass, as can be caused by lattice distortion [133].

We obtained the NLDE by evaluating the exponentials at the Brillouin Zone corner $\mathbf{K}_{+} = (0, 4\pi/3)$. There is another inequivalent corner, $\mathbf{K}_{-} \equiv (0, -4\pi/3)$, near which perturbations in momentum, i.e., long-wavelength quasiparticle excitations, are governed by a similar first-order wave equation. By considering equations of motions derived around *both* Brillouin corners, we can obtain the four-vector notation. The

coupled equations evaluated at $\mathbf{K}_- = (0, -4\pi/3)$ are

$$i\hbar\dot{\psi}_A = \frac{-t_h a\sqrt{3}}{2}(\partial_x + i\partial_y)\psi_B + U\psi_A^*\psi_A\psi_A\,, \tag{2.42}$$

$$i\hbar\dot{\psi}_B = \frac{-t_h a\sqrt{3}}{2}(-\partial_x + i\partial_y)\psi_A + U\psi_B^*\psi_B\psi_B\,. \tag{2.43}$$

Following the same steps as before we obtain

$$i\hbar\begin{pmatrix}\dot{\psi}_B\\ \dot{\psi}_A\end{pmatrix} = \frac{it_h a\sqrt{3}}{2}\vec{\sigma}\cdot\vec{\bigtriangledown}\begin{pmatrix}\psi_B\\ \psi_A\end{pmatrix} + U\begin{pmatrix}\psi_B^*\psi_B\psi_B\\ \psi_A^*\psi_A\psi_A\end{pmatrix}. \tag{2.44}$$

We combine Eqs. (2.44) and (2.35) into one equation involving a single 4-component object and attach $\pm$ subscripts to the wave functions Ψ to specify the corner of the Brillouin Zone. The resulting expression is

$$i\partial_t\begin{pmatrix}\Psi_+\\ \Psi_-\end{pmatrix} + i\begin{pmatrix}\tilde{\sigma}\cdot\tilde{\bigtriangledown} & \mathbf{0}\\ \mathbf{0} & -\vec{\sigma}\cdot\vec{\bigtriangledown}\end{pmatrix}\begin{pmatrix}\Psi_+\\ \Psi_-\end{pmatrix} - U\begin{pmatrix}\mathbf{N}_+\\ \mathbf{N}_-\end{pmatrix} = 0\,. \tag{2.45}$$

where the nonlinear terms are grouped into the 2-vectors $\mathbf{N}_+$ and $\mathbf{N}_-$ defined by

$$\mathbf{N}_+ = \begin{pmatrix}(\psi_A^*\psi_A\psi_A)_+\\ (\psi_B^*\psi_B\psi_B)_+\end{pmatrix},\quad \mathbf{N}_- = \begin{pmatrix}(\psi_B^*\psi_B\psi_B)_-\\ (\psi_A^*\psi_A\psi_A)_-\end{pmatrix} \tag{2.46}$$

and the four-spinors are given by

$$\Psi \equiv \begin{pmatrix}\Psi_+\\ \Psi_-\end{pmatrix} \equiv \begin{pmatrix}\psi_{A+}\\ \psi_{B+}\\ \psi_{B-}\\ \psi_{A-}\end{pmatrix}, \tag{2.47}$$

$$\Psi^\dagger \equiv \begin{pmatrix}\Psi_+^* & \Psi_-^*\end{pmatrix} \equiv \begin{pmatrix}\psi_{A+}^* & \psi_{B+}^* & \psi_{B-}^* & \psi_{A-}^*\end{pmatrix}. \tag{2.48}$$

Here again the $\pm$ subscripts refer to the specific corner of the Brillouin zone.

We can reduce Eq. (2.45) to a more compact form by introducing the following 4x4 matrices. Our convention in Eqs. (2.49)-(2.51), in keeping with Ref. [114], is that boldface signifies a 2x2 matrix, excepting the Pauli matrices, which are conventionally

already 2x2.

$$\Sigma_0 = \begin{pmatrix} \mathbf{1} & \mathbf{0} \\ \mathbf{0} & \mathbf{1} \end{pmatrix}, \Sigma_1 = \begin{pmatrix} \sigma_x & \mathbf{0} \\ \mathbf{0} & -\sigma_x \end{pmatrix}, \Sigma_2 = \begin{pmatrix} \sigma_y & \mathbf{0} \\ \mathbf{0} & -\sigma_y \end{pmatrix}, \tag{2.49}$$

$$A_+ = \begin{pmatrix} \mathbf{A} & \mathbf{0} \\ \mathbf{0} & \mathbf{0} \end{pmatrix}, A_- = \begin{pmatrix} \mathbf{0} & \mathbf{0} \\ \mathbf{0} & \mathbf{A} \end{pmatrix}, \tag{2.50}$$

$$B_+ = \begin{pmatrix} \mathbf{B} & \mathbf{0} \\ \mathbf{0} & \mathbf{0} \end{pmatrix}, B_- = \begin{pmatrix} \mathbf{0} & \mathbf{0} \\ \mathbf{0} & \mathbf{B} \end{pmatrix}. \tag{2.51}$$

The boldface notation **A** and **B** denote the 2×2 matrices defined in Eq. (2.38). Also, the boldface entries **1** and **0** in the matrices in Eq. (2.46) refer to the 2×2 unit matrix and zero matrix respectively. Then Eq. (2.45) becomes

$$(i\Sigma^\mu\partial_\mu - U\Psi^\dagger A_+\Psi A_+ - U\Psi^\dagger B_+\Psi B_+ - U\Psi^\dagger A_-\Psi A_- - U\Psi^\dagger B_-\Psi B_-)\Psi = 0\,. \tag{2.52}$$

We substitute into Eq. (2.52) the Dirac matrices in the Chiral representation:

$$\gamma^0 \equiv \begin{pmatrix} \mathbf{0} & \mathbf{1} \\ \mathbf{1} & \mathbf{0} \end{pmatrix}, \gamma^1 \equiv \begin{pmatrix} \mathbf{0} & -\sigma_x \\ \sigma_x & \mathbf{0} \end{pmatrix}, \gamma^2 = \begin{pmatrix} \mathbf{0} & -\sigma_y \\ \sigma_y & \mathbf{0} \end{pmatrix}, \tag{2.53}$$

where $\mu \in \{0, 1, 2\}$ in keeping with (2+1) dimensions, and multiply on the left by γ^0. Finally, for the nonlinear term we introduce

$$N \equiv -U\,\Psi^\dagger \sum_{Q \in A_+, A_-, B_+, B_-} Q\Psi Q.$$

Implementing Dirac matrix notation as described, the NLDE of Eq. (2.52) takes on its final form,

$$(i\gamma^\mu\partial_\mu + \gamma^0 N)\Psi = 0\,. \tag{2.54}$$

Eq. (2.54) is the most compact form of the massless NLDE in 4-component spinor notation.

2.4 Symmetries and Constraints

The NLDE as expressed by Eq. (2.36) or Eq. (2.40) looks like the Dirac equation for a two-spinor, as stated in the graphene problem [48], with the addition of two

nonlinear on-site interaction terms, one for each A and B sublattice; similarly, the more compact form developed in Sec. 2.3 also appears to be a Dirac equation for a four-component spinor, with an additional term. However, one should not be too hasty in assigning characteristics based on appearances. We therefore make a careful and thorough exploration of the symmetries and other important mathematical properties of the NLDE. In what follows we follow a similar route as in Ref. [114]. First we check the linear version with the delta interactions turned off to ensure that Eq. (2.40) is indeed the massless Dirac equation in (2+1) dimensions with all the necessary symmetries. For each symmetry we then check the nonlinear interaction terms to determine whether they preserve or break the symmetry.

2.4.1 Locality

We do not necessarily require the evolution of the wavefunction as described by an NLDE to be governed by a local theory. A local theory is one in which the terms in the linear equations of motion involve only factors of the wavefunction and its derivatives evaluated at the same space-time coordinate. Nonlocality arises in low energy limits of some quantum field theories. However, the nonlinearity in our NLDE is manifestly local. Thus our NLDE is closer to the standard Dirac equation on the classical level (no quantum effects), modified by the on-site interaction term. In Sec. 2.5 we discuss the possibility of non-local nonlinearities, including for graphene.

2.4.2 Poincaré Symmetry

A Poincaré transformation takes the spatiotemporal point defined by the the 4-vector r_ν into the point r'^μ according to

$$r'^\mu = \Lambda^{\mu\nu} r_\nu + d^\mu \,, \tag{2.55}$$

where $\Lambda^{\mu\nu}$ is the coordinate matrix representation of the Lorentz group and d^μ is a space-time translation. The wave function Ψ transforms as

$$\Psi'(r') = M(\Lambda)\Psi(r)\,,$$

where the matrices $M(\Lambda)$ form a representation of the subgroup of the Lorentz group consisting of spatial rotations and boosts. Boosts can be thought of as rotations in imaginary time by imaginary angles mixing space and time coordinates. We restrict these transformations to (2+1) dimensions. The proof of Lorentz covariance of the standard massless Dirac equation, Eq. (2.41), is arrived at with the aid of the transformations for the wave function and partial derivatives

$$\Psi(r) = M^{-1}(\Lambda)\Psi'(\mathbf{r}')\,, \tag{2.56}$$

$$\frac{\partial}{\partial x_i} = \Lambda_{ji}\frac{\partial}{\partial x'_j}\,. \tag{2.57}$$

This yields the conditions for the Dirac matrices:

$$\gamma_j = \Lambda_{ji} M \gamma_i M^{-1}\,. \tag{2.58}$$

The standard form of the Dirac matrices obtained this way can be found in the literature [86] and are identical to the results of our theory.

Thus imposing Lorentz covariance on the NLDE as expressed in Eq. (2.54) requires Ψ to transform under the irreducible representation of a subgroup of SL(2,C), the 2×2 complex matrices of unit determinant. The four-dimensional representation of SL(2,C), $D^{(1/2,1/2)}$, is formed by taking the direct product of the two-dimensional representations $D^{(1/2,0)}$ and $D^{(0,1/2)}$

$$D^{(1/2,1/2)} = D^{(1/2,0)} \otimes D^{(0,1/2)}\,. \tag{2.59}$$

This subgroup of SL(2,C) is isomorphic to a subgroup of the Lorentz group, the one obtained by restricting Lorentz transformations to the plane of the honeycomb lattice. So, the upper two components of Ψ transform as a spinor under $D^{(1/2,0)}$, the lower two

as a spinor under $D^{(0,1/2)}$, and Ψ itself as a four-component spinor or *bispinor*[146].

The next task is to examine the behavior of Ψ, as defined in Eq. (2.48) and governed by Eq. (2.54), under rotations in the $x-y$ plane. In order to obtain Poincaré covariance we must show that it is the same as that of a four-component spinor in the standard Dirac_{3+1} theory restricted to the 2D plane. The honeycomb lattice is invariant under rotations by $\pm 2\pi/3$ but the four components of Ψ are also defined by the particular corner of the Brillouin Zone. Since we're considering a discrete lattice it is natural to discuss discrete rotations which realign lattice points and in the continuum limit map the continuous rotations of QED_{2+1} onto our theory. Rotations by $\pm\pi/3$ exchange A and B sites, and take the theory to that of the opposite $\vec{K}$ point: $\vec{K}_+$ does not go to $\vec{K}_-$ but the result after calculating the relative phase exponentials gives back the same theory. To see this we chose a different primitive unit cell, the one obtained by a rotation of $2\pi/3$ about the $\vec{n}_1, \vec{n}_2$ origin in Fig Figure 2.1. This is because the direction of $\vec{K}'_+$ (defined as $\vec{K}_+$ rotated by $\pi/3$) differs from that of $\vec{K}_-$ by $2\pi/3$. Thus under this discrete rotation

$$
\begin{aligned}
b_k &\rightarrow b_{k-2n_1}\,, && (2.60)\\
b_{k-n_1} &\rightarrow b_{k-n_1-n_2}\,, && (2.61)\\
b_{k-n_2} &\rightarrow b_{k-n_1}\,, && (2.62)\\
a_k &\rightarrow a_{k-n_1}\,, && (2.63)\\
a_{k+n_1} &\rightarrow a_{k-2n_1+n_2}\,, && (2.64)\\
a_{k+n_2} &\rightarrow a_{k-2n_1}\,. && (2.65)
\end{aligned}
$$

Also, we observe that

$$
\begin{aligned}
\vec{K}'_+ \cdot \vec{\delta}_3 &= \vec{K}_- \cdot \vec{\delta}_1 && (2.66)\\
\vec{K}'_+ \cdot \vec{\delta}_1 &= \vec{K}_- \cdot \vec{\delta}_2 && (2.67)\\
\vec{K}'_+ \cdot \vec{\delta}_2 &= \vec{K}_- \cdot \vec{\delta}_3\,. && (2.68)
\end{aligned}
$$

Putting these together, we obtain

$$
\begin{aligned}
i\hbar\,\dot{a}_{k-n_1} &= -t_h(b_{k-2n_1}\,e^{i\vec{K}_-\cdot\vec{\delta}_1} + b_{k-n_1-n_2}\,e^{i\vec{K}_-\cdot\vec{\delta}_2} \\
&\quad + b_{k-n_1}\,e^{i\vec{K}_-\cdot\vec{\delta}_3}) + U a^*_{k-n_1} a_{k-n_1} a_{k-n_1}\,, \qquad (2.69) \\
i\hbar\,\dot{b}_{k-2n_1} &= -t_h(a_{k-n_1}\,e^{-i\vec{K}_-\cdot\vec{\delta}_1} + a_{k-2n_1+n_2}\,e^{-i\vec{K}_-\cdot\vec{\delta}_2} \\
&\quad + a_{k-2n_1}\,e^{-i\vec{K}_-\cdot\vec{\delta}_3}) + U b^*_{k-2n_1} b_{k-2n_1} b_{k-2n_1}\,. \qquad (2.70)
\end{aligned}
$$

Now, we redefine the index k: in Eq. (2.69), $k \to k + n_1$, while in Eq. (2.70), $k \to k + 2n_1$. Then

$$
\begin{aligned}
i\hbar\,\dot{a}_k &= -t_h(b_{k-n_1}\,e^{i\vec{K}_-\cdot\vec{\delta}_1} + b_{k-n_2}\,e^{i\vec{K}_-\cdot\vec{\delta}_2} + b_k\,e^{i\vec{K}_-\cdot\vec{\delta}_3}) + U a^*_k a_k a_k \qquad (2.71) \\
i\hbar\,\dot{b}_k &= -t_h(a_{k+n_2}\,e^{-i\vec{K}_-\cdot\vec{\delta}_1} + a_{k+n_2}\,e^{-i\vec{K}_-\cdot\vec{\delta}_2} + a_k\,e^{-i\vec{K}_-\cdot\vec{\delta}_3}) + U b^*_k b_k b_k. \qquad (2.72)
\end{aligned}
$$

To summarize, a rotation by $\pi/3$ which takes $\vec{K}_+ \to \vec{K}'_+$ is identical to the unrotated theory but with $\vec{K}_+ \to \vec{K}_-$. Note that the redefinition of the index k is different for the two equations because old and new primitive cells are related by a rotation. Rotating by $\pm 2\pi/3$ exchanges A and B sites once more and returns Ψ to its original configuration. Since Ψ has four components, the effect of making one full rotation of 2π is that the components acquire a net phase so that $\Psi \to -\Psi$. This *Berry phase* [128] endows Ψ with the characteristic double-valuedness of a genuine 4-spinor. However, we must be cautious when discussing chirality and helicity, since we treat (2+1) dimensions and can use only the first two Pauli matrices. As in the (3+1) theory, one can define a *pseudo-chirality operator* in (2+1) dimensions, γ^5, as the product of the other four γ matrices. In the Weyl, or Chiral, representation we have

$$
\gamma^5 \equiv i\gamma^0\gamma^1\gamma^2\gamma^3 = \begin{pmatrix} \mathbf{1} & \mathbf{0} \\ \mathbf{0} & \mathbf{-1} \end{pmatrix}, \qquad (2.73)
$$

where again the boldface indicates a 2x2 submatrix. This is the natural representation for Ψ in that the NLDE of Eq. (2.54) maps into this representation in a natural way: states of well defined chirality correspond to the upper and lower 2-spinors. Thus the

upper and lower spinors

$$\Psi_+ \equiv \begin{pmatrix} \psi_+ \\ \mathbf{0} \end{pmatrix}, \quad \Psi_- \equiv \begin{pmatrix} \mathbf{0} \\ \psi_- \end{pmatrix} \tag{2.74}$$

are eigenfunctions of γ^5,

$$\gamma^5 \Psi_+ = \Psi_+, \quad \gamma^5 \Psi_- = -\Psi_- . \tag{2.75}$$

The question of Poincaré covariance of the nonlinear Dirac equation remains. We check first coordinate translations. The wave function is required to transform as

$$\Psi'(r+d) = \Psi(r) . \tag{2.76}$$

Thus the nonlinear terms which have two factors of Ψ are invariant under translations. Under spatial rotations we observe that the interaction terms in the NLDE remain unchanged within the context of the full theory. We include both $\vec{K}_+$ and $\vec{K}_-$ points in the full theory. As for the case of boosts, we note that for the linear equation the components of the wave function transform in accordance with the transformation of the space-time coordinates in their arguments. This is exactly canceled by the reciprocal transformations of the partial derivatives. This is not the case for the nonlinear terms. One has some matrix product with two factors of the wave function. Thus the *nonlinear* Dirac equation is not invariant under Lorentz boosts.

For any truly fundamental theory of nature it is demanded that the governing equations be invariant with respect to the Poincaré group. Sometimes this requirement is loosened as in the quantization of gauge theories, when fixing the gauge causes relativistic covariance to be non-manifest. Yet the theory itself certainly remains invariant. Other times the breaking of Poincaré covariance implies that we are dealing with an effective theory in which deeper physical processes are at work. Our case is an example of the latter. By including on-site interactions we break "relativistic" invariance of the linear theory by introducing self-interactions which can be viewed as evidence of "deeper physics" in our two-dimensional universe.

2.4.3 Hermiticity

We require the Hamiltonian be Hermitian in order to guarantee that physically measurable quantities (observables) are real. Thus each term must be independently Hermitian. In particular, we must show that $N^\dagger = N$. The proof follows:

$$\begin{aligned} N^\dagger &= (U\Psi^\dagger A_+ \Psi A_+)^\dagger \\ &= U A_+^\dagger \Psi^\dagger A_+^\dagger (\Psi^\dagger)^\dagger \\ &= U A_+ \Psi \dagger A_+ \Psi \\ &= U \Psi^\dagger A_+ \Psi A_+ \\ &= N\,, \end{aligned} \tag{2.77}$$

where the last two steps work because A_+ is real and symmetric. The nonlinear terms are indeed Hermitian.

2.4.4 Current Conservation

Current conservation is expected in ordinary QED for a closed system, i.e., an isolated volume of space. However, most theories of quantum gravity do introduce Lorentz violating terms which bring in charge non-conservation effects. The conserved current for the linear Dirac equation is

$$j^\mu = \bar{\Psi}\gamma^\mu \Psi\,, \tag{2.78}$$

where $\bar{\Psi} \equiv \Psi^\dagger \gamma^0$. We check that this current is also conserved for the NLDE. The 3-divergence of the current in (2+1) spatial dimensions is

$$\begin{aligned} \partial_\mu j^\mu &= \partial_\mu(\bar{\Psi}\gamma^\mu\Psi) \\ &= \partial_\mu(\Psi^\dagger\gamma^0\gamma^\mu\Psi) \\ &= \partial_\mu\Psi^\dagger\gamma^0\gamma^\mu\Psi + \Psi^\dagger\gamma^0\gamma^\mu\partial_\mu\Psi \\ &= \partial_\mu\Psi^\dagger\gamma^0\gamma^\mu\Psi + \Psi^\dagger\gamma^0\gamma^\mu\partial_\mu\Psi \\ &= -\partial_\mu\Psi^\dagger\gamma^\mu\gamma^0\Psi + \Psi^\dagger\gamma^0\gamma^\mu\partial_\mu\Psi\,, \end{aligned} \tag{2.79}$$

where $\mu \in \{0, 1, 2\}$ and we have used the anti-commuting properties of the Dirac matrices. Taking the adjoint of the Dirac equation, Eq. (2.41), yields

$$(i\gamma^\mu \partial_\mu \Psi)^\dagger = (-\gamma^0 N \Psi)^\dagger \,, \tag{2.80}$$

which implies

$$-\partial_\mu \Psi^\dagger \gamma^\mu = -i\Psi^\dagger N^\dagger \gamma^0 \,. \tag{2.81}$$

Then the (2+1)-divergence of the current is

$$\begin{aligned} \partial_\mu j^\mu &= -i\Psi^\dagger N^\dagger \gamma^0 \gamma^0 \Psi + \Psi^\dagger \gamma^0 (i\gamma^0 N \Psi) & (2.82) \\ &= -i\Psi^\dagger (N^\dagger - N)\Psi = 0 \,. & (2.83) \end{aligned}$$

Thus current is conserved. This is in fact the statement that hermiticity implies current conservation.

2.4.5 Chiral Current

The conserved chiral current for the linear Dirac equation is

$$j_5^\mu \equiv \bar{\Psi} \gamma^\mu \gamma_5 \Psi \,. \tag{2.84}$$

Then the (2+1)-divergence of the chiral current is

$$\partial_\mu j_5^\mu = \partial_\mu (\bar{\Psi} \gamma^\mu \gamma_5 \Psi) \,. \tag{2.85}$$

Following a similar route as in Sec. 2.4.4, we find

$$\partial_\mu j_5^\mu = -i\Psi^\dagger (N\gamma_5 + \gamma_5 N)\Psi \tag{2.86}$$

where we have used the hermiticity of N. This means that in order for chiral current to be conserved we must have

$$\{N, \gamma_5\} = 0 \,, \tag{2.87}$$

where the curly braces signify the anti-commutator. The anti-commutator is

$$\{N, \gamma_5\} = U\Psi^\dagger A_+ \Psi A_+ \gamma_5 + \gamma_5 U \Psi^\dagger A_+ \Psi A_+ \,. \tag{2.88}$$

Writing this out in explicit matrix form we find that

$$\{N, \gamma_5\} = +2N\,, \tag{2.89}$$
$$\{N, \gamma_5\} = -2N\,, \tag{2.90}$$

for the $\pm$ subscript terms, respectively. Evidently chiral current is not conserved. This fact is reminiscent of the anomalous non-conservation of chiral current in the case of some field theories upon quantization, which is mediated by instantons. It is interesting to consider that our nonlinear terms might be treated as quantum-induced nonlinearities.

2.4.6 Universality

Universality refers to the invariance of a theory under rescaling of the solution. For the case of the linear Dirac equation, $\Psi \rightarrow \lambda\Psi$ leaves the theory unchanged. Because the nonlinear term in the NLDE contains one factor of Ψ and one factor of its adjoint, it scales as λ^2, thus breaking the invariance of the nonlinear theory. For a treatment of NLDEs which are universal in this sense, but not relevant to the present solid state system, see Ref. [114].

2.4.7 Discrete Symmetries

2.4.8 Parity

In the case of the standard massless Dirac equation invariance under a parity transformation requires Ψ to transform as

$$\Psi \rightarrow \Psi' = \hat{P}\Psi = \gamma^0\Psi\,, \tag{2.91}$$

where, in contrast to the Chiral representation presented in Eq. (2.53), in the Dirac representation

$$\gamma^0 = \begin{pmatrix} \mathbf{1} & \mathbf{0} \\ \mathbf{0} & \mathbf{-1} \end{pmatrix}. \tag{2.92}$$

We proceed to determine if the NLDE remains invariant under the transformation of Eq. (2.91). The parity operator acting on the honeycomb lattice inverts both coordinate axes, $\vec{\nabla} \to -\vec{\nabla}$, and thus exchanges A and B sites while also exchanging $\vec{K}$-point indices. The transformed *linear* equations ($U = 0$) are

$$i\gamma^{\mathbf{0}} \begin{pmatrix} \dot{\Psi}_- \\ \dot{\Psi}_+ \end{pmatrix} + ic_l \begin{pmatrix} -\tilde{\sigma} \cdot \tilde{\bigtriangledown} & \mathbf{0} \\ \mathbf{0} & \vec{\sigma} \cdot \vec{\bigtriangledown} \end{pmatrix} \gamma^{\mathbf{0}} \begin{pmatrix} \Psi_- \\ \Psi_+ \end{pmatrix} = 0\,. \tag{2.93}$$

Interchanging upper and lower spinors we obtain the equivalent form

$$i \begin{pmatrix} \dot{\Psi}_+ \\ \dot{\Psi}_- \end{pmatrix} + ic_l \begin{pmatrix} \tilde{\sigma} \cdot \tilde{\bigtriangledown} & \mathbf{0} \\ \mathbf{0} & -\vec{\sigma} \cdot \vec{\bigtriangledown} \end{pmatrix} \begin{pmatrix} \Psi_+ \\ \Psi_- \end{pmatrix} = 0\,. \tag{2.94}$$

Thus the linear equations are invariant under the Parity operator. Next we check the nonlinear term in the NLDE.With the transformed nonlinear term added to Eq. (2.93) we obtain

$$i \begin{pmatrix} \dot{\Psi}_- \\ -\dot{\Psi}_+ \end{pmatrix} + ic_l \begin{pmatrix} -\tilde{\sigma} \cdot \tilde{\bigtriangledown} & \mathbf{0} \\ \mathbf{0} & \vec{\sigma} \cdot \vec{\bigtriangledown} \end{pmatrix} \begin{pmatrix} \Psi_- \\ -\Psi_+ \end{pmatrix} - U \begin{pmatrix} N_- \\ -N_+ \end{pmatrix} = 0\,, \tag{2.95}$$

which after similar steps as above gives us back the NLDE. Therefore parity is a symmetry of the nonlinear Dirac equation. Parity is conserved in standard QED and also in the theory of the strong interactions, but violated by weak interactions. We are dealing with a theory which resembles QED and thus in order to reap the benefits from that theory it is certainly desirable that ours retains parity invariance.

2.4.9 Charge Conjugation

In order to maintain symmetry under charge conjugation one requires the nonlinear term to transform as

$$(\gamma^0 N)' = \hat{C}\gamma^0 N^* \hat{C}^{-1}\,, \tag{2.96}$$

where in the chiral representation

$$\hat{C} = \gamma^1$$

and the wavefunction transforms in the standard way

$$\Psi \to \gamma^1\gamma^0\Psi^{\dagger T}\,. \tag{2.97}$$

We determine if the NLDE maintains this symmetry. Let F be one of the nonlinear terms. Then

$$\begin{aligned}(\gamma^0 N)' &= (\gamma^1\gamma^0\Psi^{\dagger T})^{\dagger} A_+ (\gamma^1\gamma^0\Psi^{\dagger T}) A_+ \\ &= \Psi^T\gamma^0\gamma^1 A_+ \gamma^1\gamma^0\Psi^* A_+ \end{aligned} \tag{2.98}$$

Also, we have

$$\begin{aligned}\hat{C}\gamma^0 N^* \hat{C}^{-1} &= \gamma^1\gamma^0(\Psi^\dagger A_+ \Psi A_+)^*\gamma^1 \\ &= \gamma^1\gamma^0\Psi^T A_+ \Psi^* A_+ \gamma^1 \end{aligned} \tag{2.99}$$

Thus the NLDE breaks charge conjugation symmetry.

2.4.10 Time Reversal

The usual time reversal $t \to -t$ requires that Ψ transform as

$$\Psi \to \Psi' = \hat{\Theta}\Psi = i\gamma^1\gamma^3\Psi\,, \tag{2.100}$$

where $\hat{\Theta}$ is the time-reversal operator and

$$i\gamma^1\gamma^3 = \begin{pmatrix} -\sigma_y & \mathbf{0} \\ \mathbf{0} & -\sigma_y \end{pmatrix}, \tag{2.101}$$

In our theory the intrinsic effect of time reversal is to change the direction of momentum so that $\vec{K}$ points are switched without exchanging A and B indices. Combining these effects, we determine whether or not the linear part of the NLDE, i.e., the linear Dirac equation, remains invariant:

$$-i\frac{\partial}{\partial t}i\gamma^1\gamma^3\begin{pmatrix}\Psi_-\\ \Psi_+\end{pmatrix}+ic_l\begin{pmatrix}\tilde{\sigma}\cdot\tilde{\bigtriangledown} & \mathbf{0}\\ \mathbf{0} & -\vec{\sigma}\cdot\vec{\bigtriangledown}\end{pmatrix}i\gamma^1\gamma^3\begin{pmatrix}\Psi_-\\ \Psi_+\end{pmatrix}=0 \qquad (2.102)$$

Then

$$-i\frac{\partial}{\partial t}\begin{pmatrix}\Psi_+\\ \Psi_-\end{pmatrix}+ic_l\begin{pmatrix}\tilde{\sigma}\cdot\tilde{\bigtriangledown} & \mathbf{0}\\ \mathbf{0} & -\vec{\sigma}\cdot\vec{\bigtriangledown}\end{pmatrix}\begin{pmatrix}\Psi_+\\ \Psi_-\end{pmatrix}=0. \qquad (2.103)$$

The appearance of the negative sign in front of the time derivative indicates that these are the equations satisfied by the negative energy solutions, or holes. Thus time reversal takes the equations describing electrons into holes and those for holes into electrons but keeps the overall theory invariant. We proceed to consider the nonlinear term. With the transformed nonlinear term we obtain

$$-i\frac{\partial}{\partial t}\begin{pmatrix}\Psi_+\\ \Psi_-\end{pmatrix}+ic_l\begin{pmatrix}\tilde{\sigma}\cdot\tilde{\bigtriangledown} & \mathbf{0}\\ \mathbf{0} & -\vec{\sigma}\cdot\vec{\bigtriangledown}\end{pmatrix}\begin{pmatrix}\Psi_+\\ \Psi_-\end{pmatrix}-iU\begin{pmatrix}N_+\\ N_-\end{pmatrix}=0\,. \qquad (2.104)$$

Here we see that the interaction term has acquired a factor of i so the NLDE is not invariant under time reversal. Thus, as we see in the standard model of particle physics, CP and T are not conserved independently but CPT is conserved. A note on CPT: although it is believed that CPT is a manifest symmetry in nature, charge conservation, parity, and time reversal may be individually violated under various circumstances within the standard model of elementary particles. For example, the theory of neutral kaons violates CP. It would be interesting to investigate how our theory fits into these special cases of symmetry violation, given that parity and time-reversal symmetries are maintained while charge conjugation is not.

2.5 Discussion and Conclusions

The nonlinear Dirac equation we have presented introduces a completely new class of nonlinear phenomena in Bose-Einstein condensates. Although our work is related to graphene, in that the BEC is taken to be trapped on a honeycomb lattice, we have

switched bosons for fermions. The form of the nonlinearity is then a natural physical result of binary interactions between bosons. In fact, it is a spinor generalization of the kind of nonlinearity one finds in the nonlinear Schrodinger equation, i.e., proportional to the local condensate density. The same equation will occur for light subject to a Kerr nonlinearity when propagating through a photonic crystal with a honeycomb lattice structure [147–149]. Numerical solutions to these equations should be tractable using methods discussed in the literature [150–152].

We showed that the NLDE breaks Poincaré covariance, and therefore the principle of relativity. This suggests that small nonlinearities of this form could be looked for by such symmetry breaking in a variety of systems where Dirac or Dirac-like equations apply. For instance, even for fermions there is a small mean field effect. We could just as easily have considered ultra-cold fermions on an optical lattice. This would appear at first sight to be the exact analog of graphene; however, our work shows that Poincaré covariance will be broken by mean field effects, even if on a small level. Indeed, for graphene one should expect similar effects due to Coulomb interactions. The latter nonlinearity can be expected to be non-local due to the power law behavior of $1/r$ for the Coulomb potential, just as dipole-dipole interactions between ultra-cold atoms lead to a non-local nonlinear Schrodinger equation in a 3D continuum (in 2D dipole-dipole interactions, which have a power law of $1/r^3$, are local). Thus, in graphene, we make the conjecture that there is a non-local nonlinear correction term to the massless Dirac equation which breaks Poincaré covariance. Similar corrections can be looked for in quantum electrodynamics under the proper circumstances [141]. All generalizations of the scalar nonlinear Schrodinger equation relevant to BECs are candidates for generalized nonlinear Dirac equations. For example, pseudospin structure leads to a vector NLSE. One can therefore anticipate a vector NLDE as well.

We have thoroughly explored both continuous and discrete symmetries of the NLDE. In particular, we showed that pseudo-chiral current is not conserved, the NLDE is not covariant under Lorentz boosts, and it breaks charge conjugation as well as time reversal symmetry. On the other hand, the NLDE is hermitian, local, conserves current, and is symmetric under parity. In a future work we will treat soliton and vortex solutions of the NLDE, as a first step towards a complete classification of nonlinear relativistic phenomena in BECs.

Acknowledgments

We acknowledge useful discussions with Alex Flournoy and Mark Lusk. This work was supported by the National Science Foundation under Grant PHY-0547845 as part of the NSF CAREER program.

CHAPTER 3

FOUNDATIONAL TOPICS IN THE NONLINEAR DIRAC EQUATION: SPINOR FORMALISM, SPIN-STATISTICS, LAGRANGIAN ANALYSIS, AND REDUCTION TO THE NONLINEAR SCHRÖDINGER EQUATION

3.1 Introduction

Having established the basic foundation of the NLDE, we turn now to several topics which help understand the physics of the NLDE. Two key questions arise: first, that the BEC background for the NLDE must acquire properties of a spin-1/2 space, since the geometric phase is a natural consequence of the continuum theory near a Dirac point. Such phase structure also implies the possibility of non-standard statistics for quasi-particles. Indeed, quasi-particles in a BEC are collective states, and need not be bound by the same physical properties of the fundamental constituent bosons. In our case, we will see that quasi-particles in the NLDE background possess a non-trivial spin structure and obey fermionic statistics.

Lagrangian analysis provides a deeper understanding of the structure of partial differential equations in addition to shedding light on the vortex and soliton structure of a system. In this chapter we construct the classical Hamiltonian for the NLDE, and use this to derive the Lagrangian by the standard method. Qualitative analysis of the Lagrangian will help us understand the nature of relativistic vortices. We investigate the classical energy functional approach as well, and determine the structure of the effective potential and investigate the classical fixed points. Any type of NLDE should be reducible to some type of NLSE, often the standard cubic form plus additional correction terms. We derive the NLSE from the NLDE by considering low

energy fluctuations in a symmetric background where both spinor components at a single Dirac point are equal, $|\delta\psi_B|^2 \simeq |\delta\psi_A|^2$, but with an extreme asymmetry in the fluctuations, i.e., $|\delta\psi_{B,t}|^2 \ll |\delta\psi_{A,x}|^2$. Solitons in the 1D case are obtained and analyzed, as well as quantized vortices for the 2D case.

In addition to the topics above, we present a review of basic spinor theory and interpret this in the context of the honeycomb lattice. We also present a study of the behavior of the nonlinearity of the NLDE under Lorentz transformations.

3.2 The Spin-Statistics Theorem and Honeycomb Lattice Elementary Excitations

The physics of particles in (2+1)-dimensions is unique in that collective states may exhibit drastically different properties than their constituent particles. Total wavefunctions may acquire fractional phase values (fractional statistics) upon interchange of pairs of particles. Particles which exhibit such behavior are known as anyons, with the term semion reserved for the special case of half-integer multiples of π accumulated upon interchange. This phenomenon may be interpreted within a basic quantum mechanical picture as well as at the level of relativistic field theory. The effect may be illustrated using a simple path integral picture in which exchange of two particles involves a braiding of paths in configuration space. The key point is that in $(2+1)$-dimensions, a particular configuration of a given winding cannot be smoothly deformed into another so that the number of windings involved places many-particle states into topological classes. The relative phase winding which distinguishes one particular topological state from another need not be integer valued [153].

To illustrate this at the field theory level we start with a few general assumptions and provide only a sketch, where specific details may be found in Ref. [153]. The main assumption is that we work in a (2+1)-dimensional space-time with a field possessing conserved current, i.e., with a vanishing 4-divergence, and that we examine only the long-wavelength physics. At the level of the action the reduced dimensionality

restricts the types of terms which may appear, the conserved current condition means that the field may be expressed as the curl of some gauge field, and restricting to long distances allows one to omit more complicated higher order derivative terms from the model. The dynamics of the gauge field then appears as a Chern-Simons term with the usual form of a product of gauge field and derivative. The Chern-Simons term in (2+2)-dimensions is an example of a topological field theory for which certain invariant quantities may be computed independent of the particular form of the gauge field. This means that integrating over the curvature 2-form, for example, of the gauge bundle (the strength of the gauge field) reduces to a topological invariant, a number which describes the configuration of the field at spatial infinity, where the space is homeomorphic to S^1. Such invariants correspond to vortex configurations of the gauge field, specifically the phase winding, which may endow the particle with a fractional charge or fractional exchange statistics. If in addition, we add a scalar field to our model, and couple this to the Chern-Simons field, the resulting low-energy effective theory obtained by integrating out either the gauge field or the scalar field returns us to a Chern-Simons theory for the dressed scalar or gauge field. This method of trading one theory for an alternative perspective, the dressed scalar or the dressed gauge perspective, constitutes a duality. The work of Seradjeh and Franz [154], and Ryu et. al. [155], provide concrete realizations of these concepts for graphene-like systems.

The phenomenon of non-standard exchange statistics may be treated within the framework of differential topology, using the theory of fiber bundles with connections. Letting (E, π, M, F, G) be a fiber bundle with typical fiber F (more compactly $E \xrightarrow{\pi} M$), the differentiable manifolds E and M are the total space and base space, respectively, $\pi : E \longrightarrow M$ defines a surjection called the projection from the total space to the base space, and the Lie group G is the structure group acting on the fiber F. In physics the fiber at a point of the base space $p \in M$, denoted by F_p, is usually

taken to be either a real vector space, $F_p \in \mathbb{R}^n$, with structure group $GL(n, \mathbb{R})$ as in the case of the tangent bundle $T_p M$; a complex vector space, $F_p \in \mathbb{C}^n$, with structure group $GL(n, \mathbb{C})$; or a vector space whose elements form a spinor representation of the spin group, $F_p \in \mathrm{Spin}(n)$, the universal covering group of $SO(n)$. The structure group maps the fiber F_p into the neighboring fiber $F_{p'}$ isomorphically through what are called transition functions, whose values are taken in the structure group. The process of smoothly patching together neighboring fibers is specified by the particular form of the local transition functions and may lead to interesting non-trivial global topological structure such as fractional statistics. As we shall see, this is what happens in the case of long-wavelength excitations of a BEC in a honeycomb lattice where quasi-particles obey fermionic statistics to first order in the particle interactions.

The connection between spin and statistics arises naturally in our study of the BEC with Dirac points. We will see that the bi-partite structure of the honeycomb lattice endows the condensate wavefunction with a geometric phase, or Berry phase, so that a spinor formulation becomes necessary as is quite familiar from the study of electrons in graphene. The presence of a geometric phase endows the condensate with a non-trivial topological structure and has a direct effect on low-energy quasi-particle statistics. We can see how this works by taking a path integral point of view which shows that the condensate splits into topologically distinct sectors corresponding to different numbers of windings taken between two localized states (vortices). Moreover, this topological structure is only a feature of the continuum limit theory where energies are infinitesimal compared to the characteristic energy of the lattice scale. It is easy to see that as long as the coordinate exchange of two states involves smooth, slowly varying paths which remain within the continuum regime, there will be no ambiguity regarding the net accumulated phase for that particular exchange process. We find that quasi-particles obey fermionic statistics even though the fundamental

constituents are bosons.

The Berry phase associated with a rotation in the plane has a significant consequence for correlators involving pairs of quasi-particle operators. To illustrate this, we define the quasi-particle operator $\hat{\phi} \equiv \sum_j (\hat{\mathbf{u}}_j - \hat{\mathbf{v}}_j^\dagger)$, where $\hat{\mathbf{u}}_j$ ($\hat{\mathbf{u}}_j^\dagger$) and $\hat{\mathbf{v}}_j$ ($\hat{\mathbf{v}}_j^\dagger$) destroy (create) quasi-particles in the spinor states $\mathbf{u}_j \equiv (u_{j,A},\, u_{j,B})^T$ and $\mathbf{v}_j \equiv (v_{j,A},\, v_{j,B})^T$, respectively. In a field theory formulation, these operators become quantum fields whose Lagrangian is given by,

$$\mathcal{L} = \int d^3r\, \bar{\mathbf{\Phi}} \left(\gamma^\mu \partial_\mu \cdot \mathbb{1} - \mathrm{M}\right) \mathbf{\Phi}, \tag{3.1}$$

where we have concatenated the spinors into one structure, $\mathbf{\Phi} \equiv (\mathbf{u},\, \mathbf{v})$, and indicated the expanded space by the unit operator. The matrix M contains the interaction terms proportional to the particle interaction U in addition to the terms proportional to $\mu \pm E_j$, where μ is the chemical potential of the BEC and E_j are the quasi-particle eigenenergies. The "mass" term in Eq. (3.40) is not Lorentz invariant but accumulates an extra term, under a Lorentz transformation, proportional to U^2 which comes from the transformation properties of the $|\Psi_{A(B)}|^2$ factors in $\mathbf{M}$. Thus, to first order in U, $\mathcal{L}$ is Lorentz invariant. Now, consider the vacuum-to-vacuum correlation function $\langle 0|\mathbf{\Phi}(r)\mathbf{\Phi}(r')|0\rangle$ where r and r' are the $(2+1)$-dimensional space-time coordinates for two quasi-particle excitations. By analytic continuity, a spatial rotation is equivalent to one involving time since our theory is CPT invariant [52]. This means that a change in the order of the fields inside the correlation function is equivalent to exchanging the spatial positions of r and r' which gives an extra factor of -1 from the geometric phase. In essence, the spin-statistics theorem allows us to identify time-reordering with spatial exchange in the plane which then ties the operator algebra to the geometric phase [156–159]. We can then deduce the anti-commuting property for quasi-particles,

$$\langle 0|\Phi(r)\Phi(r') + \Phi(r')\Phi(r)|0\rangle = 0. \tag{3.2}$$

Equation 3.2 is the canonical commutation relation for fermions, which holds to first order in the interaction U.

3.3 Spinor Formalism in the Dirac Equation

In the following analysis we present a review of the basic theory of the Dirac equation and a physical lattice interpretation of Dirac spinors.

3.3.1 Energy Versus Chiral Representation

The Dirac equation was orignally solved in the Dirac basis for a free particle of mass m in the form

$$p_0\,\Phi(x) = \vec{\sigma}\cdot\vec{p}\,\chi(x) + m\,\Phi(x) \tag{3.3}$$
$$p_0\,\chi(x) = \vec{\sigma}\cdot\vec{p}\,\Phi(x) - m\,\chi(x), \tag{3.4}$$

where Φ and χ are 2-component spinors: the positive and negative energy 2-spinors respectively. This is also called *the energy representation* because each 2-spinor is a pure positive or negative energy state. For a massless particle these become

$$p_0\,\Phi(x) = \vec{\sigma}\cdot\vec{p}\,\chi(x) \tag{3.5}$$
$$p_0\,\chi(x) = \vec{\sigma}\cdot\vec{p}\,\Phi(x). \tag{3.6}$$

For a particle with 4-momentum (E , $\vec{p}$) the solutions are (apart from a normalization factor)

$$\psi_1 = e^{\,i(\,\vec{p}\,\cdot\,\vec{r}\,-\,E\,t)} \begin{pmatrix} 1 \\ 0 \\ \frac{p_z}{E} \\ \frac{p_x+ip_y}{E} \end{pmatrix}, \quad \psi_2 = e^{\,i(\,\vec{p}\,\cdot\,\vec{r}\,-\,E\,t)} \begin{pmatrix} 0 \\ 1 \\ \frac{p_x-ip_y}{E} \\ \frac{p_z}{E} \end{pmatrix}, \tag{3.7}$$

$$\psi_3 = e^{-i(\vec{p}\cdot\vec{r}-Et)}\begin{pmatrix} \frac{p_z}{E} \\ \frac{p_x+ip_y}{E} \\ 1 \\ 0 \end{pmatrix}, \quad \psi_4 = e^{-i(\vec{p}\cdot\vec{r}-Et)}\begin{pmatrix} \frac{p_x-ip_y}{E} \\ \frac{-p_z}{E} \\ 0 \\ 1 \end{pmatrix}, \tag{3.8}$$

where Φ and χ are the upper and lower 2-spinors respectively and it should be noted here that they *are not* helicity eigenstates. ψ_1 and ψ_2 are the positive energy solutions and ψ_3 and ψ_4 are the negative energy solutions. We get a different form for the 2-spinor equations (3) and (4) if we instead use the chiral representation for the Dirac matrices from the start. We then obtain

$$p_0\,\Psi_R(x) = \vec{\sigma}\cdot\vec{p}\,\Psi_R(x) \tag{3.9}$$
$$p_0\,\Psi_L(x) = -\vec{\sigma}\cdot\vec{p}\,\Psi_L(x)\,. \tag{3.10}$$

The subscripts here are used to emphasize that these 2-spinors *are* in fact helicity eigenstates. Now we arrive at the form of the equations we first derived for the linear Dirac equation in graphene where equations identical to (9) and (10) were obtained (if $p_z = 0$) for K_+ and K_- corners of the Brillouin zone respectively. Recalling the identification

$$\Psi_R = \Psi_+ = \begin{pmatrix} \psi_{A+} \\ \psi_{B+} \end{pmatrix} \tag{3.11}$$

and,

$$\Psi_L = \Psi_- = \begin{pmatrix} \psi_{B-} \\ \psi_{A-} \end{pmatrix}. \tag{3.12}$$

Now we find the plane wave solutions to be

$$p_0\begin{pmatrix} \psi_{A+} \\ \psi_{B+} \end{pmatrix} = \vec{\sigma}\cdot\vec{p}\begin{pmatrix} \psi_{A+} \\ \psi_{B+} \end{pmatrix}, \tag{3.13}$$
$$p_0\begin{pmatrix} \psi_{B-} \\ \psi_{A-} \end{pmatrix} = -\vec{\sigma}\cdot\vec{p}\begin{pmatrix} \psi_{B-} \\ \psi_{A-} \end{pmatrix}. \tag{3.14}$$

The solutions we seek are of the form (first for K_+ and positive energy)

$$\psi_{A+}(\vec{r}) = e^{i(\vec{p}\cdot\vec{r} - E\,t)}\tilde{\psi}_{A+} \tag{3.15}$$
$$\psi_{B+}(\vec{r}) = e^{i(\vec{p}\cdot\vec{r} - E\,t)}\tilde{\psi}_{B+}. \tag{3.16}$$

We thus obtain the result

$$E\tilde{\psi}_{A+} = p_x\tilde{\psi}_{B+} - ip_y\tilde{\psi}_{B+} \tag{3.17}$$
$$E\tilde{\psi}_{B+} = p_x\tilde{\psi}_{A+} + ip_y\tilde{\psi}_{A+}\,. \tag{3.18}$$

With $\tilde{\psi}_{A+} = 1$ we get

$$\tilde{\psi}_{B+} = \frac{E}{p_x - ip_y}\,, \tag{3.19}$$

similarly at the K_- point with $\tilde{\psi}_{B-} = 1$ we get

$$\tilde{\psi}_{A-} = \frac{-E}{p_x - ip_y}. \tag{3.20}$$

The positive-energy helicity eigenstates are

$$\Psi_1 = e^{i\,(\vec{p}\cdot\vec{r} - E\,t)}\begin{pmatrix} 1 \\ \frac{p_x + ip_y}{E} \\ 0 \\ 0 \end{pmatrix}\quad,\quad \Psi_2 = e^{i\,(\vec{p}\cdot\vec{r} - E\,t)}\begin{pmatrix} 0 \\ 0 \\ 1 \\ \frac{p_x + ip_y}{-E}\,, \end{pmatrix} \tag{3.21}$$

where Ψ_1 and Ψ_2 are the positive and negative helicity eigenstates respectively. In a similar way we find the negative energy helicity eigenstates to be

$$\Psi_3 = e^{i\,(\vec{p}\cdot\vec{r} + E\,t)}\begin{pmatrix} 1 \\ \frac{p_x + ip_y}{-E} \\ 0 \\ 0 \end{pmatrix}\quad,\quad \Psi_4 = e^{i\,(\vec{p}\cdot\vec{r} + E\,t)}\begin{pmatrix} 0 \\ 0 \\ 1 \\ \frac{p_x + ip_y}{E} \end{pmatrix}, \tag{3.22}$$

where Ψ_3 and Ψ_4 are positive and negative helicity states respectively. Let us interpret the components in terms of the relative A and B sublattice excitations. Looking at the components we see that the absolute value of the relative phase between adjacent

A and B sites is the same for positive and negative energies but the sign is opposite. This can be understood by thinking about the shape of the wavefunctions as we tune the lattice momentum away (increasing) from the corner of the Brillouin zone. In the state that was the conduction state (when k is slightly less than K_+) the relative phase between A and B sublattices continues to decrease (lowering its energy) while for the state that was the valence state the opposite is true. But looking at the components of Ψ_1 and Ψ_3 this is not what we see: the relative phase ϕ (comparing the components 1 and $(p_x + ip_y)/E$ we see that $\tan\phi = p_y/p_x$ for Ψ_1) becomes more negative for one state and more positive for the other but is always equal in magnitude. This is because ϕ measures the relative phase from the *perspective of the reset zero point of momentum*, ie. K-point, or equivalently relative phase between A and B sublattices.

In (21) and (22) we see the symmetry between the chiral 2-spinors that comprise the upper and lower parts of these solutions: in terms of the 2-spinors, exchanging K_+ and K_- points has the same effect as changing the sign of the energy. This is certainly familiar from Standard Model physics since a neutrino with positive helicity can be viewed as an anti-neutrino with negative helicity moving in the opposite direction. How do we interpret this in terms of excitations of the A and B sublattices? For a given k (K_+ or K_-) and ordering of phase (positive energy or negative energy), if we simply take K_+ to K_- then we will have the opposite ordering of phase (relative to the orientation of the new k value) and so to preserve the state we can simply then switch the ordering of phase by taking E to $-E$. Or simply that a quasi-particle with energy E propagating in the positive direction originates from the same branch of the spectrum as its antiparticle with energy $-E$ propagating in the opposite direction.

3.3.2 Lorentz Non-Covariance of the NLDE

Here we check the Lorentz transformation properties of the nonlinear term of the NLDE. The nonlinear terms in the NLDE are

$$\gamma^0 U \Psi^\dagger(r_\mu) \sum_{Q \in A_+, A_-, B_+, B_-} Q \Psi(r_\mu) Q. \tag{3.23}$$

In order to maintain Lorentz covariance any additional terms to the standard Dirac equation must form contractions in space-time indices in such a way as to result in Lorentz scalars; these are by definition the invariant objects under Lorentz transformations: any factors of gamma matrices must have their space-time indices contracted with other gamma matrices or with the space-time derivatives and any factors of Ψ must be contracted as $\bar{\Psi}\Psi$ where $\bar{\Psi} = \Psi^\dagger \gamma^0$. The bilinear terms in our equation are not independently, nor taken together, the contraction of two Lorentz 4-vectors. Let us develop this more thoroughly starting with the linear Dirac equation for a particle of mass m. Using the notation and approach taken in Bjorken and Drell we can show that under a Lorentz transformation the Dirac equation becomes

$$\left[i\hbar S(a) \gamma^\mu S^{-1}(a) a^\nu{}_\mu \frac{\partial}{\partial x^{\nu\prime}} - mc \right] \psi'(x') = 0\,. \tag{3.24}$$

We arrive at this expression by inserting the Lorentz transformed wavefunction,

$$\psi(x) = S^{-1}(a) \psi'(x')\,, \tag{3.25}$$

and the transformed partial derivatives where the $a^\nu{}_\mu$ are the Lorentz transformation matrices for coordinates and $S(a)$ are the transformation matrices acting on the components of the wavefunction induced by the $a^\nu{}_\mu$. Next we left multiplying by $S(a)$. The purpose behind this step is to keep the mass term in an explicitly invariant form since we know that the mass does not change under a Lorentz transformation. The prime on the coordinates indicates the Lorentz transformed coordinates but we must also allow for the mixing of the components of the wavefunction under a Lorentz transformation thus $\psi(x) \rightarrow \psi'(x')$. From this we see that in order for the Dirac equation to have the same form in the transformed frame it must be that

$$S(a)\gamma^{\mu}S^{-1}(a)a^{\nu}{}_{\mu} = \gamma^{\nu}\,. \tag{3.26}$$

Note that if we contract both sides using the Lorentz transformations we get

$$S(a)\gamma^{\mu}S^{-1}(a)a^{\nu}{}_{\mu}\,a_{\nu}{}^{\sigma} = \gamma^{\nu}a_{\nu}{}^{\sigma} \tag{3.27}$$

or,

$$S(a)\gamma^{\mu}S^{-1}(a)\delta_{\mu}{}^{\sigma} = \gamma^{\nu}a_{\nu}{}^{\sigma} \tag{3.28}$$

$$\Rightarrow \qquad S(a)\gamma^{\sigma}S^{-1}(a) = \gamma^{\nu}a_{\nu}{}^{\sigma}\,. \tag{3.29}$$

This expresses the property that a Lorentz transformation of the γ matrices from the point of view of the matrix indices (the left hand side) is equivalent to a Lorentz transformation on the space-time indices using the space-time matrices $a^{\nu}{}_{\mu}$: the γ's form a 4-vector with respect to their space-time indices.

Since the transformed γ matrices must still obey the same Clifford algebra (the same anti-commutation rules) it can be shown that they must be related to the untransformed γ's by a unitary transformation thus we leave the right hand side unprimed. By working from the infinitesimal proper Lorentz transformations we can get the form for finite transformations $S(a)$

$$\psi'(x') = S\psi(x) = \exp\left(-\frac{i}{4}\omega\sigma_{\mu\nu}I_{n}^{\mu\nu}\right)\psi(x)\,. \tag{3.30}$$

Here $I_{n}^{\mu\nu}$ is the 4x4 space-time matrix for a unit Lorentz rotation about the axis in the direction labeled n and the $\sigma_{\mu\nu}$ are given by $\sigma_{\mu\nu} = \frac{i}{2}\left[\gamma_{\mu},\gamma_{\nu}\right]$. Also, the Lorentz rotation angle or rapidity is defined in terms of the relative velocity by $\tanh(\omega) = v/c$.

Now let us see what happens when we return to our problem. In our NLDE we have no mass term but four nonlinear terms. Let us focus on one of the nonlinear

terms. By following the steps above we see that the first nonlinear term transforms like

$$\gamma^0\Psi^\dagger(x)A_+\Psi(x)A_+ \;\rightarrow\; S\gamma^0\Psi'^\dagger(x')(S^{-1})^\dagger A_+S^{-1}\Psi'(x')A_+S^{-1}\,. \tag{3.31}$$

These two expressions do not have the same form. The A_+ matrices in the untransformed term have the effect of picking out the first element of Ψ and leaving zeros for the other elements so that in the end there are no mixed products of components in any of the nonlinear terms. The transformed expression, on the other hand, is a complicated mixing of components of $\Psi'(x')$. In particular we see that since S^{-1} is itself a Lorentz transformation, the effect of multiplying $\Psi'(x')$ by A_+S^{-1} (in the full equation) is not to simply pick out the first element of $\Psi'(x')$ (as was the case for A_+ acting on Ψ), but here instead $A_+S^{-1}\Psi'(x')$ results in a column vector whose first element is a mixture of all the elements of $\Psi'(x')$ where the exact form of the mixed term is determined by the specific choice of Lorentz rotation angle in S^{-1}.

As an example let us see what happens when we apply a Lorentz boost in the positive x-direction. Then,

$$S^{-1}\Psi'(x') = \exp\left(\frac{i}{2}\omega\sigma_{01}\right)\Psi'(x')\,, \tag{3.32}$$

where we compute in the chiral representation

$$\begin{aligned}\sigma_{01} &= \frac{i}{2}\left[\gamma_0,\gamma_1\right] &(3.33)\\ &= -\frac{i}{2}\left[\gamma^0,\gamma^1\right] &(3.34)\\ &= -\begin{pmatrix}\sigma_x & 0\\ 0 & -\sigma_x\end{pmatrix}. &(3.35)\end{aligned}$$

Back substituting, expanding the exponential, separating and regrouping even and odd power terms we get

$$A_+ S^{-1}\Psi'(x') = A_+ \left\{ -\cos(\omega/2) \begin{pmatrix} 1 & 0 \\ 0 & 1 \end{pmatrix} - i\sin(\omega/2) \begin{pmatrix} \sigma_x & 0 \\ 0 & -\sigma_x \end{pmatrix} \right\} \Psi'(x'). \quad (3.36)$$

Expanding out the right hand side completely gives

$$\begin{aligned} A_+ S^{-1}\Psi'(x') &= (-1) \begin{pmatrix} 1 & 0 & 0 & 0 \\ 0 & 0 & 0 & 0 \\ 0 & 0 & 0 & 0 \\ 0 & 0 & 0 & 0 \end{pmatrix} \\ &\times \begin{pmatrix} \cos(\omega/2) & i\sin(\omega/2) & 0 & 0 \\ i\sin(\omega/2) & \cos(\omega/2) & 0 & 0 \\ 0 & 0 & \cos(\omega/2) & -i\sin(\omega/2) \\ 0 & 0 & -i\sin(\omega/2) & \cos(\omega/2) \end{pmatrix} \begin{pmatrix} \psi'_{A+} \\ \psi'_{B+} \\ \psi'_{B-} \\ \psi'_{A-} \end{pmatrix} \\ &= \begin{pmatrix} -\cos(\omega/2) & -i\sin(\omega/2) & 0 & 0 \\ 0 & 0 & 0 & 0 \\ 0 & 0 & 0 & 0 \\ 0 & 0 & 0 & 0 \end{pmatrix} \begin{pmatrix} \psi'_{A+} \\ \psi'_{B+} \\ \psi'_{B-} \\ \psi'_{A-} \end{pmatrix} \\ &= \begin{pmatrix} -\cos(\omega/2)\psi'_{A+} - i\sin(\omega/2)\psi'_{B+} \\ 0 \\ 0 \\ 0 \end{pmatrix}. \end{aligned} \quad (3.37)$$

As we expect, a Lorentz boost in the chiral representation does not mix chiral states. Only components within each chiral 2-spinor get mixed. The point in all this is that in one frame, the unprimed frame here, it is possible to define sublatice wavefunctions which remain well defined but in the primed frame if we try to define sublattice wavefunctions, they will mix in time due to the nonlinear terms: the NLDE is not Lorentz invariant.

3.4 Lagrangian and Energy Functional of the Nonlinear Dirac Equation

In this section, we obtain insights into the nonlinear solutions by casting the NLDE into a Lagrangian form. We follow this by analyzing the corresponding energy functional theory.

3.4.1 Lagrangian Analysis

Before we obtain exact vortex solutions to the nonlinear Dirac equation it is helpful to study the theory at the Lagrangian level in order to gain insight into the underlying principles as well as acquire a qualitative sense of the kinds of solutions to expect. The nonlinear Dirac equation for the components of a two-spinor is

$$i\,\psi_{A,t} + i\hbar c_l(\partial_x - i\partial_y)\psi_B - U\,|\psi_A|^2\,\psi_A = 0 \tag{3.38}$$
$$i\,\psi_{B,t} + i\hbar c_l(\partial_x + i\partial_y)\psi_A - U\,|\psi_B|^2\,\psi_B = 0\,. \tag{3.39}$$

These are the Euler-Lagrange equations to the Lagrangian density

$$\mathcal{L} = \tag{3.40}$$
$$i\,(\psi_A^*\psi_A + \psi_B^*\psi_B)_t + i\hbar c_l\,[\psi_A^*(\partial_x - i\partial_y)\psi_B + \psi_B^*(\partial_x + i\partial_y)\psi_A] - \frac{U}{2}(|\psi_A|^4 + |\psi_B|^4)\,,$$

where Eqs. (3.38)-(3.39) are obtained through the prescription

$$\partial_\mu\left(\frac{\delta\mathcal{L}}{\delta\psi^*_{A,\mu}}\right) + \frac{\delta\mathcal{L}}{\delta\psi^*_A} = 0\,. \tag{3.41}$$

The positive sign on the second term is correct, since we are taking functional derivatives with respect to the conjugate of the field and it's derivatives. The more common approach is to differentiate the Lagrange density with respect to the field and it's derivatives and take the conjugate of the resulting equations afterwards. This leads to the same result. Eq.(3.40) describes the dynamics of two self-interacting, scalar, bosonic fields coupled through the spatial derivative terms with interaction strength strength U and c_l is the characteristic speed. The Hamiltonian density can be derived using the formula

$$\mathcal{H} = \pi_A\psi_{A,t} + \pi_B\psi_{B,t} - \mathcal{L}\,, \tag{3.42}$$

where π_A and π_B are the canonical momenta associated with ψ_A and ψ_B respectively. These are defined in the usual way:

$$\pi_j = \frac{\delta \mathcal{L}}{\delta \psi_{j,t}}, \tag{3.43}$$

where j labels the field, A or B sublattice in our theory. We get,

$$\mathcal{H} = -i\hbar c_l \psi_A^*(\partial_x - i\partial_y)\psi_B - i\hbar c_l \psi_B^*(\partial_x + i\partial_y)\psi_A + \frac{U}{2}(|\psi_A|^4 + |\psi_B|^4). \tag{3.44}$$

Returning to the Lagrangian, in plane polar coordinates it is

$$\mathcal{L} = i\left(\psi_A^*\psi_A + \psi_B^*\psi_B\right)_t + i\hbar c_l \left[\psi_A^* e^{i\theta}(\partial_r - i\frac{1}{r}\,\partial_\theta)\psi_B + \psi_B^* e^{-i\theta}(\partial_r + i\frac{1}{r}\,\partial_\theta)\psi_A\right]$$
$$-\frac{U}{2}(|\psi_A|^4 + |\psi_B|^4). \tag{3.45}$$

For static (time-independent) classical solutions, and for strong interactions, we may write

$$\mathcal{L} = \tag{3.46}$$
$$U\left[i\frac{\hbar c_l}{U}\psi_A^* e^{i\theta}(\partial_r - i\,\frac{1}{r}\,\partial_\theta)\psi_B + i\frac{\hbar c_l}{U}\psi_B^* e^{-i\theta}(\partial_r + i\,\frac{1}{r}\,\partial_\theta)\psi_A - \frac{1}{2}(|\psi_A|^4 - |\psi_B|^4)\right].$$

A qualitative analysis of this expression tells us that for U large and attractive ($|U| \gg \hbar c_l, U < 0$), the quartic interactions dominate and the fields minimize their energy by forming regions of high density. For a normalized field, this is best done by forming single solitons. In a dynamic sense, the kinetic terms become costly as the forming soliton becomes more condensed and the field gradient increases sharply. The minimal solution may find a stable point in field space by staggering one field with the gradient of the other $\psi_A > 0$, $\psi_{B,x} < 0$ so that the the kinetic terms help to further lower the energy. This describes a bright vortex/soliton pair configuration for the two spinor components. We must be careful though in our claim that $|U| \gg \hbar c_l$, since c_l contains the lattice spacing a, we must impose a more stringent restriction: specifically that

$|U| \gg t_h$. The reason for this is that the mean field equations that we want to solve are only valid so long as we are in the quasi-particle domain, i.e., wavelengths that are large compared to the lattice spacing.

For the case where U is large and repulsive and assuming a finite two-dimensional box with the usual normalization conditions, the contact interaction is always positive where the field strength is non-vanishing and the tendency is for the condensate to lower it's energy by finding the most favorable combination of fields and gradients that forces the kinetic terms to be negative. The formation of a local region with large spatial variation in the fields on an otherwise uniform positive energy background describes a dark vortex/soliton pair. It may also be energetically favorable for the condensate to develop a multitude of such configurations, close enough spatially, so that the moduli of the fields oscillate in some spin texture pattern. This type of arrangement describes a skyrmion texture.

More generally, we may seek stationary solutions with characteristic energy $\hbar\omega$. These are not necessarily ground states of the theory. Time derivatives in the Lagrangian in Eq. (3.45) get replaced by multiplication by $-i\omega$ so that we have

$$\mathcal{L} = \omega\left(|\psi_A|^2 + |\psi_B|^2\right) - \tag{3.47}$$
$$i\hbar c_l\left[\psi_A^* e^{i\theta}(\partial_r - i\frac{1}{r}\partial_\theta)\psi_B - \psi_B^* e^{-i\theta}(\partial_r + i\frac{1}{r}\partial_\theta)\psi_A\right] - \frac{U}{2}(|\psi_A|^4 + |\psi_B|^4)\,.$$

Uniform solutions are possible and obtained by setting the derivatives terms to zero. The Hamiltonian density for these states is

$$\mathcal{H} = \frac{U}{2}(|\psi_A|^4 + |\psi_B|^4). \tag{3.48}$$

This is just the field theory representation for uniform density, single particle states with energy

$$E_A = \omega = \frac{U}{2}|\psi_A|^4\,, \tag{3.49}$$

$$E_B = \omega = \frac{U}{2}|\psi_B|^4 \tag{3.50}$$

$$\Rightarrow \quad |\psi_A|^2 = |\psi_B|^2 = \sqrt{\frac{2\,\omega}{U}}\,. \tag{3.51}$$

Let us look at small fluctuations of these spatially uniform stationary states. To do this, we can substitute the ansatz $\psi_A = e^{-i\omega t}v_A(r,t)$ and $\psi_B = e^{-i\omega t}v_B(r,t)$ in Eq. (3.45), where $\hbar\omega$ is the energy of the uniform background field density, and,

$$\begin{aligned}\mathcal{L} &= \omega|v_A|^2 + iv_A^*v_{A,t} + \omega|v_B|^2 + iv_B^*v_{B,t} \\ &+ i\hbar c_l v_A^* e^{i\theta}(\partial_r - i\,\frac{1}{r}\,\partial_\theta)v_B + i\hbar c_l v_B^* e^{-i\theta}(\partial_r + i\,\frac{1}{r}\,\partial_\theta)v_A - \frac{U}{2}(|v_A|^4 + |v_B|^4)\,.\end{aligned} \tag{3.52}$$

The Hamiltonian density for the fields v_A and v_B is given by

$$\begin{aligned}\mathcal{H} &= -i\,\hbar\,c_l v_A^* e^{i\theta}(\partial_r - i\,\frac{1}{r}\,\partial_\theta)v_B - i\hbar c_l v_B^* e^{-i\theta}(\partial_r + i\,\frac{1}{r}\,\partial_\theta)v_A \\ &- \omega\,(|v_A|^2 + |v_B|^2) + \frac{U}{2}\,(|v_A|^4 + |v_B|^4)\,.\end{aligned} \tag{3.53}$$

The potential energy density for v_A is

$$\mathcal{PE}_A = -\omega\,|v_A|^2 + \frac{U}{2}\,|v_A|^4\,. \tag{3.54}$$

Decomposing v_A in terms of it's amplitude and phase, $v_A = \sqrt{\rho_A}\,e^{i\phi_A}$, as expected, we see that the ground states lie at the minima of (3.54)

$$v_{A,0} = \sqrt{\frac{\omega}{U}}\,e^{i\phi_A}\,. \tag{3.55}$$

The ground state is infinitely degenerate parametrized by the phase ϕ_A. An identical result occurs for the other spinor component v_B.

As with the simplest model of a field theory with broken symmetry, ϕ^4 theory in two spatial dimensions, our theory admits solutions with topologically nontrivial structures whose phase winds around the boundary at spatial infinity. Stable states are then characterized by an integer winding number. We should note that these two-dimensional vortices do not have finite energy as we shall soon show, and that the total energy diverges logarithmically consistent with Derrick's theorem. Luckily this problem can be handled by introducing an outside gauge potential that couples to the vortex and conveniently cancels the infinite part of the vortex energy. Thus a divergent global vortex in $(2+1)$-dimensions is rendered finite when promoted to a gauged vortex theory.

Physically, the result that we have found here is easy to understand. We could think of starting with a spatially uniform stationary state with total energy ω, and adding a small local perturbation to it. The perturbation does not run away because of the repulsive self-interaction (the outside slope of the Lagrangian potential term), nor does it collapse due to the local support of the ambient non-zero background (the inside slope of the potential). Another more interesting scenario is when the correction to the uniform field cannot be accessed by perturbations but is itself a topologically stable excited state whose phase wraps around the circle at infinity so that a zero point of the nonuniform part of the field must exist where the unwrapping of the phase occurs. These are the vortex solutions that we have already discussed.

3.4.2 Energy Functional Analysis for Relativistic Vortices

We can obtain map of the energy landscape for a vortex configuration by eliminating the angular dependence in the energy functional that gives the NLDE as a variational extremum and then identifying the effective potential energy. If we assume the vortex/soliton form $\psi_A = i\, e^{-i\theta} F(r)$, $\psi_B = G(r)$, then the total energy is given by

$$E \;=\; \int_0^R dr\,[-\hbar c_l\, FG' + \hbar c_l\, GF' + V_{\text{eff}}(F,G)]\;, \tag{3.56}$$

where,

$$V_{\text{eff}} \;\equiv\; \frac{\mu^2}{2U}\left(\frac{U}{\mu}F^2 - 1\right)^2 + \frac{\mu^2}{2U}\left(\frac{U}{\mu}G^2 - 1\right)^2 + \hbar c_l \frac{G\,F}{r} - \frac{\mu^2}{U} + \mu N\,. \tag{3.57}$$

We regulate the energy by introducing an upper cutoff R. Evidently the FG' and GF' terms indicate an attractive force for configurations where $\text{sgn}(FG') > 0$ and $\text{sgn}(\text{F'G}) < 0$ respectively. In the F, G-plane the centripetal term in V_{eff} dominates for small r and forms a saddle point at the origin (of the F, G-plane) becoming singular when $r = 0$. Because of the saddle-point, points on the F and G axes have zero potential energy but are unstable. If we want to study solutions that begin at the saddle-point, i.e., $F(0) = G(0) = 0$, or on the G-axis, say, near the saddle-point, we must include the full contribution from the kinetic terms. In fact, we see that a path in the G-axis defined by $p(t) :\, = t\,\hat{e}_G$, $0 < t < t_f$, will change the total energy by $\Delta E = c_l t_f\, F'(0)$. This can be made arbitrarily large and negative by adjusting the value of F' at $r = 0$. The V-landscape flattens rapidly as r increases from zero so that it may be possible to attempt a solution for which $F(0) = 0, F'(0) < 0$, and $G(0) > 0$. For large r, F' and G' must go to zero and the centripetal term becomes negligible so that V_{eff} has nine extrema, two of which are absolute minima for the total energy E. The absolute minima occur at the points P and P' given by $P(G, F) = (-q, q)$ and $P'(G, F) = (q, -q)$ where we define $q > 0$. To determine the value of q, we can differentiate Eq.(3.57) and solve for minima in the usual manner. We then expect one of the stable solutions to start at $F(0) = 0\,,\, G(0) > 0$ and approach $F(\infty) = -\,q\,,\, G(\infty) = q$ and the other so start at $F(0) = 0$, $G(0) < 0$ and approach $F(\infty) = q$, $G(\infty) = -\,q$. These describe a bright soliton at the core of a vortex where the soliton approaches a non-zero value for large r. We obtain the

following asymptotic (large r) critical points for V_{eff} in the F, G-plane:

- $(\sqrt{\mu/U},\ \sqrt{\mu/U})$ - local minimum
- $(\sqrt{\mu/U}, 0)$ - saddle point
- $(\sqrt{\mu/U}, -\sqrt{\mu/U})$ - local minimum
- $(-\sqrt{\mu/U},\ \sqrt{\mu/U})$ - local minimum
- $(-\sqrt{\mu/U},\ 0)$ - saddle point
- $(-\sqrt{\mu/U},\ -\sqrt{\mu/U})$ - local minimum
- $(0,\ \sqrt{\mu/U})$ - saddle point
- $(0,\ -\sqrt{\mu/U})$ - saddle point
- $(0,\ 0)$ - local maximum

The two stable solutions begin at $(0, \pm G)$, where $G > 0$, and flow asymptotically $(r,\ 0 \to \infty)$ towards the stable fixed points $(\mp\sqrt{\mu/U},\ \pm\sqrt{\mu/U})$, respectively, for which the determinant of the Hessian of V_{eff} is positive.

3.5 Reduction of the Time-Dependent NLDE to the Time-Dependent NLSE with Correction Terms

In certain limits it is possible to reduce the NLDE to a NLSE which differs from the usual version by some additional correction terms. To reduce the massless nonlinear Dirac equation to the usual nonlinear Schrödinger equation with a small additional correction term, we consider an ansatz for classical low-energy fluctuations near a stable stationary state solution of the massless nonlinear Dirac equation and show that these fluctuations reduce to a nonlinear Schrödinger equation.

3.5.1 One-Dimensional Case

Working in one spatial dimension, solutions of the NLDE can be chosen as such that

$$\psi(x,t) = e^{-i\omega_0 t}\begin{pmatrix}\psi_A(x,t)\\ \psi_B(x,t)\end{pmatrix}. \tag{3.58}$$

Here we have factored out the common frequency component. The equations of motion become

$$\begin{aligned}\omega_0\psi_A + i\psi_{A,t} &= -i\psi_{B,x} + U|\psi_A|^2\psi_A &(3.59)\\ \omega_0\psi_B + i\psi_{B,t} &= -i\psi_{A,x} + U|\psi_B|^2\psi_B\,, &(3.60)\end{aligned}$$

where the component fields are understood to be functions of x and t and spatial and time derivatives are indicated by the appropriate subscripts on the fields. Equation (9.5) can be written as

$$\psi_B = -i\frac{(\psi_{B,t} + \psi_{A,x})}{(\omega_0 - U|\psi_B|^2)}\,. \tag{3.61}$$

We then assume the following approximations

$$\begin{aligned}&1. \quad |\psi_B|^2 \simeq |\psi_A|^2 &(3.62)\\ &2. \quad |\psi_{B,t}| \ll |\psi_{A,x}| &(3.63)\\ &3. \quad |U| \ll \omega_0\,. &(3.64)\end{aligned}$$

Equation (3.61) reduces to

$$\begin{aligned}\psi_B &\simeq -i\psi_{A,x}\left(\omega_0 - U|\psi_A|^2\right)^{-1}. &(3.65)\\ \psi_B &\simeq -\frac{i}{\omega_0}\psi_{A,x}\left(1 + \frac{U}{\omega_0}|\psi_A|^2 + h.c.\right). &(3.66)\end{aligned}$$

Substituting this back into Eq. (9.4) gives us

$$
\begin{aligned}
i\psi_{A,t} \simeq & -\frac{1}{\omega_0}\psi_{A,xx}\left(1+\frac{U}{\omega_0}|\psi_A|^2\right)-\frac{1}{\omega_0}\left(1+\frac{U}{\omega_0}|\psi_A|^2\right)'\psi_{A,x} \\
& -\omega_0\left(1-\frac{U}{\omega_0}|\psi_A|^2\right)\psi_A\,,
\end{aligned}
\tag{3.67}
$$

which reduces to

$$
\begin{aligned}
& i\psi_{A,t} \simeq \\
& -\frac{1}{\omega_0}\psi_{A,xx}+U|\psi_A|^2\psi_A-\frac{U}{\omega_0^2}\left(|\psi_A|^2\psi_{A,xx}+|\psi_{A,x}|^2\psi_A+\psi_A^*\psi_{A,x}^2\right)-\omega_0\psi_A.
\end{aligned}
\tag{3.68}
$$

This is the nonlinear Schrödinger modified by the addition of two extra terms: one proportional to the interaction constant U; the other proportional to the frequency common to both spinor components. We can recombine some of the terms to get

$$
\begin{aligned}
& i\psi_{A,t} \simeq \\
& -\frac{1}{\omega_0}\psi_{A,xx}+\left(U|\psi_A|^2-\omega_0\right)\psi_A-\frac{U}{\omega_0^2}\left(|\psi_A|^2\psi_{A,xx}+|\psi_{A,x}|^2\psi_A+\psi_A^*\psi_{A,x}^2\right).
\end{aligned}
\tag{3.69}
$$

The reduction of the NLDE to the NLSE relies on our initial ansatz where we have factored out the time dependence common to both component fields. The physical significance of this step is that we are starting from a massless nonlinear Dirac equation so, in a sense, we are extracting a portion of the total energy to act as the particle mass in the reduced equation.

3.5.2 Topological Solitons

We may seek stationary solutions to Eq. (3.70)

$$
\psi_A(x,t)=e^{i\omega' t}v(x)\,,
\tag{3.70}
$$

which, upon substitution into Eq. (3.70), gives us the time independent NLSE

$$
-\omega' v=-\frac{1}{\omega_0}v_{xx}+\left(U|v|^2-\omega_0\right)v-\frac{U}{\omega_0^2}\left(|v|^2v_{xx}+|v_x|^2v+v^*v_x^2\right),
\tag{3.71}
$$

or,

$$\frac{1}{\omega_0}v_{xx} + \left(\omega_0 - \omega' - U|v|^2\right)v + \frac{U}{\omega_0^2}\left(|v|^2 v_{xx} + |v_x|^2 v + v^* v_x^2\right) = 0\,. \tag{3.72}$$

We may construct the Lagrangian that approximately describes Eq. (3.69) and obtain

$$\mathcal{L} = i\psi_A^*\psi_{A,t} - \frac{1}{\omega_0}|\psi_{A,x}|^2 - U|\psi_A|^4 + \omega_0|\psi_A|^2 - \frac{U}{\omega_0^2}|\psi_A\psi_{A,x}|^2. \tag{3.73}$$

This is the usual Lagrangian density for the NLSE but with the last two terms on the right hand side added as corrections. If we compute the corresponding Euler-Lagrange equations, we find that we are missing the second term of the correction in Eq. (3.69). Nevertheless, we proceed along this path since the omitted term is small. The appearance of the positive "mass" term (fourth term on the r.h.s) indicates the possibility for interesting dynamics analogous to the phenomenon of spontaneous symmetry breaking in ϕ^4 field theory. We can cast the Lagrangian density into a form that is standard in quantum field theory

$$\begin{aligned}
\mathcal{L} &= i\psi_A^*\psi_{A,t} + \frac{1}{m^2}|\psi_{A,x}|^2 - m^2|\psi_A|^2 - U|\psi_A|^4 - \frac{U}{m^4}|\psi_A\psi_{A,x}|^2 && (3.74)\\
&= i\psi_A^*\psi_{A,t} + \frac{1}{m^2}|\psi_{A,x}|^2 - m^2|\psi_A|^2 - V(\psi_A, \psi_{A,x})\,, && (3.75)
\end{aligned}$$

where we have defined the potential

$$V(\psi_A, \psi_{A,x}) = \lambda_1|\psi_A|^4 + \lambda_2|\psi_A\psi_{A,x}|^2, \tag{3.76}$$

and the mass and couplings are given by

$$\begin{aligned}
m^2 &= -\omega_0\,, && (3.77)\\
\lambda_1 &= U\,, && (3.78)\\
\lambda_2 &= U/m^4. && (3.79)
\end{aligned}$$

At low energies the dominant terms are the mass term and potential terms. Since $\lambda_2 \ll \lambda_1$ the potential V is almost independent of $\psi_{A,x}$ and we expect that good approximations to the ground states can be found by minimizing the quantity

$$\begin{aligned} P(\psi_A, \psi_{A,x}) &= m^2|\psi_A|^2 + U|\psi_A|^4 + \frac{U}{m^4}|\psi_A\psi_{A,x}|^2 && (3.80)\\ &\simeq m^2|\psi_A|^2 + U\,|\psi_A|^4 && (3.81)\\ &= -\omega_0\,|\psi_A|^2 + U|\psi_A|^4. && (3.82) \end{aligned}$$

Now we express ψ_A in terms of density and phase fields $\psi_A = \psi e^{i\phi}$, where ψ and ϕ are functions of x and t, then we have

$$P = -\omega_0\psi^2 + U\psi^4\,, \tag{3.83}$$

where minimizing for positive values of U gives

$$\begin{aligned} P' &= -2\omega_0\psi_0 + 4U\psi_0^3 = 0\,, && (3.84)\\ \Rightarrow\ \psi_0 &= \pm\sqrt{\frac{\omega_0}{2U}}\,. && (3.85) \end{aligned}$$

The $U(1)$ symmetry is broken and we interpret the ground state in terms of a massive mode: $\tilde{\psi} = \psi - \psi_0$; and a massless mode: $\tilde{\phi} = \phi - \phi_0$, where ϕ_0 is an arbitrary fixed phase. To see this we simply make the substitution

$$\begin{aligned} \psi &= \psi_0 + \tilde{\psi} \equiv a + \tilde{\psi} && (3.86)\\ \phi &= \phi_0 + \tilde{\phi} \equiv b + \tilde{\phi} && (3.87) \end{aligned}$$

into Eq. (3.74). In one spatial dimension we cannot construct topologically nontrivial solutions (static, nonzero energy solutions). This is because if we choose different constant moduli for $x \sim -\infty$ and $x \sim +\infty$, the form of the solution for finite x is not forced to have any spatial variation (thus additional energy from the kinetic term) since it costs nothing to unwind such a state by simply rotating the phase. In contrast, for illustration, if we take ψ to be real we remove one field dimension so that

the spatial and field space have dimension-one and ψ can be nontrivially "wrapped" around x. For the moment we neglect the correction term proportional to U/m^4 and the minima of the potential are at the constants found in Eq. (3.85). Continuing with the case of a real field, the energy functional can be constructed by examining the Lagrange density. We find

$$E = \int dx \left[\frac{1}{2}\frac{\partial}{\partial t}\left(\psi_A^2\right) - \frac{1}{m^2}\left(\frac{\partial \psi_A}{\partial x}\right)^2 + m^2\psi_A^2 + U\psi_A^4 + \frac{U}{m^4}\psi_A^2\left(\frac{\partial \psi_A}{\partial x}\right)^2 \right]. \quad (3.88)$$

Classical solutions are ones which minimize the total energy so we are free to add a constant to Eq. (3.90); this will make the solutions more transparent. In addition, we seek static solutions so we can assume the field to have only spatial dependence

$$E = \int dx \left[-\frac{1}{m^2}\left(\frac{d\psi_A}{dx}\right)^2 + m^2\psi_A^2 + U\psi_A^4 + \frac{m^4}{4U} + \frac{U}{m^4}\psi_A^2\left(\frac{d\psi_A}{dx}\right)^2 \right], \quad (3.89)$$

$$E = \int dx \left[-\frac{1}{m^2}\left(\frac{d\psi_A}{dx}\right)^2 + U\left(\psi_A^2 + \frac{m^2}{2U}\right)^2 + \frac{U}{m^4}\psi_A^2\left(\frac{d\psi_A}{dx}\right)^2 \right]. \quad (3.90)$$

For weak interactions, the term proportional to U/m^4 is small so one approach is to neglect this term and find an exact solution to the resulting static field equation. An appropriately parameterized form of this exact solution may then be substituted back into Eq. (3.90), where the minimized total energy yields the minimal values of the parameters. The static field equation is

$$\frac{1}{2m^2}\frac{d^2\psi_A}{dx^2} + U\left(\psi_A^2 + \frac{m^2}{2U}\right)\psi_A = 0. \quad (3.91)$$

Multiplying both sides by the derivative of ψ_A gives

$$\frac{1}{2m^2}\frac{d^2\psi_A}{dx^2}\frac{d\psi_A}{dx} + U\left(\psi_A^2 + \frac{m^2}{2U}\right)\psi_A\frac{d\psi_A}{dx} = 0\,, \quad (3.92)$$

or, more compactly stated,

$$\frac{d}{dx}\left[\frac{1}{4m^2}\left(\frac{d\psi_A}{dx}\right)^2+\frac{U}{4}\left(\psi_A^2+\frac{m^2}{2U}\right)^2\right]=0\,. \tag{3.93}$$

This can be integrated to give (setting the integration constant to zero)

$$\frac{1}{m^2}\left(\frac{d\psi_A}{dx}\right)^2+U\left(\psi_A^2+\frac{m^2}{2U}\right)^2=0\,. \tag{3.94}$$

Then we have

$$\frac{d\psi_A}{dx} = \pm\sqrt{\omega_0 U}\left(\psi_A^2-\frac{\omega_0}{2U}\right), \tag{3.95}$$

$$\frac{d\psi_A}{\left(\psi_A^2-\frac{\omega_0}{2U}\right)} = \pm\sqrt{\omega_0 U}dx\,, \tag{3.96}$$

$$\frac{d\left(\sqrt{\frac{2U}{\omega_0}}\psi_A\right)}{\left[1-\left(\sqrt{\frac{2U}{\omega_0}}\psi_A\right)^2\right]} = \pm\frac{\omega_0}{\sqrt{2}}dx\,, \tag{3.97}$$

$$\Rightarrow\ \tanh^{-1}\left(\sqrt{\frac{2U}{\omega_0}}\psi_A\right) = \pm\frac{\omega_0}{\sqrt{2}}x\,. \tag{3.98}$$

Finally, we get

$$\psi_A(x)=\sqrt{\frac{\omega_0}{2U}}\tanh\left(\pm\frac{\omega_0}{\sqrt{2}}x\right). \tag{3.99}$$

We may write this in terms of the constant value of the field at infinity, Eq. (3.85),

$$\psi_A(x)=\psi_0\tanh\left(\pm\sqrt{2}U\psi_0^2 x\right). \tag{3.100}$$

The positive and negative signs in Eq. (3.107) refer to kink and anti-kink solutions that interpolate between the two inequivalent ground states, for $x\to\pm\infty$, in Eq. (3.85).

3.5.3 Soliton Energy

The energy density for this solution can be calculated by substituting Eq. (3.107) into Eq. (3.90) while neglecting the term proportional to U/m^6. We obtain

$$\mathcal{E} = \frac{\omega_0^2}{2U} \operatorname{sech}^4 \left(\frac{\omega_0}{\sqrt{2}} x \right). \tag{3.101}$$

Integrating to get the total energy,

$$\begin{aligned} E &= \frac{\omega_0^2}{2U} \int_{-\infty}^{+\infty} dx \operatorname{sech}^4 \left(\frac{\omega_0}{\sqrt{2}} x \right) && (3.102) \\ &= \frac{\sqrt{2}\omega_0}{2U} \int_{-\infty}^{+\infty} dx \operatorname{sech}^4 (x) && (3.103) \\ &= \frac{\sqrt{2}\omega_0}{2U} \int_{-\infty}^{+\infty} dx \left[\operatorname{sech}^2 (x) - \operatorname{sech}^2 (x) \tanh^2(x) \right] && (3.104) \\ &= \frac{2\sqrt{2}\omega_0}{3U}. && (3.105) \end{aligned}$$

We can see the effect of the neglected term in Eq. (3.90) by noticing that it can be regarded as a nonlinear rescaling of the mass in the quadtratic term of the potential (nonlinear in that the scaling factor involves the mass itself). The energy functional can be written

$$E = \int dx \left\{ -\frac{1}{m^2} \left(\frac{d\psi_A}{dx} \right)^2 + \left[1 + \frac{U}{m^6} \left(\frac{d\psi_A}{dx} \right)^2 \right] m^2 \psi_A^2 + U \psi_A^4 \right\}. \tag{3.106}$$

The factor U/m^6 is negative and, assuming $|U/m^6| \ll 1$, has the effect of reducing the strength of the negative mass term, effectively lowering the central peak of the so called "mexican hat" potential. The important fact of the presence of the square of the derivative in this same term means that this modification only takes place in the region where the solution is making the transition from one ground state to the other but does note affect the asymptotic form of the solution. The net effect is that it is less costly for the solution to interpolate more slowly between the different ground states, extending through the central bump of the potential over a greater spatial distance.

A variational approach can be used to get an approximate solution when including the extra term in the potential. We try the simplest ansatz by rescaling the argument of the solution Eq. (3.107)

$$\psi_A(x) = \sqrt{\frac{\omega_0}{2U}}\tanh\left(a\frac{\omega_0}{\sqrt{2}}x\right). \tag{3.107}$$

If we substitute this into Eq. (3.90) and using $m^2 = -\omega_0$, we can expect the integral to converge since the constant $m^4/4U$ has been added to the energy density. When integrated, this term renders the total energy finite. We obtain

$$\begin{aligned}
E(a) &= \int dx \left\{ \frac{a^2\omega_0^2}{4U}\mathrm{sech}^4\left(\frac{a\omega_0 x}{\sqrt{2}}\right) + U\left[\frac{\omega_0}{2U}\tanh^2\left(\frac{a\omega_0 x}{\sqrt{2}}\right) - \frac{\omega_0}{2U}\right]^2 \right. \\
&+ \left. \frac{a^2\omega_0^2}{8U}\mathrm{sech}^4\left(\frac{a\omega_0\, x}{\sqrt{2}}\right)\tanh^2\left(\frac{a\omega_0 x}{\sqrt{2}}\right)\right\} \\
&= \int dx \left\{ \frac{a^2\omega_0^2}{4U}\mathrm{sech}^4\left(\frac{a\omega_0\, x}{\sqrt{2}}\right) + \frac{\omega_0^2}{4U}\mathrm{sech}^4\left(\frac{a\omega_0 x}{\sqrt{2}}\right) \right. \\
&+ \left. \frac{a^2\omega_0^2}{8U}\mathrm{sech}^4\left(\frac{a\omega_0 x}{\sqrt{2}}\right)\tanh^2\left(\frac{a\omega_0\, x}{\sqrt{2}}\right)\right\} \\
&= \frac{\sqrt{2}(a^2+1)\omega_0}{4aU}\int_{-\infty}^{+\infty} dx\,\mathrm{sech}^4(x) + \frac{\sqrt{2}a\omega_0}{8U}\int_{-\infty}^{+\infty} dx\,\mathrm{sech}^4(x)\tanh^2(x) \qquad (3.108) \\
E(a) &= \frac{\sqrt{2}(a^2+1)\omega_0}{3aU} \\
&+ \frac{\sqrt{2}a\omega_0}{8U}\int_{-\infty}^{+\infty} dx\,\left[\mathrm{sech}^2(x)\tanh^2(x) - \mathrm{sech}^2(x)\tanh^4(x)\right]dx\,, \qquad (3.109) \\
E(a) &= \frac{\sqrt{2}(a^2+1)\omega_0}{3aU} + \frac{\sqrt{2}a\omega_0}{30U} = \frac{11\sqrt{2}a\omega_0}{30U} + \frac{\sqrt{2}\omega_0}{3aU}. \qquad (3.110)
\end{aligned}$$

Minimizing Eq. (3.110), we get

$$\begin{aligned}
\frac{dE}{da} &= \frac{11\sqrt{2}\,\omega_0}{30U} - \frac{\sqrt{2}\omega_0}{3a^2U} = 0 \qquad (3.111) \\
\Rightarrow \quad a &= \sqrt{10/11} \approx 0.953\,. \qquad (3.112)
\end{aligned}$$

3.5.4 Nonlinear Sigma Model

It is interesting to see that the Lagrangian density we found in Eq. (3.74) can be generalized to include identical kinetic and potential terms for ψ_B; the other component of the spinor identified with the K_+ corner of the brillouin zone; as well as terms for both fields belonging to the opposite (K_-) corner of the Brillouin zone. The reason for this is that the constraints/approximations used to derive Eq. (3.74) are symmetric in ψ_A and ψ_B: there is no contradiction if the same set of approximations of Eqs. (3.62)-(3.64) are used by interchanging ψ_A and ψ_B. The Lagrangian density that describes such a theory of four complex scalar fields is

$$\mathcal{L} = \sum_{j=1}^{4} \left(i\psi_j^* \frac{\partial \psi_j}{\partial t} + \frac{1}{m^2} \left| \frac{\partial \psi_j}{\partial x} \right|^2 - m^2 \left| \psi_j \right|^2 - U \left| \psi_j \right|^4 - \frac{U}{m^4} \left| \psi_j \frac{\partial \psi_j}{\partial x} \right|^2 \right) . \qquad (3.113)$$

For the case of real scaler fields the Lagrangian has a $O(4)$ symmetry but for complex fields the symmetry is enlarged to $SU(4)$. The $O(4)$ subgroup of $SU(4)$ describes rotations between the moduli of the four complex fields while leaving their individual phases unchanged. The remaining subgroups of $SU(4)$ act on the individual phases of the fields as $U(1)_j$ transformations where the index here refers to the jth field. Equation (3.113) is a form of the well studied nonlinear sigma model (NLSM). As in the case of ordinary ϕ^4 theory, the nonlinear terms in the NLSM do not break the overall symmetry, in this case $SU(4)$, but a non-zero vacuum expectation of any of the fields causes an apparent breaking of $SU(4)$ at the level of the field equations. The NLSM differs from ordinary ϕ^4 theory in that the breaking of the larger symmetry group of the former, gives rise to a greater number of massless Goldstone modes than in the latter theory.

3.5.5 Two-Dimensional Case

Previously we saw that in two dimensions the equations of motion contained a factor of $e^{i\theta}$ for the the polar angle dependence so that solutions that are localized

in both spatial dimensions must appear as soliton-vortex pairs. We see now that a reduction process similar to that presented in the last section removes the explicit angular dependence. The equations of motion may be written compactly as

$$\begin{aligned} i\psi_{A,t} &= -i\mathcal{D}^*\psi_B + U|\psi_A|^2\psi_A & (3.114)\\ i\psi_{B,t} &= -i\mathcal{D}\,\psi_A + U|\psi_B|^2\psi_B\,, & (3.115) \end{aligned}$$

where we have simply abbreviated the differential operators by using $\mathcal{D} = \partial_x + i\partial_y$. We work again with the ansatz

$$\psi(\vec{r},t) = e^{-i\omega_0 t}\begin{pmatrix} \psi_A(\vec{r},t) \\ \psi_B(\vec{r},t) \end{pmatrix}. \tag{3.116}$$

Substituting into Eqs.(3.114) and (3.114) gives

$$\begin{aligned} \omega_0\psi_A + i\psi_{A,t} &= -i\mathcal{D}^*\psi_B + U|\psi_A|^2\psi_A & (3.117)\\ \omega_0\psi_B + i\psi_{B,t} &= -i\mathcal{D}\psi_A + U|\psi_B|^2\psi_B\,. & (3.118) \end{aligned}$$

Following the same steps as before, in particular approximations Eqs. (3.62)-(3.64), Eq. (3.118) can then be written as

$$\psi_B \simeq -\frac{i}{\omega_0}(\mathcal{D}\psi_A)\left(1 + \frac{U}{\omega_0}|\psi_A|^2 + h.c.\right). \tag{3.119}$$

Substituting Eq. (3.119) back into Eq. (3.117)

$$\begin{aligned} i\psi_{A,t} &= -i\mathcal{D}^*\left[-\frac{i}{\omega_0}(\mathcal{D}\psi_A)\left(1 + \frac{U}{\omega_0}|\psi_A|^2 + h.c.\right)\right] + U|\psi_A|^2\psi_A - \omega_0\psi_A & (3.120)\\ i\psi_{A,t} &= -\frac{1}{\omega_0}(|\mathcal{D}|^2\psi_A)\left(1 + \frac{U}{\omega_0}|\psi_A|^2 + h.c.\right)\\ &- \frac{U}{\omega_0^2}(\mathcal{D}\psi_A)(\mathcal{D}^*|\psi_A|^2) + U|\psi_A|^2\psi_A - \omega_0\psi_A & (3.121)\\ i\psi_{A,t} &= -\frac{1}{\omega_0}(\vec{\nabla}^2\psi_A)\left(1 + \frac{U}{\omega_0}|\psi_A|^2 + h.c.\right)\\ &- \frac{U}{\omega_0^2}(\mathcal{D}\psi_A)(\mathcal{D}^*|\psi_A|^2) + U|\psi_A|^2\psi_A + \omega_0\psi_A\,. & (3.122) \end{aligned}$$

Finally we obtain

$$i\psi_{A,t} = -\frac{1}{\omega_0}\vec{\nabla}^2\psi_A + (U|\psi_A|^2 - \omega_0)\psi_A - \frac{U}{\omega_0^2}\left[|\psi_A|^2(\vec{\nabla}^2\psi_A) + (\mathcal{D}\psi_A)(\mathcal{D}^*|\psi_A|^2)\right]. \quad (3.123)$$

We want to construct the Langrangian such that Eq. (3.123) can be obtained by the usual Euler-Lagrange prescription

$$\partial_\mu\left(\frac{\partial\mathcal{L}}{\partial\psi^*_{A,\mu}}\right) - \frac{\partial\mathcal{L}}{\partial\psi^*_A} = 0\,. \quad (3.124)$$

For most of the terms in Eq. (3.123), the task of constructing the necessary terms is straight forward except for those terms containing derivatives of the conjugate of the field. To construct the Lagrangian density that corresponds to Eq. (3.123), we write out all derivatives explicitly,

$$\begin{aligned} & i\psi_{A,t} + \frac{1}{\omega_0}\left(\psi_{A,xx} + \psi_{A,yy}\right) + U\psi^*_A\psi_A\psi_A - \omega_0\psi_A \\ & -\frac{U}{\omega_0^2}\left[\psi^*_A\psi_A\left(\psi_{A,xx} + \psi_{A,yy}\right) + \left(\psi_{A,x} + i\psi_{A,y}\right)\left(\psi_{A,x} - i\psi_{A,y}\right)\psi^*_A\right. \\ & \left. + \left(\psi_{A,x} + i\psi_{A,y}\right)\left(\psi^*_{A,x} - i\psi^*_{A,y}\right)\psi_A\right] = 0 \end{aligned} \quad (3.125)$$

$$\Longrightarrow$$

$$\begin{aligned} & i\psi_{A,t} + \frac{1}{\omega_0}\left(\psi_{A,xx} + \psi_{A,yy}\right) + U\psi^*_A\psi_A\psi_A - \omega_0\psi_A \\ & -\frac{U}{\omega_0^2}\left(\psi^*_A\psi_A\psi_{A,xx} + \psi^*_A\psi_A\psi_{A,yy} + \psi^2_{A,x}\psi^*_A + \psi^2_{A,y}\psi^*_A\right. \\ & \left. +\psi_{A,x}\psi^*_{A,x}\psi_A - i\psi_{A,x}\psi^*_{A,y}\psi_A + i\,\psi_{A,y}\psi^*_{A,x}\psi_A + \psi_{A,y}\psi^*_{A,y}\psi_A\right) = 0. \end{aligned} \quad (3.126)$$

Once more, as with the one-dimensional case, we encounter a problem in constructing the exact Lagrangian but here the situation is worse: we now have an additional four terms on the left hand side of Eq. (3.126) whose Lagrangian terms will be difficult to construct . Instead, we can see that if only the first two terms on the left hand side of Eq. (3.123) were present, this would be the usual result for ϕ^4 and we expect to see vortex solutions with the modulus of the radial solution being zero at the origin and approaching a constant for large distances. The mapping of the phase at infinity

onto the boundary of the 2D manifold is just the problem of wrapping the $U(1)$ circle around the boundary circle corresponding to spatial infinity; this is the same as the fundamental homotopy group and is isomorphic to $\mathbb{Z}$. For weak interactions we then would expect similar behavior for the solution since the correction term is small. We choose the form

$$\psi_A(r,\theta,t) = Ce^{-i\omega t}e^{in\theta}\psi(r)\,, \tag{3.127}$$

such that

$$\begin{aligned} \lim_{r\to\infty}|\psi_A| &= C & (3.128)\\ \Rightarrow\ \lim_{r\to\infty}|\psi(r)| &= 1\,, & (3.129)\\ \text{also, } \lim_{r\to 0}|\psi_A| &= 0\,. & (3.130) \end{aligned}$$

In plane-polar coordinates, Eq. (3.123) becomes

$$\begin{aligned} i\psi_{A,t} &= -\frac{1}{\omega_0}\left(\frac{\partial^2}{\partial r^2}+\frac{1}{r^2}\frac{\partial^2}{\partial\theta^2}+\frac{1}{r}\frac{\partial}{\partial r}\right)\psi_A + (U|\psi_A|^2-\omega_0)\psi_A \\ &- \frac{U}{\omega_0^2}|\psi_A|^2\left(\frac{\partial^2}{\partial r^2}+\frac{1}{r^2}\frac{\partial^2}{\partial\theta^2}+\frac{1}{r}\frac{\partial}{\partial r}\right)\psi_A \\ &- \frac{U}{\omega_0^2}\left[e^{i\theta}\left(\frac{\partial}{\partial r}+i\frac{1}{r}\frac{\partial}{\partial\theta}\right)\psi_A\right]\left[e^{-i\theta}\left(\frac{\partial}{\partial r}-i\frac{1}{r}\frac{\partial}{\partial\theta}\right)|\psi_A|^2\right]. \end{aligned} \tag{3.131}$$

Inserting Eq. (3.127) gives

$$\begin{aligned} \omega\psi &= -\frac{1}{\omega_0}\left(\frac{\partial^2}{\partial r^2}-\frac{n^2}{r^2}+\frac{1}{r}\frac{\partial}{\partial r}\right)\psi + (UC^2\psi^2-\omega_0)\psi \\ &- \frac{U}{\omega_0^2}C^2\psi^2\left(\frac{\partial^2}{\partial r^2}-\frac{n^2}{r^2}+\frac{1}{r}\frac{\partial}{\partial r}\right)\psi \\ &- \frac{U}{\omega_0^2}C^2\psi\left[\left(\frac{\partial}{\partial r}-\frac{n}{r}\right)\psi\right]\left[\left(\frac{\partial}{\partial r}-\frac{n}{r}\right)\psi+\left(\frac{\partial}{\partial r}+\frac{n}{r}\right)\psi\right]. \end{aligned} \tag{3.132}$$

Canceling some terms and using condensed notation, we have

$$\begin{aligned}\omega\psi &= -\frac{1}{\omega_0}\left(\psi_{rr}-\frac{n^2}{r^2}\psi+\frac{1}{r}\psi_r\right)+(UC^2\psi^2-\omega_0)\psi \\ &- \frac{U}{\omega_0^2}C^2\psi^2\left(\psi_{rr}-\frac{n^2}{r^2}\psi+\frac{1}{r}\psi_r\right)-\frac{U}{\omega_0^2}C^2\psi\left(\psi_r-\frac{n}{r}\psi\right)2\psi_r\,. \qquad (3.133)\end{aligned}$$

More simplifying leads to

$$\begin{aligned}&\frac{1}{\omega_0}\left\{\psi_{rr}+\frac{1}{r}\psi_r+\left[\omega_0\left(\omega_0+\omega\right)-\frac{n^2}{r^2}\right]\psi\right\} \\ &= UC^2\psi^3-\frac{U}{\omega_0^2}C^2\psi^2\left(\psi_{rr}-\frac{n^2}{r^2}\psi+\frac{1}{r}\psi_r\right)-2\frac{U}{\omega_0^2}C^2\psi\left(\psi_r^2-\frac{n}{r}\psi\psi_r\right). \qquad (3.134)\end{aligned}$$

This can be further simplified by making the coordinate change $\xi=\sqrt{\omega_0\left(\omega_0+\omega\right)}x$

$$\begin{aligned}&\left(\omega_0+\omega\right)\left[\psi_{\xi\xi}+\frac{1}{\xi}\psi_\xi+\left(1-\frac{n^2}{\xi^2}\right)\psi\right] \\ &= UC^2\psi^3-\frac{U}{\omega_0}\left(\omega_0+\omega\right)C^2\psi^2\left(\psi_{\xi\xi}-\frac{n^2}{\xi^2}\psi+\frac{1}{\xi}\psi_\xi\right) \\ &- 2\frac{U}{\omega_0}\left(\omega_0+\omega\right)C^2\psi\left(\psi_\xi^2-\frac{n}{\xi}\psi\psi_\xi\right). \qquad (3.135)\end{aligned}$$

Finally, dividing through by $(\omega_0+\omega)$ gives

$$\begin{aligned}\left[\psi_{\xi\xi}+\frac{1}{\xi}\psi_\xi+\left(1-\frac{n^2}{\xi^2}\right)\psi\right] &= \frac{UC^2}{\left(\omega_0+\omega\right)}\psi^3-\frac{U}{\omega_0}C^2\psi^2\left(\psi_{\xi\xi}-\frac{n^2}{\xi^2}\psi+\frac{1}{\xi}\psi_\xi\right) \\ &- 2\frac{U}{\omega_0}C^2\psi\left(\psi_\xi^2-\frac{n}{\xi}\psi\psi_\xi\right). \qquad (3.136)\end{aligned}$$

There are several limits of this equation that are interesting:

1. For small r we expect that $\psi\to 0$ so in this case the nonlinear terms on the right hand side become negligible so that:

$$\left[\psi_{\xi\xi}+\frac{1}{\xi}\psi_\xi+\left(1-\frac{n^2}{\xi^2}\right)\psi\right] = 0\,. \qquad (3.137)$$

This is Bessel's equation and the solutions are the well known Bessel functions $J_n(x)$ and $Y_n(x)$. The ones we are interested in are the Bessel functions of the

first kind, $J_n(x)$, since these are regular at the origin. Of these, we further restrict solutions to those for which $n > 0$ since these are zero at the origin.

2. We seek solutions with constant square modulus for large r. In this limit, all derivatives may be set to zero in Eq. (3.136). This allows us to solve for C in terms of the constants U, ω_0, and ω. For large ξ (large r), $\psi \to 1$, and Eq. (3.136) reduces to $1 = UC^2/(\omega_0 + \omega)$, or simply $C = \sqrt{(\omega_0 + \omega)/U}$.

3. For $U \to 0$ we should retrieve the usual equation for the radial part of the wavefunction. This is indeed the case since, in this limit, all terms on the right hand side of Eq. (3.136) go vanish and we are left with Bessel's equation as expected.

3.6 Conclusion

In this chapter we have focused on a few important topics, focusing heavily on the relation between the NLDE and the NLSE, and the approximate conditions under which a reduction from NLDE to NLSE is possible. The physical context in which our NLDE is found, results in an intriguing modified NLSE with the usual cubic term plus additional unusual nonlinear terms containing first and second order derivatives of the spinor components. A mass term appears when we consider the dynamics of small classical fluctuations, where the mass corresponds to the total energy of the ambient background. For the 1D case, we find solitons with tanh form, with a slightly flattened shape due to the additional interaction terms. The modification to the tanh form is proportional to U/μ^4, where U is the particle interaction and μ the chemical potential of the BEC, and thus can be made small by reducing the interaction strength relative to the total energy. By analyzing the Lagrangian, we make clear the role that symmetry breaking plays in the solitons and vortices. We obtain the explicit asymptotic properties of quantized vortices in the 2D case, and find that the radial functions behave as Bessel functions of the first kind near the

core, have constant non-zero value far from the core, and where the radial form in the region between these two limits depends strongly on its quantized rotational energy through the nonlinearity.

CHAPTER 4

RELATIVISTIC LINEAR STABILITY EQUATIONS FOR THE NONLINEAR DIRAC EQUATION IN BOSE-EINSTEIN CONDENSATES

Publication: L. H. Haddad and Lincoln D. Carr, Europhysics Letters, **94**, 56002 (2011).

Abstract

We present relativistic linear stability equations (RLSE) for quasi-relativistic cold atoms in a honeycomb optical lattice. These equations are derived from first principles and provide a method for computing stabilities of arbitrary localized solutions of the nonlinear Dirac equation (NLDE), a relativistic generalization of the nonlinear Schrödinger equation. We present a variety of such localized solutions: skyrmions, solitons, vortices, and half-quantum vortices, and study their stabilities via the RLSE. When applied to a uniform background, our calculations reveal an experimentally observable effect in the form of Cherenkov radiation.

4.1 Introduction

Progress in condensed matter and particle physics has been periodically marked by significant mutual exchanges between the two disciplines, many proposals for which are realized in model systems of ultracold quantum gases in optical lattices [160–162]. Recent active areas of research include holographic dualities such as AdS/CFT [163], theoretical constructions of superstrings in ultracold quantum gases [164], chiral confinement in quasi-relativistic Bose-Einstein condensates (BECs) [165], and our own derivation of the *nonlinear Dirac equation* (NLDE) describing ultracold bosons in a honeycomb optical lattice [166]. Generically, Dirac theories arising from a honeycomb lattice geometry appear in a variety of interesting settings [20, 167, 168]. Our investigation into relativistic effects in BECs is motivated by this spirit of cross fertilization with the aim of tying in theory to experiment.

In this Letter, we develop the *relativistic linear stability equations* (RLSE) for the NLDE. Moreover, we find emergent nonlinear localized solutions [19] to the NLDE, including solitons, vortices, skyrmions, and half-quantum vortices, the latter so-far unobserved in BECs. Although most of these objects have been studied in multicomponent BECs, such models lie within the usual Schrödinger many-body paradigm. In contrast to this paradigm, our investigations reside within a relativistic framework in which the elementary excitations are governed by a Dirac-like equation. This provides a fundamentally different context distinguished by the presence of a non-trivial Berry phase when circling a vortex core. The presence of a Berry phase and, indeed, the full Dirac structure of our theory was first pioneered by condensed matter theorists within the context of Graphene [50, 169, 170]. In the case of a Bose-Einstein condensate confined in a trap and subjected to a periodic lattice potential, questions regarding stability may be addressed by applying the method of Bogoliubov theory directly at the lattice scale. Unfortunately, for lattices with interesting geometries, this approach stops short without shedding light on the fascinating emergent physics that

is revealed by examining the long-wavelength fluctuations interacting with the lattice background. Consequently, in order to determine the quasi-particle states and energies we cannot rely on the Bogoliubov-de Gennes equations (BdGE) since these are based on nonrelativistic quantum mechanics. Instead, we derive, from first principles, the RLSE which give the correct low energy dynamics for an arbitrary background condensate. The RLSE are reducible to the BdGE in certain limits, and so may naturally be considered relativistic generalizations of the latter. Based on the RLSE we predict Cherenkov radiation that can be measured in experiments: the combination of lattice and particle interactions results in a rich spatial distribution that is not seen in the BdGE for the uniform case [171].

The RLSE is relevant to a broad range of optical lattice constructions. For example, the RLSE also applies to bosons in a square optical lattice with a staggered gauge field similar to the arrangement described in the work by L. K. Lim et al. [172] and, generally, to any boson-lattice system with a bi-partite lattice structure and linear dispersion [173]. It is also important to emphasize that the optical lattice set-up that we describe here is well founded experimentally. Experiments with cold bosons in two-dimensional lattices are commonplace, and have been studied extensively [70]. The application of the RLSE to soliton and vortex solutions as well as to the uniform case gives richer physical results than one finds in either the usual single component BECs or in the case of hyperfine multi-component BECs. The unique feature of our theory is that it reveals a relativistic Fermi structure within a cold bosonic system and the RLSE are the key equations for probing this system.

In the laboratory, the NLDE can be obtained by cooling bosons into the lowest Bloch band of a honeycomb optical lattice [109]; the lattice is constructed by establishing three phase-locked interfering laser beams in a plane while freezing out excitations in the vertical direction as in Figure 4.1. To obtain the desired Dirac structure, particles are first condensed into the lowest energy state (zero crystal mo-

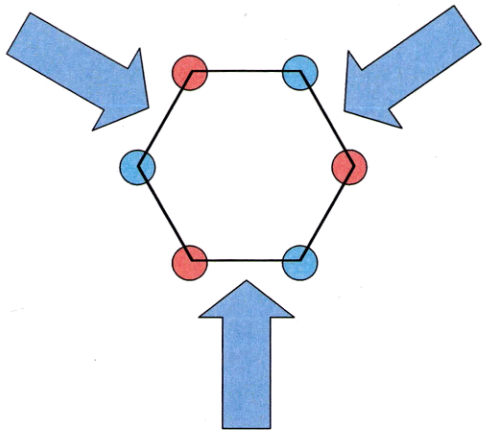

(a)

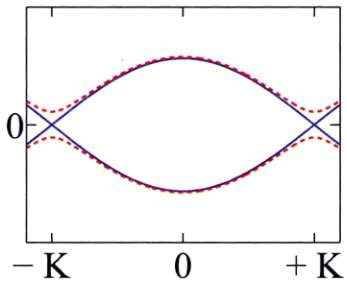

(b)

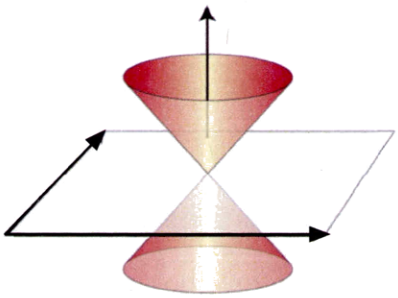

(c)

Figure 4.1: *The honeycomb optical lattice.* (a) Cross section of the band structure showing K and K' points for gapped and ungapped systems. (b) The velocity and acceleration of the lattice, with A and B sub-lattices, are functions of the frequency offsets for interfering lasers. (c) Two-dimensional Dirac cone at K and K'.

mentum) of the lattice and then adiabatically translated to the Dirac point at the band edge (see Figure 4.1) by adiabatically tuning the relative phases between the laser beams. We emphasize that the Dirac point, which is key to the NLDE and our predictions, is maintained even in the presence of the shallow harmonic trap endemic to atomic BECs [174]. Nonlinear phenomena in BECs have been studied extensively over the past decade [19, 63], from single-component vortices in rotating, trapped BECs [175] to complex multi-component order parameters [42, 176] resulting from interactions between the different components and the possibility of nontrivial topo-

logical windings of the internal symmetry space around a singular vortex core. Some form of BdGE analysis plays a central role in such constructions as a means of probing stability as well as for gaining a deeper understanding of the low-energy fluctuations.

4.2 Derivation of the RLSE

Since the system we describe in this letter is a BEC confined strictly to two spatial dimensions, it is appropriate to recall the justification for such a construction before presenting the RLSE. For uniform 2D systems the Mermin-Wagner theorem forbids the formation of a true condensate defined by an infinite phase coherence length. This comes from the fact that the density of states diverges in the 2D case for finite T. Instead, one sees the formation of a *quasi-condensate* characterized by local phase coherence restricted to finite size regions. The size of these regions greatly exceeds the healing length so that all of our solutions are realizable in this picture. However, the inclusion of a harmonic confining potential allows the formation of a true 2D condensate. The potential places a lower bound on the energy for fluctuations and, since it is these long wavelength fluctuations that are responsible for destroying long range order, the trap provides a means of expanding the spatial range of validity of the mean field description.

To obtain the low energy excitations of solutions of the NLDE, we must find the correct set of equations that describe quasi-particle states analogous to the BdGE equations for the general case. These are obtained from the Hamiltonian for a weakly interacting Bose gas, $\hat{H} = \int d\mathbf{r}\, \hat{\psi}^\dagger H_0 \hat{\psi} + \frac{U}{2} \int d\mathbf{r}\, \hat{\psi}^\dagger \hat{\psi}^\dagger \hat{\psi} \hat{\psi}$, $H_0 \equiv \hbar^2 \nabla^2 / 2M + V(\mathbf{r})$, and working through four steps [59]. (1) Take $\hat{\psi} = \Psi_c(\mathbf{r}) + \delta\hat{\psi}_\mathbf{q}(\mathbf{r})$ (condensate + quasi-particles), with $\delta\hat{\psi}_\mathbf{q}$ small. (2) Impose a constraint on Ψ_c to eliminate linear terms in $\delta\hat{\psi}_\mathbf{q}(\mathbf{r})$, keep only quadratic terms in $\delta\hat{\psi}_\mathbf{q}(\mathbf{r})$, and expand as a sum of particle and hole creation operators. (3) Invoke Bloch-state expansions for $\Psi_c(\mathbf{r})$ and $\delta\hat{\psi}_\mathbf{q}(\mathbf{r})$ and take the lowest band. (4) Take the long-wavelength limit while taking momentum with respect to the Dirac point $\mathbf{K}$, such that $\mathbf{k} \ll \mathbf{q} \ll \mathbf{K}$, where $\mathbf{q}$ is the momentum of the

condensate relative to the Dirac point $\mathbf{K}$ and $\mathbf{k}$ is the quasi-particle momentum measured relative to $\mathbf{q}$, and finally diagonalize the quasi-particle part of the Hamiltonian. One finds the RLSE

$$\tilde{\mathscr{D}}\mathbf{u_k} - U\tilde{\Psi}\mathbf{v_k} = \tilde{E}_\mathbf{k}\mathbf{u_k}, \tag{4.1}$$
$$\tilde{\mathscr{D}}^*\mathbf{v_k} - U\tilde{\Psi}\mathbf{u_k} = -\tilde{E}_\mathbf{k}\mathbf{v_k}\ , \tag{4.2}$$

where the matrix coefficients are defined as

$$\begin{aligned}
\tilde{\Psi} &\equiv \mathrm{diag}(|\Psi_A|^2, |\Psi_B|^2), && (4.3)\\
\tilde{E}_\mathbf{k} &\equiv \mathrm{diag}(E_\mathbf{k}, E_\mathbf{k}), && (4.4)\\
[\tilde{\mathscr{D}}]_{1,1} &\equiv m_{\text{eff}} - \mu + 2U|\Psi_A|^2 - i\nabla\phi_A\cdot\nabla \\
&\quad + |\nabla\phi_A| - i\left(\nabla^2\phi_A\right), && (4.5)\\
[\tilde{\mathscr{D}}]_{2,2} &\equiv m_{\text{eff}} - \mu + 2U|\Psi_B|^2 - i\nabla\phi_B\cdot\nabla \\
&\quad + |\nabla\phi_B| - i\left(\nabla^2\phi_B\right), && (4.6)\\
[\tilde{\mathscr{D}}]_{1,2} &= [\tilde{\mathscr{D}}]^*_{2,1} \equiv \mathcal{D}^*. && (4.7)
\end{aligned}$$

Here, $\mathcal{D} = (\partial_x + i\partial_y)$ is the single particle Dirac operator. Also, $\Psi = (\Psi_A, \Psi_B)$ is the BEC order parameter at the $\mathbf{K}$ Dirac point, with normalization on sublattice components $\int d\mathbf{r}\,(|\Psi_A|^2 + |\Psi_B|^2) = 1$. Analogous equations hold for the inequivalent Dirac point at $-\mathbf{K}$. Cast in this highly compact form, Eqs. (7.107)-(7.108) are reminiscent of the BdGE and may be solved for the *spinor quasi-particle amplitudes* $\mathbf{u_k}(\mathbf{r}) = [u_{\mathbf{k},A}(\mathbf{r}), u_{\mathbf{k},B}(\mathbf{r})]^T$ and $\mathbf{v_k}(\mathbf{r}) = [v_{\mathbf{k},A}(\mathbf{r}), v_{\mathbf{k},B}(\mathbf{r})]^T$ and the quasi-particle energy E_k. The components of these 2-spinors represent quantum fluctuations of the sublattice condensate order parameters Ψ_A and Ψ_B which in general are nonuniform $\mathbb{C}$-functions on the plane. The presence of the local phase of the condensate $\phi_{A(B)}(\mathbf{r})$ indicates the complex interaction between the local superfluid velocity of the condensate $\mathbf{v}_{s,A(B)}(\mathbf{r}) \equiv \nabla\phi_{A(B)}(\mathbf{r})$ and the spinor quasi-particles $\mathbf{u_k}(\mathbf{r})$ and $\mathbf{v_k}(\mathbf{r})$. We have taken $\hbar = c_l = 1$ for simplicity, where c_l is the effective speed of light in the NLDE. Note also that we have included an effective mass m_{eff} (anisotropic lattice)

that competes with the chemical potential μ.

It is important to note that for a moving condensate, the negative-energy modes cannot be removed and are crucial indicators of Cherenkov radiation. However, in our case, the Dirac Hamiltonian is *not* positive-definite since our theory is defined at zero lattice energy, not the lowest energy Bloch state, so we must respect the presence of both energy raising *and* lowering modes. Another important feature is that the RLSE are reducible to the BdGE when the local lattice potential energy is the main contributor to the condensate chemical potential and the condensate is slowly varying (quasi-uniform background), i.e., $|\mu| >> U$, $E_j \to |\mu| \approx |\Sigma_0|$, where $\Sigma_0 = \Sigma_{0A(B)} \equiv -\int d\mathbf{r}\, w^*_{A(B)} H_0 w_{A(B)}$ is the local self energy for an arbitrary lattice site, with $w_{A(B)} = w(\mathbf{r} - \mathbf{r}_{A(B)})$ the Wannier functions.

4.3 Physical Parameters and Regimes

We list first the fundamental dimensionful parameters that we use. They are as follows: the average particle density n_0, the chemical potential μ, the lattice spacing a, the s-wave scattering length a_s, the mass of the constituent bosons M, and the lattice well depth V_0. Several relevant composite quantities may be constructed from these. These are the effective speed of light $c_l = t_h a\sqrt{3}/2\hbar$, the sound speed $c_s = \sqrt{Un_0/M}$, the interaction strength $U = 4\pi\hbar^2 a_s/M$, the healing length $\xi = t_h a\sqrt{3}/2\hbar n_0 U$, and the hopping energy $t_h = \int d^2r\, w^* \hat{H}_0 w$, where t_h depends on a and V_0, respectively, through the overlap of Wannier functions and the lattice potential inside $\hat{H}_0$. Two fundamentally important constraints regarding these quantities should be stated. First, in order to avoid reaching the Landau velocity at the band edge and creating unwanted excitations we require $c_l < c_s$, where c_s is the sound speed. Thus we require $t_h a\sqrt{3}/2\hbar < \sqrt{Un_0/M}$ or $(t_h a\sqrt{3}/2\hbar)(4\pi\hbar^2 a_s\, n_0/M)^{-1/2} < 1$. For ^{87}Rb with $t_h = \hbar \times 10^3\,\mathrm{Hz}$, $a = 0.5 \times 10^{-7}\,\mathrm{m}$, $a_s = 5 \times 10^{-9}\,\mathrm{m}$, $n_0 = 2 \times 10^{12}\,\mathrm{cm}^{-3}$, we get $c_l/c_s \lesssim 0.17$. Second, in order for our long-wavelength approximation to be correct, we require the NLDE healing length $\xi \equiv t_h a\sqrt{3}/2\hbar n_0 U \gg a$; using the same values

for the physical parameters, we find $\xi \approx 9.43\, a$.

Next, we discuss the physical regimes for our theory. In this discussion we take $n_0 U/t_h \ll 1$. At length scales much larger than the healing length, $\xi k \ll 1$ where k is a characteristic quasi-particle momentum, excitations are comprised of correlated particle-hole pairs that propagate with a dispersion given by $E \propto k^{1/2}$. This is a *Bose gas* of composite particles in the sense that excitations of opposite spin are paired up (albeit non-locally) to form bosons. In contrast, for $\xi k \gg 1$, excitations are particle-like which corresponds to the case where spin eigenstates are excited independently. These states reflect the bipartite structure of the lattice, multi-component with a Dirac-like dispersion $\propto k$, but are local objects and so also reflect the bosonic nature of the fundamental constituent particles. In this sense, they form a *hybrid Dirac-Bose gas.*

4.4 Uniformly Moving Condensate

Now we return to the RLSE and solve them for the simplest case of a uniform background $\Psi(\mathbf{r}) \equiv \sqrt{n_0}\, e^{i\mathbf{q}\cdot\mathbf{r}}(1, C_0)^T$, where $C_0 \in \mathbb{C}$ contains a relative phase, n_0 is the average particle density, and $\mathbf{q}$ is the condensate momentum measured with respect to the Dirac point. In order to obtain the coherence factors and quasi-particle dispersion, we must then solve a 4×4 eigenvalue problem; the RLSE yield: $E_{\mathbf{k}} = c_l' \hbar \mathbf{q} \cdot \mathbf{k} \pm \sqrt{(c_l \hbar k)^2 + n_0 U c_l \hbar k}$. In keeping with the usual Bogoliubov notation found in the literature, we may write $E_{\mathbf{k}} = (c_l'/c_l)\, \mathbf{q} \cdot \vec{\epsilon}_k^{\,0} \pm E_k^0$ where $\vec{\epsilon}_k^{\,0} \equiv c_l \hbar \mathbf{k}$ is the single quasi-particle energy for zero interaction and $E_k^0 = \sqrt{(\epsilon_k^0)^2 + n_0 U \epsilon_k^0}$ is the quasi-particle energy for a static background. The associated coherence factors can then be written as $|u_{k,A(B)}| = (E_k^0 + c_l \hbar k)/\sqrt{4 E_k^0 c_l \hbar k}$, $|v_{k,A(B)}| = |u_{k,A(B)}|(+ \to -)$. The full interacting Hamiltonian is given by $\hat{H}_{\mathrm{RLSE}} = \frac{1}{4} U n_0^2 A + c_l \hbar q - \sum_k'(2\epsilon_k^0 + n_0 U) + \sum_k' E_k \hat{c}_k^\dagger \hat{c}_k$, where A is the area of the plane. The first three terms are the mean-field and quantum corrections to the condensate energy and the last accounts for the number of quasi-particles present in the system. The constant c_l' is defined in

terms of the overlap integral between Wannier states at neighboring lattice sites by $c_l' = \sqrt{3}a\tau/2\hbar$, where $\tau_{A,B} \equiv -\int d\mathbf{r}\, w_A^* \nabla w_B$ and $\tau = |\tau_{A,B}|$ [6].

The low energy behavior of the uniform condensate has a rich structure. The $\mathbf{q} = \mathbf{0}$ case corresponds to a condensate with zero crystal momentum measured from the Dirac point but with momentum $\mathbf{K}$ relative to the lowest Bloch state of the crystal. The idea of a condensate in motion relative to its background has been treated in both free-space as well as the case of a moving background lattice [64, 70]. Physically, the lattice potential is moving relative to the stationary condensate (laboratory frame). Two-body collisions reduce the momentum of some particles relative to the lattice (slowing down) and increase the momentum of others (speeding up) corresponding to a finite depletion of the condensate. In the laboratory frame, a two-particle collision appears as one particle gaining a component of momentum to the left and the other a component to the right. This is consistent with the well known particle-hole symmetry of the Dirac Hamiltonian: negative energy states can be interpreted as positive energy states that propagate in the opposite direction. In our theory these are quasi-particles with momentum $\mathbf{K} - \mathbf{k}$ (for the $\mathbf{K}$-Dirac point) relative to the lowest Bloch state.

For $\mathbf{q}$=0 then, we get $E_k^{(\pm)} \equiv \pm E_k^0 = \pm\sqrt{(\epsilon_k^0)^2 + n_0 U \epsilon_k^0}$. The two energy regimes evident here are separated by the condition $c_l\hbar k/n_0 U \equiv \xi k \approx 1$. At short wavelength, $k\xi \gg 1$ so that $E_k^{(\pm)} \approx \pm(c_l\hbar k + n_0 U/2)$, where the dominant first term reflects only the presence of the honeycomb lattice, while the second term is a small mean-field Hartree shift due to the interaction with the background. When $k\xi \ll 1$, we find $E_k^{(\pm)} \approx \pm\sqrt{k/\xi}$. These are collective excitations induced by the particle interactions just above the condensate energy. The presence of negative energy modes means that the condensate may lower its energy through spontaneous emission of radiation. This process can be suppressed by introducing an anisotropy in the lat-

[6] Note that whereas for the effective speed of light we have $[c_l] = m \cdot s^{-1}$, in contrast $[c_l'] = m^2 \cdot s^{-1}$ since $\tau_{A,B}$ is an integral over the gradient operator rather than the Laplacian.

tice by breaking the A-B sublattice degeneracy with a deeper optical lattice in one direction [133]. This results in an additional term in the dispersion opening up a mass gap $2m_{\text{eff}}$ at the Dirac point. For the negative energy modes we then have $E_k^{(-)}(m_{\text{eff}}) = 2m_{\text{eff}} - \sqrt{(\epsilon_k^0)^2 + n_0 U \epsilon_k^0}$ so that excitations require a minimum momentum determined by $c_l \hbar k_{\min} = \sqrt{4m_{\text{eff}}^2 + n_0^2 U^2}$. Alternatively, we can consider the effect of the confining potential: this sets a lower bound for quasi-particle energy given by $|E_{k(\min)}^{(-)}| \sim \sqrt{(c_l \hbar 2\pi/R_\perp)^2 + n_0 U\, c_l \hbar 2\pi/R_\perp}$, where $R_\perp$ is the characteristic trap radius in the 2D plane.

4.5 Cherenkov Radiation

This usually refers to the anisotropic emission of electromagnetic radiation from a source whose speed exceeds the local speed of light in some medium [177]. This concept generalizes to any source moving through a medium at a speed that exceeds the phase velocity of the elementary excitations of the medium. For example, a BEC moving in the laboratory frame, or with respect to a background, will "radiate" (emit particles) when its speed exceeds the sound speed. Moreover, the radiation will be emitted in a cone subtended by a specific angle in the direction opposite the motion of the BEC. The RLSE can be used to demonstrate this effect in the present context of a BEC in a honeycomb optical lattice.

For a BEC with momentum $\mathbf{q} > \mathbf{0}$ measured from the Dirac point, examination of the angular dependence of E_k reveals an intriguing structure for the emission of Cherenkov radiation. We observe the following properties for E_k. (1) When $v < c_l$, where $v = c_l' q$ is the condensate speed, all excitations have positive energy regardless of the angle of emission. (2) When $v > c_l$, quasi-particle energies are positive only for emission angles (measured relative to $\mathbf{q}$) for which $\theta < \theta_c \equiv \cos^{-1}(-c_l/v)$ while all other modes have negative energy corresponding to the emission of radiation in a backwards cone bounded by θ_c. When $v = c_l$, $\theta_c = \pi$ marks the onset of radiation, in which case radiation is only emitted in the direction opposite $\mathbf{q}$. This unique

directional property of the radiation suggests an obvious detectable signature in the laboratory: a time-of-flight analysis of a BEC prepared with precise values of the parameters should show a predictable shift in the momentum distributions between the forward and backward directions.

4.6 Nonlinear Localized Modes

In situations where the nonlinearity of the NLDE is Lorentz invariant, solutions may be obtained directly by exploiting the associated conservation equations [103]. This is not the case for our NLDE so we must employ other means. To obtain solutions of the NLDE that are localized in x, y for $U > 0$, we substitute the plane-polar ansatz $\Psi_A(\mathbf{r}) = c_A \exp[ip_A(\theta)]F_A(r)$, $\Psi_B(\mathbf{r}) = c_B \exp[ip_B(\theta)]F_B(r)$ into the NLDE. Then $c_A = i$, $c_B = 1$, and there are two possible combinations for the angular functions: (i) $p_A(\theta) = (l-1)\theta, p_B(\theta) = l\theta$; (ii) $p_A(\theta) = (l-1/2)\theta, p_B(\theta) = (l+1/2)\theta$, with $l \in \mathbb{Z}$. In particular, $l = 0$ in (i) corresponds to a vortex configuration in Ψ_A filled in at the core with a nonzero soliton for Ψ_B. Solutions of this type exist for different relative values of μ and U and for several asymptotic values of the components: $\lim_{r\to\infty}(\Psi_A, \Psi_B) \in \{(-i\sqrt{\frac{\mu}{U}}, 0), (-i\sqrt{\frac{\mu}{U}}, \sqrt{\frac{\mu}{U}}), (0,0)\}$. For $l = 1$, we obtain the same types of solutions but with Ψ_A and Ψ_B exchanged. For $l > 1$, centripetal terms are present for both $F_A(r)$ and $F_B(r)$ so that we must have $\Psi_A(0) = \Psi_B(0) = 0$ and both components are vortices with zero core densities. For the $l = 1$ case, we also obtain a *skyrmion* solution for which the pseudospin $\mathbf{S} = \bar{\Psi}(\mathbf{r})\sigma\Psi(\mathbf{r})$ (with Pauli vector σ) exhibits an integral number of flips near the core and approaches a constant value far from the core. This feature is encoded in a topologically conserved charge $(1/8\pi)\int_\Omega d\mathbf{r}\, \epsilon^{ij}\mathbf{S}\cdot\partial_i\mathbf{S}\times\partial_j\mathbf{S}$ which one recognizes as the Pontryagin index that classifies the mapping $S^1_{\text{spin}} \to S^1_{\partial\Omega}$ where the two circles S^1_{spin} and $S^1_{\partial\Omega}$ parameterize the rotations between the densities $\rho_{A(B)}$ and the polar angle rotation on the 2D boundary $\partial\Omega$ at spatial infinity. In general, similar types of solutions exist for (ii) above. Analytical and numerical solutions are plotted in Figure 4.2 for which different

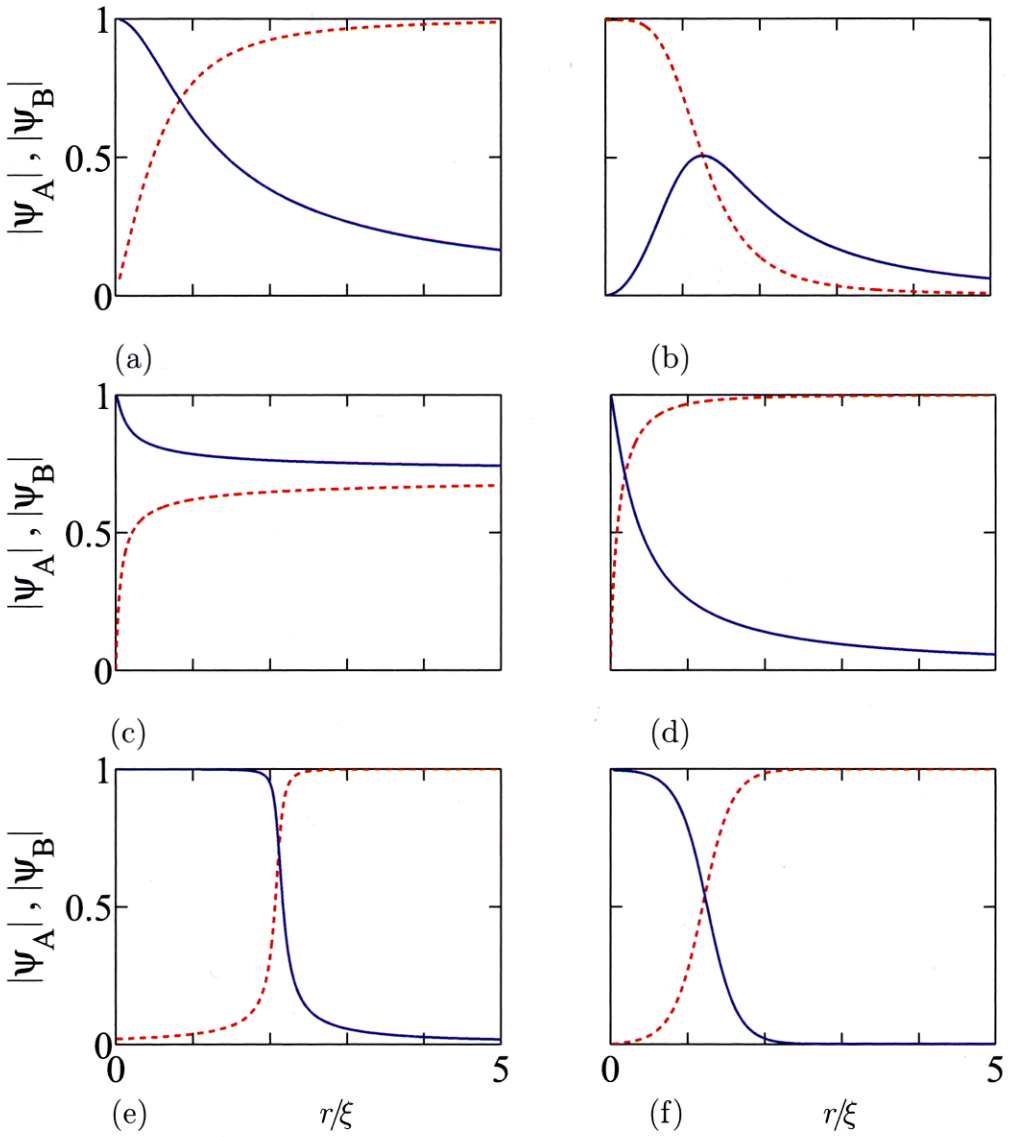

Figure 4.2: *Localized solutions of the NLDE.* Ψ_A (red dashed curves) and Ψ_B (blue solid curves), in units of NLDE healing length ξ: (a) vortex/soliton, (b) ring-vortex/soliton, (c) half-quantum vortex, (d) planar skyrmion, (e) line skyrmion, and (f) line-soliton.

values of μ/U and l allow us to obtain the different asymptotic forms.

Besides vortices with integer phase winding, we also find solutions with fractional phase winding, called *half-quantum vortices* (HQVs). Ordinarily, analyticity (single-valuedness) of the order parameter forbids the rotation of the phase of Ψ around the core to take on fractional values. In the NLDE, Ψ can acquire a coherent internal Berry phase in addition to an external phase whose angles are identified with the polar angle θ [178, 179]. Such states may have half-integer winding in both the internal and external phase angles while remaining single-valued overall. We obtain HQVs with asymptotic form $\lim_{r\to\infty} \Psi_{\rm HQV}(\mathbf{r}) = 2i\sqrt{n_0/2}\, e^{-i\theta/2}[\cos(\theta/2), i\sin(\theta/2)]^{\rm T}$; the complete solution is shown in Figure 4.2 (c).

We also obtain one-dimensional kink-soliton, skyrmion, and line-soliton solutions. The kink and skyrmion solutions are obtained by a straight-forward substitution of the ansatz $\Psi(x) = \eta\,[\cos(\varphi)\,,\,\sin(\varphi)]^T$ into the NLDE and then considering the distinct cases where $\varphi =$ constant (kink) or $\eta =$ constant (skyrmion). The line-soliton solution is obtained when both η and φ are functions of x with the additional condition that, at the origin, η remains below a certain value. This ensures that $\mu^2 < \sqrt{U/8} < (U+1)/2U \;\Rightarrow\; U < 3.365$ and $\mu^2 < 0.649$, which allows the wavefunction to collapse away from the y-axis while the nonzero wavefunction near and along the y-axis has a Lorentzian form in the x-direction due to the attractive effect from the kinetic terms.

4.7 Localized Mode Stability

We can now apply the RLSE to our localized solutions. In particular, for the case where the condensate wavefunction is in the vortex/soliton configuration, we have obtained the exact solution: $\Psi_{vs}(\mathbf{r},t) = e^{-i\mu t/\hbar}\sqrt{\frac{n_0}{1+(r/\xi)^2}}\left(ie^{i\theta}r/\xi\,,\,1\right)^T$. The upper component is a vortex with rotation speed $v = c_l\xi/r$, and the lower component is a soliton centered at the core of the vortex. We solved the RLSE numerically for the vortex/soliton and found that the lowest excitation, with angular momentum $m=-1$

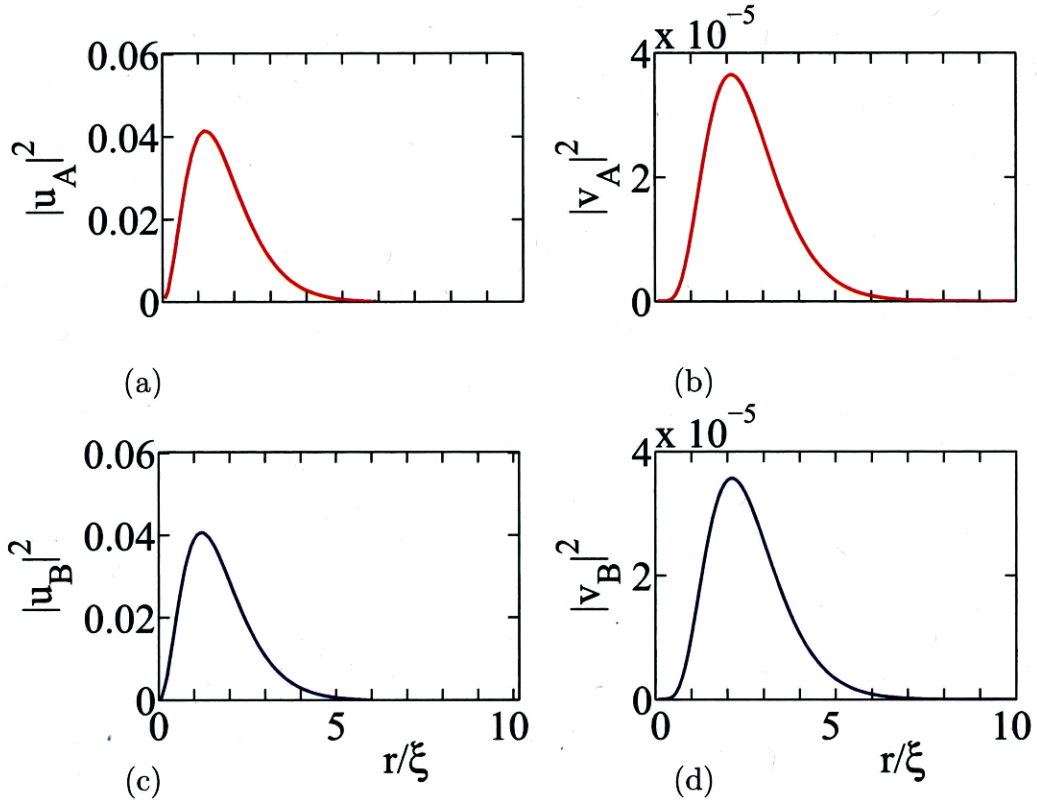

Figure 4.3: *Plots of lowest quasi-particle excitation for the vortex/soliton configuration.*

(relative to the condensate), has the eigenenergy $E_{-1} = -3.9274 + 0.0020\,i$, in units of $n_0 U$. This excitation, having angular momentum equal in magnitude but opposite to the vortex rotation, perturbs the vortex by adding a component of the state that has zero rotation, effectively driving the vortex energy towards the Dirac point. The corresponding coherence factors are shown in Figure 4.3. They peak in the region $\xi \leq r \leq 2\xi$ with $|u_{A(B),-1}|^2 \sim 10^{-2}$ and $|v_{A(B),-1}|^2 \sim 10^{-5}$ so that $u_{A(B),-1} >> v_{A(B),-1}$, which results in a positive normalization integral $\int d^2r\,(|\mathbf{u}_{-1}|^2 - |\mathbf{v}_{-1}|^2)$. This combination of positive norm and negative energy signals the presence of the *anomalous* mode which also occurs for vortices in single-component trapped BECs [180]. To the left of the peaks, near the core where $0 < r < \xi$, excitations are particle-like. There, the tangential rotation speed of the vortex exceeds the critical velocity for emission of Cherenkov radiation so that, in the presence of a mechanism for dissipation, particles are freely radiated out of the condensate. In contrast, for $r \approx 5\xi$, we find that $|\mathbf{u}_{-1}| \approx |\mathbf{v}_{-1}|$ so that excitations are roughly equal admixtures of particles and holes and no radiation is expected.

The anomalous mode has a direct physical interpretation in terms of the precession of the vortex around the central core. To see this, we first compute the density fluctuation in the anomalous mode:

$$\begin{aligned} \delta\mathbf{n}_{vs,-1} &= \left|\langle\hat{\psi}\rangle\right|^2 - |\Psi_{vs}|^2 \\ &= \left(\mathbf{u}_{-1}^T \Psi_{vs}^* - \Psi_{vs}^T \mathbf{v}_{-1}\right) e^{-iE_{-1}t/\hbar} + \left(\Psi_{vs}^T \mathbf{u}_{-1}^* - \mathbf{v}_{-1}^{T*} \Psi_{vs}^*\right) e^{iE_{-1}t/\hbar}. \end{aligned} \quad (4.8)$$

Substituting the expressions for Ψ_{vs}, $\mathbf{u}_{-1}$ and $\mathbf{v}_{-1}$ into Eq. (4.8) allows us to obtain the density fluctuations for the individual components of the condensate. For the upper component (vortex), we obtain

$$\delta n_{vs,A,-1} = f_A(r)\, e^{-i(\theta - |\mathrm{Re}E_{-1}|t/\hbar)}\, e^{\mathrm{Im}E_{-1}t/\hbar} + g_A(r)\, e^{i(\theta - |\mathrm{Re}E_{-1}|t/\hbar)}\, e^{-\mathrm{Im}E_{-1}t/\hbar}, \quad (4.9)$$

with the radial functions given by $f_A(r) = n_0^{1/2} u_{A,-1}(r)\,(r/\xi)/\sqrt{1+(r/\xi)^2}$ and $g_A(r) = n_0^{1/2} v_{A,-1}(r)\,(r/\xi)/\sqrt{1+(r/\xi)^2}$. Fluctuations are strongest near $r \approx 1.5\,\xi$ with the main contribution coming from the first term in Eq. (4.9), which describes *particle* excitations with only a minimal *hole* component. For the fluctuations of the lower component of the condensate (soliton), we obtain an expression similar to Eq. (4.9) but with the radial functions given by $f_B(r) = n_0^{1/2} u_{B,-1}(r)/\sqrt{1+(r/\xi)^2}$ and $g_B(r) = n_0^{1/2} v_{B,-1}(r)/\sqrt{1+(r/\xi)^2}$. The fluctuations of the soliton contain non-zero angular terms which is a consequence of the coupling between the vortex and soliton through the Dirac kinetic terms; in time, through quantum fluctuations, the soliton will develop a finite rotation. The first term in Eq. (4.9) grows exponentially and is proportional to $\exp[i\,(|\mathrm{Re}E_{-1}|\,t/\hbar - \theta\,)] \times \exp(\,\mathrm{Im}E_{-1}t/\hbar)$. The complex factor describes the precession of the density fluctuation in the anti-clockwise direction. The additional factor that grows in time does not appear in the analog case for a vortex in the Gross-Pitaevskii formalism and arises here from the coupling of the spinor components through the derivative terms in the Dirac Hamiltonian.

We can use Eq. (4.8) to estimate the finite lifetime of the vortex due to this effect. By requiring that the total number of particles be conserved, we compute the value: $\tau = \hbar \ln 2/(2\,\mathrm{Im}E_{-1}) \approx 1.88s$. We note that this value does not take into account interactions between the vortex and thermal cloud at finite temperature which would further reduce the value of τ. Thus, we expect the lifetime for Dirac vortices to be shorter than vortices in condensates which are stationary with respect to the lattice. This is expected since the lattice provides a source of friction (dissipation) and bosons are free to drop to lower energy states. This is of course not the case for fermions in graphene, for example, due to the presence of the Fermi level which coincides with the Dirac point. For several of our solutions, we find that the characteristic time associated with this instability is experimentally reasonable. The lowest quasi-particle energies for the other localized solutions are: $-3.9276 + 0.0019\,i$; $2.634 \times 10^2 + 9.96 \times$

$10^4 i$; $-3.9274 + 0.0019\,i$; $7.8409 \times 10^{-3} - 9.9993 \times 10^2\,i$; $7.9349 \times 10^{-3} - 9.9993 \times 10^2\,i$; for the ring-vortex/soliton, half-quantum vortex, planar skyrmion, line-skyrmion, and line-soliton respectively, where all quantities are given in units of $n_0 U$.

4.8 Conclusion

In conclusion, we have shown that an effective quasi-relativistic system with a Dirac-like structure may be designed using ordinary cold bosonic atoms as the underlying degrees of freedom. We solved the resulting NLDE for different classes of nonlinear modes including half-quantum vortices. We derived and solved relativistic linear stability equations and gave explicit criteria for experimental observation of Cherenkov radiation, as well as predicting an anomalous mode for the vortex/soliton solution. Density profiles may be observed by time-of-flight techniques to detect both massive and massless Dirac fermions in the laboratory [15, 133]; nonlinear modes involving phase winding can be created by techniques analogous to those used at JILA [181]; and we anticipate that Bragg scattering can be used to populate the Dirac cones at both $\mathbf{K}$ and $\mathbf{K}'$ points, leading to arbitrary superpositions over our localized solution types between the two cones, and thereby populating all four components of the Dirac spinor.

Acknowledgments

We thank Ken O'Hara, Jeff Steinhauer, and Michael Wall for useful discussions. This work was supported by the NSF and the Aspen Center for Physics.

CHAPTER 5

ESTABLISHING THE RELATIVISTIC LINEAR STABILITY EQUATIONS: MICROSCOPIC LATTICE DERIVATION, TRANSITION OF OPERATORS FROM LATTICE TO CONTINUUM, PROPERTIES OF SPINOR COHERENCE FACTORS AND INTERACTING GROUND STATE

5.1 Introduction

In this chapter, we provide the complete analysis for the low-energy structure of BECs in honeycomb lattices to support and build on the material presented in Chapter 4. This includes a review of the standard Bogoliubov theory for unconfined BECs with arbitrary spatial profiles, and the complete derivation of the RLSE which relies heavily on the use of Wannier functions combined with geometry to prove all of our results, for each step at the microscopic level. We apply the RLSE to a uniform condensate, for which we provide detailed calculations to obtain the terms describing interactions of the quasi-particles with the phase of the condensate. This last step allows us to obtain the prediction of Cherenkov radiation as we have presented in Chapter 4.

5.2 Standard Theory for a Free Condensate

In this section we reproduce the standard derivation for a nonuniform condensate as presented in the original article by A. L. Fetter in Ref. [66]. Beginning with the many-body Hamiltonian for interacting bosons, we first perform the Bogoliubov transformation, and then specialize the potential to include the lattice; compute the interacting system first, then turn on the lattice rather than the other way around. We start again with the Hamiltonian

$$\hat{H} = \int d^2r\hat{\psi}^\dagger H_0\hat{\psi} + \frac{g}{2}\int d^2r\hat{\psi}^\dagger\hat{\psi}^\dagger\hat{\psi}\hat{\psi}\,, \tag{5.1}$$

$$\text{where,}\quad H_0 \equiv -\frac{\hbar^2}{2m}\nabla^2 + V(\vec{r})\,, \tag{5.2}$$

and, $V(\vec{r})$ is the lattice potential and g is the contact interaction coupling strength. In what follows we proceed in the same manner as in Fetter's seminal 1972 paper. As before , we decompose the wavefunction as the sum

$$\hat{\psi}(\vec{r}) = \zeta(\vec{r})\,\hat{a}_0 + \hat{\phi}(\vec{r}), \tag{5.3}$$

where we have separated out an operator component to the condensate part that satisfies the bosonic commutation relation:

$$[\hat{a}_0\,,\,\hat{a}_0^\dagger] = 1\,. \tag{5.4}$$

It is clear that the first term on the right hand side of Eq.(5.3) describes the condensate since it destroys a particle in the mean field ζ which, by itself, is a good approximation to $\hat{\psi}$. The second term destroys a particle in a number of single-particle basis states of the noninteracting system and describes the part of $\hat{\psi}$ that deviates from the mean field. In the Bogoliubov limit $\hat{a}_0 \to N_0^{1/2}$ but we compute the commutator before taking this limit to retain the effect of the presence of a macroscopic condensate field. We can obtain the commutation relations for $\hat{\phi}$ and $\hat{\phi}^\dagger$ by starting with the commutator for $\hat{\psi}$ and $\hat{\psi}^\dagger$ and using Eqs. (5.3) and (5.4). Starting from

$$\left[\hat{\psi}(\vec{r}),\hat{\psi}^\dagger(\vec{r}\,')\right] = \delta(\vec{r}-\vec{r}\,')\,, \tag{5.5}$$

$$\left[\hat{\psi}(\vec{r}),\hat{\psi}(\vec{r}\,')\right] = 0\,, \tag{5.6}$$

$$\left[\hat{\psi}^\dagger(\vec{r}),\hat{\psi}^\dagger(\vec{r}\,')\right] = 0\,. \tag{5.7}$$

We then have

$$\left[\hat{\psi}(\vec{r}),\hat{\psi}^{\dagger}(\vec{r}')\right] = \left[\zeta(\vec{r})\,\hat{a}_0 + \hat{\phi}(\vec{r})\,,\,\zeta^*(\vec{r}')\,\hat{a}_0^{\dagger} + \hat{\phi}^{\dagger}(\vec{r}')\right] \tag{5.8}$$

$$= \zeta(\vec{r})\,\zeta^*(\vec{r}')\left[\hat{a}_0\,,\hat{a}_0^{\dagger}\right] + \zeta(\vec{r})\left[\hat{a}_0\,,\hat{\phi}^{\dagger}(\vec{r}')\right] + \zeta^*(\vec{r}')\left[\hat{\phi}(\vec{r})\,,\,\hat{a}_0^{\dagger}\right] + \left[\hat{\phi}(\vec{r})\,,\,\hat{\phi}^{\dagger}(\vec{r}')\right] \tag{5.9}$$

$$\Rightarrow$$

$$\left[\hat{\phi}(\vec{r})\,,\,\hat{\phi}^{\dagger}(\vec{r}')\right] = \delta(\vec{r}-\vec{r}') - \zeta(\vec{r})\,\zeta^*(\vec{r}')\,, \tag{5.10}$$

where we have used Eq. (5.4) and .

$$\left[\hat{a}_0\,,\hat{\phi}^{\dagger}(\vec{r}')\right] = \left[\hat{\phi}(\vec{r})\,,\,\hat{a}_0^{\dagger}\right] = 0\,. \tag{5.11}$$

Also,

$$\left[\hat{\psi}(\vec{r}),\hat{\psi}(\vec{r}')\right] = \left[\zeta(\vec{r})\,\hat{a}_0 + \hat{\phi}(\vec{r})\,,\,\zeta(\vec{r}')\,\hat{a}_0 + \hat{\phi}(\vec{r}')\right] \tag{5.12}$$

$$= \zeta(\vec{r})\,\zeta(\vec{r}')\,[\hat{a}_0\,,\hat{a}_0] + \zeta(\vec{r})\left[\hat{a}_0\,,\hat{\phi}(\vec{r}')\right] + \zeta(\vec{r}')\left[\hat{\phi}(\vec{r})\,,\,\hat{a}_0\right] + \left[\hat{\phi}(\vec{r})\,,\,\hat{\phi}(\vec{r}')\right] \tag{5.13}$$

$$\Rightarrow$$

$$\left[\hat{\phi}(\vec{r})\,,\,\hat{\phi}(\vec{r}')\right] = 0\,. \tag{5.14}$$

Similarly,

$$\left[\hat{\psi}^{\dagger}(\vec{r}),\hat{\psi}^{\dagger}(\vec{r}')\right] = \left[\zeta^*(\vec{r})\,\hat{a}_0^{\dagger} + \hat{\phi}^{\dagger}(\vec{r})\,,\,\zeta^*(\vec{r}')\,\hat{a}_0^{\dagger} + \hat{\phi}^{\dagger}(\vec{r}')\right] \tag{5.15}$$

$$= \zeta^*(\vec{r})\,\zeta^*(\vec{r}')\left[\hat{a}_0^{\dagger}\,,\hat{a}_0^{\dagger}\right] + \zeta^*(\vec{r})\left[\hat{a}_0^{\dagger}\,,\hat{\phi}^{\dagger}(\vec{r}')\right] + \zeta^*(\vec{r}')\left[\hat{\phi}^{\dagger}(\vec{r})\,,\,\hat{a}_0^{\dagger}\right] + \left[\hat{\phi}^{\dagger}(\vec{r})\,,\,\hat{\phi}^{\dagger}(\vec{r}')\right] \tag{5.16}$$

$$\Rightarrow$$

$$\left[\hat{\phi}^{\dagger}(\vec{r})\,,\,\hat{\phi}^{\dagger}(\vec{r}')\right] = 0\,. \tag{5.17}$$

In the Bogoliubov limit the condensate wavefunction has no operator part and ψ may be written as

$$\hat{\psi}(\vec{r}) \;=\; \Psi(\vec{r}) \;+\; \hat{\phi}(\vec{r})\,, \tag{5.18}$$

where the condensate wavefunction has well defined phase and particle density and so may be written as

$$\Psi(\vec{r}) \;=\; \sqrt{\frac{N_0}{A}}\, e^{iS(\vec{r})} \sqrt{\rho(\vec{r})}\,. \tag{5.19}$$

Here A is the area of the planar system. The radial part is normalized as

$$A^{-1} \int d^2r \rho(\vec{r}) \;=\; 1. \tag{5.20}$$

With these definitions the usual bosonic commutation relations become

$$\left[\hat{\phi}(\vec{r}),\; \hat{\phi}^\dagger(\vec{r}\,')\right] \;=\; e^{iS(\vec{r})}\, e^{-iS(\vec{r}\,')}\, \bar{\delta}(\vec{r},\; \vec{r}\,'), \tag{5.21}$$

$$\text{where,}\;\; \bar{\delta}(\vec{r},\; \vec{r}\,') \;=\; \delta(\vec{r} - \vec{r}\,') \;-\; A^{-1} \sqrt{\rho(\vec{r})} \sqrt{\rho(\vec{r}\,')}\,. \tag{5.22}$$

As before, we transform to the new Hamiltonian

$$\hat{K} \;=\; \hat{H} \;-\; \mu \hat{N} \;=\; \hat{H} \;-\; \mu \int d^2r\; \hat{\psi}^\dagger\, \hat{\psi}\,. \tag{5.23}$$

Now, inserting Eq. (5.3) into Eq. (5.23), expanding through second order in the operator part and eliminating the linear terms by forcing the condensate wavefunction to obey the equation

$$\left[H_0 \;-\; \mu \;+\; g\,|\Psi|^2\right] \Psi \;=\; 0. \tag{5.24}$$

These steps are the same as before but now for a single component wavefunction. We arrive at the Bogoliubov Hamiltonian $\hat{K} \;=\; \hat{K}_0 \;+\; \hat{K}_2$ where

$$\hat{K}_0 = \int d^2r\ \Psi^*(\vec{r}) \left[H_0 - \mu + \frac{g}{2}\ |\Psi(\vec{r})|^2 \right] \Psi(\vec{r})$$

$$\text{and}, \quad \hat{K}_2 = \int d^2r\ \hat{\phi}^\dagger(\vec{r}) \left[H_0 - \mu + 2g\ |\Psi(\vec{r})|^2 \right] \hat{\phi}(\vec{r})$$

$$+ \frac{g}{2} \int d^2r\ \left\{ [\Psi^*(\vec{r})]^2\ \hat{\phi}(\vec{r})\ \hat{\phi}(\vec{r}) + \hat{\phi}^\dagger(\vec{r})\ \hat{\phi}^\dagger(\vec{r})\ [\Psi(\vec{r})]^2 \right\}, \quad (5.25)$$

where in addition to the kinetic operator we also have an arbitrary external potential in the first two terms. Eq.(5.25) is quadratic in the field operators and so may be diagonalized with the appropriate field redefinition. Next, we diagonalize Eq.(5.25) with the linear transformation

$$\hat{\phi}(\vec{r}) = e^{iS(\vec{r})} \sum_j{}' \left[u_j(\vec{r})\ \hat{\alpha}_j - v_j^*(\vec{r})\ \hat{\alpha}_j^\dagger \right], \quad (5.26)$$

$$\hat{\phi}^\dagger(\vec{r}) = e^{-iS(\vec{r})} \sum_j{}' \left[u_j^*(\vec{r})\ \hat{\alpha}_j^\dagger - v_j(\vec{r})\ \hat{\alpha}_j \right]. \quad (5.27)$$

The prime on the summation sign indicates that we are omitting the condensate from the sum. The α_j's and $\alpha_j^\dagger$'s inherit standard bosonic commutation relations from $\hat{\phi}$ and $\hat{\phi}^\dagger$ and the transformation coefficients obey the completeness relations

$$\sum_j{}' \left[u_j(\vec{r})\ u_j^*(\vec{r}\,') - v_j^*(\vec{r})\ v_j(\vec{r}\,') \right] = \bar{\delta}(\vec{r}, \vec{r}\,') \quad (5.28)$$

$$\sum_j{}' \left[u_j(\vec{r})\ v_j^*(\vec{r}\,') - v_j^*(\vec{r})\ u_j(\vec{r}\,') \right] = 0 \quad (5.29)$$

$$\sum_j{}' \left[u_j^*(\vec{r})\ v_j(\vec{r}\,') - v_j(\vec{r})\ u_j^*(\vec{r}\,') \right] = 0\,. \quad (5.30)$$

Substituting Eqs. (5.26) and (5.27) into Eq. (5.25) and, after some tedious algebra as we have previously shown, we arrive at

$$
\begin{aligned}
\hat{K} &= \int d^2r\ \Psi^*(\vec{r}) \left[H_0 - \mu + \frac{g}{2}\ |\Psi(\vec{r})|^2 \right] \Psi(\vec{r}) \\
&+ \sum_{j,k}{}' \int d^2r \left\{ \hat{\alpha}_j \hat{\alpha}_k^\dagger \left[v_j \mathcal{L} v_k^* - \frac{1}{2} g\,|\Psi|^2\ (u_j v_k^* + u_k^* v_j) \right] \right. \\
&+ \hat{\alpha}_j^\dagger \hat{\alpha}_k \left[u_j^* \mathcal{L} u_k - \frac{1}{2} g\,|\Psi|^2\ (v_j^* u_k + v_k u_j^*) \right] \\
&- \hat{\alpha}_j \hat{\alpha}_k \left[v_j \mathcal{L} u_k - \frac{1}{2} g\,|\Psi|^2\ (u_j u_k + u_j v_k) \right] \\
&- \left. \hat{\alpha}_j^\dagger \hat{\alpha}_k^\dagger \left[u_j \mathcal{L} v_k - \frac{1}{2} g\,|\Psi|^2\ (u_j^* u_k^* + v_j^* v_k^*) \right] \right\}, \qquad (5.31)
\end{aligned}
$$

where we have used the condensed notation

$$
\mathcal{L} = -\frac{\hbar^2}{2m} [\nabla + i\,\nabla S(\vec{r})]^2 + V(\vec{r}) - \mu + 2g\ |\Psi(\vec{r})|^2\ . \qquad (5.32)
$$

The next step determines the functional form of the transformation coefficients and further simplifies the Hamiltonian as we continue to work towards diagonalization. Assume the following coupled eigenvalue equations as constraints

$$
\begin{aligned}
\mathcal{L}\, u_j - g\ |\Psi|^2\ v_j &= E_j u_j \qquad (5.33) \\
\mathcal{L}^*\, v_j - g\ |\Psi|^2\ u_j &= -E_j v_j\ ; \qquad (5.34)
\end{aligned}
$$

so that Eq.(5.31) reduces to

$$
\begin{aligned}
\hat{K} &= \int d^2r\ \Psi^*(\vec{r}) \left[H_0 - \mu + \frac{g}{2}\ |\Psi(\vec{r})|^2 \right] \Psi(\vec{r}) \\
&+ \frac{1}{2} \sum_{j,k}{}' \int d^2r \left[(E_j + E_k)(\alpha_j^\dagger \alpha_k u_j^* u_k - \alpha_j \alpha_k^\dagger v_j v_k^*) \right. \\
&+ \left. (E_j - E_k)(\alpha_j \alpha_k u_k v_j - \alpha_j^\dagger \alpha_k^\dagger u_j^* v_k^*) \right]. \qquad (5.35)
\end{aligned}
$$

Multiplying Eq. (5.33) by u_k^* and Eq. (5.34) by v_k^* and integrating, we get

$$
(E_j - E_k^*) \int d^2r (u_j^* u_k - v_j^* v_k) = 0\ , \qquad (5.36)
$$

which further leads to

$$\int d^2r \left[u_j^*(\vec{r})u_k(\vec{r}) \; - \; v_j^*(\vec{r})v_k(\vec{r})\right] \;\; = \;\; \delta_{j,k} \; . \tag{5.37}$$

Similarly, multiplying by v_k and u_k and integrating gives

$$\int d^2r \left[u_j(\vec{r})v_k(\vec{r}) \; - \; u_k(\vec{r})v_j(\vec{r})\right] \;\; = \;\; 0 \; . \tag{5.38}$$

Using the results of Eqs.(5.36) - (5.38) , the final diagonal form of the Hamiltonian is

$$\begin{aligned} \hat{K} \;\; &= \;\; \int d^2r \; \Psi^*(\vec{r}) \left[H_0 \; - \; \mu \; + \; \frac{g}{2} \; |\Psi(\vec{r})|^2\right] \Psi(\vec{r}) \\ &- \;\; \sum_j{}' E_j \int d^2r \, |v_j(\vec{r})|^2 \; + \; \sum_j{}' E_j \alpha_j^\dagger \alpha_j \;\; . \end{aligned} \tag{5.39}$$

5.3 Bogoliubov Theory for a Condensate at Dirac Point of a Honeycomb Lattice

So far, what we have presented is simply a review of the main points in the Bogoliubov transformation for a nonuniform Bose gas [66]. Our notation is slightly different in that we have kept H_0 in our equations to allow for a more general single-particle Hamiltonian which includes an arbitrary external potential. For our particular interest, we would like to know how the structure of the transformation changes as the lattice strength is turned up from zero to the tight-binding limit. Namely, what do Eqs.(5.33), (5.34) and (5.39) map to in the presence of a strong, two-dimensional lattice potential?

In going from the case where the lattice potential is turned off, we can imagine adiabatically tuning $V(\vec{r})$ so that the order parameter (the average field of the many-body system) gradually settles into a solution that is well described by a set of Bloch states. Since Bloch states form a complete orthonormal set there is certainly nothing preventing us from expressing any well behaved function in terms of such a basis but, only as we increase the depth of the potential wells of the lattice do the individual

states, labeled by wave-number $\vec{k}$, become stationary states of the system. The first step then is to make the leap to the tight-binding limit and trust that a straightforward substitution of Bloch states (or linear combinations of them) into the key equations will determine the correct structure of the theory in the tight-binding limit.

The first assumption is that, in the tight-binding limit, we can further decompose the condensate and operator parts of the wavefunction in terms of the individual sublattices. To compute the commutation relations , Eqs. (5.10), (5.11), (5.14), and (5.17), corresponding to taking the tight-binding limit, the condensate and quasi-partcle terms in Eq. (5.3) may be expanded as follows:

$$\zeta(\vec{r}) = \zeta_A(\vec{r}) + \zeta_B(\vec{r}), \tag{5.40}$$
$$\hat{\phi}(\vec{r}) = \hat{\phi}_A(\vec{r}) + \hat{\phi}_B(\vec{r}), \tag{5.41}$$

with,

$$\zeta_A(\vec{r}) \equiv \sum_A e^{i\vec{k}\cdot(\vec{r}-\vec{r}_A)}\, w_{A_i}(\vec{r}-\vec{r}_A), \tag{5.42}$$
$$\zeta_B(\vec{r}) \equiv \sum_B e^{i\vec{k}\cdot(\vec{r}-\vec{r}_B)}\, w_{B_i}(\vec{r}-\vec{r}_B), \tag{5.43}$$
$$\hat{\phi}_A(\vec{r}) \equiv \sum_A \hat{a}_i\, e^{i\vec{k}\cdot(\vec{r}-\vec{r}_A)}\, w(\vec{r}-\vec{r}_A) \tag{5.44}$$
$$\hat{\phi}_B(\vec{r}) \equiv \sum_B \hat{b}_i\, e^{i\vec{k}\cdot(\vec{r}-\vec{r}_B)}\, w(\vec{r}-\vec{r}_B). \tag{5.45}$$

Equation (5.3) becomes

$$\hat{\psi}(\vec{r}) = \hat{a}_0 \sum_A e^{i\vec{k}\cdot(\vec{r}-\vec{r}_A)}\, w_{A_i}(\vec{r}-\vec{r}_A) + \hat{b}_0 \sum_B e^{i\vec{k}\cdot(\vec{r}-\vec{r}_B)}\, w_{B_i}(\vec{r}-\vec{r}_B)$$
$$+ \sum_A \hat{a}_i\, e^{i\vec{k}\cdot(\vec{r}-\vec{r}_A)}\, w(\vec{r}-\vec{r}_A) + \sum_B \hat{b}_i\, e^{i\vec{k}\cdot(\vec{r}-\vec{r}_B)}\, w(\vec{r}-\vec{r}_B). \tag{5.46}$$

This decomposition also assumes that overlap between any two sites is small enough so that the field operator algebra, that is continuously parameterized by the points on the two-dimensional manifold, breaks up into a discrete set of algebras parameterized

by each lattice site. The w_{A_i} and w_{B_i} are localized at the lattice sites A_i and B_i respectively but the subscripts indicate that these are generally different for each site. Note the important difference between the condensate and quasi-partcle parts. The first and second summations on the right hand side of Eq.(5.46) destroy particles in the single-particle wavefunction described by the sum over modified Bloch states; these are states with well-defined density and phase for the A and B sublattice condensates. Because of this, the condensate is really a two-state system. On the other hand, the third and fourth summations destroy particles at individual lattice sites creating a many-body superposition of single-particle states. Computing the lattice counterpart to Eq.(5.10) using Eq.(5.46), we get

$$\begin{aligned}
\left[\hat{\psi}(\vec{r})\,,\,\hat{\psi}^\dagger(\vec{r}\,')\right] &= \left[\hat{a}_0, \hat{a}_0^\dagger\right] \sum_{A,A'} e^{-i\vec{k}\cdot(\vec{r}\,'-\vec{r}_{A'})}\, w^*_{A'_i}(\vec{r}\,'-\vec{r}_{A'})\, e^{i\vec{k}\cdot(\vec{r}-\vec{r}_A)}\, w_{A_i}(\vec{r}-\vec{r}_A) \\
&+ \left[\hat{b}_0, \hat{b}_0^\dagger\right] \sum_{B,B'} e^{-i\vec{k}\cdot(\vec{r}\,'-\vec{r}_{B'})}\, w^*_{B'_i}(\vec{r}\,'-\vec{r}_{B'})\, e^{i\vec{k}\cdot(\vec{r}-\vec{r}_B)}\, w_{B_i}(\vec{r}-\vec{r}_B) \\
&+ \sum_A \left[\hat{a}_i\,,\,\hat{a}_i^\dagger\right] e^{-i\vec{k}\cdot(\vec{r}\,'-\vec{r}_A)}\, w^*(\vec{r}\,'-\vec{r}_A)\, e^{i\vec{k}\cdot(\vec{r}-\vec{r}_A)}\, w(\vec{r}-\vec{r}_A) \\
&+ \sum_B \left[\hat{b}_i\,,\,\hat{b}_i^\dagger\right] e^{-i\vec{k}\cdot(\vec{r}\,'-\vec{r}_B)}\, w^*(\vec{r}\,'-\vec{r}_B) e^{i\vec{k}\cdot(\vec{r}-\vec{r}_B)}\, w(\vec{r}-\vec{r}_B) \quad (5.47) \\
&= \delta(\vec{r}\,-\,\vec{r}\,') \quad (5.48)
\end{aligned}$$

$$\begin{aligned}
\Longrightarrow \quad & \\
& \sum_A \left[\hat{a}_i\,,\,\hat{a}_i^\dagger\right] e^{-i\vec{k}\cdot(\vec{r}\,'-\vec{r}_A)}\, w^*(\vec{r}\,'-\vec{r}_A)\, e^{i\vec{k}\cdot(\vec{r}-\vec{r}_A)}\, w(\vec{r}-\vec{r}_A) \\
&+ \sum_B \left[\hat{b}_i\,,\,\hat{b}_i^\dagger\right] e^{-i\vec{k}\cdot(\vec{r}\,'-\vec{r}_B)}\, w^*(\vec{r}\,'-\vec{r}_B) e^{i\vec{k}\cdot(\vec{r}-\vec{r}_B)}\, w(\vec{r}-\vec{r}_B) \\
&= \delta(\vec{r}\,-\,\vec{r}\,') \\
&- \sum_{A,A'} e^{-i\vec{k}\cdot(\vec{r}\,'-\vec{r}_{A'})}\, w^*_{A'_i}(\vec{r}\,'-\vec{r}_{A'})\, e^{i\vec{k}\cdot(\vec{r}-\vec{r}_A)}\, w_{A_i}(\vec{r}-\vec{r}_A) \\
&- \sum_{B,B'} e^{-i\vec{k}\cdot(\vec{r}\,'-\vec{r}_{B'})}\, w^*_{B'_i}(\vec{r}\,'-\vec{r}_{B'})\, e^{i\vec{k}\cdot(\vec{r}-\vec{r}_B)}\, w_{B_i}(\vec{r}-\vec{r}_B)\,. \quad (5.49)
\end{aligned}$$

This can be written in condensed notation

$$\sum_A \left[\hat{\phi}_{A_i}(\vec{r}), \hat{\phi}^\dagger_{A_i}(\vec{r}\,')\right] + \sum_B \left[\hat{\phi}_{B_i}(\vec{r}), \hat{\phi}^\dagger_{B_i}(\vec{r}\,')\right] =$$
$$\delta(\vec{r} - \vec{r}\,') - \sum_A \zeta^*_{A_i}(\vec{r}\,')\,\zeta_{A_i}(\vec{r}) - \sum_B \zeta^*_{B_i}(\vec{r}\,')\,\zeta_{B_i}(\vec{r})\,. \tag{5.50}$$

The full Hamiltonian for the system is symmetric in the sublattice labels A and B which allows us to write

$$\sum_A \left[\hat{\phi}_{A_i}(\vec{r}), \hat{\phi}^\dagger_{A_i}(\vec{r}\,')\right] = \frac{1}{2}\delta(\vec{r} - \vec{r}\,') - \sum_A \zeta^*_{A_i}(\vec{r}\,')\,\zeta_{A_i}(\vec{r})\,, \tag{5.51}$$
$$\sum_B \left[\hat{\phi}_{B_i}(\vec{r}), \hat{\phi}^\dagger_{B_i}(\vec{r}\,')\right] = \frac{1}{2}\delta(\vec{r} - \vec{r}\,') - \sum_B \zeta^*_{B_i}(\vec{r}\,')\,\zeta_{B_i}(\vec{r})\,. \tag{5.52}$$

These are the lattice analogues of Eq.(5.10). Next, we compute the counterpart to Eq.(5.11). This is straightforward and needs no detailed calculation since our initial assumption; that the operators for condensate and non-condensate particles commute; still holds. We obtain

$$\left[\hat{a}_0\,,\, \hat{\phi}^\dagger_A(\vec{r}\,')\right] = \left[\hat{\phi}_A(\vec{r})\,,\, \hat{a}^\dagger_0\right] = 0\,, \tag{5.53}$$
$$\left[\hat{a}_0\,,\, \hat{\phi}^\dagger_B(\vec{r}\,')\right] = \left[\hat{\phi}_B(\vec{r})\,,\, \hat{a}^\dagger_0\right] = 0\,, \tag{5.54}$$
$$\left[\hat{b}_0\,,\, \hat{\phi}^\dagger_A(\vec{r}\,')\right] = \left[\hat{\phi}_A(\vec{r})\,,\, \hat{b}^\dagger_0\right] = 0\,, \tag{5.55}$$
$$\left[\hat{b}_0\,,\, \hat{\phi}^\dagger_B(\vec{r}\,')\right] = \left[\hat{\phi}_B(\vec{r})\,,\, \hat{b}^\dagger_0\right] = 0\,. \tag{5.56}$$

Similarly Eq.(5.14) becomes

$$\left[\hat{\phi}_A(\vec{r})\,,\, \hat{\phi}_A(\vec{r}\,')\right] = 0\,, \tag{5.57}$$
$$\left[\hat{\phi}_A(\vec{r})\,,\, \hat{\phi}_B(\vec{r}\,')\right] = 0\,, \tag{5.58}$$
$$\left[\hat{\phi}_B(\vec{r})\,,\, \hat{\phi}_B(\vec{r}\,')\right] = 0\,. \tag{5.59}$$

Eq.(5.17) becomes

$$\left[\hat{\phi}_A^\dagger(\vec{r}\,),\, \hat{\phi}_A^\dagger(\vec{r}\,')\right] \;=\; 0\,, \tag{5.60}$$

$$\left[\hat{\phi}_A^\dagger(\vec{r}\,),\, \hat{\phi}_B^\dagger(\vec{r}\,')\right] \;=\; 0\,, \tag{5.61}$$

$$\left[\hat{\phi}_B^\dagger(\vec{r}\,),\, \hat{\phi}_B^\dagger(\vec{r}\,')\right] \;=\; 0\,. \tag{5.62}$$

Next, we take the Bogoliubov limit in which the condensate part of the wavefunction becomes a pure complex number by letting $\hat{a}_0\,,\ \hat{b}_0 \;\rightarrow\; N_0^{1/2}$,

$$\hat{\psi}(\vec{r}\,) \;=\; \Psi_A(\vec{r}\,) \;+\; \Psi_B(\vec{r}\,) \;+\; \hat{\phi}_A(\vec{r}\,) \;+\; \hat{\phi}_B(\vec{r}\,)\,, \tag{5.63}$$

where the condensate wavefunction is defined as

$$\Psi(\vec{r}\,) = \;\Psi_A(\vec{r}\,) \;+\; \Psi_B(\vec{r}\,)\,, \tag{5.64}$$

and,

$$\Psi_A(\vec{r}\,) \;=\; \zeta_A(\vec{r}\,)\, N_0^{1/2} \tag{5.65}$$

$$\Psi_B(\vec{r}\,) \;=\; \zeta_B(\vec{r}\,)\, N_0^{1/2}\,. \tag{5.66}$$

Expressing the condensate in terms of a local particle number and phase,

$$\Psi_A(\vec{r}\,) \;=\; \sum_A e^{i\vec{k}\cdot(\vec{r}-\vec{r}_A)}\, w_{A_i}(\vec{r}-\vec{r}_A) \;=\; \sum_A e^{i\vec{k}\cdot(\vec{r}-\vec{r}_A)} \sqrt{n_{A_i}}\, e^{iS_{A_i}}\, w(\vec{r}-\vec{r}_A)\,, \tag{5.67}$$

$$\Psi_B(\vec{r}\,) \;=\; \sum_B e^{i\vec{k}\cdot(\vec{r}-\vec{r}_B)}\, w_{B_i}(\vec{r}-\vec{r}_B) \;=\; \sum_B e^{i\vec{k}\cdot(\vec{r}-\vec{r}_B)} \sqrt{n_{B_i}}\, e^{iS_{B_i}}\, w(\vec{r}-\vec{r}_B)\,, \tag{5.68}$$

where we assume the local functions normalized as

$$\int d^2r\, w^* w \;=\; 1\,, \tag{5.69}$$

so that

$$\int d^2r\, \Psi_A^*(\vec{r})\, \Psi_A(\vec{r}) \;=\; \sum_A n_{A_i} \;=\; N_{0,A}\;, \tag{5.70}$$

$$\int d^2r\, \Psi_B^*(\vec{r})\, \Psi_B(\vec{r}) \;=\; \sum_B n_{B_i} \;=\; N_{0,B}\;, \tag{5.71}$$

where the total number of condensate particles is defined in terms of the total in each sublattice

$$N_0 \;\equiv\; N_{0,A} \,+\, N_{0,B}\;. \tag{5.72}$$

Substituting Eq.(5.64) into Eq.(5.24), we get

$$\left[H_0 \,-\, \mu \,+\, g\,|\Psi_A|^2 \,+\, g\Psi_A^*\Psi_B \,+\, g\Psi_B^*\Psi_A \,+\, g\,|\Psi_B|^2\right](\Psi_A \,+\, \Psi_B) \;=\; 0\;. \tag{5.73}$$

Next, we substitute Eq.(5.67) and (5.68) into Eq.(5.73) and multiply on the left by

$$e^{-i\vec{k}\cdot(\vec{r}-\vec{r}_{A_j})}\, w^*(\vec{r}-\vec{r}_{A_j})\;, \tag{5.74}$$

and integrate over the plane. Here the subscript A_j indicates that this quantity is associated with the jth site of the A sublattice. We restrict to the condition of nearest-neighbor interactions which greatly simplifies the resulting expression since all A-A and B-B transitions, except for on-site kinetic and potential terms, are eliminated and the later may be neglected as an overall self-energy. Then, only integrals involving neighboring A-B sites remain in the sum. Similarly, in the interactions only on-site terms are non-negligible, i.e., overlap of functions w belonging to the same site. Eq.(5.73) then reduces to

$$\begin{aligned}
&-t_h\left[\sqrt{n_{B_j}}\, e^{iS_{B_j}}\, e^{i\vec{k}\cdot(\vec{r}_{A_j}-\vec{r}_{B_j})} \,+\, \sqrt{n_{B_{j-n_1}}}\, e^{iS_{B_{j-n_1}}}\, e^{i\vec{k}\cdot(\vec{r}_{A_j}-\vec{r}_{B_{j-n_1}})}\right.\\
&\left.+\sqrt{n_{B_{j-n_2}}}\, e^{iS_{B_{j-n_2}}}\, e^{i\vec{k}\cdot(\vec{r}_{A_j}-\vec{r}_{B_{j-n_2}})}\right] \,-\, \mu\sqrt{n_{A_j}}\, e^{iS_{A_j}} + U\left|\sqrt{n_{A_j}}\, e^{iS_{A_j}}\right|^2 \sqrt{n_{A_j}}\, e^{iS_{A_j}}\\
&=\; 0\;.
\end{aligned} \tag{5.75}$$

The hopping integral and interaction energy are respectively,

$$t_h = -\int d^2r\, w^*(\vec{r}-\vec{r}_{A_j})\, H_0\, w(\vec{r}-r_{B_j}) \tag{5.76}$$

and ,

$$U = g\int d^2r\, w_j^*\, w_j^*\, w_j\, w_j\ , \tag{5.77}$$

where A_j and B_j refer to nearest neighbor sites. In terms of the nearest neighbor vectors $\vec{\delta}_1$, $\vec{\delta}_2$, and $\vec{\delta}_3$, we get

$$\begin{aligned} &-t_h\left[\sqrt{n_{B_j}}\, e^{iS_{B_j}}\, e^{i\vec{k}\cdot\vec{\delta}_3} + \sqrt{n_{B_{j-n_1}}}\, e^{iS_{B_{j-n_1}}}\, e^{i\vec{k}\cdot\vec{\delta}_1} + \sqrt{n_{B_{j-n_2}}}\, e^{iS_{B_{j-n_2}}}\, e^{i\vec{k}\cdot\vec{\delta}_2}\right] \\ &-\mu\sqrt{n_{A_j}}\, e^{iS_{A_j}} + U\left|\sqrt{n_{A_j}}\, e^{iS_{A_j}}\right|^2 \sqrt{n_{A_j}}\, e^{iS_{A_j}} = 0. \end{aligned} \tag{5.78}$$

Next we insert particular values for the nearest-neighbor displacement vectors $\vec{\delta}$ and evaluate $\vec{k}$ at the Brillouin zone corner, defined by $\vec{k} = \vec{K} = (0, 4\pi/3)$, $\vec{\delta}_1 = (\frac{1}{2\sqrt{3}}, -\frac{1}{2})$, $\vec{\delta}_2 = (\frac{1}{2\sqrt{3}}, \frac{1}{2})$, $\vec{\delta}_3 = (-\frac{1}{\sqrt{3}}, 0)$, to obtain

$$\begin{aligned} &-t_h\left[\sqrt{n_{B_k}}\, e^{iS_{B_k}}\, e^0 + \sqrt{n_{B_{k-n_1}}}\, e^{iS_{B_{k-n_1}}}\, e^{-i2\pi/3} + \sqrt{n_{B_{k-n_2}}}\, e^{iS_{B_{k-n_2}}}\, e^{i2\pi/3}\right] \\ &-\mu\sqrt{n_{A_k}}\, e^{iS_{A_k}} + U\left|\sqrt{n_{A_k}}\, e^{iS_{A_k}}\right|^2 \sqrt{n_{A_k}}\, e^{iS_{A_k}} = 0\ . \end{aligned} \tag{5.79}$$

Reducing the exponentials gives

$$\begin{aligned} &-t_h\left[\sqrt{n_{B_k}}\, e^{iS_{B_k}} + \sqrt{n_{B_{k-n_1}}}\, e^{iS_{B_{k-n_1}}}\, (-1/2 - i\sqrt{3}/2)\right. \\ &\left. + \sqrt{n_{B_{k-n_2}}}\, e^{iS_{B_{k-n_2}}}\, (-1/2 + i\sqrt{3}/2)\right] \\ &-\mu\sqrt{n_{A_k}}\, e^{iS_{A_k}} + U\left|\sqrt{n_{A_k}}\, e^{iS_{A_k}}\right|^2 \sqrt{n_{A_k}}\, e^{iS_{A_k}} = 0\ . \end{aligned} \tag{5.80}$$

Regrouping terms gives us

$$\begin{aligned} &-t_h\left[\left(\sqrt{n_{B_k}}\, e^{iS_{B_k}} - \sqrt{n_{B_{k-n_1}}}\, e^{iS_{B_{k-n_1}}}\right)(1/2 + i\sqrt{3}/2)\right. \\ &\left. + \left(\sqrt{n_{B_k}}\, e^{iS_{B_k}} - \sqrt{n_{B_{k-n_2}}}\, e^{iS_{B_{k-n_2}}}\right)(1/2 - i\sqrt{3}/2)\right] \\ &-\mu\sqrt{n_{A_k}}\, e^{iS_{A_k}} + U\left|\sqrt{n_{A_k}}\, e^{iS_{A_k}}\right|^2 \sqrt{n_{A_k}}\, e^{iS_{A_k}} = 0\ . \end{aligned} \tag{5.81}$$

Dividing through by the lattice spacing, a, and taking the continuum limit, the first two terms that contain differences become derivatives of the condensate wavefunction with respect to the lattice translation vectors. Abusing the notation a bit, we redefine the components of the condensate wavefunction in terms of the density and phase as

$$\Psi_A(\vec{r}) \equiv \sqrt{\rho_A(\vec{r})}\, e^{iS_A(\vec{r})}\,, \tag{5.82}$$

$$\Psi_B(\vec{r}) \equiv \sqrt{\rho_B(\vec{r})}\, e^{iS_B(\vec{r})}\,. \tag{5.83}$$

Here the density and phase are the continuum limits of those in Eq.(5.81). Eq.(5.81) becomes

$$-t_h \left[\frac{\partial \Psi_B}{\partial n_1}(1/2 + i\sqrt{3}/2) + \frac{\partial \Psi_B}{\partial n_2}(1/2 - i\sqrt{3}/2)\right] - \mu\,\Psi_A + U\,|\Psi_A|^2\,\Psi_A = 0\,. \tag{5.84}$$

After transforming to x and y coordinates and working through some algebra, we arrive at

$$\frac{i\,t_h\,a\,\sqrt{3}}{2\,\hbar}\,(\partial_x - i\partial_y)\,\Psi_B - U\,|\Psi_A|^2\,\Psi_A + \mu\,\Psi_A = 0\,. \tag{5.85}$$

The same steps lead to a similar equation for Ψ_B

$$\frac{i\,t_h\,a\,\sqrt{3}}{2\,\hbar}\,(\partial_x + i\partial_y)\,\Psi_A - U\,|\Psi_B|^2\,\Psi_B + \mu\Psi_B = 0\,. \tag{5.86}$$

Replacing the constant in front of the derivative terms by the speed of sound in the condensate, we obtain

$$i\,\hbar c_l\,(\partial_x + i\partial_y)\,\Psi_A - U\,|\Psi_B|^2\,\Psi_B + \mu\,\Psi_B = 0\,, \tag{5.87}$$

$$i\,\hbar c_l\,(\partial_x - i\partial_y)\,\Psi_B - U\,|\Psi_A|^2\,\Psi_A + \mu\,\Psi_A = 0\,. \tag{5.88}$$

Eqs. (5.87) and (5.88) comprise the nonlinear Dirac equation for one Dirac point.

5.3.1 Transition of Operators Between Lattice and Continuum Limits

We should establish a more rigorous connection between operators at the lattice scale and those that are defined after taking the long-wavelength limit. In particular, when working with operator terms in the Hamiltonian in the long-wavelength limit we may wish to diagonalize certain terms inducing off-diagonal terms elsewhere. We may ask what the relationship is between the operators used to diagonalize before taking the long-wavelength and those that diagonalize after taking this limit. On the lattice scale it is clear that an operator that creates a boson on the A sublattice, say, and one that creates a boson in some superposition of A and B are related by some sort of spatial rotation while at long distances the transformation must map to some unitary operation acting on the pseudospin structure of the wavefunction.

On the lattice scale, the operator that creates a boson in the single-particle state with momentum $\hbar\,\vec{k}$, where a is the lattice spacing, is given by

$$\hat{c}^{\dagger}_{\vec{k}} = \sum_{A,B} < w_{A_i(B_i)}|\vec{k} > \hat{c}^{\dagger}_{\vec{k},A_i(B_i)} \,, \tag{5.89}$$

where, $\hat{c}^{\dagger}_{\vec{k},A_i(B_i)}$ creates a boson at some site on the lattice and the projection is defined as

$$< w_{A_i(B_i)}|\vec{k} > \equiv \int d^2r e^{i\vec{k}\cdot\vec{r}}\, w^*(\vec{r} - \vec{r}_{A_i(B_i)}) \,. \tag{5.90}$$

The summation is defined over the entire lattice. Because of the isotropy of the system we may consider states with a given magnitude $k = |\vec{k}|$ and also, define $\hat{a}^{\dagger}_{k,i} \equiv \hat{c}^{\dagger}_{k,A_i}$ and $\hat{b}^{\dagger}_{k,i} \equiv \hat{c}^{\dagger}_{k,B_i}$. We are being very loose here with the lattice notation as we are using the single index i to denote a site which is determined by a two-dimensional lattice vector. With these definitions, the operator that creates a boson with momentum $\hbar\,k$ on the A sublattice is

$$\hat{a}_k^\dagger \equiv \sum_A < w_{A_i}|k > \hat{c}_{k,A_i}^\dagger \,, \tag{5.91}$$

similarly, for the B sublattice, we have

$$\hat{b}_k^\dagger \equiv \sum_B < w_{B_i}|k > \hat{c}_{k,B_i}^\dagger \,. \tag{5.92}$$

Then, at the lattice scale, a unitary operator that creates a superposition state over A and B must be

$$\begin{aligned} \hat{q}_k^\dagger &= U_{(L)aq}^* \, \hat{a}_k^\dagger + U_{(L)bq}^* \, \hat{b}_k^\dagger & (5.93) \\ &= \sum_{A,B} \left(U_{(L)aq}^* < k|w_{A_i} > \hat{c}_{k,A_i}^\dagger + U_{(L)bq}^* < k|w_{B_i} > \hat{c}_{k,B_i}^\dagger \right) , & (5.94) \end{aligned}$$

with $|U_{(L)aq}|^2 + |U_{(L)bq}|^2 = 1$ and the subscript (L) indicates that these operator is defined at the lattice scale. We can connect a pure state to a superposition state through a spatial rotation. For example, since we have honeycomb lattice symmetry, a rotation by an integer multiple of $\pi/3$ produces

$$\begin{aligned} R(n\pi/3)\,\psi_A(\vec{r}) &= R(n\pi/3) \sum_A w(\vec{r} - \vec{r}_A)\, e^{i\vec{k}\cdot(\vec{r}-\vec{r_A})} \\ &= \sum_A \left[R(n\pi/3) w(\vec{r} - \vec{r}_A)\right] \left[R(n\pi/3) e^{i\vec{k}\cdot(\vec{r}-\vec{r_A})}\right] \\ &= \sum_B w(\vec{r} - \vec{r}_B)\, e^{i\vec{k}\cdot(\vec{r}-\vec{r_B})} \\ &= \psi_B(\vec{r}) \,, \end{aligned} \tag{5.95}$$

so that,

$$\tilde{\mathbf{R}}_{n\pi/3} \, |0, ..., n_{A,k} = 1, ..., 0 > = \, |0, ..., n_{B,k} = 1, ..., 0 > , \tag{5.96}$$

where $\tilde{\mathbf{R}}_{n\pi/3}$ is the action of a rotation by $n\,\pi/3$ on the many body state with a single boson in a state with momentum $\vec{p} = \hbar\,\vec{k}$ on sublattice A, i.e.,

$$|0,...,n_{A,k}=1,...,0> \equiv \hat{a}_k^\dagger\,|\mathcal{O}>\ . \tag{5.97}$$

Note also that the induced transformation possesses the involution property

$$\begin{aligned}
\tilde{\mathbf{R}}^2_{n\pi/3}\,|0,...,n_{A,k}=1,...,0> &= \tilde{\mathbf{R}}_{n\pi/3}\,|0,...,n_{B,k}=1,...,0> \\
&= |0,...,n_{A,k}=1,...,0> \qquad (5.98)\\
\Rightarrow \qquad \tilde{\mathbf{R}}^2_{n\pi/3} &= \mathbf{1}\,. \qquad (5.99)
\end{aligned}$$

For a mixed operator acting on the ground state we have

$$\begin{aligned}
\hat{q}_k^\dagger\,|\mathcal{O}> &= C^*_{k,aq}\,|0,...,n_{A,k}=1,...,0> + C^*_{k,bq}\,|0,...,n_{B,k}=1,...,0> \\
&= C^*_{k,aq}\,\hat{a}_k^\dagger\,|\mathcal{O}> + C^*_{k,bq}\,\tilde{\mathbf{R}}_{n\pi/3}\,\hat{a}_k^\dagger\,|\mathcal{O}> \qquad (5.100)\\
\Rightarrow \qquad \hat{q}_k^\dagger &= \left(C^*_{k,aq} + C^*_{k,bq}\,\tilde{\mathbf{R}}_{n\pi/3}\right)\hat{a}_k^\dagger \qquad (5.101)\\
&= \left(\mathbf{1} + e^{i\,\alpha}\,\tilde{\mathbf{R}}_{n\pi/3}\right)\hat{a}_k^\dagger\,, \qquad (5.102)
\end{aligned}$$

where in the last step we have replaced complex constants by a phase difference in the second term. To define spatial rotations in two-dimensions we require one generator but since we are rotating complex functions we must also specify a relative phase rotation by a phase angle δ embedded in the spatial rotation. For an infinitesimal spatial rotation ϵ, continuity in the phase of the wavefunction demands that δ must also be small so that $e^{i\,\delta/2} = 1 + i\delta/2 + h.c.$. We obtain

$$\left(\mathbf{1} + e^{i\,\alpha}\,\tilde{\mathbf{R}}_\epsilon\right) \equiv e^{\vec{\epsilon}\cdot\vec{\mathbf{Q}}_{(L)}} = \mathbf{1}_{(L)} + \epsilon_1\,\mathbf{Q}_{(L),1} + \epsilon_2\,\mathbf{Q}_{(L),2} + h.c. \tag{5.103}$$

where the bold notation indicates the action on the state space induced by the spatial and phase rotations in the plane. For a spatial plus phase rotation in two-dimensions we require the matrices

$$\begin{bmatrix} 1 & 0 \\ 0 & 1 \end{bmatrix}\ ,\ \begin{bmatrix} 0 & -e^{i\,\delta/2} \\ e^{-i\,\delta/2} & 0 \end{bmatrix}\ . \tag{5.104}$$

For small δ we can expand the second matrix

$$\begin{bmatrix} 0 & -e^{i\delta/2} \\ e^{-i\delta/2} & 0 \end{bmatrix} \approx \begin{bmatrix} 0 & -(1+i\delta/2) \\ (1-i\delta/2) & 0 \end{bmatrix} \tag{5.105}$$

$$\approx \begin{bmatrix} 0 & -1 \\ 1 & 0 \end{bmatrix} - i\delta/2 \begin{bmatrix} 0 & 1 \\ 1 & 0 \end{bmatrix} . \tag{5.106}$$

Extracting a factor of $-i$ we obtain the Pauli matrices that are relevant to the plane. With the expansion parameter in Eq.(5.103) defined such that $\epsilon_1 = \epsilon\,\delta/2$ and $\epsilon_2 = \epsilon$ we are now able to make the transition to the continuum limit through the mappings

$$\mathbf{1}_{(L)} \rightarrow \begin{bmatrix} 1 & 0 \\ 0 & 1 \end{bmatrix} \equiv \mathbf{1}_{(C)}\,, \tag{5.107}$$

$$\mathbf{Q}_{(L),1} \rightarrow -i \begin{bmatrix} 0 & 1 \\ 1 & 0 \end{bmatrix} \equiv \mathbf{Q}_{(C),1}\,, \tag{5.108}$$

$$\mathbf{Q}_{(L),2} \rightarrow -i \begin{bmatrix} 0 & -i \\ i & 0 \end{bmatrix} \equiv \mathbf{Q}_{(C),2}\ . \tag{5.109}$$

The subscripts L and C indicate that the operators are defined at the lattice scale and continuum limit respectively. It is important to note that this transition is defined up to a phase factor. This phase allows us to adjust the rotation in the plane of the lattice to match the correct value for the Berry phase in the continuum limit which may be determined through geometric considerations. The final step is to identify $\mathbf{Q}_{(C),1}$ and $\mathbf{Q}_{(C),2}$ as the generators of unitary transformations acting on the internal pseudospin space of the continuum limit states.

5.3.2 The Tight-Binding Limit Form of Bogoliubov Transformations

Next, we determine the form of the linear transformations in the tight-binding limit. Eqs. (5.26) and (5.27) define local, point-wise, linear transformations. In the tight-binding limit the continuous parameters are replaced by a discrete set of on-site parameters. The lattice versions of Eqs.(5.26) and (5.27) are obtained by replacing the left hand sides by

$$\hat{\phi}(\vec{r}) = \hat{\phi}_A(\vec{r}) + \hat{\phi}_B(\vec{r}) \tag{5.110}$$

$$= \sum_A \hat{a}_i \, e^{i\vec{k}\cdot(\vec{r}-\vec{r}_A)} \, w(\vec{r}-\vec{r}_A) + \sum_B \hat{b}_i \, e^{i\vec{k}\cdot(\vec{r}-\vec{r}_B)} \, w(\vec{r}-\vec{r}_B) \,, \tag{5.111}$$

and, similarly for the right hand sides, we decompose the u_j and v_j parameters into ones labeled by the particular sublattice as well as taking on discrete labels for each site. Thus, we have

$$u_j(\vec{r}) = u_{j,A}(\vec{r}) + u_{j,B}(\vec{r}) = \sum_{A'} u_{j,A_i}(\vec{r}-\vec{r}_A) + \sum_B u_{j,B_i}(\vec{r}-\vec{r}_B) \,. \tag{5.112}$$

Explicitly, Eq.(5.26) becomes

$$\begin{aligned} &\sum_A \hat{a}_i \, e^{i\vec{k}\cdot(\vec{r}-\vec{r}_A)} \, w(\vec{r}-\vec{r}_A) + \sum_B \hat{b}_i \, e^{i\vec{k}\cdot(\vec{r}-\vec{r}_B)} \, w(\vec{r}-\vec{r}_B) \quad = \\ &e^{iS(\vec{r})} \sum_j{}' \left\{ \left[\sum_A u_{j,A_i}(\vec{r}-\vec{r}_A) + \sum_B u_{j,B_i}(\vec{r}-\vec{r}_B) \right] \hat{\alpha}_j \right. \\ &\qquad \left. - \left[\sum_A v^*_{j,A_i}(\vec{r}-\vec{r}_A) + \sum_B v^*_{j,B_i}(\vec{r}-\vec{r}_B) \right] \hat{\alpha}^\dagger_j \right\} . \end{aligned} \tag{5.113}$$

Rearanging the summations on the right hand side gives

$$\begin{aligned} &\sum_A \hat{a}_i \, e^{i\vec{k}\cdot(\vec{r}-\vec{r}_A)} \, w(\vec{r}-\vec{r}_A) + \sum_B \hat{b}_i \, e^{i\vec{k}\cdot(\vec{r}-\vec{r}_B)} \, w(\vec{r}-\vec{r}_B) \quad = \\ &e^{iS(\vec{r})} \sum_A \left\{ \sum_j{}' \left[u_{j,A_i}(\vec{r}-\vec{r}_A) \, \hat{\alpha}_j - v^*_{j,A_i}(\vec{r}-\vec{r}_A) \, \hat{\alpha}^\dagger_j \right] \right\} \\ &+ e^{iS(\vec{r})} \sum_B \left\{ \sum_j{}' \left[u_{j,B_i}(\vec{r}-\vec{r}_B) \, \hat{\alpha}_j - v^*_{j,B_i}(\vec{r}-\vec{r}_B) \, \hat{\alpha}^\dagger_j \right] \right\} . \end{aligned} \tag{5.114}$$

Since the transformation coefficients are well localized around each lattice site, we can approximate the phase factor by its value at the each lattice site, i.e.,

$$\begin{aligned} e^{iS(\vec{r})} &\simeq \sum_A \delta(\vec{r}-\vec{r}_A) \, e^{iS(\vec{r}_A)} + \sum_B \delta(\vec{r}-\vec{r}_B) \, e^{iS(\vec{r}_B)} \\ &\equiv \sum_A e^{iS_{A_i}} + \sum_B e^{iS_{B_i}} \,. \end{aligned} \tag{5.115}$$

Also, since the new operators, the $\hat{\alpha}_j$'s , are now multiplied by transformation coefficients that are localized at each site, we can split the algebra by denoting those quasi-partcle operators that pertain to the A and B sublattices as $\hat{\alpha}_j$ and $\hat{\beta}_j$ respectively. Eq.(5.114) becomes

$$\begin{aligned}
&\sum_A \hat{a}_i\, e^{i\vec{k}\cdot(\vec{r}-\vec{r}_A)}\, w(\vec{r}-\vec{r}_A) + \sum_B \hat{b}_i\, e^{i\vec{k}\cdot(\vec{r}-\vec{r}_B)}\, w(\vec{r}-\vec{r}_B) \quad = \\
&\sum_A e^{iS_{A_i}} \left\{ \sum_j{}' \left[u_{j,A_i}(\vec{r}-\vec{r}_A)\,\hat{\alpha}_j \;-\; v^*_{j,A_i}(\vec{r}-\vec{r}_A)\,\hat{\alpha}_j^\dagger \right] \right\} \\
+ &\sum_B e^{iS_{B_i}} \left\{ \sum_j{}' \left[u_{j,B_i}(\vec{r}-\vec{r}_B)\,\hat{\beta}_j \;-\; v^*_{j,B_i}(\vec{r}-\vec{r}_B)\,\hat{\beta}_j^\dagger \right] \right\} . \qquad (5.116)
\end{aligned}$$

From this expression we can read off the transformation matrices between the $\hat{a}$'s and $\hat{b}$'s and $\hat{\alpha}$'s and $\hat{\beta}$'s. Multiplying both sides of Eq.(5.116) by $e^{-i\vec{k}\cdot(\vec{r}-\vec{r}_{A_l})}\, w^*(\vec{r}-\vec{r}_{A_l})$ and integrating over the plane give

$$\begin{aligned}
\hat{a}_l \;=\; &\sum_j{}' \left\{ \left[e^{iS_{A_l}} \int d^2r\, e^{-i\vec{k}\cdot(\vec{r}-\vec{r}_{A_l})}\, w^*(\vec{r}-\vec{r}_{A_l})\, u_{j,A_l}(\vec{r}-\vec{r}_{A_l}) \right] \hat{\alpha}_j \right. \\
- &\left. \left[e^{iS_{A_l}} \int d^2r\, e^{-i\vec{k}\cdot(\vec{r}-\vec{r}_{A_l})}\, w^*(\vec{r}-\vec{r}_{A_l})\, v^*_{j,A_l}(\vec{r}-\vec{r}_{A_l}) \right] \hat{\alpha}_j^\dagger \right\} . \qquad (5.117)
\end{aligned}$$

By condensing the notation a bit we obtain

$$\hat{a}_l \;=\; \sum_j{}' \left(\tilde{u}_{j,A_l}\,\hat{\alpha}_j \;-\; \tilde{v}^*_{j,A_l}\,\hat{\alpha}_j^\dagger \right) . \qquad (5.118)$$

Here we have defined the matrix elements as

$$\tilde{u}_{j,A_l} \;\equiv\; e^{iS_{A_l}} \int d^2r\, e^{-i\vec{k}\cdot(\vec{r}-\vec{r}_{A_l})}\, w^*(\vec{r}-\vec{r}_{A_l})\, u_{j,A_l}(\vec{r}-\vec{r}_{A_l}) , \qquad (5.119)$$

$$\tilde{v}^*_{j,A_l} \;\equiv\; e^{iS_{A_l}} \int d^2r\, e^{-i\vec{k}\cdot(\vec{r}-\vec{r}_{A_l})}\, w^*(\vec{r}-\vec{r}_{A_l})\, v^*_{j,A_l}(\vec{r}-\vec{r}_{A_l}) . \qquad (5.120)$$

Returning to Eq.(5.116), if we exchange the order of summation on the right hand side we obtain

$$\sum_A \hat{a}_i \, e^{i\vec{k}\cdot(\vec{r}-\vec{r}_A)} \, w(\vec{r}-\vec{r}_A) + \sum_B \hat{b}_i \, e^{i\vec{k}\cdot(\vec{r}-\vec{r}_B)} \, w(\vec{r}-\vec{r}_B) \quad =$$

$$\sum_j{}' \left\{ \sum_A e^{iS_{A_i}} \left[u_{j,A_i}(\vec{r}-\vec{r}_A) \, \hat{\alpha}_j \; - \; v^*_{j,A_i}(\vec{r}-\vec{r}_A) \, \hat{\alpha}^\dagger_j \right] \right\}$$

$$+ \sum_j{}' \left\{ \sum_B e^{iS_{B_i}} \left[u_{j,B_i}(\vec{r}-\vec{r}_B) \, \hat{\beta}_j \; - \; v^*_{j,B_i}(\vec{r}-\vec{r}_B) \, \hat{\beta}^\dagger_j \right] \right\} \tag{5.121}$$

Eq.(5.121) may be expressed more concisely as

$$\hat{\phi}_A(\vec{r}) + \hat{\phi}_B(\vec{r}) \;=\; e^{iS(\vec{r})} \sum_j{}' \left[u_{j,A}(\vec{r}) \, \hat{\alpha}_j \; - \; v^*_{j,A}(\vec{r}) \, \hat{\alpha}^\dagger_j \right]$$

$$+ \; e^{iS(\vec{r})} \sum_j{}' \left[u_{j,B}(\vec{r}) \, \hat{\beta}_j \; - \; v^*_{j,B}(\vec{r}) \, \hat{\beta}^\dagger_j \right] \tag{5.122}$$

$$\Rightarrow$$

$$\hat{\phi}_A(\vec{r}) \;=\; e^{iS(\vec{r})} \sum_j{}' \left[u_{j,A}(\vec{r}) \, \hat{\alpha}_j \; - \; v^*_{j,A}(\vec{r}) \, \hat{\alpha}^\dagger_j \right] , \tag{5.123}$$

$$\hat{\phi}_B(\vec{r}) \;=\; e^{iS(\vec{r})} \sum_j{}' \left[u_{j,B}(\vec{r}) \, \hat{\beta}_j \; - \; v^*_{j,B}(\vec{r}) \, \hat{\beta}^\dagger_j \right] \tag{5.124}$$

where we have used the definitions

$$\hat{\phi}_A(\vec{r}) \;=\; \sum_A \hat{a}_i \, e^{i\vec{k}\cdot(\vec{r}-\vec{r}_A)} \, w(\vec{r}-\vec{r}_A) \, , \tag{5.125}$$

$$u_{j,A}(\vec{r}) \;=\; \sum_A u_{j,A_i}(\vec{r}-\vec{r}_A) \, , \tag{5.126}$$

and so forth.

Next, we specialize the completeness relations, Eqs. (5.28)-(5.30), to the tight-binding limit. Substituting Eq.(5.112) and an equivalent one for v_j, into Eq.(5.28) gives

$$\sum_j{}' \{ [u_{j,A}(\vec{r}) + u_{j,B}(\vec{r})] [u^*_{j,A}(\vec{r}') + u^*_{j,B}(\vec{r}')] \tag{5.127}$$
$$- [v^*_{j,A}(\vec{r}) + v^*_{j,B}(\vec{r})] [v_{j,A}(\vec{r}') + v_{j,B}(\vec{r}')] \}$$
$$= \delta(\vec{r} - \vec{r}') - \zeta^*_A(\vec{r}')\,\zeta_A(\vec{r}) - \zeta^*_B(\vec{r}')\,\zeta_B(\vec{r})\,. \tag{5.128}$$

If we expand the products on the left hand side in terms of the localized basis, and retain only same site products, we obtain

$$\sum_j{}' \{ [u_{j,A}(\vec{r})\,u^*_{j,A}(\vec{r}') + u_{j,B}(\vec{r})\,u^*_{j,B}(\vec{r}')] - [v^*_{j,A}(\vec{r})\,v_{j,A}(\vec{r}') + v^*_{j,B}(\vec{r})\,v_{j,B}(\vec{r}')] \}$$
$$= \delta(\vec{r} - \vec{r}') - \zeta^*_A(\vec{r}')\,\zeta_A(\vec{r}) - \zeta^*_B(\vec{r}')\,\zeta_B(\vec{r}) \tag{5.129}$$
$$\Rightarrow$$
$$\sum_j{}' [u_{j,A}(\vec{r})\,u^*_{j,A}(\vec{r}') - v^*_{j,A}(\vec{r})\,v_{j,A}(\vec{r}')] + \sum_j{}' [u_{j,B}(\vec{r})\,u^*_{j,B}(\vec{r}') + v^*_{j,B}(\vec{r})\,v_{j,B}(\vec{r}')]$$
$$= \delta(\vec{r} - \vec{r}') - \zeta^*_A(\vec{r}')\,\zeta_A(\vec{r}) - \zeta^*_B(\vec{r}')\,\zeta_B(\vec{r})\,. \tag{5.130}$$

Again, because of the A-B symmetry, we can write

$$\sum_j{}' [u_{j,A}(\vec{r})\,u^*_{j,A}(\vec{r}') - v^*_{j,A}(\vec{r})\,v_{j,A}(\vec{r}')] = \frac{1}{2}\,\delta(\vec{r} - \vec{r}') - \zeta^*_A(\vec{r}')\,\zeta_A(\vec{r}) \tag{5.131}$$
$$\sum_j{}' [u_{j,B}(\vec{r})\,u^*_{j,B}(\vec{r}') + v^*_{j,B}(\vec{r})\,v_{j,B}(\vec{r}')] = \frac{1}{2}\,\delta(\vec{r} - \vec{r}') - \zeta^*_B(\vec{r}')\,\zeta_B(\vec{r})\,. \tag{5.132}$$

Eqs.(5.29) and (5.30) split in the same way.

5.3.3 Derivation of the Constraint Equations for the Lattice: Relativistic Linear Stability Equations

Next, we determine the Bogoliubov-de Gennes equations, Eqs.(5.33) and (5.34), for the lattice. First, we note the following:

1. Terms that are contained in the transformation, such as $u_{j,A_i}(\vec{r} - \vec{r}_A)\,\hat{\alpha}_j$, can be expressed as an amplitude times a normalized function that is localized around the ith site of the A sublattice. That is, $u_{j,A_i}(\vec{r} - \vec{r}_A)\,\hat{\alpha}_j \equiv \bar{u}_{j,A_i}\,w(\vec{r} - \vec{r}_A)\,\hat{\alpha}_j$.

2. Since the operator $\hat{\alpha}_j^\dagger \hat{\alpha}_j$ acting on the full interacting excited ground state simply counts the number of quasi-particles in the j's state, the operator

$$\begin{aligned} \int d^2r \, |\bar{u}_{j,A_i} w(\vec{r} - \vec{r}_A)|^2 \, \hat{\alpha}_j^\dagger \hat{\alpha}_j &= |\bar{u}_{j,A_i}|^2 \int d^2r \, |w(\vec{r} - \vec{r}_A)|^2 \, \hat{\alpha}_j^\dagger \hat{\alpha}_j \\ &= |\bar{u}_{j,A_i}|^2 \, \hat{\alpha}_j^\dagger \hat{\alpha}_j \end{aligned} \tag{5.133}$$

can be interpreted as the number operator for quasi-particles in the jth state and at the lattice site A_i: $\hat{n}_{j,A_i} \equiv |\bar{u}_{j,A_i}|^2 \, \hat{\alpha}_j^\dagger \hat{\alpha}_j$.

3. Expressing the transformation coefficients, in Eqs.(5.33) and (5.34), in terms of the definition in (a) and using the result in (b), then, taking the long wavelength limit will give us the final result that we seek. Eqs.(5.33) and (5.34) become

$$\begin{aligned} &\mathcal{L}\left[u_{j,A}(\vec{r}) + u_{j,B}(\vec{r})\right] - g \, |\Psi_A(\vec{r}) + \Psi_B(\vec{r})|^2 \left[v_{j,A}(\vec{r}) + v_{j,B}(\vec{r})\right] = \\ &E_j \, \left[u_{j,A}(\vec{r}) + u_{j,B}(\vec{r})\right] , \end{aligned} \tag{5.134}$$

$$\begin{aligned} &\mathcal{L}^*\left[v_{j,A}(\vec{r}) + v_{j,B}(\vec{r})\right] - g \, |\Psi_A(\vec{r}) + \Psi_B(\vec{r})|^2 \left[u_{j,A}(\vec{r}) + u_{j,B}(\vec{r})\right] = \\ &- E_j \, \left[v_{j,A}(\vec{r}) + v_{j,B}(\vec{r})\right] . \end{aligned} \tag{5.135}$$

Next, we apply the following two steps:

1. We express the u's and v's as sums of terms, identical to those in (a) above , and, using the orthonormal properties of the w functions, as in (b), we multiply Eq.(5.134) and Eq.(5.135) by $w^*(\vec{r} - \vec{r_{A_i}})$ and $w^*(\vec{r} - \vec{r_{B_i}})$, alternately, and integrate over the plane in order to obtain four reduced local equations for the lattice transformation coefficients.

2. We then follow similar steps as in the case of the condensate wave equation; that is, we regroup terms to construct discrete versions of derivatives and take the long-wavelength limit in the end to arrive at the lattice version of the Bogoliubov-de Gennes equations.

Applying steps 1. and 2. produces

$$
\begin{aligned}
i\hbar c_l \mathcal{D}^* u_{j,B} - \mu u_{j,A} + 2U |\Psi_A|^2 u_{j,A} - U |\Psi_A|^2 v_{j,A} &= E_j u_{j,A}, && (5.136)\\
i\hbar c_l \mathcal{D} u_{j,A} - \mu u_{j,B} + 2U |\Psi_B|^2 u_{j,B} - U |\Psi_B|^2 v_{j,B} &= E_j u_{j,B}, && (5.137)\\
i\hbar c_l \mathcal{D} v_{j,B} - \mu v_{j,A} + 2U |\Psi_A|^2 v_{j,A} - U |\Psi_A|^2 u_{j,A} &= -E_j v_{j,A}, && (5.138)\\
i\hbar c_l \mathcal{D}^* v_{j,A} - \mu v_{j,B} + 2U |\Psi_B|^2 v_{j,B} - U |\Psi_B|^2 u_{j,B} &= -E_j v_{j,B}. && (5.139)
\end{aligned}
$$

Here, we have defined

$$
\begin{aligned}
\mathcal{D} &= \partial_x + i\partial_y && (5.140)\\
\mathcal{D}^* &= \partial_x - i\partial_y , && (5.141)
\end{aligned}
$$

and c_s and U are defined as before. Eqs.(5.136)-(5.139) seem unwieldy but we can shed some light on the situation by introducing the following matrix and vector notation

$$
\mathbf{u}_j \equiv \begin{bmatrix} u_{j,A} \\ u_{j,B} \end{bmatrix} \quad , \quad \mathbf{v}_j \equiv \begin{bmatrix} v_{j,A} \\ v_{j,B} \end{bmatrix} \tag{5.142}
$$

$$
\tilde{\mathcal{D}} \equiv \begin{bmatrix} -\mu + 2U |\Psi_A|^2 & c_s \mathcal{D}^* \\ c_s \mathcal{D} & -\mu + 2U |\Psi_B|^2 \end{bmatrix} \tag{5.143}
$$

$$
|\mathbf{\Psi}|^2 \equiv \begin{bmatrix} |\Psi_A|^2 & 0 \\ 0 & |\Psi_B|^2 \end{bmatrix} \tag{5.144}
$$

$$
\mathbf{E}_j \equiv \begin{bmatrix} E_j & 0 \\ 0 & E_j \end{bmatrix} \tag{5.145}
$$

With these definitions, Eqs.(5.136)-(5.139) can be simply written down as

$$
\begin{aligned}
\tilde{\mathcal{D}} \mathbf{u}_j - U |\mathbf{\Psi}|^2 \mathbf{v}_j &= \mathbf{E}_j \mathbf{u}_j && (5.146)\\
\tilde{\mathcal{D}}^* \mathbf{v}_j - U |\mathbf{\Psi}|^2 \mathbf{u}_j &= -\mathbf{E}_j \mathbf{v}_j . && (5.147)
\end{aligned}
$$

Eqs.(5.187) and (5.188) elegantly reflect the bipartite nature of the honeycomb lattice and how the BDG transformation coefficients inherit the symmetry of the A and B

sublattice structure. Note also the strong resemblance to the original BDG equations where the lattice is turned off. It is apparent that the quasi-particles have a spinor-like structure and that their exact form is determined by substituting a particular solution for the condensate wavefunction into Eqs.(5.187) and (5.188). As a final step, we would like to know how the Bogoliubov Hamiltonian, is modified in the tight-binding limit. We derive the final Hamiltonian by two methods to check the commutativity of the operations of diagonalizing with respect to the j, k indices and the α and β indices. The simplest approach is to follow the same steps as the zero-lattice potential which we have done in the main part of this thesis.

5.4 Calculation of RLSE Eigenvalues and Coherence Factors for a Uniform Condensate

The wavefunction for a uniform condensate is the single-particle plane wave solution of the coupled pair of equations

$$\begin{aligned} i\hbar c_l \left(\partial_x + i\partial_y\right) \Psi_A - U \left|\Psi_B\right|^2 \Psi_B + (\mu - m)\Psi_B &= 0 \qquad (5.148) \\ i\hbar c_l \left(\partial_x - i\partial_y\right) \Psi_B - U \left|\Psi_A\right|^2 \Psi_A + (\mu - m) \Psi_A &= 0\,, \qquad (5.149) \end{aligned}$$

where we have included a general mass term m. We can insert the ansatz $\Psi_A(\vec{r}) = A\, e^{i\vec{q}\cdot\vec{r}}$ and $\Psi_B(\vec{r}) = Be^{i\vec{q}\cdot\vec{r}}$, which gives

$$\begin{aligned} i\hbar c_l \left(iq_x - q_y\right) A - U|B|^2 B + (\mu - m)B &= 0\,, \qquad (5.150) \\ i\hbar c_l \left(iq_x + q_y\right) B - UA^3 + (\mu - m)\, A &= 0. \qquad (5.151) \end{aligned}$$

If we restrict to the uniform density case we can set the spinor amplitudes proportional to the square root of the average particle density $A = \sqrt{n_0}$ and $B = C_0\sqrt{n_0}$ where C_0 is the phase difference between the upper and lower components. The coupled equations reduce to

$$\begin{aligned} i\hbar c_l \left(iq_x - q_y\right) - Un_0C_0 + (\mu - m)\, C_0 &= 0\,, \qquad (5.152) \\ i\hbar c_l \left(iq_x + q_y\right) C_0 - U\, n_0 + (\mu - m) &= 0\,. \qquad (5.153) \end{aligned}$$

These give

$$C_0 = \pm \frac{(q_x + iq_y)}{q}, \tag{5.154}$$

which allows us to solve for the chemical potential giving two values for the positive and negative energy branches of the spectrum

$$\mu_\pm = m + Un_0 \pm \hbar c_l q. \tag{5.155}$$

The first two terms on the right represent the cost of adding a particle with zero momentum to the already present n_0 particles (the first due to the energy gap opened up from the anisotropy of the lattice and the second due to the interaction) while the third term adds (or subtracts) the contribution in the case of a particle (or hole) when the condensate has finite momentum q. From now on we will simply omit the $\pm$ option with the assumption that q can be either positive or negative.

For a uniform background the quasi-particle excitations will reflect this translational symmetry so we may assume the following form

$$u_{\vec{k},A}(\vec{r}) = A^{-1/2} C_{u_{\vec{k},A}} e^{i\vec{k}\cdot\vec{r}}, \tag{5.156}$$

$$u_{\vec{k},B}(\vec{r}) = A^{-1/2} C_{u_{\vec{k},B}} e^{i\vec{k}\cdot\vec{r}}, \tag{5.157}$$

$$v_{\vec{k},A}(\vec{r}) = A^{-1/2} C_{v_{\vec{k},A}} e^{i\vec{k}\cdot\vec{r}}, \tag{5.158}$$

$$v_{\vec{k},B}(\vec{r}) = A^{-1/2} C_{v_{\vec{k},B}} e^{i\vec{k}\cdot\vec{r}}, \tag{5.159}$$

where the coefficient A is the area of the plane and we have changed the indices to specify the dependence on the momentum vector $\vec{k}$.

5.5 Derivation of Condensate Phase Gradient Terms

Previously, we derived the linear stability equations for the special case where the condensate phase was a constant. For the more general case, we must return to the derivative term that contains the gradient of the condensate phase and walk through

the usual steps that lead to the tight-binding, long wavelength limit result. The term that we want to convert is

$$-\frac{\hbar^2}{2m}\left[\nabla + i\nabla S(\vec{r})\right]^2. \tag{5.160}$$

Expanding this out gives

$$-\frac{\hbar^2}{2m}\left[\nabla^2 + i\nabla^2 S + 2i\nabla S\cdot\nabla - (\nabla S)^2\right]. \tag{5.161}$$

The first term is the usual Laplacian that converts to the Dirac differential operator we have already computed. The second and fourth terms can be decomposed at the lattice scale as

$$\nabla^2 S(\vec{r}) = \sum_A (\nabla^2 S|_{A_i})\delta(\vec{r}-\vec{r}_{A_i}) + \sum_B (\nabla^2 S|_{B_i})\delta(\vec{r}-\vec{r}_{B_i}) \tag{5.162}$$

$$[\nabla S(\vec{r})]^2 = \sum_A (\nabla S|_{A_i})^2\delta(\vec{r}-\vec{r}_{A_i}) + \sum_B (\nabla S|_{B_i})^2\delta(\vec{r}-\vec{r}_{B_i}) \tag{5.163}$$

The third term requires a bit more work. In the usual BDG equations, this term appears as

$$2\,i\nabla S\cdot\nabla u_j. \tag{5.164}$$

Expanding the quasi-particle function in terms of Bloch states and approximating the gradient of the condensate phase, we get

$$\begin{aligned} 2\,i\nabla S\cdot\nabla u_k &= 2i\left[\sum_A (\nabla S|_{A_i})\delta(\vec{r}-\vec{r}_{A_i}) + \sum_B (\nabla S|_{B_i})\delta(\vec{r}-\vec{r}_{B_i})\right] \\ &\quad\cdot\nabla\left[\sum_A e^{i\vec{k}\cdot(\vec{r}-\vec{r}_A)}u_{k,A}w(\vec{r}-\vec{r}_A) + \sum_B e^{i\vec{k}\cdot(\vec{r}-\vec{r}_B)}u_{k,B}w(\vec{r}-\vec{r}_B)\right]. \end{aligned} \tag{5.165}$$

When computing the coupling of the condensate phase to the quasi-particle phase we must be careful with the interpretation of the expansion of u_k in terms of Bloch

states. The scalar product is between the gradient of the condensate phase and the gradient of the quasi-particle function so the complex exponential factor multiplying u_k must be the slow phase associated with the quasi-particle and to lowest order may be set equal to one. The remaining quasi-particle phase resides in u_{k,B_j}. This ensures that we do not mistakenly include a coupling of the condensate to itself. Multiplying through by $\int d^2r w^*(\vec{r}-\vec{r}_{A_j})$ and integrating over the plane while keeping only nearest neighbor overlap integrals, gives

$$-2i\nabla S \cdot \left[u_{k,B_j}\vec{\tau}_{A_j,B_j} \quad + \quad u_{k,B_{j-n_1}}\vec{\tau}_{A_j,B_{j-n_1}} + u_{k,B_{j-n_2}}\vec{\tau}_{A_j,B_{j-n_2}}\right], \tag{5.166}$$

where the overlap integral is defined as

$$\vec{\tau}_{A_j,B_j} \equiv -\int d^2r w^*(\vec{r}-\vec{r}_{A_j})\nabla w(\vec{r}-\vec{r}_{B_j}). \tag{5.167}$$

One may ask what became of the same-site integrals. These involve the gradient of Wannier functions integrated over the plane which vanish due to symmetry. The remaining integral can be written in terms of the vectors that connect nearest neighbor sites which are known quantities. To see this, we note that the gradient of the Wannier function localized at site B_j, say, points symmetrically in the radial direction towards that site. Because of this symmetry, the overlap integral with the nearest neighbor site A_j lies along the line that connects B_j and A_j and indeed must point towards B_j since the integration region between the two sites is weighted most heavily. Thus, we may write

$$\vec{\tau}_{A_j,B_j} \quad = \quad \tau\vec{\delta}_3, \tag{5.168}$$

where we define

$$\tau\vec{\delta}_3 \equiv -\int d^2r\, w^*(\vec{r}-\vec{r}_{A_j})\nabla w(\vec{r}-\vec{r}_{B_j}). \tag{5.169}$$

Similarly,

$$\vec{\tau}_{A_j,B_{j-n_1}} = \tau\vec{\delta}_1 \tag{5.170}$$
$$\vec{\tau}_{A_j,B_{j-n_2}} = \tau\vec{\delta}_2. \tag{5.171}$$

We have called the proportionality constant τ and used the same $\vec{\delta}$ vectors as before:

$$\vec{\delta}_1 = (\tfrac{1}{2\sqrt{3}}, -\tfrac{1}{2}) \ , \ \vec{\delta}_2 = (\tfrac{1}{2\sqrt{3}}, \tfrac{1}{2}) \ , \ \vec{\delta}_3 = (-\tfrac{1}{\sqrt{3}}, 0) \ .$$

Writing this out gives

$$-2i\tau\nabla S \cdot \left(u_{k,B_j}\vec{\delta}_3 + u_{k,B_{j-n_1}}\vec{\delta}_1 + u_{k,B_{j-n_2}}\vec{\delta}_2 \right). \tag{5.172}$$

Replacing the on-site quasi-particle c-numbers with the following expressions

$$u_{k,B_j} = u_{k,A_j} - \partial_{\vec{\delta}_3} u_{k,A_j} \ , \tag{5.173}$$
$$u_{k,B_{j-n_1}} = u_{k,A_j} - \partial_{\vec{\delta}_1} u_{k,A_j} \ , \tag{5.174}$$
$$u_{k,B_{j-n_2}} = u_{k,A_j} - \partial_{\vec{\delta}_2} u_{k,A_j}. \tag{5.175}$$

We then obtain for Eq. (5.172)

$$\begin{aligned} & -2i\tau\nabla S \cdot \left[\left(u_{k,A_j} - \partial_{\vec{\delta}_3} u_{k,A_j} \right) \vec{\delta}_3 + \left(u_{k,A_j} - \partial_{\vec{\delta}_1} u_{k,A_j} \right) \vec{\delta}_1 + \left(u_{k,A_j} - \partial_{\vec{\delta}_2} u_{k,A_j} \right) \vec{\delta}_2 \right] \\ = \ & 2i\tau\nabla S \cdot \left(\partial_{\vec{\delta}_3}\vec{\delta}_3 + \partial_{\vec{\delta}_1}\vec{\delta}_1 + \partial_{\vec{\delta}_2}\vec{\delta}_2 \right) u_{k,A_j}, \end{aligned} \tag{5.176}$$

where in the second line the u_{k,A_j} terms all vanish due to the symmetry of the δ vectors. Expressing the partial derivatives in terms of x and y coordinates

$$\partial_{\vec{\delta}_1} = \vec{\delta}_1 \cdot \nabla = \frac{1}{2\sqrt{3}}\partial_x - \frac{1}{2}\partial_y \, , \tag{5.177}$$
$$\partial_{\vec{\delta}_2} = \vec{\delta}_2 \cdot \nabla = \frac{1}{2\sqrt{3}}\partial_x + \frac{1}{2}\partial_y \, , \tag{5.178}$$
$$\partial_{\vec{\delta}_3} = \vec{\delta}_3 \cdot \nabla = \frac{-1}{\sqrt{3}}\partial_x \, , \tag{5.179}$$

so that we obtain

$$\frac{2}{\sqrt{3}}i\tau\nabla S\cdot\left[-\partial_x\vec{\delta}_3+\left(\frac{1}{2}\partial_x-\frac{\sqrt{3}}{2}\partial_y\right)\vec{\delta}_1+\left(\frac{1}{2}\partial_x+\frac{\sqrt{3}}{2}\partial_y\right)\vec{\delta}_2\right]u_{k,A_j}. \quad (5.180)$$

Finally, inserting the δ vectors gives

$$\begin{aligned}
&\frac{2}{\sqrt{3}}i\tau\nabla S\cdot\left[-\partial_x\left(-\frac{1}{\sqrt{3}}\hat{e}_x+0\hat{e}_y\right)+\left(\frac{1}{2}\partial_x-\frac{\sqrt{3}}{2}\partial_y\right)\left(\frac{1}{2\sqrt{3}}\hat{e}_x-\frac{1}{2}\hat{e}_y\right)\right.\\
&\left.+\left(\frac{1}{2}\partial_x+\frac{\sqrt{3}}{2}\partial_y\right)\left(\frac{1}{2\sqrt{3}}\hat{e}_x+\frac{1}{2}\hat{e}_y\right)\right]u_{k,A_j}\\
=\;&\frac{2}{\sqrt{3}}i\tau\nabla S\cdot\left[\left(\frac{1}{\sqrt{3}}\partial_x+\frac{1}{4\sqrt{3}}\partial_x-\frac{1}{4}\partial_y+\frac{1}{4\sqrt{3}}\partial_x+\frac{1}{4}\partial_y\right)\hat{e}_x\right.\\
&\left.+\left(-\frac{1}{4}\partial_x+\frac{\sqrt{3}}{4}\partial_y+\frac{1}{4}\partial_x+\frac{\sqrt{3}}{4}\partial_y\right)\hat{e}_y\right]\\
=\;&\frac{2}{\sqrt{3}}i\tau\nabla S\cdot\left(\frac{\sqrt{3}}{2}\partial_x\hat{e}_x+\frac{\sqrt{3}}{2}\partial_y\hat{e}_y\right)\\
=\;&i\tau\nabla S\cdot\nabla. \quad (5.181)
\end{aligned}$$

The final result returns the gradient but with a factor of τ correction. Next we determine the transformation of the squared gradient term; the last term in Eq. (5.161). We must evaluate the expression

$$\begin{aligned}
&(\nabla S\cdot\nabla S)u_{k,A}= \quad (5.182)\\
&(i\nabla S\cdot i\nabla S)\left[\sum_A e^{i\vec{k}\cdot(\vec{r}-\vec{r}_A)}u_{k,A}w(\vec{r}-\vec{r}_A)+\sum_B e^{i\vec{k}\cdot(\vec{r}-\vec{r}_B)}u_{k,B}w(\vec{r}-\vec{r}_B)\right].
\end{aligned}$$

To lowest order we choose to allow one factor of ∇S to vary over a unit cell of the lattice while approximating the other factor as a constant over one site. As usual we multiply by the Wannier function for some site and the appropriate exponential phase factor that contains the lattice momentum. When integrating over the plane, the dominant terms are ones that are the same-site integrals. We obtain

$$\nabla S \cdot \int d^2 r w^*(\vec{r} - \vec{r}_A) \nabla S w(\vec{r} - \vec{r}_A) \tag{5.183}$$

$$= \nabla S \cdot \left(\tau_2 \frac{\nabla S}{|\nabla S|} \right) \tag{5.184}$$

$$= \tau_2 |\nabla S|, \tag{5.185}$$

where, in the second step, we have approximated the integral in that we have written it proportional to ∇S where τ_2 encapsulates the variation of the gradient of S over the region where the integral has finite support. Eq. (5.161) transforms to

$$i\mathcal{D}^* u_{k,B} + \left[-i\nabla S_A \cdot \nabla + |\nabla S_A| - i(\nabla^2 S_A) \right] u_{k,A}, \tag{5.186}$$

where we have omitted dimensionful factors which must, in the end, be compared to justify the inherent assumption that all terms are of comparable order. The linear stability equations become

$$\begin{aligned}
i\hbar c_l \mathcal{D}^* u_{j,B} + \mathcal{Q}_A u_{j,A} + 2U |\Psi_A|^2 u_{j,A} - U |\Psi_A|^2 v_{j,A} &= E_j u_{j,A}, & (5.187)\\
i\hbar c_l \mathcal{D} u_{j,A} + \mathcal{Q}_B u_{j,B} + 2U |\Psi_B|^2 u_{j,B} - U |\Psi_B|^2 v_{j,B} &= E_j u_{j,B}, & (5.188)\\
i\hbar c_l \mathcal{D}^* v_{j,B} + \mathcal{Q}_A^* v_{j,A} + 2U |\Psi_A|^2 v_{j,A} - U |\Psi_A|^2 u_{j,A} &= -E_j v_{j,A}, & (5.189)\\
i\hbar c_l \mathcal{D} v_{j,A} + \mathcal{Q}_B^* v_{j,B} + 2U |\Psi_B|^2 v_{j,B} - U |\Psi_B|^2 u_{j,B} &= -E_j v_{j,B}, & (5.190)
\end{aligned}$$

where we define

$$\mathcal{Q}_{A(B)} = \left[m - \mu - i\nabla S_{A(B)} \cdot \nabla + |\nabla S_{A(B)}| - i(\nabla^2 S_{A(B)}) \right]. \tag{5.191}$$

5.6 Energy Eigenvalues

Substituting for the plane wave condensate and quasi-particle states, Eqs. (5.187)-(5.190) become

$$
\begin{aligned}
(n_0U - E_k + \vec{q}\cdot\vec{k})C_{u_{\vec{k},A}} - \kappa^* C_{u_{\vec{k},B}} - n_0U C_{v_{\vec{k},A}} + (0)C_{v_{\vec{k},B}} &= 0\,, \quad (5.192)\\
-\kappa C_{u_{\vec{k},A}} + (n_0U - E_k + \vec{q}\cdot\vec{k})C_{u_{\vec{k},B}} + (0)C_{v_{\vec{k},A}} - n_0U C_{v_{\vec{k},B}} &= 0\,, \quad (5.193)\\
-n_0U C_{u_{\vec{k},A}} + (0)C_{u_{\vec{k},B}} + (n_0U + E_k - \vec{q}\cdot\vec{k})C_{v_{\vec{k},A}} - \kappa^* C_{v_{\vec{k},B}} &= 0\,, \quad (5.194)\\
(0)C_{u_{\vec{k},A}} - n_0U C_{u_{\vec{k},B}} - \kappa C_{v_{\vec{k},A}} + (n_0U + E_k - \vec{q}\cdot\vec{k})C_{v_{\vec{k},B}} &= 0\,, \quad (5.195)
\end{aligned}
$$

where for compactness we write $\kappa \equiv (k_x + ik_y)$. The coefficients of the complex amplitudes $C_{u_{\vec{k},A}}$, $C_{u_{\vec{k},B}}$, $C_{v_{\vec{k},A}}$, and $C_{v_{\vec{k},B}}$ form a 4x4 matrix whose determinant set equal to zero yields the four eigenvalues of the system: $E_k^{(1)}, E_k^{(2)}, E_k^{(3)}, E_k^{(4)}$. The possible presence of complex eigenvalues will determine the stability of the condensate with decay rates out of the condensate through the various modes being proportional to the magnitudes of the imaginary parts. We compute the determinant of the coefficient matrix

$$
\det\begin{pmatrix} E^- & -\kappa^* & -n_0U & 0 \\ -\kappa & E^- & 0 & -n_0U \\ -n_0U & 0 & E^+ & -\kappa^* \\ 0 & -n_0U & -\kappa & E^+ \end{pmatrix} = 0,\,, \quad (5.196)
$$

where we have used the short hand notation $E^{\pm} = \left[n_0U \pm (E_k - \vec{q}\cdot\vec{k})\right]$. Computing the determinant we obtain

$$
\begin{aligned}
&E^-\left[E^-(E^{+2} - \kappa^2) - E^+(n_0U)^2\right] + \kappa^*\left[-\kappa(E^{+2} - \kappa^2) - \kappa n_0U\right]\\
&-n_0U\left[\kappa^2 n_0U + E^-E^+ n_0U - (n_0U)^3\right] = 0\,, \quad (5.197)
\end{aligned}
$$

where we use the notation $\kappa^2 \equiv \kappa^*\kappa$. Multiplying this out gives

$$
E^{-2}E^{+2} - \kappa^2(E^{-2} + E^{+2}) - 2E^-E^+(n_0U)^2 - 2\kappa^2(n_0U)^2 + \kappa^4 + (n_0U)^4 = 0\,. \quad (5.198)
$$

To further simplify the calculation we define $E^{\pm} = (x \pm y)$, then Eq. (5.198) simplifies to

$$(x^2-y^2)^2-2\kappa^2(x^2+y^2)-2(n_0U)^2(x^2-y^2)-2\kappa^2(n_0U)^2+\kappa^4+(n_0U)^4=0\,. \quad (5.199)$$

Gathering quadratic and quartic terms in y,

$$\begin{aligned} &y^4+2\left[(n_0U)^2-x^2-\kappa^2\right]y^2 \\ &+\left[x^4-2\kappa^2x^2-2(n_0U)^2x^2-2\kappa^2(n_0U)^2+\kappa^4+(n_0U)^4\right]=0\,, \end{aligned} \quad (5.200)$$

and solving for y^2,

$$\begin{aligned} y^2=&-\left[(n_0U)^2-x^2-\kappa^2\right]\pm\left[(n_0U)^4+\kappa^4+x^4-2\kappa^2(n_0U)^2\right. \\ &\left.-2x^2(n_0U)^2+2\kappa^2x^2-x^4+2\kappa^2x^2+2x^2(n_0U)^2+2\kappa^2(n_0U)^2-\kappa^4-(n_0U)^4\right]^{1/2}. \end{aligned} \quad (5.201)$$

With $y=E_k-\vec{q}\cdot\vec{k}$ and $x=n_0U$, and the explicit definition of κ, the eigenvalues are

$$E_k=\vec{q}\cdot\vec{k}\pm\sqrt{k^2\pm 2n_0Uk}\,. \quad (5.202)$$

For reasons that we will discuss later, we will retain only the positive option that appears under the radical sign. Thus, the energy spectrum is

$$E_k=\vec{q}\cdot\vec{k}\pm\sqrt{k^2+2n_0Uk}\,. \quad (5.203)$$

Reinserting the dimensionful physical constants gives

$$E_k=c_l'\hbar\vec{q}\cdot\vec{k}\pm\sqrt{(c_l\hbar k)^2+n_0Uc_l\hbar k}\,, \quad (5.204)$$

or in keeping with the usual Bogoliubov notation found in the literature, we may write

$$E_k = (c_l'/c_l)\vec{q}\cdot\vec{\epsilon}_k^{\,0}\pm E_k^0\,, \quad (5.205)$$

$$E_k^0 = \sqrt{(\epsilon_k^0)^2+n_0g\epsilon_k^0}\,, \quad (5.206)$$

where $\epsilon_k^0 = c_l \hbar k$ is the single quasi-particle energy for zero interaction, E_k^0 is the quasi-particle energy for a static background,

$$c_l = \frac{\sqrt{3} t_h a}{2\hbar}, \tag{5.207}$$

$$c_l' = \frac{\sqrt{3} \tau a}{2\hbar}. \tag{5.208}$$

Recalling that c_l has dimensions of velocity while c_l' has dimensions of $m^2 \cdot s^{-1}$, since τ is an integral over the gradient instead of the Laplacian. The form of the energy changes from a linear dependence on k to a a dependence on $k^{1/2}$, the two regions separated by the condition $c_l \hbar k / n_0 U \approx 1$. From this we may define the modified coherence length as

$$\xi' = \frac{c_l \hbar}{n_0 U}. \tag{5.209}$$

5.7 Limits of Quasi-Particle Energy

1. Uniform background $q \to 0$. For the case of zero condensate momentum, $q = 0$, we obtain

$$E_k = \pm E_k^0 = \pm \sqrt{(c_l \hbar k)^2 + n_0 U c_l \hbar k}, \tag{5.210}$$

or,

$$E_k = \pm c_l \hbar k \left(1 + \frac{n_0 U}{c_l \hbar k}\right)^{1/2}. \tag{5.211}$$

We may examine the two limits: short wavelength, $k \ll \xi'^{-1}$, and long wavelength, $k \gg \xi'^{-1}$. In the short wavelength limit $E_k^{(\pm)} = \pm c_l \hbar k + n_0 U/2$. This is the expected result for particle like excitations, i.e., lattice potential but no contact interaction, shifted by a mean-field Hartree term for the interaction with the background condensate. For these excitations the momentum is too

large for the contact interaction to be noticed except in the form of a mean-field interaction. In the long wavelength limit, the second term dominates so that we obtain

$$E_k^{(\pm)} = \pm \xi'^{-1/2} k^{1/2}. \tag{5.212}$$

The first thing we notice is that the energy depends on momentum as $k^{1/2}$. These are low-energy collective modes; excitations just above the condensate energy.

2. Zero-interaction $n_0 U \to 0$. If we turn off the interaction, the quasi-particle energy reduces to

$$E_k = c_l' \hbar \vec{q} \cdot \vec{k} \pm c_l \hbar k \,. \tag{5.213}$$

These are excitations of the noninteracting condensate where the first term describes the anisotropy due to the motion of the condensate and the second term is the usual linear dispersion for the honeycomb lattice.

3. Zero-limit check of quasi-particle momentum $k \to 0$. If we set k to zero we should expect E_k to go to zero which is indeed the case.

5.7.1 Directional Behavior of the Energy

The dot product of $\vec{q}$ and $\vec{k}$ that appears in the energy is the counterpart of the term that appears in the Bogoliubov dispersion for a moving condensate. This term gives an anisotropic distribution for the energy for a particular direction determined by $\vec{q}$ and implies a stability critical angle θ_c. Some of these modes have negative energy so that the condensate may arbitrarily lower its energy through such emissions (these are usually called energetic instabilities in the literature.) The energy may be expressed in terms of the relative angle θ between $\vec{q}$ and $\vec{k}$

$$E_k = c_l' \hbar q k \cos\theta \pm \sqrt{(c_l \hbar k)^2 + n_0 U c_l \hbar k}\,, \tag{5.214}$$

where the critical angle may be obtained by setting the energy to zero for fixed $\vec{q}$ and $\vec{k}$. The energy may be expressed as

$$E_k = \hbar k \left[v\cos\theta \pm s(k) \right] , \tag{5.215}$$

where $v = \hbar c_l' q$ is the speed of the condensate and the momentum dependent "speed of light" is defined as

$$s(k) = c_l \sqrt{1 + \frac{n_0 U}{c_l \hbar k}}\,. \tag{5.216}$$

From this expression the two regimes are evident. In the "particle" regime ($k \gg n_0 U / c_l \hbar$) s reduces to the usual effective speed of light $s \approx c_l$ for a condensate in a honeycomb lattice. In the "phonon" regime ($k \ll n_0 U / c_l \hbar$) we have $s(k) \approx \sqrt{c_l n_0 U / \hbar k}$ (we have used quotations here since "particle" and "phonon" are more appropriate for the usual weakly interacting Bose gas where no lattice is present). For the first case, the energy is approximately

$$E_k \approx \hbar k \left(v\cos\theta \pm c_l \right). \tag{5.217}$$

Assuming a positive velocity for the condensate, we see that the sign of E_k depends on the direction of quasi-particle emission as well as whether the quasi-particle is a positive or negative energy excitation. For positive energy modes, the condensate is stable if

$$\frac{v}{c_l}\cos\theta + 1 \geq 0. \tag{5.218}$$

If $v < c_l$, positive energy modes are always stable regardless of the angle of emission. For $v \geq c_l$, there is a critical angle beyond which all positive modes are unstable determined by

$$\theta_c = \cos^{-1}(-c_l/v), \tag{5.219}$$

from which we can see that for the limiting case $v \gg c_l$, we have $\theta_c \approx \pi/2$ so that emission of positive modes in the half sphere in the backwards direction are unstable. When the condensate speed is equal to the speed of light, $v = c_l$, then we find $\theta_c \approx \pi$. This marks the onset of instability. Here only emissions in the opposite direction of $\vec{q}$ are unstable.

As one would expect, the situation is quite different in the case of negative energy excitations. The stability condition reads

$$\frac{v}{c_l}\cos\theta - 1 \geq 0. \tag{5.220}$$

First, we see that when $v < c_l$, all negative energy modes are unstable. For the case $v \geq c_l$, the energy is stable for certain angles with θ_c determined by

$$\theta_c = \cos^{-1}(c_l/v). \tag{5.221}$$

This condition is identical to the case of positive excitations except that now θ_c marks the onset of instability for a wider range of emission directions. For the limiting case $v \gg c_l$, we find $\theta_c = \pi/2$ where we see that for very large condensate speeds, emissions of negative energy modes in the forward directions are actually stable. For the case where $v = c_l$ we find that $\theta_c = 0$. This is marks the point where all negative energy modes become unstable.

5.8 Coherence Factors for Uniform Background

Now we compute the coefficients $C_{v_{\vec{k},A}}$ and $C_{v_{\vec{k},B}}$ for the simplest case where $\vec{q}=0$ by solving the system of equations

$$\begin{aligned}
(n_0U-E_k)C_{u_{\vec{k},A}}-\kappa^*C_{u_{\vec{k},B}}-n_0UC_{v_{\vec{k},A}}+(0)C_{v_{\vec{k},B}} &= 0\,, && (5.222)\\
-\kappa C_{u_{\vec{k},A}}+(n_0U-E_k)C_{u_{\vec{k},B}}+(0)C_{v_{\vec{k},A}}-n_0UC_{v_{\vec{k},B}} &= 0\,, && (5.223)\\
-n_0UC_{u_{\vec{k},A}}+(0)C_{u_{\vec{k},B}}+(n_0U+E_k)C_{v_{\vec{k},A}}-\kappa^*C_{v_{\vec{k},B}} &= 0\,, && (5.224)\\
(0)C_{u_{\vec{k},A}}-n_0U\,C_{u_{\vec{k},B}}-\kappa C_{v_{\vec{k},A}}+(n_0U+E_k)C_{v_{\vec{k},B}} &= 0\,. && (5.225)
\end{aligned}$$

For a particular choice of the normalization conditions, we have

$$\begin{aligned}
\int d^2r\left[u^*_{\vec{j},A}(\vec{r})u_{\vec{k},A}(\vec{r})-v^*_{\vec{j},A}(\vec{r})v_{\vec{k},A}(\vec{r})\right] &= \delta_{\vec{j},\vec{k}}\,, && (5.226)\\
\int d^2r\left[u^*_{\vec{j},B}(\vec{r})u_{\vec{k},B}(\vec{r})-v^*_{\vec{j},B}(\vec{r})v_{\vec{k},B}(\vec{r})\right] &= \delta_{\vec{j},\vec{k}}\,. && (5.227)
\end{aligned}$$

This implies for the coefficients

$$\begin{aligned}
|C_{u_{\vec{k},A}}|^2 &= 1+|C_{v_{\vec{k},A}}|^2\,, && (5.228)\\
|C_{u_{\vec{k},B}}|^2 &= 1+|C_{v_{\vec{k},B}}|^2\,. && (5.229)
\end{aligned}$$

In all we have six equations and eight unknowns (four complex coefficients). Writing the coefficients in terms of amplitude and phase and setting two of the phases to unity

$$\begin{aligned}
C_{u_{\vec{k},A}} &= |C_{u_{\vec{k},A}}|\,, && (5.230)\\
C_{u_{\vec{k},B}} &= |C_{u_{\vec{k},B}}|e^{i\phi_u}\,, && (5.231)\\
C_{v_{\vec{k},A}} &= |C_{u_{\vec{k},A}}|\,, && (5.232)\\
C_{v_{\vec{k},B}} &= |C_{u_{\vec{k},B}}|e^{i\phi_v}\,. && (5.233)
\end{aligned}$$

We must solve

$$
\begin{aligned}
(n_0U - E_k)|C_{u_{\vec{k},A}}| - \kappa^*|C_{u_{\vec{k},B}}|e^{i\phi_u} - n_0U|C_{v_{\vec{k},A}}| + (0)|C_{v_{\vec{k},B}}|e^{i\phi_v} &= 0, \quad (5.234)\\
-\kappa|C_{u_{\vec{k},A}}| + (n_0U - E_k)|C_{u_{\vec{k},B}}|e^{i\phi_u} + (0)|C_{v_{\vec{k},A}}| - n_0U|C_{v_{\vec{k},B}}|e^{i\phi_v} &= 0, \quad (5.235)\\
-n_0U|C_{u_{\vec{k},A}}| + (0)|C_{u_{\vec{k},B}}|e^{i\phi_u} + (n_0U + E_k)|C_{v_{\vec{k},A}}| - \kappa^*|C_{v_{\vec{k},B}}|e^{i\phi_v} &= 0, \quad (5.236)\\
(0)|C_{u_{\vec{k},A}}| - n_0U|C_{u_{\vec{k},B}}|e^{i\phi_u} - \kappa|C_{v_{\vec{k},A}}| + (n_0U + E_k)|C_{v_{\vec{k},B}}|e^{i\phi_v} &= 0. \quad (5.237)
\end{aligned}
$$

Adding Eqs. (5.234) and (5.236) gives

$$
-E_k|C_{u_{\vec{k},A}}| - \kappa^*|C_{u_{\vec{k},B}}|e^{i\phi_u} + E_k|C_{v_{\vec{k},A}}| - \kappa^*|C_{v_{\vec{k},B}}|e^{i\phi_v} = 0. \quad (5.238)
$$

Adding Eqs. (5.235) and (5.237) gives

$$
-\kappa|C_{u_{\vec{k},A}}| - E_k|C_{u_{\vec{k},B}}|e^{i\phi_u} - \kappa|C_{v_{\vec{k},A}}| + E_k|C_{v_{\vec{k},B}}|e^{i\phi_v} = 0. \quad (5.239)
$$

Regrouping terms in both equations gives

$$
\begin{aligned}
-\kappa^*(|C_{u_{\vec{k},B}}|e^{i\phi_u} + |C_{v_{\vec{k},B}}|e^{i\phi_v}) &= E_k|C_{u_{\vec{k},A}}| - E_k|C_{v_{\vec{k},A}}|, \quad (5.240)\\
-\kappa(|C_{u_{\vec{k},A}}| + |C_{v_{\vec{k},A}}|) &= E_k|C_{u_{\vec{k},B}}|e^{i\phi_u} - E_k|C_{v_{\vec{k},B}}|e^{i\phi_v}. \quad (5.241)
\end{aligned}
$$

Multiplying these equations gives

$$
\begin{aligned}
&k^2(|C_{u_{\vec{k},B}}|e^{i\phi_u} + |C_{v_{\vec{k},B}}|e^{i\phi_v})(|C_{u_{\vec{k},A}}| + |C_{v_{\vec{k},A}}|) =\\
&\left[E_k|C_{u_{\vec{k},A}}| - E_k|C_{v_{\vec{k},A}}|\right] \times \left[E_k|C_{u_{\vec{k},B}}|e^{i\phi_u} - E_k|C_{v_{\vec{k},B}}|e^{i\phi_v}\right]. \quad (5.242)
\end{aligned}
$$

The kinetic part of the Hamiltonian mixes A and B sublattice components so we are free to decouple the corresponding coefficients by taking

$$
\begin{aligned}
k(|C_{u_{\vec{k},A}}| + |C_{v_{\vec{k},A}}|) &= E_k|C_{u_{\vec{k},A}}| - E_k\,|C_{v_{\vec{k},A}}|, \quad (5.243)\\
k(|C_{u_{\vec{k},B}}|e^{i\phi_u} + |C_{v_{\vec{k},B}}|e^{i\phi_v}) &= E_k|C_{u_{\vec{k},B}}|e^{i\phi_u} - E_k|C_{v_{\vec{k},B}}|e^{i\phi_v}. \quad (5.244)
\end{aligned}
$$

Combining like terms gives

$$(E_k - k)|C_{u_{\vec{k},A}}| = (E_k + k)|C_{v_{\vec{k},A}}|\,, \tag{5.245}$$

$$(E_k - k)|C_{u_{\vec{k},B}}|e^{i(\phi_u - \phi_v)} = (E_k +, k)|C_{v_{\vec{k},B}}|\,. \tag{5.246}$$

Equating the phases on both sides gives $\phi_u = \phi_v \equiv \phi$. Squaring both sides of each equation and inserting the normalization constraints, we get

$$(E_k - k)^2(1 + |C_{v_{\vec{k},A}}|^2) = (E_k + k)^2|C_{v_{\vec{k},A}}|^2 \tag{5.247}$$

$$(E_k - k)^2(1 + |C_{v_{\vec{k},B}}|^2) = (E_k + k)^2|C_{v_{\vec{k},B}}|^2, \tag{5.248}$$

which yields the solutions

$$|C_{v_{\vec{k},A}}| = \frac{(E_k - k)}{2(E_k k)^{1/2}}\,, \tag{5.249}$$

$$|C_{u_{\vec{k},A}}| = (1 + |C_{v_{\vec{k},A}}|^2)^{1/2}\,, \tag{5.250}$$

$$= \frac{(E_k + k)}{2\,(E_k k)^{1/2}}\,, \tag{5.251}$$

with identical solutions for the B sublattice. Inserting the dimensionful constants, we may label the energy eigenvalues by

$$E_k^{(+)} = +\sqrt{(\hbar c_l \hbar\, k)^2 + n_0 U c_l \hbar k} = +\,E_k^0\,, \tag{5.252}$$

$$E_k^{(-)} = -\sqrt{(\hbar c_l \hbar\, k)^2 + n_0 U c_l \hbar k} = -\,E_k^0\,, \tag{5.253}$$

and we define

$$C^{(\pm,\pm)} = \frac{(E_k^{(\pm)} \pm c_l \hbar k)}{2(E_k^{(\pm)} c_l \hbar k)^{1/2}}\,, \tag{5.254}$$

$$\mathbf{w} = \begin{pmatrix} 1 \\ e^{i\phi} \end{pmatrix}. \tag{5.255}$$

Then the quasi-particle states are

$$\mathbf{u}_{\vec{k}}^{(++)}(\vec{r}) = A^{-1/2}C^{(++)}e^{i\vec{k}\cdot\vec{r}}\mathbf{w}, \quad \mathbf{v}_{\vec{k}}^{(++)}(\vec{r}) = A^{-1/2}C^{(-+)}e^{i\vec{k}\cdot\vec{r}}\mathbf{w}, \quad (5.256)$$

$$\mathbf{u}_{\vec{k}}^{(-+)}(\vec{r}) = A^{-1/2}C^{(-+)}e^{i\vec{k}\cdot\vec{r}}\mathbf{w}, \quad \mathbf{v}_{\vec{k}}^{(-+)}(\vec{r}) = A^{-1/2}C^{(++)}e^{i\vec{k}\cdot\vec{r}}\mathbf{w}, \quad (5.257)$$

$$\mathbf{u}_{\vec{k}}^{(+-)}(\vec{r}) = A^{-1/2}C^{(+-)}e^{i\vec{k}\cdot\vec{r}}\mathbf{w}, \quad \mathbf{v}_{\vec{k}}^{(+-)}(\vec{r}) = A^{-1/2}C^{(--)}e^{i\vec{k}\cdot\vec{r}}\mathbf{w}, \quad (5.258)$$

$$\mathbf{u}_{\vec{k}}^{(--)}(\vec{r}) = A^{-1/2}C^{(--)}e^{i\vec{k}\cdot\vec{r}}\mathbf{w}, \quad \mathbf{v}_{\vec{k}}^{(--)}(\vec{r}) = A^{-1/2}C^{(+-)}e^{i\vec{k}\cdot\vec{r}}\mathbf{w}. \quad (5.259)$$

The phase angle ϕ still must be determined from Eqs. (5.234)-(5.237). It is left to determine the correct interpretation of the signs that occur in the eigenvalues since these will determine the types of instabilities present in our system. Let us examine our results for the coherence factors satisfying positive normalization conditions. In this case we take the positive forms of E_k and we have

$$|C_{u_{\vec{k},A}}|^2 = \frac{(E_k^0 + c_l\hbar k)^2}{4E_k^0 c_l\hbar k} = \frac{\left(1+\sqrt{1+n_0U/c_l\hbar k}\right)^2}{4\sqrt{1+n_0U/c_l\hbar k}}, \quad (5.260)$$

$$|C_{v_{\vec{k},A}}|^2 = \frac{(E_k^0 - c_l\hbar k)^2}{4E_k^0 c_l\hbar k} = \frac{\left(1-\sqrt{1+n_0U/c_l\hbar k}\right)^2}{4\sqrt{1+n_0U/c_l\hbar k}}, \quad (5.261)$$

and identical expressions for the B sublattice coherence factors. For the particular normalization that we have solved for, we may show by simple expansions the limiting forms

$$\xi k \to \infty \implies |C_{u_{\vec{k},A}}|^2 \approx 1\,,\ |C_{v_{\vec{k},A}}|^2 \approx (16\xi^2k^2)^{-1} \ll 1\,. \quad (5.262)$$

In the short wavelength limit the quasi-particle operators are mostly particle with the hole component being almost zero. In the long wavelength limit we obtain

$$\xi k \to 0 \implies |C_{u_{\vec{k},A}}|^2 \approx |C_{v_{\vec{k},A}}|^2 \approx (\sqrt{16\xi k})^{-1}\,. \quad (5.263)$$

Thus, we see that both coefficients are large so that, for long wavelengths, the quasi-particle operators consist of nearly equal mixtures of particle and hole components.

5.9 Interacting Ground-State

The interacting ground state is a complicated mixture of noninteracting particle and hole states as displayed by the fact that it is annihilated by the sublattice quasi-particle destruction operators

$$\hat{\alpha}_k \mid \Phi\rangle = \hat{\beta}_k \mid \Phi\rangle = 0\,. \tag{5.264}$$

Recalling the fully expanded diagonalized Hamiltonian

$$\begin{aligned}
\hat{H} &= \int d^2r \left[ic_l \Psi_A^*(\vec{r})(\partial_x + i\partial_y)\Psi_B(\vec{r}) + ic_l \Psi_B^*(\vec{r})(\partial_x - i\partial_y)\Psi_A(\vec{r})\right. \\
&+ \left.\frac{U}{2}\left|\Psi_A(\vec{r})\right|^4 + \frac{U}{2}\left|\Psi_B(\vec{r})\right|^4\right] \\
&- {\sum_j}' \int d^2r \left\{E_j^{(+)}\left[|C_{v_{\vec{k},A}}^{(+)}|^2 + |C_{v_{\vec{k},B}}^{(+)}|^2\right] + E_j^{(-)}\left[|C_{v_{\vec{k},A}}^{(-)}|^2 + |C_{v_{\vec{k},B}}^{(-)}|^2\right]\right\} \\
&+ {\sum_j}' \left[E_j^{(+)}\hat{c}_j^{(+)\dagger}\hat{c}_j^{(+)} + E_j^{(-)}\hat{c}_j^{(-)\dagger}\hat{c}_j^{(-)}\right].
\end{aligned} \tag{5.265}$$

The first and second lines are the mean-field condensate energy, the second line is the first order correction from the contact interactions, and the third line is the quasi-particle contribution to the total energy where the $\hat{c}_j$ operators are superpositions of the $\hat{\alpha}_j$ and $\hat{\beta}_j$ operators. We can obtain the ground-state energy for the case of a uniform background ($\vec{q} = 0$) by computing the expectation value of $\hat{H}$ with respect to the quasi-particle ground-state $\mid \Phi\rangle$,

$$\begin{aligned}
E_g &= \langle \Phi \mid \hat{H} \mid \Phi \rangle \\
&= \frac{U}{4}n_0^2 A - {\sum_k}' \left\{E_k^{(+)}\left[|C_{v_{\vec{k},A}}^{(+)}|^2 + |C_{v_{\vec{k},B}}^{(+)}|^2\right] + E_k^{(-)}\left[|C_{v_{\vec{k},A}}^{(-)}|^2 + |C_{v_{\vec{k},B}}^{(-)}|^2\right]\right\},
\end{aligned} \tag{5.266}$$

where $n_0 = n_{0,A} + n_{0,B}$ is the total condensate particle density and A is the area of the system. Then,

$$
\begin{aligned}
E_g &= \frac{1}{4}Un_0^2A - \sum_k{}' 2\left[E_k^0\frac{(E_k^0 - c_l\hbar k)^2}{4E_k^0 c_l\hbar k} + (-E_k^0)\frac{(-E_k^0 - c_l\hbar k)^2}{4(-E_k^0)c_l\hbar k}\right] \\
&= \frac{1}{4}Un_0^2A - \frac{1}{2}\sum_k{}'\left[\frac{2E_k^{0\,2} + 2(c_l\hbar k)^2}{c_l\hbar\, k}\right] \\
&= \frac{1}{4}Un_0^2A - \sum_k{}'\left(2c_l\hbar\, k + n_0U\right) \\
&= \frac{1}{4}Un_0^2A - \sum_k{}'\left(2\,\epsilon_k^0 + n_0U\right). \qquad (5.267)
\end{aligned}
$$

5.10 General Properties of the RLSE, Quasi-Particle States, and Energies

In the Bogoliubov result for a weakly interacting Bose gas, we require the energies E_k to be positive, reflecting the fact that we are perturbing off of a many-body state that is essentially a single-particle Schrödinger wave function governed by a with positive-definite Hamiltonian. Thus, when interpreting the symmetry inherent in the BDG equations, namely that for states u and v with positive energy E_k and positive norm, there exist negative norm states u^* and v^* with energy $-E_k$, it is clear that we must artificially remove the negative energy states from the spectrum based on the physical grounds. In our case, we do not start from a positive-definite theory. The kinetic part of the massless Dirac Hamiltonian of course allows for both positive and negative energy solutions. In its original field theory context, the combination of relativity and quantum mechanics allows for the creation of particle-antiparticle pairs, even without introducing the additional gauge structure of electromagnetic interactions. These quantum fluctuations of the vacuum manifest in an apparently problematic way. When we go to calculate the energy of the vacuum, we encounter a sum over an infinite tower of harmonic oscillators. This diverges with an overall negative sign (from the anti-commutation of the fermion fields while commutation rules in the scalar field theory gives an overall positive divergence). The way out of this is that we agree that all processes are measured relative to the vacuum so that

we simply subtract off the infinite energy of the vacuum. In the case of a system of fermions in the non-relativistic many-body problem, the stability of the ground state is supplied by the Pauli exclusion principle in the form of a Fermi surface.

5.11 Symmetries of the RLSE

Our problem is fundamentally different. We have an ultracold Bose gas that resides mostly in a single-particle Bloch-state at the Dirac point of a honeycomb optical lattice. The true ground state of the system has negative energy measured with respect to the Dirac point and is essentially a Bloch state with zero lattice momentum. This is the lowest point on the conduction band. What happens when a Bose gas is condensed at the corner of the Brillouin zone (the Dirac point)? Here the conduction and valence bands meet. The energies of small fluctuations here are measured relative to the bulk of the condensate and must allow for negative (energy lowering) as well as positive (energy raising) modes since these describe atoms that transition to Bloch states with lattice momentum slightly less than and greater than (respectively) the Dirac point. This means that we must include the states with negative energy and then ask how this affects our interpretation of the normalization condition. We demonstrate a symmetry of the linear stability equations in the following way. First, taking the complex conjugate of the equations gives

$$
\begin{aligned}
-i\hbar c_l \mathcal{D} u^*_{j,B} + \mathcal{Q}^*_A u^*_{j,A} + 2U\left|\Psi_A\right|^2 u^*_{j,A} - U\left|\Psi_A\right|^2 v^*_{j,A} &= E_j u^*_{j,A}\,, && (5.268)\\
-i\hbar c_l \mathcal{D}^* u^*_{j,A} + \mathcal{Q}^*_B u^*_{j,B} + 2U\left|\Psi_B\right|^2 u^*_{j,B} - U\left|\Psi_B\right|^2 v^*_{j,B} &= E_j u^*_{j,B}\,, && (5.269)\\
-i\hbar c_l \mathcal{D} v^*_{j,B} + \mathcal{Q}_A v^*_{j,A} + 2U\left|\Psi_A\right|^2 v^*_{j,A} - U\left|\Psi_A\right|^2 u^*_{j,A} &= -E_j\, v^*_{j,A}\,, && (5.270)\\
-i\hbar c_l \mathcal{D}^* v^*_{j,A} + \mathcal{Q}_B v^*_{j,B} + 2U\left|\Psi_B\right|^2 v^*_{j,B} - U\left|\Psi_B\right|^2 u^*_{j,B} &= -E_j v^*_{j,B}\,. && (5.271)
\end{aligned}
$$

Next, transposing the equations and applying a parity inversion $x \to -x$, $y \to -y$,

$$
\begin{aligned}
i\hbar c_l \mathcal{D}^* v^*_{j,A} + \mathcal{Q}_B v^*_{j,B} + 2U\left|\Psi_B\right|^2 v^*_{j,B} - U\left|\Psi_B\right|^2 u^*_{j,B} &= -E_j v^*_{j,B}\,, && (5.272)\\
i\hbar c_l \mathcal{D} v^*_{j,B} + \mathcal{Q}_A v^*_{j,A} + 2U\left|\Psi_A\right|^2 v^*_{j,A} - U\left|\Psi_A\right|^2 u^*_{j,A} &= -E_j v^*_{j,A}\,, && (5.273)\\
i\hbar c_l \mathcal{D}^* u^*_{j,A} + \mathcal{Q}^*_B u^*_{j,B} + 2U\left|\Psi_B\right|^2 u^*_{j,B} + U\left|\Psi_B\right|^2 v^*_{j,B} &= E_j u^*_{j,B}\,, && (5.274)\\
i\hbar c_l \mathcal{D} u^*_{j,B} + \mathcal{Q}^*_A u^*_{j,A} + 2U\left|\Psi_A\right|^2 u^*_{j,A} - U\left|\Psi_A\right|^2 v^*_{j,A} &= E_j u^*_{j,A}\,.. && (5.275)
\end{aligned}
$$

Finally, exchanging A and B sublattice labels along with the field redefinitions

$$
\begin{aligned}
u'_{j,B} &= v^*_{j,A}\,, && (5.276)\\
u'_{j,A} &= v^*_{j,B}\,, && (5.277)\\
v'_{j,B} &= u^*_{j,A}\,, && (5.278)\\
v'_{j,A} &= u^*_{j,B}\,, && (5.279)
\end{aligned}
$$

we obtain

$$
\begin{aligned}
i\hbar c_l \mathcal{D}^* u'_{j,B} + \mathcal{Q}_A u'_{j,A} + 2U\left|\Psi_A\right|^2 u'_{j,A} - U\left|\Psi_A\right|^2 v'_{j,A} &= E'_j u'_{j,A}\,, && (5.280)\\
i\hbar c_l \mathcal{D} u'_{j,A} + \mathcal{Q}_B u'_{j,B} + 2U\left|\Psi_B\right|^2 u'_{j,B} - U\left|\Psi_B\right|^2 v'_{j,B} &= E'_j u_{j,B}\,, && (5.281)\\
i\hbar c_l \mathcal{D}^* v'_{j,B} + \mathcal{Q}^*_A v'_{j,A} + 2U\left|\Psi_A\right|^2 v'_{j,A} - U\left|\Psi_A\right|^2 u'_{j,A} &= -E'_j v'_{j,A}\,, && (5.282)\\
i\hbar c_l \mathcal{D} v'_{j,A} + \mathcal{Q}^*_B v'_{j,B} + 2U\left|\Psi_B\right|^2 v'_{j,B} - U\left|\Psi_B\right|^2 u'_{j,B} &= -E'_j v'_{j,B}, && (5.283)
\end{aligned}
$$

where we define the new energy as $E'_j \equiv -E_j$. These equations are identical to the original ones except that the sign of the energy is flipped. This is positive/negative energy symmetry for the space of excitations and (unlike the BDG problem) here must be respected since we are measuring energy relative to the Dirac point as previously discussed. For the simple case of a plane wave background, this is the obvious result that inverting the direction of positive momentum Dirac-like particles (the parity inversion in the derivative terms) yields the negative energy branch of the spectrum.

5.12 Normalization of Quasi-Particle States

The normalization for the positive and negative energy solutions may be derived from the linear stability equations. Beginning with Eq. (5.188), we multiply through

by $u^*_{k,B}$,

$$\begin{aligned} & iu^*_{k,B}\mathcal{D}u_{k,A} + \mathcal{Q}_B u^*_{k,B}u_{j,B} + 2U\left|\Psi_B\right|^2 u^*_{k,B}u_{j,B} - U\left|\Psi_B\right|^2 u^*_{k,B}v_{j,B} \\ & = E_j u^*_{k,B}u_{j,B}. \end{aligned} \tag{5.284}$$

Next, we take the complex conjugate and exchange j and k indices which yields

$$\begin{aligned} & -iu_{j,B}\mathcal{D}^*u^*_{k,A} + \mathcal{Q}^*_B u_{j,B}u^*_{k,B} + 2U\left|\Psi_B\right|^2 u_{j,B}u^*_{k,B} - U\left|\Psi_B\right|^2 u_{j,B}v^*_{k,B} \\ & = E^*_k u_{j,B}u^*_{k,B}, \end{aligned} \tag{5.285}$$

where we have allowed the possibility that the energy is complex. Subtracting Eq. (5.285) from Eq. (5.284) and integrating over the plane gives

$$\begin{aligned} & i\int d^2r\left(u^*_{k,B}\mathcal{D}u_{k,A} + u_{j,B}\mathcal{D}^*u^*_{k,A}\right) + (Q_B - Q^*_B)\int d^2r u^*_{k,B}u_{j,B} \\ + \; & U\int d^2r\cdot\left|\Psi_B\right|^2\left(u_{j,B}v^*_{k,B} - u^*_{k,B}v_{j,B}\right) = (E_j - E^*_k)\int d^2r u^*_{k,B}u_{j,B}. \end{aligned} \tag{5.286}$$

Following the same steps for Eq. (5.190) yields a similar equation

$$\begin{aligned} - \; & i\int d^2r\left(v^*_{k,B}\mathcal{D}v_{k,A} + v_{j,B}\mathcal{D}^*v^*_{k,A}\right) + (Q_B - Q^*_B)\int d^2r v^*_{k,B}v_{j,B} \\ + \; & U\int d^2r\left|\Psi_B\right|^2\left(u_{j,B}v^*_{k,B} - u^*_{k,B}v_{j,B}\right) = (E_j - E^*_k)\int d^2r v^*_{k,B}v_{j,B}. \end{aligned} \tag{5.287}$$

Subtracting these two results and taking $\nabla^2 S = 0$, we get

$$\begin{aligned} i \; & \int d^2r\left(u^*_{k,B}\mathcal{D}\mathcal{Q}_A u_{k,A} + u_{j,B}\mathcal{D}^*\mathcal{Q}^*_A u^*_{k,A} + v^*_{k,B}\mathcal{D}\mathcal{Q}_A v_{k,A} + v_{j,B}\mathcal{D}^*\mathcal{Q}^*_A v^*_{k,A}\right) \\ = \; & (E_j - E^*_k)\int d^2r\left(u^*_{k,B}u_{j,B} - v^*_{k,B}v_{j,B}\right). \end{aligned} \tag{5.288}$$

A similar equation is obtained by manipulating Eq. (5.187) and Eq. (5.189)

$$\begin{aligned} i \; & \int d^2r\left(u^*_{k,A}\mathcal{D}^*\mathcal{Q}^*_B u_{k,B} + u_{j,A}\mathcal{D}\mathcal{Q}_B u^*_{k,B} + v^*_{k,A}\mathcal{D}^*\mathcal{Q}^*_B v_{k,B} + v_{j,A}\mathcal{D}\mathcal{Q}_B v^*_{k,B}\right) \\ = \; & (E_j - E^*_k)\int d^2r\left(u^*_{k,A}u_{j,A} - v^*_{k,A}v_{j,A}\right). \end{aligned} \tag{5.289}$$

Adding these equations gives

$$\begin{aligned} & i \int d^2r \left(u^*_{k,A}\mathcal{D}^*\mathcal{Q}^*_B u_{k,B} + u_{j,A}\mathcal{D}\mathcal{Q}_B u^*_{k,B} + v^*_{k,A}\mathcal{D}^*\mathcal{Q}^*_B v_{k,B} + v_{j,A}\mathcal{D}\mathcal{Q}_B v^*_{k,B}\right) \\ + \; & i \int d^2r \left(u^*_{k,A}\mathcal{D}^*\mathcal{Q}^*_B u_{k,B} + u_{j,A}\mathcal{D}\mathcal{Q}_B u^*_{k,B} + v^*_{k,A}\mathcal{D}^*\mathcal{Q}^*_B v_{k,B} + v_{j,A}\mathcal{D}\mathcal{Q}_B v^*_{k,B}\right) \\ = \; & (E_j - E^*_k) \int d^2r \left(u^*_{k,A}u_{j,A} - v^*_{k,A}v_{j,A} + u^*_{k,B}u_{j,B} - v^*_{k,B}v_{j,B}\right). \end{aligned} \tag{5.290}$$

By using properties of the derivative terms, the left hand side can be made to vanish so that we may write

$$(E_j - E^*_k) \int d^2r \left(u^*_{k,A}u_{j,A} - v^*_{k,A}v_{j,A} + u^*_{k,B}u_{j,B} - v^*_{k,B}v_{j,B}\right) = 0. \tag{5.291}$$

This is the expected normalization condition similar to the BDG case.

5.13 Positive and Negative Energy States: Lattice Versus Interaction Effects

In our problem, the number of possible states is expanded since the normalization couples A and B states. For nonzero normalization constant, we see that by setting $j = k$, the energy must be real and the normalization condition can be expressed as

$$\int d^2r \left(u^*_{k,A}u_{j,A} - v^*_{k,A}v_{j,A} + u^*_{k,B}u_{j,B} - v^*_{k,B}v_{j,B}\right) = \delta_{jk}. \tag{5.292}$$

In order for the quasi-particle operator to obey the usual Bose commutation relations (as we have already seen), we are allowed *positive* as well as *negative* energy solutions provided the normalization constant for these states is *positive* and *negative* respectively. The presence of negative norm states introduces no physical inconsistency but a minor reinterpretation of the Fourier components is needed. Requiring Bosonic commutation rules for the quasi-particle part of the wavefunction forces the condition

$$\left(|u_j|^2 - |v_j|^2\right)\left[\hat{\alpha}_j, \hat{\alpha}^\dagger_j\right] = 1. \tag{5.293}$$

If we take $(|u_j|^2 - |v_j|^2) = -1$, this forces $\left[\hat{\alpha}_j, \hat{\alpha}_j^\dagger\right] = -1$ or, $\left[\hat{\alpha}_j^\dagger, \hat{\alpha}_j\right] = 1$ so that we must interpret $\hat{\alpha}_j^\dagger$ and $\hat{\alpha}_j$ as the *destruction* and *creation* operators, respectively, for a Boson (quasi-hole) with momentum $-j$ which are of course the negative energy states of our theory. Thus, for negative energy states, we require that

$$\int d^2r \left(u_{k,A}^* u_{j,A} - v_{k,A}^* v_{j,A} + u_{k,B}^* u_{j,B} - v_{k,B}^* v_{j,B}\right) = -\delta_{jk}. \tag{5.294}$$

Since excitations of the two sublattices are not normalized independently, as seen in Eq. (5.292) and Eq. (5.294), there exists the possibility for solutions that appear as holes in one sublattice and particles in the other while the total energy is fixed positive or negative. To elaborate on this, the fact that Eq. (5.292) shows that sublattice amplitudes are not independently normalized, means that the amplitudes u and v for one of the sublattices, say B, may appear as a hole (negative normalization for that sublattice)

$$\int d^2r \left(u_{k,B}^* u_{j,B} - v_{k,B}^* v_{j,B}\right) = -\delta_{jk}\,, \tag{5.295}$$

forcing the other two amplitudes (for the A sublattice) to be positively normalized but multiplied by a factor of 2:

$$\int d^2r \left(u_{k,A}^* u_{j,A} - v_{k,A}^* v_{j,A}\right) = 2\delta_{jk}\,. \tag{5.296}$$

This means that for positive E_j (quasi-particle propagation), one sublattice may appear to support *two quasi-particles* while the other sublattice supporting *one quasi-hole.* There also exists the possibility of zero norm states in which case the energy may be *complex.* Some representative characteristics of the possible states are summarized in Table 5.1 and Table 5.2 below.

subnorms	character	amplitudes	$\hbar c_l k \gg U$	$\hbar c_l k \ll U$
$--$	hole/hole	$\lvert u_{k,A}\rvert < \lvert v_{k,A}\rvert$	$u_{k,A} \approx 1, v_{k,A} \approx 0$	$u_{k,A} \approx v_{k,A}$
		$\lvert u_{k,B}\rvert < \lvert v_{k,B}\rvert$	$u_{k,B} \approx 1, v_{k,B} \approx 0$	$u_{k,B} \approx v_{k,B}$
$+-$	particle/hole	$\lvert u_{k,A}\rvert > \lvert v_{k,A}\rvert$		
		$\lvert u_{k,B}\rvert < \lvert v_{k,B}\rvert$		
-0	hole/undet	$\lvert u_{k,A}\rvert < \lvert v_{k,A}\rvert$		
		$\lvert u_{k,B}\rvert = \lvert v_{k,B}\rvert$		

Table 5.1: Character of Negative Norm Excitations. The dots indicate that the same condition applies as in the previous line.

subnorms	character	amplitudes	$c_l \hbar k \gg U$	$c_l \hbar k \ll U$
$++$	particle/particle	$\lvert u_{k,A}\rvert > \lvert v_{k,A}\rvert$	$u_{k,A} \approx 1, v_{k,A} \approx 0$	$u_{k,A} \approx v_{k,A}$
		$\lvert u_{k,B}\rvert > \lvert v_{k,B}\rvert$	$u_{k,B} \approx 1, v_{k,B} \approx 0$	$u_{k,B} \approx v_{k,B}$
$+-$	particle/hole	$\lvert u_{k,A}\rvert > \lvert v_{k,A}\rvert$		
		$\lvert u_{k,B}\rvert < \lvert v_{k,B}\rvert$		
$+0$	particle/undet	$\lvert u_{k,A}\rvert > \lvert v_{k,A}\rvert$		
		$\lvert u_{k,B}\rvert = \lvert v_{k,B}\rvert$		

Table 5.2: Character of Positive Norm Excitations. The dots indicate that the same condition applies as in the previous line.

5.14 Analytical Solutions of the RLSE for Arbitrary Vortex Background

In plane polar coordinates, the RLSE reduce to the system

$$i\,\hbar c_l\, e^{-i\theta}(\partial_r - i\frac{1}{r}\partial_\theta)u_{j,B} + (m-\mu)u_{j,A} + U|\Psi_A|^2(2u_{j,A} - v_{j,A}) = E_j u_{j,A}\,, \quad (5.297)$$

$$i\,\hbar c_l\, e^{i\theta}(\partial_r + i\frac{1}{r}\partial_\theta)u_{j,A} + (m-\mu)u_{j,B} + U|\Psi_b|^2(2u_{j,B} - v_{j,B}) = E_j u_{j,B}\,, \quad (5.298)$$

$$i\,\hbar c_l\, e^{-i\theta}(\partial_r - i\frac{1}{r}\partial_\theta)v_{j,B} + (m-\mu)v_{j,A} + U|\Psi_A|^2(2v_{j,A} - u_{j,A}) = -E_j v_{j,A}\,, \quad (5.299)$$

$$i\,\hbar c_l\, e^{i\theta}(\partial_r + i\frac{1}{r}\partial_\theta)v_{j,A} + (m-\mu)v_{j,B} + U|\Psi_B|^2(2v_{j,B} - u_{j,B}) = -E_j v_{j,B}\,. \quad (5.300)$$

We make an observation regarding the form of the solution that we seek. From a classical point of view, small fluctuations of the vortex correspond to small displacements which can be computed by taking the dot product of a variation of the coordinates with the gradient of the condensate wavefunction. The small classical variations that we obtain in this way can then be converted to quantum fluctuations by reinterpreting their amplitudes as operators. For Ψ_A we get

$$\begin{aligned}
\delta\Psi_A &= \delta\vec{r}\cdot\vec{\nabla}\Psi_A && (5.301)\\
&\sim (\delta r\hat{r} + \delta\theta\hat{\theta})\cdot(\hat{r}\partial_r + \hat{\theta}\frac{\partial_\theta}{r})(e^{-i\theta}F_0) && (5.302)\\
&\sim (\delta r\hat{r} + \delta\theta\hat{\theta})\cdot(\frac{dF_0}{dr}\hat{r} - i\,\frac{F_0}{r}\hat{\theta}) && (5.303)\\
&\sim \frac{dF_0}{dr}\delta r - i\,\frac{F_0}{r}\delta\theta. && (5.304)
\end{aligned}$$

To reproduce actual fluctuations of the condensate we should allow for positive as well as negative coordinate variations in Eq. (5.304) so that another form would be

$$\delta\Psi_A \sim \frac{dF_0}{dr}\delta r + i\,\frac{F_0}{r}\delta\theta. \quad (5.305)$$

To obtain a finite angular momentum fluctuation for Ψ_B we must temporarily include a nonzero angular dependence which we set to zero at the end. Apart from a

normalization factor we expect the following quasi-particle radial functions

$$\text{for } \Psi_A: \qquad f_{A1} = \frac{dF_0}{dr} - i\frac{F_0}{r}, \quad f_{A2} = \frac{dF_0}{dr} + i\frac{F_0}{r}, \tag{5.306}$$

$$\text{for } \Psi_B: \qquad f_{B1} = \frac{dG_0}{dr} - i\frac{G_0}{r}, \quad f_{B2} = \frac{dG_0}{dr} + i\frac{G_0}{r}. \tag{5.307}$$

We may construct the following solutions from these

$$f_A^- = f_{A1} - f_{A2} = -2\,i\frac{F_0}{r}, \tag{5.308}$$

$$f_A^+ = f_{A1} + f_{A2} = 2\frac{dF_0}{dr}, \tag{5.309}$$

$$f_B^- = f_{B1} - f_{B2} = -2\,i\frac{G_0}{r}, \tag{5.310}$$

$$f_B^+ = f_{B1} + f_{B2} = 2\frac{dG_0}{dr}. \tag{5.311}$$

As we have previously discussed, f_A^- and f_B^- describe modes that are associated with fluctuations in the phase of the vortex and f_A^+ and f_B^-+ are associated with fluctuations in the number density.

Next, we eliminate the angular dependence in the same way as for the condensate wavefunction except that now we have to sum over all allowed quasi-particle angular momenta measured relative to the condensate angular momentum which has $l = -1$ for the upper spinor component and $l = 0$ for the lower one. We choose the general structure for quasi-particle states as follows

$$u_{\vec{k},A}(\vec{r}) = A^{-1/2} C_{u_{\vec{k},A}} e^{i(l-1)\theta} f_{u_{k,A}}(r), \tag{5.312}$$

$$u_{\vec{k},B}(\vec{r}) = A^{-1/2}\, C_{u_{\vec{k},B}} e^{il\theta} f_{u_{k,B}}(r), \tag{5.313}$$

$$v_{\vec{k},A}(\vec{r}) = A^{-1/2}\, C_{v_{\vec{k},A}} e^{i(l-1)\theta} f_{v_{k,A}}(r), \tag{5.314}$$

$$v_{\vec{k},B}(\vec{r}) = A^{-1/2}\, C_{v_{\vec{k},B}} e^{il\theta} f_{v_{k,B}}(r). \tag{5.315}$$

Substituting these into the equations of motion gives

$$i\hbar c_l C_{u_{k,B}} \left(\frac{d}{dr} + \frac{l}{r}\right) f_{u_{k,B}} + C_{u_{k,A}}(m-\mu) f_{u_{k,A}}$$
$$+U|\Psi_A|^2(2C_{u_{k,A}} f_{u_{k,A}} - C_{v_{k,A}} f_{v_{k,A}}) = E_k C_{u_{k,A}} f_{u_{k,A}}\,, \tag{5.316}$$

$$i\hbar c_l C_{u_{k,A}} \left(\frac{d}{dr} + \frac{1-l}{r}\right) f_{u_{k,A}} + C_{u_{k,B}}(m-\mu) f_{u_{k,B}}$$
$$+U|\Psi_B|^2(2C_{u_{k,B}} f_{u_{k,B}} - C_{v_{k,B}} f_{v_{k,B}}) = E_k C_{u_{k,B}} f_{u_{k,B}}\,, \tag{5.317}$$

$$i\hbar c_l C_{v_{k,B}} \left(\frac{d}{dr} + \frac{l}{r}\right) f_{v_{k,B}} + C_{v_{k,A}}(m-\mu) f_{v_{k,A}}$$
$$+U|\Psi_A|^2(2C_{k,A} f_{v_{k,A}} - C_{u_{k,A}} f_{u_{k,A}}) = -E_k C_{v_{k,A}} f_{v_{k,A}}\,, \tag{5.318}$$

$$i\hbar c_l C_{u_{k,A}} \left(\frac{d}{dr} + \frac{1-l}{r}\right) f_{v_{k,A}} + C_{v_{k,B}}(m-\mu) f_{v_{k,B}}$$
$$+U\ |\Psi_B|^2(2C_{v_{k,B}} f_{v_{k,B}} - C_{u_{k,B}} f_{u_{k,B}}) = -E_k C_{v_{k,B}} f_{v_{k,B}}\,. \tag{5.319}$$

To determine the characteristic energies of this system we can examine the equations in the limit $r \to \infty$ since here they simplify considerably. We seek a solution for $r \to \infty$ so that generically we have $|\Psi_A|^2 \approx n_0(1 - 1/\xi^2)$ and $|\Psi_B|^2 \approx n_0/\xi^2$. Taking the complex conjugate of Eq. (5.318) and subtracting it from Eq. (5.316), while doing the same with Eqs. (5.319) and (5.317), and transforming to dimensionless variables, we obtain

$$i\,\hbar c_l \left(\frac{d}{d\xi} + \frac{l}{\xi}\right) f_B^- - f_A^- + 3(1 - 1/\xi^2) f_A^- \;=\; \epsilon_k f_A^+\,, \tag{5.320}$$

$$i\,\hbar c_l \left(\frac{d}{d\xi} + \frac{1-l}{\xi}\right) f_A^- - f_B^- + 3(1/\xi^2) f_B^- \;=\; \epsilon_k f_B^+, \tag{5.321}$$

where we have replaced the energy by $\epsilon_k = E_k/n_0 U$. Here we note that $\epsilon_k \ll 1$, since the quasi-particle energy is far less than the mean-field interaction energy of the condensate. We want to retain terms that are lowest order in $1/\xi$ which means that the derivative terms and the terms proportional to $1/\xi$ remain and we can throw away the $1/\xi^2$ terms that come from the condensate wavefunctions. In the similar derivation

that occurs for the non-lattice version of this problem, i.e., where the condensate is in a single-particle wavefunction that satisfies the nonlinear Schrödinger equation and the associated Bogoliubov-de Gennes equations are second order pde's, the $1/\xi^2$ terms from the condensate must remain in the equations so that the correct long distance behavior can be obtained. Our equations simplify considerably,

$$i\,\hbar c_l \left(\frac{d}{d\xi} + \frac{l}{\xi}\right) f_B^- + 2 f_A^- = \epsilon_k f_A^+ , \tag{5.322}$$

$$i\,\hbar c_l \left(\frac{d}{d\xi} + \frac{1-l}{\xi}\right) f_A^- - f_B^- = \epsilon_k f_B^+ . \tag{5.323}$$

Since $\epsilon_k \ll 1$, the states labeled by the $+$ and $-$ superscripts decouple and an approximate solution can be obtained by setting the right hand sides to zero and solving the system

$$i\,\hbar c_l \left(\frac{d}{d\xi} + \frac{l}{\xi}\right) f_B^- + 2 f_A^- = 0 , \tag{5.324}$$

$$i\,\hbar c_l \left(\frac{d}{d\xi} + \frac{1-l}{\xi}\right) f_A^- - f_B^- = 0 . \tag{5.325}$$

Differentiating the second equation and substituting the result into the first equation and doing the reverse of this produces two uncoupled equations for f_A^- and f_B^-

$$\left[\frac{d^2}{d\xi^2} + \frac{1}{\xi}\frac{d}{d\xi} - \frac{(1-l)^2}{\xi^2} - 2\right] f_A^- = 0 , \tag{5.326}$$

$$\left[\frac{d^2}{d\xi^2} + \frac{1}{\xi}\frac{d}{d\xi} - \frac{l^2}{\xi^2} - 2\right] f_B^- = 0 . \tag{5.327}$$

These are modified Bessel's equations whose solutions are well understood and describe bound states, i.e., excited states of the vortex that decay exponentially as $r \to \infty$. These decaying solutions are modified Bessel functions of the second kind whose asymptotic forms are given by

$$f_A^-(\xi) \approx \sqrt{\frac{\pi}{2\sqrt{2}\,\xi}}\, e^{-\sqrt{2}\xi}, \tag{5.328}$$

$$f_B^-(\xi) \approx \sqrt{\frac{\pi}{2\sqrt{2}\,\xi}}\, e^{-\sqrt{2}\xi}. \tag{5.329}$$

If we add the same equations instead of subtracting them, we obtain

$$i\left(\frac{d}{d\xi}+\frac{l}{\xi}\right) f_B^+ = \epsilon_k\, f_A^-, \tag{5.330}$$

$$i\left(\frac{d}{d\xi}+\frac{1-l}{\xi}\right) f_A^+ - f_B^+ = \epsilon_k\, f_B^-. \tag{5.331}$$

Again, we may obtain approximate solutions by setting the right hand sides to zero and solving

$$i\left(\frac{d}{d\xi}+\frac{l}{\xi}\right) f_B^+ = 0, \tag{5.332}$$

$$i\left(\frac{d}{d\xi}+\frac{1-l}{\xi}\right) f_A^+ - f_B^+ = 0. \tag{5.333}$$

Decoupling, we obtain

$$\left[\frac{d^2}{d\xi^2}+\frac{1}{\xi}\frac{d}{d\xi}-\frac{(1-l)^2}{\xi^2}\right] f_A^+ = 0, \tag{5.334}$$

$$\left(\frac{d}{d\xi}+\frac{l}{\xi}\right) f_B^+ = 0. \tag{5.335}$$

The solutions to these equations are easy to obtain and are

$$f_A^+(\xi) = \frac{c_1^+}{\xi^{\pm(1-l)}}, \tag{5.336}$$

$$f_B^+(\xi) = \frac{c_2^+}{\xi^l}. \tag{5.337}$$

We have seen that f_A^- and f_B^- decay more rapidly than f_A^+ and f_B^+. This is exactly what we expect since the first two correspond to fluctuations in the circulation velocity

potential of the vortex while the last two correspond to fluctuations in the number density which are expected to fall off more slowly.

5.15 Conclusion

In this chapter, we have derived the RLSE and applied them to the case of a uniform BEC. and compute the coherence factors for the uniform case to obtain the coherence factors, energy eigenvalues and studied their limiting forms as a function of the quasi-partcle momentum relative to the natural parameters of the system, i.e., the particle interaction, lattice spacing, and hopping energy. Moreover, we have shed light on the normalization of positive and negative energy quasi-particle states, including symmetries of the RLSE, and delineated the different types of spinor excitations where we have seen how the particle-hole picture for ordinary weakly interacting BECs is another dimensional scale to the Dirac particle-antiparticle paradigm familiar from studies of graphene. The interacting, metastable, ground state energy was determined with corrections beyond the mean field result, and has a clear limit to its counterpart describing non-interacting bosons in the honeycomb lattice. Finally, we have solved, by approximate analytical methods, the RLSE for the case of vortex, and interpret our results by analogy with the semiclassical picture that small fluctuations of the vortex are equivalent to fluctuations in its shape and spatial position, i.e., fluctuations in the location of the core and the phase angle. We obtain decaying and non-decaying solutions, where the former correspond to bound state fluctuations of the vortex and the latter are free-scattering states.

CHAPTER 6

THE NONLINEAR DIRAC EQUATION: RELATIVISTIC VORTICES AND EXPERIMENTAL REALIZATION IN BOSE-EINSTEIN CONDENSATES

L. H. Haddad, K. M. O'Hara, and Lincoln D. Carr, Physical Review Letters, under review, 2012.

Abstract

We present a detailed experimental procedure for preparing relativistic vortices, governed by the nonlinear Dirac equation, in a two-dimensional Bose-Einstein condensate (BEC) in a honeycomb optical lattice. Our setup contains Dirac points, in direct analogy to graphene. We determine a range of practical values for all relevant physical parameters needed to realize relativistic vortices in BEC of ^{87}Rb atoms. Discrete spectra for seven distinct vortices are computed in the presence of a weak harmonic trap, which include Anderson-Toulouse and Mermin-Ho skyrmion textures, and half-quantum vortices. We find that most vortices are stable with a lifetime between 1 and 10 seconds.

6.1 Main Text

Multi-component Bose-Einstein condensates (BECs) present an ideal setting for studying complex vortex structures [44]. Such vortices allow for topologically intriguing configurations ranging from skyrmions to knots [38, 43, 182]. The usual method for adding a spinor structure to a BEC relies on hyperfine degrees of freedom or different atomic species. Instead, we use the band structure and linear dispersion relation around the Dirac points at the Brillouin zone edge of a honeycomb optical lattice to realize a four-component Dirac spinor, in direct analogy to graphene [183]. This gives us both pseudospin as well as a relativistic structure. To accomplish this, we propose starting with a BEC of weakly interacting alkali metal atoms in the lowest Bloch state of a 2D honeycomb optical lattice, then using Bragg scattering to populate Bloch states at the two inequivalent Dirac points, followed by the application of a Laguerre-Gaussian laser beam to deliver a net angular momentum to the BEC which excites a plethora of vortex structures. The vortices we obtain are solutions of the nonlinear Dirac equation (NLDE), whose stability is determined by the relativistic linear stability equations (RLSE) [52, 184]. Our work on the NLDE+RLSE system opens up the field of relativistic simulations in BECs at velocities ten orders of magnitude slower than the speed of light.

In this letter we combine the study of Dirac points with superfluid vortices, an environment reminiscent of particle physics models where relativistic vortices are commonplace [185, 186]. Stability of a BEC at the Dirac points presents a challenge, since Bloch states there have finite crystal momentum and nonzero energy. We handle this problem by introducing an intermediate asymmetry between the A and B sublattice potential depths which opens up a mass gap. Using a gap enables us to construct initial and final Bloch states, $\psi_{A,\mathbf{0}}$ and $\psi_{A,\mathbf{K}}$ (with Dirac point momentum $\mathbf{K}$), as superpositions of the two degenerate states at the Dirac point with velocities c_l and $-c_l$, respectively. This produces a state with group velocity equal to zero, relative to

the lattice. Stationarity of the BEC with respect to the lattice and the lab frame is significant experimentally, since the BEC can remain confined in an external trapping potential indefinitely and does not suffer from dynamical instabilities associated with relative motion between the BEC and lattice. The end result is a metastable state in which thermal losses can be managed by maintaining the system at very low temperatures. For realistic experimental parameters our relativistic vortices are stable for up to 10 seconds, as long or longer than the lifetime of typical BECs.

Parameter	Symbol/Definition	Constraint	Value	Range
(a) Temperature	T	$\ll \hbar\omega_z$	8 nK	$\sim 100\,\mathrm{pK} < T < \sim 80\,\mathrm{nK}$
(b) Chemical potential	μ	$\ll \hbar\omega_z$	2.36 nK	$< 4.10\,\mathrm{nK}$
(c) Transverse oscillator length	$L_z = (\hbar/M\omega_z)^{1/2}$	$\ll R_\perp$	$3.0\,\mu\mathrm{m}$	$< 2.10\,\mu\mathrm{m}$
(d) Healing length	$\xi = 1/\sqrt{8\pi\bar{n}a_s}$	$\lesssim L_z$	$2.14\,\mu\mathrm{m}$	$\lesssim 1.66\,\mu\mathrm{m}$
(e) Effective speed of light	$c_l = t_h a\sqrt{3}/2\hbar$	$< c_{s,2\mathrm{D}}$	$2.69 \times 10^{-2}\,\mathrm{cm/s}$	$< 5.40 \times 10^{-2}\,\mathrm{cm/s}$
(f) Dirac nonlinearity	$U = L_z\, g\, \bar{n}^2\, 3\sqrt{3}\, a^2/8$	$\ll t_h,\ \mu$	0.393 nK	$< 2.36\,\mathrm{nK}$
(g) Quasi-particle momentum	$k = p/\hbar$	$\ll \sqrt{8}/a$	$6.27 \times 10^2\,\mathrm{cm}^{-1}$	$6.27 \times 10^2\,\mathrm{cm}^{-1} \lesssim k \ll 5.66 \times 10^4\,\mathrm{cm}^{-1}$
(h) Dirac healing length	$\xi_{\mathrm{Dirac}} = t_h a\sqrt{3}/2U$	$\gg a,\ \ll R_\perp$	$5.25\,\mu\mathrm{m}$	$0.50\,\mu\mathrm{m} \ll \xi_{\mathrm{Dirac}} \ll 50.0\,\mu\mathrm{m}$
(i) Lattice depth	V_0	$\gg E_R$	$2.59\,\mu\mathrm{K}$	$0.79\,\mu\mathrm{K} < V_0 < 5.95\ \ \mu K$

Table 6.1: *Physical parameters and constraints for the NLDE typical for a BEC of* ^{87}*Rb atoms.* (a,b) Relative energies for the 3D to 2D dimensional reduction, with the vertical trap oscillator energy $\hbar\omega_z$. (c,d,h) Relative lengths for the 3D to 2D dimensional reduction. (e) Landau criterion imposed to avoid dynamical instabilities, where the 2D speed of sound in the continuum $c_{s,2\mathrm{D}} \equiv \sqrt{3g\bar{n}/2M} = 2.97 \times 10^{-2}\,\mathrm{cm/s}$. (f) The weakly interacting and superfluid (not Mott insulating) regime. (g) The linear Dirac cone approximation which requires that quasi-particle momenta $\hbar k$ remain small compared to the Dirac point momentum $\hbar K$. (h) Long-wavelength limit, which sets the scale for the 2D Dirac healing length. (i) The lowest-band and tight-binding approximation. For the values in the table, we use the ratio of lattice depth to recoil energy $V_0/E_R = 16$, lattice constant $a = 2\lambda/3 = 0.55\,\mu\mathrm{m}$, and planar trap radius $R_\perp = 100\,a$, average particle density $\bar{n} = 1.5 \times 10^{18}\,\mathrm{m}^{-3}$, hopping energy $t_h = 4.31\,\mathrm{nK}$, and atomic mass of ^{87}Rb.

Relativistic vortices are realized in the emergent nonlinear Dirac background, in the long wavelength limit of a 2D honeycomb lattice. The usual BEC parameters in 3D are renormalized, once for the dimensional reduction [68], and again after integrat-

ing over the lattice Wannier functions and going to long wavelengths. Consequently, NLDE physics is only experimentally realizable in practice when several energy and length constraints are satisfied. We list these constraints in Table 6.1 along with their mathematical definitions. For our calculations, we use the semiclassical estimate [77] of the hopping parameter $t_h \equiv 1.861\,(V_0/E_R)^{3/4}\,E_R \exp\!\left(-1.582\sqrt{V_0/E_R}\right)$. It is helpful to consolidate the constraint inequalities to arrive at expressions relating the temperature T and length scales of the system, a_s, a, d, L_z, and $R_\perp$:

$$1 \lesssim \left(\frac{8\pi a_s}{d^3}\right)^{3/2} L_z^3 < \frac{2^5\sqrt{2}\,\pi^{1/2}(d^3 a_s)^{1/2}}{3\sqrt{3}\,a^2\left[1+\pi a/(4\sqrt{2}R_\perp)\right]}\,, \tag{6.1}$$

$$T < \hbar^2/k_B M L_z^2\,, \tag{6.2}$$

where d is the average inter-particle distance defined in terms of the particle density $d = \bar{n}^{-1/3}$. All other quantities are defined in Table 6.1. The temperature T in Eq. (6.2) depends indirectly on the ratio V_0/E_R through $\bar{n}$. We can get an idea of how the particle density affects T by evaluating the inequalities for different values of $\bar{n}$ while fixing $V_0/E_R = 16$. For example, $\bar{n} = 10^{16}\,\mathrm{m}^{-3}$ gives $26.259\,\mu\mathrm{m} \lesssim L_z < 86.934\,\mu\mathrm{m}$ and $T < 8.17 \times 10^{-3}\,\mathrm{nK}$, whereas for $\bar{n} = 10^{20}\,\mathrm{m}^{-3}$ we find $0.263\,\mu\mathrm{m} \lesssim L_z < 0.187\,\mu\mathrm{m}$ and $T < 162\,\mathrm{nK}$. From this we see that a practical value for T requires that densities to be considerably larger than $10^{16}\,\mathrm{m}^{-3}$, a consequence of the additional constraints in Eqs. (6.1)-(6.2).

The honeycomb lattice is composed of two degenerate hexagonal lattices, A and B, which leads to the band crossing and the Dirac cones. The lattice potential is straightforward to implement experimentally [187, 188] using light tuned either to the blue or to the red of an atomic resonance. For the red-detuned lattice, all three laser fields are polarized parallel to the plane of propagation so that the polarization of the net field is spatially dependent. This polarization gradient produces a spin-dependent lattice potential which is key to our method, allowing for differentiation

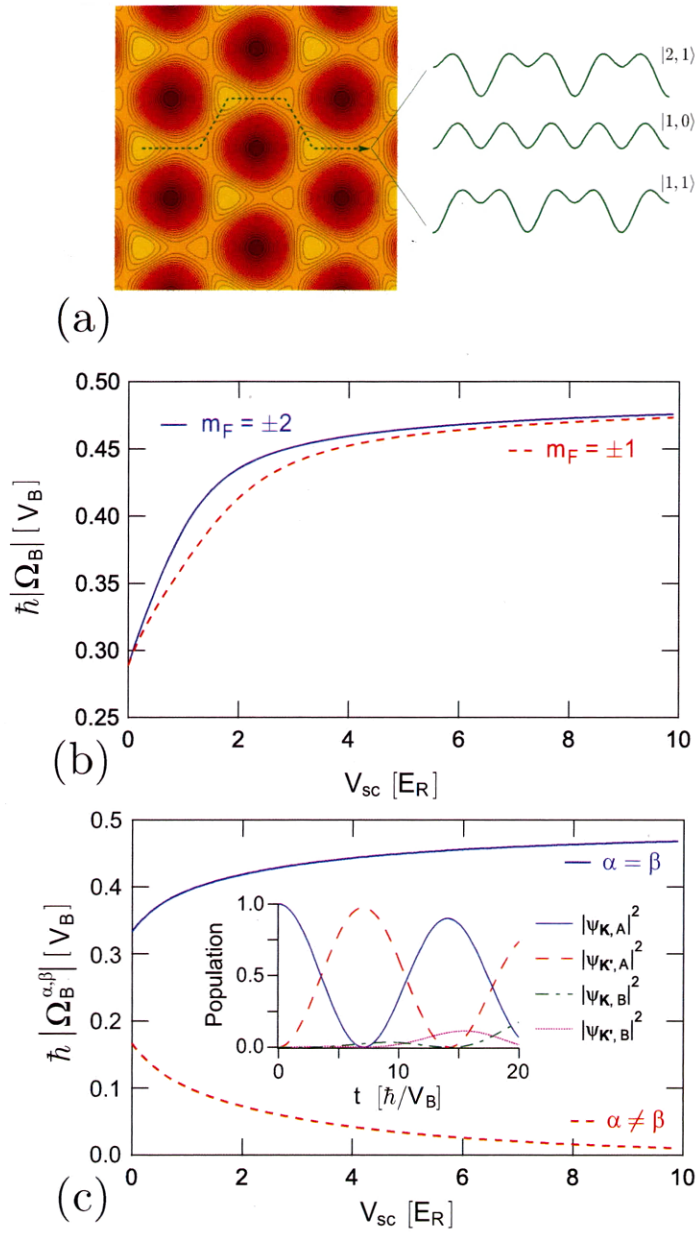

Figure 6.1: (color online) *Bragg scattering in a spin-dependent honeycomb lattice.* (a) Honeycomb potential for ^{87}Rb atoms in state $|F, m_F\rangle = |2, 1\rangle$ for the case when the wavelength of the lattice light $\lambda_L = 830\,\text{nm}$. (b) Rabi frequencies for the $m_F = \pm 2$ (solid blue) and ± 1 (dashed red) states.(c) Rabi frequency for transitions between non-equivalent Dirac points for cases where the sub-lattice index remains the same (solid blue) or changes (dashed red) as functions of the depth of the scalar part V_{sc} of the optical lattice potential. (Inset) Time dependence of the sublattice populations at the Dirac points $\mathbf{K}$ and $\mathbf{K}'$ for an optical lattice depth of $V_{\text{sc}} = 4E_R$.

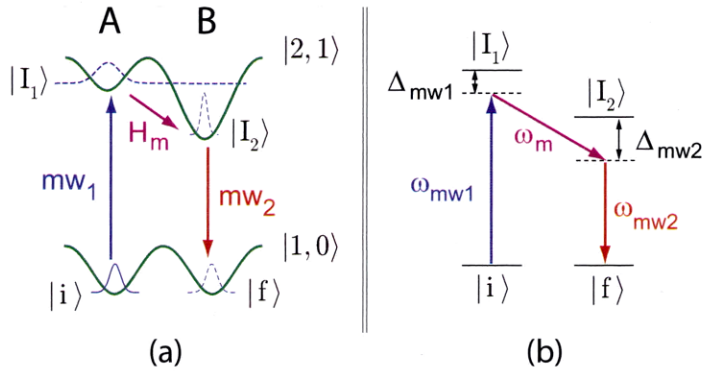

Figure 6.2: (color online) *Coherent transfer between sublattices A and B.* (a) Three step process of exciting atoms from the A sublattice with hyperfine state $|1,0\rangle$ (no sublattice asymmetry) to the hyperfine state $|2,1\rangle$ via the rf/mw transition mw_1, then from the A sublattice to the B sublattice via the perturbation $\mathrm{H_m}$, and finally back to the $|1,0\rangle$ hyperfine state via the mw_2 transition (mw = microwave). (b) The same process showing the associated rf/mw frequencies and the detunings Δ_{mw1} and Δ_{mw2}.

between different hyperfine ground states. Figure 6.1(a) shows the optical potential produced for ^{87}Rb atoms in different hyperfine states when the lattice is formed from $\lambda_L = 830\,\mathrm{nm}$ light [188].

Preparation of the BEC at a Dirac point is accomplished by first condensing into the lattice via evaporative cooling, then inducing Bragg scattering between crystal momenta $\mathbf{0}$ and $\mathbf{K}$ using auxiliary laser fields. We start with the BEC in the lowest-energy Bloch state and hyperfine state $m_F \neq 0$ with the spin-dependent potential turned on so that a mass gap is in place. The gap is defined as $2\,|m_s|c_l^2$, which measures the difference in potential depths between the A and B sublattices as shown in Figure 6.2(a). Note that $m_s c_l$ is the corresponding mass term in the NLDE, with c_l the effective speed of light (see Table 6.1). The lattice depth is then increased adiabatically [188]. Only the sublattice with the lowest energy is occupied at this point, assumed here to be the A sublattice. Bragg scattering to a Bloch state at a Dirac point can be accomplished by applying two laser fields with wavevectors $\mathbf{k}_{\mathrm{b1}}$ and $\mathbf{k}_{\mathrm{b2}}$, which satisfy $\mathbf{k}_{\mathrm{b1}} - \mathbf{k}_{\mathrm{b2}} = \mathbf{K}$ and have frequencies ω_{b1} and ω_{b2}. These frequencies satisfy $\omega_{\mathrm{b1}} - \omega_{\mathrm{b2}} = \Delta\omega = [E_A(\mathbf{K}) - E_A(\mathbf{0})]/\hbar$. Here, the function $E_A(\mathbf{k})$

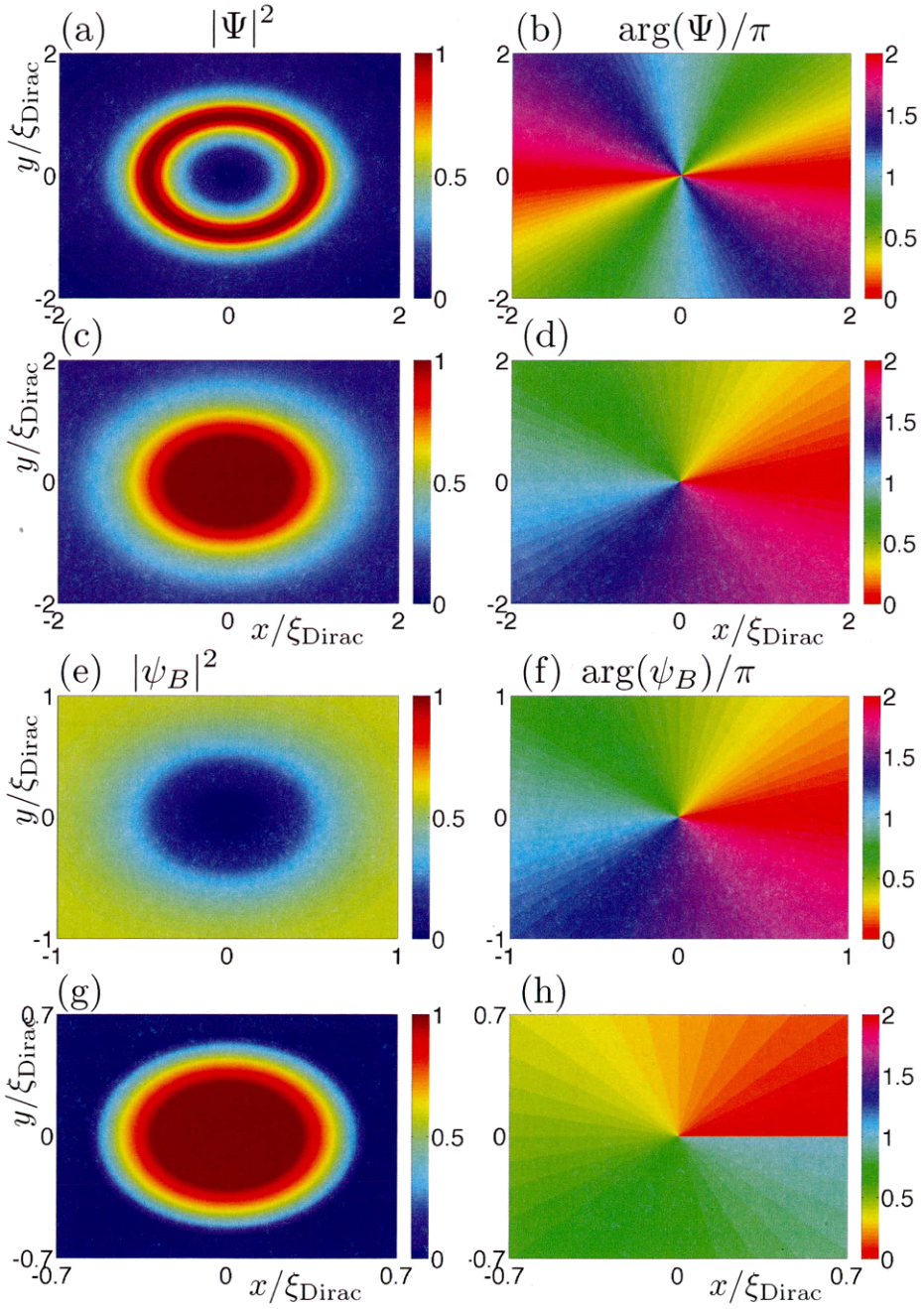

Figure 6.3: (color online) *Relativistic vortices.* Density and phase of (a,b) $\ell = 2$ ring-vortex, (c,d) B sublattice of Mermin-Ho skyrmion, (e,f) ring-vortex/soliton, (g,h) half-quantum vortex, or semion. All of these vortices and more can be made by variations on the experimental techniques which we have discussed.

gives the dispersion relation for the lower (A) band. Application of this potential results in Rabi oscillation between the initial state $\psi_{A,\mathbf{0}}$ (ground state), and the final state $\psi_{A,\mathbf{K}}$ (Dirac point) with a Rabi frequency Ω_B, where ψ_A, ψ_B are wavefunctions; $|\psi_{A(B)}|^2$ is the BEC density distribution on the A (B) sublattice. Figure 6.1(b) shows numerical calculations for $|\hbar\,\Omega_B|$ as a function of the depth of the honeycomb lattice $V_{\rm sc}$ in units of the depth of the Bragg scattering lattice V_B. We should keep in mind that $V_B \ll E_R$. The entire population of atoms in state $\psi_{A,\mathbf{0}}$ can be transferred to $\psi_{A,\mathbf{K}}$ by applying the Bragg scattering potential for a time $\tau_\pi = \pi/\Omega$ provided that the amplitude of the Bragg potential is chosen such that $\hbar/\tau_\pi$ is significantly smaller than the energy splitting between the upper and lower bands, i.e., $2\,|m_s|c_l^2$. Note that because of the gap, all the atoms are presently in a state with zero group velocity.

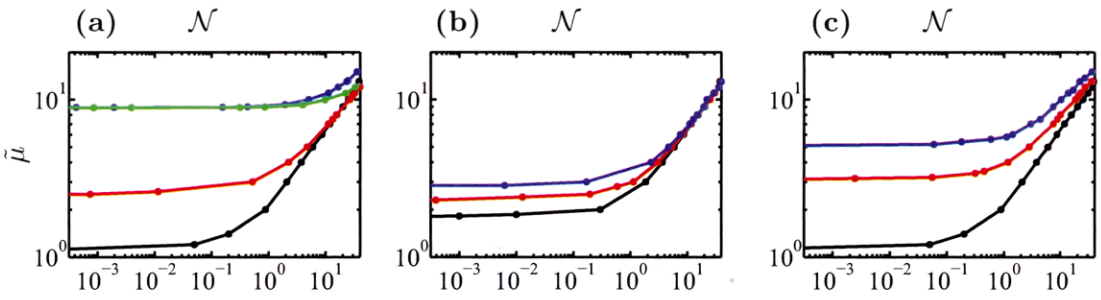

Figure 6.4: (color online) *Spectra for relativistic vortices confined in a harmonic potential.*(a) Vortex/soliton (black curve), Anderson-Toulouse skyrmion (red), Mermin-Ho skyrmion (blue), and half-quantum vortex (green). (b) Topological vortices for $\ell = 2, 3, 4$ (black, red, blue). (c) Radial ground state and first two excited states of the vortex without skyrmion symmetry (black, red, blue). In each figure, the renormalized chemical potential is plotted as a function of the normalization, both quantities described in the supplementary materials section. There are two regimes characterized by power law: $\tilde{\mu} \propto \mathcal{N}^\alpha$. The weakly interacting free-particle regime occurs for small $\mathcal{N}$, whereas the strongly interacting vortex regime is in the region of large $\mathcal{N}$). Note that the vertical and horizontal axes labels are dimensionless.

With the BEC at the Dirac point but only in the A sublattice sites, we populate the B sublattice by first transferring atoms to a hyperfine state that does not experience the vector light shift and therefore no mass gap. We can then populate

the B sublattice Bloch state by applying a periodic perturbation which modulates the amplitude of one of the lattice laser fields. This provides an anisotropy in the tunneling matrix elements, which results in a net transfer of atoms to the B sublattice, as depicted in both panels of Figure 6.2. Finally, the transfer of atoms to the non-equivalent Dirac point $\mathbf{K}'$ can be accomplished again by Bragg scattering from a lattice formed using auxiliary laser fields [189]. The Rabi frequency and resulting time-dependent populations for the $\mathbf{K}$ and $\mathbf{K}'$ points are depicted in Figure 6.1(c).

We obtain seven physically distinct NLDE vortices. A brief review of the NLDE, RLSE, and a table detailing the physical characteristics of each vortex type are included in supplementary materials. The vortex/soliton is a bright soliton or density peak in the center in the first component with a vortex of phase winding 2π around the outside in the second. The ring-vortex/soliton is also a bright soliton in the first component, but the vortex component is a ring peaked near the healing length $r = \xi_{\text{Dirac}}$. The Anderson-Toulouse skyrmion has the same core structure as the vortex/soliton, but the spinor components are continuously interchanged as the distance from the core increases, while staying within the bounds $0 < |\psi_A|, |\psi_B| < 1$ and conserving total density $|\psi_A|^2 + |\psi_B|^2 = 1$. The Mermin-Ho skyrmion again has similar behavior near the core but the soliton (vortex) amplitude decreases (increases) monotonically away from the core within the bounds $\cos(\pi/4) < \psi_A < 1$ and $0 < \psi_B < \cos(\pi/4)$. The half-quantum vortex or semion is characterized by a phase discontinuity such that far from the core the amplitudes have the form $\psi_A \propto \cos(\theta/2)$ and $\psi_B \propto \sin(\theta/2)$; the additional π phase is accounted for by a rotation between the Dirac spinor components. So far, all of these solutions have one unit of angular momentum, $\ell = 1$ with $\ell \in \mathbb{N}$, either a phase winding of 2π in one component or a winding of π in each component. Additionally, for arbitrary phase winding ($\ell > 1$) ring-vortices and topological vortices exist with $\ell - 1$ (ℓ) units of winding in the first (second) spinor component, but differ in their asymptotic form. Component ampli-

tudes for the ring-vortex peak at around one healing length from the core and quickly decay for large r. On the other hand, topological vortices retain non-zero density far from the core. Several representative vortices are plotted in Figure 6.3. All of the vortices here can be created using straightforward variations of the transition sequence depicted in Figure 6.2. In the supplementary materials, we explain how vortices are realized in practical experiments.

For most of the vortices described in the previous paragraph, we find lifetimes τ to be long compared to the lifetime of the BEC itself. Using the method which we present in the supplementary materials section, we obtain the following values for τ: 9.13 s, 10.43 s, 11.51 s, 1.57×10^{-7} s, 1.57×10^{-7} s, 1.25 s, 1.29×10^{-5} s; for the vortex/soliton, ring-vortex/soliton, Anderson-Toulouse, Mermin-Ho, half-quantum, $\ell = 2$ ring-vortex, and $\ell = 2$ topological vortex, respectively. To complete our description, we have computed the discrete spectra pertaining to the case of planar confinement by a weak harmonic trap. These are plotted in Figure 6.4. Note that ring-vortices are minimally affected by the presence of a weak trap, since they are highly localized objects and lie very near the center of the trap.

In conclusion, we have described in detail a method for constructing a stable BEC at the Dirac points of a honeycomb optical lattice. Our system allows for relativistic vortex excitations in a macroscopic Dirac spinor wavefunction, providing a means of studying high energy field theoretic vortices in a condensed matter setting. We have completely specified the required physical parameters, lifetimes, and spectra for harmonically bound vortices as a prescription guide for the experimentalist. Variations on the NLDE have tremendous potential for a host of relativistic simulations in BECs. Interesting examples include Soler models [190] and the extended Gross-Neveu model [126]. Our work puts such efforts on a solid experimental footing.

Acknowledgments

This material is based in part upon work supported by the National Science Foundation under grant numbers PHY-1067973, PHY-1011156, and the Air Force Office of Scientific Research grant number FA9550-08-1-0069. L.D.C. thanks the Alexander von Humboldt foundation and the Heidelberg Center for Quantum Dynamics for additional support.

6.2 Supplementary Materials

Vortex type	Winding	Analytic form of $\Psi(\mathbf{r})$	Topology
Vortex/soliton	$\ell = 1$	$\left[ie^{-i\theta}\frac{(r/r_0)}{\sqrt{1+(r/r_0)^2}},\ \frac{1}{\sqrt{1+(r/r_0)^2}}\right]^T$	$\lvert\psi_A(\infty)\rvert = 1$
Ring-vortex/soliton	$\ell = 1$	$\left[ie^{-i\theta}\frac{(r/r_0)}{\sqrt{1+(r/r_0)^4}},\ \frac{1}{\sqrt{1+(r/r_0)^4}}\right]^T$	non-topological
Anderson-Toulouse skyrmion	$\ell = 1$	$\left[ie^{-i\theta}\cos\varphi(r/r_0),\ \sin\varphi(r/r_0)\right]^T$	$\varphi(\infty) = 0$
Mermin-Ho skyrmion	$\ell = 1$	$\left[ie^{-i\theta}\cos\varphi(r/r_0),\ \sin\varphi(r/r_0)\right]^T$	$\varphi(\infty) = \pi/4$
Half-quantum vortex	$\ell = 1$	$[i\cos\theta/2,\ \sin\theta/2]^T$	$\lvert\Psi(\infty)\rvert = 1$
Ring-vortex	$\ell = 2, 3, 4, ...$	$\left[ie^{-i\ell\theta}\frac{(r/r_0)^{3\ell-2}}{\sqrt{1+(r/r_0)^{8(\ell-1/2)}}},\ e^{i(\ell-1)\theta}\frac{(r/r_0)^{\ell-1}}{\sqrt{1+(r/r_0)^{8(\ell-1/2)}}}\right]^T$	non-topological
General topological vortex	$\ell = 2, 3, 4, ...$	Numerical shooting method	$\lvert\psi_A(\infty)\rvert = 1$

Table 6.2: *Vortex solutions of the NLDE.* Solutions are described by their phase winding, closed-form expression, and topological properties. Solutions which retain non-zero density far from the core have an associated conserved topological charge, and we state their asymptotic form. Note that r_0 is the length scale associated with the chemical potential or the interaction strength depending on the particular solution.

NLDE Solutions – The NLDE treats the entire Dirac four-spinor. In its simplest realization without mass gaps and in tight binding the upper two components, called a *Weyl spinor*, are decoupled from the lower two, and can be written $\Psi = (\psi_A, \psi_B)^T$. We obtain vortex solutions by expressing the spinor components in the form: $\psi_A(r,\theta,t) = \pm i\, f_A(r) e^{i(\ell-1)\theta}\, e^{-i\mu t/\hbar}$, $\psi_B(r,\theta,t) = f_B(r) e^{i\ell\theta}\, e^{-i\mu t/\hbar}$, and writing the NLDE in plane-polar coordinates:

$$-\hbar c_l\left(\partial_r+\frac{\ell}{r}\right)f_B(r)+U\left|f_A(r)\right|^2 f_A(r) = \mu f_A(r) \tag{6.3}$$

$$\hbar c_l\left(\partial_r+\frac{1-\ell}{r}\right)f_A(r)+U\left|f_B(r)\right|^2 f_B(r) = \mu f_B(r), \tag{6.4}$$

where ℓ is the integer phase winding and the other parameters are defined in Table 6.1. For the case $\mu = 0$, Eqs. (8.6)-(8.7) give closed form expressions for the radial amplitudes f_A and f_B. These are the ring-vortex/soliton ($\ell = 1$) and general ring-vortex ($\ell > 1$) solutions. For the case $\mu \neq 0$, closed form solutions exist in some cases while others are obtained using a numerical shooting method. Solutions of the NLDE are listed in Table 6.2.

Experimental Realization of Vortices – Relativistic vortices can be excited by starting with all the atoms in the A sublattice at the Dirac point, then applying co-propagating Gaussian and Laguerre-Gaussian laser beams, where the Laguerre-Gaussian beam carries a single unit of orbital angular momentum. The transfer of angular momentum to the atoms occurs via the stimulated Raman transition [191]. The spatial variation of the beam results in mainly the B sublattice being populated (the vortex) throughout most of the 2D lattice, except within a small disk which becomes the core of the vortex. On the other hand, the A sublattice is left depleted everywhere (the soliton) except near the core of the vortex. This describes excitation of the vortex/soliton or Anderson-Toulouse skyrmion [184]. The Mermin-Ho vortex can be obtained by the same process, but by only partially transferring atoms to the B sublattice. The sublattice amplitudes far from the vortex core are tuned to satisfy $|\psi_B|^2 = |\psi_A|^2 < 1$, where $|\psi_{A(B)}|^2$ is the density of the BEC in the first (second) four-spinor component in the NLDE, and $\mathbf{v}_{A(B)} = \hbar/M\nabla\phi_{A(B)}$ is the associated relativistic fluid velocity, with $\phi_{A(B)} = Arg(\psi_{A(B)})$ the phase, as depicted in Figure 6.3. The half-quantum vortex or semion can be excited by using a fractional optical vortex beam in order to provide the required angular phase jump [192, 193]. General topo-

logical vortices have phase winding $\ell > 1$, non-zero chemical potential μ, and satisfy $|\psi_A|, |\psi_B| \neq 0$ far from the center of the trap. These can be created by first rotating the lattice to excite the desired $\ell - 1$ state in the A sublattice, then following up with the Laguerre-Gaussian transition to produce the correct ℓ versus $\ell - 1$ winding differential in the spinor components. We note that there is an alternative approach to the rotating lattice method. General topological vortex excitations may be induced by subsequent applications of a two-photon transition with co-propagating Laguerre-Gaussian/Gaussian beams which transfer the condensate between $m = 0$ states, i.e., from $F = 1$, $m = 0$ to $F = 2$, $m = 0$ or vice versa. Each two-photon transition would change the orbital angular momentum of both the A and B sublattices by the orbital angular momentum carried by the Laguerre-Gaussian beams, while maintaining the desired winding differential between the A and B sublattices. Finally, ring-vortices characterized by $\mu = 0$ and $|\psi_A|, |\psi_B| = 0$ far from the center of the trap, can be obtained from the other vortices by inducing depletion of the BEC from the outer edge of the trap towards the core. Plots for several vortices are shown in Figure 6.3 with more details regarding solutions of the NLDE discussed in Ref. [184].

RLSE Solutions – The RLSE form a relativistic generalization of the Bogoliubov-de Gennes equations analogous to the relationship between the NLDE and nonlinear Schrödinger equation. Thus, in the RLSE the quasi-particle amplitudes u and v are each vector in form, to match the four-spinor (two-spinor at one Dirac point) they perturb from. The RLSE can be expressed in 2×2 matrix-vector form:

$$\tilde{\mathscr{D}}\mathbf{u_k} - U\tilde{\Psi}\mathbf{v_k} = \tilde{E}_\mathbf{k}\mathbf{u_k}, \tag{6.5}$$

$$\tilde{\mathscr{D}}^*\mathbf{v_k} - U\tilde{\Psi}\mathbf{u_k} = -\tilde{E}_\mathbf{k}\mathbf{v_k}\,, \tag{6.6}$$

where $\tilde{\mathscr{D}}$ and $\tilde{\Psi}$ are 2×2 matrices which contain the first-order derivatives $(\partial_x + i\partial_y)$ and the background BEC components ψ_A, ψ_B, and $\tilde{E}_\mathbf{k}$ is the 2×2 eigenvalue matrix. Note that U is the particle interaction. When broken down, Eqs. (7.116)-(7.117) form

a 4×4 eigenvalue problem in the quasi-particle amplitudes $u_{k,A(B)}$ and $v_{k,A(B)}$ (with momentum $\mathbf{k}$) associated with particle and hole excitations of the A(B) sublattices at a Dirac point. Vortices possess cylindrical symmetry so we express Eqs. (7.116)-(7.117) in plane-polar coordinates, factor the quasi-particle amplitudes into radial and angular parts, then substitute in the particular solution for $\psi_{A(B)}$. We then obtain a set of first-order coupled ODE's in the radial coordinate to be solved consistently for the functions $u_{A(B)}(r)$, $v_{A(B)}(r)$ and the associated eigenvalues. We discretize the derivatives and functions using a forward-backward average finite-difference scheme, then solve the resulting discrete matrix eigenvalue problem using a standard numerical diagonalization method.

Vortex Lifetimes – To compute vortex lifetimes, we solve the RLSE to obtain the quasi-particle spatial functions and eigenvalues. In general, for vortex solutions of the NLDE certain eigenvalues and eigenmodes key to understanding the physical motion correspond to Nambu-Goldstone modes, i.e., anomalous with a small imaginary component [175]. When thermal losses are small, it is the imaginary part of the linear eigenvalues which depletes the BEC. We define the vortex lifetime by computing the time for depletion to reach a significant fraction of the total fixed number of atoms in the system, and consider only depletion coming from the mode with the largest imaginary term in its eigenvalue. The lifetime is then given by $\tau = [\hbar/\mathrm{Im}(E)] \ln(R_\perp/I)$, expressed in terms of the largest linear eigenvalue E and the planar radius of the BEC $R_\perp$, in units of the lattice constant a (see Table 6.1). Note also that the spatial integral I here is specific to each vortex type. For the experimental parameters of Table 6.1, we find the longest lived solutions to be the vortex/soliton and Anderson-Toulouse vortex with $\tau = 11.51\,\mathrm{s}$, compared to the typical lifetime of a ^{87}Rb condensate in an optical lattice of less than a second [194].

Chemical Potential Spectra – In order to have a clear comparative prediction for energies involved in creating our vortices, we solve the NLDE using a numerical

shooting method in the presence of a weak harmonic trap of frequency $\omega_\perp = 2\pi \times 0.0387\,\mathrm{Hz}$ along the direction of the lattice. This is the frequency associated with a planar BEC radius equal to 100 times the lattice constant. In this case vortices come in radially quantized states. For simplicity, we focus mainly on the lowest radial excitation. Using a generalization of the method in [195], we have obtained the dimensionless (renormalized) chemical potential $\tilde{\mu} \equiv \mu/\hbar\omega_\perp$ as a function of the normalization $\mathcal{N} = \sqrt{3}\,\hbar\omega_\perp NU/3t_h^2$ for each vortex type, as shown in Figure 6.4. Here, N is the number of atoms in the system with the other quantities defined in Table 6.1.

CHAPTER 7

THE NONLINEAR DIRAC EQUATION: METASTABLE RELATIVISTIC VORTICES IN A BOSE-EINSTEIN CONDENSATE

L. H. Haddad, K. M. O'Hara, and Lincoln D. Carr, Physical Review A, to be submitted, 2012.

Abstract

We present a detailed study of relativistic vortices for bosons within the mean-field nonlinear Dirac framework of a honeycomb optical lattice. The combined quasi-relativistic structure of the Dirac point and s-wave scattering for bosons leads to a large number of combinations of vortex and soliton solutions in the (2+1)-dimensional spinor amplitudes, most of which we obtain in analytical form. We present a detailed derivation of these solutions which include skyrmions, half-quantum vortices, Mermin-Ho and Anderson-Toulouse vortices for vortex winding $\ell = 1$. For $\ell \geq 2$ we obtain topological as well as non-topological vortices in the form of an asymptotic Bessel solution, algebraic closed-form solutions, and using standard numerical shooting methods. We demonstrate the continuous spectral mapping between the vortex and free particle limits for all of these solutions. A full derivation of the relativistic linear stability equations (RLSE) is presented by two independent methods. We prove that the standard Bogoliubov-de Genne equations (BdGE) and nonlinear Schrödinger equation (NLSE) are nonrelativistic limits of the RLSE and nonlinear Dirac equation (NLDE), respectively. The RLSE are necessary to determine the sta-

bility of generic nonuniform relativistic mean-field backgrounds. We solve the RLSE for our localized solutions and find *anomalous* as well as *dynamically unstable* modes in the linear spectrum for most solutions. Using parameters for ^{87}Rb for our vortex backgrounds, we find the imaginary parts of the linear eigenvalues to be two to three orders of magnitude smaller than the interaction strength and give vortex lifetimes ~ 10 s. To realize the nonlinear Dirac structure in the laboratory, we propose using Bragg scattering to obtain a condensate at the $\mathbf{K}$ and $\mathbf{K}'$ points of the reciprocal lattice, and co-propagating Laguerre-Gaussian and Gaussian laser beams to induce the two-photon Raman transitions in ^{87}Rb needed to create our vortex solutions.

7.1 Introduction

Vortices and solitons appear in physical settings which span a wide range of energy scales and disciplines. Well known examples are solitary waves in water, quantized vortices in ^{4}He, and Bogomol'nyi-Prasad-Sommerfield states in supersymmetric field theories [196]. Vortices are relevant from a technological standpoint in quantum computing for example [197], as well as in more theoretical areas of research such as galactic halos in Bose-Einstein condensate theories of dark matter [198]. In Bose-Einstein condensates (BECs), vortices as stable rotating solutions of the nonlinear Schrödinger equation (NLSE) are ubiquitous [17, 199]. Indeed, the presence of a persistent quantized rotation may be considered a defining property of superfluidity. Although a variety of types of vortices are possible in atomic condensates [44], the Laplacian inherent to the Schrödinger Hamiltonian constrains the number of observable vortex structures in the BEC. For instance, a BEC made up of spin-F bosons gives rise to a $(2F+1)$-component order parameter which nevertheless solves a multicomponent NLSE. An alternative method of constructing a multicomponent BEC is

to add the internal degrees of freedom by placing a condensate in a two-dimensional honeycomb optical lattice. Atoms are condensed into the lowest energy Bloch state then translated to a corner of the Brillouin zone using laser assisted Bragg scattering. At wavelengths large compared to the lattice constant, the microscopic details of the lattice manifest as an additional $\mathrm{SL}(2,\mathrm{C})$ spin group symmetry, i.e., a Dirac point structure emerges [52].

Multicomponent solitons in $(2+1)$-dimensions may be classified as *topological* if they are associated with a topologically conserved quantity, otherwise they are deemed *nontopological*. Topological solitons may be further labeled by the relevant homotopy group. In the case of a non-trivial first homotopy group, an overall macroscopic phase wraps around the circular boundary consisting of radial lengths much larger than the healing length, while the internal spin degrees of freedom remain topologically unconstrained. These are simply referred to as *vortices* and are distinguished by a nonvanishing radial profile at infinity. In contrast to these, when the wrapping around the circular boundary includes the internal spin degrees of freedom in a nontrivial way, the second-homotopy group is the relevant group and the order parameter is called a *vortex texture* or *skyrmion* [44, 200].

In this article, we study *relativistic quantum vortices* in the superfluid phase of a Bose gas at the Dirac point of a honeycomb optical lattice. We first provide the experimental steps for creating relativistic vortices. We then focus heavily on explicit vortex solutions of the NLDE. We begin with a preliminary asymptotic solution using Bessel functions, which provides a basic insight into the structure of the NLDE. Algebraic solutions are then obtained by considering the zero-chemical potential case. These are characterized by the condition that the derivative and repulsive interactions cancel exactly. However, for the general case of a non-zero chemical potential, analytical solutions are only possible when one unit of winding is considered; we use a numerical approach to obtain vortices with arbitrarily large winding number. A com-

bination of numerical and analytical techniques yields skyrmion and half-quantum vortices (texture vortices). Having obtained our solutions, we compute their corresponding discrete chemical potential spectra in the presence of a weak harmonic potential. This gives us the low-temperature μ versus U landscape for relativistic vortices, where μ and U are the chemical potential and lattice renormalized particle interaction, respectively. For example, for finite chemical potential μ we find that a series of phase transitions occur as U is tuned from zero upward: we encounter a Mermin-Ho skyrmion transitioning into a half-quantum vortex, followed by the Anderson-Toulouse skyrmion, then finally into a vortex/soliton (a bright soliton at the core of a singly-wound topological vortex). To compute lifetimes of our solutions, we derive a relativistic generalization of Bogoliubov's equations and solve these for each solution type. Predictably, we find that vortices with low winding are more stable than those with large winding number.

In high energy physics and cosmology, relativistic vortices appear as cosmic superstrings [201–203], in foundational studies in string theory such as mirror symmetry of Calabi-Yau manifolds [204, 205], and in various brane world scenarios [206]. In general, vortices are endemic to gauge theories where spontaneous symmetry breaking occurs. This includes both the Abelian [185, 203] (as with Nielsen-Olesen vortices in the Abelian Higgs model) as well as the non-Abelian case [207] (non-Abelian Yang-Mills for example). Supersymmetric field theories which exhibit weak-strong duality rely fundamentally on the presence of solitons and vortices which provide the natural degrees of freedom in the dual theory [186, 203].

In a previous paper, we derived a BEC version of the nonlinear Dirac equation for the case of weak interparticle interactions [52]. This has attracted attention from diverse fields of research [20, 21, 32, 103, 110, 120, 121, 168, 208–224]. In the present paper, we solve the NLDE by several methods to obtain a large class of vortex and skyrmion solutions. Solutions of the NLDE are effectively long wavelength limit

lattice envelopes, and so can cover a large number of sites. The healing length in our effectively 2D system is typically about 10 times the lattice constant, and we require the healing length to be small compared to the size of the cylindrical container. In typical experiments, the number of lattice sites is on the order of 100 in a linear direction, thus our solutions may be described accurately. These solution types differ by asymptotic conditions on the amplitude for r much greater than the healing length (far from the core) or r much less than the healing length (deep inside the core), use of the internal degree of freedom in the spinor structure, and with respect to quantization of rotation: Weyl spinor components always differ by one unit of rotation.

In our work, the question of condensate and vortex stability arises in two ways. First, for bosons, the Dirac point is not bounded below so that a solution of the NLDE is connected to a continuum of lower energy scattering states through which decay may occur. We address this issue by noting that for a uniform condensate at the Dirac point the linear eigenvalues are *real*: positive and negative valued for excitations above and below the Dirac point, respectively. This means that a uniform condensate is *dynamically stable*. Furthermore, the thermodynamic instability implied by the negative eigenvalues can be controlled by reducing the number of thermal excitations in the system. This is accomplished by taking the system to be at very low temperatures ($T \ll \mu$), reducing the number of collisions between condensate and thermal atoms. This eliminates the dominant mechanism for dissipation and justifies a metastable interpretation of the condensate [225].

Second, relativistic vortices are excited states of the (Dirac point) condensate, and we expect to encounter stability issues beyond those which arise in the uniform case. In particular, we find an "internal dissipation" which occurs as a transfer of energy between the two components of a Weyl spinor. For ordinary spinor BECs, a similar coupling occurs through the interaction terms in the Hamiltonian, whereas for relativistic vortices, the interaction only couples spinor components to themselves,

while intercomponent coupling occurs through the kinetic term. Our linear stability analysis reveals anomalous frequencies with small imaginary parts for several vortex solutions. For these solutions, one spinor component always lags behind the other by one unit of rotation, and it is the anomalous modes which reduce the rotation of one component, while increasing rotation of the other. Strictly speaking, these complex eigenvalues preclude metastability except in an approximate sense. Nevertheless, calculation of lifetimes based on complex frequencies gives values that are long compared to the life of the condensate.

Our results are organized as follows. In Sec. 7.2 we map out a detailed prescription for constructing a condensate at opposite Dirac points and creating our vortices in the laboratory. We also include a thorough analysis of the physical parameters and constraints used throughout our work. In Sec. 7.3 we solve the NLDE presenting closed form and numerical solutions with density and phase plots depicting each solution type. In Sec. 7.3.2 we solve the NLDE numerically for radial excited states in a harmonic trapping potential and obtain the discrete spectra for all of our solutions. In Sec. 7.5 we motivate and provide a full derivation of the RLSE by two methods. In Sec. 7.6 we solve the RLSE and obtain lifetimes for all of our vortex solutions. In Sec. 7.7 we summarize our results.

7.2 Experimental Realization of the NLDE

In the laboratory, the NLDE is realizable within a region of parameter space precisely delineated by constraints on particle density, energies, length scales, etc. We will discuss these parameters in this section. It is natural to relate our parameters to those in other areas of research, such as nonlinear optics, in which Dirac dynamics plays an important role. Creating vortex solutions of the NLDE requires several steps which are not standard to the usual methods for ordinary BEC vortices. For example, transferring a condensate from the lowest Bloch mode to the state at the Dirac point with zero group velocity and amplitude exclusively in one sublattice requires a lattice

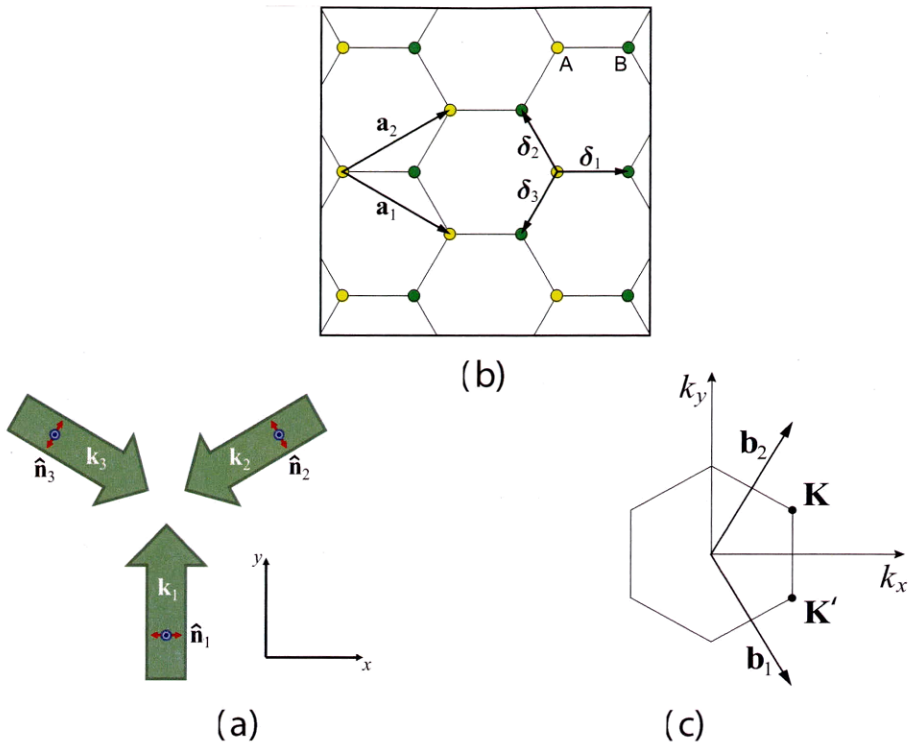

Figure 7.1: (color online) *The honeycomb optical lattice.* (a) A honeycomb lattice potential can be produced by three co-planar laser beams detuned to the red (blue) of an atomic resonance with polarizations in the plane (orthogonal to the plane). (b) The honeycomb lattice can be described by a hexagonal Bravais lattice with a two-point basis yielding the A and B sublattices. (c) The reciprocal lattice is shown. The single-particle dispersion is linear in the vicinity of two non-equivalent Dirac points at crystal momentum $\mathbf{K}$ and $\mathbf{K}'$.

potential that is sensitive to the internal hyperfine structure of the atoms. Using this feature, combined with the ability to manipulate the internal atomic state (e.g. using microwave/radio-frequency fields), one is able to scatter atoms into the proper Bloch state at the edge of the sublattice Brillouin zone. Here, there are two degenerate states with positive and negative group velocities, where positive energy excitations are "holes" and "particles", respectively. Thus, we end up with a condensate in a mixed final state which does not propagate in the laboratory frame. For the final step of exciting our vortices, we "stir" the condensate using a laser which delivers a net angular momentum (with respect to a point which becomes the core of the vortex)

to one or both spinor components.

7.2.1 Renormalized Parameters and Physical Constraints

To obtain the correct renormalized parameters for the NLDE we proceed by two steps. First, we follow the transformation of the 3D NLSE parameters as we reduce to the 2D NLSE. Second, we take the long-wavelength limit of the 2D theory at the Dirac point to get the NLDE, which induces a second renormalization of the parameters.

7.2.2 Transition from 3D to 2D NLSE

A BEC comprised of N atoms of mass M is described by a wavefunction $\psi(\mathbf{r},t)$ which solves the time-dependent nonlinear Schrödinger equation. The single-particle density is defined as $|\psi(\mathbf{r},t)|^2$ and the BEC density is defined as $\rho(\mathbf{r},t)^2 \equiv N|\psi(\mathbf{r},t)|^2$, and the phase is $\phi \equiv \arg[\psi(\mathbf{r},t)]$, with the superfluid velocity given by $\mathbf{v}_s \equiv \nabla\phi$. The two-particle interaction strength is $g = 4\pi\hbar^2 a_s/M$ and the healing length is $\xi = 1/\sqrt{8\pi\bar{n}a_s}$, where a_s is the s-wave scattering length for binary collisions between atoms. We take $a_s > 0$ so that $g > 0$, i.e., we consider only repulsive interactions, leaving attractive interactions for future studies. Throughout our work, we treat the case of an axisymmetric system associated with a harmonic trapping potential with two large dimensions described by a radius $R = \sqrt{x^2+y^2}$, and a small dimension transverse to the plane described by the length L_z. The average density which appears in ξ is then defined as $\bar{n} \equiv N/(\pi R^2 L_z)$. Note that $\psi(\mathbf{r},t)$ has dimensions of length$^{-3/2}$ so that g has dimensions of energy$\times$length^3. Another important quantity is the speed of sound in the condensate, which is defined as $c_s = \sqrt{g\bar{n}/M}$.

Transforming to the 2D regime requires that $a_s \ll L_z \lesssim \xi$ [73, 226], which ensures that the condensate remains in the ground state in the transverse direction, and $L_z \ll R$, which ensure that excitations along the plane have much lower energy than those in the transverse direction. The wavefunction can then be separated into longitudinal and transverse modes, following similar arguments as in Ref. [68],

Parameter	Symbol/Definition	Value	Range
Plank's constant	$\hbar$	$1.06 \times 10^{-34}\,\mathrm{j \cdot s}$	N/A
Boltzman's constant	k_B	$1.38 \times 10^{-23}\,\mathrm{j \cdot K^{-1}}$	N/A
Mass of ^{87}Rb	M	$1.44 \times 10^{-25}\,\mathrm{kg}$	N/A
Number of atoms	N	3.00×10^{4}	$10^2 - 10^{10}$
Wave number of laser light	k_L	$7.57 \times 10^{6}\,\mathrm{m^{-1}}$	4.19×10^{6} - $4.19 \times 10^{7}\mathrm{m^{-1}}$
Lattice constant	$a = 4\pi/3k_L$	$0.55\,\mu\mathrm{m}$	$0.30 - 0.70\,\mu\mathrm{m}$
Recoil energy	$E_R = \hbar^2 k_L^2/2M$	$0.16\,\mu\mathrm{K}$	$0.049 - 4.90\,\mu\mathrm{K}$
Lattice potential	$V_0 = 16E_R$	$2.60\,\mu\mathrm{K}$	$0.784 - 78.4\,\mu\mathrm{K}$
Hopping energy	$t_h = 1.861(V_0/E_R)^{3/4} \times E_R \exp\left(-1.582\sqrt{V_0/E_R}\right)$	$4.31\,\mathrm{nK}$	$3.49\,\mathrm{nK} - 1.90\,\mu\mathrm{K}$
Scattering length	a_s	$5.77\,\mathrm{nm}$	$5.00 - 10.0\,\mathrm{nm}$
Average particle density	$\bar{n}$	$1.5 \times 10^{18}\,\mathrm{m^{-3}}$	$10^{15} - 10^{21}\,\mathrm{m^{-3}}$
Two-body interaction	$g = 4\pi\hbar^2 a_s/M$	$41.0\,\mathrm{K \cdot nm^3}$	$22.36 - 52.18\,\mathrm{K \cdot nm^3}$
Healing length	$\xi = 1/\sqrt{8\pi\bar{n}a_s}$	$2.14\,\mu\mathrm{m}$	$\lesssim 3.00\,\mu\mathrm{m}$
Sound speed	$c_s = \sqrt{g\bar{n}/M}$	$2.43 \times 10^{-2}\,\mathrm{cm/s}$	$5.83 \times 10^{-3} - 0.825\,\mathrm{cm/s}$
Sound speed (2D)	$c_{s,2\mathrm{D}} = (3/2)^{1/2} c_s$	$2.97 \times 10^{-2}\,\mathrm{cm/s}$	$7.14 \times 10^{-3} - 1.01\,\mathrm{cm/s}$
Healing length (2D)	$\xi_{2\mathrm{D}} = (2/3)^{1/2}\xi$	$1.75\,\mu\mathrm{m}$	$\lesssim 2.45\,\mu\mathrm{m}$
Transverse trap energy	$\hbar\omega_z$	$0.63\,\mathrm{nK}$	$0.21 - 5.65\,\mathrm{nK}$
Transverse oscillator length	$L_z = (\hbar/M\omega_z)^{1/2}$	$3.00\,\mu\mathrm{m}$	$1.00 - 5.00\,\mu\mathrm{m}$
Average particle density (2D)	$\bar{n}_{2\mathrm{D}} = L_z\,\bar{n}$	$4.50 \times 10^{12}\,\mathrm{m^{-2}}$	$10^{9} - 5.00 \times 10^{15}\,\mathrm{m^{-2}}$
Effective speed of light	$c_l = t_h a\sqrt{3}/2\hbar$	$2.69 \times 10^{-2}\,\mathrm{cm/s}$	$< 5.40 \times 10^{-2}\,\mathrm{cm/s}$
Dirac kinetic coefficient	$\bar{c}_l = \hbar c_l$	$2.07\,\mathrm{nK \cdot \mu m}$	$< 5.72\,\mathrm{nK \cdot \mu m}$
Dirac nonlinearity	$U = L_z\, g\, \bar{n}^2\, 3\sqrt{3}\, a^2/8$	$0.393\,\mathrm{nK}$	$< 2.36\,\mathrm{nK}$
Dirac healing length	$\xi_{\mathrm{Dirac}} = t_h a\sqrt{3}/2U$	$5.25\,\mu\mathrm{m}$	$0.50 - 50.0\,\mu\mathrm{m}$

Table 7.1: *Physical Parameters for the NLDE typical for a BEC of ^{87}Rb atoms.* The renormalized parameters are expressed in terms of fundamental quantities. The range of possible values account for the physical constraints discussed in the main text.

$$\psi(\mathbf{r}, t) = (AL_z)^{-1/2} f(x, y) h(z) e^{-i\mu t/\hbar}, \tag{7.1}$$

where $f(x, y)$ and $h(z)$ are the dimensionless spatial functions that describe the longitudinal and transverse normal modes, respectively, and μ is the chemical potential. Projecting onto the ground state of the transverse dimension $h_{\mathrm{gs}}(z)$, gives us an effectively 2D wave equation. In the case where $L_z \sim \xi$, $h_{\mathrm{gs}}(z)$ is just the ground state of the one-dimensional particle-in-a-box solution [68], we then have: $h_{\mathrm{gs}}(z) = \sqrt{2}\sin(\pi z/L_z)$. This reduces the 3D nonlinear Schrödinger equation to the 2D form. It may be convenient to express L_z and R in terms of the trap frequencies ω_x, ω_y, and

ω_z, in which case we may write: $L_z = (\hbar/M\omega_z)^{1/2}$, $R = \sqrt{\hbar M^{-1}(1/\omega_x + 1/\omega_y)}$. The transformation is then completed by defining the renormalized 2D chemical potential and interaction as

$$\mu_{2D} \equiv \mu + \frac{\hbar^2\pi^2}{2ML_z^2}\,, \quad g_{2D} \equiv \frac{3}{2}\frac{g}{L_z}\,. \tag{7.2}$$

The 2D renormalized average density can be related to the 3D average density using the transverse oscillator length or frequency:

$$\bar{n}_{2D} \equiv \frac{N}{A} = L_z\,\bar{n} = \left(\frac{\hbar}{M\omega_z}\right)^{1/2}\bar{n}\,. \tag{7.3}$$

Using this definition and the 2D single-particle wavefunction, $\psi(x,y) = A^{-1/2}f(x,y)$, we can write the 2D condensate density as $\rho_{2D}(x,y) = N\,|\psi(x,y)|^2$. The 2D renormalized healing length can also be constructed which we find acquires only an extra numerical factor,

$$\xi_{2D} \equiv \left(\frac{2}{3}\right)^{1/2}\frac{1}{\sqrt{8\pi\bar{n}a_s}} = \left(\frac{2}{3}\right)^{1/2}\xi\,. \tag{7.4}$$

Similarly, we find the 2D speed of sound to be: $c_{s,2D} = \sqrt{g_{2D}\bar{n}_{2D}/M} = (3/2)^{1/2}c_s$. It is important to keep track of the effect of the reduced dimensionality on the dimensions of the constants: $\psi(x,y)$ now has dimensions of length^{-1}, g_{2D} has dimensions energy$\times$length^2, and $\bar{n}_{2D}$ has dimensions length^{-2}.

7.2.3 Derivation of NLDE from 2D NLSE.

The derivation of the nonlinear Dirac equation begins with the second quantized Hamiltonian for a 2D system with the bosonic field operators $\hat{\psi} \equiv \hat{\psi}(\vec{r},t) = \hat{\psi}(x,y,t)$ obeying bosonic commutation relations in the Heisenberg picture. We then expand in terms of Bloch states belonging to A or B sites of the honeycomb lattice which breaks up the bosonic field operator into a sum over the two sublattices. The spatial

dependence in this expansion is encapsulated in the exponential Bloch wave and the Wannier functions $w(x, y)$ which are then integrated out leaving only number-operator terms in the form of a *Dirac-Hubbard Hamiltonian.* Finally, the operator terms are reduced to c-numbers by averaging over on-site coherent states and the long-wavelength limit is taken. We again recover a continuum theory but with a Weyl spinor wavefunction $\Psi = (\psi_A,\, \psi_B)$.

7.2.3.1 Normalization Condition.

The key point in discerning the correct normalization (and thus other related quantities) is the contraction of the many-body bosonic operators between localized coherent states. The parameter $|c_{i,j}|^2$ which labels the coherent state at site (i, j), emerges as the number of atoms at each site, so that $c_{i,j}$ itself becomes the continuous amplitude $\psi_A(\mathbf{r}, t)$ and $\psi_B(\mathbf{r}, t)$ in the long-wavelength limit. Note that the complex moduli of these amplitudes are pure dimensionless particle numbers, not densities, since they result from taking the spatial integral over the lattice. With the area per lattice site given by $A_l = \sqrt{3}a^2/4$, the local time-dependent sublattice densities can be reconstructed as: $\rho_{A(B)}(\mathbf{r}, t) = |\psi_{A(B)}(\mathbf{r}, t)|^2/A_l$. Then, the dimensionally correct sublattice mean-field wavefunctions must be given by $\psi_{A(B)}(\mathbf{r}, t)/\sqrt{A_l} = (16/3a^4)^{1/4}\, \psi_{A(B)}(\mathbf{r}, t)$, where a is the usual lattice spacing. The correct normalization procedure can now be deduced by writing down the total number of particles in the system

$$N = (16/3a^4)^{1/2} \int_0^{2\pi} d\phi \int r\, dr (|\psi_A(r, \phi; t)|^2 + |\psi_B(r, \phi; t)|^2), \tag{7.5}$$

where the upper limit of the radial integral is taken large enough so that the integrand is negligible. The total number of atoms of the system, N, appears on the right-hand-side.

7.2.3.2 Renormalized Atomic Interaction.

The $3D$ to $2D$ reduction and continuum regime result in an effective atomic interaction U, a renormalized version of the usual interaction g. We arrive at the explicit form for U by first approximating the lowest band on-site Wannier functions by the ground state of the harmonic oscillator potential. Integrating over the area of one site, we obtain a new local interaction strength:

$$\begin{aligned} U &\equiv g_{2D} \left(\frac{\sqrt{3}a^2}{4}\right)^2 \bar{n}_{2D}^2 \int dxdy \, |w_i(x,y)|^4 \\ &= g_{2D} \left(\frac{\sqrt{3}a^2}{4}\right)^2 \bar{n}_{2D}^2 \left(\frac{1}{2\pi\ell^2}\right) , \end{aligned} \tag{7.6}$$

where ℓ is the oscillator length of a lattice potential well. It is often more practical to express the area of one site in terms of the lattice constant: $\pi\ell^2 = \sqrt{3}a^2/4$, and all other parameters in terms of the corresponding 3D parameters. The interaction then takes the form

$$U = L_z \, g \, \bar{n}^2 \, \frac{3\sqrt{3}\, a^2}{8} . \tag{7.7}$$

Note, that U has dimensions of energy.

7.2.3.3 Natural Parameters of the NLDE

We can now identify the main parameters which appear in the NLDE. The dimensionful coefficient which multiplies the Dirac kinetic term is the effective speed of light $c_l \approx 0.272\,\mathrm{cm/s}$ (compare to the analogous coefficient for relativistic electrons: $c \approx 3.00 \times 10^8\,\mathrm{m/s}$). In terms of fundamental constants, we find $c_l \equiv t_h a\sqrt{3}/2\hbar$, where a is the lattice constant and t_h is the hopping energy. The natural length scale of the NLDE is the healing length: $\xi_{\mathrm{Dirac}} \equiv \hbar c_l/U = t_h a\sqrt{3}/2U$, which characterizes the distance over which a disturbance of the condensate will return to its uniform value.

We see that ξ_{Dirac} has the correct dimension of length. To simplify the notation, for the remainder of our paper we will omit the 2D subscript on all parameters and assume that these pertain to the 2D NLDE. Finally, the quantity U which appears in the NLDE determines the strength of the nonlinearity. We have provided a full list of relevant parameters associated with the NLDE in Table 7.1.

7.2.4 Physical Constraints

The realization of the NLDE in a condensate of ^{87}Rb atoms requires that several constraints are satisfied which we now list and discuss:

1. *Landau Criterion.* In order to avoid the instabilities associated with propagation faster than the sound speed in the condensate, we require that the effective speed of light is less than the 2D renormalized speed of sound.

2. *Long-wavelength Limit.* The NLDE describes propagation of the long-wavelength Bloch envelope of a BEC near the Dirac point. Thus, a necessary condition for realizing the NLDE in the laboratory is that the healing length (defined in the effective Dirac theory) must be much larger than the lattice constant.

3. *Relative Lengths for 2D Theory.* In order to obtain an effectively 2D system, the vertical oscillator length must be much smaller than the trap size along the direction of the plane of the condensate.

4. *Relative Energies for 2D Theory.* Analogous to the previous restriction, this condition relates to the 2D structure but pertains to the energies of the system. The key point is that we must avoid excitations vertical to the plane of the condensate while enabling them along the plane: the chemical potential and temperature must be less than the lowest transverse excitation energy.

5. *Weakly Interacting Regime.* The NLDE and RLSE are derived for a weakly interacting Bose gas. This ensures both the stability of the condensate as well

as the effective nonlinear Dirac mean field description. We then require the interaction energy to be significantly less than the total energy of the system.

6. *Dirac Cone Approximation.* For a condensate in the regime where the NLDE description is valid, we require that the linear approximation to the exact dispersion remain valid. As in the case of graphene, large deviations from the Dirac point induce second order curvature corrections to the dispersion. Thus, we must quantify the parameter restrictions which allow for a quasi-relativistic interpretation.

7. *Lowest Band Approximation.* We derive the NLDE and RLSE assuming that the lowest band is the main contribution to the dispersion.

Having stated each constraint, we can now address each one in detail and explore the conditions under which each is satisfied. In the following, we consider a BEC comprised of ^{87}Rb atoms where all numbers used are listed in Table 7.1 and are experimentally realsitic [227]. Stated mathematically, the Landau criterion requires that $c_l/c_{s,2\mathrm{D}} < 1$. Using the definitions for the effective speed of light and the sound speed found in the first part of this section, we compute $c_l/c_{s,2\mathrm{D}} = 0.904$, which satisfies the inequality. The long-wavelength limit is defined by $\xi_{\mathrm{Dirac}}/a \gg 1$, for which we find: $\xi_{\mathrm{Dirac}}/a = 9.48$. Next, for an effectively 2D system, the required length constraint implies the condition $L_z \ll R$. Taking $R \approx 100\,a$ (a typical condensate size), and using a realistic value for the vertical oscillator length (Table 7.1), we obtain $L_z = 5.45\,a$, which satisfies the constraint. Moreover, we require a healing length close to or less than the transverse oscillator length. With $\xi = 2.14\,\mu$m and $L_z = 3.00\,\mu$m, we find that this condition holds. The energy constraints may be stated as: $\mu, k_B T \ll \hbar\omega_z$. We can solve the NLDE for the lowest excitation to obtain an expression for the chemical potential [184]: $\mu = \hbar c_l k + U|\Psi|^2$. Next, we evaluate this expression using the lowest excitation in a planar condensate of radius $R \approx 100a$,

which has wavenumber $k \approx \pi/2R = 5.57 \times 10^4\,\mathrm{m}^{-1}$. The interaction U is computed using Eq. (7.7) for the binary interaction g and mass M pertaining to a condensate of ^{87}Rb atoms. Finally, for a uniform condensate, we take $|\Psi|^2 \approx 1$, and the constraint on the chemical potential becomes: $0.45\,\mathrm{nK} < 0.63\,\mathrm{nK}$, which is satisfied. For the temperature, we require: $T \ll \hbar\omega_z/k_B$. Using the data in Table 7.1 for the vertical oscillator frequency, we obtain the upper bound for the temperature: $T \ll 48.2\,\mathrm{nK}$. This is a reasonable requirement given that BEC occurs for T in tens or hundreds of nanoKelvins or as low as picoKelvins. Next, we check that we are in the weakly interacting regime, i.e., that $U/\mu \ll 1$. We use the value for the chemical potential μ, which we have just computed, and compare this to the interaction energy U, we find: $U/\mu = 0.62$. An essential feature of NLDE is that characteristic fluctuations are close enough to the Dirac point so that the linear Dirac cone approximation remains valid. To quantify this, we expand the exact dispersion near the Dirac point to obtain: $\mu(k) = U \pm t_h\left(a\sqrt{3}k/2 + a^2k^2/8 - a^3\sqrt{3}k^3/48 + ...\right)$, where k is the small momentum parameter which measures the deviation away from the Dirac point. Notice that the first term gives the linear dispersion of the Dirac equation while higher order corrections describe the bending of the band structure as we move away from the Dirac point. The second order term tells us that the NLDE description is valid as long as $ak/\sqrt{8} \ll 1$, which determines a lower bound on the wavelength for fluctuations of the condensate away from the Dirac point: $\lambda_{\min} \gg (2\pi/\sqrt{8})a$. The requirement of maintaining the linear dispersion then places an additional constraint on the chemical potential, namely that: $|\mu| \ll U + 6t_h \simeq 26.25\,\mathrm{nK}$. Using the value for the chemical potential found earlier, we see that $\mu = 0.45\,\mathrm{nK} \ll 26.25\,\mathrm{nK}$. Finally, since we are treating the case of weak short range interactions at very low temperatures, the lowest band approximation is sufficient to describe the physics of the NLDE.

7.2.5 Lattice Construction

The honeycomb optical lattice potential is straightforward to implement experimentally [187, 188]. The lattice is formed from three linearly polarized laser beams with co-planar wavevectors separated by an angle of 120° (see Figure 7.1). For a honeycomb lattice formed with blue-detuned light, all three beams have parallel polarizations orthogonal to the plane of propagation. Conversely, the red-detuned lattice has all three laser fields polarized parallel to the plane of propagation. In the latter case, the polarizations make an angle of 120° with respect to one another and the polarization of the net field is spatially dependent. Due to this polarization gradient, the red-detuned optical lattice potential is *spin-dependent* as described below.

Optical fields produce an ac Stark shift according to $V = -\frac{1}{2} E_i^{(+)} E_i^{(-)} \alpha_{ij}$ where $\mathbf{E}^{(\pm)}$ denote the positive/negative frequency components of the optical field and α_{ij} is the dynamic polarizability tensor (which is dependent on the optical frequency). For alkali atoms, the potential can be written as the sum of scalar and vector components $V = -\frac{1}{2}\alpha_{\rm sc}\mathbf{E}^{(-)} \cdot \mathbf{E}^{(+)} - \frac{1}{2}\alpha_{\rm vec} i \left(\mathbf{E}^{(-)} \times \mathbf{E}^{(+)}\right) \cdot \mathbf{F}$ where $\mathbf{F}$ is the total angular momentum operator [228]. Here we assume that the detuning of the laser beams from resonance is large in comparison to the hyperfine splitting in the excited state manifolds and neglect a third (tensor) contribution that only becomes significant near resonance. While the scalar light shift is independent of the atom's spin, the vector light shift produces a spin-dependent potential that acts as a spatially dependent effective magnetic field, i.e., $V(\mathbf{r}) = V_{\rm sc}(\mathbf{r}) + m_F\, g_F\, \mu_B\, B_{\rm eff}(\mathbf{r})$. Assuming that each of the beams shown in Figure 7.1 have equal amplitudes E_0, the potential they produce is given by

$$\begin{aligned} V(\mathbf{r}) \;=\; & -2\,V_{\rm sc}\,\{3 + 2\,\hat{\mathbf{n}}_1\cdot\hat{\mathbf{n}}_2\,\cos[(\mathbf{k}_1-\mathbf{k}_2)\cdot\mathbf{r}] + 2\,\hat{\mathbf{n}}_2\cdot\hat{\mathbf{n}}_3\,\cos[(\mathbf{k}_2-\mathbf{k}_3)\cdot\mathbf{r}] \\ & +2\,\hat{\mathbf{n}}_1\cdot\hat{\mathbf{n}}_3\,\cos[(\mathbf{k}_1-\mathbf{k}_3)\cdot\mathbf{r}]\} - 4\,V_{\rm vec}\,\{\hat{\mathbf{n}}_1\times\hat{\mathbf{n}}_2\sin[(\mathbf{k}_1-\mathbf{k}_2)\cdot\mathbf{r}] \\ & +\hat{\mathbf{n}}_1\times\hat{\mathbf{n}}_3\,\sin[(\mathbf{k}_1-\mathbf{k}_3)\cdot\mathbf{r}] + \hat{\mathbf{n}}_2\times\hat{\mathbf{n}}_3\,\sin[(\mathbf{k}_2-\mathbf{k}_3)\cdot\mathbf{r}]\}\cdot\mathbf{F}, \end{aligned} \tag{7.8}$$

where $\hat{\mathbf{n}}_i$ are unit vectors denoting the polarization of each beam, $V_{\rm sc} = \alpha_{\rm sc} E_0^2/8$, and $V_{\rm vec} = \alpha_{\rm vec} E_0^2/8$. In Eq. 7.8 we have neglected to include relative phase differences between the beams which only act to translate the lattice in two-dimensions without changing its topology [7]. The detuning from resonance controls the strength of the vector light shift relative to that of the scalar light as described in Ref. [188]

The honeycomb lattice produced by the scalar light-shift is described by a hexagonal Bravais lattice with a two-point basis as shown in Figure 7.1(b). In a red-detuned spin-dependent lattice, the depths of the A and B sublattices can be asymmetric, e.g., $|F, m_F\rangle = |2, 1\rangle$ or $|1, 1\rangle$, or symmetric, e.g., $|F, m_F\rangle = |1, 0\rangle$, depending on the internal state of the atom. An A/B sublattice asymmetry produces a mass gap at the Dirac points.

7.2.6 Preparing a BEC at a Dirac Point

Study of the NLDE will require that the BEC be prepared at a Dirac point, i.e., $\mathbf{K}$ or $\mathbf{K}'$ in Figure 7.1(c). Several experimental methods can potentially accomplish this: first, loading a BEC into the lowest-energy Bloch state and subsequently applying a constant acceleration for a fixed duration; second, loading an initially stationary BEC directly into a Bloch state at a Dirac point $\mathbf{K}$ by adiabatically applying a moving lattice potential which maintains a constant velocity $\hbar\mathbf{K}/M$; and third, loading a BEC into the lowest-energy Bloch state and subsequently populating a Dirac point by Bragg scattering using auxiliary fields. The first two methods have potential deficiencies. With regard to the first method, a dynamical instability may exist for intermediate values of the crystal momenta as it linearly increases from $\mathbf{0}$ to $\mathbf{K}$ [229]. For the second method, the timescale required for adiabaticity is divergent since there is no gap for crystal momenta along the Brillouin zone boundary in the absence of a lattice potential. Hence, we consider here the method of populating a Dirac point

[7] If the relative phases between the beams vary slowly, the atoms will adiabatically follow the optical lattice potential.

by inducing Bragg scattering between crystal momenta $\mathbf{0}$ and $\mathbf{K}$ using auxiliary laser fields.

It is straightforward to populate the lowest-energy Bloch state of a honeycomb lattice by adiabatically increasing the lattice depth as demonstrated in Ref. [188] where both the BEC and the lattice are stationary in the lab frame. Here we will assume that the BEC is in a hyperfine state with $m_F \neq 0$ and a spin-dependent potential is used. This is so that only the sublattice with the lowest energy, assumed here to be the A sublattice, becomes occupied [188]. Starting from this initial condition, we can transfer atoms to the Dirac point by Bragg scattering to thr associated Bloch state using two laser fields with wavevectors $\mathbf{k}_{\mathrm{b1}}$ and $\mathbf{k}_{\mathrm{b2}}$. These obey the condition $\mathbf{k}_{\mathrm{b1}} - \mathbf{k}_{\mathrm{b2}} = \mathbf{K}$ such that ω_{b1} and ω_{b2}. Also, we have that $\omega_{\mathrm{b1}} - \omega_{\mathrm{b2}} = \Delta\omega = [E_A(\mathbf{K}) - E_A(\mathbf{0})]/\hbar$. Here, the function E_A gives the dispersion relation for the lower (A) band of a honeycomb lattice with A/B sublattice asymmetry. These fields produce a Stark shift potential:

$$V_{\mathrm{Bragg}}(\mathbf{r}) = \frac{1}{2} V_B \left[\cos(\mathbf{K}\cdot\mathbf{r} - \Delta\omega\, t) + 1\right], \tag{7.9}$$

where V_B sets the strength of the potential. This potential couples the Bloch wavefunctions $\psi_{A,\mathbf{K}}(\mathbf{r}) = e^{i\mathbf{K}\cdot\mathbf{r}}\, u_{A,\mathbf{K}}(\mathbf{r})$ and $\psi_{A,\mathbf{0}}(\mathbf{r}) = u_{A,\mathbf{0}}(\mathbf{r})$ where $u_{A,\mathbf{K}}(\mathbf{r})$ and $u_{A,\mathbf{0}}(\mathbf{r})$ have the same periodicity as the lattice. Thus, both functions can be written in the form

$$u_{A,\mathbf{K}}(\mathbf{r}) = \sum_{\mathbf{Q}} C_{\mathbf{Q}}^{A,\mathbf{K}}\, e^{i\,\mathbf{Q}\cdot\mathbf{r}}, \tag{7.10}$$

where the sum over $\mathbf{Q}$ includes all vectors in the reciprocal lattice space. The coefficients $C_{\mathbf{Q}}^{A,\mathbf{K}}$ can be calculated for a honeycomb lattice of arbitrary scalar and vector potential depths, V_{sc} and V_{vec} respectively, by numerically computing the band structure for the potential given in Eq. 7.8 [77]. Application of the Bragg scattering

potential then results in Rabi oscillation between $\psi_{A,\mathbf{0}}$ and $\psi_{A,\mathbf{K}}$ with a Rabi frequency Ω_B given by

$$\Omega_B = \frac{V_B}{2\hbar} \sum_{\mathbf{Q}} (C_{\mathbf{Q}}^{A,\mathbf{K}})^* \, C_{\mathbf{Q}}^{A,\mathbf{0}}. \tag{7.11}$$

A particularly useful feature of using a honeycomb lattice potential with A/B sublattice asymmetry for preparation is that both the initial and final Bloch states ($\psi_{A,\mathbf{0}}$ and $\psi_{A,\mathbf{K}}$) have a group velocity relative to the lattice equal to zero. This is because we are transferring atoms to a superposition of the two degenerate states at the Dirac point: one with velocity c_l and the other with velocity $-c_l$. The former state is continuously connected to "particle" excitations, when the crystal momentum is increased, while the latter is continuously connected to "holes". If the lattice is stationary with respect to the lab frame, the condensate will then also be stationary both before and after transfer to the Dirac point. This is experimentally convenient since the condensate does not move out of the field of view and can remain confined in an external trapping potential at all times. Note that the condensate would not remain stationary if it were transferred to the Dirac point by Bragg scattering in a lattice with A/B sublattice symmetry, i.e., no mass gap. In this case, the lower and upper s-bands are degenerate at the Dirac point and the eigenstates can be chosen from a two-dimensional subspace of degenerate states spanned by two Bloch wavefunctions. Application of the V_{Bragg} potential breaks this degeneracy and excites the eigenstate which moves in the same direction as that of the walking standing wave potential V_{Bragg} with a group velocity having a magnitude of c_l in the frame of the lattice. The orthogonal eigenstate has a group velocity with the same magnitude but in the opposite direction and is not coupled by V_{Bragg} to the Bloch state with zero crystal momentum.

Once the condensate has been prepared at a Dirac point in a lattice with A/B sublattice asymmetry by Bragg scattering, the atoms can be transferred to a hy-

perfine state that does not experience the vector light shift and therefore no mass gap, e.g., $|F, m_F\rangle = |1, 1\rangle \rightarrow |1, 0\rangle$, using a radio-frequency (rf) or microwave (mw) field. For a spatially homogeneous rf/mw field, the transition matrix element is proportional to the spatial overlap of the initial and final spatial wavefunctions which are not orthogonal since they experience different lattice potentials. A spatially homogeneous rf/mw field cannot change the crystal momentum which is therefore conserved in the transition. In the absence of a vector light shift, the A and B sublattices are symmetric and there is no mass gap, yielding two degenerate Bloch states at the Dirac point $\mathbf{K}$. Two orthogonal basis states that span the degenerate subspace of eigenstates can be chosen to be states which have probability current density $\mathbf{j} \equiv -i\frac{\hbar}{2M}(\Psi^*\nabla\Psi - \Psi\nabla\Psi^*) = \mathbf{0}$ but are respectively localized on either the A or B sublattice sites. A state prepared at the Dirac point of a lattice with a mass gap will have significant spatial overlap with one of these basis states and vanishing overlap with the orthogonal state. For example, for parameters identical to those realized in [188], i.e., $V_{\text{sc}} = 4\,E_R$ and $V_{\text{vec}}/V_{\text{sc}} = 0.065$. The magnitude of the inner product between the initial and final states for wavefunctions localized on the same sublattice is $|\langle A, \mathbf{K}, m_F = 1|\ A, \mathbf{K}, m_F = 0\rangle| = 0.995$ whereas $|\langle A, \mathbf{K}, m_F = 1|\ B, \mathbf{K}, m_F = 0\rangle| = 0$. Thus, by driving a transition between internal states with a rf/mw field, a condensate which remains stationary can be prepared at the Dirac point of a honeycomb lattice with no mass gap. The state produced will only have amplitude in sites of the A sublattice. In the next section we discuss how the condensate can be coherently transferred between A and B sublattices by modulating the lattice potential.

7.2.7 Coherent Transfer Between Sublattices

In relativistic quantum field theories, the vacuum state defines the lowest energy configuration of the system. If massless particles appear in the spectrum, then excitations of the vacuum may occur for arbitrarily small energetic disturbances. However,

for general interacting theories, particles may acquire a finite mass through radiative corrections. In this case, we say that the interaction opens a *mass gap* in the spectrum. The analogous concept for condensed matter systems is the presence of an energy or band gap separating the highest filled single-particle states of the many-body ground state from the lowest excitations of the system. In particular, for general two-dimensional hexagonal lattices, a large number of possible gap-opening mechanisms exist. For example, for electrons in graphene-like systems there are 36 possible mass gaps which preserve particle-hole symmetry [155]. For bosons in a honeycomb optical lattice, one way to open a mass gap is to introduce anisotropic tunneling between lattice sites. The ground state will then consist of alternating occupied and unoccupied regions determined by the spatial modulation of the tunneling factors [16]; long-wavelength fluctuations will then be characterized by a finite excitation energy.

As previously discussed, we consider a system with A/B sublattice asymmetry which has a mass gap $2\,|m_s|$ separating the s-bands of the A and B sublattices at the Dirac point. Note that in the fully covariant NLDE, the mass gap will appear as a factor of mc_l multiplying the spinor wavefunction, where c_l is the effective speed of light. Transitions between Bloch states $\psi_{A,\mathbf{K}}$ and $\psi_{B,\mathbf{K}}$ can be driven by applying a periodic perturbation $H_m(\mathbf{r})\cos\omega_{\mathbf{s}}\mathbf{t}$ where $\hbar\omega_s = 2\,|m_s|$, and $H_m(\mathbf{r})$ is chosen to exclusively couple pairs of Wannier states w_A and w_B localized on adjacent A and B sites of a given unit cell, e.g., $\langle w_A(\mathbf{r}-\mathbf{r}_A)|\,H_m\,|w_B(\mathbf{r}-\mathbf{r}'_A-\boldsymbol{\delta}_1)\rangle = \hbar\,\Omega_m\,\delta_{\mathbf{r}_A,\mathbf{r}'_A}$ where $\boldsymbol{\delta}_1$ is the displacement between an A site and *one* of its three neighboring B sites. A perturbation which only couples pairs of Wannier states separated by one of the nearest neighbor displacement vectors, e.g., $\boldsymbol{\delta}_1$, conserves the crystal momentum so that $\langle\psi_{A,\mathbf{K}+\mathbf{q}}|\,H_m\,|\psi_{B,\mathbf{K}+\mathbf{q}'}\rangle = e^{i(\mathbf{K}+\mathbf{q})\cdot\boldsymbol{\delta}_1}\,\Omega_m\,\delta_{\mathbf{q},\mathbf{q}'}$.

A suitable perturbation H_m can be experimentally realized by modulating the amplitude of one of the lattice laser fields, which provides an anisotropic modulation of the tunneling matrix elements that discriminates tunneling in one direction, while

simultaneously frequency modulating the other two fields, which periodically shakes the lattice along the same direction. Amplitude modulation of the field $\mathbf{E}_1$ and frequency modulation of $\mathbf{E}_2$ and $\mathbf{E}_3$ in Figure 7.1, for example, yields a periodic perturbation with a spatial dependence given by

$$\begin{aligned} H_m(\mathbf{r}) &= V_m \left[\cos(\mathbf{k}_1 - \mathbf{k}_2)\cdot\mathbf{r} + \cos(\mathbf{k}_1 - \mathbf{k}_3)\cdot\mathbf{r} \right. \\ &\quad \left. + \sqrt{3}\,\frac{V_{\text{vec}}}{V_{\text{sc}}} m_F \left\{\sin(\mathbf{k}_1 - \mathbf{k}_2)\cdot\mathbf{r} + \sin(\mathbf{k}_1 - \mathbf{k}_3)\cdot\mathbf{r}\right\} - \kappa\,\hat{\boldsymbol{\delta}}_1\cdot\mathbf{r}\right], \end{aligned} \tag{7.12}$$

where κ depends on the relative amplitudes of the perturbations. The last term in the square brackets describes shaking of the lattice along the $\boldsymbol{\delta}_1$ direction while the other terms act to anisotropically modulate the tunneling matrix elements between nearest neighbors with tunneling in the $\boldsymbol{\delta}_1$ direction distinguished from the other two.

The perturbations resulting from amplitude and frequency modulation both anisotropically couple a Wannier state w_A to Wannier states w_B localized on the three neighboring sites, but discriminate tunneling in the $\boldsymbol{\delta}_1$ direction with different relative strengths. By adjusting the relative amplitude and phase of the two perturbations, nearest neighbors in the $\boldsymbol{\delta}_1$ direction can be strongly coupled with negligible coupling to neighboring sites in the other two directions. For the experimental conditions realized in Ref. [188], i.e., $V_{\text{sc}} = 3.7\,E_R$ and $\alpha = V_{\text{vec}}/V_{\text{sc}} = 0.065$ for $|m_F| = 1$ states of ^{87}Rb atoms with $\lambda_L = 830\,\text{nm}$, numerical solution [77] of Eq. (7.8) indicates that the matrix elements $\langle w_A(\mathbf{r} - \mathbf{r_A})|\, H_m\, |w_B(\mathbf{r} - \mathbf{r}'_A - \boldsymbol{\delta}_1)\rangle \simeq 0.07\,V_m\,\delta_{\mathbf{r}_A,\mathbf{r}'_A}$ are achieved for $\kappa \simeq 0.97\,k_L$. The mass gap $2\,|m_s| = \hbar\,(2\pi) \times 9.4\,\text{kHz}$ in this case. For $V_m = 0.325\,E_R$, the Rabi frequency $\Omega_m = (2\pi) \times 75\,\text{Hz}$ and complete sublattice transfer is attained by applying the perturbation for a time $\Omega_m/\pi = 7\,\text{ms}$ which has sufficient spectral resolution to resolve transitions to other bands.

To coherently transfer a condensate between sublattices when the condensate is initially in an internal state with $m_F = 0$, which does not experience an A/B sublattice asymmetry, an rf/mw transition can be applied to couple to an intermediate internal

state with $m_F \neq 0$ that does experience an A/B sublattice asymmetry. Modulation of the lattice potential with the perturbation $H_m(\mathbf{r}) \cos \omega_m t$ can then be applied to drive transitions between the A and B sublattices as described above provided that $\hbar\omega_m$ equals the mass gap for the condensate with $m_F \neq 0$. The atoms can be subsequently transferred back to the original internal state via an ensuing rf/mw transition.

If the rf/mw and lattice modulation frequencies are detuned from resonance with the intermediate states, this sequence of transitions behaves as a direct transition between Bloch states $|i\rangle = |\psi_{A,\mathbf{K}}\rangle$ and $|f\rangle = |\psi_{B,\mathbf{K}}\rangle$ with an effective Rabi frequency Ω_{AB} given by

$$\Omega_{AB} = \frac{\Omega_{\mathrm{mw1}}\,\Omega_m\,\Omega_{\mathrm{mw2}}}{\Delta_{\mathrm{mw1}}\,\Delta_{\mathrm{mw2}}}. \tag{7.13}$$

The parameters Δ_{mw1} and Δ_{mw2} control the detunings from the intermediate states. The parameters Ω_{mw1}, Ω_m, and Ω_{mw2} are the Rabi frequencies associated with the transitions out of the initial $m_F = 0$ state, from the A sublattice to the B sublattice, and finally back to the initial $m_F = 0$ state, respectively.

7.2.8 Creation of Vortices

In this section, we discuss how relativistic vortex solutions of the NLDE can be excited by modifying the technique for coherent sublattice transfer described in the previous section. The two-photon Raman transition drives Rabi oscillations between two hyperfine states in the electronic ground state of an atom by coupling through intermediate states which are optically excited electronic states. The transition matrix element between hyperfine states is proportional to the product of the two field amplitudes which drive the two-photon transition. To excite a vortex, the two optical fields are provided by co-propagating Gaussian and Laguerre-Gaussian laser beams which have a frequency difference corresponding to the energy splitting between the initial and final states but are both far-detuned from the intermediate states to reduce

spontaneous emission. The Laguerre-Gaussian beam carries a single unit of orbital angular momentum which is transferred to the atoms in the stimulated Raman transition [191]. The electric field amplitude of a Laguerre-Gaussian laser beam with radial mode index $p = 0$ and charge index $\ell = 1$ is proportional to

$$E_{\mathrm{LG}}^{p=0,\ell=1}(r,\theta) \propto r \exp\left(-\frac{r^2}{w_0^2}\right) \exp(i\theta), \tag{7.14}$$

where r and θ are respectively the radial and azimuthal coordinates relative to the optical axis and w_0 is the beam waist. The field of the Gaussian laser beam $E_{\mathrm{G}}(r,\theta) \propto \exp\left(-\frac{r^2}{w_0^2}\right)$. Thus, the effective Rabi frequency for the two photon transition $\Omega_{2\gamma} \propto \langle f| E_{\mathrm{G}}(\mathbf{r})\, E_{\mathrm{LG}}^{p=0,\ell=1}(\mathbf{r})\, |I_2\rangle$ where $|I_2\rangle$ and $|f\rangle$ are respectively the intermediate and final state spatial wavefunctions of the condensate. Due to the azimuthal phase winding $\exp(i\theta)$ of the LG field $E_{\mathrm{LG}}^{p=0,\ell=1}$, the Raman fields provide the appropriate spatial dependence to drive a transition to a final state $|f\rangle$ which has a single unit of angular momentum starting from the intermediate state $|I_2\rangle$ with no orbital angular momentum.

Starting from a condensate at the Dirac point $\mathbf{K}$ with amplitude only in the A sublattice sites, i.e., the Bloch state $\psi_{A,\mathbf{K}}$, the procedure described above would couple to a vortex/soliton solution of the NLDE which has a vortex in the B sublattice and a soliton, with no angular momentum, in the A sublattice. This solution of the NLDE in the continuum limit can be written as a Weyl spinor of the form $\Psi_f = (\psi_A, \psi_B) = (if_A(r), f_B(r)e^{i\theta})$ (see Sect. 7.3 below and Ref. [184]). The initial wavefunction of the condensate at the Dirac point $\psi_{A,\mathbf{K}}$ is described by the Weyl spinor $\Psi_i = (\psi_A, \psi_B) = (1, 0)$. Starting from the state $|i\rangle = \psi_{A,\mathbf{K}}^{m_F=0}$, the transition proceeds to an intermediate state with $m_F = 1$ at the Dirac point of the A sublattice (i.e. $|I_1\rangle = \psi_{A,\mathbf{K}}^{m_F=1}$), then to the B sublattice (i.e. $|I_2\rangle = \psi_{B,\mathbf{K}}^{m_F=1}$) by modulation of the lattice potential through application of $H_m \cos\omega_m t$. Finally, by the two-photon Raman transition, we obtain the final state $|f\rangle$. This is the vortex/soliton state in the internal state with $m_F = 0$.

If we assume that $w_0, \xi \gg a$ and take the tight binding and continuum limits, the effective Rabi Raman frequency

$$\begin{aligned} \Omega_{2\gamma} &\propto \langle I_2 |\, E_{\mathrm{G}}(\mathbf{r})\, E_{\mathrm{LG}}^{p=0,\ell=1}(\mathbf{r})\, | f \rangle \\ &\propto E_{\mathrm{G},0}\, E_{\mathrm{LG},0} \int dr\, f_B(r)\, r^2\, e^{-2r^2/w_0^2}. \end{aligned} \tag{7.15}$$

The radial dependence of the vortex in the B sublattice $f_B(r)$ is calculated below (see Sect. 7.3). The radial integral is positive definite and for $w_0 \sim \xi$ will give a non-zero Rabi frequency with an absolute value determined by the amplitudes of the fields driving the two-photon Raman transition and the dipole transition matrix elements for the 5S-5P electronic transitions in ^{87}Rb.

7.2.9 Coherent Transfer Between Dirac Points by Bragg Scattering

Once a BEC has been prepared at a Dirac point $\mathbf{K}$, coherent transfer to the non-equivalent Dirac point $\mathbf{K}'$ can be accomplished by Bragg scattering from a lattice formed using auxiliary laser fields [189]. In this case, the two additional laser fields have wavevectors $\mathbf{k}_{\mathrm{b1}}$ and $\mathbf{k}_{\mathrm{b2}}$ where $\mathbf{k}_{\mathrm{b1}} - \mathbf{k}_{\mathrm{b2}} = \mathbf{K}' - \mathbf{K} = -k_L\, \hat{\mathbf{y}}$ in the frame of the lattice. The lattice produced by these fields couples a BEC at crystal momentum $\mathbf{K} = k_L \left(\frac{\sqrt{3}}{2}\, \hat{\mathbf{x}} + \frac{1}{2}\, \hat{\mathbf{y}} \right)$ to a BEC with crystal momentum $\mathbf{K}' = k_L \left(\frac{\sqrt{3}}{2}\, \hat{\mathbf{x}} - \frac{1}{2}\, \hat{\mathbf{y}} \right)$ by Bragg scattering. Since the energies of the two coupled Dirac points are identical, resonance occurs when the optical frequencies of the auxiliary fields are equal and the standing wave they form is stationary in the frame of the honeycomb lattice.

In the frame of the lattice, the applied potential is

$$V_{\mathrm{Bragg}}(\mathbf{r}) = \frac{1}{2} V_B \left[\cos(\mathbf{K} - \mathbf{K}') \cdot \mathbf{r} + 1 \right]. \tag{7.16}$$

This potential couples the degenerate Bloch wavefunctions $\psi_{\mathbf{K}}(\mathbf{r})$ and $\psi_{\mathbf{K}'}(\mathbf{r})$. The matrix element coupling $\psi_{\mathbf{K}}$ and $\psi_{\mathbf{K}'}$ is then given by

$$\Omega_B^{\alpha,\beta} = \frac{V_B}{2\hbar} \sum_{\mathbf{Q}} \left(C_{\mathbf{Q}}^{\alpha,\mathbf{K}'} \right)^* C_{\mathbf{Q}}^{\beta,\mathbf{K}}, \tag{7.17}$$

where the coefficients $C_{\mathbf{Q}}^{\alpha,\mathbf{K}}$ are identical to those defined in Sect. 7.2.6 where the index α designates the sublattice on which the condensate is localized. These coefficients can be found by numerically computing the band structure for the potential given in Eq. (7.8) [77]. Note that there are four degenerate Bloch wavefunctions corresponding to the two possible inequivalent Dirac points ($\mathbf{K}$ and $\mathbf{K}'$) and the two possible sublattices (A and B). In the tight-binding limit, i.e., $V_{\text{sc}} \gg E_R$, the Bragg scattering lattice only couples Bloch states at the non-equivalent Dirac points that are localized on the same sublattice. In this limit, application of the Bragg scattering lattice will induce Rabi oscillations with frequency $\Omega_B^{\alpha,\alpha}$ between condensates localized on the same sublattice but at the non-equivalent Dirac points. For shallower depths of the honeycomb lattice, all four degenerate Bloch states will be coupled and the dynamics will be more complicated. However, even for a moderate lattice depth $V_{\text{sc}} = 4\,E_R$, the coupling between different sublattices is small enough that the dynamics are nearly identical to those of two coupled Bloch states.

Starting from a BEC initially prepared at a single Dirac point $\mathbf{K}$, application of the Bragg scattering potential will cause the amplitude to Rabi oscillate between $\psi_{\mathbf{K}}$ and $\psi_{\mathbf{K}'}$ with a Rabi oscillation frequency $\Omega_{\text{Bragg}} = 2\,|\langle \mathbf{K}'\,|V_{\text{Bragg}}|\,\mathbf{K}\rangle|$. The pulse duration of the auxiliary fields can be controlled to produce an arbitrary superposition of BECs at $\mathbf{K}$ and $\mathbf{K}'$ – with a $\frac{\pi}{2}$-pulse $\tau_{\pi/2} = \frac{\pi}{2}\frac{1}{\Omega_{\text{Bragg}}}$ producing an equal superposition.

7.3 Vortex Solutions of the NLDE

The NLDE describes the dynamics of a four-spinor, $\Psi \equiv (\Psi_+,\, \Psi_-)^T$, with the upper $(+)$ and lower $(-)$ two-spinors relating to opposite $\mathbf{K}$ and $\mathbf{K}'$ points of the honeycomb lattice:

$$i\gamma^{\mu}\partial_{\mu}\Psi - U\sum_{i=1}^{4}(M_i\Psi)(\Psi^{\dagger}M_i)\,\Psi = 0\,. \tag{7.18}$$

The matrices γ^{μ} are the usual Dirac matrices and the interaction terms are encapsulated in the summation with the matrices M_i constructed to give the correct cubic nonlinearites, local to each spinor component [52]. This describes a gapless theory which corresponds to massless interacting Dirac spinors. Since the interactions do not couple different spinor components, Eq. (8.3) can be split into two sets of equations (one for each of the **K** and **K′** points) of the form

$$i\hbar\,\partial_t\psi_A = -i\hbar c_l\,(\partial_x - i\partial_y)\,\psi_B + U\,|\psi_A|^2\,\psi_A \tag{7.19}$$
$$i\hbar\,\partial_t\psi_B = -i\hbar c_l\,(\partial_x + i\partial_y)\,\psi_A + U\,|\psi_B|^2\,\psi_B\,, \tag{7.20}$$

with the full solution expressed as a linear combination of solutions from each Dirac point. Note the presence of the effective speed of light, c_l, and interaction strength, U. We first look for solutions with cylindrical symmetry, i.e., vortex solutions with arbitrary integer phase winding in addition to bright soliton solutions. We can obtain a dimensionless form of the NLDE by expressing the spinor wavefunctions as: $\psi_A(r,\theta,t) = \pm i\,f_A(r)e^{i(\ell-1)\theta}\,e^{-i\mu t/\hbar}$, $\psi_B(r,\theta,t) = f_B(r)e^{i\ell\theta}\,e^{-i\mu t/\hbar}$, where ℓ is the integer vortex winding and μ is the chemical potential. In plane-polar coordinates, Eqs. (8.4)-(8.5) become

$$-\hbar c_l\left(\partial_r + \frac{\ell}{r}\right)f_B(r) + U\,|f_A(r)|^2 f_A(r) = \mu f_A(r) \tag{7.21}$$
$$\hbar c_l\left(\partial_r + \frac{1-\ell}{r}\right)f_A(r) + U\,|f_B(r)|^2 f_B(r) = \mu f_B(r). \tag{7.22}$$

Localized solutions of the NLDE may be categorized by their asymptotic forms, i.e., whether the amplitude has a zero or non-zero limit far from the core. This difference is significant since it is fundamentally related to the presence (or absence) of

an underlying topological structure. Solutions for which one or both spinor components are finite far from the core are *topological*: they may be derived as extrema for Lagrangians having effective potentials which exhibit at least one (or several) local minimum (minima) separated from the ground state (or saddle point solution) energy by a finite barrier in solution space. All other solutions, for which both spinor components fall to zero far from the core, do not have an underlying topological structure and are referred to as *non-topological*.

7.3.1 Asymptotic Bessel Solutions for Large Phase Winding

For integer winding $\ell \geq 2$, both f_A and f_B must vanish at $r = 0$ due to the presence of the centrifugal terms, so we will treat the special cases $\ell = 0, 1$ in a separate section. To obtain vortex solutions, we require spatial derivatives to vanish at infinity, so that for $r \to \infty$, Eqs. (8.6)-(8.7) yield the possible asymptotic forms: $f_{A(B)}(\infty)\left[|f_{A(B)}(\infty)|^2 - \mu/U\right] = 0$ or $f_{A(B)}(\infty) \sim r^{\alpha}$, for $0 < \alpha < 1$. The first case implies $\left|f_{A(B)}(\infty)\right| = 0,\ \pm\sqrt{\mu/U}$. For the case of non-vanishing boundary conditions and $\ell \geq 2$, the asymmetry in the angular momentum terms of the NLDE seems problematic. We recall that the factors $\partial_r + \ell/r$ and $\partial_r + (1-\ell)/r$ act as index raising and lowering operators for the Bessel functions J_n. This becomes clear when we check that Bessel functions are exact solutions in the zero interaction or low density limit given by $\hbar c_l/U|\Psi|^2 \gg 1$. In this limit, solutions of Eqs. (8.6)-(8.7) are Bessel functions of the first kind, J_l and J_{l-1}, only slightly modified by the weak interaction terms which describe scattering into other Bessel functions. We then choose the modified Bessel-Fourier expansion as our ansatz

$$f_A(r) = A\,F(r)\,e^{iQ(r)}\left[a_0 + \sum_{n=1}^{\infty} a_n J_n(r)\right] \tag{7.23}$$

$$f_B(r) = (B/A)\,f_A(r)\,, \tag{7.24}$$

where A and B are normalization constants, $J_n(r)$ is the Bessel function of the first kind of order n, a_0 and a_n are the expansion coefficients, and $Q(r)$ is the argument of the integrating factor, which we include to enlarge the parameter space. The series that we have chosen to use runs over the Bessel index rather than the usual form where the summation runs over the zeros of one Bessel function with fixed index. Our choice of expansion is certainly valid but does not offer the convenience of using the standard orthonormal relations for Bessel functions when computing the coefficients.

Once the ansatz is substituted into the NLDE, we combine the angular momentum and derivative terms in the series by using the recurrence relations for Bessel functions: $J_n/x = (J_{n-1}+J_{n+1})/2n$ and $J_n' = (J_{n-1}-J_{n+1})/2$. Substituting Eqs. (7.23)-(7.24) into Eqs. (8.6)-(8.7) gives two first-order differential equations for the integrating factor Q in addition to the recursion relations for the coefficients a_n. We find that Q must solve the first order equation

$$iQ' = -\frac{F'}{F} - \frac{a_0 \ell}{r} \pm \frac{U}{\hbar c_l} i|AF|^2 \left| a_0 + \sum_n a_n J_n \right|^2 \mp i \frac{\mu}{\hbar c_l} \frac{a_0 + \sum_n C_n' a_n J_n}{a_0 + \sum_n a_n J_n}, \tag{7.25}$$

in addition to a similar equation but where ℓ is replaced by $1-\ell$. The recursion relations for the a_n are

$$\begin{aligned} \frac{a_{n+1}}{2}\left(\frac{\ell+n+1}{n+1}\right) + \frac{a_{n-1}}{2}\left(\frac{\ell-n+1}{n-1}\right) &= -\frac{\mu A}{\hbar c_l B} C_n a_n \\ \frac{a_{n+1}}{2}\left(\frac{2-\ell+n}{n+1}\right) + \frac{a_{n-1}}{2}\left(\frac{2-\ell-n}{n-1}\right) &= \frac{\mu B}{\hbar c_l A} C_n a_n. \end{aligned} \tag{7.26}$$

In Eq. (7.25) we have absorbed a term-dependent fraction $C_n \equiv 1 - C_n'$, from the chemical potential terms, into the recursion relations. We can solve the recursion relations to get

$$A = \pm iB\,, \quad a_n = \left(\pm i \frac{C\mu}{U(2\ell-1)}\right)^{n-1} \frac{n!}{n^{n-1}}\,. \tag{7.27}$$

To obtain a vortex solution, we set $a_0 = -1/2\ell$ which cancels the factor of $F(r)$ in Eq. (7.25), provided $F = r^{1/2}$. This effectively allows the solution to vanish at the origin and also balances the behavior of the Bessel functions at long distances. The vortex solution is obtained by tuning the parameter C in Eq. (7.27) to some critical value C_{vortex}. If we examine the asymptotic region $r \gg \xi_{\text{Dirac}}$, far from the vortex core, the Bessel functions decrease at a rate proportional to $r^{-1/2}$. On the other hand, near the vortex core where $r \ll \xi_{\text{Dirac}}$, the Bessel functions have the form $J_n \sim r^n$, for $n \geq 1$. Using this information, in the regions $r \ll \xi_{\text{Dirac}}$ and $r \gg \xi_{\text{Dirac}}$, and for weak interaction U, we obtain the asymptotic integral solution of Eq. (7.25)

$$iQ \approx \pm i \frac{\mu}{\hbar c_l} r \,. \tag{7.28}$$

The vortex profile is obtained for $\ell^2 \gg 1$ and for the values $C_{\text{vortex}} = 2.5 \times (2\ell - 1)$ and $\mu/U = 1$. We have plotted this solution in Figure 7.6(a) which has a closed form given by

$$f_A(r) = A(Ur/\hbar c_l)^{1/2}\, e^{\pm i(Ur/\hbar c_l)} \sum_{n=1}^{\infty} (2.5\, i)^{n-1} \frac{n\,!}{n^{n-1}} J_n(Ur/\hbar c_l)\,, \tag{7.29}$$

where the overall constant A is determined by normalizing the wavefunction. Density and phase plots for the complex Bessel solution are shown in Figure 7.4.

7.3.2 Numerical Shooting Method for Vortices with Arbitrary Phase Winding and Chemical Potential

The radial profile for a topological vortex with arbitrary winding number ℓ can be obtained using a numerical shooting method [230]. The most direct approach is to express Eqs. (8.6)-(8.7) in terms of the dimensionless radial variable $\chi \equiv (U/\hbar c_l)r$. The functions $f_A(\chi)$ and $f_B(\chi)$ are then expanded in power series around $\chi = 0$:

$$f_A(\chi) = \sum_{j=0}^{\infty} a_j \chi^j \,, \quad f_B(\chi) = \sum_{j=0}^{\infty} b_j \chi^j \,, \tag{7.30}$$

where the a_j and b_j are the expansion coefficients. Since we are solving two coupled first order equations, we require the initial conditions $f_A(0)$ and $f_B(0)$. Substituting into Eqs. (8.6)-(8.7) gives us the core behavior

$$f_A(0) \sim \chi^{\ell-1}\,, \qquad f_B(0) \sim \chi^{\ell}\,. \tag{7.31}$$

These core values indicate that the first nonzero coefficients for a given choice of ℓ are $a_{\ell-1}$ and b_ℓ, where $a_{\ell-1}$ is sufficient to determine all other coefficients for both expansions in Eq. (8.41). For a given ℓ value, a vortex is found by tuning $a_{\ell-1}$ towards a critical value $a_{\ell-1}^{\rm vortex}$. As examples, we have found vortices for the three lowest ℓ values for which both spinor components have nonzero rotation:

$$a_1^{\rm vortex} = 0.571718...\,, \qquad \ell = 2\,, \tag{7.32}$$
$$a_2^{\rm vortex} = 0.145291...\,, \qquad \ell = 3\,, \tag{7.33}$$
$$a_3^{\rm vortex} = 0.0240267...\,, \qquad \ell = 4\,. \tag{7.34}$$

In Figure 7.2 we have plotted both components for the case $\ell = 2$ and illustrated the convergence to the vortex solution by overlaying an excitation of the vortex (a) and the free particle Bessel solution (b). The $\ell = 4$ numerical topological vortex solution density and phase are shown in Figure 7.5 and the radial solution plotted in Figure 7.6(b).

The same shooting method can be used to obtain the ring-vortex solutions for the special case of the chemical potential $\mu = 0$. These types of solutions are non-topological vortices whose tails decay to zero far from core. Although we demonstrate such solutions by analytical methods in the next section, the numerical approach allows us to illustrate the transition from the vortex limit ($\mu \ll U$) to Bessel solutions in the free particle limit ($\mu \gg U$). This transition is illustrated in Figure 7.3 for the strength of the nonlinearity U fixed to unity and the chemical potential running from 0.001 to 2. In Sec. 7.4, we provide a more thorough discussion of our numerical

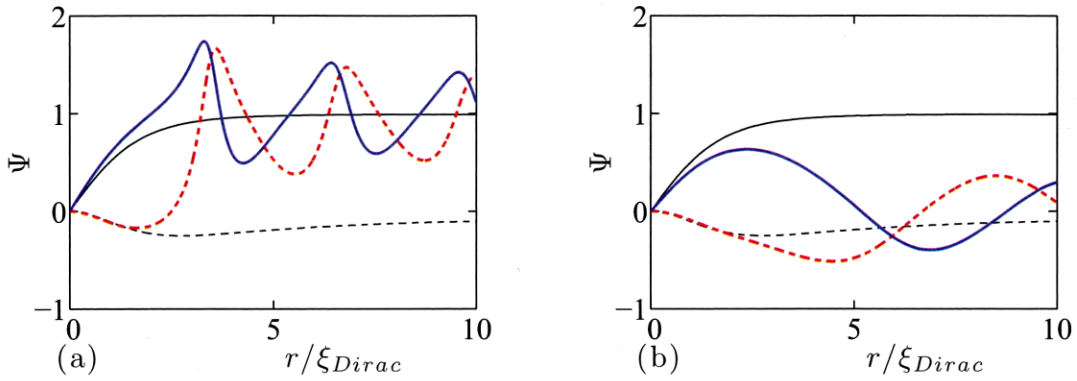

Figure 7.2: (color online) *Convergence of numerical vortex for* $\ell = 2$. (a) For $a_1 > a_1^{\text{vortex}}$, the solution overshoots to an excited state of the vortex. (b) For $a_1 < a_1^{\text{vortex}}$, the solution undershoots and converges to the linear solution Bessel functions. Note that the solid blue and dashed red plots are the A and B sublattice radial wavefunctions, respectively. The solid black and dashed black plots are the exact solutions for the A and B sublattice radial wavefunctions, respectively.

results.

7.3.3 Algebraic Solutions for Zero Chemical Potential and Phase Winding Greater than One

By setting $\mu = 0$ in Eqs. (8.6)-(8.7), it is possible to obtain exact non-topological vortex solutions which fall to zero far from the core. From a technical standpoint, eliminating the chemical potential terms in the NLDE simplifies the problem considerably in that solutions to the homogeneous non-interacting equations are simple algebraic forms: vortices are not connected to Bessel function scattering states. Starting from an algebraic ansatz $f_{A(B)} = A(B)r^{\alpha(\beta)}/(1 + Cr^{\delta})^{1/2}$, where $\alpha, \beta, \delta, C \in \mathbb{R}$ and $A, B \in \mathbb{C}$, substituting into Eqs. (8.6)-(8.7) and solving for A, B, C, α, β and δ we find

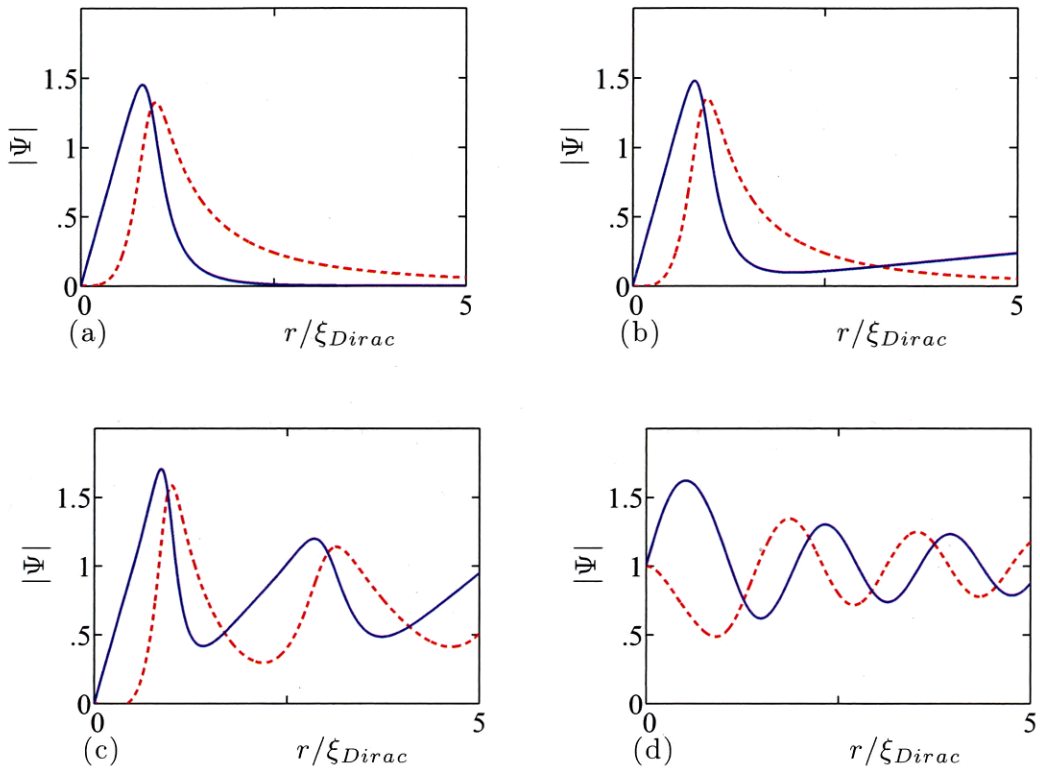

Figure 7.3: (color online) *Connection of ring-vortex solution to free particle Bessel solution.* The vortex limit is shown in (a) where we have taken the chemical potential to be small: $\mu = 0.001$. The solutions for $\mu = 0.05$ and $\mu = 0.5$ are shown (b) and (c), respectively. Finally, the free particle limit is shown in (d) for the value $\mu = 2$. Note that in (d) the spinor components become Bessel functions of the first J_0 and J_1 .

$$f_A(r) = \frac{A\,(Ur/\hbar c_l)^{\ell-1}}{\left[1+\frac{|B|^2B}{A(4\ell-2)}\,(Ur/\hbar c_l)^{8(\ell-1/2)}\right]^{1/2}} \tag{7.35}$$

$$f_B(r) = \frac{B\,(Ur/\hbar c_l)^{3\ell-2}}{\left[1+\frac{|B|^2B}{A(4\ell-2)}\,(Ur/\hbar c_l)^{8(\ell-1/2)}\right]^{1/2}}\,, \tag{7.36}$$

which we have plotted in Figure 7.6(c) and (d) for the angular windings $\ell = 1, 4$. Density and phase plots for the $\ell = 2$ case are shown in Figure 7.7.

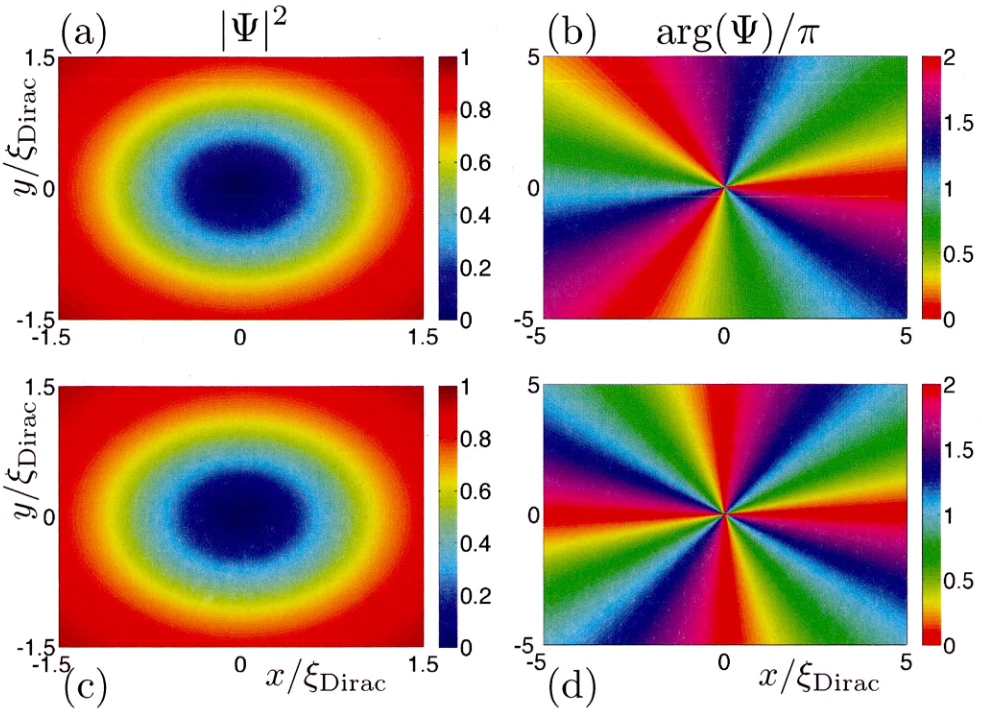

Figure 7.4: (color online) *Phase and density for the Bessel topological vortex for* $\ell = 4$. (a,b) A sublattice density and phase. (c,d) B sublattice density and phase.

In solving for Eqs. (7.35)-(7.36), we obtain an additional constraint that relates the constants A and B: $|A|^2 A/B = |B|^2 B/CA = 4\ell - 2$, as well as the normalization condition

$$\int r dr \, \frac{|A|^2 \left(Ur/\hbar c_l\right)^{2\ell-2} + |B|^2 \left(Ur/\hbar c_l\right)^{6\ell-4}}{\left[1 + \frac{|B|^2 B}{A(4\ell-2)} \left(Ur/\hbar c_l\right)^{8(\ell-1/2)}\right]} = 1 \, . \tag{7.37}$$

It is possible to prove that this type of algebraic solution does not exist for $\mu \neq 0$ and $\ell \geq 2$.

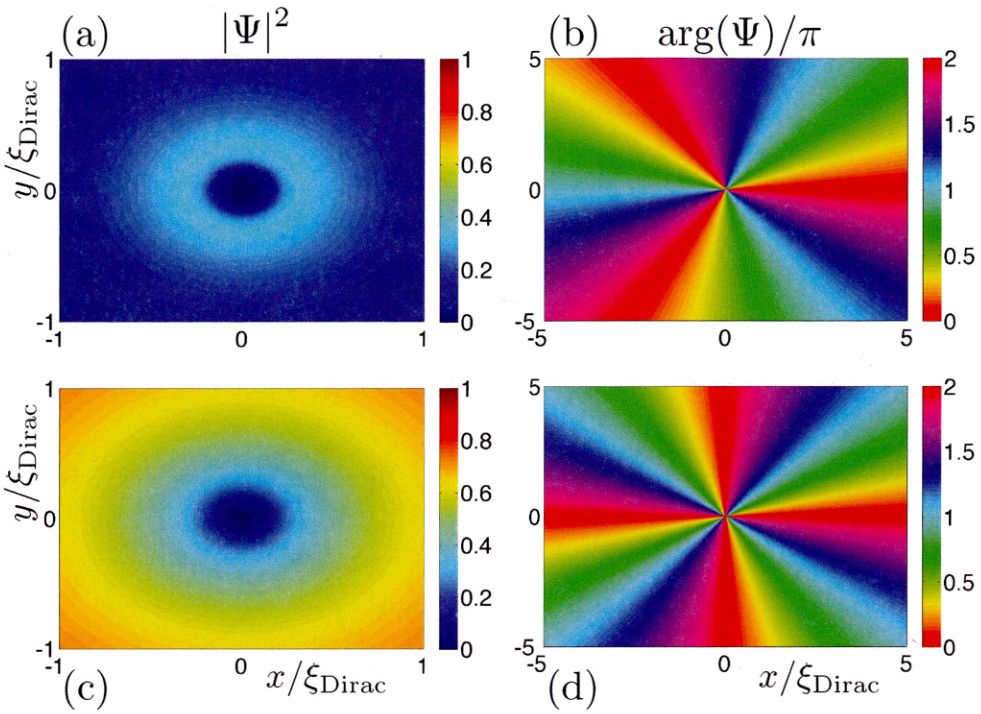

Figure 7.5: (color online) *Phase and density for the $\ell = 4$ numerical topological vortex.* (a,b) A sublattice density and phase. (c,d) B sublattice density and phase.

7.3.4 Algebraic Solutions for Zero and Unit Phase Winding

When the winding parameter $\ell = 0$ or 1, the angular momentum term will appear in only one of Eqs. (8.6)-(8.7). In this case, the NLDE is easier to solve and allows for a simple algebraic type solution, even when $\mu \neq 0$.

7.3.5 Ring-Vortex/Soliton.

For the homogeneous case ($\mu = 0$), our previous results for arbitrary values of ℓ, given by Eqs. (7.35)-(7.36), will give us the correct solution. Substituting $\ell = 1$ gives

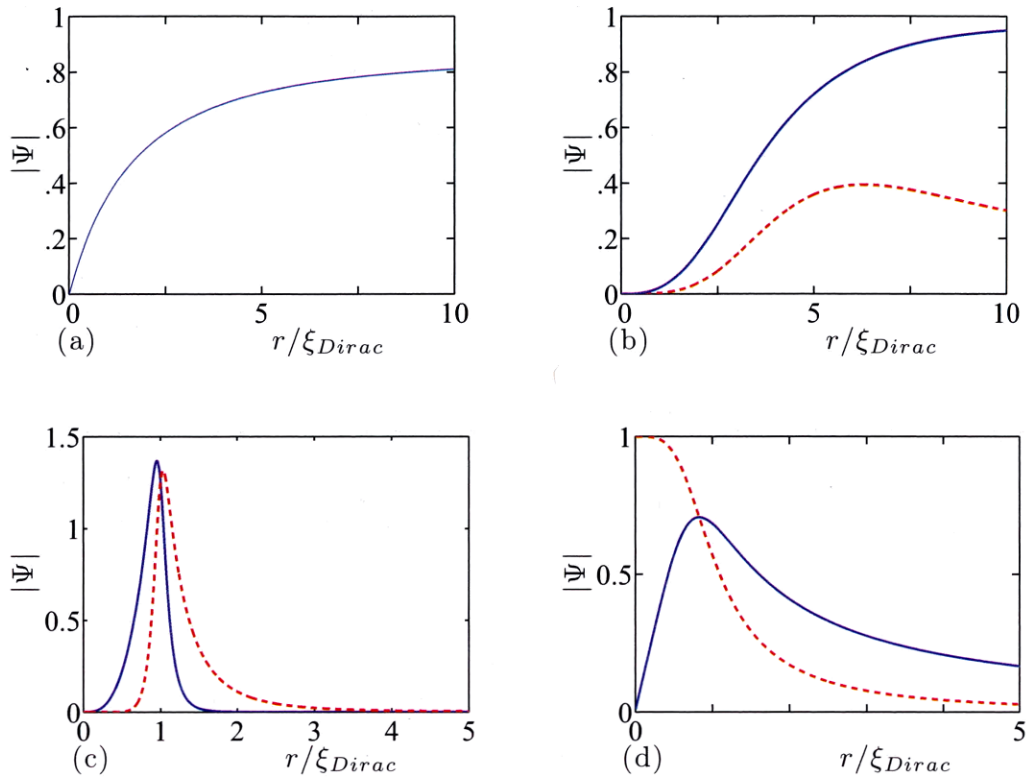

Figure 7.6: (color online) *NLDE vortex radial solutions.* Shown are: (a) Bessel solution for $\ell = 3$; (b) numerical solution for $\ell = 4$; (c) ring-vortex solution for $\ell = 4$; (d) ring-vortex/soliton solution.

$$f_A(r) = \frac{A}{\left[1 + \frac{|B|^2 B}{2A}\left(Ur/\hbar c_l\right)^4\right]^{1/2}} \tag{7.38}$$

$$f_B(r) = \frac{B\left(Ur/\hbar c_l\right)}{\left[1 + \frac{|B|^2 B}{2A}\left(Ur/\hbar c_l\right)^4\right]^{1/2}}. \tag{7.39}$$

This is the ring-vortex/soliton solution from our previous work [184] and describes a vortex whose density peaks in the shape of a ring with a bright soliton located at its center. Setting $\ell = 0$ in Eqs. (7.35)-(7.36), simply interchanges the forms for f_A and f_B. The ring-vortex/soliton radial solution is plotted in Figure 7.6(d), and density and phase are shown in Figure 7.8.

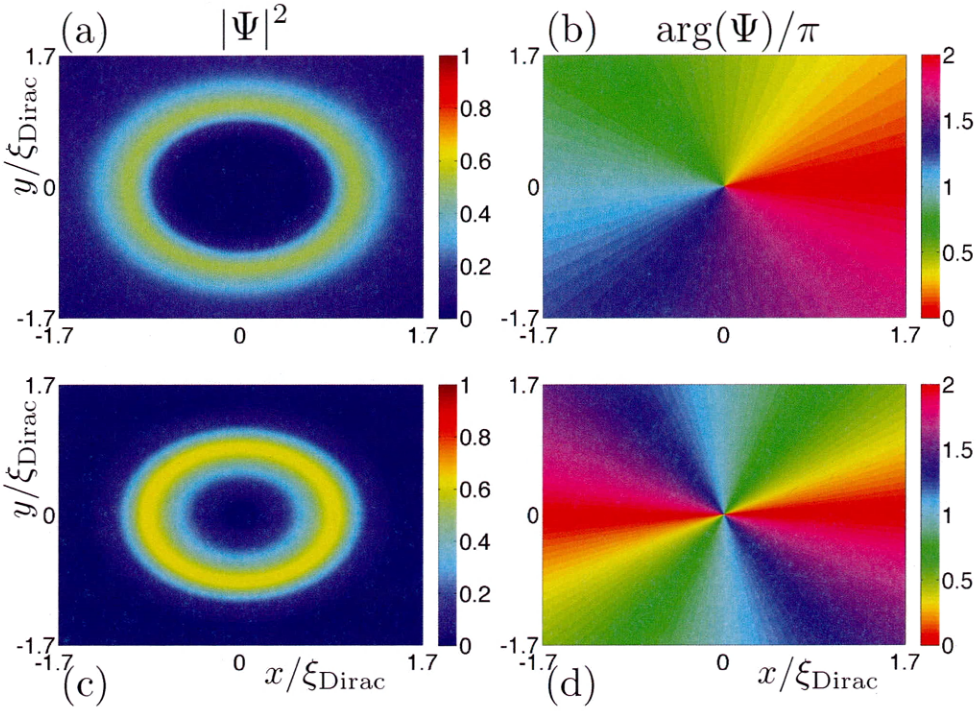

Figure 7.7: (color online) *Phase and density for the $\ell = 2$ ring-vortex.* (a,b) A sublattice density and phase. (c,d) B sublattice density and phase.

7.3.6 Vortex/Soliton.

For the case $\mu \neq 0$ and $\ell = 1$, we find the solutions

$$f_A(r) = \frac{\sqrt{\mu/U}(\mu\, r/\hbar c_l)}{[1+(\mu\, r/\hbar c_l)^2]^{1/2}} \tag{7.40}$$

$$f_B(r) = \frac{\sqrt{\mu/U}}{[1+(\mu\, r/\hbar c_l)^2]^{1/2}}\,. \tag{7.41}$$

This is the *vortex/soliton* solution from our previous work and describes an ordinary vortex, f_A, with a bright soliton, f_B, centered at the core of the vortex. This solution can also be obtained by beginning with the ansatz $f_A = \tanh[g(r)]$, $f_B = \mathrm{sech}[g(r)]$ which, upon substitution into the NLDE, may be directly integrated

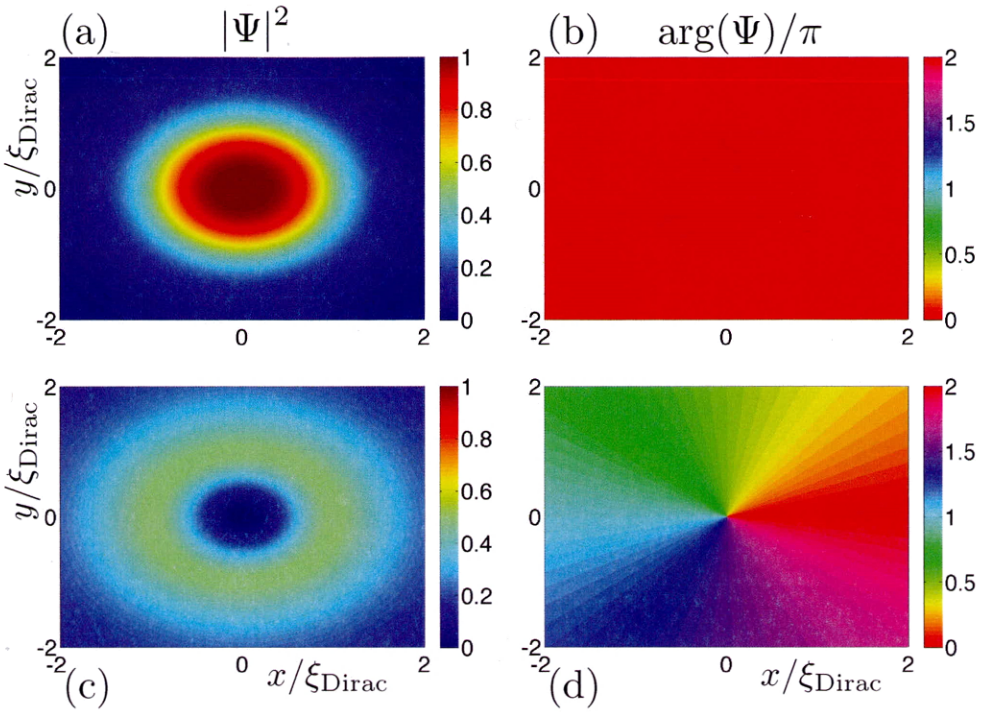

Figure 7.8: (color online) *Phase and density for the $\ell = 1$ ring-vortex/soliton.* (a,b) A sublattice density and phase. (c,d) B sublattice density and phase.

to give $g(r) = \mathrm{arcsinh}(\mu r/\hbar c_l)$; applying a standard identity then yields Eq. (7.41). For $\ell = 1$, f_B is the vortex and f_A the soliton with a phase difference of -1 between the two components. The vortex/soltion radial solution, density and phase are shown in Figure 7.11(a) and Figure 7.9, respectively.

7.3.7 Skyrmion Solutions

To obtain Skyrmion type solutions, we choose an ansatz of the form: $f_A = \eta\cos\varphi$, $f_B = \eta\sin\varphi$, where in general the parameters η and φ are both functions of the radial coordinate: $\eta(r)$, $\varphi(r)$ (for background on skyrmions in 2-dimensions see [42, 200]). The NLDE then reduces to two first order nonlinear ODEs

$$\frac{d\varphi}{dr} = \frac{(1+\ell)}{2r}\sin 2\varphi + \frac{U}{2\hbar c_l}\eta^2(1+\cos^2 2\varphi) - \frac{\mu}{\hbar c_l} \tag{7.42}$$

$$\frac{d\eta}{dr} = \eta\frac{\ell}{r}\cos 2\varphi - \eta\frac{1}{r}\cos^2\varphi + \frac{U}{\hbar c_l}\eta^3 \sin 4\varphi\,. \tag{7.43}$$

The first point to note is that the centripetal terms place a restriction on the behavior of φ for $r \to 0$: Eq. (7.42) forces the condition $\varphi \to n\pi/2$ ($n \in \mathbb{Z}$), while the only way to keep Eq. (7.43) finite at $r = 0$ is to require $\ell = 1$, which corresponds to $\varphi(0) = \pi$, or $\ell = 0$ for $\varphi(0) = \pi/2$. Thus, skyrmion solutions exist only for *one unit of angular momentum* in either the upper or the lower two-spinor component (choosing $\ell = 0$ or 1 simply transfers a unit of rotation from one component to the other.) We can further simplify the problem with the restriction that $\eta = C \equiv$ constant. To find C, we can look at the asymptotic form of the equations for $r \to \infty$, since then, assuming finite energy of course, we can set the derivative terms equal to zero and thereby obtain the asymptotic values

$$\varphi(\infty) = \frac{m\pi}{4}\,, \quad \eta = \pm\sqrt{\frac{4\,\mu/U}{3+(-1)^m}}\,, \tag{7.44}$$

where $m \in \mathbb{Z}$. Next, we combine Eqs. (7.42)-(7.43) into one equation for φ,

$$\frac{d\varphi}{dr} = \frac{1}{r}\sin 2\varphi - \frac{\mu}{\hbar c_l} + \frac{2\mu C_m}{\hbar c_l}\left[1 + \left(\cos^2\varphi - \frac{4\mu C_m}{\hbar c_l}\, r \sin 4\varphi\right)^2\right], \tag{7.45}$$

for $\ell = 1$, and,

$$\frac{d\varphi}{dr} = \frac{1}{2r}\sin 2\varphi - \frac{\mu}{\hbar c_l} + \frac{2\mu C_m}{\hbar c_l}\left[1 + \left(\sin^2\varphi - \frac{4\mu C_m}{\hbar c_l}\, r \sin 4\varphi\right)^2\right], \tag{7.46}$$

for $\ell = 0$, where $C_m = 1/2$ for odd m, and $C_m = 1/4$ for even m.

7.3.8 Anderson-Toulouse Skyrmions

As we stated previously, Eqs. (7.42)-(7.43) allow for two types of solutions labeled by the subscript m: one that asymptotically approaches $\pi/4$ and another that approaches 0. The Anderson-Toulouse solution is obtained for $\varphi(0) = \pi/2$ and $\varphi(\infty) = 0$ [231, 232].

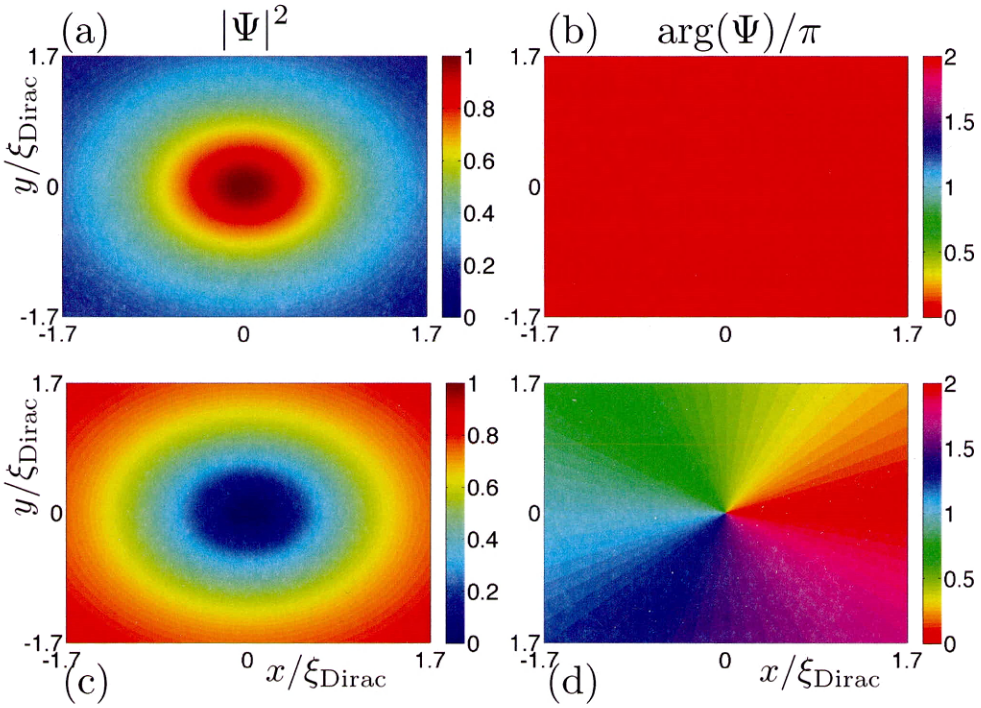

Figure 7.9: (color online) *Phase and density for the $\ell = 1$ vortex/soliton.* (a,b) A sublattice density and phase. (c,d) B sublattice density and phase.

7.3.9 Mermin-Ho Skyrmions

This is obtained for the case $\varphi(\infty) = \pi/4$ [231, 233]. Note that in both cases we have $\eta = \sqrt{2\mu/U}$.

The radial profiles for both the Mermin-Ho and Anderson-Toulouse vortices are obtained by solving Eqs. (7.45)-(7.46) using a straightforward shooting method. We

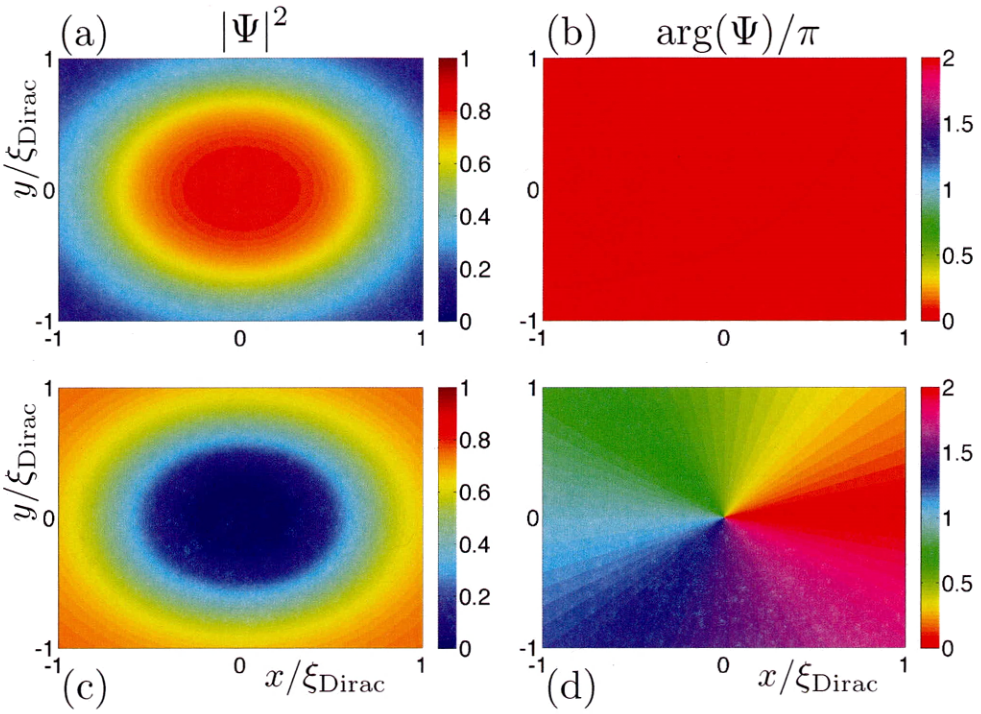

Figure 7.10: (color online) *Phase and density for the $\ell = 1$ Anderson-Toulouse skyrmion.* (a,b) A sublattice density and phase. (c,d) B sublattice density and phase.

have plotted the radial solutions for both types in Figure 7.11 and the density and phase plots are shown in Figure 7.10 and Figure 7.12.

7.3.10 Half-Quantum Vortices

We can construct a half-quantum vortex solution (a fractional vortex with half-integer winding) by forming superpositions of f_A and f_B for the Mermin-Ho vortex in part *b.* above [179, 234]. The key requirement is that both components do not vanish at infinity (see Figure 7.11(c)). We choose the linear combinations: $f_A = -ie^{i\theta/2}\sin\varphi - ie^{-i\theta/2}\cos\varphi$ and $f_B = ie^{i\theta/2}\sin\varphi - ie^{-i\theta/2}\cos\varphi$. Note that these no longer constitute a solution of the *time-independent* NLDE, but they do provide a stationary solution of the full NLDE. To see how the fractional winding comes about, we note

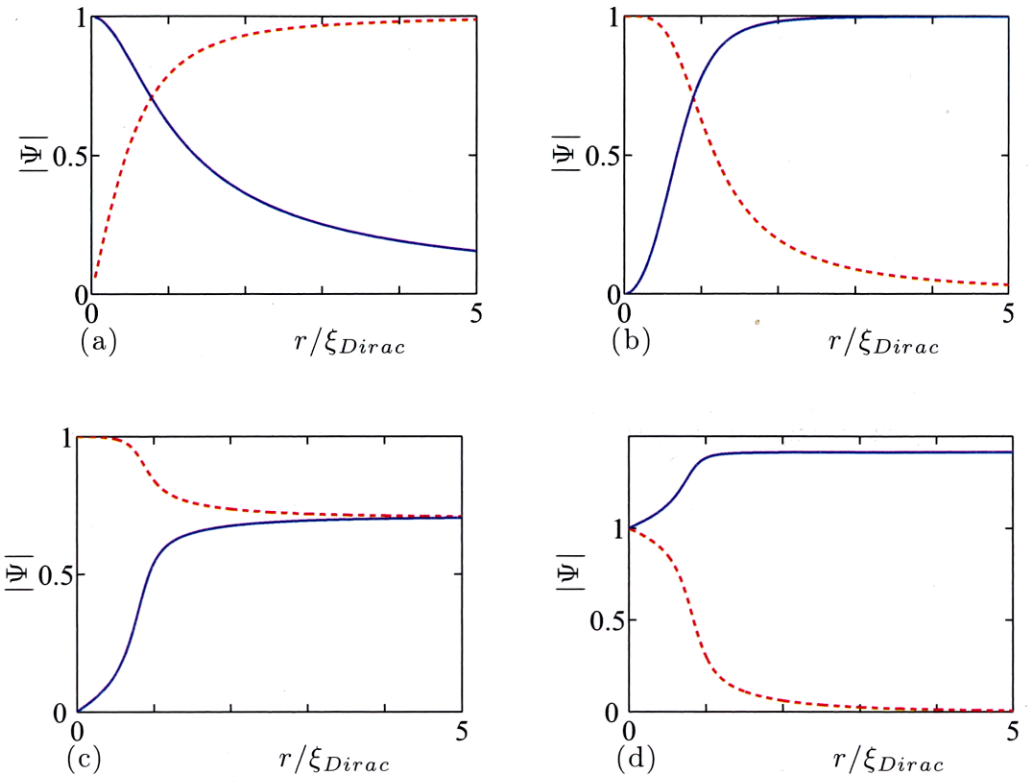

Figure 7.11: (color online) *NLDE vortex radial solutions.* Shown are: (a) vortex/soliton; (b) Anderson-Toulouse vortex; (c) Mermin-Ho vortex; (d) half-quantum vortex.

that far from the vortex core, $\varphi \to \pi/4$, and the wavefunction takes the form

$$\Psi = 2\sqrt{\mu/U}e^{-i\theta/2}\,[i\cos(\theta/2),\,\sin(\theta/2)] \tag{7.47}$$

. From this, we can compute the geometric phase that comes from encircling the core by computing the Berry phase ϕ_B:

$$\phi_B \equiv \exp\left(\oint d\theta \langle\Psi\left|\frac{\partial}{\partial\theta}\right|\Psi\rangle\right). \tag{7.48}$$

The wavefunction for the vortex transforms as a Dirac spinor under spatial rotations and acquires a factor of $\exp(-i\sigma_z\theta/2)$, where σ_z is the third Pauli matrix, so that the exponent in Eq. (7.48) becomes

Vortex type	Winding	Analytic form of $\Psi(\mathbf{r})$	Topology
Vortex/Soliton	$\ell = 1$	$\left[ie^{-i\theta}\frac{(r/r_0)}{\sqrt{1+(r/r_0)^2}},\ \frac{1}{\sqrt{1+(r/r_0)^2}}\right]^T$	$\lvert\psi_A(\infty)\rvert = 1$
Ring-Vortex/Soliton	$\ell = 1$	$\left[ie^{-i\theta}\frac{(r/r_0)}{\sqrt{1+(r/r_0)^4}},\ \frac{1}{\sqrt{1+(r/r_0)^4}}\right]$	non-topological
Anderson-Toulouse	$\ell = 1$	$\left[ie^{-i\theta}\cos\varphi(r),\ \sin\varphi(r)\right]^T$	$\varphi(\infty) = 0$
Mermin-Ho	$\ell = 1$	$\left[ie^{-i\theta}\cos\varphi(r),\ \sin\varphi(r)\right]^T$	$\varphi(\infty) = \pi/4$
Half-Quantum Vortex	$\ell = 1$	$[i\cos\theta/2,\ \sin\theta/2]^T$	$\lvert\Psi(\infty)\rvert = 1$
Ring-Vortex	$\ell = 2, 3, 4, \ldots$	$\left[ie^{-i\ell\theta}\frac{(r/r_0)^{3\ell-2}}{\sqrt{1+(r/r_0)^{8(\ell-1/2)}}},\ e^{i(\ell-1)\theta}\frac{(r/r_0)^{\ell-1}}{\sqrt{1+(r/r_0)^{8(\ell-1/2)}}}\right]^T$	non-topological
General Topological Vortex	$\ell = 2, 3, 4, \ldots$	Numerical Shooting Method	$\lvert\psi_A(\infty)\rvert = 1$
Complex Topological Vortex	$\ell \gg 1$	Approximate Asymptotic Method	$\lvert\psi_A(\infty)\rvert = 1$

Table 7.2: *Vortex solutions of the NLDE.* Solutions are described by their phase winding, closed-form expression, and topological properties. Solutions which retain non-zero density far from the core have an associated conserved topological charge, and we state their asymptotic form. Note that r_0 is the length scale associated with the chemical potential or the interaction strength depending on the particular solution.

$$\int_0^{2\pi} d\theta\, e^{i\theta/2}\left(\, -i\, e^{i\theta/2}\cos(\theta/2)\ ,\ e^{-i\theta/2}\sin(\theta/2)\ \right)$$
$$\times\frac{\partial}{\partial\theta}\, e^{-i\theta/2}\begin{pmatrix} i\, e^{-i\theta/2}\cos(\theta/2) \\ e^{i\theta/2}\sin(\theta/2)\end{pmatrix} = \int_0^{2\pi} d\theta\left(-\frac{i}{2}\right)$$
$$= -i\pi\ . \tag{7.49}$$

The radial solution of the half-quantum vortex is plotted in Figure 7.11(d) for the case where the polar angle is set equal to zero, withe the density and phase shown in Figure 7.13. We summarize the NLDE vortices along with their key properties in Table 7.2.

7.4 Spectra for Relativistic Vortices

In this section we extend our earlier numerical studies by examining the radial excitations of our vortex solutions in more depth followed by a thorough treatment of vortices bound within a weak harmonic potential. All of the solutions presented in this section were obtained by numerical shooting, thus we follow a similar procedure

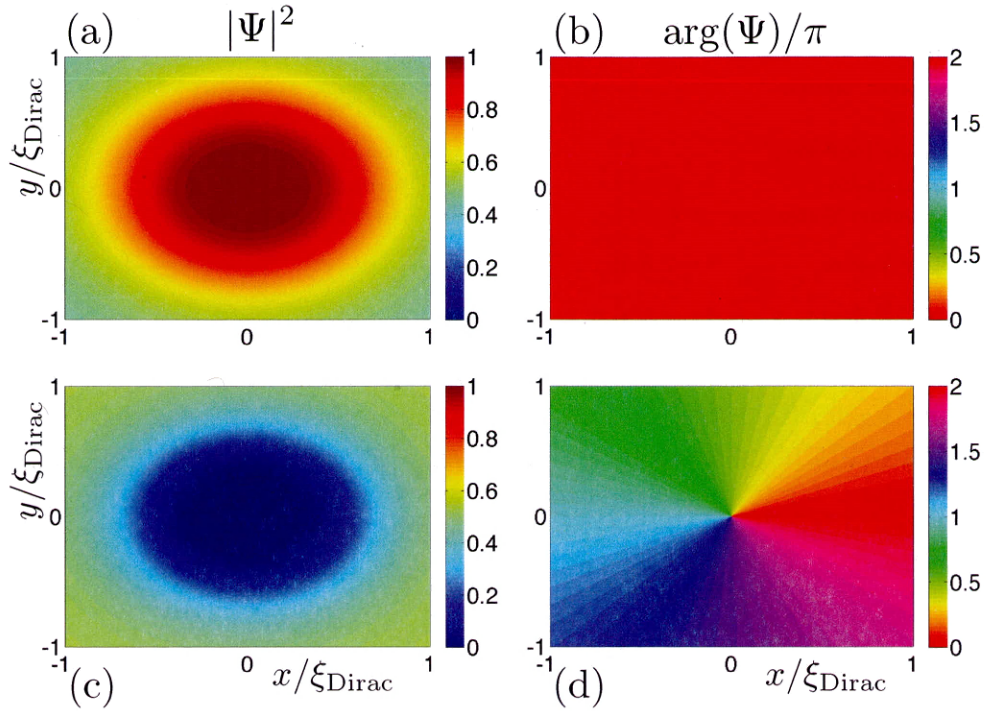

Figure 7.12: (color online) *Phase and density for the $\ell = 1$ Mermin-Ho skyrmion.* (a,b) A sublattice density and phase. (c,d) B sublattice density and phase.

as before in preparing the NLDE for a numerical analysis by first converting the NLDE to its dimensionless form.

7.4.1 Ground State and Radial Excitations of Unconfined Vortices

We first obtain a dimensionless version of the NLDE by introducing the dimensionless variable and rescaled wavefunction

$$\chi \equiv \mu r/(\hbar c_l) \quad \eta_A \equiv \sqrt{U/\mu} f_A \,, \quad \eta_B \equiv \sqrt{U/\mu} f_B \,, \tag{7.50}$$

so that the NLDE becomes

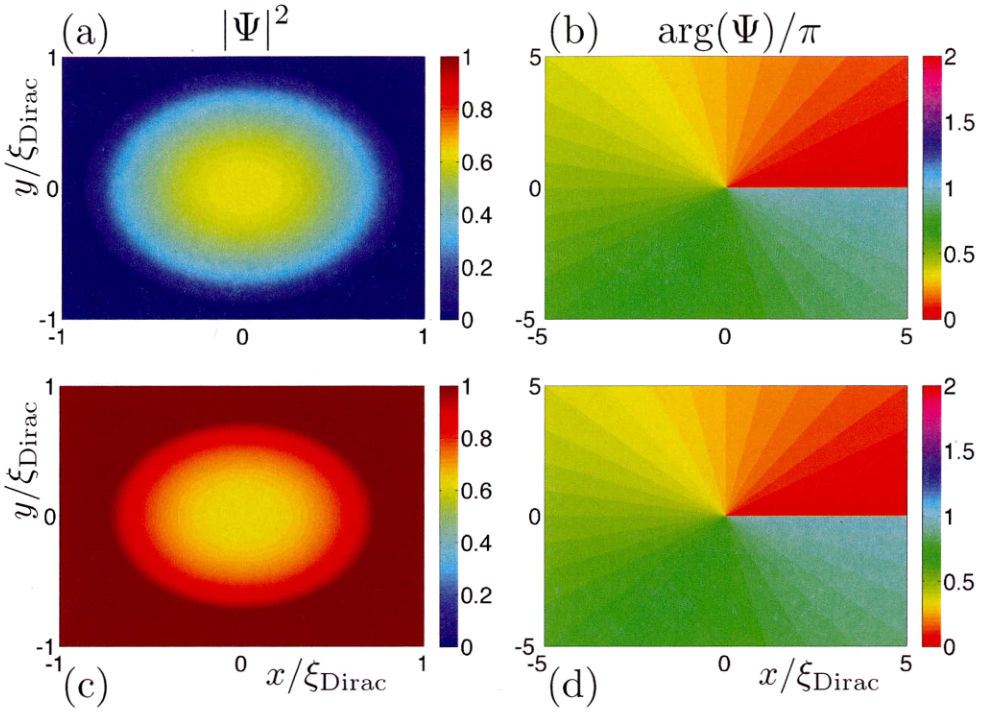

Figure 7.13: (color online) *Phase and density for the half-quantum vortex solutions.* (a,b) A sublattice density and phase. (c,b) B sublattice density and phase.

$$\left(\partial_\chi + \frac{\ell}{\chi}\right)\eta_B(\chi) - |\eta_A(\chi)|^2\eta_A(\chi) = -\eta_A(\chi) \tag{7.51}$$

$$-\left(\partial_\chi + \frac{1-\ell}{\chi}\right)\eta_A(\chi) - |\eta_B(\chi)|^2\eta_B(\chi) = -\eta_B(\chi)\,. \tag{7.52}$$

Here the dependence of the solution on the choice of angular quantum number ℓ is implied. As before we note that the asymptotic form of these equations show that convergent solutions $|\eta_{A(B)}|$ can approach either 0 or 1 for large χ. To study the analytic structure as well as a practical starting point for a numerical techniques, we can expand the solution in a power series in χ:

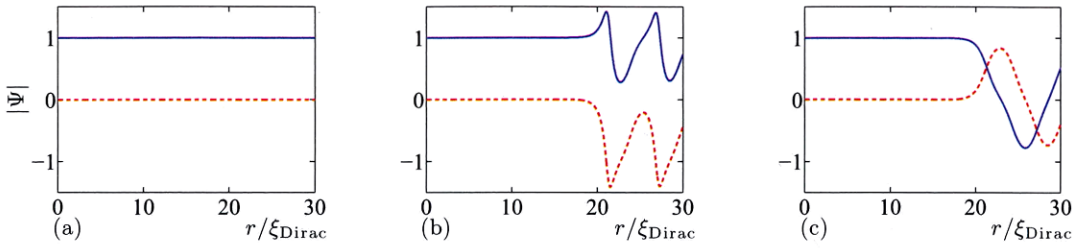

Figure 7.14: (color online) *Radial excited states for* $\ell = 1$. (a) Ground state. (b) Excited state where interaction is dominant. (c) Excited state where kinetic energy is dominant.

$$\eta_A(\chi) = \sum_{j=0}^{\infty} a_j \chi^j \,, \qquad \eta_B(\chi) = \sum_{j=0}^{\infty} b_j \chi^j . \tag{7.53}$$

Substituting these forms into the NLDE gives the relations for the expansion coefficients

$$\begin{aligned}
&(1+\ell)b_1 - a_0^3 = -a_0 \,, && (7.54)\\
&(2+\ell)b_2 - 3a_1 a_0^2 = -a_1 \,, && (7.55)\\
&(3+\ell)b_3 - 3a_2 a_0^2 - 3a_0 a_1^2 = -a_2 \,, && (7.56)\\
&\qquad\vdots \\
&(2-\ell)a_1 + b_0^3 = b_0 \,, && (7.57)\\
&(3-\ell)a_2 + 3b_1 b_0^2 = b_1 \,, && (7.58)\\
&(4-\ell)a_3 + 3b_2 b_0^2 + 3b_0 b_1^2 = b_2 \,. && (7.59)\\
&\qquad\vdots
\end{aligned}$$

Choosing a particular value for ℓ determines the values of both a_0 and b_0, and we find that there is only one independent parameter, the tunable input parameter when integrating by the shooting method.

7.4.2 Solutions for Unit Phase Winding

If we consider only positive ℓ angular quantum numbers, then the $\ell = 1$ state corresponds to one unit of rotation in ψ_B and no rotation in ψ_A. There is a constant

solution which appears with this choice of ℓ for which $\eta_A = 1$ and $\eta_B = 0$, identically. Ordinarily it might seem trivial to consider this solution, but its connection to higher radial excitations makes this a useful exercise. To see this, we solve Eqs. (7.51)-(7.52) by numerical shooting radially away from the origin. Radial excited states appear as we tune our initial value for η_A (or equivalently a_0 in the Taylor expansion) away from unity. We find that the spatially constant solution is a boundary between excitations which oscillate around $\eta_A = 1$ and $\eta_B = -1$, and those which oscillate around $\eta_A = \eta_B = 0$. In Figure 7.14, we display the onset of inward movement of ring-vortices. The blue and red dashed lines are η_A and η_B respectively. Note that the actual vortex rotation resides only in the B sublattice (blue curve). Figure 7.14(b) shows the excited state rings which appear when $a_0 = 1 + 10^{-12}$. The solution overshoots to an excited state of the vortex. In contrast, Figure 7.14(c) shows the onset of radial oscillations which result when the kinetic energy dominates the interaction energy, where in this case $a_0 = 1 - 10^{-12}$. Here the solution undershoots and takes on the form of the linear solution Bessel functions.

The NLDE allows for a solution which satisfies an additional symmetry given by the constraint $|\eta_A|^2 + |\eta_B|^2 = 1$. Solutions which satisfy this constraint are the vortex/soltion, and Anderson-Toulouse and Mermin-Ho skyrmions. In particular, for the Mermin-Ho solution, we integrate backwards starting with the boundary condition: $\eta_A = \cos(\pi/4) + 10^{-k}$, $\eta_B = \sin(\pi/4) - 10^{-k}$. Here k is a parameter tuned to give the desired values of functions at the origin, analogous to a_0 for the forward shooting. The half-quantum vortex is obtained by forming linear combinations of the numerical Mermin-Ho components, as previously discussed.

7.4.3 Solutions for Phase Winding Greater than One

For $\ell > 1$, both angular momentum terms in the NLDE are non-vanishing which forces the core condition $\eta_A(0) = 0$ and $\eta_B(0) = 0$. For these values of ℓ, there are two types of radially excited states distinguished by the property that $|\eta_{A,(B)}|$ either

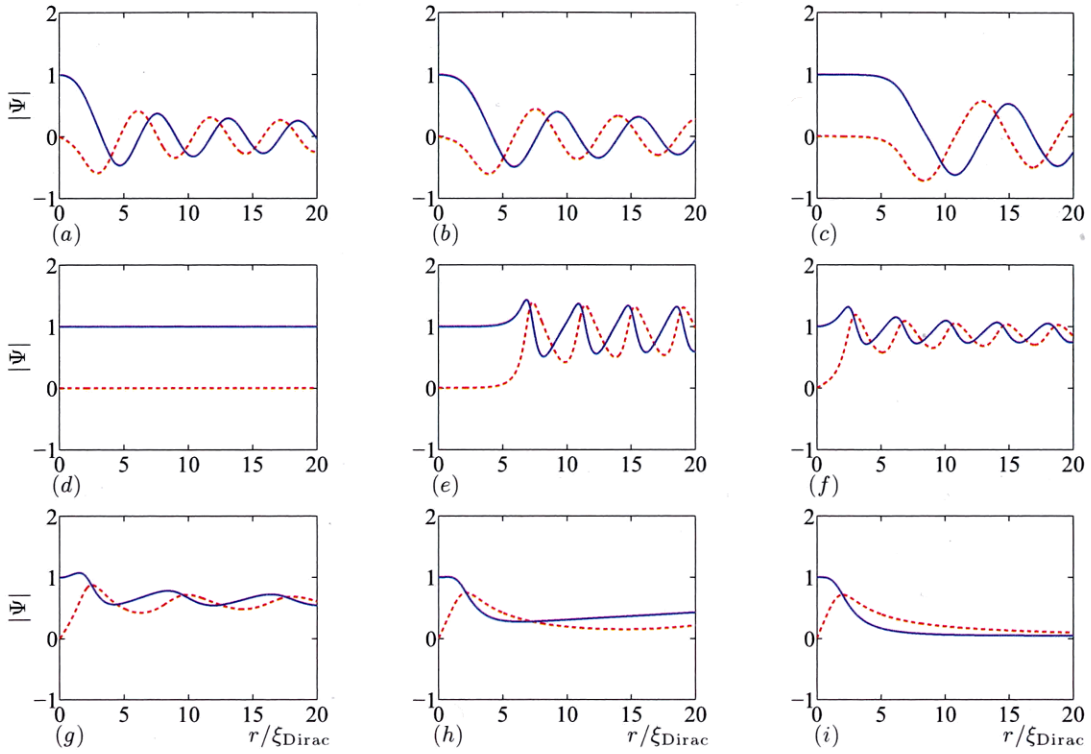

Figure 7.15: (color online) *Radial profiles for $\ell = 1$ flat solution.* (a)-(c) Dimensionless chemical potential $\tilde{\mu}$ greater than 1. (d) $\tilde{\mu}$ equal to 1. (e)-(i) $\tilde{\mu}$ less than 1. In (a) the solution is most like the noninteracting solution $\mu > U$, while the solution in (i) shows the strongly interacting case $\mu \ll U$.

oscillate around 1 or around 0.

7.4.4 Special Case of Zero Chemical Potential: Localized Ring-Vortices

To obtain these solutions we choose a particular rescaling of the NLDE which allows us to take $\mu \to 0$, so that

$$\chi \equiv U^2 r/(\hbar c_l \mu),\ \eta_A \equiv \sqrt{\mu/U} f_A,\ \eta_B \equiv \sqrt{\mu/U} f_B. \tag{7.60}$$

The resulting dimensionless NLDE is

$$-\left(\partial_\chi + \frac{\ell}{\chi}\right)\eta_B(\chi) + |\eta_A(\chi)|^2 \eta_A(\chi) = \tilde{\mu}^2\, \eta_A(\chi) \tag{7.61}$$

$$\left(\partial_\chi + \frac{1-\ell}{\chi}\right)\eta_A(\chi) + |\eta_B(\chi)|^2 \eta_B(\chi) = \tilde{\mu}^2\, \eta_B(\chi)\,. \tag{7.62}$$

For example, we look at the case $\ell = 1$. We fix $a_0 = 1$ and $b_0 = 0$ in the Taylor expansions and tune $\tilde{\mu}$ from unity toward zero. The progression for $\tilde{\mu} \to 0$ is depicted in the sequence of plots in Figure 7.15. As $\tilde{\mu}$ is reduced towards 1, oscillations about $\eta_{A(B)} \sim 0$ are pushed out towards large χ (a)-(c), flattening out the solution at $\tilde{\mu} = 1$ in (d). As $\tilde{\mu}$ is further reduced towards 0, oscillation nodes about $\eta_{A(B)} \sim 1$ move inward from large χ and finally flatten out leaving only the ring-vortex feature near $\chi = 0$. An analogous sequence for arbitrary ℓ can be obtained. The difference for $\ell < 1$, is that since both components must vanish at the origin, we must take $b_0, a_0 = 0$ but then specify the first derivative of η_A at the origin. We fix $a_0 = 0.001$ in the Taylor expansion then tune $\tilde{\mu}$ as before. The vortex solutions with flat non-zero asymptotic forms mark the point in the chemical potential parameter space where kinetic and interaction terms of the NLDE are perfectly balanced. These form a boundary between two solution regimes: one where the kinetic energy is dominant, and the other where the interaction is dominant. The results also demonstrate how the ring-vortex solutions smoothly connect to free Besssl solutions, with the topological solutions as intermediate states.

7.4.5 Discrete Eigenvalue Spectra for Vortices in a Weak Harmonic Trap

Next, we study the same solutions as above but for the case of a highly oblate harmonic confining potential, which defines the 2D system. In this case, the oscillator frequencies satisfy $\omega_z \gg \omega \equiv \omega_x, \omega_y$. Since Eqs. (8.6)-(8.7) are already defined for a 2-dimensional system (the z-dependence has been integrated out), we require that the harmonic potential be dependent only on the planar directions x and y. We then take $V(r) = (1/2)M\omega^2(x^2+y^2)^2 = (1/2)M\omega^2 r^2$. We must choose a dimensional rescaling of the NLDE appropriate to the harmonic oscillator. We divide through by the harmonic oscillator energy $\hbar\omega$ and define the dimensionless variable and wavefunction in terms of this energy scale:

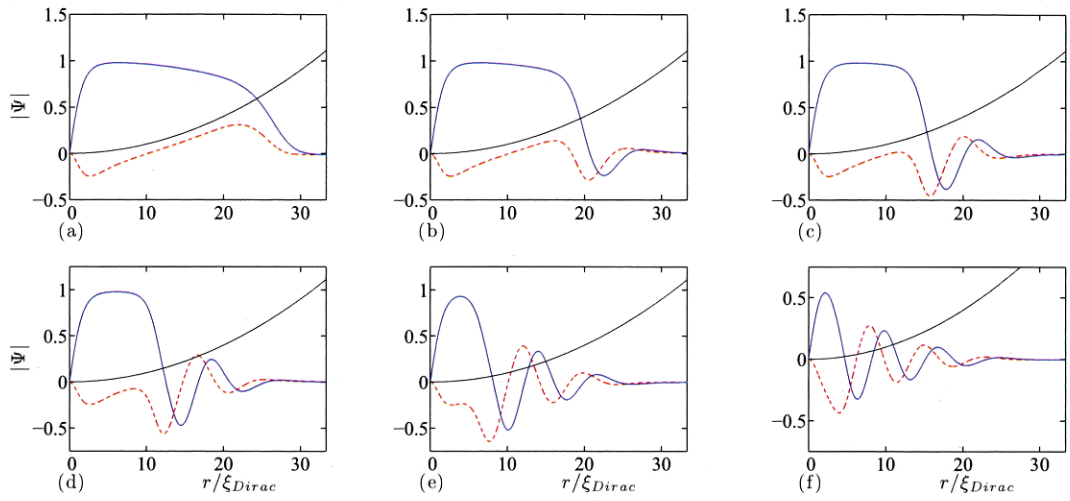

Figure 7.16: (color online) *Radial ring-vortex states for $\ell = 2$ topological solution in the harmonic trap.* (a) Ground state. (b)-(f) First through fifth excited states. The harmonic potential is shown in black.

$$\chi \equiv \hbar\omega r/(\hbar c_l)\,, \quad \eta_{A(B)} \equiv \sqrt{U/\hbar\omega}\, f_{A(B)}\,. \tag{7.63}$$

The NLDE transforms into

$$-\left(\partial_\chi + \frac{\ell}{\chi}\right)\eta_B(\chi) + |\eta_A(\chi)|^2\eta_A(\chi) + \mathcal{Q}\,\chi^2\,\eta_A(\chi) = \tilde{\mu}\,\eta_A(\chi) \tag{7.64}$$

$$\left(\partial_\chi + \frac{1-\ell}{\chi}\right)\eta_A(\chi) + |\eta_B(\chi)|^2\eta_B(\chi) + \mathcal{Q}\,\chi^2\,\eta_B(\chi) = \tilde{\mu}\,\eta_B(\chi)\,, \tag{7.65}$$

where the two dimensionless parameters in the NLDE are

$$\mathcal{Q} \equiv \frac{Mc_l^2}{2\,\hbar\omega}\,, \qquad \tilde{\mu} \equiv \frac{\mu}{\hbar\omega}\,. \tag{7.66}$$

Solutions of Eqs. (8.80)-(7.62) represent quantized states in the harmonic trap. The ground state and first five excited states for the $\ell = 2$ topological vortex are shown in Figure 7.16.

Next, we compute the discrete eigenvalue spectrum for vortices bound in a harmonic potential. As a first step, we find the normalization condition for bound states

to be

$$\int \chi d\chi (|\eta_A(\chi)|^2 + |\eta_B(\chi)|^2) = \mathcal{N}\,, \tag{7.67}$$

where the right hand side is given by

$$\mathcal{N} = \frac{\sqrt{3}\,\hbar\omega\, N\, U}{3\, t_h^2}\,. \tag{7.68}$$

To compute the spectra, we fix $\mathcal{Q}$ (which is the same as fixing ω and thus the oscillator length) and vary $\tilde{\mu}$, calculating the norm $\mathcal{N}$ for each value of $\tilde{\mu}$. This gives the paired values $(\mathcal{N}, \tilde{\mu})$. If in addition, we take the total number of particle N to be fixed, we obtain an effective relation between the chemical potential μ and the interaction U. The values for the free parameter in the Taylor expansion, a_0, normalization $\mathcal{N}$, and corresponding chemical potential $\tilde{\mu} = \mu/\hbar\omega$, are tabulated in Table 7.3 for the radial ground state of the $\ell = 2$ topological vortex shown in Figure 7.16(a). Plots of this data along with the spectra for other solutions are shown in Chapter 6. We have taken $\mathcal{Q} = 0.001$ for all of our calculations.

7.5 Relativistic Linear Stability Equations

Bogoliubov's method was originally introduced in his 1947 paper [57] (see also [235, 236] for thorough contemporary treatments), and the concept later generalized by Fetter [66] to accommodate nonuniform condensate profiles. The latter formulation gives a convenient method for computing quasi-particle states and the associated eigenvalues by simply substituting the spatial functions for a particular background condensate into a pair of coupled differential equations, and then solving the resulting eigenvalue problem. Fetter's extended method was designed with a vortex profile in mind, and has been proven successful in determining the stability of vortices in trapped condensates as well as for gaining a deeper understanding of general vortex dynamics [28, 29, 175]. The set of equations that we will derive in this section form

Free parameter a_0	Normalization $\mathcal{N}$	Chemical potential $\tilde{\mu}$
0.00000003	1.9679×10^{-5}	1.8
0.0000 0365	0.29560	2
0.0000 1018	1.85630	3
0.0000 1532 51	3.63288	4
0.0000 2089 47	5.87547	5
0.0000 2708 8395	8.62326	6
0.0000 3387 0293	11.72273	7
0.0000 4118 5861 75	15.54209	8
0.0000 4899 1422 392	20.12707	9
0.0000 5725 2724 4133	24.87695	10
0.0000 6594 2040 6807 59	30.25986	11
0.0000 75036 2691 0578 11	35.51507	12
0.0000 8451 5722 6783 7827 3795	37.30714	13

Table 7.3: *Numbers for computing spectra of $\ell = 2$ topological vortex* ground state *solution.*

the counterpart to Fetter's equations, but for trapped condensates that exhibit a Dirac point in their reciprocal lattice dispersion [184]. We call them *relativistic linear stability equations* (RLSE) because of the quasi-relativistic context of our theory and the similarity to the analog equations that appear in relativistic fluid dynamics. It is noteworthy that our result is *not* limited to the honeycomb optical lattice but applies generically to any system where the linear dispersion and bipartite structure are present, and where the contact interaction between the constituent bosons is weak.

Mathematically, the essence of our derivation is contained in two steps: (1) transformation of a spatially continuous second quantized Hamiltonian into a spatially discrete one through an operation $\mathcal{F}$; (2) diagonalization of the Hamiltonian with an appropriate unitary transformation $\mathcal{G}$. The effect of $\mathcal{F}$ is to take the system from the continuum to the tight-binding limit on the lattice, and $\mathcal{G}$ is equivalent to a Bogoliubov rotation. We will see that the final result is independent of the order

of these operations so that the full procedure can be summarized abstractly by the commutative diagram

$$\begin{array}{ccc} X & \longrightarrow & Y \\ \downarrow & & \downarrow g \\ Y' & \longrightarrow & Z \\ & f & \end{array} \tag{7.69}$$

where X, Y, Y', and Z are the categories made up of the operator algebra $\hat{\mathcal{A}}$ and Hilbert space $\mathcal{H}$ of the theory at each step, e.g., $X \equiv \{\hat{\mathcal{A}}; \mathcal{H}\}$, and f and g are the morphisms induced by the operations $\mathcal{F}$ and $\mathcal{G}$.

7.5.1 Derivation

In deriving the RLSE we have relied fundamentally on Bogoliubov's method [57] as the underlying principle, and referred to Fetter's work [66] for technical considerations regarding nonuniform condensates. First, we recall the second-quantized many-body Hamiltonian for weakly interacting bosons

$$\hat{H} = \int d^2r\, \hat{\psi}^\dagger H_0 \hat{\psi} + \frac{g}{2} \int d^2r\, \hat{\psi}^\dagger \hat{\psi}^\dagger \hat{\psi} \hat{\psi}\,, \tag{7.70}$$

$$\text{where,} \quad H_0 \equiv -\frac{\hbar^2}{2m}\nabla^2 + V(\mathbf{r})\,. \tag{7.71}$$

Here, $V(\mathbf{r})$ is the lattice potential and g is the strength of the contact interaction. The first step is to decompose the wavefunction as the sum $\hat{\psi}(\mathbf{r}) = \zeta(\mathbf{r})\,\hat{a}_0 + \hat{\phi}(\mathbf{r})$, where we have split the wavefunction into a part that describes the condensate (first term) and satisfies the bosonic commutation relation $[\hat{a}_0\,,\, \hat{a}_0^\dagger] = 1$, and a second part that describes the quasi-particle fluctuations. It is clear that the first term describes the condensate since it destroys a particle in the mean field ζ, which, by itself, is a good approximation to $\hat{\psi}$. The second term destroys a particle in a number of single particle basis states of the noninteracting system and describes the part of $\hat{\psi}$ that deviates

from the mean field. Taking the Bogoliubov limit requires $\hat{a}_0 \rightarrow N_0^{1/2}$, but we choose to compute the commutator before taking this limit in order to retain the effect of the presence of a macroscopic condensate field. We can obtain the commutation relations for $\hat{\phi}$ and $\hat{\phi}^\dagger$ by knowing that $\hat{\psi}$ and $\hat{\psi}^\dagger$ obey commutation rules for bosons. We obtain the quasi-particle commutation relations: $\left[\hat{\phi}(\mathbf{r}),\, \hat{\phi}^\dagger(\mathbf{r}')\right] = \delta(\mathbf{r} - \mathbf{r}') - \zeta(\mathbf{r})\,\zeta^*(\mathbf{r}')$, $\left[\hat{\phi}(\mathbf{r}),\, \hat{\phi}(\mathbf{r}')\right] = 0$, $\left[\hat{\phi}^\dagger(\mathbf{r}),\, \hat{\phi}^\dagger(\mathbf{r}')\right] = 0$. In the Bogoliubov limit, the condensate wavefunction has no operator part in which case $\hat{\psi}$ may be written as $\hat{\psi}(\mathbf{r}) = \Psi(\mathbf{r}) + \hat{\phi}(\mathbf{r})$. The condensate wavefunction has well defined phase and particle density and so may be expressed as: $\Psi(\mathbf{r}) = \sqrt{N_0/A}\, e^{iS(\mathbf{r})}\sqrt{\rho(\mathbf{r})}$, where A is the area covered by the planar condensate. Note that the radial part is normalized as $A^{-1}\int d^2r\, \rho(r) = 1$. With these definitions, the usual bosonic commutation relations become: $\left[\hat{\phi}(\vec{\mathbf{r}}),\, \hat{\phi}^\dagger(\mathbf{r}')\right] = e^{iS(\mathbf{r})}\, e^{-iS(\mathbf{r}')}\, \bar{\delta}(\mathbf{r},\, \mathbf{r}')$, where $\bar{\delta}(\mathbf{r}, \mathbf{r}') = \delta(\mathbf{r} - \mathbf{r}') - A^{-1}\sqrt{\rho(\mathbf{r})}\sqrt{\rho(\mathbf{r}')}$.

Next, we transform to the new Hamiltonian defined by: $\hat{K} = \hat{H} - \mu\hat{N} = \hat{H} - \mu\int d^2r\, \hat{\psi}^\dagger\, \hat{\psi}$, and we expand through second order in the operator part, eliminating the linear terms by forcing the condensate wavefunction to satisfy the constraint: $(H_0 - \mu + g\,|\Psi|^2)\Psi = 0$. We arrive at the Bogoliubov Hamiltonian: $\hat{K} = \hat{K}_0 + \hat{K}_2$, wherein zero-order and second-order operator terms are grouped into $\hat{K}_0$ and $\hat{K}_2$ respectively. These are defined as

$$\begin{aligned}
\hat{K}_0 &= \int d^2r\, \Psi^*(\mathbf{r}) \left[H_0 - \mu + \frac{g}{2}\,|\Psi(\mathbf{r})|^2\right] \Psi(\mathbf{r})\,, \\
\hat{K}_2 &= \int d^2r\, \hat{\phi}^\dagger(\mathbf{r}) \left[H_0 - \mu + 2g\,|\Psi(\mathbf{r})|^2\right] \hat{\phi}(\mathbf{r}) \\
&+\frac{g}{2}\int d^2r\, \left\{[\Psi^*(\mathbf{r})]^2\, \hat{\phi}(\mathbf{r})\hat{\phi}(\mathbf{r}) + \hat{\phi}^\dagger(\mathbf{r})\hat{\phi}^\dagger(\mathbf{r})\,[\Psi(\mathbf{r})]^2\right\}. \qquad (7.72)
\end{aligned}$$

Note that, in addition to the kinetic operator, we also have an arbitrary external potential in the first two terms, which in our case will be the periodic potential of the optical lattice. Eq.(7.72) is quadratic in the field operators and so may be diagonalized with the appropriate field redefinition. To diagonalize Eq.(7.72), we first

apply the linear transformation: $\hat{\phi}(\mathbf{r}) = e^{iS(\mathbf{r})} \sum_j' \left[u_j(\mathbf{r})\, \hat{\alpha}_j \; - \; v_j^*(\mathbf{r})\, \hat{\alpha}_j^\dagger \right]$ and $\hat{\phi}^\dagger(\mathbf{r}) = e^{-iS(\mathbf{r})} \sum_j' \left[u_j^*(\mathbf{r})\, \hat{\alpha}_j^\dagger \; - \; v_j(\mathbf{r})\, \hat{\alpha}_j \right]$, where the prime notation on the summation sign indicates that we are omitting the condensate from the sum. The $\hat{\alpha}_j$'s and $\hat{\alpha}_j^\dagger$'s inherit standard bosonic commutation relations from $\hat{\phi}$ and $\hat{\phi}^\dagger$, and the spatially dependent transformation coefficients $u_j(\mathbf{r})$ and $v_j(\mathbf{r})$ obey the completeness relations

$$\sum_j' \left[u_j(\mathbf{r})\, u_j^*(\mathbf{r}') \; - \; v_j^*(\mathbf{r})\, v_j(\mathbf{r}') \right] \;=\; \bar{\delta}(\mathbf{r}, \mathbf{r}')\,, \tag{7.73}$$

$$\sum_j' \left[u_j(\mathbf{r})\, v_j^*(\mathbf{r}') \; - \; v_j^*(\mathbf{r})\, u_j(\mathbf{r}') \right] \;=\; 0\,, \tag{7.74}$$

$$\sum_j' \left[u_j^*(\mathbf{r})\, v_j(\mathbf{r}') \; - \; v_j(\mathbf{r})\, u_j^*(\mathbf{r}') \right] \;=\; 0\,. \tag{7.75}$$

So far, our discussion has taken place in two continuous spatial dimensions constrained only at the boundary by a trapping potential. We now want to translate to a formalism that fits a two-dimensional periodic optical lattice potential with hexagonal geometry. This is done by assuming a tight-binding limit at each lattice site. Formally, this corresponds to expanding the wavefunction in terms of a Wannier basis: functions which are localized and centered on each lattice site. The nearest-neighbor approximation then allows for a decomposition of the condensate and operator parts in terms of individual sublattices labeled A and B. In this new basis, the spatial dependence of the condensate and quasi-particle functions follows:

$$\begin{aligned} \Psi(\mathbf{r}) \;&=\; \sum_A e^{i\mathbf{k}\cdot(\mathbf{r}-\mathbf{r}_A)} \sqrt{n_{A_i}} e^{iS_{A_i}} w(\mathbf{r}-\mathbf{r}_A) \\ &\qquad + \sum_B e^{i\mathbf{k}\cdot(\mathbf{r}-\mathbf{r}_B)} \sqrt{n_{B_i}}\, e^{iS_{B_i}}\, w(\mathbf{r}-\mathbf{r}_B), \end{aligned} \tag{7.76}$$

$$\begin{aligned} \hat{\phi}(\mathbf{r}) \;&=\; e^{iS(\mathbf{r})} \sum_{A,j}' \left[u_{j,A_i}(\mathbf{r}-\mathbf{r}_A)\hat{\alpha}_j - v_{j,A_i}^*(\mathbf{r}-\vec{r}_A)\hat{\alpha}_j^\dagger \right] \\ &\qquad + e^{iS(\mathbf{r})} \sum_{B,j}' \left[u_{j,B_i}(\mathbf{r}-\mathbf{r}_B)\, \hat{\beta}_j - v_{j,B_i}^*(\mathbf{r}-\mathbf{r}_B)\hat{\beta}_j^\dagger \right]. \end{aligned} \tag{7.77}$$

7.5.2 First Method - Tight-Binding Limit Followed by Diagonalization of the Quasi-Particle Hamiltonian

We substitute these expressions into the Hamiltonian then take the long-wavelength limit, while translating the exponential (crystal) momentum factors to coincide with the Dirac point. The continuum limit effectively converts the sublattice sums into integrals. By performing one of the integrations, over the A sublattice, say, while adhering to nearest neighbor overlaps, we obtain the affective Hamiltonian for the condensate and quasi-particles: $\hat{H} = \hat{K}_0 + \hat{K}_2$, where

$$\hat{K}_0 = \int d^2r \left[i\hbar c_l \, \psi_A^*(\mathbf{r}) \mathcal{D} \psi_B(\mathbf{r}) + i\hbar \, c_l \psi_B^*(\mathbf{r}) \mathcal{D}^* \psi_A(\mathbf{r}) + \frac{U}{2} \left|\psi_A(\mathbf{r})\right|^4 + \frac{U}{2} \left|\psi_B(\mathbf{r})\right|^4 \right], \tag{7.78}$$

$$\begin{aligned}
\hat{K}_2 = \sum_{j,k}{}' \int d^2r \Big\{ & \hat{\alpha}_j \hat{\beta}_k^\dagger \, \hbar c_l \, v_{j,A} \, \mathcal{D}^* v_{k,B}^* + \hat{\beta}_j \hat{\alpha}_k^\dagger \, \hbar c_l \, v_{j,B} \, \mathcal{D} v_{k,A}^* + 2U \, \hat{\alpha}_j \hat{\alpha}_k^\dagger \, v_{j,A} \left|\psi_A\right|^2 v_{k,A}^* \\
& + 2U \, \hat{\beta}_j \hat{\beta}_k^\dagger \, v_{j,B} \left|\psi_B\right|^2 v_{k,B}^* - \frac{1}{2} U \left|\psi_A\right|^2 \hat{\alpha}_j \hat{\alpha}_k^\dagger \left(u_{j,A} \, v_{k,A}^* + u_{k,A}^* \, v_{j,A}\right) \\
& - \frac{1}{2} U \left|\psi_B\right|^2 \hat{\beta}_j \hat{\beta}_k^\dagger \left(u_{j,B} \, v_{k,B}^* + u_{k,B}^* \, v_{j,B}\right) + \hat{\alpha}_j^\dagger \hat{\beta}_k \, \hbar c_l \, u_{j,A}^* \, \mathcal{D}^* u_{k,B} \\
& + \hat{\beta}_j^\dagger \hat{\alpha}_k \, \hbar c_l \, u_{j,B}^* \, \mathcal{D} u_{k,A} + 2U \, \hat{\alpha}_j^\dagger \hat{\alpha}_k \, u_{j,A}^* \left|\psi_A\right|^2 u_{k,A} + 2U \, \hat{\beta}_j^\dagger \hat{\beta}_k \, u_{j,B}^* \left|\psi_B\right|^2 u_{k,B} \\
& - \frac{1}{2} U \left|\psi_A\right|^2 \hat{\alpha}_j^\dagger \hat{\alpha}_k \left(v_{j,A}^* \, u_{k,A} + v_{k,A} \, u_{j,A}^*\right) - \frac{1}{2} U \left|\psi_B\right|^2 \hat{\beta}_j^\dagger \hat{\beta}_k \left(v_{j,B}^* \, u_{k,B} + v_{k,B} \, u_{j,B}^*\right) \\
& - \hat{\alpha}_j \hat{\beta}_k \, \hbar c_l \, v_{j,A} \, \mathcal{D}^* u_{k,B} - \hat{\beta}_j \hat{\alpha}_k \, \hbar c_l \, v_{j,B} \, \mathcal{D} u_{k,A} - 2U \hat{\alpha}_j \hat{\alpha}_k \, v_{j,A} \left|\psi_A\right|^2 u_{k,A} \\
& - 2U \, \hat{\beta}_j \hat{\beta}_k \, v_{j,B} \left|\psi_B\right|^2 u_{k,B} + \frac{1}{2} U \left|\psi_A\right|^2 \hat{\alpha}_j \hat{\alpha}_k \left(u_{j,A} \, u_{k,A} + v_{k,A} \, v_{j,A}\right) \\
& + \frac{1}{2} U \left|\psi_B\right|^2 \hat{\beta}_j \hat{\beta}_k \left(u_{j,B} \, u_{k,B} + v_{k,B} \, v_{j,B}\right) - \hat{\alpha}_j^\dagger \hat{\beta}_k^\dagger \hbar c_l \, u_{j,A}^* \, \mathcal{D}^* v_{k,B}^* \\
& - \hbar c_l \, \hat{\beta}_j^\dagger \hat{\alpha}_k^\dagger \, u_{j,B}^* \, \mathcal{D} v_{k,A}^* - 2U \, \hat{\alpha}_j^\dagger \hat{\alpha}_k^\dagger \, u_{j,A}^* \left|\psi_A\right|^2 v_{k,A}^* - 2U \, \hat{\beta}_j^\dagger \hat{\beta}_k^\dagger \, u_{j,B}^* \left|\psi_B\right|^2 v_{k,B}^* \\
& + \frac{1}{2} U \left|\psi_A\right|^2 \hat{\alpha}_j^\dagger \hat{\alpha}_k^\dagger \left(u_{j,A}^* \, u_{k,A}^* + v_{k,A}^* \, v_{j,A}^*\right) \\
& + \frac{1}{2} U \left|\psi_B\right|^2 \hat{\beta}_j^\dagger \hat{\beta}_k^\dagger \left(u_{j,B}^* \, u_{k,B}^* + v_{k,B}^* \, v_{j,B}^*\right) \Big\} .
\end{aligned} \tag{7.79}$$

Note that we have defined the condensate two-spinor in terms of the A and B sublattice components: $\Psi(\mathbf{r}) = [\psi_A(\mathbf{r}), \psi_B(\mathbf{r})]^T$. Next, we isolate the first six terms (terms

with the daggered operator to the right) and write them as a matrix contraction of two pure operator valued vectors,

$$\left(\hat{\alpha}_j \, , \, \hat{\beta}_j \right) \left(\begin{array}{cc} A_{u,v} & D_{A,B} \\ D_{B,A} & B_{u,v} \end{array} \right) \left(\begin{array}{c} \hat{\alpha}_k^\dagger \\ \hat{\beta}_k^\dagger \end{array} \right) , \tag{7.80}$$

where

$$A_{u,v} \equiv 2U v_{j,A} \left|\psi_A\right|^2 v_{k,A}^* - \frac{1}{2} U \left|\psi_A\right|^2 \left(u_{j,A} v_{k,A}^* + u_{k,A}^* v_{j,A}\right) , \tag{7.81}$$

$$B_{u,v} \equiv 2U v_{j,B} \left|\psi_B\right|^2 v_{k,B}^* - \frac{1}{2} U \left|\psi_B\right|^2 \left(u_{j,B} v_{k,B}^* + u_{k,B}^* v_{j,B}\right) , \tag{7.82}$$

$$D_{A,B} \equiv \hbar c_l v_{j,A} \mathcal{D}^* v_{k,B}^* , \tag{7.83}$$

$$D_{B,A} \equiv \hbar c_l v_{j,B} \mathcal{D} \, v_{k,A}^* . \tag{7.84}$$

The eigenvalues are then obtained by

$$\det \left(\begin{array}{cc} A_{u,v} - \lambda & D_{A,B} \\ D_{B,A} & B_{u,v} - \lambda \end{array} \right) = 0 \tag{7.85}$$

$$\Rightarrow$$

$$\left(A_{u,v} - \lambda\right)\left(B_{u,v} - \lambda\right) - D_{A,B} \, D_{B,A} = 0 , \tag{7.86}$$

$$\lambda_\pm = \frac{\left(A_{u,v} + B_{u,v}\right)}{2} \pm \frac{1}{2} \sqrt{\left(A_{u,v} - B_{u,v}\right) + 4 \, D_{A,B} \, D_{B,A}} , \tag{7.87}$$

and the corresponding eigenvectors follow:

$$\vec{V}_\pm = \left(\begin{array}{c} 1 \\ \frac{D_{B,A}}{\left(\lambda_\pm - B_{u,v}\right)} \end{array} \right) . \tag{7.88}$$

The unitary matrix that diagonalizes Eq.(7.80) is

$$\mathbf{U} = \frac{1}{\sqrt{2}} \left(\begin{array}{cc} 1 & 1 \\ \frac{D_{B,A}}{\left(\lambda_+ - B_{u,v}\right)} & \frac{D_{B,A}}{\left(\lambda_- - B_{u,v}\right)} \end{array} \right) . \tag{7.89}$$

The first six terms in Eq. (7.79) may be expressed in the new basis as

$$\lambda_{+\{jk\}} \, \hat{c}_{+,j} \, \hat{c}_{+,k}^\dagger + \lambda_{-\{jk\}} \, \hat{c}_{-,j} \, \hat{c}_{-,k}^\dagger , \tag{7.90}$$

where we have included the j,k subscripts on the eigenvalues to be fully descriptive. The new quasi-particle operators can be written in terms of the old ones as

$$\hat{c}^{\dagger}_{\pm,j} = \frac{1}{\sqrt{2}} \left[\hat{\alpha}^{\dagger}_{j} + \frac{D^{*}_{B,A}}{(\lambda^{*}_{\pm\{jk\}} - B^{*}_{u,v})} \hat{\beta}^{\dagger}_{j} \right] . \tag{7.91}$$

Note that the right hand side is k-dependent which is implied on the left. The substance of the transformation is contained in the momentum and space-dependent eigenvalues

$$\begin{aligned} \lambda_{\pm\{jk\}} &= U v_{j,A} \left|\psi_A\right|^2 v^{*}_{k,A} - \frac{1}{4} U \left|\psi_A\right|^2 (u_{j,A} v^{*}_{k,A} + u^{*}_{k,A} v_{j,A}) + U v_{j,B} \left|\psi_B\right|^2 v^{*}_{k,B} \\ &\quad - \frac{1}{4} U \left|\psi_B\right|^2 (u_{j,B} v^{*}_{k,B} + u^{*}_{k,B} v_{j,B}) \\ &\quad \pm \Bigg\{ \Bigg[U v_{j,A} \left|\psi_A\right|^2 v^{*}_{k,A} - \frac{1}{4} U \left|\psi_A\right|^2 (u_{j,A} v^{*}_{k,A} + u^{*}_{k,A} v_{j,A}) \qquad (7.92) \\ &\quad - U v_{j,B} \left|\psi_B\right|^2 v^{*}_{k,B} + \frac{1}{4} U \left|\psi_B\right|^2 (u_{j,B} v^{*}_{k,B} + u^{*}_{k,B} v_{j,B}) \Bigg]^2 \\ &\quad + (\hbar c_l)^2 v_{j,A} (\mathcal{D}^{*} v^{*}_{k,B}) v_{j,B} (\mathcal{D} v^{*}_{k,A}) \Big\}^{1/2} . \qquad (7.93) \end{aligned}$$

The next step is to constrain the quasi-particle amplitudes in Eq. (7.93) (the u's and v's) in order to diagonalize the Hamiltonian with respect to the momentum indices j and k. First, we let

$$\begin{aligned} \hbar c_l v_{j,A} \mathcal{D}^{*} v^{*}_{k,B} &= 2U v_{j,A} \left|\psi_A\right|^2 v^{*}_{k,A} - \frac{1}{2} U \left|\psi_A\right|^2 (u_{j,A} v^{*}_{k,A} + u^{*}_{k,A} v_{j,A}) \\ \hbar c_l v_{j,B} \mathcal{D} v^{*}_{k,A} &= 2U v_{j,B} \left|\psi_B\right|^2 v^{*}_{k,B} - \frac{1}{2} U \left|\psi_B\right|^2 (u_{j,B} v^{*}_{k,B} + u^{*}_{k,B} v_{j,B}) , \end{aligned} \tag{7.94}$$

and then substitute these into Eq.(7.93), which reduces the two eigenvalues to

$$
\begin{aligned}
\lambda_{+\{jk\}} &= -\mu\, v_{j,A}\, v^*_{k,A} + 2U\, v_{j,A}\, |\psi_A|^2\, v^*_{k,A} \\
&\quad -\frac{1}{2} U\, |\psi_A|^2\, (u_{j,A}\, v^*_{k,A} + u^*_{k,A}\, v_{j,A}) \\
&\quad -\mu\, v_{j,B}\, v^*_{k,B} + 2U\, v_{j,B}\, |\psi_B|^2\, v^*_{k,B} \\
&\quad -\frac{1}{2} U\, |\psi_B|^2\, (u_{j,B}\, v^*_{k,B} + u^*_{k,B}\, v_{j,B}) \\
\text{and,} & \\
\lambda_{-\{jk\}} &= 0\,, \qquad (7.95)
\end{aligned}
$$

where we have reinserted the chemical potential terms. It is important that Eqs. (7.94) depend only on one index so that quasi-particle amplitudes for different eigeneneregies are not coupled. Dividing Eqs. (7.94) through by $v_{j,A}$ and $v_{j,B}$, respectively, cancels all j-index terms except for ones that appear as $u_{j,A}/v_{j,A}$ and $u_{j,B}/v_{j,B}$. To completely decouple the j-k modes, we must ensure that $u_{j,A}/v_{j,A} = u_{j,B}/v_{j,B} = \eta(\vec{r})$, i.e., the amplitudes for any given quasi-particle mode have the same relative spatial form. We can then rewrite $\lambda_{+\{jk\}}$ as

$$
\begin{aligned}
\lambda_{+\{jk\}} &= \frac{1}{2}\hbar c_l\, v_{j,A} \mathcal{D}^* v^*_{k,B} - \frac{1}{2}\mu\, v_{j,A}\, v^*_{k,A} \\
&\quad + U v_{j,A}\, |\psi_A|^2\, v^*_{k,A} - \frac{1}{4} U\, |\psi_A|^2\, (u_{j,A} v^*_{k,A} + u^*_{k,A} v_{j,A}) \\
&\quad + \frac{1}{2}\hbar c_l\, v_{j,B}\, \mathcal{D}\, v^*_{k,A} - \frac{1}{2}\mu\, v_{j,B}\, v^*_{k,B} \\
&\quad + U v_{j,B}\, |\psi_B|^2\, v^*_{k,B} - \frac{1}{4} U\, |\psi_B|^2\, (u_{j,B} v^*_{k,B} + u^*_{k,B} v_{j,B})\,. \qquad (7.96)
\end{aligned}
$$

Finally, we impose the constraints

$$
\begin{aligned}
-\frac{1}{4} E_k v^*_{k,A} &= \frac{1}{4}\hbar c_l \mathcal{D}^* v^*_{k,B} - \frac{1}{4}\mu v^*_{k,A} + \frac{1}{2} U\, |\psi_A|^2\, v^*_{k,A} - \frac{1}{4} U\, |\psi_A|^2\, u^*_{k,A} \quad (7.97) \\
-\frac{1}{4} E_j v_{j,A} &= \frac{1}{4}\hbar c_l \mathcal{D}^* v_{j,B} - \frac{1}{4}\mu v_{j,A} + \frac{1}{2} U\, |\psi_A|^2\, v_{j,A} - \frac{1}{4} U\, |\psi_A|^2\, u_{j,A}\,. \quad (7.98)
\end{aligned}
$$

Multiplying Eqs. (7.97) and (7.98) by $v_{j,A}$ and $v^*_{k,A}$, respectively, and using the property that $\int d^2r\, v_{j,B}\, \mathcal{D}\, v^*_{k,A} = \int d^2r (\mathcal{D}^* v_{j,B})\, v^*_{k,A}$, we may separate out 1/2 of each derivative term in Eq. (7.96), which reduces the non-derivative terms in the first line

of Eq. (7.96) to

$$-\frac{1}{4}(E_k + E_j)\, v^*_{k,A}\, v_{j,A} \ . \tag{7.99}$$

We may reduce the second line using the other half of each derivative term, thereby condensing the eigenvalues down to

$$\lambda_{+\{jk\}} = -\frac{1}{4}(E_k + E_j)\,(v^*_{k,A}\, v_{j,A} + v^*_{k,B}\, v_{j,B}) \ . \tag{7.100}$$

The next six terms in Eq.(7.79) may be diagonalized in a similar way yielding the eigenvalues

$$\begin{aligned}
\lambda_{+\{jk\}} &= -\mu\, u^*_{j,A}\, u_{k,A} + 2\,U\, u^*_{j,A}\, |\psi_A|^2\, u_{k,A} \\
&\quad -\frac{1}{2}\,U\, |\psi_A|^2\, (v^*_{j,A}\, u_{k,A} + v_{k,A}\, u^*_{j,A}) \\
&\quad -\mu\, u^*_{j,B}\, u_{k,B} + 2\,U\, u^*_{j,B}\, |\psi_B|^2\, u_{k,B} \\
&\quad -\frac{1}{2}\,U\, |\psi_B|^2\, (v^*_{j,B}\, u_{k,B} + v_{k,B}\, u^*_{j,B}) \\
\text{and,} & \\
\lambda_{-\{jk\}} &= 0 \, .
\end{aligned} \tag{7.101}$$

Following our previous steps, we obtain

$$\lambda_{+\{jk\}} = \frac{1}{4}(E_k + E_j)\,(u^*_{k,A}\, u_{j,A} + u^*_{k,B}\, u_{j,B}) \ . \tag{7.102}$$

Combining Eqs. (7.100) and (7.102), and inserting the quasi-particle operators, reduces the first twelve terms in Eq. (7.79) to the expression

$$\frac{1}{4}\sum_{j,k}{}' \int d^2r\, (E_j + E_k) \left[\hat{c}^\dagger_{+,j}\hat{c}_{+,k}\,(u^*_{k,A}\, u_{j,A} + u^*_{k,B}\, u_{j,B}) - \hat{c}_{+,j}\hat{c}^\dagger_{+,k}\,(v^*_{k,A}\, v_{j,A} + v^*_{k,B}\, v_{j,B})\right] . \tag{7.103}$$

For the special case where $j = k$, we may further combine the terms at the cost of an extra c-number term to arrive at

$$
\begin{aligned}
&-\frac{1}{2}\sum_{k}{}' \int d^2r\, 2E_k(v^*_{k,A}v_{k,A} + v^*_{k,B}v_{k,B}) \\
&+\frac{1}{4}\sum_{j,k}{}' \int d^2r(E_j + E_k)\hat{c}^\dagger_{+,j}\hat{c}_{+,k}(u^*_{k,A}u_{j,A} - v^*_{k,A}v_{j,A} \\
&\qquad +u^*_{k,B}u_{j,B} - v^*_{k,B}v_{j,B}).
\end{aligned} \tag{7.104}
$$

Applying the completeness relations $\int d^2r\,(u^*_{k,A}\,u_{j,A} - v^*_{k,A}\,v_{j,A}) = \delta_{i,j}$ and $\int d^2r\,(u^*_{k,B}\,u_{j,B} - v^*_{k,A}\,v_{j,B}) = \delta_{i,j}$, contracts Eq. (7.104) down to

$$
-\sum_{k}{}' \int d^2r\, E_k\,(|v_{k,A}|^2 + |v_{k,B}|^2) + \sum_{k}{}' E_k\,\hat{c}^\dagger_{+,k}\hat{c}_{+,k}. \tag{7.105}
$$

Diagonalizing the rest of Eq.(7.79) (terms with no daggered operators and ones with only daggered operators) by capitalizing on the j-k symmetry of terms such as $\int d^2r\, u_{k,A}\, v_{j,A}$, and anti-symmetry of the $(E_j - E_k)$ factor, we obtain the final form of the interacting Hamiltonian

$$
\begin{aligned}
\hat{H} \;=\; &\int d^2r\, \Big[i\hbar c_l\,\psi^*_A(\mathbf{r})(\partial_x + i\partial_y)\psi_B(\mathbf{r}) \;+\; i\hbar c_l\,\psi^*_B(\mathbf{r})(\partial_x - i\partial_y)\psi_A(\mathbf{r}) \\
&+\frac{U}{2}\,|\psi_A(\mathbf{r})|^4 + \frac{U}{2}\,|\psi_B(\mathbf{r})|^4\Big] - \sum_{j}{}' E_j \int d^2r\, \mathbf{v}^{T*}_j\mathbf{v}_j + \sum_{j}{}' E_j\hat{c}^\dagger_{+,j}\,\hat{c}_{+,j}\,,
\end{aligned} \tag{7.106}
$$

with the resulting constraints on quasi-particle amplitudes given by

$$
\begin{aligned}
i\,\hbar c_l\,\mathcal{D}^* u_{j,B} - \mu u_{j,A} + 2U\,|\psi_A|^2\,u_{j,A} - U\,|\psi_A|^2\,v_{j,A} &= E_j u_{j,A}\,, && (7.107)\\
i\,\hbar c_l\,\mathcal{D}\,u_{j,A} - \mu u_{j,B} + 2U\,|\psi_B|^2\,u_{j,B} - U\,|\psi_B|^2\,v_{j,B} &= E_j u_{j,B}\,, && (7.108)\\
i\,\hbar c_l\,\mathcal{D}\,v_{j,B} - \mu v_{j,A} + 2U\,|\psi_A|^2\,v_{j,A} - U\,|\psi_A|^2\,u_{j,A} &= -E_j v_{j,A}\,, && (7.109)\\
i\,\hbar c_l\mathcal{D}^* v_{j,A} - \mu v_{j,B} + 2U\,|\psi_B|^2\,v_{j,B} - U\,|\psi_B|^2\,u_{j,B} &= -E_j v_{j,B}\,. && (7.110)
\end{aligned}
$$

7.5.3 Second Method - Diagonalize the Quasi-Particle Hamiltonian then Impose Tight-Binding

Although the first method is cumbersome, it is the more rigorous approach and instills confidence in the final constraint equations. A shorter approach is to first

obtain the usual Bogoliubov equations for a condensate not confined in a lattice, and then apply the tight-binding limit directly. The Bogoliubov Hamiltonian is

$$\hat{H} = \int d^2r\, \Psi^*(\mathbf{r}) \left[H_0 - \mu + \frac{g}{2} |\Psi(\mathbf{r})|^2 \right] \Psi(\mathbf{r}) - \sum_j{}' E_j \int d^2r\, |v_j(\vec{r})|^2 + \sum_j{}' E_j \alpha_j^\dagger \alpha_j \,, \tag{7.111}$$

with the constraint equations (BdGE) given by

$$\mathcal{L}\, u_j - g\, |\Psi|^2\, v_j = E_j u_j \tag{7.112}$$

$$\mathcal{L}^*\, v_j - g\, |\Psi|^2\, u_j = -E_j v_j \,. \tag{7.113}$$

In Eqs. (7.112)-(7.113), $\mathcal{L}$ is a differential operator which combines terms that couple the quasi-particle and condensate velocities. An additional implicit constraint is that Ψ satisfies the nonlinear Schrödinger equation. To pass to the tight-binding limit, we express all spatial functions in Eqs. (7.111)-(7.113) in terms of Wannier functions for the individual sublattices, and evaluate the Bloch plane wave factors at the Dirac point momemtum. Adhering to nearest-neighbor overlap for on-site Wannier functions, we integrate out spatial degrees of freedom (which splits the honeycomb lattice into A and B sublattices), regroup terms into finite differences, and then take the continuum limit. Eq. (7.111) then transforms to Eq. (7.106), while Eqs. (7.112)-(7.113) transform to Eqs. (7.107)-(7.110) with several additional derivative terms contained in $\mathcal{L}$ as follows

$$-\frac{\hbar^2}{2m} \left[\nabla^2 + i\nabla^2\phi + 2i\, \nabla\phi \cdot \nabla - (\nabla\phi)^2 \right] u_j \,, \tag{7.114}$$

where ϕ is the condensate phase. After going through the steps that culminate in the tight-binding continuum limit, these terms transform to

$$i\hbar c_l \mathcal{D}^* u_{k,B(A)} + \left[-i\hbar\tau_1 \nabla\phi_{A(B)} \cdot \nabla + \hbar\tau_2 |\nabla\phi_{A(B)}| - i\hbar\tau_3 (\nabla^2\phi_{A(B)}) \right] u_{k,A(B)} \,, \tag{7.115}$$

where the coefficients encapsulate the spatial integrals as follows: $\tau_1 \propto |\int d\mathbf{r}\, w_A^* \nabla w_B|$, $\tau_2 \propto |\int d\mathbf{r}\, w_A^* (\nabla\phi) w_A|$, $\tau_3 \propto \int d\mathbf{r}\, w_A^* |\nabla\phi|^2 w_A$. These extra terms depend on the condensate phase $\phi_{A(B)}$, and so couple the superfluid velocity to the quasi-particle excitations. In particular, the term with coefficient τ_1 depends on the direction of quasi-particle emission relative to the motion of the condensate. The *relativistic linear stability equations*, Eqs. (7.107)-(7.110), may be expressed in compact notation as

$$\tilde{\mathscr{D}}\mathbf{u_k} - U\tilde{\Psi}\mathbf{v_k} = \tilde{E}_\mathbf{k}\mathbf{u_k}, \tag{7.116}$$
$$\tilde{\mathscr{D}}^*\mathbf{v_k} - U\tilde{\Psi}\mathbf{u_k} = -\tilde{E}_\mathbf{k}\mathbf{v_k}\ , \tag{7.117}$$

where

$$\begin{aligned}
\tilde{\Psi} &\equiv \mathrm{diag}(|\psi_A|^2, |\psi_B|^2), && (7.118)\\
\tilde{E}_\mathbf{k} &\equiv \mathrm{diag}(E_\mathbf{k}, E_\mathbf{k}), && (7.119)\\
[\tilde{\mathscr{D}}]_{1,1} &\equiv -\mu + 2U|\psi_A|^2 - i\hbar\tau_1 \nabla\phi_A\cdot\nabla \\
&\quad + \hbar\tau_2 |\nabla\phi_A| - i\hbar\tau_3 \left(\nabla^2\phi_A\right), && (7.120)\\
[\tilde{\mathscr{D}}]_{2,2} &\equiv -\mu + 2U|\psi_B|^2 - i\hbar\tau_1 \nabla\phi_B\cdot\nabla \\
&\quad + \hbar\tau_2 |\nabla\phi_B| - i\hbar\tau_3 \left(\nabla^2\phi_B\right), && (7.121)\\
[\tilde{\mathscr{D}}]_{1,2} &= [\tilde{\mathscr{D}}]_{2,1}^* \equiv i\hbar c_l \mathcal{D}^*. && (7.122)
\end{aligned}$$

7.5.4 Proof of NLDE Limit to NLSE

The standard Dirac equation has a well defined non-relativistic limit to the Schrödinger equation. The proof uses the fact that, in the low energy limit, the mass term (the term multiplied by mc^2) is the largest contribution to the energy. One spinor equation is back-substituted into the remaining equation and the approximation reduces this down to an expression that has the correct Schrödinger kinetic term. It is natural to ask if there exists some limit in which our nonlinear Dirac equation reduces to the nonlinear Schrödinger equation, and, if so, how to tune the parameters in order to observe this transition in the laboratory. To show that the NLDE can be reduced to

the NLSE, we start from the discrete nonlinear Dirac equation for one Dirac point, which is an intermediate step in deriving the NLDE:

$$
\begin{aligned}
-t_h\left(\psi_{B_j}e^{i\mathbf{k}\cdot\delta_3}+\psi_{B_{j-n_1}}e^{i\mathbf{k}\cdot\delta_1}+\psi_{B_{j-n_2}}e^{i\mathbf{k}\cdot\delta_2}\right)-t_0\psi_{A_j}+U\left|\psi_{A_j}\right|^2\psi_{A_j} &= 0\,, \quad (7.123)\\
-t_h\left(\psi_{A_j}e^{-i\mathbf{k}\cdot\delta_3}+\psi_{A_{j+n_1}}e^{-i\mathbf{k}\cdot\delta_1}+\psi_{A_{j+n_2}}e^{-i\mathbf{k}\cdot\delta_2}\right)-t_0\psi_{B_j}+U\left|\psi_{B_j}\right|^2\psi_{B_j} &= 0\,. \quad (7.124)
\end{aligned}
$$

Physically, t_h, t_0, U, and $\mathbf{k}$ are the hopping, same site, and on-site interaction energies and crystal momentum, respectively. The δ's, $\mathbf{n}$'s, and 2D vector indices $\mathbf{j}$ are the lattice vectors described in our original derivation [52]. For weak interactions, we can make the on-site energy much larger than the contact interaction strength by adjusting the lattice potential so that $|t_0| \gg U$. After inserting the correct values for the lattice vectors and solving Eq. (7.124) for ψ_{B_j}, to lowest order in U/t_0, we obtain

$$
\psi_{B_\mathbf{j}}=\frac{t_h}{-t_0}\left(\psi_{A_j}+\psi_{A_{j+n_1}}e^{i2\pi/3}+\psi_{A_{j+n_2}}e^{-i2\pi/3}\right). \quad (7.125)
$$

From Eq. (7.125) we may write down the corresponding expressions for neighboring sites by shifting the indices using the lattice vectors $\mathbf{n_j}$:

$$
\begin{aligned}
\psi_{B_{j-n_1}} &= \frac{t_h}{-t_0}\left[\psi_{A_{j-n_1}}+\psi_{A_j}e^{i2\pi/3}+\psi_{A_{j+(n_2-n_1)}}e^{-i2\pi/3}\right] \quad (7.126)\\
\psi_{B_{j-n_2}} &= \frac{t_h}{-t_0}\left[\psi_{A_{j-n_2}}+\psi_{A_{j-(n_2-n_1)}}e^{i2\pi/3}+\psi_{A_j}e^{-i2\pi/3}\right]. \quad (7.127)
\end{aligned}
$$

Substituting Eqs. (7.125)-(7.127) into Eq. (7.123), expanding complex factors and regrouping the terms to form finite differences, we arrive at the expression

$$
\begin{aligned}
&\frac{t_h^2}{2t_0}\left\{\left(\psi_{j+n_1}-2\psi_j+\psi_{j-n_1}\right)+\left(\psi_{j+n_2}-2\psi_j+\psi_{j-n_2}\right)\right.\\
&+\left(\psi_{j+(n_2-n_1)}-2\psi_j+\psi_{j-(n_2-n_1)}\right)\\
&-i\sqrt{3}\left[\left(\psi_{j+n_1}-\psi_j\right)+\left(\psi_j-\psi_{j-n_1}\right)-\left(\psi_{j+n_2}-\psi_j\right)\right.\\
&-\left(\psi_j-\psi_{j-n_2}\right)+\left(\psi_{j+(n_2-n_1)}-\psi_j\right)\\
&\left.\left.+\left(\psi_j-\psi_{j-(n_2-n_1)}\right)\right]\right\}-t_0\psi_j+U\left|\psi_j\right|^2\psi_j=0\,. \quad (7.128)
\end{aligned}
$$

It is somewhat surprising that this is a version of the discrete nonlinear Schrödinger equation for the honeycomb lattice in the sense that, in the continuum limit, it gives the usual nonlinear Schrödinger equation with cubic nonlinearity. Substituting the correct continuum limit forms for the finite differences and then expressing the result in $x-y$ coordinates:

$$\frac{t_h^2 a^2}{2t_0}\left[\left(\frac{3}{4}\frac{\partial^2}{\partial x^2}+\frac{1}{4}\frac{\partial^2}{\partial y^2}-\frac{\sqrt{3}}{2}\partial_x\partial_y\right)\psi+\left(\frac{3}{4}\frac{\partial^2}{\partial x^2}+\frac{1}{4}\frac{\partial^2}{\partial y^2}+\frac{\sqrt{3}}{2}\partial_x\partial_y\right)\psi+\frac{\partial^2\psi}{\partial y^2}\right.$$
$$\left.-i\frac{\sqrt{3}}{a}\left(\sqrt{3}\frac{\partial\psi}{\partial x}-\frac{\partial\psi}{\partial y}-\sqrt{3}\frac{\partial\psi}{\partial x}-\frac{\partial\psi}{\partial y}+2\frac{\partial\psi}{\partial y}\right)\right]-t_0\psi+U\left|\psi\right|^2\psi=0\,, \qquad (7.129)$$

which finally reduces to

$$\frac{t_h^2\hbar^2 a^2}{2t_0}\left(\frac{\partial^2\psi}{\partial x^2}+\frac{\partial^2\psi}{\partial y^2}\right)-t_0\,\psi+U\left|\psi\right|^2\psi=0\,. \qquad (7.130)$$

This is the time-independent nonlinear Schrödinger equation. Note that we have reintroduced the correct number of factors of $\hbar$ and the lattice constant a. By defining the effective mass and chemical potential as

$$M_{\text{eff}}=-\frac{t_0}{t_h^2 a^2}\,,\quad \mu=t_0\,, \qquad (7.131)$$

we may write Eq. (7.130) in the more familiar form

$$-\frac{\hbar^2}{2\,m}\nabla^2\psi-\mu\,\psi+U\left|\psi\right|^2\psi=0\,. \qquad (7.132)$$

7.5.5 Proof of RLSE limit to BdGE

For states with energies that are large measured from the Dirac point (deviations from the linear theory), we expect the relativistic formalism to no longer be appropriate and expect to recover a non-relativistic Schrödinger framework for quasi-particle dynamics. Based on our discussion in Sec. 7.3, we expect to find an analogous mapping between the RLSE and the BdGE. This is indeed possible and easy to demonstrate

by writing the RLSE in discrete form similar to the method we used to show the connection between the NLDE and NLSE, i.e., by manipulating the discrete version of Eqs. (7.107)-(7.110) followed by taking the continuum limit. Grouping the equations pairwise, solving Eq. (7.108) for $u_{j,B}$, and back-substituting into Eq. (7.107), we arrive at an intermediate form where the Dirac kinetic term $\mathcal{D}$ has been converted to the Schrödinger ∇^2 form. To complete the reduction, we require the following approximation. At each lattice site, the chemical potential μ is made up of contributions from H_0 (kinetic and lattice potential energy) and from the contact interaction energy U. If the lattice potential is deep and the interaction weak, then the contribution from H_0 dominates the chemical potential, and we find $\mu \approx -t_0$ where t_0 is a self energy. If we then examine the regime where $\mu \gg U, \nabla\phi_{A(B)}, E_k$, we see that the factor multiplying the ∇^2 term appears as $-t_h^2\hbar^2a^2/2t_0$, where t_h, t_0, and a are the hopping energy, self energy, and lattice constant, respectively. We are then free to read off the effective quasi-particle mass as $m_{\text{eff}} = t_0/t_h^2a^2$. Performing the same algebraic steps with Eqs. (7.109)-7.110), and using the same approximations, completes the reduction of the RLSE to the BdGE.

7.6 Stability of Vortex Solutions

Having obtained the RLSE by two different methods, and in light of the natural mapping that we found between these and the BdGE, we are confident that Eqs. (7.116)-(7.117) give us the correct way to compute the low-energy structure (quasi-particle states and eigenenergies) for any of the solutions in Sec. 7.3. The most immediate and pragmatic concern is the combined effect of the honeycomb lattice geometry and the inter-particle interaction on the lifetime of a vortex state. It should be emphasized that the presence of an infinite tower of negative energy states below the Dirac point seems to imply that a condensate residing there will eventually decay provided there is a mechanism for energy dissipation into noncondensate modes (i.e., secondary interactions with thermal atoms). Generically, negative energy states

are present for moving condensates for which excitations subtended by a backward cone have negative frequencies [66]. Moreover, when a vortex is present, small displacements of the core from the symmetry axis of the trap results in a precession of the core, which, when combined with dissipation, causes the vortex to spiral to the edge of the condensate. In the case of zero-lattice potential, this dynamical process is known to be driven by the anomalous modes in the linear spectrum (modes with negative energy and positive norm) [175]. The time for a vortex to spiral to the edge of the trap would then define its lifetime. We note that, in our case, this precessional motion is most likely canceled by introducing rotation to the trap as in the ordinary case with no lattice [29, 175].

To undertake a full treatment of the lifetime would mean computing this spiraling time and then comparing it with the lifetime that we compute here due to the dynamical instability from the complex frequencies. The lifetime of the vortex would then be the smaller of the two values. Nevertheless, in cases where dissipation is weak and the vortex is centered on the symmetry axis of the trap, the dominant source of instability arises from the complex eigenvalues in the solution of the RLSE. We will limit our analysis to the effect of the latter, and regard the negative, real, part of the eigenvalues from a standpoint of metastability. Physically, the complex eigenvalue gives rise to fluctuations in the angular rotation of the vortex spinor components [184]. In the case of the NLDE, this is a result of internal "friction" between the two spinor components displayed in the complex derivative terms of the Dirac kinetic energy. This drag force between the two vortex components (or between vortex and soliton) eventually causes substantial depletion of the condensate. This is the measure that we will use to compute vortex lifetimes.

7.6.1 Solving the RLSE

To determine stability of our vortex solutions, we expand Eqs. (7.116)-(7.117) and express them in plane-polar coordinates, factor the quasi-particle amplitudes into ra-

dial and angular parts, then substitute in the particular solution for $\psi_{A(B)}$. We then obtain a set of first-order coupled ODE's in the radial coordinate to be solved consistently for the functions $u_{A(B)}(r)$, $v_{A(B)}(r)$ and the eigenvalues E_k. We discretize the derivatives and functions using a forward-backward average finite-difference scheme, then solve the resulting discrete matrix eigenvalue problem using MATLAB function Eig. In Figure 7.17 we have plotted the real and imaginary parts of the lowest eigenvalues for the vortex/soliton solution from Eq. (7.41). The lowest modes are anomalous with negative real parts and positive, non-zero but small, imaginary parts. In Figure 7.18 the imaginary parts of the five lowest anomalous modes are plotted as a function of the ratio U/μ depicting the transition from moderate interaction strength: $U/\mu \approx 1$, to the extremely low chemical potential or large interaction limit: $U/\mu >> 1$.

To illustrate convergence of the RLSE eigenvalues for the vortex/soliton, in Appendix Figure 7.19 we have plotted the real and imaginary parts of the eigenvalue for the lowest excitation mode as a function of the number of steps (length of the square matrix along one side).

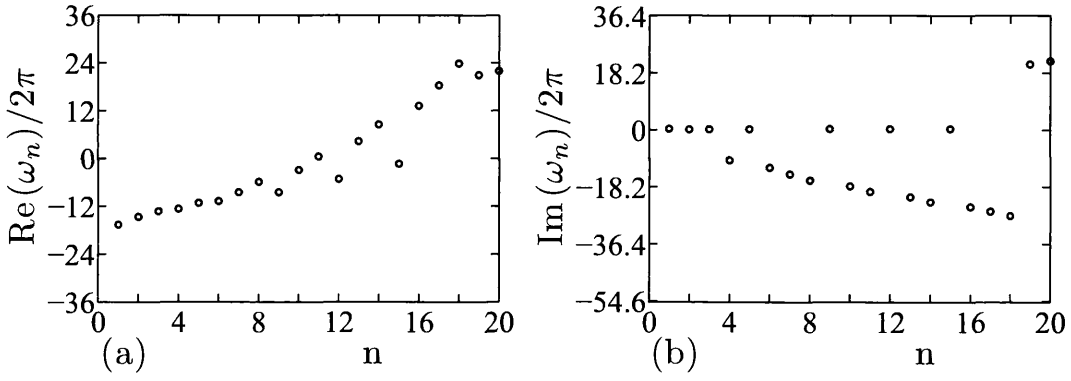

Figure 7.17: (color online) *Anomalous mode frequencies for the vortex/soliton.* The real part of the anomalous mode frequencies are plotted in (a), the Imaginary parts are plotted in (b). The horizontal axis labels the excitation mode.

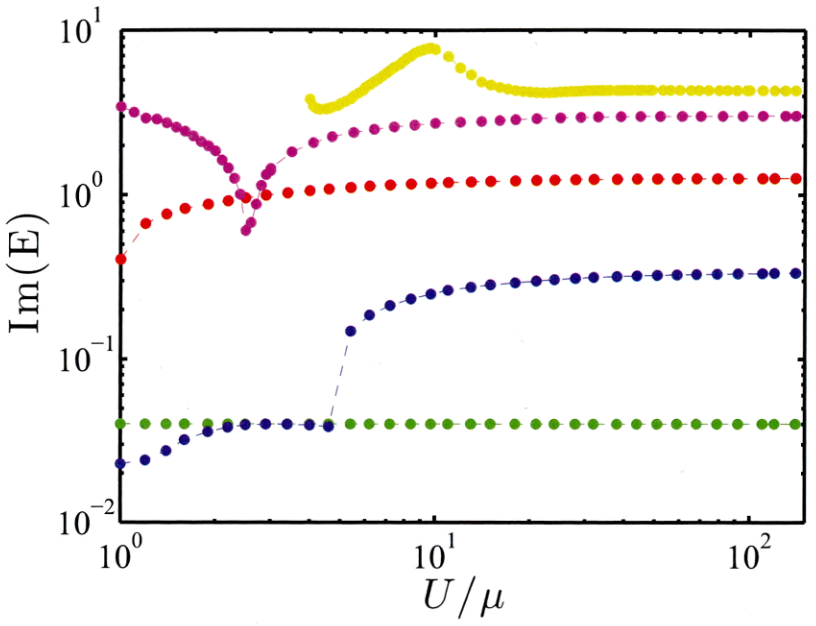

Figure 7.18: (color online) *Imaginary parts of the five lowest quasi-particle excitation energies for the ring/vortex solution.* The excitations are ordered lowest to highest from bottom to top along the right edge of the figure. The horizontal axis indicates the ratio of the interaction strength to the chemical potential. The vertical axis is in units of U.

7.6.2 Computing Vortex Lifetimes

Once the quasi-particle spatial functions and eigenvalues are determined for a particular vortex solution, we can determine the lifetime by calculating the time it takes for the depletion to become large relative to the total number of atoms in the system. We illustrate the method using the vortex/soliton solution. We start by writing down the total particle density operator to lowest order in the quasi-particle operator $\hat{\phi}$:

$$\begin{aligned} \hat{n} &= \hat{\psi}^\dagger \hat{\psi} \approx \sum_{i \in \{A,B\}} \left(|\psi_i|^2 + \psi_i^* \hat{\phi}_i + \psi_i \hat{\phi}_i^\dagger \right) \\ &= n_{\rm C} + \hat{n}_{\rm NC}, \end{aligned} \tag{7.133}$$

Solution type	Lowest excitation energy	Lifetime
Complex topological vortex	$2.085 - 3.90 \times 10^2 i$	4.31×10^{-5} s
Topological vortex	$7.65 \times 10^{-3} - 9.96 \times 10^2 i$	1.29×10^{-5} s
Ring-vortex	$-3.9069 - 1.54 \times 10^{-2} i$	1.25 s
Ring-vortex/soliton	$-3.9276 + 1.9 \times 10^{-3} i$	10.43 s
Vortex/soliton	$-3.9274 + 2.0 \times 10^{-3} i$	9.13 s
Mermin-Ho vortex	$2.634 \times 10^2 + 9.96 \times 10^4 i$	1.57×10^{-7} s
Anderson-Toulouse vortex	$-3.9274 + 1.9 \times 10^{-3} i$	11.51 s
Half-quantum vortex	$2.634 \times 10^2 + 9.96 \times 10^4 i$	1.57×10^{-7} s

Table 7.4: *Stability properties of NLDE vortices.* All energies are in units of the interaction strength U.

where it is understood that a factor of the average 2D particle density $\bar{n}$ must be included before interpreting the final result. The condensate and noncondensate contributions to the density, $n_{\rm C}$ and $\hat{n}_{\rm NC}$, are given by

$$n_{\rm C} \equiv |\psi_A|^2 + |\psi_B|^2 \tag{7.134}$$

$$\hat{n}_{\rm NC} \equiv \psi_A^* \hat{\phi}_A + \psi_A \hat{\phi}_A^\dagger + \psi_B^* \hat{\phi}_B + \psi_B \hat{\phi}_B^\dagger \, . \tag{7.135}$$

Next, we restrict to the mode with the largest imaginary term in its eigenvalue which has $\ell = -1$ relative to the vortex background and has the effect of reducing the rotation of the vortex. We will denote its eigenvalue by $\mathrm{E}_{-1} = (-3.9274 + 0.002\, i)\, U$, where U is the interaction energy. The quasi-particle operators can then be approximated by

$$\hat{\phi}_{A,-1}(r,\theta,t) \approx e^{-iE_{-1}t/\hbar}\, u_{A,-1}(r)\,\hat{\alpha}_j + e^{iE_{-1}t/\hbar}\, v^*_{A,-1}(r)\,\hat{\alpha}^\dagger_j \quad (7.136)$$

$$\hat{\phi}_{B,-1}(r,\theta,t) \approx e^{-iE_{-1}t/\hbar}\, u_{B,-1}(r)\,\hat{\beta}_j + e^{iE_{-1}t/\hbar}\, v^*_{B,-1}(r)\,\hat{\beta}^\dagger_j. \quad (7.137)$$

Notice that these expressions do not depend on the polar angle because we are in the rotating frame of the vortex. We recall that the spatial functions have the properties $u_{A,-1}(r)$, $u_{B,-1}(r) \sim 10^{-2}$ and $v_{A,-1}(r)$, $v_{B,-1}(r) \sim 10^{-5}$ [184], where all are peaked in the "notch" region $\xi_{\rm Dirac} < r < 2\xi_{\rm Dirac}$, and where the absolute values of the slopes of the soliton and vortex are maximum. In this region, the normalization integrals (one for each sublattice) are given by

$$\int d^2r\, \left[|u_{A(B),-1}(r)|^2 - |v_{A(B),-1}(r)|^2\right] > 0\,. \quad (7.138)$$

This combination of positive norm and negative $\mathrm{Re}(\mathrm{E}_{-1})$ signals the presence of the anomalous mode. Next, we fix the total number of particles N of the system and take all N particles to be in the condensate at $t = 0$. We can then compute the depletion out of the vortex/soliton state as a function of time,

$$N_{\rm NC,vs}(t) = \bar{n} \int d^2r\, \left[\langle n_\alpha||\hat{n}_{\rm NC,vs}||0\rangle + |\langle n_\beta||\hat{n}_{\rm NC,vs}||0\rangle|\right], \quad (7.139)$$

where $|0\rangle$ and $|n_{\alpha(\beta)}\rangle$ are the initial and final A(B) sublattice quasi-particle number states, respectively. Retaining only the terms which grow exponentially in time, and using the fact that the $v_{A(B)}$ terms are three orders of magnitude smaller than the $u_{A(B)}$ terms, Eq. (7.139) reduces to

$$N_{\rm NC,vs}(t) = e^{{\rm Im}(E_{-1})t/\hbar}\, 2\pi\, \bar{n} \int_0^{10\xi_{\rm Dirac}} r dr\, \frac{[(r/\xi_{\rm Dirac})u_{A,-1}(r) + u_{B,-1}(r)]}{\sqrt{1+(r/\xi_{\rm Dirac})^2}}\,, \quad (7.140)$$

where we have inserted spatial dependence of the vortex/soliton and taken the size of the condensate to be equal to ten times the healing length. To compute the lifetime $\tau_{\rm vs}$, we can determine the time it takes for the depletion number to grow to roughly

the number of atoms initially in the condensate. Thus, we set Eq. (7.140) equal to $\int d^2r\, \bar{n}$ for time t equal to the lifetime $\tau_{\rm vs}$, which gives

$$\tau_{\rm vs} = \frac{\hbar}{{\rm Im}(E_{-1})} \ln(50/I) = \frac{\hbar}{(0.002)\, U} \ln(50/I) \ . \tag{7.141}$$

The dimensionless integral I contains the overlap of the vortex background with the quasi-particle functions and measures the nonuniformity of particle being ejected from the condensate:

$$I \equiv (\pi 10^2)^{-1/2} \int_0^{10} r' dr' \left[r' u_{A,-1}(r') + u_{B,-1}(r') \right] / \sqrt{1 + r'^2} \, . \tag{7.142}$$

Note the insertion of the normalization factor for the wavefunction $(\pi 10^2)^{-1/2}$. Evaluating the integral numerically gives $I \approx 0.0065$. Using the values for parameters in Table 7.1, we find the lifetime of the vortex/soliton state to be: $\tau_{\rm vs} = 9.13\,{\rm s}$. We have computed lifetimes for all of our solutions and listed them in Table 7.4.

7.7 Conclusion

We have found eight different types of vortex solutions to the NLDE using asymptotic, numerical, and analytical methods in addition to performing a detailed analysis of their lifetimes, elucidating the low-energy landscape for these solutions. Vortex lifetimes were computed based on dynamical instabilities induced by quantum fluctuations: complex eigenvalues appear in the linear spectrum for all vortex types as a result of the couplings between spinor components through Dirac derivative terms. Nevertheless, for four of our solutions, the imaginary parts are smaller than the interaction energy by several orders of magnitude resulting in experimentally realistic lifetimes of about ten seconds.

In the experimental part of our paper, we have provided a clear path towards realizing relativistic vortices in the laboratory: detailed instructions on lattice construction, condensation of bosons at both $\mathbf{K}$ and $\mathbf{K}'$ points, and a method for creating

relativistic vortices are explained using established experimental techniques. Importantly, our proposed method for populating the Dirac points by laser assisted Bragg scattering provides a dynamically stable approach by maintaining a zero group velocity for the condensate. We have discussed specific conditions for energy, density, interaction strength, and lattice depth for observing a transition from the NLDE/RLSE regime to that of the NLSE/BdGE. The density profiles of our solutions should be observable by the usual time-of-flight techniques used to detect Dirac fermions in the laboratory [15, 133].

Interesting new problems naturally arise given the interdisciplinary nature of our work. The following are a few examples. First, the study of nonlinear partial differential equations provides an extensive array of techniques for probing, solving, and classifying equations which could be used for a more complete investigation of the NLDE. Second, by including rotation, one would expect a qualitative change in the anomalous mode structure as a function of trap rotation speed. In the future, we plan to generalize our analysis to the case of a rotating trap in analogy to ordinary trapped BECs in the absence of a lattice. This would provide a more complete understanding of relativistic vortex stabilities and their relationship to ordinary single and multi-component vortices. Third, our solutions suggest a possible mapping to vortices in Chern-Simons theory [237–239]. This seems to indicate a deeper connection between the NLDE and high energy models which could lead to cold atomic simulations of more exotic relativistic field theories. Finally, our results should be easily reproduced within an optics setting by adhering to the momentum space bounds we have provided, thus contributing to the long-standing mutual exchange between condensed matter and nonlinear optics.

Acknowledgments

This material is based in part upon work supported by the National Science Foundation under grant numbers PHY-1067973, PHY-1011156, and the Air Force Office of Scientific Research grant number FA9550-08-1-0069. L.D.C. thanks the Alexander von Humboldt foundation and the Heidelberg Center for Quantum Dynamics for additional support.

7.8 Appendix A: Convergence of Numerical Solutions of the NLDE and RLSE

We show convergence of the numerical solutions of the NLDE by looking at the $l = 2$ ring-vortex solution. To obtain the solution, we use a simple forward-difference scheme to discretize the radial derivatives in Eqs. (8.6)-(8.7) and then integrate out from the core of the vortex with the following values for the parameters: $\mu/U = 1$, $f_A(0) = 10^{-4}$. The results are plotted in Figure 7.20 for four different values of the number of steps N. Note also that we have included the exact solution for comparison (dotted and dashed-dotted curves). Also, we have normalized the exact solution so that the peaks of the solid curves match.

Convergence of the RLSE can be shown by computing the eigenvalues for a particular background solution and varying the number of grid points N used in the $4N \times 4N$ matrix problem. In Figure 7.19 we have plotted the real and imaginary parts of the lowest eigenvalue for the $l = 1$ vortex/soliton background as a function of the grid size N.

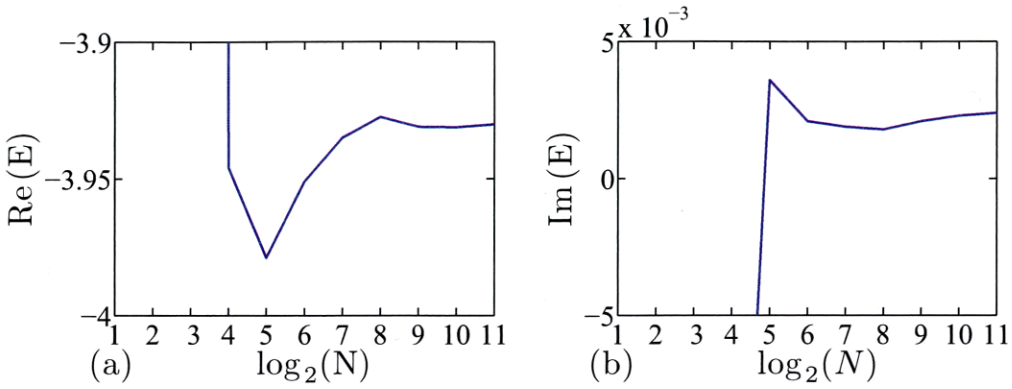

Figure 7.19: (color online) *Convergence of RLSE for the vortex/soliton.* Real (a) and imaginary (b) parts of the lowest anomalous mode. The horizontal axis shows the number of steps and the energy of the lowest excitation is plotted on the vertical axis.

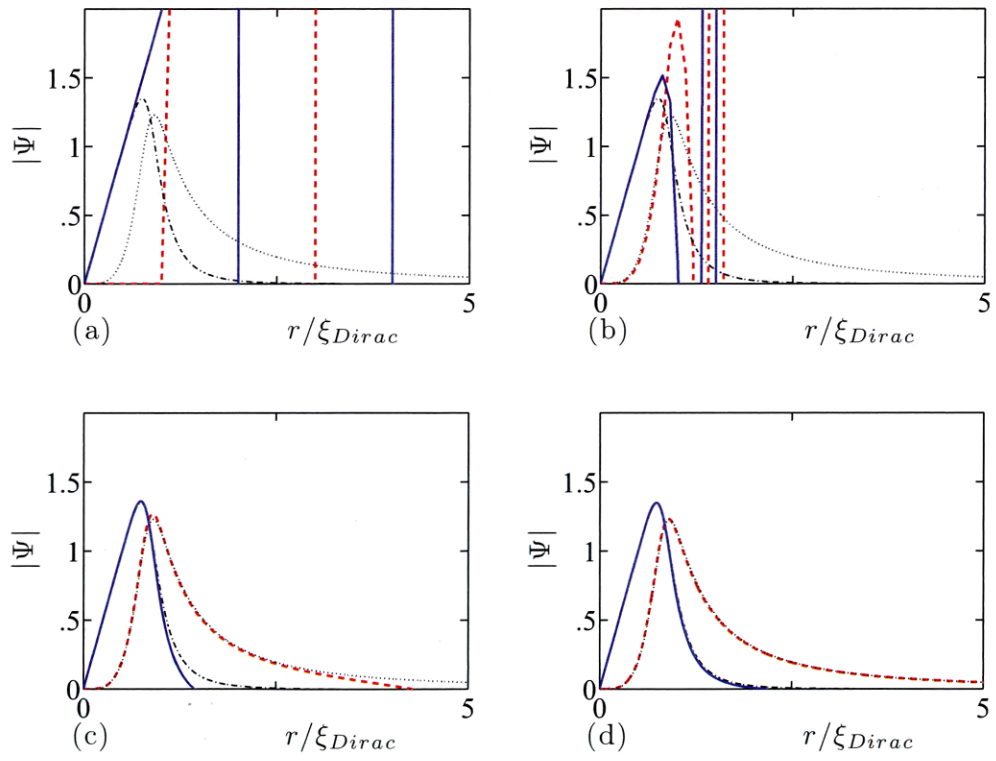

Figure 7.20: (color online) *Convergence of the $l = 2$ ring-vortex solution.* The black (dotted and dashed-dotted) curves are the exact solutions. The blue (solid) and red (dashed) plots are the numerical results for the upper and lower spinor components, respectively. Plots are shown for four values of the number of steps N:(a)$N = 10^2$, (b)$N = 10^3$, (c)$N = 10^4$, (d)$N = 10^5$. We have set $\mu = 0$ and $U = 1$ for all plots.

CHAPTER 8

THE NONLINEAR DIRAC EQUATION: RELATIVISTIC SOLITONS AND MASS GAPS

L. H. Haddad, C. M. Weaver, and Lincoln D. Carr, Physical Review A, under review, 2012.

Abstract

We present a thorough analysis of solitons which solve the one-dimensional (1D) zigzag and armchair nonlinear Dirac equation (NLDE) for a Bose-Einstein condensate (BEC) in a honeycomb lattice, where the two types of NLDEs correspond to the two independent directions in analogy to the narrowest of graphene nanoribbons. Analytical as well as numerical soliton two-component spinor solutions are obtained. These include analytical spatially infinite arrays of bright two-spinor solitons. In addition, we find a gray line-soliton and compute its discrete spectra for several spatially quantized states in a harmonic potential. The strong region of the harmonic trap provides a unique opportunity to study the BEC analog of Klein-tunneling. By solving the relativistic linear stability equations (RLSE) for a BEC of ^{87}Rb atoms, we find that most of our solutions are either stable or unstable on times scales longer than the lifetime of experiments. Nambu-Goldstone modes are detected in the linear spectra for all of our solutions. We study the effect of various types of mass gaps on the solution space of the NLDE. In particular, the gap produced by a modulation of the nearest-neighbor hopping allows for a general mapping of our embedded solitons into

the gapped theory, in addition to a second mapping from a Poincaré invariant subspace of the NLDE to the massive Thirring model, the latter a well known integrable theory.

8.1 Introduction

The nonlinear Dirac equation (NLDE) appears in a variety of physical settings, typically as classical field equations for relativistic interacting fermions [103, 126]. The $(1+1)$-dimensional NLDE with scalar-scalar or vector-vector interaction is the prototypical effective model for interacting fermions, and has been the subject of much analysis over the past decades [111–116]. Dirac-like spin-orbit couplings for interacting cold atoms have also been investigated, simulating some features of quark confinement [211]. Moreover, soliton solutions of the NLDE appear in one-dimensional (1D) nonlinear optical structures [120, 123], acoustic physics [122], and electron propagation in graphene [21, 121, 221–223, 240, 241]. In all of these cases the combination of Dirac kinetic term and nonlinearity leads to a plethora of solitary wave solutions whose properties depend on the particular form of the interaction term [215, 242]. Our own recent work has placed the NLDE in the context of a Bose-Einstein condensate (BEC) [52]. Significantly, our particular form of the NLDE has opened up research in other fields of physics [20, 32, 110, 168, 208–210, 212–214, 216]. For the NLDE in a BEC, the relativistic structure arises naturally as bosons propagate in a shallow periodic honeycomb lattice potential, and yields a rich soliton landscape which we explore in detail in this article.

The 1D NLDE may be obtained by dimensionally reducing the full two-dimensional (2D) honeycomb lattice theory [52] to a one-dimensional theory by making the trap frequency large in one of the planar directions. A schematic of the beams, harmonic

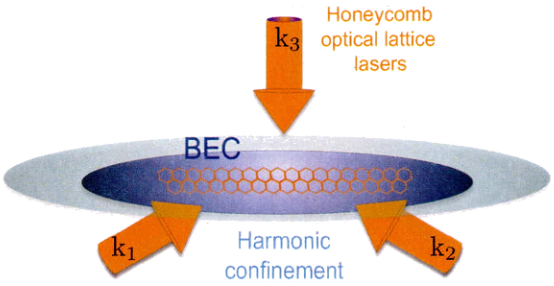

Figure 8.1: (color online) *Quasi-one-dimensional BEC in a honeycomb optical lattice with harmonic confinement.*

potential, and narrow band of the reduced honeycomb lattice is shown in Figure 8.1.

Thus, there are two independent forms of the 1D NLDE corresponding to the armchair and zigzag patterns in the narrowest possible graphene nanoribbons [183], but here related to the honeycomb optical lattice potential. The NLDE operator is complex in the armchair direction and real along the zigzag direction. From here on we will refer to these two forms as the *armchair NLDE* and *zigzag NLDE* [243]. The exact honeycomb lattice potential with an additional harmonic trap in the y-direction for the zigzag and armchair geometries are plotted in Figure 8.2 and are given explicitly by

$$U_{\text{armchair}}(\mathbf{r}) = \tag{8.1}$$
$$-\frac{\alpha E_0^2}{4}\left(3+2\cos\left[(\mathbf{k}_1-\mathbf{k}_2)\cdot\mathbf{r}\right]+2\cos\left[(\mathbf{k}_2-\mathbf{k}_3)\cdot\mathbf{r}\right]+2\cos\left[(\mathbf{k}_1-\mathbf{k}_3)\cdot\mathbf{r}\right]\right)$$
$$+\frac{1}{2}M\omega^2 y^2\,,$$
$$U_{\text{zigzag}}(\mathbf{r}) = \tag{8.2}$$
$$-\frac{\alpha E_0^2}{4}\left(3+2\cos\left[(\mathbf{k}_2-\mathbf{k}_1)\cdot\mathbf{r}\right]+2\cos\left[(\mathbf{k}_1-\mathbf{k}_3)\cdot\mathbf{r}\right]+2\cos\left[(\mathbf{k}_2-\mathbf{k}_3)\cdot\mathbf{r}\right]\right)$$
$$+\frac{1}{2}M\omega^2 y^2\,,$$

where $\mathbf{k}_1$, $\mathbf{k}_2$, $\mathbf{k}_3$ are the wavenumbers for the lattice laser beams, α is the polarizability of the atoms, E_0 is the amplitude of the beams, M is the mass of the atoms, and ω is the trap frequency along the narrow direction. pinor soliton solutions associated

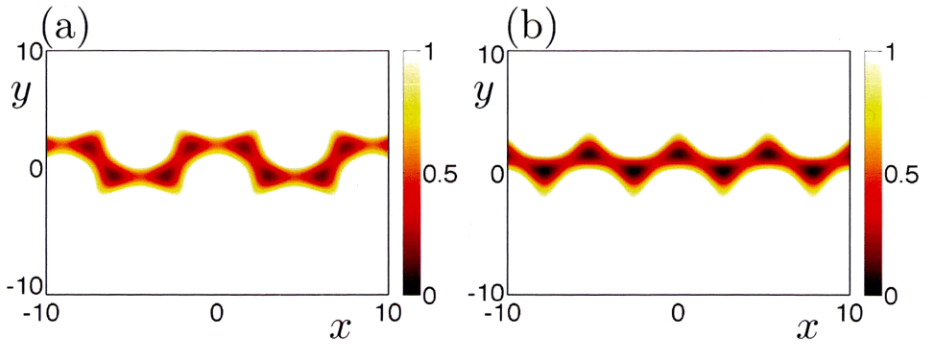

Figure 8.2: (color online) *Optical lattice nanoribbons.* (a) Potential of the armchair geometry. (b) Potential for the zigzag geometry.

with propagation along these two directions are related by a complex Pauli matrix rotation. To obtain soliton solutions we first solve the zigzag NLDE using an envelope function ansatz, which leads directly to an exact closed form for an infinite array of bright solitons along the x-axis. From this solution we then obtain a form which solves the armchair NLDE. Both types of solutions describe solitons embedded in the continuous spectrum of the $(2+1)D$ NLDE [244]. We determine the stability of our solitons by solving the relativistic linear stability equations (RLSE), an analog of the Bogoliubov de-Gennes system [184]. The solution of the RLSE gives us the linear perturbation spectrum due to the presence of small quantum fluctuations in the BEC.

The NLDE solution space can be expanded by opening a mass gap in the spectrum, accomplished by imposing an asymmetry in the A/B sublattice depths, a directed (anisotropic) next-nearest neighbor hopping, or by modulating the nearest neighbor hopping [155]. The latter method effectively connects two inequivalent Dirac points in which case a full four-spinor description is needed. The presence of a mass gap greatly enlarges the spectrum of soliton solutions by incorporating gap solitons, which possess unique features distinct from their embedded counterparts [120]. Significantly, we find that the gapped four-spinor version of the NLDE has a direct mapping to the massive Thirring model [125, 126], a theory which is well known to be integrable in

both the quantum and classical sense. At the level of the wavefunction, the real and imaginary parts of the NLDE spinor components are mapped to the upper and lower spinor components in the Thirring model, respectively. The Thirring spinors possess exact relativistic invariance and so are comprised of equal admixtures of positive and negative energy solutions in the NLDE picture. The fact that our mapping works for a subspace of NLDE solutions suggests integrability but is certainly not conclusive. A complete analysis of the problem would require constructing a Lax pair representation of the NLDE, in addition to using other formal methods such as general Painlevé analysis, singular manifold methods, or Darboux and Bäcklund transformations [103, 245–250]. For the latter test, the key question to address is whether or not our mapping to the Thirring model can be classified as an auto-Bäcklund or hetero-Bäcklund transformation.

8.2 Soliton Solutions of the NLDE

In this section we solve the NLDE without a mass gap. The parameters which enter directly into the NLDE and will therefore appear in all of our solutions, are the effective speed of light $c_l = t_h a\sqrt{3}/2\hbar$ and the particle interaction $U = L_z g\bar{n}^2 3\sqrt{3}a^2/8$, where U is the 2D optical lattice renormalized version of the usual interaction $g = 4\pi\hbar^2 a_s/M$. Appearing in these definitions are the average particle density $\bar{n} = N/V$, the s-wave scattering length a_s, the vertical oscillator length L_z, the mass M of the constituent atoms in the BEC, the lattice constant a, and the hopping energy t_h. For the hopping energy, we use a semiclassical estimate given by $t_h \equiv 1.861\,(V_0/E_R)^{3/4}\,E_R \exp\left(-1.582\sqrt{V_0/E_R}\right)$ [77]. A complete discussion of NLDE parameters and constraints can be found in [cite our NP paper on the axiv]

The NLDE for two inequivalent Dirac points describes the dynamics of a Dirac four-spinor of the form $\Psi \equiv (\Psi_+,\, \Psi_-)^T$, with the upper $(+)$ and lower $(-)$ two-spinors relating to opposite $\mathbf{K}$ and $\mathbf{K}'$ points of the honeycomb lattice. The full NLDE in this case is

$$i\hbar\gamma^{\mu}\partial_{\mu}\Psi - U\sum_{i=1}^{4}(M_i\Psi)(\Psi^{\dagger}M_i)\,\Psi = 0\,. \tag{8.3}$$

The matrices γ^{μ} are the usual Dirac matrices and the interaction terms are encapsulated in the summation with the matrices M_i constructed to give the correct cubic nonlinearites, local to each spinor component [52]. The interactions do not couple different spinor components so we focus on the equations for a two-spinor in rectangular coordinates

$$\begin{aligned} i\hbar\,\partial_t\psi_A &= -i\hbar c_l\,(\partial_x - i\partial_y)\,\psi_B + U\,|\psi_A|^2\,\psi_A & (8.4)\\ i\hbar\,\partial_t\psi_B &= -i\hbar c_l\,(\partial_x + i\partial_y)\,\psi_A + U\,|\psi_B|^2\,\psi_B\,, & (8.5) \end{aligned}$$

with the full solution expressed as a linear combination of solutions from each Dirac point. Note the presence of the effective speed of light, c_l, and interaction strength, U. Eqs. (8.4)-(8.5) allow for one-dimensional (1D) solutions by taking ψ_A and ψ_B to vary in only one direction while remaining constant in the other. We are interested in stationary states so we take the time-dependence to be the usual exponential factor with the chemical potential as the frequency. We then write: $\psi_A(x,t) = \exp(-i\mu t/\hbar)f_A(x)$ and $\psi_B(x,t) = \exp(-i\mu t/\hbar)f_B(x)$, where $f_A(x)$ and $f_B(x)$ are taken to be functions of the single variable x and μ is the usual chemical potential. Note that choosing the y-direction adjusts the relative phase between the spinor components. Eqs. (8.4)-(8.5) become

$$\begin{aligned} \mu f_A(x) &= -i\hbar c_l\,\partial_x f_B(x) + U\,|f_A(x)|^2 f_A(x) & (8.6)\\ \mu f_B(x) &= -i\hbar c_l\,\partial_x f_A(x) + U\,|f_B(x)|^2 f_B(x)\,. & (8.7) \end{aligned}$$

This is the time-independent 1D NLDE for the armchair direction of the honeycomb lattice. Notice that taking $f_A \to i f_A$ we converts the real zigzag version corresponding to the y-direction. It is natural to retain the x notation when discussing either form

of the NLDE, thus we write the zigzag version as

$$\mu f_A(x) = -\hbar c_l \, \partial_x f_B(x) + U \, |f_A(x)|^2 f_A(x) \tag{8.8}$$
$$\mu f_B(x) = \hbar c_l \, \partial_x f_A(x) + U \, |f_B(x)|^2 f_B(x) \, . \tag{8.9}$$

8.3 Bright Soliton Train

An exact real solution of the NLDE may be obtained using the form

$$\Psi(x) = \eta(x) \begin{pmatrix} \cos\varphi(x) \\ \sin\varphi(x) \end{pmatrix} , \tag{8.10}$$

where we have assumed only that the wavefunction is real. Substituting Eq. (8.10) into Eqs. (8.8)-(8.9), multiplying by $\cos\varphi$ and $\sin\varphi$, respectively, then adding the resulting equations gives

$$\frac{d\varphi}{dx} = -\frac{\mu}{\hbar c_l} \left[1 - \eta^2 \, (U/\mu)(\cos^4\varphi + \sin^4\varphi) \right] \tag{8.11}$$

To obtain a second equation we multiply Eqs. (8.8)-(8.9) by $\cos\varphi$ and $\sin\varphi$, respectively, then subtract the resulting equations which yields

$$\frac{d(\ln\eta)}{dx} = \frac{U}{4\hbar c_l} \eta^2 \sin(4\varphi) \, . \tag{8.12}$$

Note that we have divided through by η to arrive at Eqs. (8.11)-(8.12). Equations (8.11)-(8.12) can be combined by back substitution to get

$$\left[\frac{\sin(4\varphi)}{\cos^4\varphi + \sin^4\varphi} \right] \left(\varphi + \frac{\mu x}{\hbar c_l} \right)' = 4 \, (\ln\eta)' \tag{8.13}$$

where the prime notation indicates differentiation with respect to x. From Eq. (8.13), we may obtain a formal expression for η:

$$\eta^4 = \exp\left[\int dx \, \frac{\sin(4\varphi)}{\cos^4\varphi + \sin^4\varphi} \left(\varphi + \frac{\mu x}{\hbar c_l} \right)' \right] . \tag{8.14}$$

To solve Eq. (8.14), we choose the linear form $\varphi(x) = \kappa x$, obtain an explicit form for $\eta(x)$ which we then substitute into Eq. (8.11) to determine the constant κ and obtain a relation for the chemical potential μ and the interaction U. Equation (8.14) becomes

$$\eta^4 = \exp\left[(\kappa + \mu/\hbar c_l) \int dx \, \frac{\sin(4\kappa x)}{\cos^4\kappa x + \sin^4\kappa x}\right] . \tag{8.15}$$

Integrating gives

$$\eta(x) = \left(\cos^4\kappa x + \sin^4\kappa x\right)^{-(1+\mu/\kappa\hbar c_l)/4} . \tag{8.16}$$

Substituting this result into Eq. (8.11) and using the linear ansatz, gives the expression

$$\kappa = -\frac{\mu}{\hbar c_l}\left[1 - \frac{U}{\mu}\left(\cos^4\kappa x + \sin^4\kappa x\right)^{1-(1+\mu/\kappa\hbar c_l)/2}\right] . \tag{8.17}$$

In order for this expression to be true, it must be that the exponent of the spatial functions is identically zero. Equation (8.17) then gives the two conditions

$$\frac{1}{2} - \frac{\mu}{2\kappa\hbar c_l} = 0 , \tag{8.18}$$

$$-\frac{\mu}{\hbar c_l}\left(1 - \frac{U}{\mu}\right) = \kappa , \tag{8.19}$$

which may be solved to give

$$\kappa = \frac{\mu}{\hbar c_l} , \tag{8.20}$$

$$\mu = 2\,U . \tag{8.21}$$

The corresponding solution is then

$$\Psi_{\text{zigzag}}(x) = \left(\cos^4\kappa x + \sin^4\kappa x\right)^{-1/2} \begin{pmatrix} \cos\kappa x \\ \sin\kappa x \end{pmatrix} , \tag{8.22}$$

where $\kappa = 2U/(\hbar c_l)$. The spinor components in Eq. (8.22) are plotted in Figure 8.3 along with the density. Equation (8.22) was obtained for the zigzag NLDE and can be modified to get the associated armchair solution by taking $\psi_A \to i\psi_A$ to get

$$\Psi_{\text{armchair}}(x) = \left(\cos^4\kappa x + \sin^4\kappa x\right)^{-1/2} \begin{pmatrix} i\cos\kappa x \\ \sin\kappa x \end{pmatrix} \tag{8.23}$$

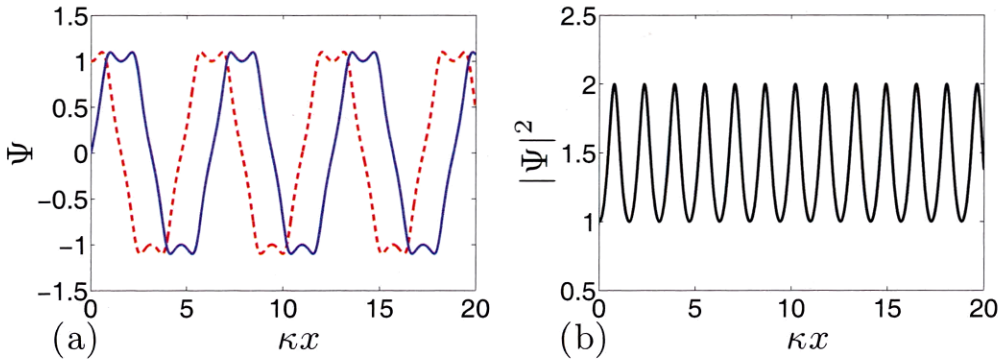

Figure 8.3: (color online) *Bright soliton train.* (a) The upper (red) and lower (blue) component solutions. (b) The spatial variation of the square of the total density.

8.3.1 Soliton Expansion and Conserved Charges

We can obtain an exact solution for general values of the chemical potential by choosing series expansion ansatz for η in terms of the quantity $\cos^4\varphi + \sin^4\varphi$. This form is convenient since we note that $(\cos^4\varphi + \sin^4\varphi)' = -\sin(4\varphi)$. We then write

$$\eta = \sum_{\text{n}=-\infty}^{\infty} a_n(\cos^4\varphi + \sin^4\varphi)^n. \tag{8.24}$$

With this form, Eq. (8.12) becomes

$$\frac{d\varphi}{dx} = -\frac{U}{4\hbar c_l}\frac{\left[\sum_{\text{n}=-\infty}^{\infty} a_n(\cos^4\varphi + \sin^4\varphi)^n\right]^3}{\sum_{\text{n}=-\infty}^{\infty} n a_n(\cos^4\varphi + \sin^4\varphi)^{n-1}}. \tag{8.25}$$

Similarly, Eq. (8.11) becomes

$$\frac{d\varphi}{dx} = \frac{U}{\hbar c_l}\left[\sum_{n=-\infty}^{\infty} a_n(\cos^4\varphi + \sin^4\varphi)^n\right]^2(\cos^4\varphi + \sin^4\varphi) - \frac{\mu}{\hbar c_l}. \tag{8.26}$$

For our initial ansatz to be valid, the expansion coefficients in Eqs. (8.25)-(8.26) must be solved for consistently such that both equations are simultaneously true. Thus, setting Eq. (8.25) equal to Eq. (8.26)

$$\frac{\left[\sum_{n=-\infty}^{\infty} a_n(\cos^4\varphi + \sin^4\varphi)^n\right]^3}{4\sum_{n=-\infty}^{\infty} n a_n(\cos^4\varphi + \sin^4\varphi)^{n-1}} = \frac{\mu}{U} - \left[\sum_{n=-\infty}^{\infty} a_n(\cos^4\varphi + \sin^4\varphi)^n\right]^2(\cos^4\varphi + \sin^4\varphi). \tag{8.27}$$

The expansion coefficients a_n may be obtained by performing a formal term-by-term multiplication and division and then matching the coefficients for corresponding powers of the argument $\cos^4\varphi + \sin^4\varphi$. Once we obtain a formal recursion for the coefficients in terms of μ/U, we can obtain the formal expression for Eq. (8.25),

$$\sum_{n=-\infty}^{\infty}\left[c_n(\cos^4\varphi + \sin^4\varphi)^n + b_n\right]\frac{d\varphi}{dx} - 1 = 0. \tag{8.28}$$

where the coefficients c_n are obtained by the matching process in the previous step and the constants b_n are the result of dividing like powers of the argument on the left hand side of Eq. (8.27). Each term in the summation is integrable and associated with an infinite number of conserved charges. For example, the case $n = 0$ gives back the linear form for φ,

$$(c_0\,\varphi - x + b_0 x)' = 0 \tag{8.29}$$

$$\Rightarrow\ [(c_0\,\varphi - x + b_0 x)^m]' = 0\,, \tag{8.30}$$

for any integer m and where b_0 is the integration constant. The associated conserved charges are

$$Q_0^{(m)} = (c_0\,\varphi - x + b_0 x)^m \ . \tag{8.31}$$

For $n = 1$, the integral and conserved charges are

$$(3\varphi + \sin 4\varphi + b_1 x)' = 0\,, \tag{8.32}$$
$$Q_1^{(m)} = (3\varphi + \sin 4\varphi + b_1 x)^m \ , \tag{8.33}$$

for $n = 2$,

$$\left(19\,\varphi + 3\sin 4\varphi + \frac{1}{8}\sin 8\varphi + b_2 x\right)' = 0\,, \tag{8.34}$$
$$Q_2^{(m)} = \left(19\,\varphi + 3\sin 4\varphi + \frac{1}{8}\sin 8\varphi + b_2 x\right)^m \ , \tag{8.35}$$

and for n=3,

$$\left(63\,\varphi + \frac{111}{8}\sin 4\varphi + \frac{9}{8}\sin 8\varphi + \frac{1}{24}\sin 12\varphi + b_3 x\right)' = 0\,, \tag{8.36}$$
$$Q_3^{(m)} = \left(63\,\varphi + \frac{111}{8}\sin 4\varphi + \frac{9}{8}\sin 8\varphi + \frac{1}{24}\sin 12\varphi + b_3 x\right)^m . \tag{8.37}$$

Terms in the series for negative n-values are also exactly integrable but in terms of inverse tangent functions. For example, integrating the $n = -3$ term gives

$$\left[16\,(3+\cos 4\varphi)^2\right]^{-1}\left[-19\sqrt{2}\arctan\left[1-\sqrt{2}\tan\varphi\right](3+\cos 4\varphi)^2\right.$$
$$\left.-19\sqrt{2}\arctan\left[1+\sqrt{2}\tan\varphi\right](3+\cos 4\varphi)^2 + 70\sin 4\varphi + 9\sin 8\varphi + b_{-3}x\right]' = 0\,. \tag{8.38}$$

Each conserved charge above corresponds to an independent solution for φ matched with a particular envelope function

$$Q_n^{(m)} = \text{constant}\,, \tag{8.39}$$
$$\eta_n(x) = \left(\cos^4\varphi + \sin^4\varphi\right)^n \ , \tag{8.40}$$

where the charge equation may in principle be inverted to obtain the function $\varphi(x)$.

8.3.2 Numerical Solitons

The profile for a topological soliton ($\mu \neq 0$) can be obtained using a numerical shooting method [230]. The most direct approach is to express Eqs. (8.8)-(8.9) in terms of the dimensionless spatial variable $\chi \equiv (U/\hbar c_l)x$. The functions $f_A(\chi)$ and $f_B(\chi)$ are then expanded in power series around $\chi = 0$

$$f_A(\chi) = \sum_{j=0}^{\infty} a_j \chi^j \,, \quad f_B(\chi) = \sum_{j=0}^{\infty} b_j \chi^j \,, \tag{8.41}$$

where the a_j and b_j are the expansion coefficients. Since we are solving two coupled first order equations, we require the initial conditions $f_A(0)$ and $f_B(0)$. Substituting into Eqs. (8.8)-(8.9) gives us the behavior of the solution at the origin:

$$f'_A(0) \sim \frac{1}{\hbar c_l}\left[\mu - U f_B(0)^2\right] f_B(0) \tag{8.42}$$

$$f'_B(0) \sim -\frac{1}{\hbar c_l}\left[\mu - U f_A(0)^2\right] f_A(0). \tag{8.43}$$

The form of the 1D NLDE shows that for any index $j \geq 0$, a_{2j+1} and b_{2j} are related through a recursion formula, likewise a_{2j} and b_{2j+1} are also related. To obtain a soliton solutions using the shooting method, we first fix either a_0 or b_0 then vary the other until we obtain convergence to a the desired precision. Although it seems that both a_0 and b_0 are free parameters, fixing one to a different value before shooting results in a spatially translated final solution. We take $b_0 = 0$ and solve for the value $a_0 = a_0^{\text{soliton}}$ which gives the desired form. Figure 8.4(c) shows our numerical shooting results for the line soliton. This is obtained for

$$a_0^{\text{soliton}} = 0.94640402384. \tag{8.44}$$

In Figure 8.4(a) and (b) we show the solution for values of $a_0 > a_0^{\text{soliton}}$. At larger values of a_0, the interaction energy becomes more pronounced and we start to pick

up some of the excited soliton states which can be seen in Figure 8.4(a) and (b). For values $a_0 < a_0^{\text{soliton}}$, the effect of the interaction is reduced, Figure 8.4(d) and (e), until finally we see the free particle sine and cosine forms appearing in Figure 8.4(f).

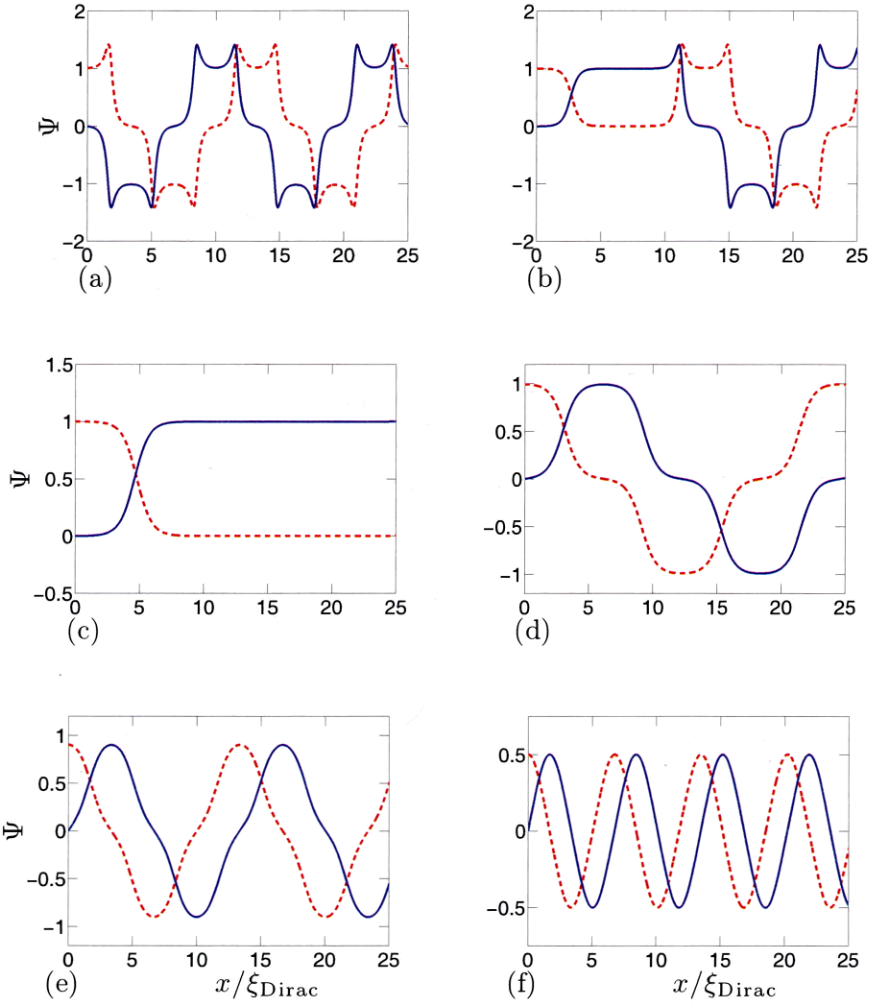

Figure 8.4: (color online) *Numerical solutions of the NLDE.* (a) $a_0 = 1.1$. (b) $a_0 = 0.9992922$. (c) $a_0 = 0.999292150145$. (d) $a_0 = 0.99$. (e) $a_0 = 0.9$. (f) $a_0 = 0.5$.

The solution in Figure 8.4(c) is an example of a gray soliton since the density of atoms is constant everywhere except near the line where the A and B sublattice amplitudes meet. A comparison of the gray soliton and bright soliton densities is shown in Figure 8.5. We can see that the line soliton is at the boundary between two

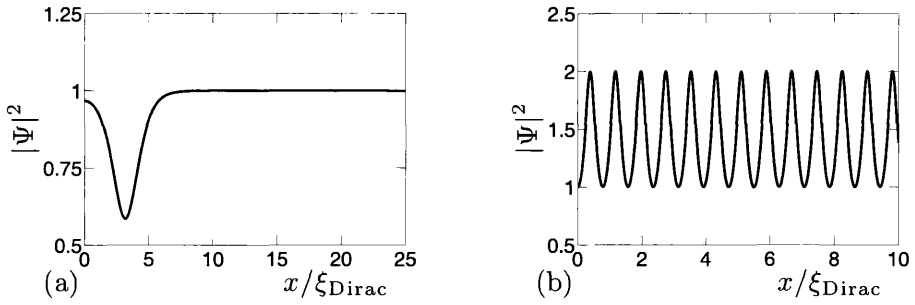

Figure 8.5: (color online) *Soliton densities.* (a) Gray soliton density. The notch can be shifted by using a different value of b_0. (b) Bright soliton density for the case $n = 1$. In (b), the individual peaks are locally Lorentzian.

regimes: the strongly interacting bright soliton regime shown in Figure 8.4(a), and the weakly interacting free-particle regime in Figure 8.4(f).

8.4 Mass Gaps for the NLDE

The introduction of a mass gap into our system greatly expands its versatility, allowing for a richer structures in the nonlinear landscape. Masses in general graphene-like systems with fermions have been studied extensively [155], and provide a foundation for our analysis of mass gaps within the analog bosonic system. In this section we define and then discuss the various key types of gaps possible for bosons in the honeycomb optical lattice, then present the particular features of solitons in the presence of a gap and discuss how they relate back to our gapless solitons. We provide some detailed discussion of the continuous spectrum of the NLDE in the appendix. Several type of lattice modifications can be used to open a gap in the spectrum while still preserving spin rotation symmetry [155]. One way to open a gap is through a staggered chemical potential between the two sublattices. This is obtained by changing the relative depths of the sublattice potentials tuned so that $\mu_A = \mu + m_s c_l$ and $\mu_B = \mu - m_s c_l$, where c_l is the effective speed of light. The mass difference term $m_s c_l$ results from a different self energy at each site when we go to the tight-binding limit.

This opens a spectral gap of $2|m_s|c_l$. A second way to open a gap is by introducing a directed next-nearest-neighbor hopping amplitude in the presence of fluxes which opens a gap $2|\eta|c_l$. Finally, we may introduce a modulation of the nearest neighbor hopping with a wave vector that mixes the two opposite Dirac points (equivalent to a Kekulé dimerization pattern in graphene) and opens a gap of $2|\Delta c_l|$ where Δ is the complex parameter $\Delta = \mathrm{Re}\,\Delta + i\,\mathrm{Im}\,\Delta$. Here the phase of Δ controls the angles of the dimerization pattern. Combining all of these effects produces the gapped version of the full NLDE in Eq. (8.3),

$$i\hbar\gamma^\mu\partial_\mu\Psi + (|\Delta|c_l\beta e^{i\theta\gamma_5} + m_s c_l\alpha_3 + i\eta c_l\alpha_1\alpha_2)\Psi - U\sum_{i=1}^{4}(M_i\Psi)(\Psi^\dagger M_i)\Psi = 0. \quad (8.45)$$

where the matrices M_i were defined in our earlier work [52], and θ defines the direction of the dimerization pattern.

8.4.1 General Embedded and Gap Solitons

Equation (8.45) has an important simplified form for the spatial values $m_s, \eta = 0$. This allows for a straightforward solution based on solutions that we have already obtained. If we combine the spinor components and define: $\psi_1 \equiv \psi_{A+} = \psi_{B-}$ and $\psi_2 \equiv \psi_{B+} = \psi_{A-}$, i.e., the spinor equations for opposite Dirac points have the same form, and we find that ψ_1 and ψ_2 satisfy the equations

$$i\hbar\,\partial_t\begin{pmatrix}\psi_1\\ \psi_2\end{pmatrix} = \begin{pmatrix} U|\psi_1|^2 + |\Delta|c_l\cos\theta & -i\hbar c_l\mathcal{D}^* \\ -i\hbar c_l\mathcal{D} & U|\psi_2|^2 + |\Delta|c_l\cos\theta\end{pmatrix}\begin{pmatrix}\psi_1\\ \psi_2\end{pmatrix}, \quad (8.46)$$

which, for stationary solutions with chemical potential μ_g (redefined for the gapped case), reduce to the time-independent NLDE with mass gap:

$$\begin{aligned} -i\hbar c_l\mathcal{D}^*\psi_2 + U|\psi_1|^2\psi_1 &= (\mu_g + |\Delta|c_l\cos\theta)\,\psi_1 \\ -i\hbar c_l\mathcal{D}^*\psi_1 + U|\psi_1|^2\psi_2 &= (\mu_g + |\Delta|c_l\cos\theta)\,\psi_2\,, \end{aligned} \quad (8.47)$$

where subscripted μ_g indicates the chemical potential in the gapped theory. Eq. (8.47) is exactly the two-spinor NLDE modified by the gap $|\Delta|\cos\theta$ along with the identifications $\psi_1 \equiv \psi_A$, $\psi_2 = \psi_B$. This means that all of our previous solutions are valid here, and we can read off the chemical potential μ for the gapless theory with the identification $\mu_g = \mu - |\Delta|c_l\cos\theta$ for the gaped theory. The characteristic features of the different types of gapped solutions are as follows:

1. For the special case where $\theta = n\pi$, solutions with non-zero μ in the gapless theory map to solitons that are either inside the gap or are embedded in the continuous spectrum, depending on the phase integer n. For example, a soliton solution with chemical potential $\mu = 2U$ maps to $\mu_g = 2U \pm |\Delta|c_l$. The *positive* sign sets the soliton *inside* the gap when $|\mu_g| < |\Delta|c_l$, which is satisfied if $|\Delta|c_l > U > |\Delta|c_l/2$, for positive μ_g. The *negative* sign *embeds* the soliton within the continuous spectrum. In this case the chemical potential $\mu_g = 2U + |\Delta|c_l$. Thus, the chemical potential of the gapless solution is shifted up by $|\Delta|c_l$.

2. For zero-chemical potential solutions, we find the condition $\mu_g = \pm|\Delta|c_l$ (for $\theta = n\pi$). These correspond to solitons whose components both vanish for $x \to \infty$. Again, these solutions have their chemical potentials shifted by $|\Delta|c_l$, reside at the *lower* (*negative* sign) and *upper* (*positive* sign) edges of the gap.

3. By tuning the gap phase angle θ, we can continuously adjust the chemical potential μ_g setting it inside or outside the gap.

4. It is important to note that for the general case where m_s, $\eta \neq 0$, exact solutions are still likely to be found but further analysis is required, since we cannot use the same mapping as we have done here.

8.4.2 Mapping to the Integrable Thirring Model

As discussed in the last section, the mass gaps $m_s c_l$, ηc_l, and $|\Delta| c_l e^{\pm i\theta}$ are for inequivalent lattice depths, next-nearest-neighbor hopping, and modulation of nearest-neighbor hopping, respectively. Taking $m_s = \eta = 0$ and restricting to the $x-$direction, the NLDE for finite-energy stationary solutions can be written compactly as

$$(\mu \mathbb{1} - \mathbb{D})\, \Psi = 0\,, \tag{8.48}$$

where $\mathbb{1}$ is the 4×4 unit matrix and $\mathbb{D}$ is defined as

$$\mathbb{D} \equiv \begin{pmatrix} U|\psi_{A+}|^2 & -i\hbar c_l \frac{d}{dx} & |\Delta| e^{i\theta} & 0 \\ -i\hbar c_l \frac{d}{dx} & U|\psi_{B+}|^2 & 0 & |\Delta| e^{i\theta} \\ |\Delta| e^{-i\theta} & 0 & U|\psi_{B-}|^2 & i\hbar c_l \frac{d}{dx} \\ 0 & |\Delta| e^{-i\theta} & i\hbar c_l \frac{d}{dx} & U|\psi_{A-}|^2 \end{pmatrix}, \tag{8.49}$$

8.4.3 Derivation of the Mapping

Equation (8.49) has a symmetry which allows for a consistent solution of the form

$$\psi_{A+} = \psi_{B+} \equiv \psi\,, \quad \psi_{A-} = \psi_{B-} \equiv \psi^*\,. \tag{8.50}$$

Substituting this ansatz into Eq. (8.49) transforms the lower two equations into the conjugates of the upper two. The four-spinor wavefunction in Eq. (8.48) becomes $\Psi = (\psi, \psi, \psi^*, \psi^*)^T$, and $\mathbb{D}$ becomes

$$\mathbb{D} = \begin{pmatrix} U|\psi|^2 & -i\,\hbar c_l \frac{d}{dx} & |\Delta| e^{i\theta} & 0 \\ -i\,\hbar c_l \frac{d}{dx} & U|\psi|^2 & 0 & |\Delta| e^{i\theta} \\ |\Delta| e^{-i\theta} & 0 & U|\psi|^2 & i\,\hbar c_l \frac{d}{dx} \\ 0 & |\Delta| e^{-i\theta} & i\,\hbar c_l \frac{d}{dx} & U|\psi|^2 \end{pmatrix}. \tag{8.51}$$

By inspection we see that Eq. (8.51) is equivalent to the single equation

$$\mu\psi = -i\,\hbar c_l \frac{d}{dx}\psi + |\Delta| c_l e^{i\theta}\psi^* + U|\psi|^2\psi\,. \tag{8.52}$$

Next, we show that the real and imaginary parts of Eq. (8.52) satisfy the classical field equations for the massive Thirring model [126]. Splitting $\psi(x)$ into real and imaginary parts: $\psi(x) = u(x) + iv(x)$, and taking the modulation angle $\theta = \pi$, Eq. (8.52) becomes

$$\mu(u+iv) = -i\hbar c_l \frac{d}{dx}(u+iv) + |\Delta| c_l (u-iv) + U(u^2+v^2)(u+iv). \tag{8.53}$$

Finally, equating real and imaginary parts on both sides yields equations for u and v:

$$\mu u = \hbar c_l \frac{d}{dx} v - |\Delta| c_l u + U(u^2+v^2)u \tag{8.54}$$

$$\mu v = -\hbar c_l \frac{d}{dx} u + |\Delta| c_l v + U(u^2+v^2)v\,. \tag{8.55}$$

If we consider negative energy solutions of the NLDE so that $\mu = -|\mu|$, and also take $v \to -v$, we obtain

$$\hbar c_l \frac{du}{dx} + (|\Delta| c_l + |\mu|)v + U(u^2+v^2)v = 0 \tag{8.56}$$

$$\hbar c_l \frac{dv}{dx} + (|\Delta| c_l - |\mu|)u - U(u^2-v^2)u = 0\,. \tag{8.57}$$

With the definitions: $m \equiv |\Delta|/\hbar$, $E \equiv |\mu|/\hbar c_l$, $g^2 \equiv U/\hbar c_l$, we obtain

$$\frac{du}{dx} + (m+E)v + g^2(u^2+v^2)v = 0 \tag{8.58}$$

$$\frac{dv}{dx} + (m-E)u - g^2(u^2+v^2)u = 0\,. \tag{8.59}$$

This is the *massive Thirring model* for interacting fermions with vector-vector interaction. We note that Eqs. (8.58)-(8.59) form an integrable system: see for example [126] for early work; [96] for connection to nonlinear optics; and [103] for a generalization to arbitrary powers of the interaction. Note that the *massless* Thirring model is obtained by setting the gap parameter $|\Delta|$ to zero.

8.4.4 NLDE Gap Solitons from the Thirring Mapping

Equations (8.58)-(8.59) can be derived by minimizing the action for fermions with vector-vector interaction written in the usual compact form found in the literature

$$L = \bar{\Psi}(i\gamma^{\mu}\partial_{\mu} - m)\Psi + \frac{g^2}{2}\left(\bar{\Psi}\gamma_{\mu}\Psi\right)^2 , \tag{8.60}$$

where, here one must recall that in 1D the γ_{μ} matrices are the usual Pauli matrices and we have omitted factors of the speed of light c to be consistent with the literature. It is important to emphasize that the interaction term here is a Lorentz invariant quantity in contrast to its NLDE counterpart. Soliton solutions can be found using the parameterization

$$\tilde{\psi}(x) \equiv \begin{pmatrix} u(x) \\ v(x) \end{pmatrix} = R(x) \begin{pmatrix} \cos\phi(x) \\ \sin\phi(x) \end{pmatrix} . \tag{8.61}$$

A first integral of Eqs. (8.58)-(8.59) can be obtained using conservation of the energy-momentum tensor [103], to arrive at

$$\phi(x) = \tan^{-1}(\alpha \tanh \beta x) , \tag{8.62}$$

where

$$\alpha = \sqrt{\frac{m-E}{m+E}} , \qquad \beta = \sqrt{m^2 - E^2} , \tag{8.63}$$

and

$$R(x) = \frac{\sqrt{2}\,\beta \operatorname{sech}\beta x}{g\sqrt{(m+E)(1+\alpha^2 \tanh^2 \beta x)}} . \tag{8.64}$$

It is significant that these solutions are stable for $0 < E < m$, i.e., when the energy is inside the gap, consequently such solutions are usually referred to as *gap solitons.*

Having obtained our solution, we now map it back to the NLDE four-spinor components to arrive at

$$\psi_{A+}(x) = \frac{\sqrt{2\hbar c_l\,\alpha\beta/U}\,\operatorname{sech}\beta x}{(1+\alpha^2\tanh^2\beta x)}\,(1-i\,\alpha\tanh\beta x)\,, \tag{8.65}$$

$$\psi_{B+}(x) = \frac{\sqrt{2\hbar c_l\,\alpha\beta/U}\,\operatorname{sech}\beta x}{(1+\alpha^2\tanh^2\beta x)}\,(1-i\,\alpha\tanh\beta x)\,, \tag{8.66}$$

$$\psi_{B-}(x) = \frac{\sqrt{2\hbar c_l\,\alpha\beta/U}\,\operatorname{sech}\beta x}{(1+\alpha^2\tanh^2\beta x)}\,(1+i\,\alpha\tanh\beta x)\,, \tag{8.67}$$

$$\psi_{A-}(x) = \frac{\sqrt{2\hbar c_l\,\alpha\beta/U}\,\operatorname{sech}\beta x}{(1+\alpha^2\tanh^2\beta x)}\,(1+i\,\alpha\tanh\beta x)\,, \tag{8.68}$$

with the parameters mapped to the NLDE parameters by

$$\alpha = \sqrt{\frac{|\Delta|-|\mu|}{|\Delta|+|\mu|}}\,, \qquad \beta = \sqrt{\Delta^2-\mu^2}\,. \tag{8.69}$$

The real and imaginary parts of these solutions are plotted in Figure 8.6 for several values of the parameters α, β, and U.

8.4.5 Implications of the Mapping: Integrability of a Relativistic Subspace of Solutions

The massive Thirring model is completely integrable. In light of the mapping we have presented this seems to suggest that the 1D NLDE may be integrable as well. It is useful to recall though that our mapping pertains to a restricted subspace of the NLDE defined by the constraint

$$\psi_{A+} = \psi_{B+} \equiv \psi\,, \text{ and } \quad \psi_{A-} = \psi_{B-} \equiv \psi^*\,. \tag{8.70}$$

As a result, we have proven only that a subspace (closed under the NLDE operator) of the total solution space of the NLDE is integrable. Note that, not counting symmetries and normalization, the requirement of Eq. (8.70) constrains the solution space from 8 degrees of freedom down to 2. A conclusive test for integrability would

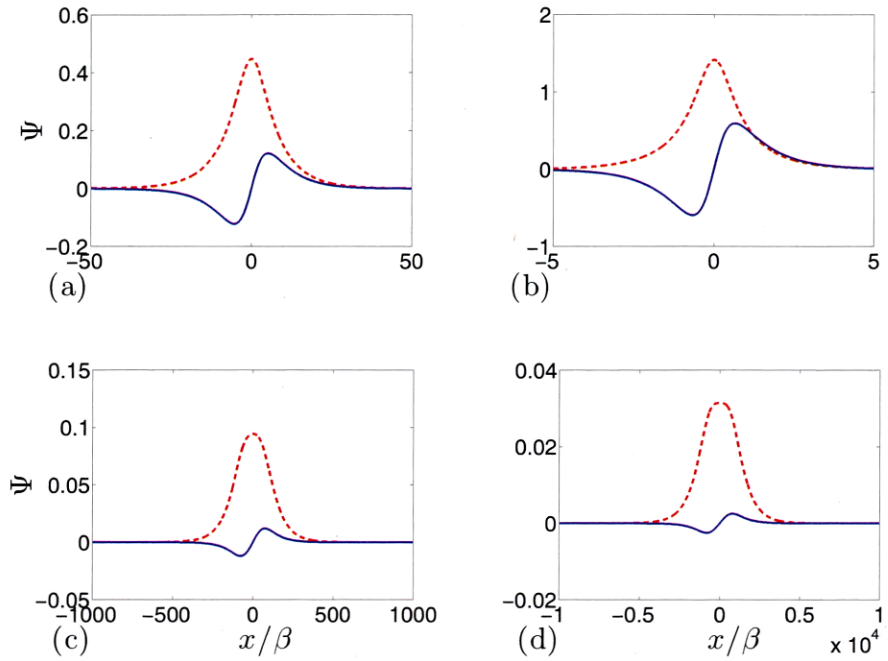

Figure 8.6: (color online) *Real and imaginary parts of Thirring solutions.* (a) $|\Delta| = 1$, $|\mu| = 0.99$. (b) $|\Delta| = 1$, $|\mu| = 0$. (c) $|\Delta| = 0.1$, $|\mu| = 0.099$. (d) $|\Delta| = 0.01$, $|\mu| = 0.0099$

require constructing an explicit Lax pair equivalent form of the NLDE, a possible future project.

Another key point to our mapping is that although the nonlinearity in the NLDE is not a Lorentz invariant [52], the interaction term in the Thirring model is an invariant vector-vector form. This implies that the NLDE solution space contains a Lorentz invariant subspace, namely the one involved in the Thirring mapping. Specifically, in terms if the spinor solutions, the mapping is

$$\begin{aligned}
\begin{pmatrix} u \\ v \end{pmatrix} &= \frac{1}{2}\begin{pmatrix} \psi + \psi^* \\ -i(\psi - \psi^*) \end{pmatrix} \\
&= \frac{1}{2}\psi\begin{pmatrix} 1 \\ -i \end{pmatrix} + \frac{1}{2}\psi^*\begin{pmatrix} 1 \\ i \end{pmatrix} \\
&= \frac{1}{2}\int_{-\infty}^{+\infty} dk \left[\tilde{\psi}(k)\, e^{-ikx}\begin{pmatrix} 1 \\ -i \end{pmatrix} + \tilde{\psi}^*(k)\, e^{ikx}\begin{pmatrix} 1 \\ i \end{pmatrix}\right],
\end{aligned} \tag{8.71}$$

where the last step expresses the Thirring solution in terms of positive and negative energy Fourier modes. This says that the subspace of the NLDE involved in the mapping is a symmetric superposition (equal admixture) of particle an anti-particle states, a general defining feature of a relativistic theory.

8.5 Stability of Soliton Solutions

To compute soliton lifetimes we must solve the relativistic linear stability equations (RLSE) in the 1D case. The honeycomb lattice geometry combined with the particle interaction has a characteristic signature effect on the stability of our soliton solutions. In particular, for the zero gap case, the presence of negative energy states below the Dirac point means that a BEC will eventually decay by radiating into the continuum of scattering states. However, this process requires a mechanism for energy dissipation into noncondensate modes. This comes from secondary interactions with thermal atoms. Thus, as long as the system is at very low temperatures our main concern for depletion of the BEC comes from possible imaginary eigenvalues in the linear spectrum.

To determine stability of a particular soliton solution, we insert the spatial function for the soliton into the RLSE as a background for the quasi-particle coherence functions. This gives a set of first-order coupled ODE's in one spatial variable to be solved consistently for the quasi-particle energies E_k and amplitudes $\mathbf{u_k}$ and $\mathbf{v_k}$, where the subscript denotes the mode with momentum $k = |\mathbf{k}|$. Since we are perturbing from a spin-1/2 BEC background, $\mathbf{u_k}$ and $\mathbf{v_k}$ have vector form describing quasi-particle and quasi-hole excitations of the A and B sublattice, respectively. We discretize the derivatives and spatial functions in the RLSE using a forward-backward average finite-difference scheme, then solve the resulting discrete matrix eigenvalue problem using the MATLAB function Eig. we find that the lowest modes are anomalous corresponding to Nambu-Goldstone modes, with negative energy and positive norm defined as $N = \sum_k (|\mathbf{u_k}|^2 - |\mathbf{v_k}|^2)$.

8.5.1 Linear Eigenvalues

We solve the RLSE for each of the zigzag and armchair bright soliton trains and find the eigenvalues for the lowest quasi-particle modes to be $E_1 = -|E_1|$: $|E_1|/U = 3.8275$. For the solitons obtained through the Thirring mapping, we find: $|E_1|/U = 3.9129, 3.9129, 3.9150, 3.9211$, corresponding to the plots in Figure 8.6(a)-(d), respectively, for the specified values of Δ and μ. Strictly speaking, in the case of the Thirring solutions inside the gap, quantum fluctuations are only important for modes with energy larger than the gap energy. Thus our results here pertain to the limiting case of a small gap parameter. We note that for the gray line soliton in Figure 8.4(c), the lowest eigenvalue is $E_1/U = 7.9349 \times 10^{-3} - 9.9993 \times 10^2\, i$. This is the only value which has a nonzero imaginary part and another calculation step is needed to determine stability, which we cover in the next section. Significantly, apart form the line soliton, all of our solitons have real eigenvalues and are thus dynamically stable solutions of the NLDE. This means that at very low temperature, we expect these solitons to remain viable over the lifetime of the BEC.

8.5.2 Computing the Line Soliton Lifetime

To determine stability of the line soliton, we must compute it's lifetime $\tau_{\rm ls}$ and compare it with the lifetime of the BEC. To find $\tau_{\rm ls}$, we calculate the time it takes for the depletion to become large relative to the total number of atoms in the system based on the imaginary part of the linear eigenvalue. First we express the total particle density operator to lowest order in the quasi-particle operator $\hat{\phi}$:

$$\begin{aligned} \hat{n} &= \hat{\psi}^\dagger \hat{\psi} \approx \sum_{i \in \{A,B\}} \left(|\psi_i|^2 + \psi_i^* \hat{\phi}_i + \psi_i \hat{\phi}_i^\dagger \right) \\ &= n_{\rm C} + \hat{n}_{\rm NC}, \end{aligned} \tag{8.72}$$

where the condensate and noncondensate contributions to the density, $n_{\rm C}$ and $\hat{n}_{\rm NC}$, are given by

$$n_{\rm C} \equiv |\psi_A|^2 + |\psi_B|^2 \tag{8.73}$$
$$\hat{n}_{\rm NC} \equiv \psi_A^* \hat{\phi}_A + \psi_A \hat{\phi}_A^\dagger + \psi_B^* \hat{\phi}_B + \psi_B \hat{\phi}_B^\dagger \, . \tag{8.74}$$

Next, we restrict to the mode with the largest imaginary term in its eigenvalue: $E_1 = (7.9349 \times 10^{-3} - 9.9993 \times 10^2 \, i) \, U$, in units of the interaction energy. The quasi-particle operators can then be approximated by

$$\hat{\phi}_{A,1}(x,t) \approx e^{-iE_1 t/\hbar} \, u_{A,1}(x) \, \hat{\alpha}_j + e^{iE_1 t/\hbar} \, v_{A,1}^*(x) \, \hat{\alpha}_j^\dagger \tag{8.75}$$
$$\hat{\phi}_{B,1}(x,t) \approx e^{-iE_1 t/\hbar} \, u_{B,1}(x) \, \hat{\beta}_j + e^{iE_1 t/\hbar} \, v_{B,-1}^*(x) \, \hat{\beta}_j^\dagger . \tag{8.76}$$

We fix the total number of particles N of the system and take all N particles to be in the condensate at $t = 0$. We can then compute the depletion out of the line soliton state as a function of time

$$N_{\rm NC}(t) = \bar{n} \int dx \, \left[\langle n_\alpha || \hat{n}_{\rm NC} || 0 \rangle + | \langle n_\beta || \hat{n}_{\rm NC} || 0 \rangle | \right] , \tag{8.77}$$

where $|0\rangle$ and $|n_{\alpha(\beta)}\rangle$ are the initial and final A(B) sublattice quasi-particle number states, respectively. Note that we have included a factor of the average particle density of the BEC, $\bar{n}$. Retaining only the terms which grow exponentially in time, we define the lifetime $\tau_{\rm ls}$ by computing the time it takes for the depletion number to grow to roughly the number of atoms initially in the condensate. Thus, we set Eq. (8.77) equal to $\int dx \, \bar{n}$ with time t set equal to the lifetime $\tau_{\rm ls}$, which gives

$$\tau_{\rm ls} = \frac{\hbar}{{\rm Im}(E_{-1})} \times I, \tag{8.78}$$

where I contains the spatial part of the contraction in Eq. (8.77), i.e., the overlap of the soliton background with the quasi-particle functions, which encodes the spatial dependence of particle being ejected from the condensate. We find the lifetime of the line soliton to be: $\tau_{\rm ls} = 3.76 \times 10^{-6}$s, much longer than typical BEC lifetimes on the

order of nanoseconds.

8.6 Soliton Spectra in a Harmonic Trap

In real experiments, solitons reside in a BEC within a harmonic magnetic trap. Consequently, in the case of extended dark or gray solitons the trap boundary affects the soliton in a nontrivial way. This occurs in the form of spatial quantization which will have a significant effect at large healing length (comparable to the trap size) or equivalently for weak particle interactions. Most of our solutions are bright solitons occurring in series, and the boundary only affects peaks very near the trap edge. But the spacing between bright peaks can be adjusted to place a node in the soliton series in the region where the harmonic potential becomes appreciable. Thus, interesting boundary effects become noticeable only when the soliton asymptotically approaches a non-zero constant value at large distances, i.e., a dark or gray soliton. In this section we study the behavior of our line soliton solution in the presence of a harmonic trap by computing the chemical potential spectra for the ground state and several excited states. A very interesting feature arises when we attempt to confine relativistic solitons which is the phenomenon of Klein-tunneling: the non-decaying transmission of particle through a large potential barrier. This is the BEC analog of the familiar effect predicted for relativistic electrons.

8.6.1 Quantized Excitations

For the case of a highly oblate harmonic confining potential which defines a 2D system, the oscillator frequencies satisfy $\omega_z \gg \omega \equiv \omega_x, \omega_y$. If in addition to this condition we also take $\omega_y \ll \omega_x$, with the soliton in the x-direction, we may treat only the effects of spatial quantization along the soliton direction. We then take the trapping potential to be: $V(x) = (1/2)M\omega^2 x^2$. We proceed numerically by incorporating this potential into the NLDE and then transforming to dimensionless equations by defining

$$\chi \equiv \hbar\omega\, x/(\hbar c_l)\,, \quad \eta_{A(B)} \equiv \sqrt{U/\hbar\omega}\, f_{A(B)}\,, \tag{8.79}$$

thereby obtaining the dimensionless form of the NLDE

$$\begin{aligned} -\tilde{\mu}\,\eta_A(\chi) &= \partial_\chi \eta_B(\chi) - |\eta_A(\chi)|^2 \eta_A(\chi) - \mathcal{Q}\,\chi^2\,\eta_A(\chi)\,, & (8.80)\\ -\tilde{\mu}\,\eta_B(\chi) &= -\partial_\chi \eta_A(\chi) - |\eta_B(\chi)|^2 \eta_B(\chi) - \mathcal{Q}\,\chi^2\,\eta_B(\chi)\,, & (8.81) \end{aligned}$$

where the two rescaled parameters in the NLDE are

$$\mathcal{Q} \equiv \frac{Mc_l^2}{2\,\hbar\omega}\,, \qquad \tilde{\mu} \equiv \frac{\mu}{\hbar\omega}\,. \tag{8.82}$$

We have plotted the ground state and first two excited states in Figure 8.7 along with their respective densities for the unconfined case where $Q = 0$. To obtain these results we used a numerical shooting method as discussed previously using the following data: for the ground state, $a_0 = 0.9949684287783$, $\tilde{\mu} = 1$; $a_0 = 0.99496892372588591202$, $\tilde{\mu} = 1.00000103$, for the first excited state; and, $a_0 = 0.993$, $\tilde{\mu} = 1.001$, for the second excited state.

8.6.2 Eigenvalue Spectra and Macroscopic Klein-Tunneling

By solving Eqs. (8.80)-(8.81) with a finite oscillator length, i.e., a non-zero value for $\mathcal{Q}$, we can obtain the spatially quantized ground state and excited states for the line soliton. For $\mathcal{Q} = 0.001$, we find the free parameter a_0 for the ground state at $a_0 = 0.94640402384$ and for the first and second excited states at $a_0 = 0.89882708125$ and $a_0 = 0.8523151$, respectively. These are plotted in Figure 8.8 along with the corresponding densities. The dark spots near the origin in the density plots correspond to the density dips in the plots in Figure 8.7. The number of dips identifies the ground state, and first and second excited state.

Note that the tail ends of these solutions oscillate. This is not a relic of the numerics involved, but is an inherent feature of the Dirac equation itself. To demonstrate

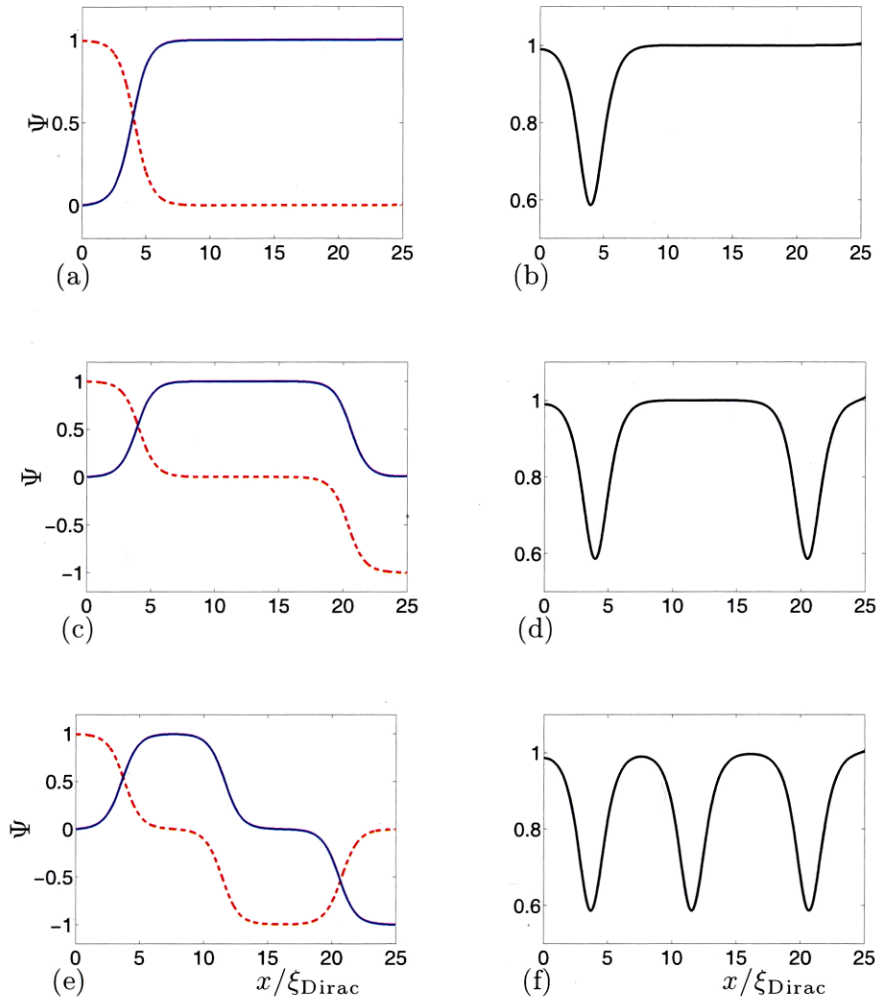

Figure 8.7: (color online) *Numerical shooting results for the line soliton.* Sublattice amplitudes and density. (a,b) Ground state. (c,d) First excited state. (e,f) Second excited state.

the source of this effect, we rewrite Eqs. (8.80)-(8.81) for clarity so that

$$\eta_B' = \left(\mathcal{Q}\,\chi^2 - \tilde{\mu} + |\eta_A|^2\right)\eta_A\,, \tag{8.83}$$

$$\eta_A' = -\left(\mathcal{Q}\,\chi^2 - \tilde{\mu} + |\eta_B|^2\right)\eta_B\,. \tag{8.84}$$

We can see that near the origin, the trap potential is weak and the chemical potential term dominates so that we have $\eta_B' < 0$ and $\eta_A' > 0$. However, as we move away from the origin and into the strong potential region the term quadratic in χ grows, even-

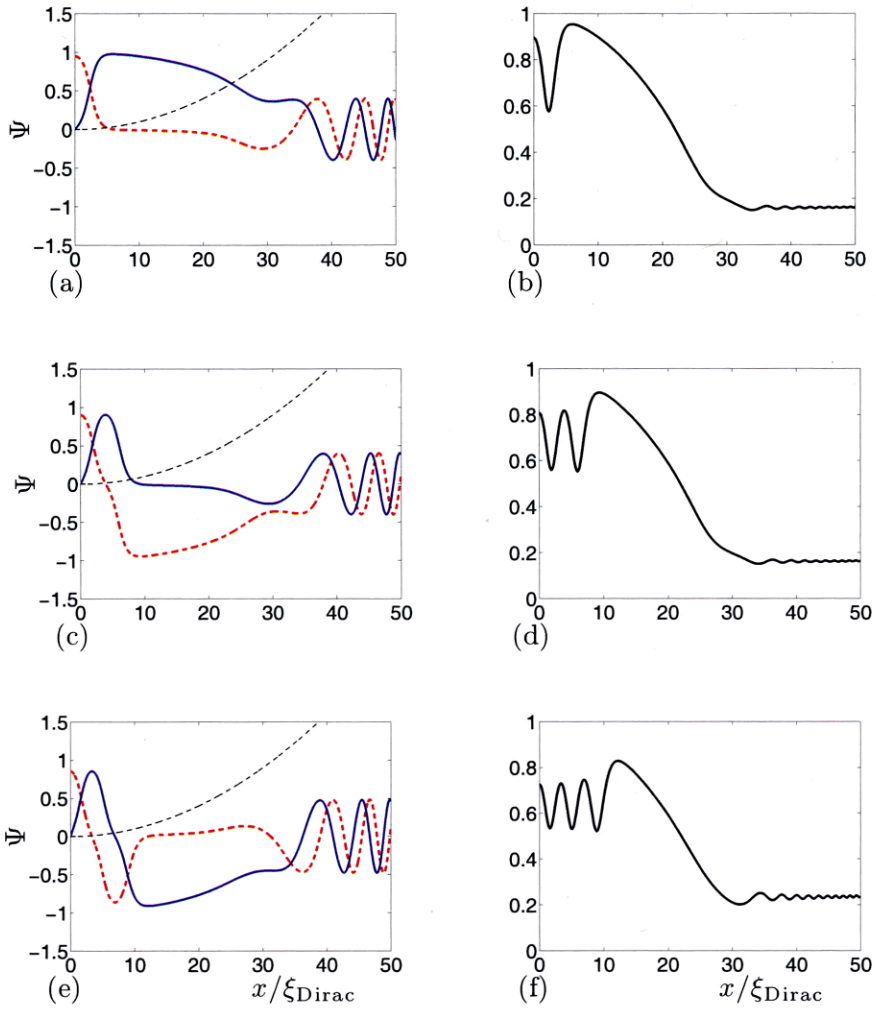

Figure 8.8: (color online) *Numerical shooting results for the line soliton in a harmonic trap.* Sublattice amplitudes and density. (a,b) Ground state. (c,d) First excited state. (e,f) Second excited state. The black dashed plot is the harmonic trapping potential.

tually overwhelming the other terms where η_A and η_B solve the asymptotic equations

$$\eta_B' = \mathcal{Q}\chi^2\eta_A \tag{8.85}$$
$$\eta_A' = -\mathcal{Q}\chi^2\eta_B\,, \tag{8.86}$$

whose solutions are

$$\eta_B(\chi) = \frac{1}{3}\sin\left[(\mathcal{Q}\chi^2)\chi\right] \tag{8.87}$$

$$\eta_A(\chi) = \frac{1}{3}\cos\left[(\mathcal{Q}\chi^2)\chi\right]. \tag{8.88}$$

These oscillate with a spatially increasing frequency $k \equiv \mathcal{Q}\chi^2$, so it is clear that the tail oscillations are coming from the unbounded potential barrier. Of course for an ordinary Schrödinger particle described by a single wavefunction $\psi(x)$, this effect does not arise since the analogous case for a particle in a 1D harmonic potential gives

$$-\frac{\hbar^2}{2M}\psi'' = \left(E - \mathcal{Q}x^2\right)\psi, \tag{8.89}$$

where deep inside the strong potential region the quadratic term is much larger than the characteristic energy E, and ψ obeys the equation

$$\psi'' \approx \frac{2M\mathcal{Q}}{\hbar^2}x^2\psi\,, \tag{8.90}$$

for which we obtain either exponential growth or decay and omit the non-physical growing solution. This choice is clearly not an option in Eqs. (8.85)-(8.86). What we have uncovered is an example of macroscopic Klein-tunneling. This effect is predicted for ordinary relativistic electrons inside a large potential barrier, but in our case it pertains to a BEC, and so it is a macroscopic phenomenon occurring at very low energies. Physically, the barrier potential forces a positive energy particle into negative energy states so that the total wavefunction does not decay to zero but acquires a component within the continuum of negative energy scattering states below the Dirac point. We can interpret this in our problem by recalling the positive and negative energy scattering states for massless Dirac quasi-particles in the honeycomb lattice. The eigenstates in the non-interacting massles case traveling in the positive x-direction solve the two-spinor equation

$$E\,\Psi(x) = ic_l\,\sigma_x \hat{p}_x \Psi \tag{8.91}$$

where σ_x is the usual first Pauli matrix. The two independent solutions are the Weyl spinors

$$\Psi_+(x,p_x) = e^{-ip_x x/\hbar}\begin{pmatrix} 1 \\ 1 \end{pmatrix}, \tag{8.92}$$

$$\Psi_-(x,p_x) = e^{-ip_x x/\hbar}\begin{pmatrix} 1 \\ -1 \end{pmatrix}, \tag{8.93}$$

where it is straightforward to show that $E\,\Psi_\pm = \pm c_l p_x \Psi_\pm$, where $\Psi_\pm$ are the positive and negative energy states (above and below the Dirac point) and differ by the relative phase between the A and B sublattice amplitudes (upper and lower spinor components). From these we can construct a superposition of positive and negative energy quasi-particles traveling to the right and to the left, respectively, by forming

$$\Psi(x,\pm p_x) \equiv \frac{1}{2}\left[\Psi(x,+p_x) + \Psi(x,-p_x)\right] \tag{8.94}$$

$$= \begin{pmatrix} \cos p_x x/\hbar \\ \sin p_x x/\hbar \end{pmatrix}. \tag{8.95}$$

From this expression we see that Eqs. (8.87)-(8.88) describe a mixing into positive and negative energy states, the hallmark feature of Klein-tunneling [251]. For the practical purpose of confining the BEC, it seems possible to modify the trapping potential by breaking it up into a series of smaller step functions to soften the trap edge. Figure 8.9 shows the ground state when the harmonic trap potential is replaced by the function

$$V(\chi) = \frac{1}{2}\left\{1 + \tanh\left[0.1(\chi - 20)\right]\right\}, \tag{8.96}$$

for which we see a dramatic decrease in the tail oscillations.

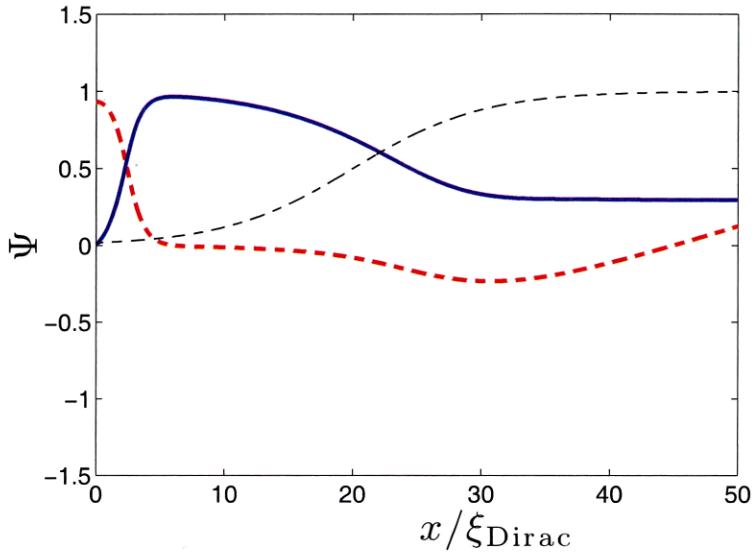

Figure 8.9: (color online) *Ground state of the line soliton in a trap with soft boundary.* The step form for the trap potential has a dramatic effect on the amplitude and frequency of the tail oscillations. The black dashed plot is the potential of Eq. (8.96).

To obtain the functional relation between the chemical potential μ and the interaction U for a particular excitation inside the harmonic trap, we first derive an expression for the normalization of the wavefunction for the new rescaled NLDE in Eqs. (8.80)-(8.81). This is found to be

$$\int d\chi(|\eta_A(\chi)|^2 + |\eta_B(\chi)|^2) = \mathcal{N}\,, \tag{8.97}$$

where the right hand side is given by

$$\mathcal{N} = \frac{\sqrt{3}\,\hbar\omega\, N\, U}{3\, t_h^2}\,, \tag{8.98}$$

where N is the number of atoms in the system. To compute the chemical potential spectra, we fix $\mathcal{Q}$ (which is the same as fixing ω and thus the oscillator length) and vary $\tilde{\mu}$, calculating the norm $\mathcal{N}$ for each value of $\tilde{\mu}$. This gives the paired values $(\mathcal{N}, \tilde{\mu})$.

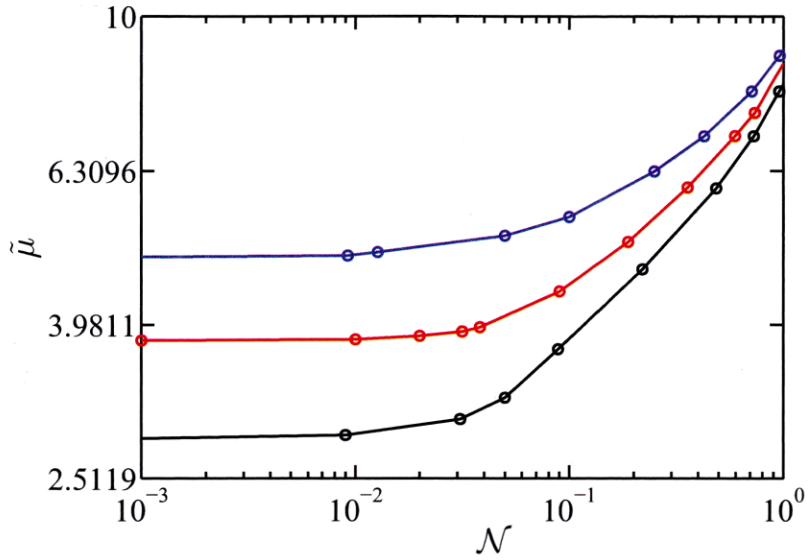

Figure 8.10: (color online) *Discrete spectra of the line soliton in a harmonic trap.* Ground state (black). First excited state (red). Second excited state (blue). The vertical axis is labeled by the renormalized chemical potential $\tilde{\mu}$, and the normalization $\mathcal{N}$ is along the horizontal axis. Both quantities are dimensionless.

These values for the line soliton ground state, and first and second excited states are graphed in Figure 8.10. The plots show two regimes: weakly interacting at small $\mathcal{N}$ versus strongly interacting for large $\mathcal{N}$. Note that $\mathcal{N}$ depends on both the total number of atoms and the interaction U, as one would expect. For small $\mathcal{N}$ ($\sim 10^{-3}$), the solutions correspond to the single-particle bound states of a massless Dirac spinor trapped inside a harmonic potential. Here the quantization can be seen by noting that the three states shown in the figure intersect the vertical axis at $\tilde{\mu} = 2.83,\ 3.80,\ 4.88$, or in terms of the oscillator frequency ω: $\mu = 2.83\,\hbar\omega,\ 3.80\,\hbar\omega,\ 4.88\,\hbar\omega$, for the ground state and first two excited states, respectively, which displays approximate integer multiples n of the energy $\hbar\omega$: $\mu \approx (2.8 + n)\hbar\omega$. For large $\mathcal{N}$ (~ 1), solutions are bound gray solitons with spectra characterized by a power law: $\tilde{\mu} \propto \mathcal{N}^{\alpha}$.

8.7 Conclusion

In this article we have presented an exact closed form bright soliton train in addition to a gray line soliton obtained through a numerical shooting method. We find a similarity between the analytical bright solitons and those obtained by using a soliton series expansion technique. Each term in the soliton expansion resembles the envelope function of the soliton train and suggests the possibility of additional exact solution. Also, we find that each term in the expansion is an exactly integrable quantity uniquely associated with a conserved charge, which seems to suggest possible integrability of the NLDE. A likely fruitful research direction would be a rigorous test for integrability using a standard analytical method. Solution of the NLDE by inverse scattering would also lead to a much deeper understanding of its solution space.

By introducing a mass gap into our system we have uncovered a mapping between the NLDE and the massive Thirring model. The significance of the mapping is twofold: it allows for a direct incorporation of Thirring solitons into the larger space of NLDE solutions, while also revealing a completely integrable Poincaré invariant subspace of the NLDE. From the standpoint of stability, gap solitons are robust objects due to their isolation from single particle scattering states. In the case of embedded solitons, we find that all of our bright solitons are stable based on analysis using the relativistic linear stability equations. However, the line soliton is found to be dynamically unstable due to the presence of a complex eigenvalue in its linear spectrum, with a lifetime of $3.76\,\mu$s

We have computed the discrete spectra for several bound states of the line soliton and found two asymptotic regions. One at small interaction where the chemical potential for excited states differ by a constant multiple of the oscillator energy, $\mu \approx (2.8+n)\hbar\omega$, and the other limit for large interaction where the chemical potential obeys a power law: $\mu \propto U^{\alpha}$. We have shown that confinement in a harmonic trap leads to a macroscopic realization of Klein-tunneling and suggests future investigations

extending the full physics of the Klein paradox to the BEC.

Acknowledgments

This material is based in part upon work supported by the National Science Foundation under grant number PHY-1067973. L.D.C. thanks the Alexander von Humboldt foundation and the Heidelberg Center for Quantum Dynamics for additional support.

8.8 Appendix A: Continuous Spectrum of the NLDE

8.8.1 Four-Spinor Spectrum

Here we present some important details regarding the continuous spectrum of the nonlinear Dirac operator in the presence of mass gap. The information we present here provides a context for the solitons described in the main body of this article. We first consider a BEC that is a macroscopic superposition of excitations at two opposite Dirac points. In this case, a variety of superpositions of the four-spinor components are possible. The full NLDE in the chiral representation splits into equations for each Dirac point:

$$i\hbar\,\partial_t\Phi = \hbar c_l\,\vec{\sigma}\cdot\vec{p}\,\Phi + (m_s-\eta)c_l\,\Phi - U\sum_{M_i^{(u)}}(M_i^{(u)}\Phi)(\Phi^\dagger M_i^{(u)})\,\Phi \tag{8.99}$$

$$i\hbar\,\partial_t\chi = -\hbar c_l\,\vec{\sigma}\cdot\vec{p}\,\chi - (m_s-\eta)c_l\,\chi - U\sum_{M_i^{(l)}}(M_i^{(l)}\chi)(\chi^\dagger M_i^{(l)})\,\chi\,, \tag{8.100}$$

with the two-spinors defined in terms of excitations of the A and B sublattices at two opposite Dirac points ($\pm$),

$$\Phi = \begin{pmatrix}\psi_{A+}\\ \psi_{B+}\end{pmatrix}\,,\quad \chi = \begin{pmatrix}\psi_{B-}\\ \psi_{A-}\end{pmatrix}\,, \tag{8.101}$$

and $M_i^{(u)}$ and $M_i^{(l)}$ are the upper and lower submatrices along the diagonals of the M_i. For our problem the eigenvalue ω is identified with the chemical potential $\mu = \hbar\omega$.

We can find the continuous spectrum of the NLDE operator by substituting in plane wave stationary states for the various component wavefunctions and then solving the associated characteristic equation. In this way we obtain

$$\mu(k)_{\pm} = U \pm c_l \sqrt{\hbar^2 k^2 + (m_s - \eta)^2}\,. \tag{8.102}$$

The corresponding Fourier states labeled by the helicity h and energy eigenvalue are

$$\Psi^{(+)}_{h_+} = e^{i\,(\hbar k x - \omega_+ t)} \begin{pmatrix} 1 \\ A \\ 0 \\ 0 \end{pmatrix}, \quad \Psi^{(+)}_{h_-} = e^{i\,(\hbar k x - \omega_+ t)} \begin{pmatrix} 0 \\ 0 \\ 1 \\ -A \end{pmatrix}, \tag{8.103}$$

$$\Psi^{(-)}_{h_+} = e^{i\,(\hbar k x - \omega_- t)} \begin{pmatrix} 1 \\ -A \\ 0 \\ 0 \end{pmatrix}, \quad \Psi^{(-)}_{h_-} = e^{i\,(\hbar k x - \omega_- t)} \begin{pmatrix} 0 \\ 0 \\ 1 \\ A \end{pmatrix}, \tag{8.104}$$

where we have used the following definitions:

$$\omega_{\pm} = \mu_{\pm}/\hbar, \quad A = \frac{(c_l/\hbar)\,p}{[(\mu - U) - c_l(m_s - \eta)]}, \tag{8.105}$$

$$p^2 = (\hbar/c_l)^2[(\mu - U)^2 - c_l^2(m_s - \eta)^2]. \tag{8.106}$$

8.8.2 Resonances at $k = 0$

At the gap edge where $k = 0$, the eigenvalues reduce to

$$\mu(0)_{\pm} = U \pm (m_s - \eta)c_l. \tag{8.107}$$

The resonances at the gap edges are the given by

$$\Psi_{h_+}^{(+)} = e^{-i\omega_+ t} \begin{pmatrix} 1 \\ 1 \\ 0 \\ 0 \end{pmatrix}, \Psi_{h_-}^{(+)} = e^{-i\omega_+ t} \begin{pmatrix} 0 \\ 0 \\ 1 \\ -1 \end{pmatrix}, \tag{8.108}$$

$$\Psi_{h_+}^{(-)} = e^{-i\omega_- t} \begin{pmatrix} 1 \\ -1 \\ 0 \\ 0 \end{pmatrix}, \Psi_{h_-}^{(-)} = e^{-i\omega_- t} \begin{pmatrix} 0 \\ 0 \\ 1 \\ 1 \end{pmatrix}. \tag{8.109}$$

8.8.3 Two-Spinor Spectrum

In the Chiral representation, the NLDE decouples into pairs of equations, one for each Dirac point. As before, we solve for plane-wave stationary states with total energy $E = \mu$ with $\psi_A \sim A\exp(i\mathbf{k}\cdot\mathbf{r})$ and $\psi_B \sim B\exp(i\mathbf{k}\cdot\mathbf{r})$ are. As before, we find that the eigenvalue satisfies the equation

$$\mu(k) = U \pm c_l\sqrt{\hbar^2k^2 + (m_s - \eta)^2}\,, \tag{8.110}$$

with a gap size $2|m_s - \eta|c_l$. The shape of $\mu(k)$ is a hyperbola centered at $\mu = U$ and asymptotically approaching the straight lines $U \pm c_l\hbar k$, for $k \to \pm\infty$ or in the limit of small gap size. The continuous spectrum is defined as the union of interval $(-\infty, U - m_s c_l + \eta c_l] \cup [U + m_s c_l - \eta c_l, +\infty)$. Next, we examine two special points in the spectrum.

8.8.4 Static Solutions for Zero Chemical Potential

If we look at the two points where $E = 0$ that occur where the lower branch crosses the k-axis, we find static solutions with $k = \pm k_0 = \pm(1/\hbar c_l)\sqrt{U^2 - c_l^2(m_s - \eta)^2}$. These are time-independent solutions with plane-wave spatial dependence that form the boundary between positive and negative eigenvalue. Here, the momentum just balances the interaction U adjusted by the gap size. At a single Dirac point, there is just one state and has positive helicity

$$\Psi^{(-)}_{h_+} = \sqrt{1/2}\, e^{ik_0 x} \begin{pmatrix} 1 \\ -A \\ 0 \\ 0 \end{pmatrix}. \tag{8.111}$$

The nonzero current associated with this state is

$$\begin{aligned} J^\mu &= \bar{\Psi}^{(-)}_{h_+} \gamma^\mu \Psi^{(-)}_{h_+} \\ &= \Psi^{(-)\dagger}_{h_+} \gamma^0 \gamma^\mu \Psi^{(-)}_{h_+}. \end{aligned} \tag{8.112}$$

so that

$$J^0 = \frac{1}{2} + \frac{1}{2} = 1\,, \tag{8.113}$$

$$J^x = (c_l/\hbar) \frac{p}{U + c_l(m_s - \eta)}\,, \tag{8.114}$$

This is a static plane wave with non-zero current.

8.8.5 Resonances at $k = 0$

These are solutions at the edge of the gap, $\mu_\pm(0) = U \pm (m_s - \eta)$. There are two uniform solutions

$$\Psi^{(+)}_{h_+} = e^{-i\omega_+ t} \begin{pmatrix} 1 \\ 1 \\ 0 \\ 0 \end{pmatrix}, \quad \Psi^{(-)}_{h_+} = e^{-i\omega_- t} \begin{pmatrix} 1 \\ -1 \\ 0 \\ 0 \end{pmatrix}, \tag{8.115}$$

where $\omega_\pm = \mu_\pm(0)/\hbar$.

CHAPTER 9

EFFECTIVE QUANTUM FIELD THEORY FOR BOSONS IN THE HONEYCOMB LATTICE

L. H. Haddad and Lincoln D. Carr, Physical Review A, to be submitted, 2012.

Abstract

We develop the continuum field theory for bosons near the Dirac points of a honeycomb lattice and find that the system is described by a relativistic quantum field theory for Dirac spinors. We derive the effective field theory at the quantum critical point and find that this is described by a nonlinear Dirac action with additional higher order terms in the superfluid order parameter and its derivatives. The presence of the Dirac points result in the characteristic phase differences between the two sublattices which results in the exact spinor structure for the continuum theory.

9.1 Introduction

The theory of ultracold bosons in a honeycomb lattice, the mean fields for bosons defined relative to the Dirac point can be interpreted as quasi-particle fields propagating on a background which provides an $SU(2)$ Berry phase. Here we use the Hubbard-Stratonovich formalism to obtain the continuum field theory for bosons. As a preliminary step, we first derive the many-body Hamiltonian in the lattice by expanding the field operators in terms of Wannier states and focusing on the geometry of the lattice to arrive at a Hamiltonian for Dirac spinors.

9.2 Microscopic Derivation of the Many-body Hamiltonian for Bosons in a Honeycomb Lattice

9.2.1 First-Order Nearest-Neighbor Hopping

Consider a BEC in a honeycomb optical lattice where we work with characteristic momentum near the Dirac point. We consider the case of zero particle interactions. We do this in order to isolate the part of the Hamiltonian which describes low energy quasi-particle excitations near the Dirac point and show that we arrive at the massless Dirac Hamiltonian in (2+1)-dimensions. The second quantized Hamiltonian for the condensate in the lattice is

$$\hat{H} = \int d^2 r \hat{\psi}^\dagger H_0 \hat{\psi}, \tag{9.1}$$

$$H_0 \equiv -\frac{\hbar^2}{2m}\nabla^2 + V(\vec{r}). \tag{9.2}$$

The field operators $\hat{\psi} = \hat{\psi}(\vec{r}, t)$ obey bosonic commutation relations in the Heisenberg picture and $V(\vec{r})$ is the potential of the honeycomb lattice. The goal is to derive the effective Hamiltonian for quasi-particles interacting with the lattice background. Toward this end, we express the many-body wavefunction in terms of a Bloch expansion. In the tight-binding approximation we can decompose the fields into sums of terms specific to each lattice site

$$\hat{\psi} = \hat{\psi}_A + \hat{\psi}_B \,, \tag{9.3}$$

$$\hat{\psi}_A \equiv \sum_A e^{i\vec{k}\cdot(\vec{r}-\vec{r}_A)} u(\vec{r}-\vec{r}_A)\cdot\hat{a}\;\phi_{q,A}(\vec{r}) \,, \tag{9.4}$$

$$\hat{\psi}_B \equiv \sum_B e^{i\vec{k}\cdot(\vec{r}-\vec{r}_B)} u(\vec{r}-\vec{r}_B)\cdot\hat{b}\;\phi_{q,B}(\vec{r}) \,. \tag{9.5}$$

Inserting these into Eq. (9.1) and restricting the sum to nearest-neighbors gives

$$\begin{aligned}\hat{H} = \int d^2r \sum_{<A,B>} \Big[& \hat{a}^\dagger\, e^{-i\vec{k}\cdot\vec{\chi}_A} u(\vec{\chi}_A)\phi^*_{q,A}(\vec{r}) H_0 \hat{a}\, e^{i\vec{k}\cdot\vec{\chi}_A} u(\vec{\chi}_A)\phi_{q,A}(\vec{r}) \\ & + \hat{a}^\dagger\, e^{-i\vec{k}\cdot\vec{\chi}_A} u(\vec{\chi}_A)\phi^*_{q,A}(\vec{r}) H_0 \hat{b}\, e^{i\vec{k}\cdot\vec{\chi}_B} u(\vec{\chi}_B)\phi_{q,B}(\vec{r}) \\ & + \hat{b}^\dagger\, e^{-i\vec{k}\cdot\vec{\chi}_B} u(\vec{\chi}_B)\phi^*_{q,B}(\vec{r}) H_0 \hat{a}\, e^{i\vec{k}\cdot\vec{\chi}_A} u(\vec{\chi}_A)\phi_{q,A}(\vec{r}) \\ & + \hat{b}^\dagger\, e^{-i\vec{k}\cdot\vec{\chi}_B} u(\vec{\chi}_B)\phi^*_{q,B}(\vec{r}) H_0 \hat{b}\, e^{i\vec{k}\cdot\vec{\chi}_B} u(\vec{\chi}_B)\phi_{q,B}(\vec{r}) \Big]\end{aligned} \tag{9.6}$$

$$\vec{\chi}_A \equiv \vec{r}-\vec{r}_A \,, \quad \vec{\chi}_B \equiv \vec{r}-\vec{r}_B \,, \vec{\chi}_{AB} = \vec{r}_A - \vec{r}_B \,. \tag{9.7}$$

We are interested in the behavior of low momentum excitations relative to the Dirac point momentum at the corner of the Brillouin zone. This is equivalent to expanding the quasi-particle functions about their designated lattice sites and keeping only the lowest order terms; this works because $\phi_{q,A}$ and $\phi_{q,B}$ do not vary much over the nearest-neighbor separation distance. Thus,

$$\begin{aligned}\phi_{q,A}(\vec{r}) &\simeq \phi_{q,A}(\vec{r}_A) + \vec{\nabla}\phi_{q,A}|_{\vec{r}_A}\cdot(\vec{r}-\vec{r_A}) + \dots \,, \\ \phi_{q,B}(\vec{r}) &\simeq \phi_{q,B}(\vec{r}_B) + \vec{\nabla}\phi_{q,B}|_{\vec{r}_B}\cdot(\vec{r}-\vec{r_B}) + \dots\end{aligned} \tag{9.8}$$

Keeping only zeroth order terms and substituting back into Eq. (9.6) gives

$$\begin{aligned}\hat{H} = \int d^2r \sum_{<A,B>} \Big[& \hat{a}^\dagger\, e^{-i\vec{k}\cdot\vec{\chi}_A} u(\vec{\chi}_A)\phi^*_{q,A}(\vec{r}_A) H_0 \hat{a}\, e^{i\vec{k}\cdot\vec{\chi}_A} u(\vec{\chi}_A)\phi_{q,A}(\vec{r}_A) \\ & + \hat{a}^\dagger\, e^{-i\vec{k}\cdot\vec{\chi}_A} u(\vec{\chi}_A)\phi^*_{q,A}(\vec{r}_A) H_0 \hat{b}\, e^{i\vec{k}\cdot\vec{\chi}_B} u(\vec{\chi}_B)\phi_{q,B}(\vec{r}_B) \\ & + \hat{b}^\dagger\, e^{-i\vec{k}\cdot\vec{\chi}_B} u(\vec{\chi}_B)\phi^*_{q,B}(\vec{r}_B) H_0 \hat{a}\, e^{i\vec{k}\cdot\vec{\chi}_A} u(\vec{\chi}_A)\phi_{q,A}(\vec{r}_A) \\ & + \hat{b}^\dagger\, e^{-i\vec{k}\cdot\vec{\chi}_B} u(\vec{\chi}_B)\phi^*_{q,B}(\vec{r}_B) H_0 \hat{b}\, e^{i\vec{k}\cdot\vec{\chi}_B} u(\vec{\chi}_B)\phi_{q,B}(\vec{r}_B) \Big] \,.\end{aligned} \tag{9.9}$$

Isolating the integrals, we get

$$\begin{aligned}\hat{H} &= \sum_{<A,B>}\Big[\hat{a}^\dagger\hat{b}\;\phi^*_{q,A}(\vec{r}_A)\phi_{q,B}(\vec{r}_B)\,e^{i\vec{k}\cdot\vec{\chi}_{AB}}\int d^2re^{-i\vec{k}\cdot\vec{r}}u(\vec{\chi}_A)H_0e^{i\vec{k}\cdot\vec{r}}u(\vec{\chi}_B)\\ &+\hat{b}^\dagger\hat{a}\;\phi^*_{q,B}(\vec{r}_B)\phi_{q,A}(\vec{r}_A)\,e^{-i\vec{k}\cdot\vec{\chi}_{AB}}\int d^2re^{-i\vec{k}\cdot\vec{r}}u(\vec{\chi}_B)H_0e^{i\vec{k}\cdot\vec{r}}u(\vec{\chi}_A)\Big]\\ &+\sum_A\hat{a}^\dagger\hat{a}\;\phi^*_{q,A}(\vec{r}_A)\phi_{q,A}(\vec{r}_A)\int d^2re^{-i\vec{k}\cdot\vec{r}}u(\vec{\chi}_A)H_0e^{i\vec{k}\cdot\vec{r}}u(\vec{\chi}_A)\\ &+\sum_B\hat{b}^\dagger\hat{b}\;\phi^*_{q,B}(\vec{r}_B)\phi_{q,B}(\vec{r}_B)\int d^2re^{-i\vec{k}\cdot\vec{r}}u(\vec{\chi}_B)H_0e^{i\vec{k}\cdot\vec{r}}u(\vec{\chi}_B)\,. \qquad (9.10)\end{aligned}$$

The last two terms give an overall self energy so focus only on the first two terms. Writing the integrals as the hopping energy t_h gives

$$\hat{H}=-t_h\,a\sum_{<A,B>}\Big[\hat{a}^\dagger\hat{b}\;\phi^*_{q,A}(\vec{r}_A)\phi_{q,B}(\vec{r}_B)\,e^{i\vec{k}\cdot\vec{\chi}_{AB}}+\hat{b}^\dagger\hat{a}\;\phi^*_{q,B}(\vec{r}_B)\phi_{q,A}(\vec{r}_A)\,e^{-i\vec{k}\cdot\vec{\chi}_{AB}}\Big]\,, \qquad (9.11)$$

where a is the lattice spacing. Evaluating the exponentials at the Brillouin zone with the proper vectors χ_{AB} for nearest-neighbors and using the condensed notation: $\phi_{q,B_j}=\phi_{q,B}(\vec{r}_{B_j})$ and $\phi_{q,A_j}=\phi_{q,A}(\vec{r}_{A_j})$, we get

$$\begin{aligned}\hat{H} &= -t_h\,a\sum_{A,B}\Big[\hat{a}^\dagger\hat{b}\;\phi^*_{q,A_j}\phi_{q,B_j}+\hat{a}^\dagger\hat{b}\;\phi^*_{q,A_j}\phi_{q,B_{j-n_1}}(-1/2-i\sqrt{3}/2) \qquad (9.12)\\ &+\hat{a}^\dagger\hat{b}\;\phi^*_{q,A_j}\phi_{q,B_{j-n_2}}(-1/2+i\sqrt{3}/2)+\hat{b}^\dagger\hat{a}\;\phi^*_{q,B_j}\phi_{q,A_j}\\ &+\hat{b}^\dagger\hat{a}\;\phi^*_{q,B_j}\phi_{q,A_{j+n_1}}(-1/2+i\sqrt{3}/2)+\hat{b}^\dagger\hat{a}\;\phi^*_{q,B_j}\phi_{q,A_{j+n_1}}(-1/2+i\sqrt{3}/2)\Big]\,.\end{aligned}$$

Adding and subtracting some terms, regrouping, and inserting the differences Δn_1 and Δn_2 in order to ensure that the fields have the proper spatial dimensionality. Here n_1 and n_2 are coordinates in the direction of the lattice vectors. In terms of x and y coordinates they are $n_1=(\sqrt{3}/2)x-(1/2)y$, $n_2=(\sqrt{3}/2)x+(1/2)y$. We then get

$$\begin{aligned}
\hat{H} &= -t_h\, a \sum_{A,B} \Bigg[\hat{a}^\dagger \hat{b}\; \phi^*_{q,A_j} \frac{(\phi_{q,B_j} - \phi_{q,B_{j-n_1}})}{\Delta n_1} \, (1/2 + i\sqrt{3}/2)\; \Delta n_1 \Delta n_2 \\
&\quad + \hat{a}^\dagger \hat{b}\; \phi^*_{q,A_j} \frac{(\phi_{q,B_j} - \phi_{q,B_{j-n_2}})}{\Delta n_2} \, (1/2 - i\sqrt{3}/2)\; \Delta n_1 \Delta n_2 \\
&\quad + \hat{b}^\dagger \hat{a}\; \phi^*_{q,B_j} \frac{(\phi_{q,A_{j+n_1}} - \phi_{q,A_j})}{\Delta n_1} \, (-1/2 + i\sqrt{3}/2)\; \Delta n_1 \Delta n_2 \\
&\quad + \hat{b}^\dagger \hat{a}\; \phi^*_{q,B_j} \frac{(\phi_{q,A_{j+n_2}} - \phi_{q,A_j})}{\Delta n_2} \, (-1/2 - i\sqrt{3}/2)\; \Delta n_1 \Delta n_2 \Bigg] . \qquad (9.13)
\end{aligned}$$

In the long wavelength limit, or equivalently taking Δn_1 and Δn_2 to zero, the sum becomes an integral

$$\begin{aligned}
\hat{H} &= -t_h\, a \lim_{\Delta n_1, \Delta n_2 \to 0} \sum_{A,B} \Bigg[\hat{a}^\dagger \hat{b}\; \phi^*_{q,A_j} \frac{\Delta \phi_{q,B_j}}{\Delta n_1} (1/2 + i\sqrt{3}/2) \Delta n_1 \Delta n_2 \\
&\quad + \hat{a}^\dagger \hat{b}\, \phi^*_{q,A_j} \frac{\Delta \phi_{q,B_j}}{\Delta n_2} \, (1/2 - i\sqrt{3}/2)\, \Delta n_1 \Delta n_2 \\
&\quad + \hat{b}^\dagger \hat{a}\; \phi^*_{q,B_j} \frac{\Delta \phi_{q,A_j}}{\Delta n_1} \, (-1/2 + i\sqrt{3}/2)\, \Delta n_1 \Delta n_2 \\
&\quad + \hat{b}^\dagger \hat{a}\, \phi^*_{q,B_j} \frac{\Delta \phi_{q,A_j}}{\Delta n_2} \, (-1/2 - i\sqrt{3}/2)\, \Delta n_1 \Delta n_2 \Bigg] \\
&= -t_h \int\int dn_1 dn_2 \Big[\hat{a}^\dagger \hat{b}\; \phi^*_{q,A}\, \partial_{n_1} \phi_{q,B}\, (1/2 + i\sqrt{3}/2) + \hat{a}^\dagger \hat{b}\; \phi^*_{q,A}\, \partial_{n_2} \phi_{q,B}\, (1/2 - i\sqrt{3}/2) \\
&\quad + \hat{b}^\dagger \hat{a}\; \phi^*_{q,B}\, \partial_{n_1} \phi_{q,A}\, (-1/2 + i\sqrt{3}/2) + \hat{b}^\dagger \hat{a}\; \phi^*_{q,B}\, \partial_{n_2} \phi_{q,A}\, (-1/2 - i\sqrt{3}/2) . \Big] \qquad (9.14)
\end{aligned}$$

Transforming to orthogonal x and y coordinates using

$$\begin{aligned}
n_1 &= (1/\sqrt{3})\, x - y\,, \; n_2 = (1/\sqrt{3})\, x + y \\
&\Rightarrow \quad y = (1/2)(n_2 - n_1)\,, \; x = (\sqrt{3}/2)(n_1 + n_2), \qquad (9.15)
\end{aligned}$$

we get

$$\begin{aligned}
\partial_{n_1} &= (\partial_{n_1} x)\partial_x + (\partial_{n_1} y)\partial_y = (\sqrt{3}/2)\partial_x - (1/2)\partial_y\,, \\
\partial_{n_2} &= (\partial_{n_2} x)\partial_x + (\partial_{n_2} y)\partial_y = (\sqrt{3}/2)\partial_x + (1/2)\partial_y\,. \qquad (9.16)
\end{aligned}$$

Putting these together gives

$$\begin{aligned}\hat{H} &= -t_h\, a \int\int dx\, dy \left\{ \hat{a}^\dagger \hat{b}\, \phi^*_{q,A} \left[(\sqrt{3}/2)\partial_x - (1/2)\partial_y \right] \phi_{q,B}\ (1/2 + i\sqrt{3}/2) \right. \\ &\quad -t_h\, a \int\int dx\, dy \left\{ \hat{a}^\dagger \hat{b}\, \phi^*_{q,A} \left[(\sqrt{3}/2)\partial_x - (1/2)\partial_y \right] \phi_{q,B}\ (1/2 + i\sqrt{3}/2) \right. \\ &\quad \left. \left. + \hat{b}^\dagger \hat{a}\, \phi^*_{q,B} \left[(\sqrt{3}/2)\partial_x + (1/2)\partial_y \right] \phi_{q,A}\, (-1/2 - i\sqrt{3}/2) \right\} . \end{aligned} \tag{9.17}$$

Finally, after multiplying out and recombining the terms, and rotating the coordinate system, we obtain the expression

$$\begin{aligned}\hat{H} &= -t_h\, a(\sqrt{3}/2) \int\int dx\, dy \left[\hat{a}^\dagger \hat{b}\, \phi^*_{q,A} \left(\partial_x \phi_{q,B} - i\partial_y \phi_{q,B} \right) + \hat{b}^\dagger \hat{a}\, \phi^*_{q,B} \left(\partial_x \phi_{q,A} + i\partial_y \phi_{q,A} \right) \right] \\ &= -t_h (\sqrt{3}/2) \int\int dx\, dy \left[\hat{\psi}^\dagger_A \left(\partial_x \hat{\psi}_B - i\partial_y \hat{\psi}_B \right) + \hat{\psi}^\dagger_B \left(\partial_x \hat{\psi}_A + i\partial_y \hat{\psi}_A \right) \right] . \end{aligned} \tag{9.18}$$

This is the second quantized Dirac Hamiltonian for one pseudospin valley of the honeycomb lattice. By going through the same steps for the opposite corner of the Brillouin zone we get the usual 4-spinor Hamiltonian for a free massless particle:

$$\hat{H} = -i\, t_h\, a(\sqrt{3}/2) \int d^2 r\, \hat{\psi}^\dagger \left(\gamma^\mu \partial_\mu \right) \hat{\psi} , \tag{9.19}$$

where

$$\hat{\psi} \equiv \begin{pmatrix} \hat{a}\, \phi_{q,A+} \\ \hat{b}\, \phi_{q,B+} \\ \hat{b}\, \phi_{q,B-} \\ \hat{a}\, \phi_{q,A-} \end{pmatrix} . \tag{9.20}$$

We can see that the inclusion of higher order corrections through Eq. (9.8) will introduce symmetry breaking terms reflecting a greater resolution of the lattice structure. For example, adding another term would result in a Hamiltonian with an additional quadratic term in the spatial derivatives which a quadratic correction to the linear Dirac dispersion.

9.2.2 Second-Order Nearest-Neighbor Hopping Correction

At this point it would be instructive to examine the theory to the next order in the lattice spacing. Returning to Eq. (9.8), we now include the second terms that involve gradients of the quasi-particle wavefunctions, and by following the same steps as for the zeroth order case, we should expect the appearance of kinetic terms with second derivatives in the spatial directions. We work in the tight-binding limit, consequently there are two additional second order corrections which are negligible and we do not consider here. The first is the effect from extending the calculation to include three nearby sites spanning a length of $2\vec{n}_1$ (or $2\vec{n}_2$). Such triples are mediated by two A (or B)-sites, in particular by the relative difference in amplitudes between the two sites of the same type, thus effectively the gradient in the A or B-field. From this argument it is clear that we have inherently chosen to neglect gradients in the mediating field in favor of the field itself. A second contribution which we neglect is the next-nearest-neighbor hopping, which again is justified in the tight-binding limit.

Proceeding as in the last section, we get

$$\begin{aligned}\hat{H} \equiv \sum_{<A,B>} \Big[& \hat{a}^\dagger \hat{b}\, \phi^*_{q,A}(\vec{r}_A) e^{i\vec{k}\cdot\vec{\chi}_{AB}} \vec{\nabla}\phi_{q,B}|_{\vec{r}_B} \cdot \int d^2r (\vec{r} - \vec{r_B}) e^{-i\vec{k}\cdot\vec{r}} u(\vec{\chi}_A) H_0 e^{i\vec{k}\cdot\vec{r}} u(\vec{\chi}_B) \\ & + \hat{b}^\dagger \hat{a}\, \phi^*_{q,B}(\vec{r}_B) e^{-i\vec{k}\cdot\vec{\chi}_{AB}} \vec{\nabla}\phi_{q,A}|_{\vec{r}_A} \cdot \int d^2r (\vec{r} - \vec{r_A}) e^{-i\vec{k}\cdot\vec{r}} u(\vec{\chi}_B) H_0 e^{i\vec{k}\cdot\vec{r}} u(\vec{\chi}_A) \Big] . \quad (9.21)\end{aligned}$$

For simplicity, we write the integrals as $\vec{T}_A$ and $\vec{T}_B$ respectively, and condense the field and gradient notation with the understanding that they are evaluated at the sites labeled by their subscripts, which gives

$$\hat{H} \equiv \sum_{<A,B>} \left[\hat{a}^\dagger \hat{b}\, \phi^*_{q,A} e^{i\vec{k}\cdot\vec{\chi}_{AB}} \vec{\nabla}\phi_{q,B} \cdot \vec{T}_B + \hat{b}^\dagger \hat{a}\, \phi^*_{q,B} e^{-i\vec{k}\cdot\vec{\chi}_{AB}} \vec{\nabla}\phi_{q,A} \cdot \vec{T}_A \right] . \quad (9.22)$$

Following the same procedure as in the previous section, we obtain

$$\hat{H} =$$
$$\sum_{A,B} \Bigg[\hat{a}^\dagger \hat{b}\, \phi^*_{q,A_j} \frac{(\vec{\nabla}\phi_{q,B_j} \cdot \vec{T}_{B_j} - \vec{\nabla}\phi_{q,B_{j-n_1}} \cdot \vec{T}_{B_{j-n_1}})}{\Delta n_1} (1/2 + i\sqrt{3}/2)\Delta n_1 \Delta n_2$$
$$+ \hat{a}^\dagger \hat{b}\, \phi^*_{q,A_j} \frac{(\vec{\nabla}\phi_{q,B_j} \cdot \vec{T}_{B_j} - \vec{\nabla}\phi_{q,B_{j-n_2}} \cdot \vec{T}_{B_{j-n_2}})}{\Delta n_2} (1/2 - i\sqrt{3}/2)\Delta n_1 \Delta n_2$$
$$+ \hat{b}^\dagger \hat{a}\, \phi^*_{q,B_j} \frac{(\vec{\nabla}\phi_{q,A_{j+n_1}} \cdot \vec{T}_{A_{j+n_1}} - \vec{\nabla}\phi_{q,A_j} \cdot \vec{T}_{A_j})}{\Delta n_1} (-1/2 + i\sqrt{3}/2)\Delta n_1 \Delta n_2$$
$$+ \hat{b}^\dagger \hat{a}\, \phi^*_{q,B_j} \frac{(\vec{\nabla}\phi_{q,A_{j+n_2}} \cdot \vec{T}_{A_{j+n_2}} - \vec{\nabla}\phi_{q,A_j} \cdot \vec{T}_{A_j})}{\Delta n_2} (-1/2 - i\sqrt{3}/2)\Delta n_1 \Delta n_2 \Bigg] . \quad (9.23)$$

The first moments, $\vec{T}_{B_j}$ and $\vec{T}_{A_j}$, point in the direction from one site to one of it's nearest-neighbors, since these integrals contain the overlap of symmetric Wannier functions and so are weighted along the line joining neighboring sites. This allows us to simplify the integrals by writing them proportional to the $\vec{\delta}$ vectors that point between neighboring sites. The magnitude of these is independent of the site and so can be factored out of the whole expression. Physically, this number characterizes to second order (in momentum) propagation of quasi-particle fields, and is identified with the reciprocal of the effective mass. With $\vec{\delta}_1 = (1/2\sqrt{3}, -1/2)$, $\vec{\delta}_2 = (1/2\sqrt{3}, 1/2)$, $\vec{\delta}_3 = (-1/\sqrt{3}, 0)$, the moments are

$$\vec{T}_{B_j} = \int d^2r(\vec{r}-\vec{r}_{B_j})e^{-i\vec{k}\cdot\vec{r}}u(\vec{\chi}_{A_j})H_0e^{i\vec{k}\cdot\vec{r}}u(\vec{\chi}_{B_j}) \tag{9.24}$$

$$= \frac{\sqrt{3}}{m}\,\vec{\delta}_3 \tag{9.25}$$

$$= \frac{\sqrt{3}}{m}\,(-\frac{1}{\sqrt{3}},0)\,, \tag{9.26}$$

$$\vec{T}_{B_{j-n_1}} = \int d^2r(\vec{r}-\vec{r}_{B_{j-n_1}})e^{-i\vec{k}\cdot\vec{r}}u(\vec{\chi}_{A_j})H_0e^{i\vec{k}\cdot\vec{r}}u(\vec{\chi}_{B_{j-n_1}}) \tag{9.27}$$

$$= \frac{\sqrt{3}}{m}\,\vec{\delta}_1 \tag{9.28}$$

$$= \frac{\sqrt{3}}{m}\,(\frac{1}{2\sqrt{3}},-\frac{1}{2})\,, \tag{9.29}$$

$$\vec{T}_{B_{j-n_2}} = \int d^2r(\vec{r}-\vec{r}_{B_{j-n_2}})e^{-i\vec{k}\cdot\vec{r}}u(\vec{\chi}_{A_j})H_0e^{i\vec{k}\cdot\vec{r}}u(\vec{\chi}_{B_{j-n_2}}) \tag{9.30}$$

$$= \frac{\sqrt{3}}{m}\,\vec{\delta}_2 \tag{9.31}$$

$$= \frac{\sqrt{3}}{m}\,(\frac{1}{2\sqrt{3}},\frac{1}{2})\,, \tag{9.32}$$

$$\vec{T}_{A_j} = \int d^2r(\vec{r}-\vec{r}_{A_j})e^{-i\vec{k}\cdot\vec{r}}u(\vec{\chi}_{B_j})H_0e^{i\vec{k}\cdot\vec{r}}u(\vec{\chi}_{A_j}) \tag{9.33}$$

$$= \frac{\sqrt{3}}{m}\,(-\vec{\delta}_3) \tag{9.34}$$

$$= \frac{\sqrt{3}}{m}\,(\frac{1}{\sqrt{3}},0)\,, \tag{9.35}$$

$$\vec{T}_{A_{j+n_1}} = \int d^2r(\vec{r}-\vec{r}_{A_{j+n_1}})e^{-i\vec{k}\cdot\vec{r}}u(\vec{\chi}_{B_j})H_0e^{i\vec{k}\cdot\vec{r}}u(\vec{\chi}_{A_{j+n_1}}) \tag{9.36}$$

$$= \frac{\sqrt{3}}{m}\,(-\vec{\delta}_1) \tag{9.37}$$

$$= \frac{\sqrt{3}}{m}\,(-\frac{1}{2\sqrt{3}}\,,\frac{1}{2})\,, \tag{9.38}$$

$$\vec{T}_{A_{j+n_2}} = \int d^2r(\vec{r}-\vec{r}_{A_{j+n_2}})e^{-i\vec{k}\cdot\vec{r}}u(\vec{\chi}_{B_j})H_0e^{i\vec{k}\cdot\vec{r}}u(\vec{\chi}_{A_{j+n_2}}) \tag{9.39}$$

$$= \frac{\sqrt{3}}{m}\,(-\vec{\delta}_2) \tag{9.40}$$

$$= \frac{\sqrt{3}}{m}\,(-\frac{1}{2\sqrt{3}},-\frac{1}{2})\,. \tag{9.41}$$

$$\tag{9.42}$$

Next, expanding the dot-products gives

$$\vec{\nabla}\phi_{q,B_j}\cdot\vec{T}_{B_j} = -\frac{1}{m}\,\partial_x\phi_{q,B_j}\,, \tag{9.43}$$

$$\vec{\nabla}\phi_{q,B_{j-n_1}}\cdot\vec{T}_{B_{j-n_1}} = \frac{1}{2m}\,\partial_x\phi_{q,B_{j-n_1}} - \frac{\sqrt{3}}{2m}\,\partial_y\phi_{q,B_{j-n_1}}\,, \tag{9.44}$$

$$\vec{\nabla}\phi_{q,B_{j-n_2}}\cdot\vec{T}_{B_{j-n_2}} = \frac{1}{2m}\,\partial_x\phi_{q,B_{j-n_2}} + \frac{\sqrt{3}}{2m}\,\partial_y\phi_{q,B_{j-n_2}}\,, \tag{9.45}$$

$$\vec{\nabla}\phi_{q,A_j}\cdot\vec{T}_{A_j} = \frac{1}{m}\,\partial_x\phi_{q,A_j}\,, \tag{9.46}$$

$$\vec{\nabla}\phi_{q,A_{j+n_1}}\cdot\vec{T}_{A_{j+n_1}} = -\frac{1}{2m}\,\partial_x\phi_{q,A_{j+n_1}} + \frac{\sqrt{3}}{2m}\,\partial_y\phi_{q,A_{j+n_1}}\,, \tag{9.47}$$

$$\vec{\nabla}\phi_{q,A_{j+n_2}}\cdot\vec{T}_{A_{j+n_2}} = -\frac{1}{2m}\,\partial_x\phi_{q,A_{j+n_2}} - \frac{\sqrt{3}}{2m}\,\partial_y\phi_{q,A_{j+n_2}}\,. \tag{9.48}$$

Inserting these expressions into $\hat{H}$ and taking the limit $\Delta n_1\,\Delta n_2 \to dn_1\,dn_2$, leads to

$$\begin{aligned}
\hat{H} = a\int dn_1 dn_2 \Bigg[& \hat{a}^\dagger\hat{b}\,\phi^*_{q,A}\partial_{n_1}\left(-\frac{1}{m}\partial_x\phi_{q,B} - \frac{1}{2m}\partial_x\phi_{q,B} + \frac{\sqrt{3}}{2m}\partial_y\phi_{q,B}\right)\left(1/2 + i\sqrt{3}/2\right) \\
+ & \hat{a}^\dagger\hat{b}\,\phi^*_{q,A}\partial_{n_2}\left(-\frac{1}{m}\partial_x\phi_{q,B} - \frac{1}{2m}\partial_x\phi_{q,B} - \frac{\sqrt{3}}{2m}\partial_y\phi_{q,B}\right)\left(1/2 - i\sqrt{3}/2\right) \\
+ & \hat{b}^\dagger\hat{a}\,\phi^*_{q,B}\partial_{n_1}\left(-\frac{1}{2m}\partial_x\phi_{q,A} + \frac{\sqrt{3}}{2m}\partial_y\phi_{q,A} - \frac{1}{m}\partial_x\phi_{q,A}\right)\left(-1/2 + i\sqrt{3}/2\right) \\
+ & \hat{b}^\dagger\hat{a}\,\phi^*_{q,B}\partial_{n_2}\left(-\frac{1}{2m}\partial_x\phi_{q,A} - \frac{\sqrt{3}}{2m}\partial_y\phi_{q,A} - \frac{1}{m}\partial_x\phi_{q,A}\right)\left(-1/2 - i\sqrt{3}/2\right)\Bigg]\,.
\end{aligned} \tag{9.49}$$

The next step is to write all derivatives and differentials in terms of x and y coordinates and insert the Jacobian factor $2/\sqrt{3}$ along with $\partial_{n_1} = (\sqrt{3}/2)\partial_x - (1/2)\partial_y$, $\partial_{n_2} = (\sqrt{3}/2)\partial_x + (1/2)\partial_y$, so that

$$
\begin{aligned}
\hat{H} &= a\frac{2}{\sqrt{3}}\int\frac{dxdy}{2m}\left[\hat{a}^\dagger\hat{b}\,\phi^*_{q,A}\left(\frac{\sqrt{3}}{2}\partial_x-\frac{1}{2}\partial_y\right)\left(-3\partial_x+\sqrt{3}\partial_y\right)\phi_{q,B}\left(1/2+i\sqrt{3}/2\right)\right.\\
&+ \hat{a}^\dagger\hat{b}\,\phi^*_{q,A}\left(\frac{\sqrt{3}}{2}\partial_x+\frac{1}{2}\partial_y\right)\left(-3\partial_x-\sqrt{3}\partial_y\right)\phi_{q,B}\left(1/2-i\sqrt{3}/2\right)\\
&+ \hat{b}^\dagger\hat{a}\,\phi^*_{q,B}\left(\frac{\sqrt{3}}{2}\partial_x-\frac{1}{2}\partial_y\right)\left(-3\partial_x+\sqrt{3}\partial_y\right)\phi_{q,A}\left(-1/2+i\sqrt{3}/2\right)\\
&+ \left.\hat{b}^\dagger\hat{a}\,\phi^*_{q,B}\left(\frac{\sqrt{3}}{2}\partial_x+\frac{1}{2}\partial_y\right)\left(-3\partial_x-\sqrt{3}\partial_y\right)\phi_{q,A}\left(-1/2-i\sqrt{3}/2\right)\right]. \qquad (9.50)
\end{aligned}
$$

After multiplying out all the factors and regrouping like terms we obtain a much simpler expression

$$
\begin{aligned}
&\hat{H} = \qquad (9.51)\\
&\int\frac{dxdy}{2m}\left[\hat{a}^\dagger\hat{b}\,\phi^*_{q,A}\left(-3\partial_x^2+6i\partial_{xy}^2-\partial_y^2\right)\phi_{q,B}+\hat{b}^\dagger\hat{a}\,\phi^*_{q,B}\left(3\partial_x^2+6i\partial_{xy}^2+\partial_y^2\right)\phi_{q,A}\right].
\end{aligned}
$$

We are free to transform the coordinates in both expressions to recover the Schrödinger Laplacian form as long as we include the correct Jacobian factor. Thus, we define

$$
\begin{aligned}
\partial_x &\rightarrow u\,\partial_x+v\,\partial_y \qquad (9.52)\\
\partial_y &\rightarrow w\,\partial_x+z\,\partial_y\,. \qquad (9.53)
\end{aligned}
$$

Inserting this transformation into the first expression in for $\hat{H}$ and imposing the proper constraints to ensure that the transformed expression is the Laplacian in 2D, we obtain the conditions

$$
\begin{aligned}
-3u^2+6iuw-w^2 &= 1\,, \qquad (9.54)\\
-6uv+6i(uz+vw)-2wz &= 0\,, \qquad (9.55)\\
-3v^2+6ivz-z^2 &= 1\,. \qquad (9.56)
\end{aligned}
$$

After a few algebraic steps, we find a solution

$$u = i\frac{7}{3}\sqrt{\frac{3}{4}}, \tag{9.57}$$
$$v = -2, \tag{9.58}$$
$$w = \sqrt{\frac{3}{4}}, \tag{9.59}$$
$$z = i, \tag{9.60}$$

and the Jacobian factor for this transformation is $-3\sqrt{4/3}$. The constraints for the second expression in $\hat{H}$ are

$$3u^2 + 6iuw + w^2 = 1, \tag{9.61}$$
$$6uv + 6i(uz + vw) + 2wz = 0, \tag{9.62}$$
$$3v^2 + 6ivz + z^2 = 1, \tag{9.63}$$

where, after more algebra, we find that

$$u = \frac{7}{3}\sqrt{\frac{3}{4}}, \tag{9.64}$$
$$v = -2i, \tag{9.65}$$
$$w = i\sqrt{\frac{3}{4}}, \tag{9.66}$$
$$z = 1. \tag{9.67}$$

The Jacobian factor here is $3\sqrt{4/3}$. Finally, the transformed Hamiltonian is

$$\hat{H} = \sqrt{3}a \int \frac{dxdy}{m} \left(-\hat{a}^\dagger \hat{b}\, \phi^*_{q,A} \vec{\nabla}^2 \phi_{q,B} + \hat{b}^\dagger \hat{a}\, \phi^*_{q,B} \vec{\nabla}^2 \phi_{q,A} \right). \tag{9.68}$$

For the special mode where $\phi_{q,B} = \phi_{q,A}$, we obtain the form

$$\hat{H} = \sqrt{3}a \int d^2r \left[\hat{\psi}^\dagger_A \left(\frac{-\hbar^2 \vec{\nabla}^2}{m} \right) \hat{\psi}_B + \hat{\psi}^\dagger_B \left(\frac{\hbar^2 \vec{\nabla}^2}{m} \right) \hat{\psi}_A \right]. \tag{9.69}$$

This gives the second order correction to the Hamiltonian for long-wavelength excitations corresponding to the second order expansion of the dispersion relation for

the upper and lower branches of the Dirac cone. The many-body Hamiltonian up to second-order in spatial derivatives can be expressed in condensed notation. Including the result from the previous gives

$$\hat{H} = -i \int d^2r \, \hat{\psi}^\dagger \left(\hbar c_l \, \sigma \cdot \mathbf{p} + \frac{\sqrt{3}}{m} \sigma_y \, \mathbf{p}^2 \right) \hat{\psi} \, . \tag{9.70}$$

9.3 Continuum Quantum Field Theory

We can determine the structure of the low energy excitations of the insulating phase by the usual quantum field theory technique. First we introduce the superfluid order parameters as before but now we allow it vary in two (continuous) spatial dimensions as well as time: $\psi(\mathbf{r}, \tau)$. The path integral form of the Euclidean partition function near the SF-MI phase transition is

$$Z = \int \mathcal{D}c_i(\tau) \, \mathcal{D}c_i^*(\tau) \exp\left(- \int_0^{1/T} d\tau \mathcal{L} \right) , \tag{9.71}$$

$$\mathcal{L} = \sum_i \left(c_i^* \hbar \partial_\tau c_i - \mu c_i^* c_i + \frac{1}{2} U c_i^* c_i^* c_i c_i \right) - J \sum_{<i,j>} \left(c_i^* c_j + c_j^* c_i \right) , \tag{9.72}$$

where the indices i, j are short hand for the ith and j^{th} lattice vectors $\mathbf{r}_i$ and $\mathbf{r}_j$ respectively and c and c^* are the corresponding bosonic fields. Decoupling the hopping term as before by the standard Hubbard-Stratanovich transformation by introducing the auxiliary field $\psi_i(\tau)$ into Z which gives

$$Z = \int \mathcal{D}c_i(\tau) \, \mathcal{D}c_i^*(\tau) \mathcal{D}\psi_i(\tau) \, \mathcal{D}\psi_i^*(\tau) \exp\left(- \int_0^{1/T} d\tau \mathcal{L}' \right) , \tag{9.73}$$

$$\mathcal{L}' = \sum_i \left(c_i^* \hbar \partial_\tau c_i - \mu c_i^* c_i + \frac{1}{2} U c_i^* c_i^* c_i c_i - \psi_i c_i^* - \psi_i^* c_i \right) + \sum_{<i,j>} \psi_i^* J_{ij}^{-1} \psi_j \, . \tag{9.74}$$

Note that the dependence on the Euclidean time τ is implied. The usual process involves integrating over c_i and c_i^* and then performing a derivative expansion in the

superfluid fields ψ_i to obtain the low energy, long wavelength, effective action. To connect to the Dirac theory, we still must translate the action to the edge of the Brillouin zone before performing the integral over the c_i. Resetting the zero-point for the fields to the Dirac point requires the addition of an extra phase in the hopping terms which comes from the background. Also, we must make the sublattice structure explicit in the hopping terms so that $\mathcal{L}'$ becomes

$$\mathcal{L}' = \sum_{<\mathbf{r},\mathbf{r}'>\in\{\mathcal{A},\mathcal{B}\}} \left(c^*_{\mathbf{r}} \hbar \partial_\tau c_{\mathbf{r}} - \mu c^*_{\mathbf{r}} c_{\mathbf{r}} + \frac{1}{2} U c^*_{\mathbf{r}} c^*_{\mathbf{r}} c_{\mathbf{r}} c_{\mathbf{r}} - e^{i\theta_{\mathbf{r}\mathbf{r}'}} \psi_{\mathbf{r}} J^{-1}_{\mathbf{r}\mathbf{r}'} c^*_{\mathbf{r}'} - e^{-i\theta_{\mathbf{r}'\mathbf{r}}} \psi^*_{\mathbf{r}'} J^{-1}_{\mathbf{r}\mathbf{r}'} c_{\mathbf{r}} \right)$$
$$+ \sum_{<\mathbf{r},\mathbf{r}'>} e^{i\theta_{\mathbf{r}\mathbf{r}'}} \psi^*_{\mathbf{r}} J^{-1}_{\mathbf{r}\mathbf{r}'} \psi_{\mathbf{r}'} \,, \tag{9.75}$$

where $e^{i\theta_{\mathbf{r}\mathbf{r}'}}$ is the directed background phase between nearest-neighbor sites coming from the Bloch wave expansion at the Dirac point of the lattice. The notation in the first summation refers to the $\mathcal{A}$ sublattice and $\mathcal{B}$ sublattice vector spaces. Next, we factor the partition function

$$Z = \int \mathcal{D}\psi_i(\tau)\, \mathcal{D}\psi^*_i(\tau) \exp\left[-\frac{t_h}{\hbar} \int d\tau \sum_{<\mathbf{r},\mathbf{r}'>} e^{i\theta_{\mathbf{r}\mathbf{r}'}} \psi^*_{\mathbf{r}} \psi_{\mathbf{r}'} \right]$$
$$\times \int \mathcal{D}c_i(\tau)\, \mathcal{D}c^*_i(\tau) \exp\left[-\frac{t_h}{\hbar} \int d\tau \sum_{<\mathbf{r},\mathbf{r}'>\in\{\mathcal{A},\mathcal{B}\}} \left(-e^{i\theta_{\mathbf{r}\mathbf{r}'}} \psi_{\mathbf{r}} c^*_{\mathbf{r}'} - e^{-i\theta_{\mathbf{r}'\mathbf{r}}} \psi^*_{\mathbf{r}'} c_{\mathbf{r}} \right) \right]$$
$$\times \exp\left\{ -\frac{\mathcal{L}_0[c, c^*]}{\hbar} \right\}, \tag{9.76}$$

where we have reduced the nearest-neighbor transition matrix to $J^{-1}_{\mathbf{r}\mathbf{r}'} = t_h$ and the action composed purely of Mott fields is

$$\mathcal{L}_0[c, c^*] = \int d\tau \sum_{\mathbf{r}\in\{\mathcal{A},\mathcal{B}\}} c^*_{\mathbf{r}} \left(\hbar\partial_\tau - \mu + \frac{1}{2} U c^*_{\mathbf{r}} c_{\mathbf{r}} \right) c_{\mathbf{r}} \,. \tag{9.77}$$

The functional integral over the Mott fields in the second line of Z is just the expectation value of the exponential containing the cross-terms of Mott and superfluid

fields weighted by the exponential of the action S_0:

$$Z = \int \mathcal{D}\psi_i(\tau)\,\mathcal{D}\psi_i^*(\tau)\exp\left[-\frac{t_h}{\hbar}\int d\tau \sum_{<\mathbf{r},\mathbf{r}'>} e^{i\theta_{\mathbf{r}\mathbf{r}'}}\psi_{\mathbf{r}}^*\psi_{\mathbf{r}'}\right]$$
$$\times \langle\exp\left[-\frac{t_h}{\hbar}\int d\tau \sum_{<\mathbf{r},\mathbf{r}'>\in\{\mathcal{A},\mathcal{B}\}} \left(-e^{i\theta_{\mathbf{r}\mathbf{r}'}}\psi_{\mathbf{r}}c_{\mathbf{r}'}^* - e^{-i\theta_{\mathbf{r}'\mathbf{r}}}\psi_{\mathbf{r}'}^* c_{\mathbf{r}}\right)\right]\rangle_0. \tag{9.78}$$

To evaluate this expression, we follow the usual cumulant expansion prescription but, since the Mott fields do not acquire an expectation value in the ground state, all odd power correlators vanish which simplifying the expansion

$$\langle\exp(M)\rangle_0^{\text{even}} \approx \exp\left[\frac{1}{2}\langle M^2\rangle_0 + \langle M^4\rangle_0 - \frac{1}{4}\langle M^2\rangle_0^2 + ...\right]. \tag{9.79}$$

Then the effective action up to second order in the superfluid field ψ and ψ^* is

$$\mathcal{L}^{\text{eff}}[\psi,\psi^*] = -\frac{t_h}{\hbar}\sum_{<\mathbf{r},\mathbf{r}'>}\int d\tau\, e^{i\theta_{\mathbf{r}\mathbf{r}'}}\psi_{\mathbf{r}}^*\psi_{\mathbf{r}'}$$
$$+\sum_{<\mathbf{r},\mathbf{r}'>}\int d\tau\left[\frac{t_h^2}{2\hbar^2}\langle\left(e^{i\theta_{\mathbf{r}\mathbf{r}'}}\psi_{\mathbf{r}}c_{\mathbf{r}'}^* + e^{-i\theta_{\mathbf{r}'\mathbf{r}}}\psi_{\mathbf{r}'}^*c_{\mathbf{r}}\right)^2\rangle_0 + \frac{t_h^4}{\hbar^4}\langle\left(e^{i\theta_{\mathbf{r}\mathbf{r}'}}\psi_{\mathbf{r}}c_{\mathbf{r}'}^* + e^{-i\theta_{\mathbf{r}'\mathbf{r}}}\psi_{\mathbf{r}'}^*c_{\mathbf{r}}\right)^4\rangle_0\right.$$
$$\left. - \frac{t_h^4}{4\hbar^4}\langle\left(e^{i\theta_{\mathbf{r}\mathbf{r}'}}\psi_{\mathbf{r}}c_{\mathbf{r}'}^* + e^{-i\theta_{\mathbf{r}'\mathbf{r}}}\psi_{\mathbf{r}'}^*c_{\mathbf{r}}\right)^2\rangle_0^2\right]. \tag{9.80}$$

Next, we note the following properties of the two-point and four-point functions

$$\langle c_{\mathbf{r}}(\tau)c^*_{\mathbf{r}'}(\tau')\rangle_0 = \delta(\mathbf{r}-\mathbf{r}')\langle c(\tau)c^*(\tau')\rangle_0\,, \tag{9.81}$$
$$\langle c^*_{\mathbf{r}}(\tau)c^*_{\mathbf{r}'}(\tau')\rangle_0 = \langle c_{\mathbf{r}}(\tau)c_{\mathbf{r}'}(\tau')\rangle_0 = 0\,, \tag{9.82}$$

$$\langle c_{\mathbf{r}}(\tau)c_{\mathbf{r}'}(\tau')c^*_{\mathbf{r}''}(\tau'')c^*_{\mathbf{r}'''}(\tau''')\rangle_0 = \tag{9.83}$$
$$\delta(\mathbf{r}-\mathbf{r}')\delta(\mathbf{r}'-\mathbf{r}'')\delta(\mathbf{r}''-\mathbf{r}''')\langle c(\tau)c(\tau')c^*(\tau'')c^*(\tau''')\rangle_0\,, \tag{9.84}$$

$$\langle c^*_{\mathbf{r}}(\tau)c^*_{\mathbf{r}'}(\tau')c^*_{\mathbf{r}''}(\tau'')c^*_{\mathbf{r}'''}(\tau''')\rangle_0 = 0\,, \tag{9.85}$$

$$\langle c^*_{\mathbf{r}}(\tau)c^*_{\mathbf{r}'}(\tau')c^*_{\mathbf{r}''}(\tau'')c_{\mathbf{r}'''}(\tau''')\rangle_0 = 0\,, \tag{9.86}$$

$$\langle c^*_{\mathbf{r}}(\tau)c_{\mathbf{r}'}(\tau')c_{\mathbf{r}''}(\tau'')c_{\mathbf{r}'''}(\tau''')\rangle_0 = 0\,, \tag{9.87}$$

$$\langle c_{\mathbf{r}}(\tau)c_{\mathbf{r}'}(\tau')c_{\mathbf{r}''}(\tau'')c_{\mathbf{r}'''}(\tau''')\rangle_0 = 0\,. \tag{9.88}$$

To compute the two-point function we introduce the imaginary time ordering operator T and express the answer in terms of an operator expression so that we can connect to our previous work:

$$\langle c(\tau)c^*(\tau')\rangle_0 = \langle \mathrm{T}\,\left[c(\tau)c^\dagger(\tau')\right]\rangle_0 \tag{9.89}$$
$$= \theta(\tau-\tau')\,\langle c(\tau)c^\dagger(\tau')\rangle_0 \,+\, \theta(\tau'-\tau)\langle c^\dagger(\tau')c(\tau)\rangle_0\,, \tag{9.90}$$

and in the second line we have expressed the time-ordered result in terms of the Heavyside functions. These expressions can be computed exactly by using the result that we found before for the ground state energy:

$$E^{(0)}_g = \frac{1}{2}\bar{U}g\,(g-1) \,-\, \bar{\mu}\,g\,, \tag{9.91}$$

with g the number of particles in the ground state. The problem reduces to the simple formula

$$\langle \tau' , g \,|\, c(\tau')\, c^{\dagger}(\tau) \,|\, \tau , g \rangle$$

$$= (g+1)\, \langle 0 , g+1 \,|\, \exp\left[\left(E^{(0)}_{g+1} - E^{(0)}_{g}\right)\tau'/\hbar\right] \cdot \exp\left[-\left(E^{(0)}_{g+1} - E^{(0)}_{g}\right)\tau/\hbar\right] \,|\, 0 , g+1 \rangle$$

$$= (g+1) \exp\left[-\left(E^{(0)}_{g+1} - E^{(0)}_{g}\right)(\tau - \tau')/\hbar\right], \tag{9.92}$$

so that

$$\begin{aligned} \langle c(\tau) c^{*}(\tau') \rangle_0 &= \theta(\tau - \tau')\,(g+1) \exp\left[-\left(E^{(0)}_{g+1} - E^{(0)}_{g}\right)(\tau - \tau')/\hbar\right] \\ &+ \theta(\tau' - \tau)\, g \exp\left[\left(E^{(0)}_{g-1} - E^{(0)}_{g}\right)(\tau - \tau')/\hbar\right], \end{aligned} \tag{9.93}$$

keeping in mind that

$$E^{(0)}_{g+1} - E^{(0)}_{g} = g\,U - \mu\,, \tag{9.94}$$

$$E^{(0)}_{g-1} - E^{(0)}_{g} = (g-1)U - \mu\,, \tag{9.95}$$

then

$$\begin{aligned} \langle c(\tau) c^{*}(\tau') \rangle_0 &= \theta(\tau - \tau')(g+1) \exp\left[-\left(gU - \mu\right)(\tau - \tau')/\hbar\right] \\ &+ \theta(\tau' - \tau) g \exp\left[\left(gU - U - \mu\right)(\tau - \tau')/\hbar\right]. \end{aligned} \tag{9.96}$$

For the four-point function, we can use Wick's theorem to reduce it to sums of products of two-point functions and then evaluate these using our previous results:

$$
\begin{aligned}
&\langle \mathrm{T}\left[c(\tau)c(\tau')c^*(\tau'')c^*(\tau''')\right]\rangle_0 \qquad (9.97)\\
&= \langle \mathrm{T}\left[c(\tau)c^*(\tau''')\right]\rangle_0 \langle \mathrm{T}\left[c(\tau')c^*(\tau'')\right]\rangle_0\\
&+\langle \mathrm{T}\left[c(\tau)c^*(\tau'')\right]\rangle_0 \langle \mathrm{T}\left[c(\tau')c^*(\tau''')\right]\rangle_0
\end{aligned}
$$

$$
\begin{aligned}
&= \{\theta(\tau-\tau''')\,(g+1)\exp\left[-\,(gU\,-\,\mu)\,(\tau-\tau''')/\hbar\right]\\
&+\,\theta(\tau'''-\tau)\,g\exp\left[-\,(gU\,-\,U\,-\,\mu)\,(\tau-\tau''')/\hbar\right]\}\\
&\times\{\theta(\tau'-\tau'')\,(g+1)\exp\left[-\,(gU\,-\,\mu)\,(\tau'-\tau'')/\hbar\right]\\
&+\,\theta(\tau''-\tau')\,g\exp\left[-\,(gU\,-\,U\,-\,\mu)\,(\tau'-\tau'')/\hbar\right]\}\\
&+\{\theta(\tau-\tau'')\,(g+1)\exp\left[-\,(gU\,-\,\mu)\,(\tau-\tau'')/\hbar\right]\\
&+\,\theta(\tau''-\tau)\,g\exp\left[-\,(gU\,-\,U\,-\,\mu)\,(\tau-\tau'')/\hbar\right]\}\\
&\times\{\theta(\tau'-\tau''')\,(g+1)\exp\left[-\,(gU\,-\,\mu)\,(\tau'-\tau''')/\hbar\right]\\
&+\,\theta(\tau'''-\tau')\,g\exp\left[-\,(gU\,-\,U\,-\,\mu)\,(\tau'-\tau''')/\hbar\right]\}\,. \qquad (9.98)
\end{aligned}
$$

Using these results and forming discrete derivatives in the fist summation of the effective action, we can then take the continuum limit, also, we note that the phase difference between nearest-neighbor sites have the property that $\phi \equiv \theta_{\mathbf{r}\mathbf{r}'} = -\,\theta_{\mathbf{r}'\mathbf{r}}$ where we now call the phase difference ϕ to avoid confusing it with the Heavyside step function. We obtain:

$$
\begin{aligned}
&\mathcal{L}^{\mathrm{eff}}[\psi,\psi^*] = -\frac{t_h}{\hbar}\int d\mathbf{r}\,d\tau\,i\,\left[\psi_A^*(\mathbf{r},\tau)(\partial_x - i\partial_y)\psi_B(\mathbf{r},\tau) + \psi_B^*(\mathbf{r},\tau)(\partial_x + i\partial_y)\psi_A(\mathbf{r},\tau)\right]\\
&+\sum_{i\in\{A,B\}}\int d\mathbf{r}\,d\tau\left[\frac{t_h}{2\hbar}\int d\tau'\,e^{i2\phi}\,\psi_i(\mathbf{r},\tau)\,\psi_i^*(\mathbf{r},\tau')\langle \mathrm{T}\left[c(\tau)c^*(\tau')\right]\rangle_0\right.\\
&+\frac{t_h^4}{\hbar^4}\int d\tau'\,d\tau''\,d\tau'''\,e^{i4\phi}\,\psi_i^*(\mathbf{r},\tau'')\psi_i^*(\mathbf{r},\tau''')\psi_i(\mathbf{r},\tau')\psi_i(\mathbf{r},\tau)\\
&\times\,\{\langle \mathrm{T}\left[c(\tau)c^*(\tau''')\right]\rangle_0\langle \mathrm{T}\left[c(\tau')c^*(\tau'')\right]\rangle_0 + \langle \mathrm{T}\left[c(\tau)c^*(\tau'')\right]\rangle_0\\
&\left.\times\langle \mathrm{T}\left[c(\tau')c^*(\tau''')\right]\rangle_0 - \frac{t_h^4}{4\hbar^4}\left\{\int d\tau'\,e^{i2\phi}\,\psi_i(\mathbf{r},\tau)\,\psi_i^*(\mathbf{r},\tau')\langle \mathrm{T}\left[c(\tau)c^*(\tau')\right]\rangle_0\right\}^2\right]\,. \qquad (9.99)
\end{aligned}
$$

Next, we rewrite the integral with respect to τ' in the second line above:

$$
\begin{aligned}
&\int d\tau'\, e^{i2\phi}\, \psi_i(\mathbf{r},\tau)\, \psi_i^*(\mathbf{r},\tau') \langle \mathrm{T}\left[c(\tau) c^*(\tau')\right]\rangle_0 \\
&= e^{i2\phi}\psi_i(\mathbf{r},\tau) \int_0^\tau d\tau'\; \psi_i^*(\mathbf{r},\tau') \left\{(g+1)\exp\left[-\left(gU\; -\; \mu\right)(\tau-\tau')/\hbar\right]\right\} \\
&+ e^{i2\phi}\psi_i(\mathbf{r},\tau) \int_\tau^\infty d\tau'\, \psi_i^*(\mathbf{r},\tau') \left\{g\exp\left[\left(gU\; -\; U\; -\; \mu\right)(\tau-\tau')/\hbar\right]\right\} \\
&= e^{i2\phi}\left[\frac{(g+1)}{(gU-\mu)} + \frac{g}{(gU-U-\mu)}\right] \hbar |\psi_i(\mathbf{r},\tau)|^2 \\
&- e^{i2\phi}\left[\frac{(g+1)}{(gU-\mu)^2} - \frac{g}{(gU-U-\mu)^2}\right] \hbar^2 \psi_i^*(\mathbf{r},\tau)\partial_\tau \psi_i(\mathbf{r},\tau) + \mathcal{O}(\hbar^3), \quad (9.100)
\end{aligned}
$$

where the second equality comes from integrating by parts twice with respect to τ' and dropping an overall constant. Continuing this process produces higher order derivatives and powers of the superfluid order parameter which, in the low energy and low momentum approximation, justify the truncation. Computing all other terms and combining the sublattice fields ψ_i in spinor form $\Psi \equiv (\psi_A, \psi_B)^T$, the effective action takes the final form

$$
\begin{aligned}
&\mathcal{L}^{\text{eff}}[\Psi,\bar{\Psi}] = \qquad\qquad (9.101) \\
&-\int d\mathbf{r}\, d\tau \left[\bar{\Psi}\partial_\tau \Psi + i c_l\, \bar{\Psi}\left(\sigma\cdot\nabla\right)\Psi + \frac{u}{2}\sum_{i\in\{A,B\}} |\psi_i|^4 + r|\Psi|^2 + \kappa_1 |\partial_\tau \Psi|^2 + \kappa_2 |\nabla\Psi|^2\right].
\end{aligned}
$$

Here we have defined $\bar{\Psi} \equiv (\Psi^*)^T$. The first three terms comprise the classical action for the nonlinear Dirac equation, the fourth term is a quadratic chemical potential where $r = 0$ gives the condition for the second order superfluid-insulator transition, and the last two quadratic terms describe second sound for the superfluid. Note that the final term comes from the next order correction to the gradient describing departure from linear dispersion at the Dirac point. This is computed in detail in the next section. Notably, Eq.(9.102) is the Lagrangian that describes the strongly interacting critical quantum field theory at the Dirac point of the honeycomb lattice. Notice that in the coefficients of the higher order terms, t_h occurs as a modified

hopping parameter $t'_h \equiv e^{i2\phi}t_h$. This has the effect of weighting transitions in the direction of the lattice momentum $\mathbf{K}$ by a factor of $(1+i\sqrt{3})$ and in the opposite direction of $\mathbf{K}$ by a factor of $(1-i\sqrt{3})$. The imaginary parts of these weights represent the effect of the background condensate on the hopping terms that appear at the level of the Hamiltonian. We can see their effects by noting that the induced transition amplitude from lattice site i to site j in the direction of $\mathbf{K}$ is obtained by taking the expectation value after exponentiating the imaginary parts of the hopping terms

$$\begin{aligned} T(i \to j) &= \langle n_i - 1, n_j + 1 | \exp\left[-i(i\sqrt{3}t_h)b_j^\dagger b_i (t-t_0)/\hbar\right] | n_i, n_j \rangle - \mathbb{1} \\ &\approx (t-t_0)t_h\sqrt{3}\, n_i^{1/2}(n_j+1)^{1/2}/2\hbar\,, \end{aligned} \tag{9.102}$$

while for the reverse process we get:

$$T(j \to i) \approx -(t-t_0)t_h\sqrt{3}\, n_j^{1/2}(n_i+1)^{1/2}/2\hbar\,. \tag{9.103}$$

As we would expect, the imaginary terms induce gains and losses of particles for transitions along $\mathbf{K}$ and opposite $\mathbf{K}$ respectively. Yet, it is crucial to note that the phase transition depends on $|e^{i2\phi}t_h|$, so that what we have described is just an interpretation of the phase as a mean-field effect that accounts for higher order interactions with the background condensate.

9.4 Conclusion

We have obtained the continuum quantum field theory for bosons near the Dirac point, and found that it has the same form as that of relativistic interacting Dirac spinors, but with two additional interaction terms corresponding to second sound in the superfluid, one proportional to the square of the time derivative and the other proportional the square of the gradient of the field. The equation of motion for the corresponding single-particle states is the nonlinear Dirac equation, with additional terms second order in the space-time derivatives. Together, these extra second order

terms are identical to the Klein-Gordon momentum terms. This last feature points to the interesting prospect of a possible redefinition of fields to obtain a relativistic theory of interacting fermions and bosons. Several modifications to our results offer the possibility of investigating more elaborate field theories. For example, by including mass gaps and nearest neighbor interactions, which can be tuned to be attractive or repulsive, may lead to other interesting field theories near criticality such as Gross-Neveu, Chern-Simons, Kogut-Susskind, and Yukawa theory, in addition to low energy supersymmetric theories.

CHAPTER 10

CONCLUSIONS AND OUTLOOK

In this thesis we have derived the nonlinear Dirac equation, a new mean-field theory which describes bosons in a 2D honeycomb lattice analogous to the nonlinear Schrödinger equation for general BECs in 3D. In addition, we have derived the relativistic linear stability equations (RLSE), the relativistic generalization of the Bogoliubov-de Gennes equations. We have obtained localized solutions of the NLDE which include bright and gray solitons, topological and non-topological vortices, half-quantum vortices, and skyrmion textures. Although similar solutions have been studied in ordinary BECs confined only by a magnetic trap, our solutions exhibit a Dirac spinor structure due to the presence of the honeycomb optical lattice. Thus, we obtain solitons, vortices, and textures with a Dirac spinor structure sharing features in common with both spinor BECs and particle physics models.

From the point of view of experimental realization, we have clearly defined all the physical parameters of our theory through a systematic reduction from the usual 3D BEC parameters down to the effective 2D lattice at long-wavelengths. The constraints are clearly established and a workable range of values is determined for all of our parameters. We have fully described the necessary steps to construct the lattice and transfer the BEC to any desired vortex configuration while maintaining the system in a metastable state. In addition, discrete spectra for relativistic vortices give a global perspective for vortex energies as functions of the particle interaction. A significant result of our findings is that most of the soliton solutions are perfectly stable while most vortex lifetimes are on the order of or greater than the BEC lifetime. Together, these results provide a formal prescription for realizing relativistic vortices in the laboratory.

On the theory side, we have characterized the low energy quantum fluctuations of all of our solutions by developing a new theory of relativistic quasi-particles contained in the RLSE. The RLSE describe propagation of pseudospin-1/2 quasi-particles similar to the case of graphene pseudospin valley excitations. However, we go beyond the standard graphene picture by considering the effect of tuning a bosonic contact interaction with positive s-wave scattering. By solving for the coherence factors we find that tuning the interaction U upward gradually changes the character of quasi-particle excitations from pseudospin-1/2 to pseudospin-0 or 1, i.e., to a singlet or triplet state. More precisely stated, for $U \ll \sqrt{3}\,\pi t_h a/R$, where t_h is the hopping energy, a the lattice constant, and R the condensate radius, quasi-particles are distinct and uncorrelated pseudospin-1/2 states: the lattice spin-valley structure is only weakly affected by particle interactions. On the other hand, when $U \gg \sqrt{3}\,\pi t_h a/R$, quasi-particles are highly correlated into pairs with aligned or anti-aligned pseudospin. When considering a typical vortex solution of the NLDE in the mean-field picture, quantum fluctuations appear as either bound states (fluctuations of the vortex) or free scattering states (fluctuations of the ambient background). Bound states are localized within one or two healing lengths of the vortex core and deplete the vortex by introducing equal admixtures of particles and holes,

We have analyzed the 1D NLDE, obtained experimentally by making the trap size small in one of the planar directions, which amounts to setting one spatial derivative to zero. The 1D case offers an opportunity to focus on the question of integrability, since the most common integrable systems are 1D models. One approach to proving integrability of a system is to find a reparametrization, or mapping, to another known integrable model. By doing so we gain insight into the original system and possibly new solutions. Using the complete four-spinor NLDE with mass gap as a starting point, which provides a large parameter space to work with, we have found a reparametrization which maps the imaginary and real parts of A and B sublat-

tice wavefunctions to the two independent spinor functions of the massive Thirring model. As a consequence, we were able to apply the map in reverse and obtain new soliton solutions for the massive 1D NLDE. The Thirring parameters are directly related to the mass gap parameter, chemical potential, and interaction strength in the NLDE picture. Integrability of the Thirring model is well known and has been studied extensively, which suggests a direction for further investigations of the 1D NLDE.

We have found a series solution of the 1D NLDE, when the NLDE spinor is parametrized by $\Psi(x) = \eta(x)\,[\cos\varphi(x),\, \sin\varphi(x)]^T$. Our method expands the envelope function $\eta(x)$ in powers of the quantity $\cos\varphi(x)^4 + \sin\varphi(x)^4$, which appears in the NLDE after incorporating our ansatz, and we obtain the expansion coefficients by matching. For the internal parameter function $\varphi(x)$, we arrive at a power series with each term a differential equation for $\varphi(x)$ containing either a positive or negative power of $\cos\varphi(x)^4 + \sin\varphi(x)^4$. Such terms are integrable and lead to an infinite number of conserved quantities for each term in the series. Interestingly, the terms in our series expansion match solutions which we have found by another independent method. This discussion points to symmetries of the 1D NLDE which exist and warrant deeper investigation. In particular, the conserved charges that we have found strongly suggest integrability and an underlying Lax-pair structure.

The NLDE allows for a large variety of vortex solutions, which may be classified according to how the internal degrees of freedom evolve under spatial rotations. Thus a thorough classification of our solutions into topological classes would provide a comparison with similar topological vortices in the area of spinor BECs. Spinor BECs are well established, where topological structures such as skyrmion textures are commonplace. One advantage of accessing atomic hyperfine degrees of freedom within the honeycomb lattice setting, is that this would allow for the same freedom as in the case of spinor BECs, but with the Schrödinger differential operator replaced by

the Dirac operator. In principle, the combination of internal and lattice symmetries would lead to unique nonlinear structures not yet observed in cold atomic gases.

Another possible area to investigate is the use of mixtures of more than one atomic species. Combined with a spin-dependent lattice, as we have discussed in Chapters 6 and 7, this approach offers another way to simulate relativistic mean-field theories. Specifically, the advantage of using this method lies in tuning the lattice parameters so that one type of atom experiences the lattice potential, while the other atoms experience only the harmonic trap. The corresponding continuum mean-field theory would contain Dirac spinors, as we have shown in this thesis, as well as excitations which behave according to the usual Schrödinger paradigm. Furthermore, the inclusion of interactions between the different atom types, would result in a theory of interacting Dirac spinors where interactions are mediated by the additional bosons, which could simulate a semiclassical electromagnetic field.

In Chapter 9, we established the full many-body continuum field theory for bosons in addition to the phase structure for the Hubbard and extended Hubbard models for the honeycomb lattice. We have shown that the inclusion of attractive and repulsive nearest neighbor interactions enhances the richness of the phase landscape. In the mean-field theory, nearest neighbor interactions mix the spinor components while on-site ones do not. By tuning the relative strengths and signs of these interactions, we may be able to simulate a large number of relativistic field equations, since these differ mainly by the specific ways in which the interactions combine the spinor components. By including in this picture the various mass gaps, which we have explored in Chapter 8, we obtain a large parameter space to work with, including four gap parameters and two types of interactions. This offers an intriguing low-energy scenario: by tuning the relative strengths and signs of mass gap parameters, on-site interactions, and nearest-neighbor interactions, we expect to see phase transitions connecting several different nonlinear Dirac theories.

Bose-Einstein condensates in honeycomb lattices offer the opportunity for more detailed investigations into fundamental questions around non-equilibrium BECs. In this thesis, particularly in Chapters 6 and 7, we have shown that it is possible to create a BEC at inherently metastable points in the honeycomb lattice, namely at the Dirac points. Combined with our lifetime and stability analyses, we have set the ground for questions such as non-equilibrium phase fluctuations, growth of the condensate fraction, and turbulence in non-equilibrium systems.

REFERENCES CITED

[1] M. H. Anderson, J. R. Ensher, M. R. Matthews, C. E. Wieman, and E. A. Cornell. Observation of Bose-Einstein condensation in a dilute atomic vapor. *Science*, 269:198–201, 1995.

[2] K. B. Davis, M.-O. Mewes, M. R. Andrews, N. J. van Druten, D. S. Durfee, D. M. Kurn, and W. Ketterle. Bose-Einstein condensation in a gas of sodium atoms. *Phys. Rev. Lett.*, 75:3969–3973, 1995.

[3] C. C. Bradley, C. A. Sackett, J. J. Tollett, and R. G. Hulet. Evidence of Bose-Einstein condensation in an atomic gas with attractive interactions. *Phys. Rev. Lett.*, 75:1687–1690, 1995.

[4] A. J. Leggett. Bose-Einstein condensation in the alkali gases: Some fundamental concepts. *Rev. Mod. Phys.*, 73:307–356, 2001.

[5] I. Bloch, J. Dalibard, and W. Zwerger. Many-body physics with ultracold gases. *Rev. Mod. Phys.*, 80:885–964, 2008.

[6] F. Dalfovo, S. Giorgini, L. P. Pitaevskii, and S. Stringari. Theory of Bose-Einstein condensation in trapped gases. *Rev. Mod. Phys.*, 71:463–512, 1999.

[7] C. Pethick and H. Smith. *Bose-Einstein Condensation in Dilute Gases.* Cambridge University Press, 2002.

[8] M. Lewenstein, A. Sanpera, V. Ahufinger, B. Damski, A. Sen De, and U. Sen. Ultracold atomic gases in optical lattices: mimicking condensed matter physics and beyond. *Advances in Physics*, 56:243, 2007.

[9] C. J. Myatt, E. A. Burt, R. W. Ghrist, E. A. Cornell, and C. E. Wieman. Production of two overlapping Bose-Einstein condensates by sympathetic cooling. *Phys. Rev. Lett.*, 78:586–589, 1997.

[10] D. M. Stamper-Kurn, M. R. Andrews, A. P. Chikkatur, S. Inouye, H. J. Miesner, J. Stenger, and W. Ketterle. Optical confinement of a Bose-Einstein condensate. *Phys. Rev. Lett.*, 80:2027–2030, 1998.

[11] A. I. Safonov, S. A. Vasilyev, I. S. Yasnikov, I. I. Lukashevich, and S. Jaakkola. Observation of quasicondensate in two-dimensional atomic hydrogen. *Phys. Rev. Lett.*, 81:4545–4548, 1998.

[12] R. Kaiser, C. Westbrook, and F. David, editors. *Coherent atomic matter waves.* EDP Sciences and Springer-Verlag, Les Ulis, France and Berlin, Germany, 2001.

[13] J. H. Denschlag, J. E. Simsarian, H. Haffner, C. McKenzie, A. Browaeys, D. Cho, K. Helmerson, S. L. Rolston, and W. D. Phillips. A Bose-Einstein condensate in an optical lattice. *J. Phys. B*, 35:3095–3110, 2002.

[14] A. Jacob, P. Ohberg, G. Juzeliunas, and L. Santos. Cold atom dynamics in non-Abelian gauge fields. *Appl. Phys. B*, 89:439–445, 2008.

[15] C. Wu and S. Das Sarma. The $p_{x,y}$-orbital counterpart of graphene: Cold atoms in the honeycomb optical lattice. *Phys. Rev. B*, 77:235107, 2008.

[16] S. L. Zhu, B. Wang, and L.-M. Duan. Simulation and detection of Dirac fermions with cold atoms in an optical lattice. *Phys. Rev. Lett.*, 98:260402, 2007.

[17] B. Anderson. Experiments with vortices in superfluid atomic gases. *Journal of Low Temperature Physics*, 161:574–602, 2010.

[18] L.-K. Lim, A. Hemmerich, and C. M. Smith. Artificial staggered magnetic field for ultracold atoms in optical lattices. *Phys. Rev. A*, 2010.

[19] P. G. Kevrekidis, D. J. Frantzeskakis, and R. Carretero-González. *Emergent Nonlinear Phenomena in Bose-Einstein Condensates.* Springer-Verlag, Berlin, 2008.

[20] M. J. Ablowitz and Y. Zhu. Evolution of bloch-mode envelopes in two-dimensional generalized honeycomb lattices. *Phys. Rev. A*, 82:013840, 2010.

[21] Z. H. Musslimani, M. Segev, and D. N. Christodoulides. Multicomponent two-dimensional solitons carrying topological charges. *Opt. Lett.*, 25:61–63, 2000.

[22] F. Lederer, G. I. Stegeman, D. N. Christodoulides, G. Assanto, M. Segev, and Y. Silberberg. Discrete solitons in optics. *Phys. Rep.*, 463:1–126, 2008.

[23] W. Zhang, C. A. Sackett, and R. G. Hulet. Optical detection of a Bardeen-Cooper-Schrieffer phase transition in a trapped gas of fermionic atoms. *Phys. Rev. A*, 60:504–507, 1999.

[24] G. M. Bruun and C. W. Clark. Detection of the BCS transition of a trapped Fermi gas. *J. Phys. B: At. Mol. Opt. Phys.*, 33:3953, 2000.

[25] D. S. Petrov, C. Salomon, and G. V. Shlyapnikov. Weakly bound dimers of fermionic atoms. *Phys. Rev. Lett.*, 93:090404, 2004.

[26] P. G. Saffman. *Vortex Dynamics.* Cambridge University Press, The Pitt Building, Trumpington Street, Cambridge CB2 1RP, 1992.

[27] F. Dalfovo, S. Giorgini, L. P. Pitaevskii, and S. Stringari. Theory of Bose-Einstein condensation in trapped gases. *Rev. Mod. Phys.*, 71:463–512, 1999.

[28] A. L. Fetter and A. A. Svidzinsky. Stability of a vortex in a rotating trapped Bose-Einstein condensate. *Phys. Rev. Lett.*, 84:5919–23, 2000.

[29] A. L. Fetter and A. A. Svidzinsky. Vortices in a trapped dilute Bose-Einstein condensate. *J. Phys.: Condens. Matter*, 13:R135, 2001.

[30] E. H. Lieb and R. Seiringer. Proof of Bose-Einstein condensation for dilute trapped gases. *Phys. Rev. Lett.*, 88:170409, 2002.

[31] E. H. Lieb, R. Seiringer, J. P. Solovej, and Jakob Yngvason. *The Mathematics of the Bose Gas and its Condensation.* Springer, 2005.

[32] Z. Chen and B. Wu. Bose-Einstein condensate in a honeycomb optical lattice: Fingerprint of superfluidity at the Dirac point. *Phys. Rev. Lett.*, 107:065301, 2011.

[33] G.E. Volovick. *The Universe in a Helium Droplet.* Oxford University Press, Great Clarendon Street, Oxford OX2 6DP, 2003.

[34] W.G. Unruh and R. Schutzhold, editors. *Quantum analogues: from phase transitions to black holes and cosmology.* Springer-Verlag, 233 Spring Street, New York, NY 10013, 2007.

[35] C. Chin, R. Grimm, P. Julienne, and E. Tiesinga. Feshbach resonances in ultracold gases. *Rev. Mod. Phys.*, 82:1225–1286, 2010.

[36] M. Greiner, O. Mandel, T. Esslinger, T. W. Hansch, and I. Bloch. Quantum phase transition from a superfluid to a Mott insulator in a gas of ultracold atoms. *Nature*, 415:39–44, 2002.

[37] L. Tarruell, D. Greif, T. Uehlinger, G. Jotzu, and T. Esslinger. Creating, moving and merging dirac points with a Fermi gas in a tunable honeycomb lattice. *Nature*, 483:302, 2012.

[38] A. E. Leanhardt, Y. Shin, D. Kielpinski, D. E. Pritchard, and W. Ketterle. Coreless vortex formation in a spinor Bose-Einstein condensate. *Phys. Rev. Lett.*, 90:140403, 2003.

[39] M. R. Matthews, B. P. Anderson, P. C. Haljan, D. S. Hall, C. E. Wieman, and E. A. Cornell. Vortices in a Bose-Einstein condensate. *Phys. Rev. Lett.*, 83: 2498–2501, 1999.

[40] J. E. Williams and M J. Holland. Preparing topological states of a Bose-Einstein condensate. *Nature*, 401:568–572, 1999.

[41] V. Schweikhard, I. Coddington, S. Tung P. Engels, and E. A. Cornell. Vortex lattice dynamics in rotating spinor Bose-Einstein condensates. *Phys. Rev. Lett.*, 2004.

[42] K. Kasamatsu, M. Tsubota, and M. Ueda. Spin textures in rotating two-component Bose-Einstein condensates. *Phys. Rev. A*, 71:043611, 2005.

[43] Y. Kawaguchi, M. Nitta, and M. Ueda. Knots in a spinor Bose-Einstein condensate. *Phys. Rev. Lett.*, 100:180403, 2008.

[44] Y. Kawaguchi and M. Ueda. Symmetry classification of spinor Bose-Einstein condensates. *Phys. Rev. A*, 84:053616, 2011.

[45] D. Durfee and W. Ketterle. Experimental studies of Bose-Einstein condensation. *Opt. Express*, 2:299–313, 1998.

[46] S. Inouye, D. M. Stamper-Kurn, H.-J. Miesner, A. P. Chikkatur, and W. Ketterle. Spin domains in ground-state Bose-Einstein condensates. *Nature*, 396: 345–348, 1998.

[47] T.-L. Ho. Spinor Bose condensates in optical traps. *Phys. Rev. Lett.*, 81:742–745, 1998.

[48] A. K. Geim and K. S. Novoselov. The rise of graphene. *Nature Materials*, 6: 183–191, 2007.

[49] M. Katsnelson and K. S. Novoselov. Graphene: New bridge between condensed matter physics and quantum electrodynamics. *Solid State Commun.*, 143, 2007.

[50] P. R. Wallace. The band structure of graphite. *Phys. Rev.*, 71:622–634, 1947.

[51] V. Gusynin, S. Sharapov, and J. Carbotte. Ac conductivity of graphene: from tight-binding model to 2+1-dimensional quantum electrodynamics. *International Journal of Modern Physics B*, 2007.

[52] L. H. Haddad and L. D. Carr. The nonlinear Dirac equation in Bose-Einstein condensates: Foundation and symmetries. *Physica D: Nonlinear Phenomena*, 238:1413–1421, 2009.

[53] J. C. Slonczewski and P. R. Weiss. Band structure of graphite. *Phys. Rev.*, 109: 272–279, 1958.

[54] M. I. Katsnelson and K. S. Novoselov. Graphene: New bridge between condensed matter physics and quantum electrodynamics. *Solid State Commun.*, 143:3–13, 2007.

[55] E. Antonyan, J. A. Harvey, S. Jensen, and D. Kutasov. NJL and QCD from string theory. *e-print arXiv:hep-th/0604017*, 2006.

[56] E. Antonyan, J. A. Harvey, and D. Kutasov. The Gross-Neveu model from string theory. *e-print arXiv:hep-th/0608149v1*, 2006.

[57] N. N. Bogoliubov. On the theory of superfluidity. *J. Phys. (USSR)*, 11:23–32, 1947.

[58] E. P. Gross. Structure of a quantized vortex in a Bose system. *Nuovo Cimento*, 20:454, 1961.

[59] L.P. Pitaevskii. Vortex lines in an imperfect Bose gas. *Sov. Phys. JETP*, 13: 451, 1961.

[60] Y. Castin and R. Dum. Low-temperature Bose-Einstein condensates in time-dependent traps: Beyond the $U(1)$ symmetry-breaking approach. *Phys. Rev. A*, 57:3008–3021, 1998.

[61] N. P. Proukakis and K. Burnett. Generalized mean fields for trapped Bose-Einstein condensates. *J. Res. Natl. Inst. Stand. Technol.*, 101:457, 1996.

[62] G. L. Alfimov, P. G. Kevrekidis, V. V. Konotop, and M. Salerno. Wannier functions analysis of the nonlinear Schrödinger equation with a periodic potential. *Phys. Rev. E*, 66:046608, 2002.

[63] V. M. Perez-Garcia, N. G. Berloff, P. G. Kevrekidis, and V. V. Konotop. Nonlinear phenomena in degenerate quantum gases. *Physica D: Nonlinear Phenomena*, 238:1289, 2009.

[64] V. I. Yukalov. Cold bosons in optical lattices. *Laser Physics*, 19:1, 2009.

[65] S. Sachdev. *Quantum Phase Transitions.* Cambridge University Press, The Edinburgh Building, Cambridge CB2 8RU, UK, 1999.

[66] A. L. Fetter. Nonuniform states of an imperfect Bose gas. *Annals of Physics*, 70:67–101, 1972.

[67] H. T. C. Stoof, D. B. M. Dickerscheid, and K. Gubbels. *Ultracold Quantum Fields.* Springer, 2009.

[68] L. D. Carr, Charles W. Clark, and W. P Reinhardt. Stationary solutions of the one-dimensional nonlinear Schrödinger equation. I. Case of repulsive nonlinearity. *Phys. Rev. A*, 62:063610, 2000.

[69] L. Salasnich, A. Parola, and L. Reatto. Dimensional reduction in Bose-Einstein-condensed alkali-metal vapors. *Phys. Rev. A*, 69:045601, 2004.

[70] O. Morch and M. Oberthaler. Dynamics of Bose-Einstein condensates in optical lattices. *Rev. Mod. Phys.*, 78:179–215, 2006.

[71] A. J. Leggett. Superfluidity. *Rev. Mod. Phys.*, 71:318–323, 1999.

[72] N. D. Mermin and H. Wagner. Absence of ferromagnetism or antiferromagnetism in one- or two-dimensional isotropic heisenberg models. *Phys. Rev. Lett.*, 17:1133–1136, 1966.

[73] Z. Hadzibabic and J. Dalibard. Two-dimensional Bose fluids: An atomic physics perspective. *Rivista Del Nuovo Cimento*, 34:389, 2011.

[74] Z. Hadzibabic, P. Kruger, M. Cheneau, B. Battelier, and J. Dalibard. Berezinskii-Kosterlitz-Thouless crossover in a trapped atomic gas. *Nat Phys*, 441:1118–1121, 2006.

[75] A. Griffin, T. Nikuni, and E. Zaremba. *Bose-Condensed Gases at Finite Temperatures.* Cambridge University Press, The Edinburgh Building, Cambridge CB2 8RU, UK, 2009.

[76] A. M. Rey, K. Burnett, R. Roth, M. Edwards, C. J. Williams, and C. W. Clark. Bogoliubov approach to superfluidity of atoms in an optical lattice. *J. Phys. B: At. Mol. Opt. Phys.*, 36:825, 2003.

[77] K. L. Lee, B. Grémaud, R. Han, B.-G. Englert, and C. Miniatura. Ultracold fermions in a graphene-type optical lattice. *Phys. Rev. A*, 80, 2009.

[78] M. P. A. Fisher, P. B. Weichman, G. Grinstein, and D. S. Fisher. Boson localization and the superfluid-insulator transition. *Phys. Rev. B*, 40:546–570, 1989.

[79] W. Zwerger. Mott-Hubbard transition of cold atoms in optical lattices. *J. Phys. B: At. Mol. Opt. Phys.*, 5, 2003.

[80] L. D. Carr, editor. *Understanding Quantum Phase Transitions.* Taylor & Francis, Boca Raton, Fl., 2010.

[81] V. L. Berezinskii. Destruction of long-range order in one-dimensional and two-dimensional system possessing a continous symmetry group. *Sov. Phys. JETP*, 34:610, 1971.

[82] J. M. Kosterlitz and D. J. Thouless. Ordering, metastability and phase transitions in two dimensional systems. *J. Phys. C: Solid State Phys.*, 6:1181, 1973.

[83] D. J. Bishop and J. D. Reppy. Study of the superfluid transition in two-dimensional ^{4}He films. *Phys. Rev. Lett.*, 40:1727–1730, 1978.

[84] D. J. Resnick, J. C. Garland, J. T. Boyd, S. Shoemaker, and R. S. Newrock. Kosterlitz-Thouless transition in proximity-coupled superconducting arrays. *Phys. Rev. Lett.*, 47:1542–1545, 1981.

[85] K. Jensen, A. Karch, D. T. Son, and E. G. Thompson. Holographic Berezinskii-Kosterlitz-Thouless transitions. *Phys. Rev. Lett.*, 105:041601, 2010.

[86] J. D. Bjorken and S. D. Drell. *Relativistic Quantum Mechanics.* McGraw-Hill, New York, NY., 1964.

[87] H. M. Pilkuhn. *Relativistic Quantum Mechanics.* Springer-Verlag Berlin Heidelberg New York, 2005.

[88] M. Nakahara. *Geometry, Topology and Physics.* Institute of Physics Publishing, 1990.

[89] D. D. Ivanenko. Notes to the theory of interaction via particles. *Zhurn. Experim. Teoret. Fiz.*, 8:260–266, 1938.

[90] W. Heisenberg. On quantization of nonlinear equations. *Nachr. Acad. Wiss. Göttingen*, 8:111–127, 1953.

[91] W. Heisenberg. Doubts and hopes in quantum electrodynamics. *Physica*, 19: 897–908, 1953.

[92] R. Finkelstein, R. Le Levier, and M. Ruderman. Nonlinear spinor fields. *Phys. Rev.*, 83:326–329, 1951.

[93] R. Finkelstein, C. Fronsdal, and P. Kaus. Nonlinear spinor field. *Phys. Rev.*, 103:1571–1574, 1956.

[94] F. Gürsey. On the conform-invariant spinor wave equations. *Nuovo Cim.*, 3: 988–1006, 1956.

[95] W. Fushchych and R. Zhdanov. *Symmetries and Exact Solutions of Nonlinear Dirac Equations.* Mathematical Ukraina Publisher, Ukraine, 1997.

[96] N. Akozbek and S. John. Optical solitary waves in two- and three-dimensional nonlinear photonic band-gap structures. *Phys. Rev. E*, 57:2287–2319, 1998.

[97] W.-K. Ng and Parwani R. R. Nonlinear Dirac equations. *SIGMA*, 5:20, 2009.

[98] M. J. Esteban, M. Lewin, and E. Seré. Stationary states of the nonlinear Dirac equation: A variational approach. *Commun. Math. Phys.*, 171:323–350, 1995.

[99] K. Takahashi. Soliton solutions of nonlinear Dirac equations. *J. Math. Phys.*, 20:1232–1238, 1979.

[100] S. Machihara, K. Nakanishi, and K Tsugawa. Well-posedness for nonlinear Dirac equations in one dimension. *Kyoto J. of Math*, 50:403–451, 2010.

[101] A. Komech and A. Komech. Global attraction to solitary waves for a nonlinear Dirac equation with mean field interaction. *SIAM Journal of Mathematical Analysis*, 42:2944–2964, 2010.

[102] T. Candy. Global existence for an L^2 critical nonlinear Dirac equation in one dimension. *Adv. Differential Equations*, 16:643–666, 2011.

[103] F. Cooper, A. Khare, B. Mihaila, and A. Saxena. Solitary waves in the nonlinear Dirac equation with arbitrary nonlinearity. *Phys. Rev. E*, 82:036604, 2010.

[104] M. J. Esteban and E. Seré. An overview on linear and nonlinear Dirac equations. *Discrete and Continuous Dynamical Systems*, 8:381–397, 2002.

[105] T. Cazenave and L. Vazquez. Existence of localized solutions for a classical nonlinear Dirac field. *Commun. Math. Phys.*, 105:35–47, 1986.

[106] L. Vazquez. Localised solutions of a non-linear spinor field. *J. Phys. A*, 10: 1361–1368, 1977.

[107] J. Bagger and E. Witten. Matter couplings in N = 2 supergravity. *Nucl. Phys. B*, 222:1–10, 1983.

[108] A. Haydys. Nonlinear Dirac operator and quaternionic analysis. *Commun. Math. Phys.*, 281:251–261, 2008.

[109] P. Soltan-Panahi, J. Struck, P. Hauke, A. Bick, W. Plenkers, G. Meineke, C. Becker, P. Windpassinger, M. Lewenstein, and K. Sengstock. Multi-component quantum gases in spin-dependent hexagonal lattices. *Nat Phys*, 7:434–440, 2010.

[110] J. Kusk Block and N. Nygaard. Honeycomb optical lattices with harmonic confinement. *Phys. Rev. A*, 81:053421, 2010.

[111] W. Fushchich and R. Zhdanov. Symmetries and exact solutions of nonlinear Dirac equations. *Phys. Rep.*, 172:123, 1989.

[112] F.M. Toyama, Y. Hosono, B. Ilyas, and Y. Nogami. Reduction of the nonlinear Dirac equation to a nonlinear Schrödinger equation with a correction term. *J. Phys. A*, 27:3139–3148, 1994.

[113] L. Hu. U(1) connection, nonlinear Dirac-like equations and Seiberg-Witten equations. *Int. J. Theor. Phys.*, 37:2115–2125, 2000.

[114] W.-K. Ng and R. R. Parwani. Nonlinear Dirac equations. *SIGMA*, 5:023, 2009.

[115] T. Cazenave and L. Vazquez. Existence of localized solutions for a nonlinear classical Dirac field. *Commun. Math. Phys.*, 105:35–47, 1986.

[116] M. J. Esteban and E. Seré. Stationary states of the nonlinear Dirac equation: A variational approach. *Commun. Math. Phys.*, 171:323–350, 1995.

[117] M. J. Esteban and E. Seré. An overview on linear and nonlinear Dirac equations. *Discrete and Cont. Dyn. Syst.*, 8:381–397, 2002.

[118] A. Maccari. Chaos, solitons and fractals in the nonlinear Dirac equation. *Phys. Lett. A*, 336:117, 2005.

[119] W. Fushchych and R. Zhdanov. *Symmetries and exact solutions of nonlinear Dirac equations.* Mathematical Ukraina Publisher, Kyiv, 1997.

[120] O. Peleg, G. Bartal, B. Freedman, O. Manela, M. Segev, and D. N. Christodoulides. Conical diffraction and gap solitons in honeycomb photonic lattices. *Phys. Rev. Lett.*, 98:103901, 2007.

[121] O. Bahat-Treidel, O. Peleg, and M. Segev. Symmetry breaking in honeycomb photonic lattices. *Opt. Lett.*, 33:2251–2253, 2008.

[122] D. Torrent and J. Sánchez-Dehesa. Acoustic analogue of graphene: Observation of Dirac cones in acoustic surface waves. *Phys. Rev. Lett.*, 108:174301, 2012.

[123] M. J. Ablowitz, S. D. Nixon, and Y. Zhu. Conical diffraction in honeycomb lattices. *Phys. Rev. A*, 79:053830, 2009.

[124] R. Gerritsma, G. Kirchmair, F. Zahringer, E. Solano, R. Blatt, and C. F. Roos. Quantum simmulation of the Dirac equation. *Nature*, 463:68–71, 2010.

[125] W. E. Thirring. A soluble relativistic field theory. *Ann. Phys.*, 3(1):91–112, 1958.

[126] S. Y. Lee, T. K. Kuo, and A. Gavrielides. Exact localized solutions of two-dimensional field theories of massive fermions with fermi interactions. *Phys. Rev. D*, 12:2249, 1975.

[127] K. S. Novoselov, A. K. Geim, S.V. Morozov, D. Jiang, M. I. Katsnelson, I.V. Grigorieva, S.V. Dubonos, and A.A. Firsov. Two-dimensional gas of massless Dirac fermions in graphene. *Nature*, 438:197–200, 2005.

[128] Y. B. Zhang, Y. W. Tan, H. L. Stormer, and P. Kim. Experimental observation of the quantum Hall effect and Berry's phase in graphene. *Nature*, 438:201–204, 2005.

[129] Y. Hatsugai, T. Fukui, and H. Aoki. Topological aspects of quantum Hall effect in graphene. *Int. J. of Mod. Phys. B*, 21:1133–1139, 2007.

[130] C. Wu, D. Bergman, L. Balents, and S. D. Sarma. Flat bands and Wigner crystallization in the honeycomb optical lattice. *Phys. Rev. Lett.*, 99:070401, 2007.

[131] L.-M. Duan, E. Demler, and M. D. Lukin. Controlling spin exchange interactions of ultracold atoms in optical lattices. *Phys. Rev. Lett.*, 91:090402, 2003.

[132] L. M. Duan. Effective Hamiltonian for fermions in an optical lattice across Feshbach resonance. *Phys. Rev. Lett.*, 95:243202, 2005.

[133] S. L. Zhu, B. Wang, and L.-M. Duan. Simulation and detection of Dirac fermions with cold atoms in an optical lattice. *Phys. Rev. Lett.*, 98:260402, 2007.

[134] L. Lih-King, C. Morais Smith, and A. Hemmerich. Staggered-vortex superfluid of ultracold bosons in an optical lattice. *Phys. Rev. Lett.*, 100:130402, 2008.

[135] G. Juzeliunas, J. Ruseckas, M. Lindberg, L. Santos, and P. Ohberg. Quasirelativistic behavior of cold atoms in light fields. *Phys. Rev. A*, 77:011802, 2008.

[136] W. Congjun and S. Das Sarma. The $p_{x,y}$-orbital counterpart of graphene: Cold atoms in the honeycomb optical lattice. *Phys. Rev. B*, page 235107, 2008.

[137] J. Ruostekoski, J. Javanainen, and G. V. Dunne. Manipulating atoms in an optical lattice: Fractional fermion number and its optical quantum measurement. *Phys. Rev. A*, 77:013603, 2008.

[138] J. Ruostekoski, G. V. Dunne, and J. Javanainen. Particle number fractionalization of an atomic fermi-dirac gas in an optical lattice. *Phys. Rev. Lett.*, 88: 180401, 2002.

[139] R. V. Mishmash and L. D. Carr. Ultracold atoms in 1D optical lattices: Mean field, quantum field, computation, and soliton formation. *Mathematics and Computers in Simulation*, 80:732, 2009.

[140] R. V. Mishmash and L. D. Carr. Quantum entangled dark solitons formed by ultracold atoms in optical lattices. *Phys. Rev. Lett.*, 103:140403, 2007.

[141] A. Ferrando, H. Michinel, M. Seco, and D. Tommasini. Nonlinear phase shift from photon-photon scattering in vacuum. *Phys. Rev. Lett.*, 99:150404, 2007.

[142] A. M. Rey. *Ultracold bosonic atoms in optical lattices.* PhD thesis, University of Maryland, 2004.

[143] P. B. Blakie and C. W. Clark. Wannier states and Bose-Hubbard parameters for 2D optical lattices. *J. Phys. B*, 37:1391, 2004.

[144] E. Taylor and E. Zaremba. Bogoliubov sound speed in periodically modulated Bose-Einstein condensates. *Phys. Rev. A*, 68:053611, 2003.

[145] B. Wu and J. Shi. Critical velocities for a superfluid in a periodic potential. *e-print cond-mat/0607098*, 2006.

[146] J. Hladik. *Spinors in Physics.* Springer-Verlag, 1999.

[147] N. Akozbek and S. John. Optical solitary waves in two- and three-dimensional nonlinear photonic band-gap structures. *Phys. Rev. E*, 57:2287–2319, 1998.

[148] I. Merhasin and B. Malomed. Four-wave solitons in waveguides with a cross-grating. *Phys. Lett. A*, 327:296–311, 2004.

[149] I. Merhasin and B. Malomed. Four-wave solitons in bragg cross-gratings. *J. Opt. B*, 6:S323–S332, 2004.

[150] P. Krekora, Q. Su, and R. Grobe. Relativistic electron localization and the lack of zitterbewegung. *Phys. Rev. Lett.*, 93:043004, 2004.

[151] P. Krekora, Q. Su, and R. Grobe. Klein paradox in spatial and temporal resolution. *Phys. Rev. Lett.*, 92:040406, 2002.

[152] P. Krekora, K. Cooley, Q. Su, and R. Grobe. Creation dynamics of bound states in supercritical fields. *Phys. Rev. Lett.*, 95:070403, 2005.

[153] A. Zee. *Quantum Field Theory in a Nutshell.* Princeton University Press, 41 William Street, Princeton, New Jersey 08540, 2010.

[154] B. Seradjeh and M. Franz. Fractional statistics of topological defects in graphene and related structures. *Phys. Rev. Lett.*, 101:146401, 2008.

[155] S. Ryu, C. Mudry, C. Hou, and C. Chamon. Masses in graphenelike two-dimensional electronic systems: Topological defects in order parameters and their fractional exchange statistics. *Phys. Rev. B*, 80:205319, 2009.

[156] I. Duck, W. Pauli, and E. C. G. Sudarshan. *Pauli and the Spin-Statistics Theorem.* World Scientific Publishing Company, Incorporated, 27 Warren Street, Suite 401-402 Hackensack, NJ 07601 USA, January 1998.

[157] W. Pauli. The connection between spin and statistics. *Phys. Rev.*, 58:716, 1940.

[158] J. Schwinger. The theory of quantized fields. I. *Phys. Rev.*, 82:914, 1951.

[159] J. Schwinger. The theory of quantized fields. II. *Phys. Rev.*, 91:713, 1953.

[160] L. J. Garay, J. R. Anglin, J. I. Cirac, and P. Zoller. Sonic analog of gravitational black holes in Bose-Einstein condensates. *Phys. Rev. Lett.*, 85:4643, 2000.

[161] A. Rapp, G. Zarand, C. Honerkamp, and W. Hofstetter. Color superfluidity and "baryon" formation in ultracold fermions. *Phys. Rev. Lett.*, 98:160405, 2007.

[162] Y. Yu and K. Yang. Supersymmetry and the goldstino-like mode in Bose-Fermi mixtures. *Phys. Rev. Lett.*, 100:090404, 2008.

[163] S. A. Hartnoll. *Understanding Quantum Phase Transitions.* Taylor & Francis, Boca Raton, Fl., 2010.

[164] M. Snoek, S. Vandoren, and H. T. C. Stoof. Theory of ultracold superstrings. *Phys. Rev. A*, 74:033607, 2009.

[165] M. Merkl, A. Jacob, F. E. Zimmer, P. Ahberg, and L. Santos. Chiral confinement in quasirelativistic Bose-Einstein condensates. *Phys. Rev. Lett.*, 104: 073603, 2010.

[166] L. H. Haddad and L. D. Carr. The nonlinear Dirac equation in Bose-Einstein condensates: Foundation and symmetries. *Physica D: Nonlinear Phenomena*, 238:1413, 2009.

[167] C. Becker, P. Soltan-Panahi, J. Kronjager, S. Dorscher, K. Bongs, and K. Sengstock. Ultracold quantum gases in triangular optical lattices. *New J. Phys.*, 12:065025, 2010.

[168] O. Bahat-Treidel, O. Peleg, M. Segev, and H. Buljan. Breakdown of Dirac dynamics in honeycomb lattices due to nonlinear interactions. *Phys. Rev. A*, 82:013830, 2010.

[169] G. W. Semenoff. Condensed-matter simulation of a three-dimensional anomaly. *Phys. Rev. Lett.*, 53:2449, 1984.

[170] F. D. M. Haldane. Model for a quantum hall effect without Landau levels: Condensed-matter realization of the "parity anomaly". *Phys. Rev. Lett.*, 61: 2015, 1988.

[171] A. L. Fetter. Nonuniform states of an imperfect Bose gas. *Ann. Phys.*, 70:67, 1972.

[172] L.-K. Lim, A. Lazarides, A. Hemmerich, and C. Morais Smith. Strongly interacting two-dimensional Dirac fermions. *Europhys. Lett.*, 88:36001, 2009.

[173] X.-J. Liu, X. Liu, C. Wu, and J. Sinova. Quantum anomalous Hall effect with cold atoms trapped in a square lattice. *Phys. Rev. A*, 81:033622, 2010.

[174] J. K. Block and N. Nygaard. Honeycomb optical lattices with harmonic confinement. *Phys. Rev. A*, 81:053421, 2010.

[175] D. L. Feder, A. A. Svidzinsky, A. L. Fetter, and C. W. Clark. Anomalous modes drive vortex dynamics in confined Bose-Einstein condensates. *Phys. Rev. A*, 62: 053606, 2000.

[176] E. J. Mueller. Spin textures in slowly rotating Bose-Einstein condensates. *Phys. Rev. A*, 69:033606, 2004.

[177] J. V. Jelley. *Cherenkov Radiation and its Applications.* Pergamon Press, London, 1958.

[178] A.-C. Ji, W. M. Liu, J. L. Song, and F. Zhou. Dynamical creation of fractionalized vortices and vortex lattices. *Phys. Rev. Lett.*, 101:010402, 2008.

[179] K. G. Lagoudakis, T. Ostatnický, A. V. Kavokin, Y. G. Rubo, R. André, and B. Deveaud-Plédran. Observation of half-quantum vortices in an exciton-polariton condensate. *Science*, 326:974, 2009.

[180] A. L. Fetter. Rotating trapped Bose-Einstein condensates. *Rev. Mod. Phys.*, 81:647, 2009.

[181] M. R. Matthews, B. P. Anderson, P. C. Haljan, D. S. Hall, C. E. Wieman, and E. A. Cornell. Vortices in a Bose-Einstein condensate. *Phys. Rev. Lett.*, 83: 2498–2501, 1999.

[182] An-Chun Ji, W. M. Liu, J. L. Song, and F. Zhou. Dynamical creation of fractionalized vortices and vortex lattices. *Phys. Rev. Lett.*, 101:010402, 2008.

[183] A. K. Geim and K. S. Novoselov. The rise of graphene. *Nature*, 6, 2007.

[184] L. H. Haddad and L. D. Carr. Relativistic linear stability equations for the nonlinear Dirac equation in Bose-Einstein condensates. *EPL (Europhysics Letters)*, 94:56002, 2011.

[185] H. B. Nielsen and P. Olesen. Vortex-line models for dual strings. *Nucl. Phys. B*, 61:45–61, 1973.

[186] N. Seiberg and E. Witten. Electric-magnetic duality, monopole condensation, and confinement in N=2 supersymmetric Yang-Mills theory. *Nuclear Physics B*, 426:19–52, 1994.

[187] G. Grynberg, B. Lounis, P. Verkerk, J.-Y. Courtois, and C. Salomon. Quantized motion of cold cesium atoms in 2-dimensional and 3-dimensional optical potentials. *Phys. Rev. Lett.*, 70:2249–2252, 1993.

[188] P. Soltan-Panahi, J. Struck, P. Hauke, A. Bick, W. Plenkers, G. Meineke, C. Becker, P. Windpassinger, M. Lewenstein, and K. Sengstock. Multi-component quantum gases in spin-dependent hexagonal lattices. *Nat Phys*, 7:434–440, 2011.

[189] P. T. Ernst, S. Goetze, J. S. Krauser, K. Pyka, D.-S. Luehmann, D. Pfannkuche, and K. Sengstock. Probing superfluids in optical lattices by momentum-resolved Bragg spectroscopy. *Nat Phys*, 6:56–61, 2010.

[190] A. F. Rañada, M. F. Rañada, M. Soler, and L. Vázquez. Classical electrodynamics of a nonlinear Dirac field with anomalous magnetic moment. *Phys. Rev. D*, 10:517–525, 1974.

[191] M. F. Andersen, C. Ryu, Pierre Cladé, Vasant Natarajan, A. Vaziri, K. Helmerson, and W. D. Phillips. Quantized rotation of atoms from photons with orbital angular momentum. *Phys. Rev. Lett.*, 97:170406, 2006.

[192] J. Leach, E. Yao, and M. J. Padgett. Observation of the vortex structure of a non-integer vortex beam. *New J. Phys.*, 6:71, 2004.

[193] I. V. Basistiy, V. A. Pas'ko, V. V. Slyusar, M. S. Soskin, and M. V. Vasnetsov. Synthesis and analysis of optical vortices with fractional topological charges. *J. Opt. A*, 6:S166, 2004.

[194] S. Trotzky, L. Pollet, F. Gerbier, U. Schnorrberger, I. Bloch, N.V. Prokof'ev, B. Svistunov, and M. Troyer. Suppression of the critical temperature for superfluidity near the Mott transition. *Nat Phys*, 6:998–1004, 2010.

[195] L. D. Carr and Charles W. Clark. Vortices and ring solitons in Bose-Einstein condensates. *Phys. Rev. A*, 74:043613, 2006.

[196] S. Kawai and S. Sasaki. BPS vortices in nonrelativistic M2-brane Chern-Simons-matter theory. *Phys. Rev. D*, 80:025007, 2009.

[197] T. Ohmi and M. Nakahara. Quantum computing with p-wave superfluid vortices. *Journal of the Physical Society of Japan*, 79(1):104602, 2010.

[198] B. Kain and H. Y. Ling. Vortices in Bose-Einstein condensate dark matter. *Phys. Rev. D*, 82:064042, September 2010.

[199] M. Tsubota and K. Kasamatsu. Quantized vortices and quantum turbulence. *arXiv:1202.1863v1*, 2012.

[200] B. J. Schroer. The spectrum of Bogomol'nyi solitons in gauged linear sigma models. *Nucl. Phys. B*, 475:440, 1996.

[201] J. Polchinski. Cosmic superstrings revisited. *Int. J. of Mod. Phys. A*, 20:3413, 2005.

[202] K. Lee. The dual formulation of cosmic strings and vortices. *Phys. Rev. D*, 48: 2493–2498, 1993.

[203] L. G. Aldrovandi and F. A. Schaposnik. Non-Abelian vortices in Chern-Simons theories and their induced effective theory. *Phys. Rev. D*, 76:045010, 2007.

[204] D. Rickles. Mirror symmetry and other miracles in superstring theory. *Foundations of Physics*, pages 1–27, 2010.

[205] *Trieste lectures on mirror symmetry*, number 13, Strada Costiera, 11, I - 34151, Trieste Italy, 2002. ICTP spring school on superstrings and related matters, ICTP.

[206] M. Li. 't Hooft vortices on D-branes. *Journal of High Energy Physics*, 9807:3, 1998.

[207] R. Auzzi, S. Bolognesi, J. Evslin, K. Konishi, and A. Yung. Non-Abelian superconductors: Vortices and confinement in N=2 SQCD. *Nucl. Phys. B*, 673: 187, 2003.

[208] C.-H. Park and S. G. Louie. Making massless Dirac fermions from a patterned two-dimensional electron gas. *Nano Letters*, 9:1793–1797, 2009.

[209] A. Szameit, M. C. Rechtsman, O. Bahat-Treidel, and M. Segev. PT-symmetry in honeycomb photonic lattices. *Phys. Rev. A*, 84:021806, 2011.

[210] P. J. Dellar, D. Lapitski, S. Palpacelli, and S. Succi. Isotropy of three-dimensional quantum lattice Boltzmann schemes. *Phys. Rev. E*, 83:046706, 2011.

[211] M. Merkl, A. Jacob, F. E. Zimmer, P. Ahberg, and L. Santos. Chiral confinement in quasirelativistic Bose-Einstein condensates. *Phys. Rev. Lett.*, 104: 073603, 2010.

[212] C. Becker, P. Soltan-Panahi, J. Kronjager, S. Dorscher, K. Bongs, and K. Sengstock. Ultracold quantum gases in triangular optical lattices. *New J. Phys.*, 12:065025, 2010.

[213] E. Kapit and E. Mueller. Optical-lattice Hamiltonians for relativistic quantum electrodynamics. *Phys. Rev. A*, 83(3):033625, 2011.

[214] W. Zhang, P. Zhang, S. Duan, and X. G. Zhao. Quasi-energy spectra of a charged particle in planar honeycomb lattices. *New J. Phys.*, 11:063032, 2009.

[215] W. K. Ng and R. R. Parwani. Nonlinear Schrödinger-Pauli equations. *arXiv:0807.1877*, 2008.

[216] P. D. Gupta, S. Raj, and D. Chaudhuri. Some exact stationary state solutions of a nonlinear Dirac equation in 2+1 dimensions. *Journal of Physics A: Mathematical and General*, page 8, 2010.

[217] W.-K. Ng and R. R. Parwani. Information and particle physics. *Modern Physics Letters A*, 26:681–689, 2011.

[218] L. Fu and C. L. Kane. Topological insulators with inversion symmetry. *Phys. Rev. B*, 76:045302, 2007.

[219] M. Z. Hasan and C. L. Kane. Colloquium: Topological insulators. *Rev. Mod. Phys.*, 82:3045, 2010.

[220] H. Buljan, G. Bartal, O. Cohen, T. Schwartz, O. Manela, T. Carmon, M. Segev, J. W. Fleischer, and D. N. Christodoulides. Partially coherent waves in nonlinear periodic lattices. *Studies in Applied Mathematics*, 115:173–208, 2005.

[221] N. K. Efremidis, J. Hudock, D. N. Christodoulides, J. W. Fleischer, O. Cohen, and M. Segev. Two-dimensional optical lattice solitons. *Phys. Rev. Lett.*, 91: 213906, 2003.

[222] O. Manela, M. Segev, D. N. Christodoulides, and D. Kip. Hofstadter butterflies in nonlinear Harper lattices, and their optical realizations. *New J. Phys.*, 12: 053017, 2010.

[223] D. N. Christodoulides and R. I. Joseph. Vector solitons in birefringent nonlinear dispersive media. *Opt. Lett.*, 13:53–55, 1988.

[224] S. Bitner, B. Dietz, M. Miski-Oglu, P. Oria Iriarte, A. Richter, and F. Schaefer. Observation of a Dirac point in microwave experiments with a photonic crystal modeling graphene. *Phys. Rev. B*, 82:014301, 2010.

[225] P. O. Fedichev and G. V. Shlyapnikov. Dissipative dynamics of a vortex state in a trapped Bose-condensed gas. *Phys. Rev. A*, 60:1779–1782, 1999.

[226] D. S. Petrov, M. Holzmann, and G. V. Shlyapnikov. Bose-Einstein condensation in quasi-2D trapped gases. *Phys. Rev. Lett.*, 84:2551–2555, 2000.

[227] C. D. Fertig, K. M. O'Hara, J. H. Huckans, S. L. Rolston, W. D. Phillips, and J. V. Porto. Strongly inhibited transport of a degenerate 1D Bose gas in a lattice. *Phys. Rev. Lett.*, 94:120403, 2005.

[228] I. H. Deutsch and P. S. Jessen. Quantum control and measurement of atomic spins in polarization spectroscopy. *Opt. Comm.*, 283:681–694, 2010.

[229] D. M. Stamper-Kurn, A. P. Chikkatur, A. Görlitz, S. Inouye, S. Gupta, D. E. Pritchard, and W. Ketterle. Excitation of phonons in a Bose-Einstein condensate by light scattering. *Phys. Rev. Lett.*, 83:2876–2879, 1999.

[230] L. D. Carr and Charles W. Clark. Vortices in attractive Bose-Einstein condensates in two dimensions. *Phys. Rev. Lett.*, 97:010403, 2006.

[231] U. Leonhardt and G. Volovik. How to create an Alice string (half-quantum vortex) in a vector Bose-Einstein condensate. *JETP Letters*, 72:46–48, 2000.

[232] P. W. Anderson and G. Toulouse. Phase slippage without vortex cores: Vortex textures in superfluid ^{3}He. *Phys. Rev. Lett.*, 38:508–511, 1977.

[233] N. D. Mermin and T.-L. Ho. Circulation and angular momentum in the A phase of superfluid helium-3. *Phys. Rev. Lett.*, 36:594–597, 1976.

[234] M. M. Salomaa and G. E. Volovik. Half-quantum vortices in superfluid ^{3}He-A. *Phys. Rev. Lett.*, 55:1184–1187, 1985.

[235] V. Zagrebnov. The Bogoliubov model of weakly imperfect Bose gas. *Phys. Rep.*, 350:291–434, 2001.

[236] S. Adams and J. B. Bru. Critical analysis of the Bogoliubov theory of superfluidity. *Physica A: Statistical Mechanics and its Applications*, 332:60–78, 2004.

[237] R. Jackiw and Erick J. Weinberg. Self-dual Chern-Simons vortices. *Phys. Rev. Lett.*, 64:2234, 1990.

[238] G. V. Dunne, R. Jackiw, S.-Y. Pi, and C. A. Trugenberger. Self-dual Chern-Simons solitons and two-dimensional nonlinear equations. *Phys. Rev. D*, 43: 1332, 1991.

[239] P. A. Horvathy and P. Zhang. Vortices in (Abelian) Chern-Simons gauge theory. *Phys. Rep.*, 481:88, 2008.

[240] Z. H. Musslimani, M. Segev, and D. N. Christodoulides. Multicomponent two-dimensional solitons carrying topological charges. *Opt. Lett.*, 25:61–63, 2000.

[241] Y. V. Kartashov, B. A. Malomed, and L. Torner. Solitons in nonlinear lattices. *Rev. Mod. Phys.*, 83:247, 2011.

[242] K.-Y. Lee R. Jackiw and E. Weinberg. Self-dual Chern-Simons solitons. *Phys. Rev. D*, 42:3488, 1990.

[243] M. Y. Han, B. Özyilmaz, Y. Zhang, and P. Kim. Energy band-gap engineering of graphene nanoribbons. *Phys. Rev. Lett.*, 98:206805, 2007.

[244] J. Yang, B. A. Malomed, and D. J. Kaup. Embedded solitons in second-harmonic-generating systems. *Phys. Rev. Lett.*, 83:1958–1961, 1999.

[245] D. Bartolucci and G. Tarantello. Liouville type equations with singular data and their applications to periodic multivortices for the electroweak theory. *Communications in Mathematical Physics*, 229:3–47, 2002.

[246] A. Sakhnovich. Non-self-adjoint Dirac-type systems and related nonlinear equations: Wave functions, solutions, and explicit formulas. *Integral Equations and Operator Theory*, 55:127–143, 2006.

[247] S. Ting and Z.-W. Wang. An application of a generalized version of the dressing method to integration of a variable-coefficient Dirac system. *Chinese Physics Letters*, 27:090203, 2010.

[248] L. Luo. Darboux transformation and exact solutions for a hierarchy of nonlinear evolution equations. *Journal of Physics A: Mathematical and Theoretical*, 40: 4169, 2007.

[249] X.-Y. Wen and Y.-T. Gao. Darboux transformation and explicit solutions for discretized modified Korteweg-de Vries lattice equation. *Communications in Theoretical Physics*, 53:825, 2010.

[250] J. Wang. Darboux transformation and soliton solutions for the Heisenberg hierarchy. *Journal of Physics A: Mathematical and General*, 38:5217, 2005.

[251] M. I. Katsnelson, K. S. Novoselov, and A. K. Geim. Chiral tunnelling and the Klein paradox in graphene. *Nat Phys*, 2:1745–2473, 2006.